

The Role of Intramyocellular Lipid Content in the Physiological Changes Observed in Inactivity, Exercise, and Non-Alcoholic Fatty Liver Disease

Prince Kudakwashe Chivaka, BSc. (Hons),
MSc.



Thesis submitted to the University of Nottingham
for the degree of Doctor of Philosophy

(August 2022)

Thesis Abstract

Lipid stored within droplets in skeletal muscle, referred to as intramyocellular lipid (IMCL), has established and emerging roles in health and disease. Lipid droplets (LDs) act as the first destination for activated fatty acids (FAs) following their esterification to triacylglycerol (TAG). Under normal physiological conditions these FAs are then released from LDs to supply adjacent mitochondria with substrate for ATP production during fasting and exercise. It has been proposed that dysregulation of adipose tissue storage, in the context of chronic overfeeding, and basal and insulin-mediated impairments in muscle lipid oxidation in response to inactivity are responsible for the ectopic accumulation of lipid in the skeletal muscles. This accumulation can result in increased sarcoplasmic and sarcolemmal expression of intermediates of TAG synthesis and lipolysis, which attenuate the insulin signalling pathway, resulting in skeletal muscle and whole-body insulin resistance, and potentially contributing to the aetiology of non-alcoholic fatty liver disease (NAFLD). However, the associations between IMCL accumulation and insulin resistance in inactivity and NAFLD are equivocal, and the adaptations in IMCL to resistance exercise training are poorly defined. Therefore, primarily using the hyperinsulinaemic-euglycaemic clamp technique, the gold standard method in the assessment of insulin action in humans in vivo, and histochemical quantification of total and fibre-type specific IMCL content, the results of the work in this thesis contribute to our understanding of the role of IMCL in inactivity, resistance exercise training, and NAFLD.

This thesis comprises primarily of retrospective analyses of four comprehensive human volunteer studies. The studies described in **Chapter 3** explored the role of IMCL in the development of whole-body insulin resistance during acute (3 days) and chronic (56 days) bed rest in healthy, male participants maintained in energy balance throughout. Glucose disposal was decreased by a similar magnitude after 3 and 56 days of bed rest, and these observations could not be explained by IMCL accumulation. This suggests that

inactivity per se is the primary driver of whole-body insulin resistance during bed rest and that IMCL accumulation is likely to be a confounding response that occurs when participants are in positive energy balance.

It has been proposed that overfeeding, which contributes to the pathogenesis of obese NAFLD by increasing plasma FA concentration and hepatic lipid content, also leads to the ectopic accumulation of IMCL. Given that the skeletal muscles are the main sites for the disposal of glucose and that IMCL accumulation is associated with muscle insulin resistance, increased muscle lipid content may contribute to the development of whole-body insulin resistance in those with NAFLD. The study described in **Chapter 4** investigated differences in IMCL content, skeletal muscle glucose disposal, and whole-body glucose disposal between individuals with NAFLD and healthy controls to determine if muscle lipid content does in fact contribute to insulin resistance in those with NAFLD. It was observed that IMCL content was not different between healthy males and males with NAFLD, even though skeletal muscle and whole-body glucose disposal were significantly reduced in those with NAFLD. These findings suggest that IMCL accumulation is not a contributor to the development of insulin resistance in NAFLD.

The study described in **Chapter 5** explored changes in IMCL and perilipin 5 (PLIN5) content in response to a 12-week resistance training intervention, which has not been investigated in detail to date. A secondary aim was to determine the impact of the non-steroidal anti-inflammatory drug (NSAID), diclofenac, on the mRNA expression of genes involved in FA metabolism and oxidation. It was hypothesised that diclofenac would have a role in these processes based on evidence of its affinity for Peroxisome proliferator-activated receptor gamma (PPAR- γ) in vitro. This study comprised a randomised, placebo controlled, double-blind protocol in which one group of exercise-trained participants ingested diclofenac, 75 mg/daily, concurrent with the exercise protocol. IMCL content and muscle PLIN5 content did not change in response to the resistance exercise intervention, though diclofenac administration robustly altered the mRNA expression of genes involved in lipid metabolism.

This thesis presents novel insights into the role of IMCL content in the development of insulin resistance in the context of bed rest-induced immobilisation and NAFLD. It also identifies a new trajectory for future research into diclofenac, an NSAID which may alter muscle FA oxidation via a previously underexplored mechanism.

Declaration

The work described in this thesis was funded by the Centre for Sport, Exercise and Osteoarthritis Research Versus Arthritis, within the School of Life Sciences, Queen's Medical Centre, The University of Nottingham.

All histochemical analyses were performed by me. Sectioning, fluorescent and immunohistochemical staining, and imaging of vastus lateralis biopsies from the acute and chronic bed rest studies described in **Chapter 3** was performed by me at the Core Facility for Integrated Microscopy (CFIM), University of Copenhagen (www.cfim.ku.dk), with training and supervision by Professor Clara Prats and CFIM staff. Method validation was performed by me at CFIM. Hyperinsulinaemic-euglycaemic clamps and DEXA procedures and analyses were performed by Dr. Liz Simpson and Dr. Natalie Shur. Analysis of blood samples for plasma insulin, triglyceride, and FFA concentrations was performed by Sally Corden. In **Chapter 4** Dr. Liz Simpson and Dr. Prarthana Thiagarajan performed the hyperinsulinaemic-euglycaemic clamps in control volunteers and fatty liver disease patients. In **Chapter 5** Dr. Jo Mallinson and Dr. Tariq Taylor conducted the exercise intervention protocols and muscle mRNA expression analyses were performed by Dr. Despina Constantin.

Magnetic resonance spectroscopy of skeletal muscle for the quantification of IMCL:EMCL ratio and liver for the determination of intrahepatic triglyceride content was performed by the staff of the Sir Peter Mansfield Imaging Centre, The University of Nottingham.

Except where assistance by colleagues in academic and technical roles at CFIM and The University of Nottingham has been declared in the preceding statements, I attest to the fact that this thesis was composed by me and serves as an accurate record of the work I have performed. No part of this thesis has previously been submitted for the degree of Doctor of Philosophy or any other degree in higher education.

Prince Chivaka, August 2022

Acknowledgements

It is difficult to put into words how important those who should be acknowledged here have been to completing my PhD and to my academic and personal development throughout the years. But I will do my best.

Firstly, I would like to extend my sincerest gratitude to my supervisors Professor Paul Greenhaff and Dr. Liz Simpson for their time, guidance, and patience, especially during the writing of this thesis. My admiration for their vast knowledge and enthusiasm for research will persist long after the completion of my PhD.

The work presented within this thesis would not have been possible without the contributions of many members of the Physiology, Metabolism, and Nutrition research team to whom I owe my thanks. One of the things I developed a greater appreciation for during my PhD is the fact that research is a team sport. In that regard I count myself very lucky to have been part of such a fantastic group.

To Professor Clara Prats for her kindness, hospitality, and encouragement during my time in Copenhagen and for teaching me many of the methods which formed the foundation of this thesis. Thank you.

Lastly to my family. To my Baba whose pep talks on the importance of “Education, education, education” have been instrumental to all my academic pursuits, including the completion of my PhD. To my Mhamha for her endless warmth, belief, and support. And to my Siblings Grace and Nigel for their positivity and humour. Ndinokutendai mose.

Covid Impact Statement

From March 2020 to September 2020, national lockdown measures and the “work from home” directive meant that the University of Nottingham’s Medical School facilities within the Queen’s Medical Centre were closed to all students and most research, academic, and technical personnel. This prevented access to the wet laboratories and imaging equipment within the Medical School necessary to perform the work presented in **Chapters 4** and **5**.

Delays in the importation of reagents from the United States and Continental Europe from March 2020 to the final months of 2020, alongside occupancy restrictions placed on the use of laboratories within the Medical School once research activity was possible meant that the work necessary to generate the data presented in **Chapter 4** could not begin until the 16th of October 2020. This loss of time had a significant knock-on effect into 2021 such that applications for time and funding extensions were submitted to, and accepted by, the University of Nottingham and Versus Arthritis respectively.

These time restrictions meant that the data generated by the present author in **Chapters 4** and **5** constituted retrospective analyses of prior studies rather than a direct follow up to **Chapter 3**. This follow-up would have involved maintaining participants in positive energy balance during the course of an acute, 3-7 days, period of bed rest to determine if IMCL content increased under these conditions and if this increase exacerbated inactivity-induced attenuation of whole-body glucose disposal.

Conference Communications and Publications

During my doctoral study period the data presented in this thesis resulted in the following conference communications and publications.

Conference Communications

Abstracts

Shur, N.F., Simpson, E.J., Chivaka, P.K., Crossland, H., Constantin, D., Constantin-Teodosiu, D., Stephens, F.B., Lobo, D.N., Prats, C., Macdonald, I.A., and Greenhaff, P.L. (2020) Impaired insulin sensitivity and carbohydrate oxidation during bed rest in healthy participants. *Clinical Nutrition (ESPEN)*.

Chivaka, P.K., Mallinson, J., Taylor, T., Constantin, D., Constantin-Toeodsiu, D., Simpson, E.J., and Greenhaff, P.L. (2023) Diclofenac alters expression of genes regulating muscle lipid metabolism during resistance exercise training in humans, but does not change IMCL content. *Surgical Research Society Annual Meeting*.

Presentations

(09/07/2019) Arthritis Research UK Intern Dissemination Day (Nottingham Visit):

Oral presentation titled “The Influence of Short- and Long-term Immobilisation on IMCL and Insulin Resistance”.

(21/07/2020) University of Nottingham SOLS PGR Symposium 2020:

Poster presentation titled “Intramyocellular lipid content is unaffected by acute and chronic bed rest in young healthy volunteers maintained in energy balance and is not responsible for impaired glucose disposal under these conditions.”

Best Scientific Poster (Physiology and Anatomy): Winner

Best Scientific Poster (Overall): Winner

(19/04/2021) Centre for Sport, Exercise and Osteoarthritis Research, Versus Arthritis- Exercise for the Prevention and Management of Osteoarthritis and associated Comorbidities Conference:

Oral presentation titled “Intramyocellular lipid content is unaffected by acute and chronic bed rest and rehabilitation”.

(12/04/2022) The Biomedical Basis of Elite Performance 2022:

Poster presentation titled “IMCL content is unaffected by acute and chronic bed rest in healthy volunteers maintained in energy balance and is not responsible for impaired glucose disposal under these conditions.”

Early Career Researcher Poster Award: Runner-up

(10/06/2022) NIHR & BRC Gastro-intestinal and Liver Research Showcase Event:

Poster presentation titled “Intramyocellular lipid content is unaffected by acute and chronic bed rest in young healthy male volunteers maintained in energy balance and is not responsible for impaired glucose disposal under these conditions.”

Publications

Shur, N.F., Simpson, E.J., Crossland, H., Chivaka, P.K., Constantin, D., Cordon, S.M., Constantin-Teodosiu, D., Stephens, F.B., Lobo, D.N., Szewczyk, N., Narici, M., Prats, C., Macdonald, I.A., and Greenhaff, P.L. (2022) Human adaptation to immobilization: Novel insights of impacts on glucose disposal and fuel utilization. *Journal Of Cachexia, Sarcopenia and Muscle*. 13 (6), pp. 2999-3013.

Table of Contents

THESIS ABSTRACT	I
DECLARATION IV	
ACKNOWLEDGEMENTS	V
COVID IMPACT STATEMENT	VI
CONFERENCE COMMUNICATIONS AND PUBLICATIONS	VII
CONFERENCE COMMUNICATIONS	VII
PUBLICATIONS	VIII
TABLE OF CONTENTS	IX
LIST OF FIGURES	XIV
LIST OF TABLES	XXI
LIST OF ABBREVIATIONS	XXIII
1. GENERAL INTRODUCTION	1
1.1 LIPID DROPLETS AND THEIR ROLE IN HEALTH AND DISEASE	1
1.1.1 INTRAMYOCELLULAR LIPID CONTENT.....	3
1.1.2 IMPORTANCE OF FIBRE TYPE TO SKELETAL MUSCLE FUNCTION AND IMCL CONTENT ...	4
1.2 MECHANISMS REGULATING IMCL CONTENT	6
1.2.1 FA TRANSPORT INTO SKELETAL MUSCLE AND ENERGY BALANCE.....	6
1.2.2 TAG SYNTHESIS AND STORAGE IN LDLs	10
1.2.3 LDL TAG LIPOLYSIS	11
1.2.4 OXIDATION OF LDL-DERIVED FA	13
1.2.5 DE NOVO LIPOGENESIS.....	18
1.3 SKELETAL MUSCLE GLUCOSE UPTAKE AND UTILISATION	20
1.3.1 INSULIN-MEDIATED GLUCOSE UPTAKE IN SKELETAL MUSCLE	21
1.3.2 CONTRACTION-MEDIATED GLUCOSE UPTAKE IN SKELETAL MUSCLE.....	24
1.3.3 CARBOHYDRATE UTILISATION	28
1.4 INTEGRATION OF MUSCLE FA AND GLUCOSE OXIDATION	34
1.4.1 SKELETAL MUSCLE FUEL OXIDATION IN THE POSTABSORPTIVE STATE	34
1.4.2 SKELETAL MUSCLE FUEL OXIDATION IN THE POSTPRANDIAL STATE.....	36
1.4.3 METABOLIC FLEXIBILITY AND PHYSICAL ACTIVITY STATUS	37
1.4.4 SKELETAL MUSCLE FUEL OXIDATION DURING EXERCISE	38

1.4.5	TRANSCRIPTIONAL REGULATION OF SKELETAL MUSCLE FUEL OXIDATION	41
1.5	LIPID-INDUCED INSULIN RESISTANCE.....	45
1.5.1	WHAT IS INSULIN RESISTANCE?	45
1.5.2	EVIDENCE OF AN ASSOCIATION BETWEEN IMCL AND IMPAIRED GLUCOSE UPTAKE	46
1.5.3	THE LIPID OVERFLOW THEORY	48
1.5.4	MECHANISMS OF LIPID-INDUCED INSULIN RESISTANCE	51
1.6	INACTIVITY-INDUCED INSULIN RESISTANCE.....	55
1.7	THESIS STRUCTURE AND AIMS.....	57
1.8	REFERENCES.....	59
2.	GENERAL METHODS.....	105
2.1	HYPERINSULINAEMIC-EUGLYCEMIC CLAMP TECHNIQUE IN THE MEASUREMENT OF WHOLE-BODY GLUCOSE DISPOSAL.....	105
2.1.1	OVERVIEW OF THE HYPERINSULINAEMIC-EUGLYCAEMIC CLAMP	105
2.1.2	CALCULATING THE M VALUE.....	106
2.2	DETERMINATION OF BODY COMPOSITION USING DUAL-ENERGY X-RAY ABSORPTIOMETRY (DEXA).....	107
2.3	INDIRECT CALORIMETRY.....	110
2.4	PHYSICAL ACTIVITY LEVEL ASSESSMENT USING ACCELEROMETRY.....	114
2.5	ESTIMATING RESTING METABOLIC RATE FROM EQUATIONS	118
2.6	BLOOD ANALYSES.....	119
2.6.1	SERUM INSULIN CONCENTRATION	120
2.6.2	TOTAL PLASMA FREE FATTY ACID CONCENTRATION.....	122
2.6.3	PLASMA TRIGLYCERIDE CONCENTRATION	122
2.7	QUANTIFICATION OF IMCL CONTENT USING MAGNETIC RESONANCE SPECTROSCOPY (MRS).....	124
2.8	HISTOCHEMICAL QUANTIFICATION OF IMCL CONTENT	127
2.8.1	FLUORESCENT STAINING OF LIPID IN VASTUS LATERALIS MUSCLE CRYOSECTIONS WITH BODIPY 493/503	127
2.8.2	IMAGE ACQUISITION	128
2.8.3	IMAGE ANALYSIS	129
2.8.4	COMPARISON OF IMAGE ANALYSIS METHODS	135
2.8.5	REPEATABILITY OF IMCL QUANTIFICATION WITH BODIPY 493/503	143
2.9	IMMUNOHISTOCHEMICAL DETERMINATION OF MUSCLE FIBRE TYPE	151
2.9.1	CRYOSECTIONING	151
2.9.2	STAINING	151
2.9.3	IMAGE ACQUISITION	153

2.9.4 FIBRE TYPE AND IMCL MATCHING	153
2.10 STATISTICAL ANALYSIS	154
2.11 REFERENCES	155
3. THE EFFECT OF 3 AND 56 DAYS OF BED REST ON IMCL CONTENT AND GLUCOSE DISPOSAL IN HEALTHY MALE VOLUNTEERS MAINTAINED IN ENERGY BALANCE	163
3.1 INTRODUCTION	163
3.2 STUDY AIMS	167
3.3 MATERIALS AND METHODS	168
3.3.1 STUDY OVERVIEW AND ETHICS STATEMENT	168
3.3.2 STUDY PROTOCOLS	169
3.3.4 QUANTIFICATION OF IMCL CONTENT	176
3.3.5 IMMUNOHISTOCHEMICAL STAINING OF MHC FOR MUSCLE FIBRE TYPING	178
3.3.6 BLOOD ANALYSES	180
3.3.7 STATISTICAL ANALYSIS	181
3.4 RESULTS	182
3.4.1 PARTICIPANT CHARACTERISTICS.....	182
3.4.2 WHOLE-BODY GLUCOSE DISPOSAL: 3 DAYS BED REST.....	183
3.4.3 WHOLE-BODY GLUCOSE DISPOSAL: 56 DAYS BED REST.....	185
3.4.4 SUBSTRATE OXIDATION: 3 DAYS BED REST.....	187
3.4.5 SUBSTRATE OXIDATION: 56 DAYS BED REST.....	189
3.4.6 FASTING INSULIN, TAG, AND FFA CONCENTRATION.....	190
3.4.7 IMCL CONTENT: 3 DAYS BED REST.....	192
3.4.8 IMCL CONTENT BY FIBRE TYPE: 3 DAYS BED REST	194
3.4.9 IMCL CONTENT: 56 DAYS BED REST	197
3.4.10 IMCL CONTENT BY FIBRE TYPE: 56 DAYS BED REST.....	199
3.5 DISCUSSION	201
3.6 CONCLUSION	205
3.7 REFERENCES	206
4. DOES IMCL ACCUMULATION CONTRIBUTE TO IMPAIRED WHOLE-BODY GLUCOSE DISPOSAL AND PERIPHERAL INSULIN SENSITIVITY IN MALES WITH NAFLD?	220
4.1 INTRODUCTION	220
4.2 STUDY AIMS	224
4.3 MATERIALS AND METHODS	225
4.3.1 STUDY OVERVIEW AND ETHICS STATEMENT	225
4.3.2 STUDY PROTOCOL	226

4.3.3	BODY COMPOSITION	228
4.3.4	WHOLE-BODY GLUCOSE DISPOSAL	228
4.3.5	LEG GLUCOSE DISPOSAL	229
4.3.6	DETERMINATION OF IMCL:EMCL RATIO USING ¹ H-MRS	229
4.3.7	IMCL QUANTIFICATION WITH BODIPY 493/503	230
4.3.8	IMMUNOHISTOCHEMICAL STAINING FOR FIBRE TYPE	230
4.3.9	STATISTICAL ANALYSES	231
4.4	RESULTS.....	232
4.4.1	PARTICIPANT CHARACTERISTICS.....	232
4.4.2	WHOLE-BODY GLUCOSE DISPOSAL	233
4.4.3	LEG GLUCOSE DISPOSAL	235
4.4.4	¹ H-MRS QUANTIFICATION OF IMCL:EMCL RATIO	237
4.4.5	HISTOCHEMICAL QUANTIFICATION OF IMCL CONTENT	238
4.4.6	IMCL CONTENT BY FIBRE TYPE	240
4.4.7	ASSOCIATION BETWEEN IMCL CONTENT AND GLUCOSE DISPOSAL.....	242
4.5	DISCUSSION.....	243
4.6	CONCLUSION	246
4.7	REFERENCES.....	247
5.	EFFECT OF DICLOFENAC ADMINISTRATION ON IMCL CONTENT DURING 12 WEEKS OF RESISTANCE EXERCISE TRAINING IN YOUNG, HEALTHY MALE VOLUNTEERS	261
5.1	INTRODUCTION.....	261
5.2	STUDY AIMS.....	268
5.3	MATERIALS AND METHODS	268
5.3.1	STUDY OVERVIEW AND ETHICS STATEMENT	268
5.3.2	STUDY PROTOCOL	269
5.3.3	MEASURES OF MUSCLE STRENGTH AND FUNCTION	271
5.3.4	QUANTIFICATION OF IMCL CONTENT	271
5.3.5	IMMUNOHISTOCHEMICAL STAINING FOR IDENTIFICATION OF MUSCLE FIBRE TYPES	272
5.3.6	IMMUNOHISTOCHEMICAL STAINING FOR QUANTIFICATION OF PLIN5 CONTENT	272
5.3.7	MUSCLE mRNA EXPRESSION.....	275
5.3.8	STATISTICAL ANALYSIS	280
5.4	RESULTS.....	281
5.4.1	MUSCLE STRENGTH AND FUNCTION.....	281
5.4.2	HISTOCHEMICAL QUANTIFICATION OF IMCL CONTENT	282
5.4.3	IMCL CONTENT BY MUSCLE FIBRE TYPE (PLACEBO GROUP).....	284
5.4.4	IMCL CONTENT BY MUSCLE FIBRE TYPE (DICLOFENAC GROUP).....	286
5.4.5	PLIN 5 CONTENT AND COLOCALISATION WITH LDS	288

5.4.6 PREDICTED METABOLIC EVENTS FOR LIPID METABOLISM PER CHANGES IN mRNA ABUNDANCE RELATIVE TO BASELINE.....	290
5.5 DISCUSSION.....	295
5.6 CONCLUSION	299
5.7 REFERENCES.....	301
6. GENERAL DISCUSSION	315
6.1 THESIS OVERVIEW.....	315
6.1.1 ROLE OF IMCL IN PHYSIOLOGICAL ADAPTATIONS TO INACTIVITY	315
6.1.2 ROLE OF IMCL CONTENT IN THE INSULIN RESISTANCE OBSERVED IN NAFLD.....	318
6.1.3 EFFECT OF CHRONIC RESISTANCE EXERCISE AND DICLOFENAC ON IMCL CONTENT AND MUSCLE FUEL OXIDATION	319
6.2 CONSIDERATIONS EMERGING FROM THIS WORK.....	320
6.3 FUTURE DIRECTIONS	323
6.3.1 IMPACT OF INACTIVITY WITH OVERFEEDING ON FIBRE-TYPE SPECIFIC IMCL CONTENT AND LIPOTOXIC INTERMEDIATES	323
6.3.2 DOES CHRONIC DICLOFENAC ADMINISTRATION ALTER SKELETAL MUSCLE FUEL OXIDATION AT REST AND IN RESPONSE TO EXERCISE?	325
6.3.3 LIPOTOXIC INTERMEDIATES CONTENT IN THE SKELETAL MUSCLES OF INDIVIDUALS WITH NAFLD 327	
6.4 REFERENCES.....	329
7. APPENDICES.....	341
APPENDIX A.....	341
APPENDIX B.....	343
APPENDIX C.....	345

List of Figures

<i>Figure 1-1: Simplified diagram of a lipid droplet.....</i>	<i>1</i>
<i>Figure 1-2: TAG synthesis pathway.....</i>	<i>10</i>
<i>Figure 1-3: TAG lipolysis.....</i>	<i>11</i>
<i>Figure 1-4: Fatty acid activation and the carnitine shuttle</i>	<i>14</i>
<i>Figure 1-5: The four enzymatic reactions involved in a single cycle of the β-oxidation of saturated fatty-acyl chains.....</i>	<i>16</i>
<i>Figure 1-6: Simplified schematic of the key insulin-mediated intracellular events that promote GLUT4 translocation to the sarcolemma.....</i>	<i>21</i>
<i>Figure 1-7: Pathway for AMPK activation and the effect of this activation on fatty acid transport into the mitochondria.....</i>	<i>25</i>
<i>Figure 1-8: Schematic of glycogenesis pathway.....</i>	<i>29</i>
<i>Figure 1-9: ATP-utilisation phase of glycolysis</i>	<i>30</i>
<i>Figure 1-10: ATP-production phase of glycolysis</i>	<i>31</i>
<i>Figure 1-11: Diagram of the TCA cycle.....</i>	<i>33</i>
<i>Figure 2-1: The Lunar Prodigy DEXA</i>	<i>107</i>
<i>Figure 2-2: Example output for DEXA.....</i>	<i>109</i>

<i>Figure 2-3: Example schematic of the ventilated hood indirect calorimetry system.....</i>	<i>113</i>
<i>Figure 2-4: Branched equation decision tree.....</i>	<i>116</i>
<i>Figure 2-5: Standard insulin concentration curve</i>	<i>120</i>
<i>Figure 2-6: Example ¹H-MRS spectra.....</i>	<i>125</i>
<i>Figure 2-7: Example diagram of variables used in the binarisation of pixels via the Bernsen algorithm</i>	<i>130</i>
<i>Figure 2-8: (A) Binarised image of muscle biopsy sample with a single fibre bounded by an ROI in yellow.....</i>	<i>132</i>
<i>Figure 2-9: Images showing the variation in the particles recorded in the “Analyse Particles” output.....</i>	<i>134</i>
<i>Figure 2-10: Representative images of the FOV and SF.....</i>	<i>135</i>
<i>Figure 2-11: Comparison of parameter means in various samples using the SF and FOV methods.....</i>	<i>140</i>
<i>Figure 2-12: Comparison of manual vs automated ROI</i>	<i>142</i>
<i>Figure 2-14: (A) Graph showing pooled LD count data for each section/replicate.....</i>	<i>145</i>
<i>Figure 2-15: (A) Graph showing pooled LD size data for each section/replicate.....</i>	<i>146</i>

Figure 2-16: (A) Graph showing pooled IMCL content data for each section/replicate. Bars are mean \pm SEM..... 147

Figure 2-17: Comparison of (A) LD count, (B) LD size, and (C) IMCL content measurements of two independent sections..... 149

Table 2-2: Table of data showing the comparison of LD count, LD size, and IMCL content measurements in two sections of the same sample from the ECLIPSE study..... 150

Figure 2-18: Image showing the result of the immunohistochemical staining 153

Figure 3-1: Timelines for the experimental protocols of the (A) acute (3 days) bed rest study and (B) chronic (60 days) 170

Figure 3-2: Schematic of the experimental days..... 172

Figure 3-3: Representative images of Bodipy 493/503 staining in the acute and chronic bed rest studies 177

Figure 3-4: Representative scan preview image of individual vastus lateralis sample section identification in ZEN software before Axio image acquisition..... 178

Figure 3-5: Matching of IMCL content in individual fibres to MHC isoform 180

Figure 3-6: Whole-body glucose disposal during the time course of the 180-minute hyperinsulinaemic-euglycaemic clamp 184

Figure 3-7: Whole-body glucose disposal during the time course of the 180-minute hyperinsulinaemic-euglycaemic clamp 185

Figure 3-8: (A) Carbohydrate and (B) fat oxidation..... 187

Figure 3-9: (A) Carbohydrate and (B) fat oxidation..... 189

Figure 3-10: (A) LD count, (B) LD size and (C) the percentage IMCL content in the vastus lateralis muscle biopsies before and after 3 days of -6° HDT bed rest and after remobilisation 193

Figure 3-11: Representative images of fibre type staining. (B) The Immunohistochemical staining of the MHC Type 1 (Type I) isoform in red..... 194

Figure 3-12 Fibre type specific differences in LD parameters and IMCL content after 3 days of bed rest. (A) LD count. (B) LD Size. (C) IMCL content 196

Figure 3-13: (A) LD count, (B) LD size and (C) the IMCL content in the vastus lateralis muscle tissue before and after 56 days of bed rest..... 198

<i>Figure 3-14: Fibre type specific differences in LD parameters and IMCL content before and after 56 days of bed rest. (A) LD count. (B) LD Size. (C) IMCL content.....</i>	<i>200</i>
<i>Figure 4-1: Timeline for the screening and baseline experimental days in the ECLIPSE study.</i>	<i>226</i>
<i>Figure 4-2: Mean whole-body glucose disposal in control and NAFLD groups during the steady state</i>	<i>233</i>
<i>Figure 4-3: Association between (A) whole body fat mass and (B) trunk fat mass with whole body glucose disposal</i>	<i>234</i>
<i>Figure 4-4: Leg glucose disposal in control and NAFLD group participants during the steady state of the hyperinsulinaemic-euglycaemic clamp protocol</i>	<i>236</i>
<i>Figure 4-5: IMCL:EMCL ratio estimated from $-(CH_2)_n-$ and terminal $-CH_3$ resonances in 1H-MR spectra of the vastus lateralis ...</i>	<i>237</i>
<i>Figure 4-6: The (A) LD count, (B) LD size, and (C) IMCL content in vastus lateralis muscle biopsies</i>	<i>239</i>
<i>Figure 4-7: Fibre type specific (A) LD count, (B) LD size, and (C) IMCL content in the control and NAFLD groups</i>	<i>241</i>
<i>Figure 4-8: Association between (A) whole-body glucose disposal and (B) leg glucose disposal.</i>	<i>242</i>

<i>Figure 5-1: Overview of COX isoform expression, function and targeting by NSAIDs.....</i>	<i>262</i>
<i>Figure 5-2: Schematic diagram of COX-mediated prostaglandin biosynthesis.....</i>	<i>263</i>
<i>Figure 5-3: Representative images of vastus lateralis muscle fibres co-stained for IMCL and PLIN5.....</i>	<i>274</i>
<i>Figure 5-4: Mean total work output (A) and isometric strength (B) of the concentric trained legs of the participants in the Placebo and Diclofenac groups.....</i>	<i>281</i>
<i>Figure 5-5: Mean vastus lateralis muscle (A) LD count, (B) LD Size and (C) IMCL content of participants in both the placebo group and the Diclofenac group.....</i>	<i>283</i>
<i>Figure 5-6: Fibre type specific differences in mean (A) LD count, (B) LD size and (C) IMCL content at the baseline, 28d, and 84d time points for the participants in the placebo group</i>	<i>285</i>
<i>Figure 5-7: Fibre type specific differences in mean (A) LD count, (B) LD size and (C) IMCL content at the baseline, 28d, and 84d time points for the participants in the Diclofenac group</i>	<i>287</i>
<i>Figure 5-8: (A) Mean PLIN 5 content as a percentage of total muscle fibre area and (B) the percentage of LDs in the total LD pool</i>	

that were coated with PLIN 5 in both placebo and Diclofenac participants.288

Figure 5-9: Schematics of gene networks and IPA predicted changes in metabolic events related to lipid metabolic in both groups.....292

List of Tables

<i>Table 1-1: MHC protein isoforms and the genes encoding them.</i>	<i>4</i>
<i>Table 2-1: Table of data showing the comparison of principal study parameter measurements in all samples using the SF and FOV methods</i>	<i>141</i>
<i>Tables 3-2 and 3-3: Mean number of fibres counted and matched per MHC isoform, per time point for all samples of the acute and chronic bed rest studies.....</i>	<i>179</i>
<i>Table 3-1: Table of participant characteristics for both the acute and chronic bed rest studies.....</i>	<i>182</i>
<i>Table 3-4: Table of fasting insulin, triglyceride and FFA concentrations in participants of both the acute and chronic bed rest studies at all time points</i>	<i>190</i>
<i>Table 4-1: Participant characteristics for the control and NAFLD groups.....</i>	<i>232</i>
<i>Table 4-2: Blood flow and AV differences in glucose concentration across the leg in control and NAFLD participants.....</i>	<i>235</i>
<i>Table 5-1: Baseline anthropometric characteristics in the participants of the placebo group and the Diclofenac</i>	<i>269</i>

Table 5-2: Table of all genes related to lipid metabolism that had altered mRNA expression290

Tables 7-1, 7-2, 7-3, 7-4: Tables showing the change in mRNA expression from baseline (Log Fold Change)342

List of Abbreviations

ACC	Acetyl-CoA carboxylase
ACS	Acetyl-CoA Synthetase
ACP	Acyl Carrier Protein
ADP	Adenosine Diphosphate
AEE	Activity Energy Expenditure
Akt	Protein Kinase B
ALM	Appendicular Lean Mass
AMP	Adenosine Monophosphate
AMPK	AMP-Activated Protein Kinase
ANOVA	Analysis of Variance
AGPAT	1-Acylglycerol-3-Phosphate Acyltransferases
AS160	Akt substrate of 160 kDa
ATGL	Adipose Triglyceride Lipase
ATP	Adenosine Triphosphate
BCP	Bromochloropropane
BMC	Bone Mineral Content
BMI	Body Mass Index
BMR	Basal Metabolic Rate
BPM	Beats Per Minute
BSA	Bovine Serum Albumin
CaMK	Ca ²⁺ /Calmodulin-dependent Protein Kinase
CD36	Cluster of Differentiation 36
cDNA	Complementary DNA
CFIM	Core Facility for Integrated Microscopy
CoA	Coenzyme A
COX	Cyclooxygenase

CSA	Cross-Sectional Area
CV	Coefficient of Variation
CPM	Counts Per Minute
CPT	Carnitine Palmitoyltransferase
DAG	Diacylglycerol
DEXA	Dual-Energy X-ray Absorptiometry
DGAT	Diacylglycerol Acyltransferases
DNA	Deoxyribonucleic Acid
DNL	De Novo Lipogenesis
DSHB	Developmental Studies Hybridoma Bank
ECG	Electrocardiogram
ECLIPSE	Effect of Carnitine on Liver Fat and Glucose Metabolism
EDTA	Ethylenediaminetetraacetic Acid
EMCL	Extramycellar Lipid
ER	Endoplasmic Reticulum
ESA	European Space Agency
ETC	Electron Transport Chain
FA	Fatty Acid
FAD	Flavin Adenine Dinucleotide
FAS	Fatty Acid Synthase
FFA	Free Fatty Acid
FFM	Free Fat Mass
FOV	Field of View
FOXO	Fork Head Box O
G1P	Glucose-1-phosphate
G6P	Glucose-6-phosphate
GAP	GTPase-activating proteins
GEF	Guanine Nucleotide Exchange Factor

GD	Glucose Disposal
GDP	Guanosine Diphosphate
GIR	Glucose Infusion Rate
GLUT	Glucose Transporter
GPAT	Glycerol-3-Phosphate Acyltransferases
GS	Glycogen Synthase
GSK-3	Glycogen Synthase Kinase 3
GTP	Guanosine-5'-Triphosphate
HDT	Head-down Tilt
HSL	Hormone Sensitive Lipase
IBI	Interbeat Interval
IHTG	Intrahepatic Triglyceride
IKB	Ingenuity Knowledge Base
IMCL	Intramycocellular Lipid
IMF	Intermyofibrillar
IMM	Inner Mitochondrial Membrane
IMS	Intermembrane Space
IPA	Ingenuity Pathway Analysis
IPAQ	International Physical Activity Questionnaire
IRS	Insulin Receptor Substrate
LBM	Lean Body Mass
LCFA	Long-Chain Fatty ACid
LD	Lipid Droplet
LKB1	Liver Kinase B1
MAG	Monoacylglycerol
MEDES	L'Institut de Médecine et de Physiologie Spatiales
MET	Metabolic Equivalent of Task
MGL	Monoacylglycerol Lipase

MHC	Myosin Heavy Chain
MRI	Magnetic Resonance Imaging
mRNA	Messenger RNA
MRS	Magnetic Resonance Spectroscopy
mTORC2	Mammalian Target of Rapamycin (MTOR) Complex 2
NAD	Nicotinamide Adenine Dinucleotide
NAFLD	Non-Alcoholic Fatty Liver Disease
NASH	Non-Alcoholic Steatohepatitis
NEFA	Non-Esterified Fatty Acid
NICE	National Institute for Health and Care Excellence
NSAID	Non-Steroidal Anti-Inflammatory Drug
OMM	Outer Mitochondrial Membrane
PA	Phosphatidic Acid
PAI	Physical Activity Intensity
PAL	Physical Activity Level
PAP	Lipin Phosphatidic Acid Phosphatase
PCR	Polymerase Chain Reaction
PDC	Pyruvate Dehydrogenase Complex
PDH	Pyruvate Dehydrogenase
PDK1	3-phosphoinositide-dependent protein kinase 1
PDP	Pyruvate Dehydrogenase Phosphatase
PG	Prostaglandin
PGC-1α	Peroxisome Proliferator-Activated Receptor Gamma Coactivator 1-Alpha
PGM	Phosphoglucomutase
PI3K	Phosphatidylinositol-4,5-Biphosphate 3-Kinase

PIP₂	Phosphatidylinositol-4,5-bisphosphate
PIP₃	Phosphatidylinositol-3,4,5-triphosphate
PKC	Protein Kinase C
PLA₂	Phospholipase A2
PLIN	Perilipin
PPAR	Peroxisome Proliferator-Activated Receptors
PPP	Pentose Phosphate Pathway
RER	Respiratory Exchange Ratio
RHR	Resting Heart Rate
RMR	Resting Metabolic Rate
RNA	Ribonucleic acid
ROI	Region of Interest
ROS	Reactive Oxygen Species
RT-PCR	Reverse Transcription Polymerase Chain Reaction
RXR	Retinoid X Receptor
SCD	Stearoyl-CoA Desaturase
SD	Standard Deviation
SDS	Sequence Detection Systems
SEM	Standard Error of The Mean
SF	Single Fibre
SH2	Src-homology 2
SNARE	Soluble NSF attachment protein receptor
SPB	Sørensen's Phosphate Buffer
SPMIC	Sir Peter Mansfield Imaging Centre
SPSS	Statistical Package for the Social Sciences
SS	Subsarcolemmal
T2DM	Type 2 Diabetes Mellitus

TAG	Triacylglycerol
TCA	Tricarboxylic acid
TEE	Total Energy Expenditure
UK	United Kingdom
VAT	Visceral Adipose Tissue
VL	Vastus Lateralis
VLCFAs	Very Long-Chain Fatty Acids
VLDL	Very Low-Density Lipoprotein
WADA	World Anti-Doping Agency

1. General Introduction

1.1 Lipid Droplets and Their Role in Health and Disease

In the past three decades interest in lipid droplets (LDs), previously thought to be inert components of the cytoplasmic compartment, has grown exponentially. Emerging evidence from animal and in vitro studies has led some to propose that LDs may be major hubs in energy metabolism and act as key components of intracellular signalling and cell survival due to their pleiotropic interactions with various biological pathways (Walther and Farese, 2009). However, corroborating evidence from in vivo human studies is lacking. Though many of the mechanisms that govern LD interactions remain incompletely defined, recent developments, including mapping of the LD proteome (Bersuker *et al.*, 2018), the creation of the “Lipid Droplet Knowledge Portal” (Mejhert *et al.*, 2022), and advancements in our understanding of LD biogenesis (Arlt *et al.*, 2022), suggest that there is great enthusiasm to better characterise the role of LDs in health and disease.

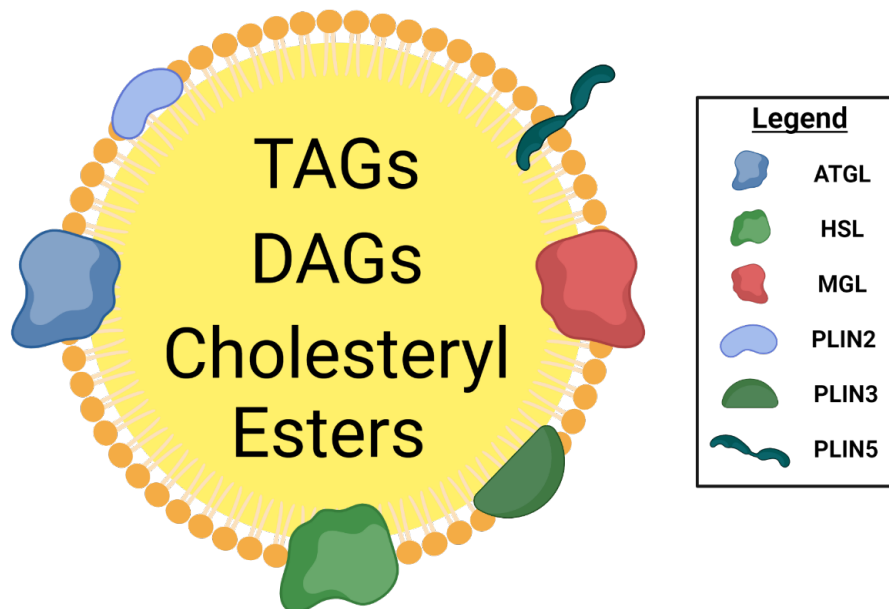


Figure 1-1: Simplified diagram of a lipid droplet. The neutral lipid core contains TAGs, DAGs, and cholesteryl esters enclosed in a phospholipid monolayer embedded with various lipases and structural proteins.

LDs are small intracellular constructs expressed ubiquitously in every domain of life, from the smallest prokaryotic organism to the largest multicellular organism (Murphy, 2012; Huang, 2018) (see **Figure 1**). LDs are composed of a hydrophobic core primarily containing neutral lipids, including triacylglycerols (TAGs), cholesteryl esters and diacylglycerols (DAGs), in that order from most abundant to least abundant (Hsieh *et al.*, 2012). This lipid core is surrounded by a phospholipid monolayer, which is unique amongst intracellular structures (Walther and Farese, 2012). The phospholipid monolayer is coated by lipases and proteins from the perilipin (PLIN) family (Greenberg *et al.*, 1991), which play a crucial role in LD biogenesis and function.

Currently, there is no conclusive model for LD formation, but there is a prevailing hypothesis supported by evidence from the Farese and Walther laboratory, who are at the forefront of research into lipid droplet biogenesis (Arlt *et al.*, 2022). Walther and Farese suggest that lipid droplets form from the accumulation of TAG and cholesterol esters in a discrete segment of the hydrophilic phase between the layers of the endoplasmic reticulum (ER) (Walther and Farese, 2009; Thiam, Farese, and Walther, 2013). This lipid eventually amalgamates to form a lens which is enlarged to form a sphere via the interaction of the nascent LD with ER-bound seipin proteins that facilitate and promote TAG synthesis (Salo *et al.*, 2016; Schuldiner and Bohnert, 2017). The increase in the curvature and tension of the ER bilayer around the forming droplet upregulates the activity ER shaping proteins, including the reticulons and atlastins, which are believed to facilitate the budding of the droplet from the ER into the cytosol (Jackson, 2019).

The excessive accumulation of LDs in ectopic tissues including the skeletal muscles and liver has been linked with the development of muscle and whole-body insulin resistance (Coen *et al.*, 2010), with oxidative stress that can damage cells and trigger apoptosis (Guebre-Egziabher *et al.*, 2013), and with the presentation of metabolic disturbances including type 2 diabetes mellitus (T2DM) (Barrett *et al.*, 2022) and non-alcoholic fatty liver disease (NAFLD) (da Silva Rosa *et al.*, 2020). The work presented in this thesis aims to contribute to our growing understanding of the role of LDs in the

development of skeletal muscle and whole-body insulin resistance in states of inactivity and in the context of NAFLD. This thesis will also investigate how resistance exercise affects LD and PLIN5 expression in skeletal muscle and the effect of non-steroidal inflammatory drug (NSAID) administration on IMCL content in this context.

1.1.1 Intramyocellular Lipid Content

The neutral lipid pool stored in LDs within skeletal muscle constitutes the bulk of what is referred to as intramyocellular lipid content (IMCL). In human muscle, LDs are found localised to two distinct regions of the muscle fibre. The first is the subsarcolemmal (SS) region, defined as the sarcoplasmic region that is within 5% of the maximal distance from the sarcolemma to the centre of the myocyte (Daemen *et al.*, 2018). The second is the intramyofibrillar (IMF) region which includes the rest of the sarcoplasm. In 1973, using electron microscopy, Hoppeler visualised sarcoplasmic LDs within nanometres of mitochondria (Hoppeler *et al.*, 1973). This landmark discovery provided some circumstantial evidence of a role for LDs in energy homeostasis, but it was not until many years later that the presence of LD-mitochondria contact sites was confirmed (Renne and Hariri, 2021). PLIN5 functions as the main architect of these contact sites which not only form between LDs and mitochondria but are the main points of LD-LD interactions and LD interactions with various organelles (Bosma, 2012; Schuldiner and Bohnert, 2017). The subcellular localisation of myocellular LDs is critical for fulfilling their main function: the provision of FAs to adjacent mitochondria for ATP production via β -oxidation, particularly in response to elevated energy demand during exercise (Hoppeler, 1986; Watt *et al.*, 2002; van Loon, 2004). Clear evidence of this was reported in early studies which used a stereological method developed by Eisenberg and Kuda in 1975 to calculate lipid droplet volume density in images obtained from electron microscopy (Eisenberg and Kuda, 1975; Broskey *et al.*, 2013). Staron and colleagues observed a 42% reduction in lipid volume within the gastrocnemius muscle of 10 runners 15 minutes after the completion of a standard marathon whilst Kayar and colleagues reported that the mean volume density of lipid decreased from 0.013 to 0.003 in muscle fibres from the tibialis anterior of 7 male runners following a 100 km run.

1.1.2 Importance of Fibre Type to Skeletal Muscle Function and IMCL Content

Gene	Protein Isoform	Muscle Fibre Type
MYH7	MHC- β	Type I
MYH2	MHC-IIA	Type IIA
MYH1	MHC-IIX	Type IIX

Table 1-1: MHC protein isoforms and the genes encoding them.

An important consideration when studying skeletal muscle is muscle fibre type composition because of the distinct contractile and metabolic properties, and lipid profiles of these muscle fibre isoforms. What defines the different fibre types are the predominant myosin heavy chain (MHC) isoforms they express (Reggiani, Bottinelli, and Stienen, 2000). Muscle fibres can be classified as Type I, Type IIA, and Type IIX depending on whether they primarily express the myosin heavy chain- β (MHC- β), MHC-IIA, or MHC-IIX isoform encoded by the MYH7, MYH2, and MYH1 genes, respectively (see **Table 1-1**). Muscle groups (soleus, gluteus maximus, triceps etc.) express different proportions of the muscle fibre types and fibre composition changes as an adaptation to exercise and as a response to aging and myopathies (Talbot and Maves, 2016).

Mature muscle fibres can co-express MHC isoforms, producing hybrid Type I/IIA, IIA/IIX, and I/IIA/IIX fibres which compose roughly 25% of all fibres (Medler, 2019). Elite endurance athletes characteristically possess a high proportion of slow twitch muscle fibres (Tesch and Karlsson, 1985) whilst athletes in sports requiring explosiveness and strength, like sprinting and Olympic weightlifting, have a relatively high abundance of fibres expressing the fast twitch MHC isoforms, especially Type IIX (Trappe *et al.*, 2015; Serrano *et al.*, 2019). Indeed, the proportion of Type I fibres increases with endurance exercise, with the gastrocnemius muscle of elite long-distance runners being composed of $79 \pm 3.5\%$ Type I fibres and of average untrained men being composed of $58 \pm 2.5\%$ Type I fibres (Fink, Costill, and Pollock, 1977). The cross-sectional area of Type I fibres is also significantly larger in elite runners

than in untrained males (Fink, Costill, and Pollock, 1977). These observations have led some to suggest that exercise may lead to the conversion of muscle fibres from one type to another, with endurance training favouring the transition of fibres to Type I and resistance training favouring transitions towards Type IIX (Wilson *et al.*, 2012). Some investigators propose that hybrid fibres represent an intermediate stage in the transition from Type I muscle fibres to Type II muscle fibres and vice versa, induced by ageing or exercise (Medler, 2019) but evidence for this phenomenon in humans, in vivo is currently inadequate (Plotkin *et al.*, 2021).

Force generation by skeletal muscle is dependent on muscle length and fibre type composition. This is because MHC isoforms vary in the speed at which they shorten, with Type I fibres having the slowest shortening velocity, Type IIX fibres having the fastest shortening velocity and Type IIA being intermediate (Smerdu *et al.*, 1994; Schiaffino, and Reggiani, 2011). Indeed, Type IIA and IIX fibres possess 3 and 4.4 times greater contractile velocity than Type I fibres, respectively (Malisoux *et al.*, 2006), which is reflected in the ability of Type II fibres to hydrolyse ATP 2-3 times faster than Type I fibres (Taylor, Essén, and Saltin, 1974), allowing for speedier cross-bridge cycling (Sugi *et al.*, 2008). For this reason, muscle fibres are colloquially split into two categories, “slow-twitch” (Type I) and “fast-twitch” (Type IIA and Type IIX) muscle fibres.

Although there is some plasticity, Type I fibres primarily rely on oxidative metabolism for ATP production whilst Type IIX fibres rely on glycolysis. Type I fibres express 20-25% more glucose transporter type 4 (GLUT4) than Type II fibres in the healthy untrained (Gaster *et al.*, 2000), and evidence shows that low intensity, high volume exercise increases GLUT4 content in these fibres (Daugaard *et al.*, 2000). Type I fibres also possess greater protein expression of hexokinase II and glycogen synthase (Albers *et al.*, 2015), greater mitochondrial density, and greater capillary-fibre contact length due to their increased vascularisation relative to Type IIA and IIX fibres, reflecting a greater capacity for aerobic respiration in Type I fibres than in any other muscle fibre type (Ørtenblad *et al.*, 2018).

It is well recognised that IMCL content is greatest in Type I muscle fibres, being at least twice as high as IMCL content in Type IIA and IIX fibres in many lean, healthy individuals (Whytock 2020). Interestingly, though trained individuals and those with T2DM have similar IMCL content, trained individuals have smaller, more numerous LDs in the IMF region of Type I fibres whilst those with T2DM have large LDs in the SS region of Type II fibres (Daemen *et al.*, 2018). Using histochemical staining of vastus lateralis muscle sections from both trained and untrained participants, Chow and colleagues showed that acute elevation of plasma free fatty acid (FFA) concentration by lipid infusion during the course of a hyperinsulinaemic-euglycaemic clamp increased IMCL content in type I fibres irrespective of training status (Chow *et al.*, 2017). The implications of these differences in the myocellular and fibre-type localisation of LDs between healthy individuals and those with metabolic impairments will be discussed in detail in **Section 1.5.2**.

1.2 Mechanisms Regulating IMCL Content

1.2.1 FA Transport into Skeletal Muscle and Energy Balance

During feeding and in the postprandial state, dietary fat is hydrolysed by salivary, stomach, and pancreatic lipases to form FAs with the assistance of bile salts released by the liver, which break down very large fat droplets into smaller fat droplets (D'Aquila *et al.*, 2016). The non-esterified/free FAs released from the lipolysis of dietary fat enter the intestinal lumen and are absorbed by enterocytes (Winkler, D'Arcy, and Hunziker, 1990). Within the enterocytes these dietary FAs are then esterified to glycerol to form TAG, which is packaged into lipoproteins referred to as chylomicrons, storage vesicles that transport TAGs into the lacteals, thoracic lymphatic duct, and then into the general circulatory system (D'Aquila *et al.*, 2016).

Adipose tissue is the main site for fat storage in healthy individuals under normal physiological conditions (Chait and den Hartigh, 2020). In this tissue FAs are esterified to TAG and stored such that TAG can be hydrolysed and FAs can be released into the circulation to supply peripheral tissues with lipid substrate for β -oxidation during periods of prolonged fasting or during exercise when energy demand is high (Langin, 2006). Albumin is required to transport

FAs released from adipose tissue into the circulation because the acyl moieties of FAs confer low solubility in aqueous mediums like blood. The high affinity binding sites on a single albumin molecule can accommodate 8 FAs (Kragh-Hansen, 1981).

The liver also plays a major role in supplying lipid during fasting, being the main site of de novo lipogenesis (DNL), the process in which excess glucose is converted to FAs (Ameer *et al.*, 2014). The liver is the site for the assembly of very low-density lipoproteins (VLDLs) into which these newly synthesised FAs are packaged in the form of TAG (Rustaeus *et al.*, 1999). Once synthesised, VLDLs are secreted into the blood, with their primary role being to facilitate the movement of liver-synthesised fats and cholesterol through the aqueous plasma to peripheral tissues like the skeletal muscle where the stored FAs can be released, taken up, and oxidised (Yli-Jokipii, *et al.*, 2003).

The vascular endothelium is impermeable to lipoproteins, thus the circulating FAs that these structures transport must be released from the TAG core before trans-endothelial transport of the FAs can occur. Lipoprotein lipases (LPLs) on the luminal surface of endothelial cells are enzymes that have phospholipase A2 activity, which allows them to break down the phospholipids forming the capsules of circulating lipoproteins, thus providing access to the TAGs stored within them, which can then be hydrolysed to form FAs and glycerol (Van Der Vusse, 1992; Braun and Severson, 1992). LPL is present in the microvasculature of most organs, except the liver (Braun and Severson, 1992). The presence of LPL in the liver would result in the release of FAs from TAGs held within VLDLs synthesised by the liver immediately after the VLDL-TAG complexes are released from hepatocytes, thus preventing the transport of VLDL-TAG into the general circulation, resulting in insufficient fasting FA supply to the peripheral tissues and skeletal muscle. LPL enzymatic activity is highest in adipose tissue, lactating mammary glands, the myocardium, and skeletal muscle (Camps *et al.*, 1990).

Once released from circulating lipoproteins, the diffusion of FAs through the sarcolemma is facilitated by several transporters including cluster of

differentiation 36 (CD36), sarcolemmal fatty acid binding protein (FABP_{pm}) and fatty acid transporter 1-4 proteins (FATP1-4) (Glatz, Luiken, and Bonen, 2010). The translocation of these transporters from the cytosol to the sarcolemma is regulated by Akt2 activity which is upregulated by cellular insulin stimulation and muscular contractions (Jain *et al.*, 2015). These FAs then undergo esterification to form TAG whilst FAs are released from the lipolysis of intramuscular TAG and undergo β -oxidation simultaneously, such that TAG synthesis and breakdown are balanced, with muscular contractions stimulating reduced incorporation of FAs into the TAG pool and increased FA oxidation (Dyck and Bonen, 1998; Sacchetti *et al.*, 2002). In studies conducted using a 10-hour constant infusion of ¹³C-palmitate tracer in fasting normoweight, healthy, young, male participants, it has been demonstrated that ~50-60% of plasma FA transported into non-contracting leg skeletal muscle from the circulation is incorporated into the intramuscular TAG pool (Sacchetti *et al.*, 2004). Based on the matched synthesis and lipolysis rates of intramuscular TAG, complete turnover of the intramuscular TAG pool of participants was estimated to take 29 hours, with lipid turnover being faster in trained individuals versus untrained individuals (Lund *et al.*, 2018). Subsequent work found that 10-13% of plasma FA was esterified to TAG at the whole-body skeletal muscle level when the palmitate enrichment of carnitines was factored into incorporation calculations (Kanaley *et al.*, 2009).

At this juncture, before discussing myocellular re-esterification of FAs to form TAG that augments muscle LDs, it is important to touch upon the role of energy balance in controlling circulating lipid availability and FA delivery to the peripheral tissues. The term “energy balance” describes the relationship between the calories consumed (energy intake) and the calories utilised (energy expenditure) by the body daily (Hill, Wyatt, and Peters, 2012). When energy intake and energy expenditure are equal, the body is said to be in energy balance. Energy intake greater than energy expenditure produces a state of positive energy balance and energy intake lower than energy expenditure creates a calorific deficit or state of negative energy balance. When energy intake remains greater than energy expenditure for a prolonged period, the body enters a state of chronic positive energy balance during which

plasma FFA concentration and TAG concentration increase significantly (Chow and Hall, 2014). This in turn results in significant increases in body weight (Forbes *et al.*, 1986; Horton *et al.*, 1995), 60-80% of which is accounted for by increases in whole-body fat mass (Hill and Commerford, 1996), and leads to the ectopic accumulation of lipid in non-adipose tissue, primarily the liver, heart, pancreas and skeletal muscle (Unger *et al.*, 2010; Ruberg *et al.*, 2010; Suganami, Tanaka, and Ogawa, 2012; Solinas, Borén, and Dulloo, 2015). Elevated plasma FA concentration is well correlated with impaired insulin-stimulated skeletal muscle glucose uptake (Abdul-Ghani, and DeFronzo, 2010), with decreases in plasma FA concentration by diet or exercise being associated with improved skeletal muscle glucose uptake and oxidation (Bajaj *et al.*, 2005). Thus, ectopic lipid accumulation induced by overfeeding plays a significant role in the aetiology of metabolic dysfunctions, as will be discussed in detail in **Section 1.5.3**. Conversely, extreme hypocaloric diets of 450 kcal/day and 700 kcal/day in obese individuals with and without T2DM have been shown to decrease overall weight, decrease IMCL content, and significantly improve multiple measures of whole-body insulin sensitivity (Jazet *et al.*, 2007; Lara-Castro *et al.*, 2008).

1.2.2 TAG Synthesis and Storage in LDs

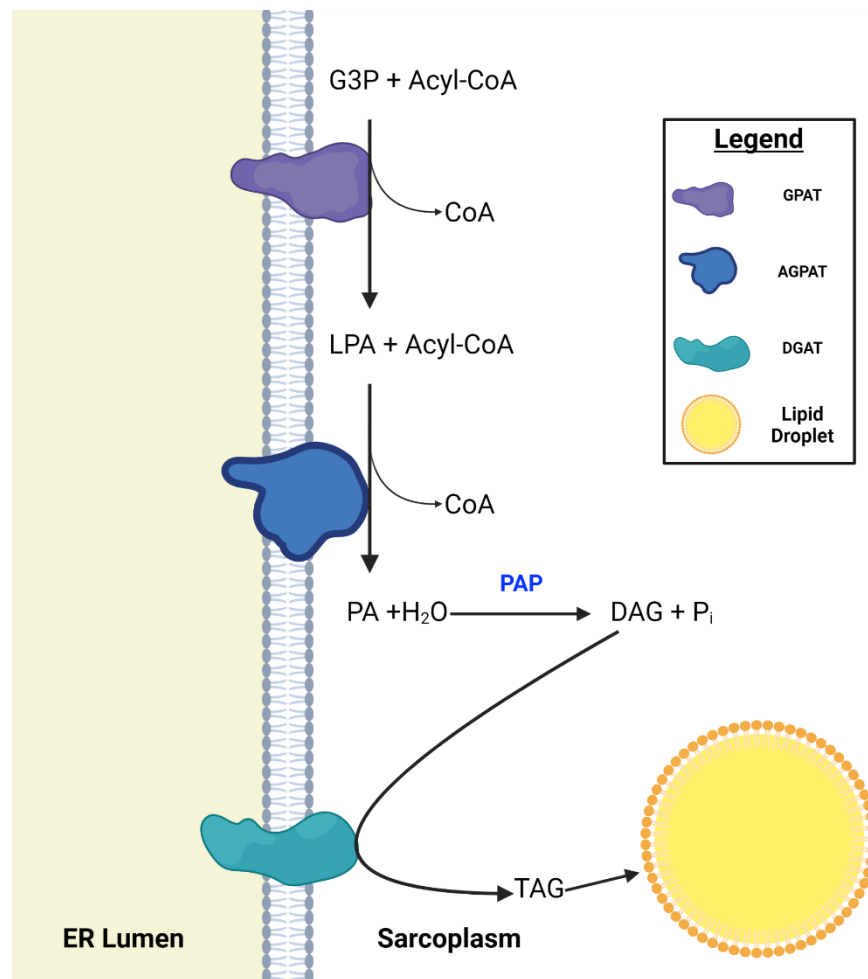


Figure 1-2: TAG synthesis pathway at the endoplasmic reticulum.

Once FAs are transported into the skeletal muscle, they are converted to TAG via the glycerol phosphate pathway which involves the stepwise addition of fatty acyl chains to a glycerol backbone (Kennedy, 1961; Kanaley *et al.*, 2009). First FAs undergo thioesterification with CoA to form fatty acyl-CoA in a reaction catalysed by acyl-CoA synthetase (ACS). These FA-CoA molecules are then converted to TAG in a series of reactions catalysed by Glycerol-3-Phosphate Acyltransferases (GPATs), 1-Acylglycerol-3-Phosphate Acyltransferases (AGPATs), Lipin Phosphatidic Acid Phosphatase (PAP) proteins, and Diacylglycerol Acyltransferases (DGATs) (Wang, Airola, and Reue, 2017) (see **Figure 1-2**). The acyltransferases are all transmembrane proteins localised to the ER membrane, the main site of TAG synthesis, and

have been detected on mitochondrial membranes, the nuclear membrane, and the LD monolayer (Kuerschner, Moessinger, and Thiele, 2008).

Though the TAG synthesis pathway on the LD monolayer is not well understood, existing evidence suggests that it proceeds in the same manner as TAG synthesis at the ER membrane (Wilfling *et al.*, 2013). In this pathway GPAT enzymes catalyse the bonding of a fatty acyl chain to glycerol-3-phosphate to form lysophosphatidic acid (LPA). Then AGPAT catalyses the transference of a fatty acyl chain from a fatty Acyl-CoA molecule to LPA to form phosphatidic acid (PA) (Shindou *et al.*, 2009). PA acts as a branching point in the TAG synthesis pathway. It can function as a precursor to phospholipid synthesis (Vance, 2004) or to the synthesis of DAG. PAPS translocate to the ER membrane and dephosphorylate PA to form DAG as shown in **Figure 1-2** (Reue and Wang, 2019). Finally, though the exact mechanism is unclear, DAG is converted to TAG by DGAT enzymes (Wang *et al.*, 2020). Efficient functioning of this pathway is critical for preventing the accumulation of intermediates of FA biosynthesis and metabolism which can antagonise components of the insulin signalling pathway as will be discussed in detail in **Section 1.5.4**.

1.2.3 LD TAG Lipolysis

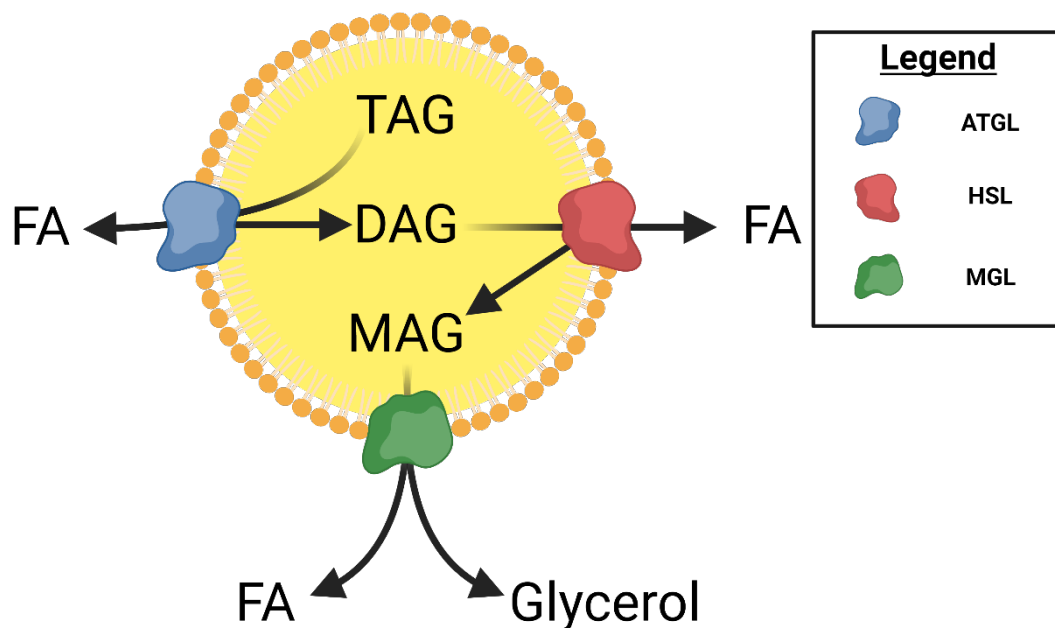


Figure 1-3: TAG lipolysis.

TAG lipolysis is a crucial biochemical process that, within the context of the work presented here, is important for facilitating the release of FAs from LDs so that they can enter adjacent mitochondria for β -oxidation (see **Figure 1-3**). This pathway is initiated by adipose triglyceride lipase (ATGL) which was identified in 2004 by the group led by Rudolf Zechner (Zimmerman *et al.*, 2004), sparking an exponential increase in research concerning the lipolysome, the network of proteins and cofactors responsible for TAG lipolysis (Hofer *et al.*, 2020). Today it is understood that ATGL is expressed in almost all tissues and catalyses the hydrolysis of TAG to DAG (Eichmann *et al.*, 2012). This is followed by the activation of hormone sensitive lipase (HSL).

HSL catalyses the lipolysis of various substrates, but it has a 10-fold enzymatic specificity for DAG compared to TAG, monoacylglycerol (MAG), and cholesterol esters, thus its main role is the lipolysis of DAG to form MAG (Holm and Østerlund, 1999). Indeed, it has been demonstrated that in response to epinephrine-induced contractions of rat soleus muscle HSL translocates to LDs and these droplets decrease in size, highlighting the importance of this enzyme in releasing stored FA (Prats *et al.*, 2006). Based on exercise intervention studies in adrenalectomised humans (Kjaer *et al.*, 2000), it is recognised that both muscle contractions and epinephrine can contribute to the phosphorylation and activation of HSL in humans depending on the duration and intensity of exercise (Watt and Spriet, 2004; Krintel *et al.*, 2008). HSL expression is significantly and consistently decreased in obese individuals and in those with T2DM, resulting in decreased DAG lipolysis (Moro *et al.*, 2009; Jocken *et al.*, 2010). This impaired lipolytic activity may partly explain why IMCL content is typically greater in these groups than in healthy lean individuals (Goodpaster *et al.*, 2001). Also, using human primary myotubes, Badin and his colleagues showed that impaired IMCL breakdown due to dysregulated HSL activity induces insulin resistance through the DAG/PKC pathway (Badin *et al.*, 2011), which will be discussed in detail in **Section 1.5.4.1**. Monoacylglycerol lipase (MGL), which is expressed ubiquitously, is the final enzyme in this pathway and it catalyses the lipolysis of MAG to glycerol and a FA chain (Tornqvist and Belfrage, 1976).

1.2.4 Oxidation of LD-Derived FA

FAs released by LDs are then transported into adjacent mitochondria for β -oxidation, the process via which acetyl-CoA is produced by the oxidation of fatty acyl chains. During this process the H^+ ions released from the fatty acyl chains are donated to form the reducing equivalents NADH and $FADH_2$, which play an integral role in ATP generation in the electron transport chain (ETC). The length of the acyl chain determines where it is oxidised. Short-, medium-, and long-chain FAs undergo β -oxidation in the mitochondria (Schönfeld and Wojtczak, 2016). Very long chain FAs (VLCFAs), composed of 20 or more carbon atoms, undergo β -oxidation in peroxisomes (Wanders *et al.*, 2021). FAs delivered to muscle from the hydrolysis of lipid stored in adipose tissue, from IMCL, from cholesterol and from dietary fat all contribute to skeletal muscle mitochondrial FA oxidation to varying degrees during rest and exercise (Achten and Jeukendrup, 2004). Transcriptional regulation of FA oxidation is primarily governed by isoforms of Peroxisome proliferator-activated receptors (PPARs) (Muoio *et al.*, 2002) and the transcriptional activator Peroxisome proliferator-activated receptor gamma coactivator 1-alpha ($PGC-1\alpha$) (Huss, Kopp, and Kelly, 2002).

The enzymes necessary for the β -oxidation of most FAs are found in the mitochondrial matrix, thus FAs must be able to enter this compartment. The outer mitochondrial membrane (OMM) contains porins, voltage-dependent anion-selective channels, which make it semi-permeable (Kerner and Hoppel, 2000). Fatty acyl chains of 8 or less carbons can diffuse into the mitochondria matrix via these porins, but long-chain and medium-chain FAs cannot (Schönfeld and Wojtczak, 2016). The mechanism which facilitates the transport of long-chain acyl groups from the sarcoplasm to the mitochondrial matrix is referred to as the “Carnitine Shuttle”.

1.2.4.1 The Carnitine Shuttle

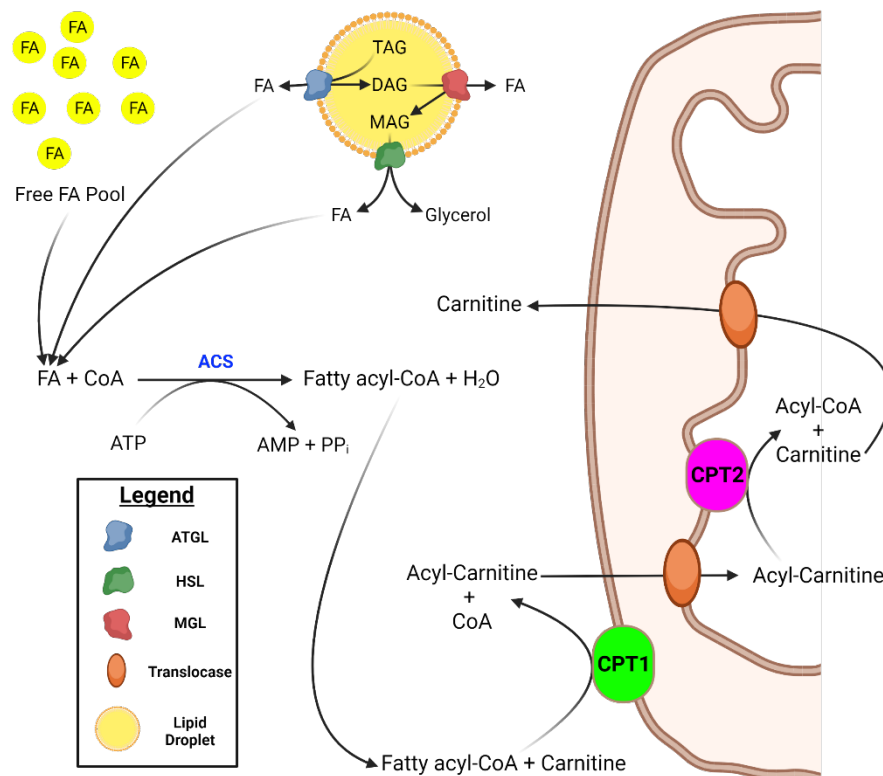


Figure 1-4: Fatty acid activation and the carnitine shuttle. FFAs or FAs derived from TAG stored in LDs which is hydrolysed sequentially by ATGL, HSL and MGL is “activated” by ACS. Resultant fatty-acyl CoA is transported into the mitochondrial matrix via the carnitine shuttle.

Before FAs can be committed to any metabolic pathway like β -oxidation, they must first be “activated” by the formation of a thioester bond with CoA, in an ATP-dependent reaction catalysed by ACS, to form fatty acyl-CoA (Hisanaga *et al.*, 2004) (see **Figure 1-4**). As the OMM is impermeable to long-chain fatty acyl chains, carnitine palmitoyltransferases (CPTs) are required to transport them. The CPT1B isoform is the main CPT isoform found in skeletal muscle (Yamazaki *et al.*, 1996). CPT1 enzymes are located within the OMM, and they catalyse the conjugation of carnitine to the fatty acyl group in acyl-CoA to form acyl-carnitines, which is the rate-limiting step in LCFA oxidation (Drynan, Quant, and Zammit, 1996). These long-chain acyl-carnitines are then transported into the intermembrane space (IMS).

Within the inner mitochondrial membrane (IMM) are carnitine-acylcarnitine translocases, bi-directional transporters which permit the

movement of these acyl-carnitines from the IMS into the mitochondrial matrix and the movement of carnitines from the mitochondrial matrix to the IMS and out into the sarcoplasm (Pande, 1975; Console *et al.*, 2014). Once in the mitochondrial matrix acyl-carnitines are directed to CPT2 enzymes. CPT2 is localised to the matrix side of the IMM, and it catalyses the dissociation of carnitines from acyl-carnitines such that units of acyl-CoA are reformed within the matrix (Violante *et al.*, 2010). This catalytic activity promotes the exchange diffusion of the dissociated carnitine from the mitochondrial matrix out to the sarcoplasm and acyl-carnitines from the IMS into the mitochondrial matrix through carnitine-acylcarnitine translocases. This reformed acyl-CoA is the starting substrate for mitochondrial β -oxidation.

1.2.4.2 Mitochondrial β -Oxidation

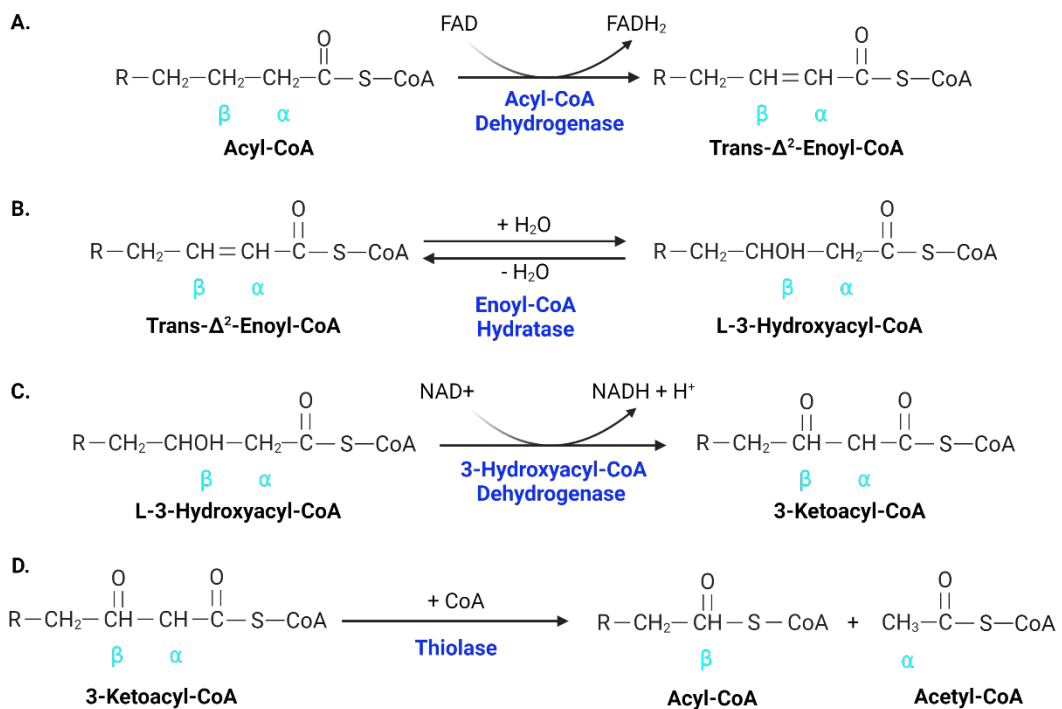


Figure 1-5: The four enzymatic reactions involved in a single cycle of the β -oxidation of saturated fatty-acyl chains. (A) Step 1 through to (D) Step 4.

The β -oxidation of acyl-CoA proceeds in a sequence of four enzymatic reactions (see **Figure 1-5**):

Step 1: In the first step of β -oxidation a hydrogen atom is removed from the α - and β -carbons of acyl-CoA, resulting in the creation of a trans double bond between these carbon atoms to form Trans- Δ^2 -Enoyl-CoA in a reaction catalysed by acyl-CoA dehydrogenase (Bonito *et al.*, 2016) (see **Figure 1-5A**). The two liberated hydrogen atoms are donated to FAD, reducing it to FADH₂.

Step 2: The second step is a reversible hydration reaction across the double bond between the α - and β -carbons of Trans- Δ^2 -Enoyl-CoA in which a hydroxyl group is added to the β -carbon and a hydrogen atom is bonded to the α -carbon via a reaction catalysed by Enoyl-CoA Hydratase. L-3-Hydroxyacyl-CoA is formed in this step.

Step 3: The hydroxyl group on the β -carbon of L-3-Hydroxyacyl-CoA is oxidised to a ketone group in a reaction catalysed by 3-hydroxyacyl-CoA dehydrogenase forming 3-Ketoacyl-CoA., with the hydrogen atom from the hydroxyl group being donated to NAD^+ to form NADH (see **Figure 1-5C**).

Step 4: In the final step of β -oxidation, CoA cleaves the bond between the α - and β -carbon of 3-Ketoacyl-CoA in a thiolytic reaction catalysed by β -ketothiolase. This results in the formation of two molecules. An acyl-CoA molecule in which the fatty acyl chain is 2 carbons shorter than it was in step 1 and a molecule of acetyl-CoA.

The disparate fates of the reducing equivalents, acyl-CoA, and acetyl-CoA produced during β -oxidation are central to energy metabolism. The FADH_2 and NAD molecules produced in step 1 and step 4, respectively, donate electrons to the electron transferring flavoproteins in the mitochondrial matrix, which transfer these electrons to ubiquinone in the ETC for ATP generation. The FADH_2 produced goes on to account for the production of 1.5 units of ATP in the ETC whilst the NADH produced in this step accounts for 2.5 units of ATP via the donation of its hydrogen ions to complex I of the ETC (Hinkle, 2005). The acetyl-CoA produced in step 4 in skeletal muscle is directed to the tricarboxylic acid (TCA) cycle. In the liver acetyl-CoA produced during β -oxidation can also act as substrate to produce ketone bodies during periods of prolonged nutrient deprivation (Fletcher *et al.*, 2019). However, it is important to note that the reducing equivalents (NADH and FADH_2) and ATP produced during β -oxidation inhibit pyruvate dehydrogenase, citrate synthase and isocitrate dehydrogenase, key enzymes which propagate the TCA cycle (Garland *et al.*, 1968). This inhibition is important in the regulation of muscle fuel selection, which is discussed in **Section 1.4**. As β -oxidation is a cyclical process, the fatty acyl-CoA produced in step 4 is returned to step 1 and truncated again. Thus, the greater the length of the FA chain the more units of ATP are generated by its complete oxidation (Reddy *et al.*, 2014).

Figure 1-5 outlines the oxidation of saturated FA chains; the oxidation of unsaturated FA chains requires additional reaction steps but still relies upon the sequential cleavage of 2 carbon atoms from the fatty acyl chain. Of note,

the breakdown of odd-chain FAs creates another bridge between β -oxidation and the TCA cycle. In the final round of the β -oxidation of odd-chain FAs, the 3-carbon propionyl-CoA is formed as an end product, which can then be enzymatically converted to succinyl-CoA (Bhagavan and Ha, 2015), a key molecule in the TCA cycle.

1.2.5 De Novo Lipogenesis

Muscle fibres can synthesise FAs de novo but to a limited extent, the bulk of FA stored and used in muscle comes from extracellular sources (Saggerson, Ghadiminejad, and Awan, 1992). As previously mentioned, the liver is the main site of DNL and, in response to decreasing circulating lipid availability caused by elevated muscle FA oxidation, this newly synthesised FA can be released into the circulation, enter skeletal muscle, and be incorporated into the LD TAG pool (Dagenais, Tancredi, and Zierler, 1976; Zierler, 1976).

De novo FA synthesis is initiated by citrate lyase, an enzyme that bridges glucose and FA metabolism and has a role in modulating TAG storage in LDs. When pyruvate flux through the TCA cycle increases, excess citrate can be shuttled out of the mitochondrial matrix into the sarcoplasm via citrate transporters (Sun *et al.*, 2010). Citrate lyase then converts cytoplasmic citrate into oxaloacetate, which can diffuse back into the mitochondria and propagate the TCA cycle, and acetyl-CoA which, amongst an array of intracellular fates, can act as the first substrate for FA synthesis (Burke and Huff, 2017). Acetyl-CoA is committed to FA synthesis when acetyl-CoA carboxylase 2 (ACC2), the muscle-specific ACC isoform, catalyses its high irreversible carboxylation to form malonyl-CoA (Abu-Elheiga *et al.*, 2000). This reaction is the rate-limiting step in FA synthesis.

The malonyl group of malonyl-CoA binds to an acyl carrier protein (ACP) in a reaction catalysed by Malonyl-CoA ACP transacylase. ACPs are important for shuttling acyl groups to fatty acid synthase (FAS) complexes, the main hubs of FA synthesis. FAS complexes have two critical components, an ACP region, and a cysteine thiol residue. In conjunction with an array of enzymes, and with NADH as a reducing equivalent, FAS complexes catalyse the sequential elongation of an acetyl-CoA primer group bound to its ACP region with carbon

atoms that are donated by the decarboxylation of malonyl groups, which transiently bind to the cysteine thiol residues (Wakil, Stoops, and Joshi, 1983). The reader is directed to a comprehensive review of FAS components, enzymes, and activity by Beld and colleagues (Beld *et al.*, 2015).

What is salient here is that the de novo FA synthesis pathway primarily produces the saturated FAs palmitate (C16:0) and stearate (C18:0) as end products. However, cells require mono- and poly-unsaturated FAs of various lengths for phospholipid synthesis and for the activation and regulation of intracellular signalling pathways (Brown *et al.*, 2019). Therefore, whilst the palmitate and stearate produced during FA synthesis can be esterified and trafficked to LDs for storage (Li and Cheng, 2014), thereby increasing IMCL content, they can also be used in the biosynthesis of mono-unsaturated FAs by Stearoyl-CoA desaturases (SCDs) (Igal, 2016) and poly-unsaturated FAs by FA desaturases (Lattka *et al.*, 2010). It is also important to note that malonyl-CoA inhibits FA oxidation in a mechanism that is discussed in **Section 1.3.2** and is critical to muscle contraction-mediated glucose uptake.

1.3 Skeletal Muscle Glucose Uptake and Utilisation

Plasma glucose concentration, representing a balance between glucose utilisation and glucose availability, is tightly regulated. Per the National Institute for Health and Care Excellence (NICE) Public Health Guideline 38 document, for metabolically healthy individuals, fasting plasma glucose concentration should be between 4-5.5 mmol/L or 72-100 mg/dL (NICE, 2012). Though the pancreas is the main regulator of plasma glucose concentration, secreting insulin from the β -cells of the Islets of Langerhans in response to postprandial elevations in blood glucose and glucagon from α -cells in response to postabsorptive decreases in blood glucose, other organs and tissues also play a vital role in this regulation (Röder *et al.*, 2016). Skeletal muscle is the main site for the disposal of glucose, accounting for upwards of 80% of intravenously infused glucose uptake under hyperinsulinaemic-euglycaemic clamp conditions (Wasserman, 2009; DeFronzo and Tripathy, 2009) and for roughly 50% of postprandial glucose uptake under normal physiological conditions (Capaldo *et al.*, 1999). To fully appreciate how ectopic lipid accumulation in skeletal muscle may contribute to decreased whole-body glucose uptake and the development of insulin resistance, it is important to first describe the glucose uptake and utilisation pathways.

Glucose is a polar molecule; it cannot cross phospholipid bilayers via diffusion. Thus, glucose transporters (GLUTs) on the cell membrane which express differences in kinetics, substrate specificity, and tissue expression are required to facilitate the ATP-dependent transport of hexose sugars into cells (Hruz and Mueckler, 2001). The primary transporter in skeletal muscle is GLUT4 which was first characterised in 1989 (James, Strube, and Mueckler, 1989) and is unique amongst GLUTs in that it is largely localised to vesicles in intracellular compartments rather than the cell membrane. The trafficking of intracellular GLUT4 vesicles to, and their enhanced expression on, the sarcolemma is largely dependent upon (1) the binding of insulin to insulin receptors (Huang and Czech, 2007) and (2) muscle contraction (Lund *et al.*, 1995). Highlighting the importance of insulin in mediating skeletal muscle glucose uptake is the fact that only around 4% of myocellular GLUT4 is localised to the sarcolemma in the absence of stimulation by insulin, with more

than 90% localised to subcellular compartments (Coster, Govers, and James, 2004). The intracellular signalling events regulating both insulin-mediated and contraction-mediated glucose uptake will be described here.

1.3.1 Insulin-Mediated Glucose Uptake in Skeletal Muscle

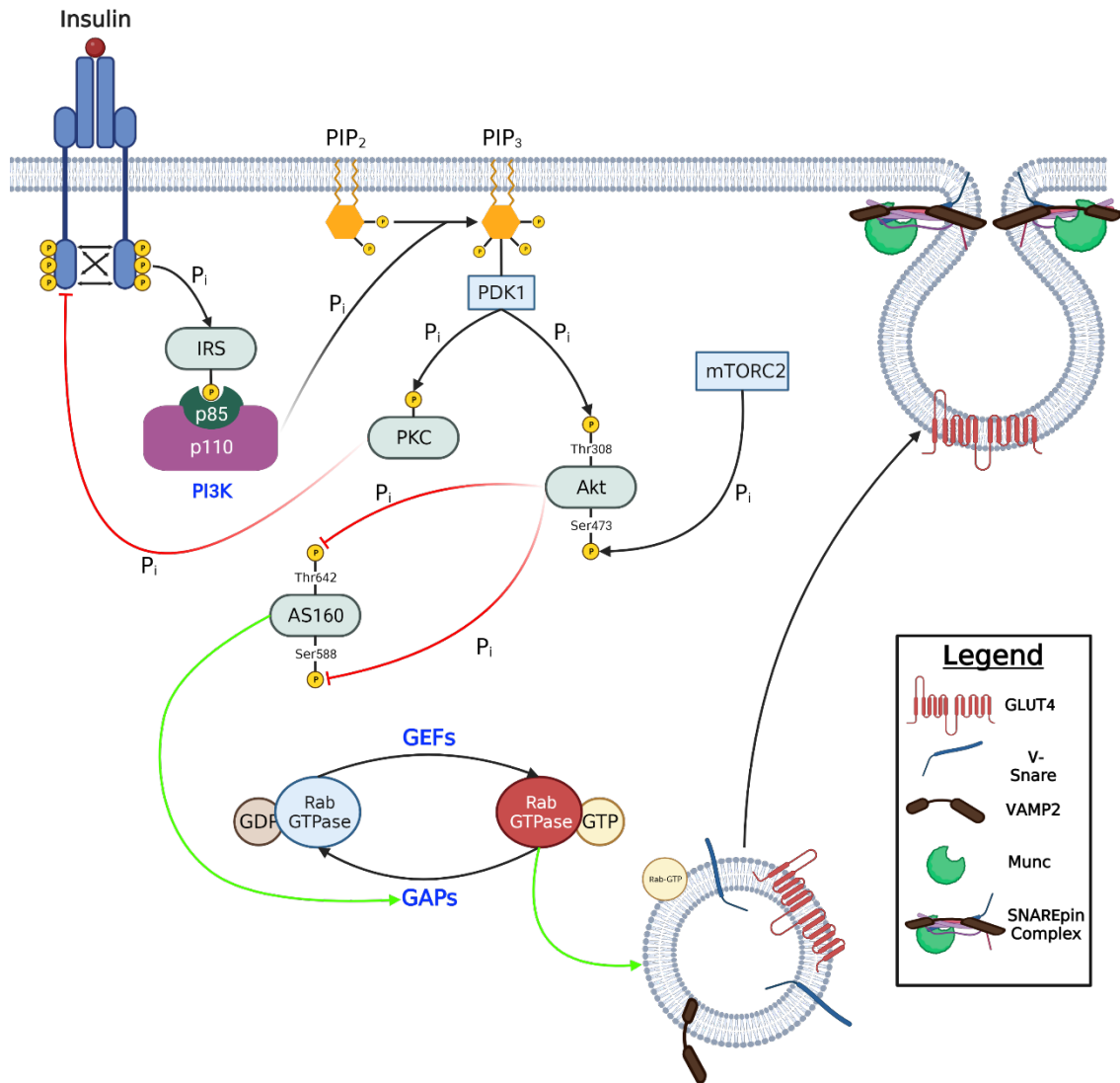


Figure 1-6: Simplified schematic of the key insulin-mediated intracellular events that promote GLUT4 translocation to the sarcolemma. Red arrows indicate inhibition. Green arrows indicate activation.

When insulin binds to the extracellular α -subunits of insulin receptor monomers, which are transmembrane tyrosine kinases (Moller *et al.*, 1989), they homodimerise or heterodimerise with insulin-like growth factor receptors (Baillyes *et al.*, 1997) (see **Figure 1-6**). The tyrosine residues in the intracellular β -subunits of the resulting functional dimers then undergo autophosphorylation

and transphosphorylation (Gammeltoft and Van Obberghen, 1986). The phosphorylated tyrosine residues on the β -subunits recruit and phosphorylate adapter proteins such as those of the Insulin Receptor Substrate (IRS) family. Phosphorylated IRS-1 and 2 have several tyrosine residues within YxxM motifs that recruit the class 1a regulatory phosphatidylinositol-4,5-bisphosphate 3-kinase (PI3K) lipid kinases via their src-homology 2 (SH2) domains (White, 2002). PI3K has two important subunits: the p85 regulatory subunit and the p110 catalytic subunit (Rathinaswamy *et al.*, 2021). The p85 subunit attaches directly to phosphorylated tyrosine residues on IRS-1/2 leading to the phosphorylation and activation of the p110 subunit. The activated p110 subunit catalyses the addition of a phosphate group to the 3' carbon of the membrane phospholipid phosphatidylinositol-4,5-bisphosphate (PIP₂) to form phosphatidylinositol-3,4,5-triphosphate (PIP₃) (Knight *et al.*, 2006). PIP₃ remains integrated in the sarcolemma where it acts as a site for the recruitment and activation of 3-phosphoinositide-dependent protein kinase 1 (PDK1). Phosphatidylinositol binding of PDK1 is necessary for the activation of many PDK1 substrates at the cell membrane, the crucial one in this case being protein kinase B (PKB) or Akt. PIP₃ co-recruits PDK1 and its substrate kinases Akt and protein kinase C (PKC) to the cell membrane via their Pleckstrin homology domains (Miao *et al.*, 2010). Once localised to the plasma membrane Akt undergoes conformational changes that expose two amino acids which must both be phosphorylated to achieve full activation. Akt is phosphorylated at Thr308 by PDK1 and then phosphorylated at Ser473 by mammalian target of rapamycin (mTOR) complex 2 (mTORC2) (Yoon, 2017). The effects of insulin on glucose uptake and metabolism are primarily mediated by this activated Akt.

Phosphorylated Akt modulates Rab GTPase protein activity and increases glucose uptake in insulin-stimulated cells by promoting the translocation of GLUT4 vesicles to the cell membrane, thus increasing cell membrane permeability to glucose. Rab GTPases are regulated by the cycling between their Guanosine-5'-Triphosphate (GTP)-bound active conformation and their Guanosine Diphosphate (GDP)-bound inactive conformation (Stenmark, 2009). This conformational cycling is controlled by the balance

between the activity of Rab GTPase-activating proteins (GAPs) and Guanine nucleotide exchange factors (GEFs). GEFs promote the release of GDP bound to Rab GTPases, such that GTP can then bind to and functionally activate the GTPases. Rab GAPs then inactivate Rab proteins by catalysing GTP hydrolysis from them, which is then replaced by GDP (Barr and Lambright, 2010).

Rab GTPases control membrane trafficking pathways which are responsible for intracellular GLUT4 vesicle formation, vesicle transport to the cell membrane, and vesicle fusion to the cell membrane (Fukuda, 2008; Stenmark, 2009). Rab GAPs contain a highly conserved domain, the GAP domain, which contains 200-300 amino acids, depending on the protein, and catalyses GTP hydrolysis (Pan *et al.*, 2006). In cells which are not stimulated by insulin, the Rab GAPs Akt substrate of 160 kDa (AS160), also known as TBC1D4, and TBC1D1 constitutively inhibit GLUT4 vesicle translocation to the cell membrane by catalysing the conversion of GTP to GDP for Rab GTPases that control GLUT4 translocation. Thus, in the resting state the rate of GLUT4 vesicle trafficking to and from the sarcolemma is comparatively low and many vesicles are retained in intracellular compartments. When myocytes are stimulated by insulin, AS160 and TBC1D1 are phosphorylated by Akt and inactivated (Middelbeek *et al.*, 2013; Cartee, 2015). In this insulin-stimulated state the molecular switch is flipped to favour the activity of Rab GEFs which catalyse the binding of GTP to Rab GTPases, activating them, upregulating the translocation of GLUT4 vesicles to the sarcolemma, and boosting glucose uptake. It has been demonstrated in 3T3-L1 adipocytes that when the phosphorylation sites of AS160 are mutated to alanine, such that Akt cannot phosphorylate them and inactivate AS160, GLUT4 translocation to the cell surface is reduced by roughly 80% (Sano *et al.*, 2003).

Soluble NSF attachment protein receptor (SNARE) proteins mediate the translocation of intracellular GLUT4-containing vesicles to the sarcolemma and the fusion of these vesicles with the sarcolemma (Han, Pluhackova, and Böckmann, 2017). A detailed review of this complex and incompletely understood process is beyond the scope of this thesis. Briefly, during GLUT4 translocation, vesicle (v-) SNAREs located on GLUT4 vesicles interact with the

relevant target (t-) SNAREs located in the sarcolemma to form 4 SNARE motifs which are assembled in twisted 4-helical bundles known as SNAREpin complexes (Hong and Lev, 2014). SNAREpin complexes are obligatory for the fusion of vesicles with the sarcolemma and the exocytosis of GLUT4 to the cell surface. The SNAREs involved in insulin-mediated GLUT4 translocation include VAMP2, Syntaxin 4 and SNAP23 which are in turn regulated by Munc18C, Synip, and Synaptotagmin (Foley, Boguslavsky and Klip, 2011). The actin cytoskeleton also plays a role as evidenced by the activation of the cytoskeleton regulatory protein GTPase Rac1 during this translocation (SyLOW *et al.*, 2013).

1.3.2 Contraction-Mediated Glucose Uptake in Skeletal Muscle

The contraction-mediated glucose uptake pathway is not as well understood as the insulin-mediated pathway. Existing evidence suggests that it is primarily facilitated by 5' adenosine monophosphate-activated protein kinase (AMPK), a heterotrimeric serine/threonine kinase that plays a major role in the regulation of metabolic substrate utilisation. AMPK is composed of an α -subunit, responsible for its catalytic activity, and regulatory β - and γ -subunits. The γ -subunit contains CBS domains which bind to both AMP and ATP (Xiao *et al.*, 2007), thereby affording this enzyme sensitivity to changes in the intracellular ratio of AMP:ATP caused, in this context, by ATP consumption during exercise (Richter and Ruderman, 2009).

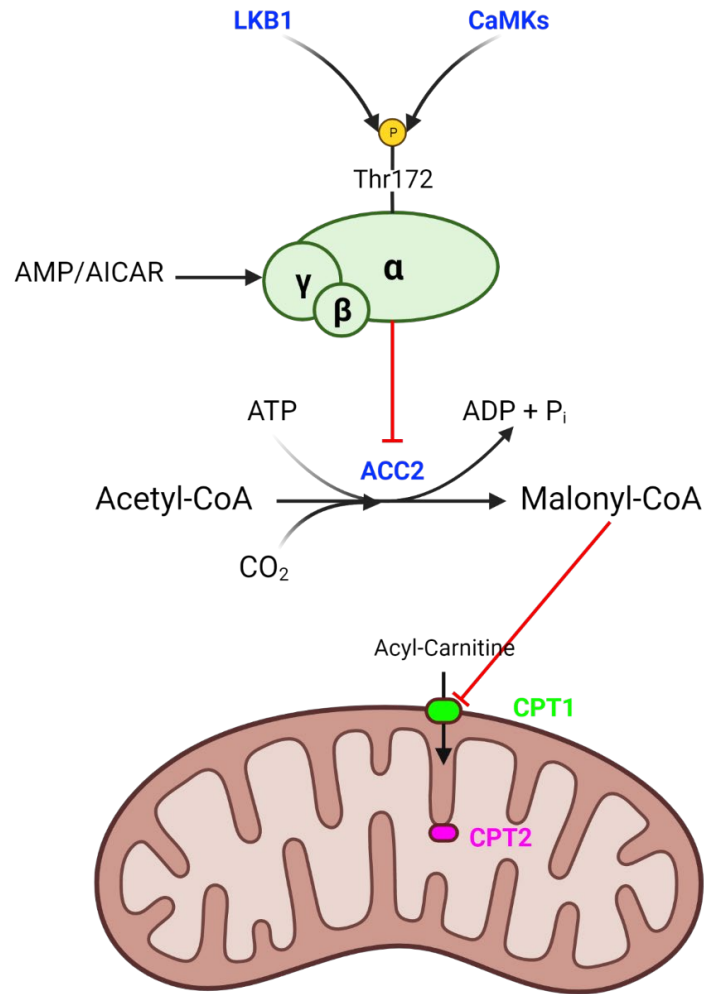


Figure 1-7: Pathway for AMPK activation and the effect of this activation on fatty acid transport into the mitochondria. Enzymes are shown in blue text. CPT1, Carnitine palmitoyltransferase I; CPT2, Carnitine palmitoyltransferase 2.

Muscular contractions increase the rate of ATP hydrolysis, forming ADP which can then be converted to AMP in a reaction catalysed by adenylate kinase. As the AMP:ATP ratio increases, more AMP binds to the CBS domains in site 3 of the γ -subunit of AMPK, thereby allosterically activating it and enhancing the phosphorylation of the threonine 172 residue in the catalytic α -subunit by upstream kinases including Liver Kinase B1 (LKB1) (Hardie *et al.*, 2003; Legendorf *et al.*, 2016) (see **Figure 1-7**). Phosphorylation of AMPK functionally activates it (Woods *et al.*, 2003) and it is the ratio of AMP:ATP that is the primary determinant of this activation, not the intracellular concentration of ATP which, unlike AMP, does not change significantly during low-moderate

intensity exercise (Hardie, Salt, and Davies, 2000). In lean, healthy individuals, but not obese individuals or those with T2DM, cytoplasmic increases in AMP concentration, and increased AMPK activation, are closely coupled with the velocity, power output, and duration of muscular contractions (Chen *et al.*, 2003; Sriwijitkamol *et al.*, 2007). This is evident in both resistance (Dreyer *et al.*, 2006) and endurance exercise modalities, with AMPK activation notably increasing in the latter from exercise intensities of 40% VO₂ peak (Chen *et al.*, 2003). An analogue of AMP, 5-Aminoimidazole-4-carboxamide ribonucleotide (AICAR), is another important allosteric activator of AMPK (Višnjić *et al.*, 2021).

Activated AMPK has three main functions, all of which fit within the rubric of increasing ATP generation to decrease the intracellular AMP:ATP ratio:

1. Upon activation, mainly through AICAR, AMPK phosphorylates AS160 (Treebark *et al.*, 2006), resulting in increased Rab GTPase activity, enhanced GLUT4 translocation to the sarcolemma and greater glucose uptake in contracting muscle, as discussed in **Section 1.3.1**.
2. Activated AMPK phosphorylates Acetyl-CoA carboxylase 2 (ACC2), the predominant ACC isoform in muscle, at Ser212 thereby inhibiting its activity (see **Figure 1-7**). ACC2 catalyses the synthesis of malonyl-CoA from acetyl-CoA (Abu-Elheiga *et al.*, 2000), a critical reaction in FA biosynthesis. Malonyl-CoA is responsible for the inhibition of CPT1 (Cook, Stephens, and Harris, 1984) which, as discussed in **Section 1.2.3.1**, is an integral part of the carnitine shuttle that transports fatty acids into the mitochondrial matrix for β -oxidation (Houten, and Wanders, 2010). Thus, by inhibiting ACC2 catalytic activity, AMPK reduces malonyl-CoA synthesis, decreases inhibition of CPT1 and promotes LCFA oxidation, thereby increasing ATP production and decreasing the intracellular AMP:ATP ratio.
3. Activated AMPK also limits the activity of pathways involved in lipid and protein synthesis, cell growth, and cell proliferation, all of which are processes that consume ATP (Steinberg, and Carling, 2019).

However, though AMPK has a recognised role in the contraction-mediated glucose uptake pathway, several studies using transgenic rodent models have found that glucose uptake via this pathway is only partially blunted by 40-60% following deactivation or knockout of AMPK (Hingst *et al.*, 2020). Therefore, other molecules are implicated in facilitating contraction-mediated glucose uptake.

The seminal findings in this regard were published by Youn and colleagues in 1991. They incubated muscle isolated from male Wistar rats in caffeine and N-(6-aminohexyl)-5-chloro-1-naphthalenesulfonamide at concentrations that were sufficient to stimulate Ca^{2+} release from the sarcoplasmic reticulum without increasing muscle tension. In so doing they observed that increases in intramyocellular Ca^{2+} concentration independently enhanced the uptake of 3-O-methyl-D-glucose in skeletal muscle (Youn, Gulve, and Holloszy, 1991). Later it was found in similar experiments that incubation of muscle with KN93, an inhibitor of the Ca^{2+} /Calmodulin-dependent Protein Kinases (CaMKs) class of regulators (Junho *et al.*, 2020), completely blunted any caffeine-induced increases in glucose uptake, indicating that the CaMK enzyme class was the key mediator in Ca^{2+} -induced glucose uptake (Wright *et al.*, 2004).

The role of the CaMK-dependent element of the contraction-mediated glucose uptake pathway in humans is debated (Jensen *et al.*, 2014) but is currently conceptualised as follows (Wright *et al.*, 2006). Muscle contractions stimulate the release of Ca^{2+} ions from the sarcoplasmic reticulum, which raises the calcium levels in the sarcoplasm. Calmodulin binds to these Ca^{2+} ions and the resultant Ca^{2+} /calmodulin complex undergoes a conformational change that allows it to bind to and activate CaMKII, the main CaMK in skeletal muscle (Rose, Kiens, and Richter, 2006). Activated CaMKII then undergoes autophosphorylation at Thr286 and Thr287 (Lucić, Greif, and Kennedy, 2008) and, in conjunction with LKB1, acts as an upstream kinase of AMPK, phosphorylating it at Thr172 as shown in **Figure 1-7** (Witczak *et al.*, 2006). Phosphorylated AMPK promotes GLUT4 translocation to the sarcolemma and t-tubules, and muscle glucose uptake as previously described. Evidence supporting this concept comes from experiments using electrical pulse

stimulation (EPS) of C2C12 myotubes, which induces muscle contractions *ex vivo* (Ojuka, Goyaram, and Smith, 2012; Nikolić, and Aas, 2019). These experiments show that the abundance of phosphorylated Thr172-AMPK and phosphorylated Thr286-CaMKII is significantly increased during muscle contractions (Hong *et al.*, 2016) and that GLUT4 translocation and glucose uptake are enhanced because of this contraction-induced phosphorylation (Witczak *et al.*, 2006). Alongside phosphorylation of AMPK, there is evidence that CaMKII enhances muscle glucose uptake by increasing the activation of myocyte enhancer factor 2 (MEF2 proteins), which are transcription factors that upregulate GLUT4 gene expression (Ojuka, Goyaram, and Smith, 2012).

1.3.3 Carbohydrate Utilisation

The first step in carbohydrate utilisation is the ATP-dependent phosphorylation of internalised glucose to form glucose-6-phosphate (G6P), a reaction which is catalysed by the hexokinase isoforms (Wilson, 2003), primarily hexokinase II in the skeletal muscle (Roberts and Miyamoto, 2015). This reaction commits glucose to downstream metabolic pathways as G6P cannot be transported out of the myocyte. It also ensures that the gradient in glucose concentration between the interstitial space and the sarcoplasm continues to favour glucose uptake by the muscle. G6P acts as the foundation for three pathways that are necessary for ATP production and cell survival: Glycogenesis, through which glucose is stored as glycogen within the cell; Glycolysis, which produces pyruvate and ATP, and the Pentose Phosphate Pathway, which generates NADH with the production of 5-carbon sugars for nucleotide synthesis as the endpoint. A discussion on the PPP is beyond the scope of this thesis.

1.3.3.1 Glycogenesis

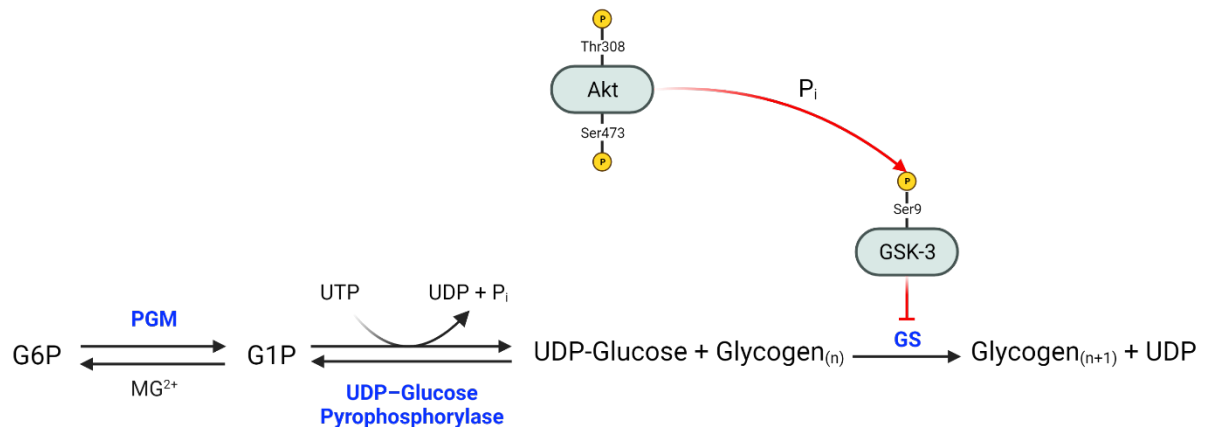


Figure 1-8: Schematic of glycogenesis pathway. In response to cellular insulin stimulation activated Akt phosphorylates GSK-3, promoting the incorporation of glucose molecules into glycogen.

Akt promotes glycogenesis through the inhibition of glycogen synthase kinase 3 (GSK-3). To form glycogen, G6P must first be converted to UDP-glucose (see **Figure 1-8**). This conversion is mediated by the enzyme phosphoglucomutase (PGM) which transforms G6P into glucose-1-phosphate (G1P), and UDP-glucose pyrophosphorylase which catalyses the reaction between uridine triphosphate and glucose-1-phosphate to form UDP-glucose with the release of pyrophosphate (Tegtmeyer *et al.*, 2014). Glycogen synthase (GS) is the enzyme that catalyses the incorporation of UDP-glucose units into glycogen (Contreras *et al.*, 2016). When Akt activity is low in the absence of cellular insulin stimulation, GSK-3 actively phosphorylates GS, inactivating it and decreasing the rate of glycogenesis. GSK-3 is phosphorylated on Ser-9 (Sutherland, Leighton, and Cohen, 1993) in its N-terminus by phosphorylated Akt in response to cellular insulin stimulation, thus reducing the active site availability of the enzyme and decreasing GSK-3 phosphorylation of GS (Cross *et al.*, 1995). Unphosphorylated GS is enzymatically active and will begin to increase the rate of glycogenesis using intracellular glucose.

1.3.3.2 Glycolysis

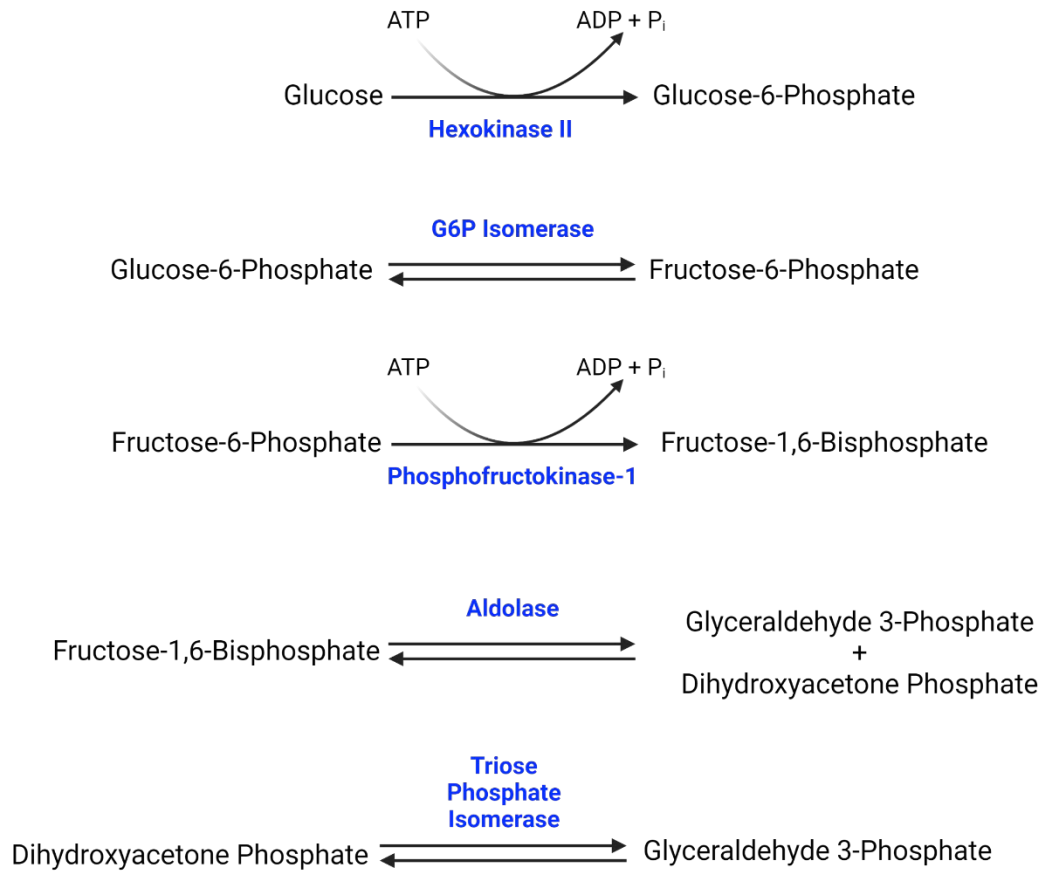


Figure 1-9: ATP-utilisation phase of glycolysis. Enzymes are shown in blue.

Glycolysis is a well characterised, 10-step enzymatic reaction in which glucose is converted to two units of pyruvate, which are further sequentially metabolised to CO₂ via the TCA cycle, with the generation of ATP and H₂O (Gnaiger, 2009). Glycolysis can largely be split into two phases: an ATP-utilisation phase (see **Figure 1-9**) followed by an ATP-production phase. As mentioned in **Section 1.3.3**, the first committed step in glucose metabolism is the phosphorylation of a glucose molecule to form G6P in an ATP-dependent reaction catalysed by hexokinase II. This is followed by the isomerisation of G6P to form fructose-6-phosphate, catalysed by G6P isomerase, and the phosphorylation of fructose-6-phosphate to form fructose-1,6-bisphosphate, a reaction which consumes another molecule of ATP. The ATP utilisation phase ends at the fourth and fifth steps of glycolysis in which a fructose-1,6-bisphosphate molecule is cleaved by aldolase to form a single glyceraldehyde

3-phosphate and a single dihydroxyacetone phosphate molecule, which is subsequently converted to a second glyceraldehyde 3-phosphate molecule by triose phosphate isomerase.

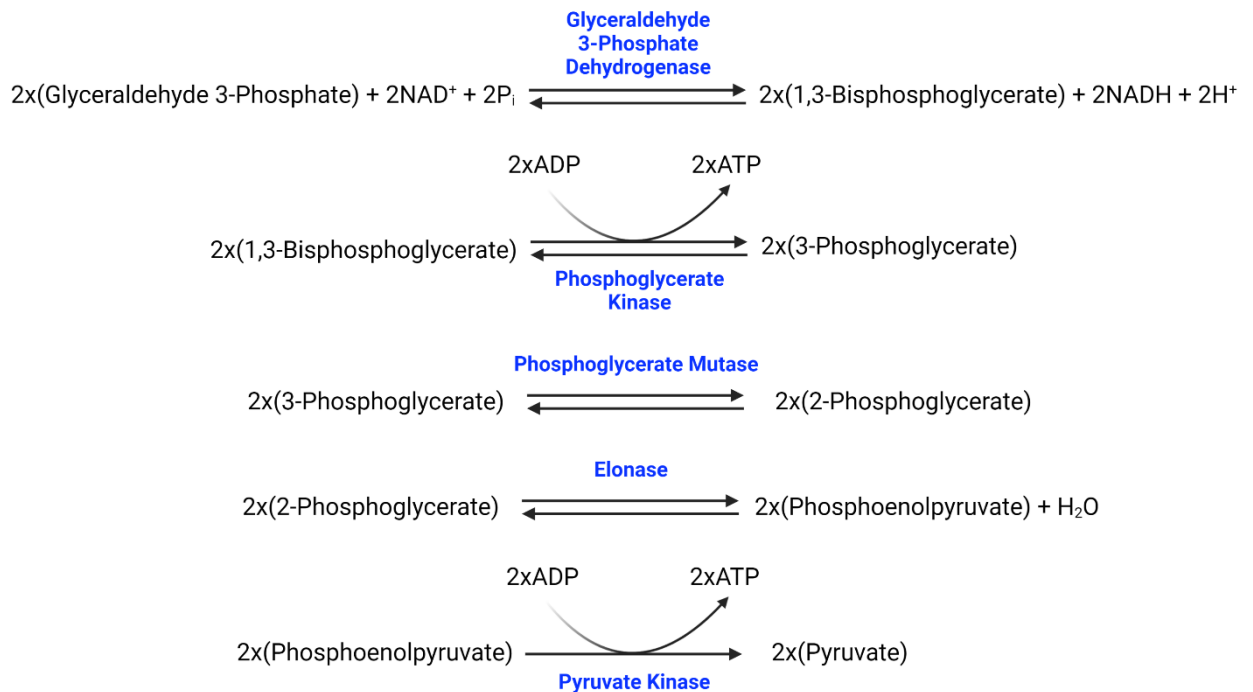


Figure 1-10: ATP-production phase of glycolysis. Enzymes are shown in blue.

The ATP-production phase is initiated when each of the two glyceraldehyde 3-phosphate molecules are oxidised by NAD^+ to form two molecules of 1,3-bisphosphoglycerate and NADH, a reaction catalysed by glyceraldehyde 3-phosphate dehydrogenase. This is followed by the first ATP producing step in which each 1,3-bisphosphoglycerate molecule is converted to 3-phosphoglycerate by phosphoglycerate kinase, generating two ATP molecules. Phosphoglycerate mutase and enolase, via a dehydration reaction, then sequentially catalyse the conversion of the two 3-phosphoglycerate molecules to form two phosphoenolpyruvate molecules as shown in **Figure 1-10**. The final step of glycolysis is the dephosphorylation of the two phosphoenolpyruvate molecules to form pyruvate, as catalysed by pyruvate kinase, to yield two units of ATP. Thus, when both the ATP-utilisation phase in which 2 molecules of ATP are used and the ATP-production phase in which 4 molecules of ATP are generated, glycolysis yields a net total of two units of

ATP for each molecule of glucose (Boiteux and Hess, 1981). In skeletal muscle the formation of G6P, fructose-6-phosphate, and pyruvate are irreversible steps but the reversal of these reactions by different enzymes is essential for gluconeogenesis in the liver (Rui, 2014).

Pyruvate has several fates. In the cytoplasm it can be anaerobically reduced to lactate via a fermentation reaction catalysed by lactate dehydrogenase, or it can undergo transamination to form alanine. Pyruvate can also traverse the mitochondrial membranes and enter the mitochondrial matrix via pyruvate carrier proteins (Halestrap, 2012; Bricker et al., 2012) where it goes through the TCA cycle.

1.3.3.3 The TCA Cycle

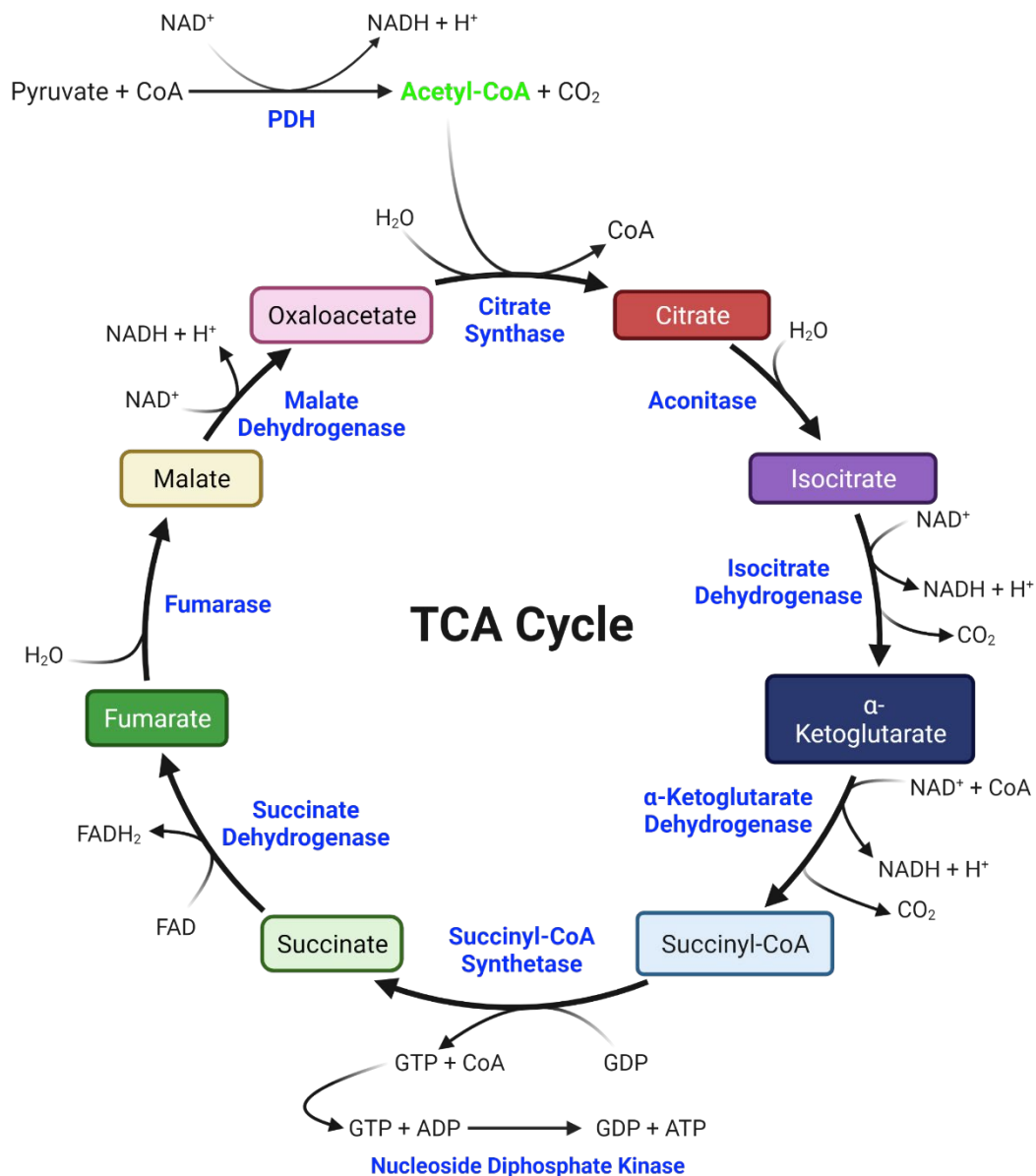


Figure 1-11: Diagram of the TCA cycle. Acetyl-CoA, through which this cycle is initiated, is shown in green. Enzymes are shown in blue.

In the mitochondrial matrix pyruvate molecules can undergo one of two irreversible reactions integral to the TCA cycle (see **Figure 1-11**). They can be carboxylated to form oxaloacetate in a reaction catalysed by pyruvate carboxylase (Jitrapakdee *et al.*, 2008). Or the pyruvate dehydrogenase complex (PDC), an assembly of the pyruvate dehydrogenase (PDH), dihydrolipoyl acetyltransferase, and dihydrolipoyl dehydrogenase enzymes, catalyses the oxidative decarboxylation of pyruvate to form acetyl-CoA (Patel

et al., 2014). This process is tightly controlled by the reversible phosphorylation of PDH, mediated by pyruvate dehydrogenase kinase (PDK) and pyruvate dehydrogenase phosphatase (PDP).

Whilst a detailed discussion of the TCA cycle is beyond the scope of this thesis, it is important to highlight that the main function of this cycle is to oxidise acetyl-CoA derived both from pyruvate and produced during β -oxidation as discussed in **Section 1.2.4.2** (Bowtell *et al.*, 2007). Thus, the regulation of PDC activation status by PDKs and PDPs is central to muscle fuel selection.

1.4 Integration of Muscle FA and Glucose Oxidation

The oxidation of FA and oxidation of glucose are tied together in a reciprocal relationship. The first attempt to characterise this relationship mechanistically was put forth by Sir Philip Randle and his colleagues in 1963 with what is now termed the glucose-FA, or Randle, cycle (Randle *et al.*, 1963). Based on previous findings that elevated plasma FA availability resulted in increased FA oxidation concurrent with decreased glucose oxidation, Randle and his colleagues proposed that these findings resulted from the inhibition of the PDC caused by changes in the production of acetyl-CoA and NADH reducing equivalents in the mitochondrial matrix. Standing on the shoulders of this ground-breaking theory, subsequent research has afforded us a clearer, modern understanding of the integration of fat and glucose oxidation during fasting, following feeding, during exercise, and in response to metabolic dysfunction and disease.

1.4.1 Skeletal Muscle Fuel Oxidation in the Postabsorptive State

In the fasting, or postabsorptive, state, 6-12 hours following feeding when nutrients have been absorbed by the gut and stored within the tissues, adipose tissue lipolysis allows for the release of FAs into the circulation, increasing plasma FA availability and FA transport to and uptake by the peripheral tissues, including the skeletal muscles (Jensen, Ekberg, and Landau, 2001). Increased intramyocellular FA availability increases the rate of β -oxidation, thereby supporting the selective utilisation of fats as fuel for ATP production during fasting, and impairs glucose oxidation (Boden *et al.*, 1994; Vaag *et al.*,

1994). FA oxidation accounts for about 66% of whole-body energy production in the fasted state (Kuzmiak-Glancy and Willis, 2014) and typically the reliance on FA oxidation for energy production is even greater than 66% in the skeletal muscles specifically (Dagenais, Tancredi, and Zierler, 1976). This preferential oxidation of FAs at rest in most tissues allows for the sparing of blood glucose and of glycogen stores. These are crucial survival adaptations that maintain glucose availability for brain cells and the wider central nervous system where, unlike almost all other tissues in the body, glucose oxidation predominates overwhelmingly, even at rest (Schönfeld and Reiser, 2013). As described by the glucose-FA cycle, the impairment of glucose oxidation by FAs in the fasted state is at three key levels of the glucose metabolism pathway:

1. Firstly, β -oxidation of FAs is the primary source for the production of acetyl-CoA and the reducing equivalents NADH and FADH₂ in the mitochondrial matrix during fasting, with enhanced β -oxidation increasing mitochondrial acetyl-CoA/CoA and NADH/NAD⁺ ratios. Elevations in Acetyl-CoA and NADH mitochondrial content can acutely reduce pyruvate flux through PDC by feedback inhibition, so as the concentration of these β -oxidation products increases, glucose oxidation is antagonised (Constantin-Teodosiu, 2013).
2. Secondly, increased production of acetyl-CoA from β -oxidation also increases citrate concentrations in the mitochondrial matrix. Excess citrate can be transported out of the mitochondria into the sarcoplasm, see **Section 1.2.3.3**, where it can directly inhibit the activity of phosphofructokinase, which catalyses the phosphorylation of fructose-6-phosphate to form fructose-1,6-bisphosphate during glycolysis (Jenkins *et al.*, 2011), thereby attenuating the glycolytic pathway (see **Section 1.3.3.2**). The inhibition of phosphofructokinase in this way also leads to the accumulation of G6P and indirect inhibition of hexokinase, resulting in the impaired retention and oxidation of glucose (Hue and Taegtmeyer, 2009).

3. Thirdly, the expression of PDKs is elevated during the postabsorptive state due to decreased plasma insulin concentration and increased FA-induced transcription of PDK genes (Holness and Sugden, 2003). PDKs target the pyruvate dehydrogenase (E1) enzymatic region of the PDC, phosphorylating the Ser293, 300, and 232 residues and reducing its activity (Abbot *et al.*, 2005; Tovar-Méndez *et al.*, 2005). This antagonism of PDCs reduces the rate at which pyruvate from glycolysis is converted to acetyl-CoA, thereby decreasing the rate of glucose oxidation, and increasing the rate of β -oxidation to meet the energy demands of the muscle (Sugden *et al.*, 2000).

1.4.2 Skeletal Muscle Fuel Oxidation in the Postprandial State

The work of Andres, Cader, and Zierler in human forearm muscle was the first to show that during the transition from the fasted to the fed state, muscle fuel oxidation switches from predominantly FA to glucose oxidation (Andres, Cader, and Zierler, 1956). Following a meal, or under hyperinsulinaemic-euglycaemic clamp conditions, plasma insulin and glucose concentrations increase. Insulin inhibits the rate of adipose tissue lipolysis, thereby suppressing the release of FAs stored in these depots into the circulation, promoting greater FA re-esterification, and reducing plasma FA concentration (Foley, 1988; Bajaj *et al.*, 2004; Choi *et al.*, 2010). Given that plasma FA concentration is a major determinant of FA oxidation, changes in plasma glucose concentration act as one of the mechanisms regulating the rate of FA oxidation in this transition from the fed to the fasted state. Most of the glucose taken up by the muscles in the postprandial state is oxidised whilst the rest is converted to glycogen as described in **Section 1.3.3.1**.

The inhibition of FA oxidation in the postprandial state, or under hyperinsulinaemic-euglycaemic clamp conditions, is largely caused by the inhibition of FA transport into the mitochondria. A study by Sidossis and Wolfe demonstrated, using the hyperinsulinaemic-euglycaemic clamp technique, that increasing plasma glucose concentration blunted the oxidation of LCFAs but not of medium chain FAs (Sidossis and Wolfe, 1996). Given that CPT1 is responsible for the transport of LCFAs into the mitochondria, these data

suggested that glucose-induced inhibition of FA oxidation is regulated at the level of CPT1. As detailed in **Section 1.3.2**, malonyl-CoA is the regulator of CPT1 activity, inhibiting it and decreasing the transport of long-chain acyl-carnitines into the mitochondria. The synthesis of malonyl-CoA is dependent upon the carboxylation of acetyl-CoA in a reaction catalysed ACC2.

Pyruvate formed during glycolysis enters the mitochondria and is converted to acetyl-CoA by the PDC. Excess citrate produced by elevated insulin-stimulated pyruvate flux through the TCA cycle can be transported into the sarcoplasm where it is converted to acetyl-CoA by citrate lyase, see **Section 1.2.5**. Greater cytosolic acetyl-CoA content upregulates the activity of ACC2 and increases the synthesis of malonyl-CoA, thereby promoting the inhibition of CPT1, decreasing the transport of LCFAs into the mitochondria and decreasing FA oxidation (Saha *et al.*, 1997). The resultant accumulation of LCFAs in the cytosol limits the uptake of FAs from the blood and favours the esterification of these FA chains to form TAG that is then stored within LDs. Feeding also attenuates PDK activation, increasing the rate at which the PDC catalyses the conversion of pyruvate to acetyl-CoA which ultimately leads to greater malonyl-CoA synthesis from citrate as previously described, resulting in impaired FA oxidation and increased glucose oxidation (Foster, 2012).

1.4.3 Metabolic Flexibility and Physical Activity Status

The ability to readily switch between preferential FA or glucose oxidation in response to changes in nutrient availability and plasma insulin concentration during the transition between the fasted and fed states is termed “metabolic flexibility” (Storlien, Oakes, and Kelley, 2004; Goodpaster and Sparks, 2017; Palmer and Clegg, 2022). The transition from FA to glucose oxidation is rapid, taking less than 30 minutes following the start of feeding in healthy individuals (Hue and Taegtmeyer, 2009). The characteristic preference for FA oxidation at rest and glucose oxidation after feeding in healthy, metabolically flexible individuals is perturbed in obese and insulin-resistant individuals.

Insulin-mediated suppression of FA oxidation and induction of glucose oxidation during feeding or during the hyperinsulinaemic-euglycaemic clamp are both blunted in obese individuals and those with T2DM, being indicative of

severe insulin resistance in both groups relative to healthy controls (Kelley *et al.*, 1990; Kelley *et al.*, 1999). There is some evidence to suggest that even in the postabsorptive state, obese individuals, and those with T2DM have lower resting FA oxidation, and higher resting glucose oxidation, rates than healthy individuals (Goodpaster, Wolfe, and Kelley, 2002; Hulver *et al.*, 2003; Carstens *et al.*, 2013). This “metabolic inflexibility” is a common finding in insulin resistant individuals and those with T2DM, though whether it precedes or is caused by insulin resistance is currently unclear (Palmer and Clegg, 2022). In vivo, using the hyperinsulinaemic-euglycaemic clamp technique in conjunction with indirect calorimetry, it has been demonstrated that insulin sensitivity and maximal oxygen uptake are positive predictors of metabolic flexibility whilst body fat percentage is negatively correlated with metabolic flexibility (Ukropcova *et al.*, 2005). Indeed, these associations were also observed in primary myotubes cultured from the vastus lateralis tissue of healthy, insulin-sensitive young males, demonstrating that differences in metabolic flexibility are evident at the level of the muscle (Ukropcova *et al.*, 2005).

Physical activity status is a major determinant of metabolic flexibility, with individuals that are habitually sedentary or who participate in bed rest interventions presenting with multiple markers of metabolic inflexibility and with impaired insulin sensitivity indicative of insulin resistance, whilst trained individuals have high metabolic flexibility (Rynders *et al.*, 2018). Indeed, it has been demonstrated that 10 days of endurance exercise, 1-hour long sessions at 70% VO_{2max} , improves metabolic flexibility in obese individuals such that their postprandial glucose and FA oxidation rates are comparable to healthy, lean controls (Battaglia *et al.*, 2012).

1.4.4 Skeletal Muscle Fuel Oxidation During Exercise

Skeletal muscle ATP content is around 5 mmol/kg wet muscle at any given time (Spriet *et al.*, 1992). In response to exercise, energy expenditure can increase more than 10-fold relative to the energy demands at rest (Romijn, 1993). This small pool of ATP would be rapidly depleted, particularly in response to exercise, unless it is consistently replenished and maintained. Therefore, both the uptake and oxidation of FA and glucose increase

significantly during the transition from rest to exercise to maintain muscle force output, with IMCL-derived FAs, adipose tissue-derived FAs, intramuscular glycogen stores, and blood glucose all providing substrate for ATP production in contracting muscle (Van Loon *et al.*, 2001). The extent to which glucose and FA oxidation contribute to whole-body energy requirements during exercise is dependent upon the exercise training modality, its duration, and its intensity (Romijn *et al.*, 1993).

During aerobic exercise maximal FA oxidation is achieved at exercise intensities from 45-65% VO_{2max} . At exercise intensities greater than this FA oxidation begins to decrease (Purdom *et al.*, 2018) and the oxidation of glucose increases to compensate in what is referred to as the “crossover” effect (Brooks, and Mercier, 1994). Mechanistically, at low-moderate exercise intensities, increased myocellular Ca^{2+} concentration (Watt, Heigenhauser, and Spriet, 2003) and stimulation of myocytes by adrenaline (Talanian *et al.*, 2006) results in the phosphorylation and activation of HSL, a key enzyme in the lipolysis of TAG stored within LDs as discussed in **Section 1.2.3**. This is accompanied by AMPK-mediated phosphorylation of PLIN proteins on the surface of LDs which recruits in activated ATGL and HSL enzymes, thereby promoting the lipolysis of LD TAGs and the supply of FAs to adjacent mitochondria for FA oxidation (Prats *et al.*, 2006). Thus, during low-moderate intensity exercise IMCL acts as a major source of FAs for ATP production (Stellingwerff *et al.*, 2007), with utilisation of LD-derived FAs being greatest at the maximal FA oxidation rate (Van Loon, 2004), which is also supported by exercise-induced increases in the intramyocellular synthesis and sarcolemmal expression of FA transporters (Talanian *et al.*, 2010).

As exercise intensity increases there is reduced FA delivery to, and oxidation by, the skeletal muscles and increased utilisation of glucose, primarily derived from the breakdown of glycogen, thereby shifting fuel utilisation to favour glucose oxidation (Spriet, 2014). The oxidation of fats at lower exercise intensities spares glycogen stores, with the depletion of these stores resulting in a precipitous decrease in muscle force output (Wahren *et al.*, 1971). Initial increases in glucose uptake in response to exercise are mediated by AMPK-induced translocation of GLUT4 to the sarcolemma

(Hargreaves and Spriet, 2018), as described in **Section 1.3.2**. The increase in the utilisation of glucose from glycogenolysis for ATP production is induced by cytoplasmic increases in Ca^{2+} and P_i concentrations and in the AMP:ATP ratio, all of which promote greater activation of glycogen phosphorylase (Hargreaves and Spriet, 2018).

Though the relationship between malonyl-CoA and CPT1 is important in the regulation of fuel selection during fed and fasted states, during exercise malonyl-CoA content in the skeletal muscles remains unchanged from exercise intensities of 35-100% $\text{VO}_{2\text{max}}$ and is independent of exercise duration or FA oxidation rates (Odland *et al.*, 1998). Instead, it is proposed that the availability of free carnitine to transport LCFAs into the mitochondrial matrix may be the determinant of FA oxidation during high intensity exercise (Hiatt *et al.*, 1989).

Van Loon and colleagues investigated the role of carnitines in muscle fuel selection during the crossover effect in 8 male cyclists (Van Loon *et al.*, 2001). The study involved participants exercising on a cycle ergometer at intensities of 40, 55, and 75% W_{max} in conjunction with intravenous infusion of glucose and palmitate tracers, blood and breath sampling, and muscle biopsy collection. They observed that whilst total carnitine concentration did not change from 40 to 55 to 75% W_{max} , muscle free carnitine concentration decreased whilst acyl-carnitine concentration increased, concurrent with the increased concentration of activated PDC. Accordingly, palmitate oxidation decreased from 55 to 75% W_{max} whilst the oxidation of glucose from muscle glycogen stores and plasma glucose increased. These changes were dissociated from plasma FFA concentration (Van Loon *et al.*, 2001).

Later work provided further insight into the mechanism via which PDC is activated during exercise. Muscular contractions stimulate Ca^{2+} release from the sarcoplasmic reticulum and Ca^{2+} uptake by the mitochondria in an exercise intensity-dependent manner (Egan and Zierath, 2013). In the mitochondria these Ca^{2+} ions then activate PDP (Huang *et al.*, 1998). It has been suggested that the increased PDC flux in the transition from rest to moderate-high intensity exercise is regulated by this increased Ca^{2+} -mediated activation of

PDPs in contracting muscle (Constantin-Teodosiu *et al.*, 2004). In line with this, maximal intensity contractions have been shown to increase the proportion of activated PDC in skeletal muscle, to decrease muscle free carnitine and glycogen content, and to increase PDH flux (Constantin-Teodosiu *et al.*, 2019).

Taken together, these findings support a pathway in which increased PDC flux decreases the flux of FA-derived acetyl-CoA into the TCA cycle, which causes the upstream accumulation of mitochondrial acyl-carnitines and decreases the cytosolic free carnitine pool. This results in the decreased ability to transport LCFAs into the mitochondrial matrix via the carnitine shuttle (see **Section 1.2.4.1**) and the inhibition of oxidation of FAs derived from IMCL and delivered to the tissues by lipoproteins (Van Loon *et al.*, 2001).

1.4.5 Transcriptional Regulation of Skeletal Muscle Fuel Oxidation

A legion of genes are responsible for regulating the interplay between muscle fuel oxidation, muscle insulin sensitivity, and IMCL content at rest, after feeding, and during exercise (Sabaratnam *et al.*, 2019; Parikh *et al.*, 2021; Verbrugge *et al.*, 2022). And though there are recent developments, such as the identification of Yes1 associated transcriptional regulator (YAP) as a key regulator of human skeletal muscle fuel oxidation (Watt *et al.*, 2021), only those genes with the greatest evidentiary support for a role in muscle fuel oxidation will be discussed, with relevance to the work presented here and brevity in mind.

1.4.5.1 Peroxisome Proliferator-Activated Receptors

FAs act as the endogenous ligands for peroxisome proliferator-activated receptors (PPARs) (Finck *et al.*, 2002), a family of nuclear receptor transcription factors that function as the main regulators of mitochondrial biogenesis and FA oxidation, of which there are three major isoforms: PPAR- α , - δ , and - γ (Lee, Olson, and Evans, 2003; Varga, Czimmerer, and Nagy, 2011). The different isoforms have variable tissue expression and functions, but all play a role in the regulation of fuel oxidation (Crossland, Constantin-Teodosiu, and Greenhaff, 2021). Upon activation by FAs PPARs heterodimerise with retinoid X receptors (RXRs) to form complexes that bind

to the regulatory regions of genes involved in lipid metabolism and promote their transcription, including LPL, FABP, SCD and CD36 (Varga, Czimmerer, and Nagy, 2011). PPAR activation is upregulated under fasting conditions, when FAs from adipose tissue lipolysis are taken up by the skeletal muscles, acting as one of the regulatory changes that underpin elevated FA oxidation in this state (Kersten *et al.*, 1999; Inagaki *et al.*, 2007; Duszka *et al.*, 2020). In mice chronic activation of PPARs has been demonstrated to significantly elevate FA oxidation in skeletal muscle, to prevent body weight gains even in response to high-fat feeding, and to decrease adiposity (Tanaka *et al.*, 2003).

PPARs also have a role in regulating carbohydrate metabolism as they upregulate the transcription of genes controlling the synthesis of PDKs, including the main muscle isoforms PDK2 and PDK4 (Degenhardt *et al.*, 2007). Given that PDKs compete with PDPs in the regulation of PDCs, this upregulation results in greater inhibition of PDC and decreased conversion of pyruvate to acetyl-CoA which promotes FA oxidation during fasting (Tsintzas *et al.*, 2006). PPARs also regulate the transcription of malonyl-CoA decarboxylase, an enzyme that promotes LCFA transport into the mitochondrial by catalysing the decarboxylation of Malonyl-CoA to form acetyl-CoA, thereby increasing FA oxidation (Young *et al.*, 2001).

1.4.5.2 Fork Head Box O

Fork head box O (FOXO) proteins are a family of transcription factors which are involved in the regulation of an array of processes in skeletal muscle, including energy metabolism (Sanchez, Candau, and Bernardi, 2014). Insulin suppresses FOXO expression by the induction of the PI3K/Akt signalling pathway in which Akt phosphorylates and inactivates FOXO1 (Zhang *et al.*, 2011). Conversely, it has been demonstrated that incubation with palmitate reduces the phosphorylation of FOXO in myocytes in vitro, activating FOXO1 (Chien, Greenhaff, and Constantin-Teodosiu, 2020). This is because the promoter region of FOXO1 contains PPAR response elements, with the transcription and activation of FOXO1 in skeletal muscle being highly responsive to PPAR activation by FAs (Nahlé *et al.*, 2008). The expression of FOXO1 is upregulated during fasting and starvation when plasma FA availability and FA uptake by the skeletal muscles are elevated due to adipose

tissue lipolysis, and there are three main mechanisms via which FOXO increases FA oxidation during these states.

Firstly, FOXO1, in conjunction with PPAR, targets response elements in the promoter region of the PDK genes (Kwon *et al.*, 2004) and induces increased skeletal muscle PDK4 mRNA transcription, thereby decreasing PDK activity and attenuating oxidative glucose metabolism in favour of FA oxidation (Furuyama *et al.*, 2003; Constantin-Teodosiu *et al.*, 2012; Chien, Greenhaff, and Constantin-Teodosiu, 2020). Secondly, FOXO1 decreases the transcription of genes involved in glucose metabolism via its interactions with PPARs (Chen *et al.*, 2019). Overexpression of dominant negative FOXO1 and FOXO3 reduces the expression of genes involved in FA metabolism, decreases GLUT4 expression, and decreases in vivo glucose uptake as determined by glucose tolerance tests in the intervention muscle by 20-35% compared to the control limb in mice (Lundell *et al.*, 2019). Lastly in vitro myocyte studies have shown that overexpression of FOXO1 increases the activity of LPLs, which release FAs from circulating lipoproteins (Kamei *et al.*, 2003), and increases the sarcolemmal expression of the FA transporter CD36, thereby increasing FA uptake and oxidation (Bastie *et al.*, 2005; Nahlé *et al.*, 2008).

1.4.5.3 CD36

CD36 is a transmembrane glycoprotein located within the sarcolemma that functions as a major FA transporter, particularly of LCFAs (Niculite, Enciu, and Hinescu, 2019). CD36 is the most efficient transporter of LCFA into the muscle and its overexpression in the sarcolemma results in enhanced FA uptake and oxidation but does not increase the esterification of FAs to TAG to the same extent (Nickerson *et al.*, 2009). Indeed, CD36 knock-out results in a precipitous decline in muscle FA uptake (Coburn *et al.*, 2000). Because the esterification of FAs taken up by CD36 form TAG does not match the rate of FA uptake, this can result in the build-up of lipotoxic intermediates that can disrupt insulin signalling and contribute to the development of muscle insulin resistance as will be discussed in **Section 1.5** (Puchałowicz and Rać, 2020). As aforementioned, CD36 transcription is induced by PPARs, particularly PPAR- γ in conjunction with FOXO1, and as the FAs it transports can activate PPARs

this establishes a feedback mechanism that potentiates FA oxidation (Maréchal *et al.*, 2018). Whilst not the most efficient transporters of FAs into the muscle, overexpression of FABPs is associated with the greatest rate of LCFA oxidation (Nickerson *et al.*, 2009; Storch and Thumser, 2010).

1.4.5.4 AMPK and Myocyte Enhancer Factor

In response to stressors including exercise and prolonged starvation AMPK acts as a central regulator of energy metabolism, targeting myriad genes as reviewed extensively elsewhere (Hardie, Ross, and Hawley, 2012; Herzig and Shaw, 2018). Of relevance here is that AMPK activation is associated with increased skeletal muscle FA oxidation via the mechanism described in **Section 1.3.2** in which it reduces the synthesis of malonyl-CoA via the inhibition of ACC2, resulting in greater transport of LCFAs into the mitochondria. AMPK also phosphorylates and inactivates SREBP-1 Sterol regulatory element-binding protein 1 (SREBP-1) which is encoded by the Sterol regulatory element-binding transcription factor 1 (SREBF1) gene and regulates the expression of ACC2 (Dif *et al.*, 2006) and most lipogenic enzymes (Dessalle *et al.*, 2012). Also, the activation of AMPK has been shown to reorganise LDs in the SS region of myotubes such that the number of LD-mitochondria interaction sites are increased, more LD-derived FAs are supplied to adjacent mitochondria, and FA oxidation is promoted (Herms *et al.*, 2015).

AMPK also regulates the uptake and oxidation of glucose. Glucose uptake in the skeletal muscle is dependent upon the translocation of GLUT4 as previously discussed (see **Section 1.3**). The promoter region of the GLUT4 gene has a 103 base pair long region containing a functional myocyte enhancer factor 2 (MEF2) binding site, which is obligatory for the expression of GLUT4 (Thai *et al.*, 1998). MEF2 transcription is inhibited by class II histone deacetylases (HDACs) which are in turn phosphorylated and inactivated by AMPK and CaMKs such that during insulin- and contraction-mediated glucose uptake HDAC activity is antagonised, the transcription of MEF proteins is upregulated, and GLUT4 expression is enhanced (Richter and Hargreaves, 2013). Thus, AMPK activation induces greater glucose uptake and metabolism

via its stimulation of enhanced GLUT4 expression and translocation to the sarcolemma as described in **Section 1.3.2** (Garcia and Shaw, 2017).

1.5 Lipid-Induced Insulin Resistance

1.5.1 What is Insulin Resistance?

The term “insulin resistance” describes a state in which insulin-sensitive tissues fail to respond appropriately to normal or elevated concentrations of insulin (Cefalu, 2001), presenting instead with impaired whole-body, insulin-mediated, glucose uptake and utilisation. The manifestation of insulin resistance can be driven by decreased peripheral insulin sensitivity, as defined by increases in the insulin concentration required to elicit half maximal tissue glucose uptake (Stuart *et al.*, 1988), decreased maximal responsiveness to insulin stimulation, as defined by robustly blunted tissue maximum glucose uptake (irrespective of any compensatory increases in plasma insulin concentration beyond physiologically normal levels), or a combination of both.

As mentioned in **Section 1.3** Skeletal muscle is the primary site for the disposal of infused glucose under hyperinsulinaemic-euglycaemic clamp conditions (Wasserman, 2009; DeFronzo and Tripathy, 2009) and postprandial glucose uptake under normal physiological conditions (Capaldo *et al.*, 1999). It is unsurprising then that impairments in skeletal muscle glucose disposal are primarily responsible for reductions in whole-body glucose disposal. This was demonstrated by the work of Mikines and his colleagues (Mikines *et al.*, 1991) who published the first study to measure whole-body glucose uptake and leg glucose uptake concurrently in humans using the hyperinsulinaemic-euglycaemic clamp technique (DeFronzo, Tobin and Andres, 1979). Six healthy young men, who did not engage in regular bouts of endurance or resistance exercise prior to the intervention, underwent 7 days of strict bed rest. Clamps with three sequential, two-hour long, steps (Mikines *et al.*, 1988) were performed at baseline and on the final day of the bed rest period, such that exogenous insulin was infused at a constant rate of 0.2, 0.7, and 5 mU.m⁻¹.kg⁻¹ to reach steady state plasma insulin concentrations of 17 ± 0.7, 36.4 ± 0.6, and 352 ± 9 µU/mL, respectively.

Using this technique, they observed that there were no statistically significant differences in whole-body glucose uptake after 7 days of bed rest at basal insulin concentrations or at steady states of 17 ± 0.7 and 352 ± 9 $\mu\text{U}/\text{mL}$. However, whole-body glucose uptake was significantly impaired at steady state insulin concentrations of 36.4 ± 0.6 $\mu\text{U}/\text{mL}$. These data indicated a decrease in whole-body insulin sensitivity without an associated decrease in maximal glucose uptake rate in response to insulin stimulation. In the leg, glucose uptake rate was significantly ($p < 0.05$) lower after 7 days of bed rest compared to pre bed rest at all steady state insulin concentrations, even at 352 ± 9 $\mu\text{U}/\text{mL}$ a concentration that is much greater than physiologically normal insulin concentration in the postabsorptive state. These data implicated both decreased insulin sensitivity and decreased maximal responsiveness to stimulation by insulin in the impairment of glucose uptake in inactive skeletal muscle after 7 days of bed rest. As the leg is predominantly muscle, these data also indicated that inactivity-induced insulin resistance at the level of the skeletal muscle accounts for a significant proportion of decreased glucose uptake rate at the whole-body level.

1.5.2 Evidence of an Association Between IMCL and Impaired Glucose Uptake

Extensive research into the role of stored myocellular lipids in promoting whole-body insulin resistance was filled in the late 1990s by the identification of an inverse association between IMCL content and whole-body insulin sensitivity by several research groups.

Phillips and colleagues studied 27 normal weight ($24.8 \text{ kg}/\text{m}^2$) women (47-55 years) (Phillips *et al.*, 1996). Biopsies were taken from the gastrocnemius muscle. A portion of this muscle was frozen, cut into 8 μm thick sections and stained with Oil Red O for histochemical quantification of IMCL content. The remaining muscle was used for the biochemical quantification of muscle TAG content. Insulin sensitivity was determined by GS activity in an assay measuring the quantity of GS required to incorporate ^{14}C -glucose into glycogen per minute. They found that in these healthy women, increased IMCL content determined both biochemically and histochemically was strongly associated with decreased insulin-stimulated glycogen synthesis, a response

that has been demonstrated to be driven by impaired glucose transport into the muscle (Dresner *et al.*, 1999).

Pan and colleagues also investigated this association in 38 young (28 ± 1 years), obese (32.7 ± 1.1 kg/m²) Pima Indians (Pan *et al.*, 1997), a much-studied ethnic group notable for having a high prevalence of T2DM, partially due to idiosyncratic genetic and metabolic adaptations (Schulz, and Chaudhari, 2015) in tandem with modifiable risk factors, like diet. Lipid content in vastus lateralis biopsies was quantified using the biochemical chloroform: methanol method for TAG extraction from homogenised muscle. Whole-body glucose disposal was determined using a two-step hyperinsulinaemic-euglycaemic clamp. They found that the greater the skeletal muscle TAG content a participant had the lower their whole-body glucose disposal rate was.

Then, Krssak and colleagues used localised proton magnetic resonance spectroscopy (¹H-MRS) of the soleus muscle to determine muscle IMCL content, a novel application of this method at the time, and the hyperinsulinaemic-euglycaemic clamp to determine whole-body glucose disposal and in a cohort of 23 young (29 ± 2 years) normal weight (24.1 ± 0.5 kg/m²) males and females (15 women) (Krssak *et al.*, 1999). Multiple regression analysis showed that both IMCL content and fasting plasma FFA concentration were inversely and independently correlated with whole-body glucose disposal. This association has since been observed in almost all studies investigating IMCL content and insulin sensitivity in groups of lean and obese individuals and in those with T2DM.

However, it is important to note that there is an exception to this association. Highly trained endurance athletes have high IMCL content, comparable to the IMCL content observed in those with T2DM, but they remain insulin sensitive, presenting with none of the metabolic dysfunctions observed in obese individuals or those with T2DM (Goodpaster *et al.*, 2001; Dubé *et al.*, 2008). Mounting evidence suggests that this disparity, which has commonly been referred to as the “Athlete’s Paradox”, is attributable to the enhanced muscle oxidative capacity and lipid turnover in athletes, sparing them from the lipotoxicity and lipid-induced insulin resistance observed in obese individuals

(Zacharewicz, Hesselink, and Schrauwen, 2018; Barret *et al.*, 2022). This hypothesis was interrogated in a study involving lipid infusion concurrent with hyperinsulinaemia (Phielix *et al.*, 2012). Glucose disposal was reduced by 63% in lean, untrained controls but by only 29% in endurance trained athletes. Oxidative capacity was greater in the athletes, with only insulin-stimulated glucose oxidation being impaired whilst in the lean, untrained group both glucose oxidation and glycogen synthesis were impaired. IMCL content was increased in the lean group in response to the clamp but not in the athletes. Also, as mentioned in **Section 1.1**, though trained individuals and those with T2DM have similar IMCL content, trained individuals have smaller, more numerous LDs in the IMF region of Type I fibres whilst those with T2DM have large LDs in the SS region of Type II fibres (Daemen *et al.*, 2018). IMF-localised LDs are primarily involved in energy production to meet the needs of contracting muscle, as evidenced by their enhanced expression of proteins involved in oxidative phosphorylation (Ferreira *et al.*, 2010) relative to SS LDs, which presumably supply FAs for phospholipid synthesis and membrane processes. The smaller surface area to volume ratio and myocellular localisation of LDs in athletes explains their ability to readily supply FAs from LDs to mitochondria.

Of course, it must be underlined that these findings of an association between IMCL content and impaired insulin sensitivity did not establish clear causation between these two factors.

1.5.3 The Lipid Overflow Theory

The “lipid overflow” theory seeks to define a causal relationship between elevated circulating and myocellular lipid content, with whole-body insulin resistance. White adipocytes are the main sites of fat storage in the human body, specialised for this function via their ability to rapidly expand and proliferate, but their capacity for this can be overwhelmed, particularly in obese individuals (Tan and Vidal-Puig, 2008). This results in the overflow of lipid from the adipose tissue to ectopic storage locations including the liver and skeletal muscle where they can accumulate and promote lipotoxicity. Lipotoxicity describes a state in which excess cytoplasmic FA and TAG availability beyond

the storage capacity of LDs results in the formation of highly reactive lipid and oxygen species that can cause significant cell damage via oxidative stress (Ly *et al.*, 2017) and can activate apoptotic machinery (Kusminski *et al.*, 2009).

The redirection of FAs to the liver can result in an increase in the size and number of LDs as intrahepatic triglyceride (IHTG) content increases. The accumulation of IHTG content caused by chronic overfeeding is central to the development of NAFLD (da Silva Rosa *et al.*, 2020). Whether IMCL content is elevated concurrently in this context, and to what extent any such alterations in IMCL content contribute to the pathogenesis of NAFLD, is presently unclear.

Studies have been conducted involving the intravenous infusion of lipid emulsions (with glycerol and saline infusion controls) into sedentary individuals and athletes, raising their plasma FFA levels into the millimolar range, significantly greater than the normal 200-300 μM FFA reference range. These infusions resulted in significant increases in IMCL content in both Type I and Type II muscle fibres (Bachmann *et al.*, 2001; Brehm *et al.*, 2010; Lee *et al.*, 2013) in healthy males (Hoeks *et al.*, 2012) and athletes (Phielix *et al.*, 2012). Similar findings have been reported within days of participants starting hypercaloric diets (Zderic *et al.*, 2004; Larson-Meyer *et al.*, 2008; Sakurai *et al.*, 2011). These increases in IMCL content were paralleled by significant decreases in insulin sensitivity as determined by decreased insulin-mediated glucose uptake, decreases that were much less severe in athletes compared to sedentary controls. DAGs and ceramides are the main lipotoxic intermediates that have been implicated in directly impairing muscle insulin sensitivity. Total myocellular DAG and ceramide content is significantly elevated in the vastus lateralis muscle of obese individuals and those with type 2 diabetes compared to lean controls (Adams *et al.*, 2004; Moro *et al.*, 2009; Bergman *et al.*, 2012). Acute and chronic endurance training decreases DAG and ceramide concentration and improves myocellular insulin sensitivity (Schenk and Horowitz, 2007; Dubé *et al.*, 2011).

Tying these evidentiary threads of the lipid overflow theory together, strong evidence supporting a causal link between elevated circulating and myocellular lipid content and impaired glucose disposal in humans was

reported in an excellent study by Szendroedi and colleagues. They performed hyperinsulinaemic-euglycaemic clamps concurrent with lipid infusion (20% v/v intralipid) in 36 young, lean, insulin-tolerant males and females, and with glycerol infusion (2.5% glycerol in 0.9% saline/90 ml/h) in 24 of these same participants on different days (Szendroedi *et al.*, 2014). They also collected blood and vastus lateralis biopsies before and during the time course of these clamps. During the lipid infusion hyperinsulinaemic-euglycaemic clamp they observed significant increases in plasma FFA and TAG concentration and a greater than two-fold increase in myocellular membrane-localised and cytosol-localised DAG concentration by 2.5 hours. In tandem with these results, glucose uptake during the lipid infusion clamp was 61% lower than during the glycerol-infusion clamp. Total and species-specific myocellular ceramide content did not change during either the lipid infusion or glycerol infusion clamps. Also, by the 4-hour timepoint of the lipid infusion clamp, activation of PKC- θ , as determined the translocation of this isoform from the cytosol to the sarcoplasm, had increased by almost 50% relative to baseline. No changes in PKC- θ activation were observed in the glycerol infusion clamp. At this same 4-hour time point in the lipid infusion clamp, the phosphorylation of Ser1101 residues on IRS-1 was increased two-fold relative to base line. IRS-1 phosphorylation was unaltered during the glycerol infusion clamp. Though phosphorylation of Akt and PI3K was increased during the glycerol infusion clamp, demonstrating robust induction of the insulin-mediated glucose uptake pathway, no such significant increase in the phosphorylation of these crucial components of the glucose uptake pathway was observed during the lipid infusion clamp.

Another component of this study was a baseline comparison of resting DAG and ceramide content, and PKC- θ activation between obese individuals, those with T2DM, and healthy controls (Szendroedi *et al.*, 2014). Membrane-localised DAG concentration was elevated in the T2DM group relative to the control and obese group. Cytosolic DAG concentration in both the obese and T2DM groups was greater than in the control group. PKC- θ activation was elevated in both the obese and T2DM groups relative to the control group, was negatively correlated with insulin sensitivity, and was positively correlated with

plasma FFA concentration and membrane-localised DAG concentration, with the C18:2 and C20:4 species having the strongest correlation with this PKC- θ activation. Glucose disposal determined via the hyperinsulinaemic-euglycaemic clamp was 78% and 88% lower in the obese and T2DM groups respectively compared to healthy controls. There were no differences between the lean control, obese, and T2DM groups in total ceramide content, with no relationship between ceramide content and insulin sensitivity identified. Though IMCL content was not measured directly in this study, it has long been recognised that obese individuals (Malenfant *et al.*, 2001; Sinha *et al.*, 2002) and those with T2DM (Goodpaster *et al.*, 2000; Goodpaster *et al.*, 2001) have greater IMCL content than healthy lean controls.

Also, though Szendroedi and colleagues reported no difference in total ceramide content between obese individuals, those with T2DM, and healthy controls, the method they used to measure myocellular ceramide content could not distinguish between cytoplasmic-localised and sarcolemmal-localised ceramide. However, it was later reported in a study by Perreault and colleagues that sarcolemmal-localised ceramide content, particularly of the C18:0 ceramide species, has a strong negative correlation with insulin sensitivity and is greater in obese individuals and those with T2DM (Perreault *et al.*, 2018). Also, this study supported the aforementioned findings of increased PKC activity, accumulation of DAG, and impaired glucose uptake in the obese and T2DM groups.

1.5.4 Mechanisms of Lipid-Induced Insulin Resistance

There had been extensive research since the turn of the century into the mechanisms via which DAGs and ceramides contribute to the development of lipid-induced insulin-resistance using cell and animal models but the studies by Szendroedi and Perreault facilitated a great leap forward in our understanding of how these mechanisms may operate in humans. Still, this remains a contentious research area. Though the preponderance of evidence supports a role for DAGs and ceramides in the perturbation of intracellular signalling pathways initiated by insulin, it is important to acknowledge there are some cell-based, rodent, and human studies that do not report impaired insulin

sensitivity and glucose uptake in response to elevated circulating or myocellular DAG or ceramide content. A well-curated, extensive summary of these studies is presented in chapter 6 of a review by Bandet and colleagues (Bandet *et al.*, 2019). Nevertheless, the mechanisms via which DAGs and ceramides interfere with insulin-mediated glucose uptake as they are currently understood are detailed below.

1.5.4.1 PKC and DAGs

Protein Kinase C is a family of serine/threonine kinases, of which there are several conventional (- α , - β , and - γ), novel (- δ , - ϵ , - η , and - θ) and atypical (- ζ and - λ) isoforms, all with the same conserved catalytic domain but differentiated by alternate N-terminal regulatory regions (Newton, 2018). The regulatory regions of all PKCs have an autoinhibitory segment containing a pseudosubstrate that occupies the substrate binding site when PKC is in its inactive state, this pseudosubstrate prevents access to the C1 domains that sense and bind to DAGs (Newton, 2018). The binding of secondary messengers or cognate proteins generates an activation signal that promotes the movement of the pseudosubstrate away from the substrate binding domain, alleviating pseudosubstrate-mediated autoinhibition of PKC, and allowing DAG to bind to the C1 domain (Steinberg, 2018).

Novel PKCs like PKC- θ are activated in response to increases in cytoplasmic DAG content alone whilst conventional PKCs like PKC- δ require a concomitant increase in cytoplasmic Ca^{2+} concentration for full activation (Giorgione *et al.*, 2006). This is attributable to the C1 domains of novel PKCs having the greatest binding affinity for DAG whilst conventional PKCs have low affinity for DAG in the absence of Ca^{2+} (Giorgione *et al.*, 2006). Atypical PKCs do not bind to and have no affinity for DAG.

Binding of DAG to the C1 domains induces the activation and translocation of PKC to the cell membrane (Itani *et al.*, 2000). Membrane associated PKC isoforms phosphorylate various proteins. Most salient here is the abundance of evidence demonstrating that activated, membrane-bound PKC targets and phosphorylates specific serine/threonine residues on insulin receptors (Bollag *et al.*, 1986; Lewis *et al.*, 1990), decreasing their kinase

activity (Chin *et al.*, 1993; Bossenmaier *et al.*, 1997). This leads to decreased phosphorylation of downstream components of the insulin-mediated glucose uptake pathway including IRS, PI3K, PDK1, and Akt (Chin, Liu, and Roth, 1994; Schmitz-Peiffer and Biden, 2008), thereby impairing glucose uptake. DAG-activated PKC isoforms can also phosphorylate serine residues on IRS-1, decreasing its activity (Schmitz-Peiffer and Biden, 2008). PKC- α , - β , - δ , - θ and - ϵ are all expressed in skeletal muscle though PKC- θ is predominant, having the greatest affinity for DAG (Bassel-Duby and Olson, 2006). PKC- θ knockout mice exhibit decreased lipid accumulation and do not present with lipid-induced insulin resistance (Kim *et al.*, 2004), even in response to high-fat feeding (Peck *et al.*, 2018).

1.5.4.2 Ceramides

Ceramides are molecules composed of a sphingosine backbone amide-linked to a FA chain (Uchida and Park, 2021). They are involved in an array of cellular processes, highlighted by their presence in or adjacent to the nuclear envelope, mitochondria, Golgi apparatus, and endoplasmic reticulum (Bionda *et al.*, 2004). They can also be localised to lipid rafts, plasma membrane constructs that contain lipids, proteins, cholesterol, and sphingolipids (Bieberich, 2018). There are three pathways for the synthesis of ceramides but the main pathway in skeletal muscle is the de novo synthesis of ceramides in the endoplasmic reticulum from palmitate taken up from the circulation (Tan-Chen *et al.*, 2020). Thus, lipid availability and the duration for which circulating FFA concentration is elevated play a major role in determining the rate at which ceramides are synthesised in the muscle (Bandet *et al.*, 2019; Tan-Chen *et al.*, 2020).

Ceramides have three main mechanisms via which they contribute to the impairment of insulin-mediated glucose uptake and the development of insulin resistance, depending on whether myocellular elevation of ceramide concentration is acute or chronic (Chavez and Summers, 2012).

Firstly, ceramides are potent activators of protein phosphatase 2A (PP2A) (Dobrowsky *et al.*, 1993) which, via the targeting of its B55 α regulatory subunit to Akt, dephosphorylates Akt at Thr308 and Ser473, thereby

inactivating it and attenuating cellular glucose uptake (Kuo *et al.*, 2008). When C2C12 myotubes are cultured in palmitate there is an increase in myocellular PP2A activity, which is accompanied by a decrease in Akt phosphorylation and activation in response to stimulation by insulin (Cazzolli *et al.*, 2001). Under these same conditions, if PP2A activity is inhibited by okadaic acid then Akt phosphorylation and activation is restored (Stratford *et al.*, 2004).

In another mechanism, elevated myocellular ceramide content stabilises the complex between PKC- ζ and Akt. PKC- ζ is a recognised inhibitor of Akt activity (Doornbos *et al.*, 1999), but under normal conditions the PKC- ζ /Akt complexes that form at rest readily dissociate when insulin binds to myocellular insulin receptors and in response to anabolic stimuli (Konishi, Kuroda, and Kikkawa, 1994; Doornbos *et al.*, 1999). However, when myocellular ceramide content is increased, PKC- ζ activity is robustly upregulated leading to enhanced stabilisation of the PKC- ζ /Akt interaction that reduces insulin-mediated phosphorylation of Akt (Bourbon, Sandirasegarane, and Kester, 2002) and impairs insulin-mediated glucose uptake (Hajduch *et al.*, 2001; Powell *et al.*, 2004).

Both the PP2A and PKC- ζ mechanisms are observed in the context of acute elevations in sarcoplasmic ceramide concentration but appear to be independent, with ceramides preferentially acting through PKC- ζ in caveolae-rich cells like myotubes and PP2A in cells with fewer caveolae (Mahfouz *et al.*, 2014).

Recently, evidence for a chronic mechanism of action for ceramides in response to nutrient oversupply in this context has been reported. Hage Hassan and colleagues observed that long-term, 4 days, incubation of C2C12 cells and human myocytes isolated from patients with T2DM with ceramide or palmitate, lead to increased phosphorylation of IRS-1, resulting in inhibition of this protein and attenuation of the insulin-mediated glucose uptake pathway (Hage Hassan *et al.*, 2016). In human skeletal muscle, the C18:0 ceramide species has the greatest association with insulin resistance (Perreault *et al.*, 2018; Tan-Chen *et al.*, 2020) and it has been shown in mice that global and

muscle-specific depletion of this species results in improved whole-body glucose uptake (Turpin-Nolan, 2019), implicating a causal relationship.

1.6 Inactivity-Induced Insulin Resistance

Physical inactivity contributes to the development of skeletal muscle and whole-body insulin resistance and is a major risk factor for T2DM (Hamburg *et al.*, 2007), the effects of physical inactivity in this regard are often investigated using step count reduction or bed rest. A single day of strict bed rest does not alter whole-body insulin sensitivity, determined by the oral glucose tolerance test, whole-body fuel oxidation, or muscle mRNA expression (Dirks *et al.*, 2018). However, decrements in glucose disposal at the level of the skeletal muscles are observed after just 24 hours of immobilisation (Burns *et al.*, 2021). On the other hand, exercise is known to improve insulin sensitivity and promote greater substrate oxidation as discussed in **Section 1.4.3**. A longitudinal multi-ethnic study of 5,829 male and female participants aged 45-84 without diabetes on baseline assessment found that, over a 10-year period, participants that regularly engaged in vigorous physical activity, as determined by physical activity questionnaires supplied monthly, were less likely to develop T2DM regardless of age or sex (Sjöros *et al.*, 2020). Even brisk walking, greater than 4 miles per hour, was associated with lower risk of T2DM. Indeed, physical activity levels establish a hierarchy of insulin sensitivity in which, regardless of age, endurance trained individuals have greater insulin sensitivity than lean, healthy individuals who in turn have greater insulin sensitivity than obese individuals, where activity level is determined by measurement of VO_{2Peak} (Amati *et al.*, 2009). The exact pathophysiological links between physical inactivity and insulin resistance remain elusive, though there is evidence highlighting some potential mechanisms.

Alibegovic and colleagues conducted a 10-day bed rest study with 20 young, 24-27 years, healthy men (Alibegovic *et al.*, 2010). Hyperinsulinaemic-euglycaemic clamps were performed before and 9 days into the bed rest intervention, and after a 4-week long retraining programme, with muscle biopsies taken at these same time points. Glucose disposal was impaired following bed rest and a reduction in the expression of hexokinase II was

observed. Microarray analysis of biopsies at these time points revealed significant basal and insulin-stimulated downregulation of the transcription of TCA genes regulating oxidative phosphorylation and genes involved in FA metabolism, with the PPARGC1A gene being the most downregulated gene overall. PPARGC1A is the gene which encodes PGC-1 α , the coactivator of PPAR- γ , a transcription factor which plays a critical role in fuel selection by promoting the transcription of genes that produce proteins which increase the rate of FA oxidation, as previously discussed in **Section 1.4.5.1**. PPARGC1A expression was decreased due to increased, inactivity-induced methylation of this gene. This supports another study reporting downregulated PPARGC1A expression in those with T2DM (Mootha *et al.*, 2003). Also, in this same study, TGF- β_2 was the most upregulated signalling pathway (Alibegovic *et al.*, 2010). Recent evidence is uncovering major roles for TGF- β in the regulation of both glucose and FA oxidation, with TGF- β suppressing FA oxidation and promoting FA storage in a context-dependent manner (Liu and Chen, 2022). These changes in mRNA expression induced by 9 days of bed rest were almost completely reversed by 4 weeks of retraining, though 15% of these changes remained unreversed following this period. These data support the hypothesis proposed by some authors that inactivity-induced insulin resistance and lipid-induced insulin resistance are linked, with inactivity reducing mitochondrial oxidative capacity and impaired FA oxidation resulting in increased IMCL content, the accumulation of lipotoxic lipid species in muscle, and whole-body insulin resistance (Befroy *et al.*, 2007; Mogensen *et al.*, 2007; Larsen *et al.*, 2009).

To investigate the role of sedentary behaviour in inactivity-induced insulin resistance, in conjunction with measurements of lipotoxic intermediates content, Reidy and colleagues studied 7 healthy males and 5 healthy females aged 60-85 years (Reidy *et al.*, 2018). They reduced the step count of these participants by 70% for 14 days, with hyperinsulinaemic-euglycaemic clamps performed before and after this reduced step count period and 14 days after they had resumed their habitual activity. Muscle biopsies were also taken at these time points. Glucose disposal fell by an average of 15% following the reduced step count period. However, it was not only restored but increased by

15% above baseline glucose disposal after participants had resumed their normal activity levels. There were no changes in the abundance of ceramide species and DAG localised to the sarcoplasm or nuclear membrane and no correlations were observed between the content of these lipotoxic intermediates and changes in glucose disposal following the 14-day reduced step count period. This observation matches similar data from a 7-day bed rest intervention in 10 healthy young men in which total ceramide content was unchanged (Dirks *et al.*, 2016).

It has been difficult to determine the effect of inactivity per se on IMCL content and the role of any changes in IMCL on the development of whole-body insulin resistance given that energy balance, which is a confounding variable that can independently increase IMCL content with overfeeding, is often uncontrolled in inactivity studies.

1.7 Thesis Structure and Aims

LDs are thought to play a role in the metabolic changes observed in the context of inactivity, disease, and exercise. This thesis aims to further elucidate the role of IMCL in these settings by addressing the following questions.

Chapter 3, Determination of whether inactivity per se causes IMCL accumulation, which contributes to insulin resistance, has been confounded by failure to account for energy balance in previous studies. Also, the effect of chronic inactivity (>7 days) on IMCL content is poorly explored. Therefore, there were two central questions. Firstly, does IMCL content change in healthy young males during periods of short- (3 days) and long-term (56 days) bed rest in which energy balance is maintained? Secondly, if so, do these changes contribute to the development of whole-body insulin resistance? In addition, it is well known that resistance exercise can improve muscle and whole-body glucose disposal robustly, in general and following bed rest. However, it is currently unknown whether exercise-induced improvements in whole-body glucose disposal following bed rest are associated with changes in IMCL content. Therefore, the tertiary question was: are improvements in whole-body glucose disposal following unilateral knee extensions post bed rest associated with changes in IMCL content?

Chapter 4, A major contributor to IHTG accumulation in NAFLD is elevated plasma FFA concentration resulting from chronic overfeeding and lipid overspill when adipose tissue FA oxidation and storage capacity is exceeded. Given that skeletal muscle insulin resistance and whole-body insulin resistance are hallmark features of NAFLD alongside IHTG accumulation, it has been suggested that lipid overspill in NAFLD may also lead to the accumulation of IMCL. This IMCL accumulation may then contribute to the development of insulin resistance in this condition. However, to date IMCL content in healthy young control volunteers has not been compared to IMCL content in those with NAFLD. There was one central question. Is IMCL content different in participants with NAFLD versus healthy controls and, if so, are these IMCL differences associated with differences in skeletal muscle and whole-body insulin resistance?

Chapter 5, The overwhelming majority of exercise intervention studies in which IMCL is determined and related to measures of muscle and whole-body insulin resistance and fuel oxidation concern endurance exercise. The effect of resistance exercise modalities on IMCL is sparsely trodden ground in this field of research. Many athletes and non-athletes take performance enabling NSAIDs including diclofenac before and after exercise to reduce inflammation, improve exercise tolerance and hasten recovery. However, evidentiary support for the use of NSAIDs in this context is lacking. Also, NSAIDs have secondary effects that are completely unexplored in humans. Therefore, there were two central questions. Firstly, does chronic resistance exercise change IMCL content and the expression of PLIN5, a key regulator of LD lipolysis? Secondly, does diclofenac, an NSAID which is a known agonist of PPAR- γ in vitro, alter muscle FA metabolism in humans in vivo?

1.8 References

- Abbot, E.L., McCormack, J.G., Reynet, C., Hassall, D.G., Buchan, K.W., and Yeaman, S.J. (2005) Diverging regulation of pyruvate dehydrogenase kinase isoform gene expression in cultured human muscle cells. *The FEBS Journal*. 272 (12), pp. 3004-3014.
- Abu-Elheiga, L., Brinkley, W.R., Zhong, L., Chirala, S.S., Woldegiorgis, G., and Wakil, S.J. (2000) The subcellular localization of acetyl-CoA carboxylase 2. *Proceedings of the National Academy of Sciences of the United States of America*. 97 (4), pp. 1444-1449.
- Abdul-Ghani, M.A., and DeFronzo, R.A. (2010) Pathogenesis of insulin resistance in skeletal muscle. *Journal of Biomedicine & Biotechnology*. 2010, 476279.
- Achten, J., and Jeukendrup, A.E. (2004) Optimizing fat oxidation through exercise and diet. *Nutrition (Burbank, Los Angeles County, Calif.)*. 20 (7-8), pp. 716-727.
- Adams, J.M., Pratipanawat, T., Berria, R., Wang, E., DeFronzo, R.A., Cameron Sullards, M. and Mandarino, L.J. (2004) Ceramide Content Is Increased in Skeletal Muscle from Obese Insulin-Resistant Humans. *Diabetes*. 53 (1), pp. 25-31.
- Adeva-Andany, M.M., Carneiro-Freire, N., Seco-Filgueira, M., Fernández-Fernández, C., and Mouriño-Bayolo, D. (2019) Mitochondrial β -oxidation of saturated fatty acids in humans. *Mitochondrion*. 46, pp. 73-90.
- Albers, P.H., Pedersen, A.J., Birk, J.B., Kristensen, D.E., Vind, B.F., Baba, O., Nøhr, J., Højlund, K., and Wojtaszewski, J.F. (2015) Human muscle fiber type-specific insulin signaling: impact of obesity and type 2 diabetes. *Diabetes*. 64 (2), pp. 485-497.
- Al-Khayat, H.A. (2013) Three-dimensional structure of the human myosin thick filament: clinical implications. *Global Cardiology Science & Practice*. 2013 (3), pp. 280-302.

Alibegovic, A.C., Sonne, M.P., Højbjerg, L., Bork-Jensen, J., Jacobsen, S., Nilsson, E., Faerch, K., Hiscock, N., Mortensen, B., Friedrichsen, M., Stallknecht, B., Dela, F., and Vaag, A. (2010) Insulin resistance induced by physical inactivity is associated with multiple transcriptional changes in skeletal muscle in young men. *American journal of physiology. Endocrinology and Metabolism*. 299 (5), pp. E752-E763.

Amati, F., Dubé, J.J., Coen, P.M., Stefanovic-Racic, M., Toledo, F.G., and Goodpaster, B.H. (2009) Physical inactivity and obesity underlie the insulin resistance of aging. *Diabetes Care*. 32 (8), pp. 1547-1549.

Ameer, F., Scanduzzi, L., Hasnain, S., Kalbacher, H., and Zaidi, N. (2014) De novo lipogenesis in health and disease. *Metabolism: Clinical and Experimental*. 63 (7), pp. 895-902.

Andres, R., Cader, G., and Zierler, K.L. (1956) The quantitatively minor role of carbohydrate in oxidative metabolism by skeletal muscle in intact man in the basal state; measurements of oxygen and glucose uptake and carbon dioxide and lactate production in the forearm. *The Journal of Clinical Investigation*. 35 (6), pp. 671-682.

Arlt, H., Sui, X., Folger, B., Adams, C., Chen, X., Remme, R., Hamprecht, F.A., DiMaio, F., Liao, M., Goodman, J.M., Farese, R.V., Jr, and Walther, T.C. (2022) Seipin forms a flexible cage at lipid droplet formation sites. *Nature Structural & Molecular Biology*. 29 (3), pp. 194-202.

Bachmann, O.P., Dahl, D.B., Brechtel, K., Machann, J., Haap, M., Maier, T., Loviscach, M., Stumvoll, M., Claussen, C.D., Schick, F., Häring, H.U., and Jacob, S. (2001) Effects of Intravenous and Dietary Lipid Challenge on Intramyocellular Lipid Content and the Relation with Insulin Sensitivity in Humans. *Diabetes*. 50 (11), pp. 2579-2584.

Badin, P.-M., Louche, K., Mairal, A., Liebisch, G., Schmitz, G., Rustan, A.C., Smith, S.R., Langin, D., and Moro, C. (2011) Altered skeletal muscle lipase expression and activity contribute to insulin resistance in humans. *Diabetes*. 60 (6), pp. 1734-1742.

- Baillyes, E.M., Navé, B.T., Soos, M.A., Orr, S.R., Hayward, A.C., and Siddle, K. (1997) Insulin receptor/IGF-I receptor hybrids are widely distributed in mammalian tissues: quantification of individual receptor species by selective immunoprecipitation and immunoblotting. *The Biochemical Journal*. 327 (1), pp. 209-215.
- Bajaj, M., Suraamornkul, S., Romanelli, A., Cline, G.W., Mandarino, L.J., Shulman, G.I., and DeFronzo, R.A. (2005) Effect of a sustained reduction in plasma free fatty acid concentration on intramuscular long-chain fatty Acyl-CoAs and insulin action in type 2 diabetic patients. *Diabetes*. 54 (11), pp. 3148-3153.
- Bandet, C.L., Tan-Chen, S., Bourron, O., Le Stunff, H., and Hajduch, E. (2019) Sphingolipid Metabolism: New Insight into Ceramide-Induced Lipotoxicity in Muscle Cells. *International Journal of Molecular Sciences*. 20 (3), 479.
- Barrett, J.S., Whytock, K.L., Strauss, J.A., Wagenmakers, A., and Shepherd, S.O. (2022) High intramuscular triglyceride turnover rates and the link to insulin sensitivity: influence of obesity, type 2 diabetes and physical activity. *Applied Physiology, Nutrition, and Metabolism*. 47 (4), pp. 343-356.
- Bassel-Duby, R., and Olson, E.N. (2006) Signaling pathways in skeletal muscle remodeling. *Annual Review of Biochemistry*. 75, pp. 19-37.
- Bastie, C.C., Nahlé, Z., McLoughlin, T., Esser, K., Zhang, W., Unterman, T., and Abumrad, N.A. (2005) FoxO1 stimulates fatty acid uptake and oxidation in muscle cells through CD36-dependent and -independent mechanisms. *The Journal of Biological Chemistry*. 280 (14), pp. 14222-14229.
- Battaglia, G.M., Zheng, D., Hickner, R.C., and Houmard, J.A. (2012) Effect of exercise training on metabolic flexibility in response to a high-fat diet in obese individuals. *American Journal of Physiology. Endocrinology and Metabolism*. 303 (12), pp. E1440-E1445.
- Befroy, D.E., Petersen, K.F., Dufour, S., Mason, G.F., de Graaf, R.A., Rothman, D.L., and Shulman, G.I. (2007) Impaired mitochondrial substrate oxidation in muscle of insulin-resistant offspring of type 2 diabetic patients. *Diabetes*. 56 (5), pp. 1376-1381.

Beld, J., Lee, D.J., Burkart, M.D. (2015) Fatty acid biosynthesis revisited: structure elucidation and metabolic engineering. *Molecular bioSystems*. 11 (1), pp. 38-59.

Bergman, B.C., Hunerdosse, D.M., Kerege, A., Playdon, M.C., and Perreault, L. (2012) Localisation and composition of skeletal muscle diacylglycerol predicts insulin resistance in humans. *Diabetologia*. 55 (4), pp. 1140-1150.

Bersuker, K., Peterson, C., To, M., Sahl, S.J., Savikhin, V., Grossman, E.A., Nomura, D.K., and Olzmann, J.A. (2018). A Proximity Labeling Strategy Provides Insights into the Composition and Dynamics of Lipid Droplet Proteomes. *Developmental Cell*. 44 (1), pp. 97-112.e7.

Bhagavan, N.V., and Ha, C.E. (2015) Chapter 16 - Lipids I: Fatty Acids and Eicosanoids. *Essentials of Medical Biochemistry*. 2nd ed. Cambridge, MA, USA: Academic Press.

Bieberich, E. (2018) Sphingolipids and lipid rafts: Novel concepts and methods of analysis. *Chemistry and Physics of Lipids*. 216, pp. 114-131.

Bionda, C., Portoukalian, J., Schmitt, D., Rodriguez-Lafrasse, C., and Ardail, D. (2004) Subcellular compartmentalization of ceramide metabolism: MAM (mitochondria-associated membrane) and/or mitochondria?. *The Biochemical Journal*. 382 (Pt 2), pp. 527-533.

Bircher, S., and Knechtle, B. (2004) Relationship between Fat Oxidation and Lactate Threshold in Athletes and Obese Women and Men. *Journal of Sports Science & Medicine*. 3 (3), pp. 174-181.

Boden, G., Chen, X., Ruiz, J., White, J.V., and Rossetti, L. (1994) Mechanisms of fatty acid-induced inhibition of glucose uptake. *The Journal of Clinical Investigation*. 93 (6), pp. 2438-2446.

Boiteux, A., and Hess, B. (1981) Design of glycolysis. *Philosophical Transactions of the Royal Society B*. 293 (1063), pp. 5-22.

Bollag, G.E., Roth, R.A., Beaudoin, J., Mochly-Rosen, D., and Koshland, D.E., Jr (1986) Protein kinase C directly phosphorylates the insulin receptor in vitro

and reduces its protein-tyrosine kinase activity. *Proceedings of the National Academy of Sciences of the United States of America*. 83 (16), pp. 5822-5824.

Bonito, C.A., Leandro, P., Ventura, F.V. and Guedes, R.C. (2016) Insights into Medium-chain Acyl-CoA Dehydrogenase Structure by Molecular Dynamics Simulations. *Chemical Biology and Drug Design*. 88 (2), pp. 281-292.

Bosma, M., Minnaard, R., Sparks, L. M., Schaart, G., Losen, M., de Baets, M.H., Duimel, H., Kersten, S., Bickel, P.E., Schrauwen, P., and Hesselink, M.K. (2012) The lipid droplet coat protein perilipin 5 also localizes to muscle mitochondria. *Histochemistry and Cell Biology*. 137 (2), pp. 205-216.

Bossenmaier, B., Mosthaf, L., Mischak, H., Ullrich, A., and Häring, H.U. (1997) Protein kinase C isoforms beta 1 and beta 2 inhibit the tyrosine kinase activity of the insulin receptor. *Diabetologia*. 40 (7), pp. 863-866.

Bourbon, N.A., Sandirasegarane, L., and Kester, M. (2002) Ceramide-induced inhibition of Akt is mediated through protein kinase Czeta: implications for growth arrest. *The Journal of Biological Chemistry*. 277 (5), pp. 3286-3292.

Bowtell, J.L., Marwood, S., Bruce, M., Constantin-Teodosiu, D., and Greenhaff, P.L. (2007) Tricarboxylic acid cycle intermediate pool size: functional importance for oxidative metabolism in exercising human skeletal muscle. *Sports Medicine (Auckland, N.Z.)*. 37 (12), pp. 1071-1088.

Braun, J.E.A., and Severson, D.L. (1992) Regulation of the synthesis, processing and translocation of lipoprotein lipase. *The Biochemical Journal*. 287 (2), pp. 337-347.

Brehm, A., Krššák, M., Schmid, A.I., Nowotny, P., Waldhäusl, W., and Roden, M. (2010). Acute elevation of plasma lipids does not affect ATP synthesis in human skeletal muscle. *American Journal of Physiology-Endocrinology and Metabolism*. 299 (1), pp. E33-E38.

Bricker, D.K., Taylor, E.B., Schell, J.C., Orsak, T., Boutron, A., Chen, Y.C., Cox, J.E., Cardon, C.M., Van Vranken, J.G., Dephoure, N., Redin, C., Boudina, S., Gygi, S.P., Brivet, M., Thummel, C.S., and Rutter, J. (2012) A mitochondrial pyruvate carrier required for pyruvate uptake in yeast, *Drosophila*, and humans. *Science*. 337 (6090), pp. 96-100.

Brooks, G.A., and Mercier, J. (1994) Balance of carbohydrate and lipid utilization during exercise: the "crossover" concept. *Journal of Applied Physiology (Bethesda, Md.: 1985)*. 76 (6), pp. 2253-2261.

Brooks, G.A., and Mercier, J. (1994) Balance of carbohydrate and lipid utilization during exercise: the "crossover" concept. *Journal of Applied Physiology (Bethesda, Md.: 1985)*. 76 (6), pp. 2253-2261.

Broskey, N.T., Daraspe, J., Humbel, B.M., and Amati, F. (2013) Skeletal muscle mitochondrial and lipid droplet content assessed with standardized grid sizes for stereology. *Journal of Applied Physiology (Bethesda, Md.: 1985)*. 115 (5), pp. 765-770.

Brown, K.M., Sharma, S., Baker, E., Hawkins, W., van der Merwe, M., and Puppa, M.J. (2019) Delta-6-desaturase (FADS2) inhibition and omega-3 fatty acids in skeletal muscle protein turnover. *Biochemistry and Biophysics Reports*. 18, 100622.

Burke, A.C., and Huff, M.W. (2017) ATP-citrate lyase: genetics, molecular biology and therapeutic target for dyslipidemia. *Current Opinion in Lipidology*. 28 (2), pp. 193-200.

Burns, A.M., Nixon, A., Mallinson, J., Cordon, S.M., Stephens, F.B., and Greenhaff, P.L. (2021) Immobilisation induces sizeable and sustained reductions in forearm glucose uptake in just 24 h but does not change lipid uptake in healthy men. *The Journal of Physiology*. 599 (8), pp. 2197-2210.

Camps, L., Reina, M., Llobera, M., Vilaró, S., and Olivecrona, T. (1990) Lipoprotein lipase: cellular origin and functional distribution. *The American Journal of Physiology*. 258 (4 Pt 1), pp. C673-C681.

Capaldo, B., Gastaldelli, A., Antonello, S., Auletta, M., Pardo, F., Ciociaro, D., Guida, R., Ferrannini, E., and Saccà, L. (1999) Splanchnic and leg substrate exchange after ingestion of a natural mixed meal in humans. *Diabetes*. 48 (5), pp. 958-966.

Carrasco, S., and Mérida, I. (2007) Diacylglycerol, when simplicity becomes complex. *Trends in Biochemical Sciences*. 32 (1), pp. 27-36.

Carstens, M.T., Goedecke, J.H., Dugas, L., Evans, J., Kroff, J., Levitt, N.S., and Lambert, E.V. (2013) Fasting substrate oxidation in relation to habitual dietary fat intake and insulin resistance in non-diabetic women: a case for metabolic flexibility?. *Nutrition & Metabolism*. 10 (1), 8.

Cartee, G.D. (2015) Roles of TBC1D1 and TBC1D4 in insulin- and exercise-stimulated glucose transport of skeletal muscle. *Diabetologia*. 58 (1), pp. 19-30.

Cazzolli, R., Carpenter, L., Biden, T.J., and Schmitz-Peiffer, C. (2001) A role for protein phosphatase 2A-like activity, but not atypical protein kinase Czeta, in the inhibition of protein kinase B/Akt and glycogen synthesis by palmitate. *Diabetes*. 50 (10), pp. 2210-2218.

Cefalu, W.T. (2001) Insulin Resistance: Cellular and Clinical Concepts. *Experimental Biology and Medicine*. 226 (1), pp. 13-26.

Chait, A., and den Hartigh, L.J. (2020) Adipose Tissue Distribution, Inflammation and Its Metabolic Consequences, Including Diabetes and Cardiovascular Disease. *Frontiers in Cardiovascular Medicine*. 7, 22.

Chavez, J.A., and Summers, S.A. (2012) A Ceramide-Centric View of Insulin Resistance. *Cell*. 15 (5), pp. 585-594.

Chen, J., Lu, Y., Tian, M., and Huang, Q. (2019) Molecular mechanisms of FOXO1 in adipocyte differentiation. *Journal of Molecular Endocrinology*. 62 (3), pp. R239-R253.

Chen, Z.P., Stephens, T.J., Murthy, S., Canny, B.J., Hargreaves, M., Witters, L.A., Kemp, B.E., and McConell, G.K. (2003) Effect of exercise intensity on skeletal muscle AMPK signaling in humans. *Diabetes*. 52 (9), 2205-2212.

Chien, H.C., Greenhaff, P.L., and Constantin-Teodosiu, D. (2020) PPAR δ and FOXO1 Mediate Palmitate-Induced Inhibition of Muscle Pyruvate Dehydrogenase Complex and CHO Oxidation, Events Reversed by Electrical Pulse Stimulation. *International Journal of Molecular Sciences*. 21 (16), 5942.

Chin, J.E., Dickens, M., Tavare, J.M., and Roth, R.A. (1993) Overexpression of protein kinase C isoenzymes alpha, beta I, gamma, and epsilon in cells

overexpressing the insulin receptor. Effects on receptor phosphorylation and signaling. *The Journal of Biological Chemistry*. 268 (9), pp. 6338-6347.

Chin, J.E., Liu, F., and Roth, R.A. (1994) Activation of protein kinase C alpha inhibits insulin-stimulated tyrosine phosphorylation of insulin receptor substrate-1. *Molecular Endocrinology (Baltimore, Md.)*. 8 (1), pp. 51-58.

Cho, Y.S., Lee, J.I., Shin, D., Kim, H.T., Jung, H.Y., Lee, T.G., Kang, L.W., Ahn, Y.J., Cho, H.S., and Heo, Y.S. (2010) Molecular mechanism for the regulation of human ACC2 through phosphorylation by AMPK. *Biochemical and Biophysical Research Communications*. 391 (1), pp. 187-192.

Choi, S.M., Tucker, D.F., Gross, D.N., Easton, R.M., DiPilato, L.M., Dean, A.S., Monks, B.R., and Birnbaum, M.J. (2010) Insulin regulates adipocyte lipolysis via an Akt-independent signaling pathway. *Molecular and Cellular Biology*. 30 (21), pp. 5009-5020.

Chow, C.C., and Hall, K.D. (2014) Short and long-term energy intake patterns and their implications for human body weight regulation. *Physiology & Behaviour*. 134, pp. 60-65.

Chow, L.S., Mashek, D.G., Wang, Q., Shepherd, S.O., Goodpaster, B.H., and Dubé, J.J. (2017) Effect of acute physiological free fatty acid elevation in the context of hyperinsulinemia on fiber type-specific IMCL accumulation. *Journal of Applied Physiology (Bethesda, Md.: 1985)*. 123 (1), pp. 71-78.

Coburn, C.T., Knapp, F.F., Jr, Febbraio, M., Beets, A.L., Silverstein, R.L., and Abumrad, N.A. (2000) Defective uptake and utilization of long chain fatty acids in muscle and adipose tissues of CD36 knockout mice. *The Journal of Biological Chemistry*. 275 (42), pp. 32523-32529.

Coen, P.M., Dubé, J.J., Amati, F., Stefanovic-Racic, M., Ferrell, R.E., Toledo, F.G., and Goodpaster, B.H. (2010) Insulin resistance is associated with higher intramyocellular triglycerides in type I but not type II myocytes concomitant with higher ceramide content. *Diabetes*. 59 (1), pp. 80-88.

Console, L., Giangregorio, N., Indiveri, C., and Tonazzi, A. (2014) Carnitine/acylcarnitine translocase and carnitine palmitoyltransferase 2 form a

complex in the inner mitochondrial membrane. *Molecular and Cellular Biochemistry*. 394 (1-2), pp. 307-314.

Constantin, D., Constantin-Teodosiu, D., Layfield, R., Tsintzas, K., Bennett, A.J., and Greenhaff, P.L. (2007) PPARdelta agonism induces a change in fuel metabolism and activation of an atrophy programme, but does not impair mitochondrial function in rat skeletal muscle. *The Journal of Physiology*. 583 (Pt 1), pp. 381-390.

Constantin-Teodosiu, D., Peirce, N.S., Fox, J., and Greenhaff, P.L. (2004) Muscle pyruvate availability can limit the flux, but not activation, of the pyruvate dehydrogenase complex during submaximal exercise in humans. *The Journal of Physiology*. 561 (Pt 2), pp. 647-655.

Constantin-Teodosiu, D., Constantin, D., Stephens, F., Laithwaite, D., and Greenhaff, P.L. (2012) The role of FOXO and PPAR transcription factors in diet-mediated inhibition of PDC activation and carbohydrate oxidation during exercise in humans and the role of pharmacological activation of PDC in overriding these changes. *Diabetes*. 61 (5), pp. 1017-1024.

Constantin-Teodosiu, D. (2013) Regulation of muscle pyruvate dehydrogenase complex in insulin resistance: effects of exercise and dichloroacetate. *Diabetes & Metabolism Journal*. 37 (5), pp. 301-314.

Contreras, C.J., Segvich, D.M., Mahalingan, K., Chikwana, V.M., Kirley, T.L., Hurley, T.D., DePaoli-Roach, A.A. and Roach, P.J. (2016) Incorporation of phosphate into glycogen by glycogen synthase. *Archives of Biochemistry and Biophysics*. 597, pp. 21-29.

Cook, G.A., Stephens, T.W., and Harris, R.A. (1984) Altered sensitivity of carnitine palmitoyltransferase to inhibition by malonyl-CoA in ketotic diabetic rats. *The Biochemical Journal*. 219 (1), pp. 337-339.

Coster, A.C., Govers, R., and James, D.E. (2004) Insulin stimulates the entry of GLUT4 into the endosomal recycling pathway by a quantal mechanism. *Traffic (Copenhagen, Denmark)*. 5 (10), pp. 763-771.

Cross, D.A., Alessi, D.R., Cohen, P., Andjelkovich, M. and Hemmings, B.A. (1995) Inhibition of glycogen synthase kinase-3 by insulin mediated by protein kinase B. *Nature*. 378 (6559), pp. 785-789.

Crossland, H., Constantin-Teodosiu, D., and Greenhaff, P.L. (2021) The Regulatory Roles of PPARs in Skeletal Muscle Fuel Metabolism and Inflammation: Impact of PPAR Agonism on Muscle in Chronic Disease, Contraction and Sepsis. *International Journal of Molecular Sciences*. 22 (18), 9775.

D'Aquila, T., Hung, Y.H., Carreiro, A., and Buhman, K.K. (2016) Recent discoveries on absorption of dietary fat: Presence, synthesis, and metabolism of cytoplasmic lipid droplets within enterocytes. *Biochimica et Biophysica Acta*. 1861 (8 Pt A), pp. 730-747.

da Silva Rosa, S.C., Nayak, N., Caymo, A.M., and Gordon, J.W. (2020) Mechanisms of muscle insulin resistance and the cross-talk with liver and adipose tissue. *Physiological Reports*. 8 (19), e14607.

Daemen, S., Gemmink, A., Brouwers, B., Meex, R., Huntjens, P.R., Schaart, G., Moonen-Kornips, E., Jörgensen, J., Hoeks, J., Schrauwen, P., and Hesselink, M. (2018). Distinct lipid droplet characteristics and distribution unmask the apparent contradiction of the athlete's paradox. *Molecular Metabolism*. 17, pp. 71-81.

Dagenais, G.R., Tancredi, R.G., and Zierler, K.L. (1976) Free fatty acid oxidation by forearm muscle at rest, and evidence for an intramuscular lipid pool in the human forearm. *The Journal of Clinical Investigation*. 58 (2), pp. 421-31.

Dagenais, G.R., Tancredi, R.G., and Zierler, K.L. (1976) Free fatty acid oxidation by forearm muscle at rest, and evidence for an intramuscular lipid pool in the human forearm. *The Journal of Clinical Investigation*. 58 (2), pp. 421-431.

Daugaard, J.R., Nielsen, J.N., Kristiansen, S., Andersen, J.L., Hargreaves, M., and Richter, E.A. (2000) Fiber type-specific expression of GLUT4 in human

skeletal muscle: influence of exercise training. *Diabetes*. 49 (7), pp. 1092-1095.

Debard, C., Laville, M., Berbe, V., Loizon, E., Guillet, C., Morio-Liondore, B., Boirie, Y., and Vidal, H. (2004) Expression of key genes of fatty acid oxidation, including adiponectin receptors, in skeletal muscle of Type 2 diabetic patients. *Diabetologia*. 47 (5), pp. 917-925.

DeFronzo, R.A., and Tripathy, D. (2009) Skeletal muscle insulin resistance is the primary defect in type 2 diabetes. *Diabetes Care*. 32 (Supplement 2), pp. S157-S163.

DeFronzo, R.A., Tobin, J.D., and Andres, R. (1979) Glucose clamp technique: a method for quantifying insulin secretion and resistance. *The American Journal of Physiology*. 237 (3), pp. E214-E223.

Degenhardt, T., Saramäki, A., Malinen, M., Rieck, M., Väisänen, S., Huotari, A., Herzig, K.H., Müller, R., and Carlberg, C. (2007) Three members of the human pyruvate dehydrogenase kinase gene family are direct targets of the peroxisome proliferator-activated receptor beta/delta. *Journal of Molecular Biology*. 372 (2), pp. 341-355.

Dessalle, K., Euthine, V., Chanon, S., Delarichaudy, J., Fujii, I., Rome, S., Vidal, H., Nemoz, G., Simon, C., and Lefai, E. (2012) SREBP-1 transcription factors regulate skeletal muscle cell size by controlling protein synthesis through myogenic regulatory factors. *PloS One*. 7 (11), e50878.

Dif, N., Euthine, V., Gonnet, E., Laville, M., Vidal, H., and Lefai, E. (2006) Insulin activates human sterol-regulatory-element-binding protein-1c (SREBP-1c) promoter through SRE motifs. *The Biochemical Journal*. 400 (1), pp. 179-188.

Dirks, M.L., Wall, B.T., van de Valk, B., Holloway, T.M., Holloway, G.P., Chabowski, A., Goossens, G.H., and van Loon, L.J. (2016) One Week of Bed Rest Leads to Substantial Muscle Atrophy and Induces Whole-Body Insulin Resistance in the Absence of Skeletal Muscle Lipid Accumulation. *Diabetes*. 65 (10), pp. 2862-2875.

- Dirks, M.L., Stephens, F.B., Jackman, S.R., Galera Gordo, J., Machin, D.J., Pulsford, R.M., van Loon, L., and Wall, B.T. (2018) A single day of bed rest, irrespective of energy balance, does not affect skeletal muscle gene expression or insulin sensitivity. *Experimental Physiology*. 103 (6), pp. 860–875.
- Dobrowsky, R.T., Kamibayashi, C., Mumby, M.C., and Hannun, Y.A. (1993) Ceramide activates heterotrimeric protein phosphatase 2A. *The Journal of Biological Chemistry*. 268 (21), pp. 15523-15530.
- Doornbos, R.P., Theelen, M., van der Hoeven, P.C., van Blitterswijk, W.J., Verkleij, A.J., and van Bergen en Henegouwen, P.M. (1999) Protein kinase Czeta is a negative regulator of protein kinase B activity. *The Journal of Biological Chemistry*. 274 (13), pp. 8589-8596.
- Dresner, A., Laurent, D., Marcucci, M., Griffin, M.E., Dufour, S., Cline, G.W., Slezak, L.A., Andersen, D.K., Hundal, R.S., Rothman, D.L., Petersen, K.F., and Shulman, G.I. (1999) Effects of free fatty acids on glucose transport and IRS-1-associated phosphatidylinositol 3-kinase activity. *The Journal of Clinical Investigation*. 103 (2), pp. 253-259.
- Dreyer, H.C., Fujita, S., Cadenas, J.G., Chinkes, D.L., Volpi, E., and Rasmussen, B.B. (2006) Resistance exercise increases AMPK activity and reduces 4E-BP1 phosphorylation and protein synthesis in human skeletal muscle. *The Journal of Physiology*. 576 (Pt 2), pp. 613-624.
- Drynan, L., Quant, P.A., and Zammit, V.A. (1996) Flux control exerted by mitochondrial outer membrane carnitine palmitoyltransferase over beta-oxidation, ketogenesis and tricarboxylic acid cycle activity in hepatocytes isolated from rats in different metabolic states. *The Biochemical Journal*. 317 (Pt 3), pp. 791-795.
- Dubé, J.J., Amati, F., Toledo, F.G., Stefanovic-Racic, M., Rossi, A., Coen, P., and Goodpaster, B.H. (2011) Effects of weight loss and exercise on insulin resistance, and intramyocellular triacylglycerol, diacylglycerol and ceramide. *Diabetologia*. 54 (5), pp. 1147-1156.

Duszka, K., Gregor, A., Guillou, H., König, J., and Wahli, W. (2020) Peroxisome Proliferator-Activated Receptors and Caloric Restriction-Common Pathways Affecting Metabolism, Health, and Longevity. *Cells*. 9 (7), 1708.

Dyck, D.J., and Bonen, A. (1998) Muscle contraction increases palmitate esterification and oxidation and triacylglycerol oxidation. *The American Journal of Physiology*. 275 (5), pp. E888-E896.

Egan, B., and Zierath, J.R. (2013) Exercise metabolism and the molecular regulation of skeletal muscle adaptation. *Cell Metabolism*. 17 (2), pp. 162-184.

Eichmann, T.O., Kumari, M., Haas, J.T., Farese, R.V., Jr, Zimmermann, R., Lass, A., and Zechner, R. (2012). Studies on the substrate and stereo/regioselectivity of adipose triglyceride lipase, hormone-sensitive lipase, and diacylglycerol-O-acyltransferases. *The Journal of Biological Chemistry*. 287 (49), pp. 41446-41457.

Eisenberg, B.R. and Kuda, A.M. (1975) Stereological analysis of mammalian skeletal muscle. II. White vastus muscle of the adult guinea pig. *Journal of Ultrastructure Research*. 51 (2), pp. 176-187.

Farese, R.V., Jr, and Walther, T.C. (2009) Lipid droplets finally get a little R-E-S-P-E-C-T. *Cell*. 139 (5), pp. 855-860.

Ferreira, R., Vitorino, R., Alves, R.M., Appell, H.J., Powers, S.K., Duarte, J.A., and Amado, F. (2010) Subsarcolemmal and intermyofibrillar mitochondria proteome differences disclose functional specializations in skeletal muscle. *Proteomics*. 10 (17), pp. 3142-3154.

Finck, B.N., Lehman, J.J., Leone, T. C., Welch, M.J., Bennett, M.J., Kovacs, A., Han, X., Gross, R.W., Kozak, R., Lopaschuk, G.D., and Kelly, D.P. (2002) The cardiac phenotype induced by PPARalpha overexpression mimics that caused by diabetes mellitus. *The Journal of Clinical Investigation*. 109 (1), pp. 121-130.

Fink, W.J., Costill, D.L., and Pollock, M.L. (1977) Submaximal and maximal working capacity of elite distance runners. Part II. Muscle fiber composition and enzyme activities. *Annals of the New York Academy of Sciences*. 301, pp. 323-327.

- Fletcher, J.A., Deja, S., Satapati, S., Fu, X., Burgess, S.C. and Browning, J.D. (2019) Impaired ketogenesis and increased acetyl-CoA oxidation promote hyperglycemia in human fatty liver. *JCI Insight*. 5 (11), e127737.
- Foley, J.E. (1988) Mechanisms of impaired insulin action in isolated adipocytes from obese and diabetic subjects. *Diabetes/Metabolism Reviews*. 4 (5), pp. 487-505.
- Foley, K., Boguslavsky, S., and Klip, A. (2011) Endocytosis, Recycling, and Regulated Exocytosis of Glucose Transporter 4. *Biochemistry*. 50 (15), pp. 3048-2061.
- Forbes, G.B., Brown, M.R., Welle, S.L., and Lipinski, B.A. (1986) Deliberate overfeeding in women and men: energy cost and composition of the weight gain. *British Journal of Nutrition*. 56 (1), pp. 1-9.
- Foster, D.W. (2012) Malonyl-CoA: the regulator of fatty acid synthesis and oxidation. *The Journal of Clinical Investigation*. 122 (6), pp. 1958-1959.
- Frayn, K.N. (2010) Fat as a fuel: emerging understanding of the adipose tissue-skeletal muscle axis. *Acta Physiologica (Oxford, England)*. 199 (4), pp. 509-518.
- Frye, J., and Clayton, Z.S. (2019) Physical inactivity-induced insulin resistance: could alterations to the vasculature be to blame?. *The Journal of Physiology*. 597 (2), pp. 375-376.
- Fukuda, M. (2008) Membrane traffic in the secretory pathway: Regulation of secretory vesicle traffic by Rab small GTPases. *Cellular and Molecular Life Sciences*. 65 (18), pp. 2801-2813.
- Furuyama, T., Kitayama, K., Yamashita, H., and Mori, N. (2003) Forkhead transcription factor FOXO1 (FKHR)-dependent induction of PDK4 gene expression in skeletal muscle during energy deprivation. *The Biochemical Journal*. 375 (Pt 2), pp. 365-371.
- Gammeltoft, S. and Van Obberghen, E. (1986). Protein kinase activity of the insulin receptor. *The Biochemical Journal*. 235 (1), pp. 1-11.

Garcia, D., and Shaw, R.J. (2017) AMPK: Mechanisms of Cellular Energy Sensing and Restoration of Metabolic Balance. *Molecular Cell*. 66 (6), pp. 789-800.

Garland, P.B., Shepherd, D., Nicholls, D.G., and Ontko, J. (1968) Energy-dependent control of the tricarboxylic acid cycle by fatty acid oxidation in rat liver mitochondria. *Advances in Enzyme Regulation*. 6, pp. 3-30.

Gaster, M., Poulsen, P., Handberg, A., Schroder, H.D., and Beck-Nielsen, H. (2000) Direct evidence of fiber type-dependent GLUT-4 expression in human skeletal muscle. *American Journal of Physiology. Endocrinology and Metabolism*. 278 (5), pp. E910-E916.

Giorgione, J.R., Lin, J.H., McCammon, J.A., and Newton, A.C. (2006) Increased membrane affinity of the C1 domain of protein kinase Cdelta compensates for the lack of involvement of its C2 domain in membrane recruitment. *The Journal of Biological Chemistry*. 281 (3), pp. 1660-1669.

Glatz, J.F., Luiken, J.J. and Bonen, A. (2010) Membrane fatty acid transporters as regulators of lipid metabolism: implications for metabolic disease. *Physiological Reviews*. 90 (1), pp. 367-417.

Gnaiger, E. (2009) Capacity of oxidative phosphorylation in human skeletal muscle: New perspectives of mitochondrial physiology. *The International Journal of Biochemistry & Cell Biology*. 41 (10), pp. 1837-1845.

Gong, H., Liu, L., Ni, C.X., Zhang, Y., Su, W.J., Lian, Y.J., Peng, W., Zhang, J.P., and Jiang, C.L. (2016) Dexamethasone rapidly inhibits glucose uptake via non-genomic mechanisms in contracting myotubes. *Archives of Biochemistry and Biophysics*. 603, pp. 102-109.

Goodpaster, B.H., and Sparks, L.M. (2017) Metabolic Flexibility in Health and Disease. *Cell Metabolism*. 25 (5), pp. 1027-1036.

Goodpaster, B.H., He, J., Watkins, S., and Kelley, D.E. (2001) Skeletal muscle lipid content and insulin resistance: evidence for a paradox in endurance-trained athletes. *The Journal of Clinical Endocrinology and Metabolism*. 86 (12), pp. 5755-5761.

Goodpaster, B.H., Theriault, R., Watkins, S.C., and Kelley, D.E. (2000). Intramuscular lipid content is increased in obesity and decreased by weight loss. *Metabolism: Clinical and Experimental*. 49 (4), pp. 467-472.

Goodpaster, B.H., Wolfe, R.R., and Kelley, D.E. (2002) Effects of obesity on substrate utilization during exercise. *Obesity Research*. 10 (7), pp. 575-584.

Greenberg, A.S., Egan, J.J., Wek, S.A., Garty, N.B., Blanchette-Mackie, E.J., and Londos, C. (1991) Perilipin, a major hormonally regulated adipocyte-specific phosphoprotein associated with the periphery of lipid storage droplets. *Journal of Biological Chemistry*. 266 (17), pp. 11341-11346.

Guebre-Egziabher, F., Alix, P. M., Koppe, L., Pelletier, C. C., Kalbacher, E., Fouque, D., and Soulage, C. O. (2013) Ectopic lipid accumulation: A potential cause for metabolic disturbances and a contributor to the alteration of kidney function. *Biochimie*. 95 (11), 1971-1979.

Hage Hassan, R., Pacheco de Sousa, A. C., Mahfouz, R., Hainault, I., Blachnio-Zabielska, A., Bourron, O., Koskas, F., Górski, J., Ferré, P., Fougelle, F., and Hajduch, E. (2016) Sustained Action of Ceramide on the Insulin Signaling Pathway in Muscle Cells: IMPLICATION OF THE DOUBLE-STRANDED RNA-ACTIVATED PROTEIN KINASE. *The Journal of Biological Chemistry*. 291 (6), pp. 3019-3029.

Hajduch, E., Balendran, A., Batty, I.H., Litherland, G.J., Blair, A.S., Downes, C.P., and Hundal, H.S. (2001) Ceramide impairs the insulin-dependent membrane recruitment of protein kinase B leading to a loss in downstream signalling in L6 skeletal muscle cells. *Diabetologia*. 44 (2), pp. 173-183.

Halestrap, A.P. (2012) The Mitochondrial Pyruvate Carrier: Has It Been Unearthed at Last? *Cell Metabolism*. 16 (2), pp. 141-143.

Hamburg, N.M., McMackin, C.J., Huang, A.L., Shenouda, S.M., Widlansky, M.E., Schulz, E., Gokce, N., Ruderman, N.B., Keaney, J.F., Jr, and Vita, J.A. (2007) Physical inactivity rapidly induces insulin resistance and microvascular dysfunction in healthy volunteers. *Arteriosclerosis, Thrombosis, and Vascular Biology*. 27 (12), pp. 2650-2656.

- Han, J., Pluhackova, K., and Böckmann, R.A. (2017) The Multifaceted Role of SNARE Proteins in Membrane Fusion. *Frontiers in Physiology*. 8, 5.
- Hardie, D.G., Ross, F.A., and Hawley, S.A. (2012) AMPK: a nutrient and energy sensor that maintains energy homeostasis. *Nature Reviews. Molecular Cell Biology*. 13 (4), pp. 251-262.
- Hardie, D.G., Salt, I.P., and Davies, S.P. (2000) Analysis of the role of the AMP-activated protein kinase in the response to cellular stress. *Methods in Molecular Biology (Clifton, N.J.)*. 99, pp. 63-74.
- Hardie, D.G., Scott, J.W., Pan, D.A., and Hudson, E.R. (2003) Management of cellular energy by the AMP-activated protein kinase system. *FEBS Letters*. 546 (1), pp. 113-120.
- Hargreaves, M., and Spriet, L.L. (2018) Exercise Metabolism: Fuels for the Fire. *Cold Spring Harbor Perspectives in Medicine*. 8 (8), a029744.
- Herms, A., Bosch, M., Reddy, B.J., Schieber, N.L., Fajardo, A., Rupérez, C., Fernández-Vidal, A., Ferguson, C., Rentero, C., Tebar, F., Enrich, C., Parton, R.G., Gross, S.P., and Pol, A. (2015) AMPK activation promotes lipid droplet dispersion on detyrosinated microtubules to increase mitochondrial fatty acid oxidation. *Nature Communications*. 6, 7176.
- Herzig, S., and Shaw, R.J. (2018) AMPK: guardian of metabolism and mitochondrial homeostasis. *Nature reviews. Molecular Cell Biology*. 19 (2), pp. 121-135.
- Hiatt, W.R., Regensteiner, J.G., Wolfel, E.E., Ruff, L., and Brass, E.P. (1989) Carnitine and acylcarnitine metabolism during exercise in humans. Dependence on skeletal muscle metabolic state. *The Journal of Clinical Investigation*. 84 (4), pp. 1167-1173.
- Hill, J.O., and Commerford, R. (1996) Physical activity, fat balance, and energy balance. *International Journal of Sport Nutrition*. 6 (2), pp. 80-92.
- Hill, J.O., Wyatt, H.R., and Peters, J.C. (2012) Energy balance and obesity. *Circulation*. 126 (1), pp. 126-132.

Hingst, J.R., Kjøbsted, R., Birk, J.B., Jørgensen, N.O., Larsen, M.R., Kido, K., Larsen, J.K., Kjeldsen, S., Fentz, J., Frøsig, C., Holm, S., Fritzen, A.M., Dohmann, T.L., Larsen, S., Foretz, M., Viollet, B., Schjerling, P., Overby, P., Halling, J.F., Pilegaard, H., Hellsten, Y., and Wojtaszewski, J. (2020) Inducible deletion of skeletal muscle AMPK α reveals that AMPK is required for nucleotide balance but dispensable for muscle glucose uptake and fat oxidation during exercise. *Molecular Metabolism*. 40, 101028.

Hinkle, P.C. (2005) P/O ratios of mitochondrial oxidative phosphorylation. *Biochimica et Biophysica Acta*. 1706 (1-2), pp. 1-11.

Hisanaga, Y., Ago, H., Nakagawa, N., Hamada, K., Ida, K., Yamamoto, M., Hori, T., Arii, Y., Sugahara, M., Kuramitsu, S., Yokoyama, S., and Miyano, M. (2004) Structural basis of the substrate-specific two-step catalysis of long chain fatty acyl-CoA synthetase dimer. *The Journal of Biological Chemistry*. 279 (30), pp. 31717-31726.

Hoeks, J., Mensink, M., Hesselink, M.K.C., Ekroos, K., and Schrauwen, P. (2012) Long- and medium-chain fatty acids induce insulin resistance to a similar extent in humans despite marked differences in muscle fat accumulation. *Journal of Clinical Endocrinology and Metabolism*. 97 (1), pp. 208-216.

Hofer, P., Taschler, U., Schreiber, R., Kotzbeck, P., and Schoiswohl, G. (2020) The Lipolysome-A Highly Complex and Dynamic Protein Network Orchestrating Cytoplasmic Triacylglycerol Degradation. *Metabolites*. 10 (4), 147.

Holm, C., and Østerlund, T. (1999) Hormone-sensitive lipase and neutral cholesteryl ester lipase. *Methods in Molecular Biology (Clifton, N.J.)*. 109, pp. 109-121.

Holness, M. J., and Sugden, M.C. (2003) Regulation of pyruvate dehydrogenase complex activity by reversible phosphorylation. *Biochemical Society Transactions*. 31 (Pt 6), pp. 1143-1151.

Hong, W., and Lev, S. (2014) Tethering the assembly of SNARE complexes. *Trends in Cell Biology*. 24 (1), pp. 35-43.

- Hoppeler, H. (1986) Exercise-induced ultrastructural changes in skeletal muscle. *International Journal of Sports Medicine*. 7 (4), pp. 187-204.
- Hoppeler, H., Luthi, P., Claassen, H., Weibel, E.R., and Howald, H. (1973) The ultrastructure of the normal human skeletal muscle: a morphometric analysis on untrained men, women and well-trained orienteers. *Pflugers Archiv: European Journal of Physiology*. 344 (3), pp. 217-232.
- Horton, T.J., Dow, S., Armstrong, M., and Donahoo, W.T. (2009) Greater systemic lipolysis in women compared with men during moderate-dose infusion of epinephrine and/or norepinephrine. *Journal of applied physiology (Bethesda, Md.: 1985)*. 107 (1), pp. 200-210.
- Horton, T.J., Drougas, H., Brachey, A., Reed, G.W., Peters, J.C., and Hill, J.O. (1995) Fat and carbohydrate overfeeding in humans: different effects on energy storage. *American Journal of Clinical Nutrition*. 62 (1), pp. 19-29.
- Houten, S.M., and Wanders, R.J. (2010) A general introduction to the biochemistry of mitochondrial fatty acid β -oxidation. *Journal of Inherited Metabolic Disease*. 33 (5), pp. 469-477.
- Hruz, P.W. and Mueckler, M.M. (2001) Structural analysis of the GLUT1 facilitative glucose transporter. *Molecular Membrane Biology*. 18 (3), pp. 183-193.
- Hsieh, K., Lee, Y.K., Londos, C., Raaka, B.M., Dalen, K.T., and Kimmel A.R. (2012) Perilipin family members preferentially sequester to either triacylglycerol- or cholesteryl ester-specific intracellular lipid storage droplets. *Journal of Cell Science*. 125 (17), pp. 4067-4076.
- Huang, B., Gudi, R., Wu, P., Harris, R.A., Hamilton, J., and Popov, K.M. (1998) Isoenzymes of pyruvate dehydrogenase phosphatase. DNA-derived amino acid sequences, expression, and regulation. *The Journal of Biological Chemistry*. 273 (28), pp. 17680-17688.
- Huang, A.H.C. (2018) Plant Lipid Droplets and Their Associated Proteins: Potential for Rapid Advances. *Plant Physiology*. 176 (3), pp. 1894-1918.

Hue, L., and Taegtmeyer, H. (2009) The Randle cycle revisited: a new head for an old hat. *American journal of physiology. Endocrinology and Metabolism*. 297 (3), pp. E578-E591.

Hulver, M.W., Berggren, J.R., Cortright, R.N., Dudek, R.W., Thompson, R.P., Pories, W.J., MacDonald, K.G., Cline, G.W., Shulman, G.I., Dohm, G.L., and Houmard, J.A. (2003) Skeletal muscle lipid metabolism with obesity. *American Journal of Physiology. Endocrinology and Metabolism*. 284 (4), pp. E741-E747.

Huss, J.M., Kopp, R.P., and Kelly, D.P. (2002) Peroxisome proliferator-activated receptor coactivator-1alpha (PGC-1alpha) coactivates the cardiac-enriched nuclear receptors estrogen-related receptor-alpha and -gamma. Identification of novel leucine-rich interaction motif within PGC-1alpha. *The Journal of Biological Chemistry*. 277 (43), pp. 40265-40274.

Igal, R.A. (2016) Stearoyl CoA Desaturase-1: New insights into a central regulator of cancer metabolism. *Biochimica et Biophysica Acta*. 1861 (12 Pt A), pp. 1865-1880.

Inagaki, T., Dutchak, P., Zhao, G., Ding, X., Gautron, L., Parameswara, V., Li, Y., Goetz, R., Mohammadi, M., Esser, V., Elmquist, J.K., Gerard, R.D., Burgess, S.C., Hammer, R.E., Mangelsdorf, D.J., and Kliewer, S.A. (2007) Endocrine regulation of the fasting response by PPARalpha-mediated induction of fibroblast growth factor 21. *Cell Metabolism*. 5 (6), pp. 415-425.

Itani, S.I., Zhou, Q., Pories, W.J., MacDonald, K.G., and Dohm, G.L. (2000) Involvement of protein kinase C in human skeletal muscle insulin resistance and obesity. *Diabetes*. 49 (8), pp. 1353-1358.

Jain, S.S., Luiken, J.J.F.P., Snook, L.A., Han, X.X., Holloway, G.P., Glatz, J.F.C., and Bonen, A. (2015) Fatty acid transport and transporters in muscle are critically regulated by Akt2. *FEBS Letters*. 589 (19 Part B), pp. 2769-2775.

James, D.E., Strube, M., and Mueckler, M. (1989) Molecular Cloning and Characterization of an Insulin-regulatable Glucose Transporter. *Nature*. 338 (6210), pp. 83-87.

Jazet, I.M., Schaart, G., Gastaldelli, A., Ferrannini, E., Hesselink, M.K., Schrauwen, P., Romijn, J.A., Maassen, J.A., Pijl, H., Ouwens, D.M., and Meinders, A.E. (2008) Loss of 50% of excess weight using a very low energy diet improves insulin-stimulated glucose disposal and skeletal muscle insulin signalling in obese insulin-treated type 2 diabetic patients. *Diabetologia*. 51 (2), pp. 309-319.

Jenkins, C.M., Yang, J., Sims, H.F., and Gross, R.W. (2011) Reversible high affinity inhibition of phosphofructokinase-1 by acyl-CoA: a mechanism integrating glycolytic flux with lipid metabolism. *The Journal of Biological Chemistry*. 286 (14), pp. 11937-11950.

Jensen, M.D., Ekberg, K., and Landau, B.R. (2001) Lipid metabolism during fasting. *American journal of physiology. Endocrinology and Metabolism*. 281 (4), pp. E789-E793.

Jensen, T.E., Angin, Y., Sylow, L., and Richter, E.A. (2014b) Is contraction-stimulated glucose transport feedforward regulated by Ca^{2+} ?. *Experimental Physiology*. 99 (12), pp. 1562-1568.

Jensen, T.E., Sylow, L., Rose, A.J., Madsen, A.B., Angin, Y., Maarbjerg, S.J., and Richter, E.A. (2014a) Contraction-stimulated glucose transport in muscle is controlled by AMPK and mechanical stress but not sarcoplasmic reticulum Ca^{2+} release. *Molecular Metabolism*. 3 (7), pp. 742-753.

Jitrapakdee, S., St Maurice, M., Rayment, I., Cleland, W.W., Wallace, J.C., and Attwood, P.V. (2008) Structure, mechanism and regulation of pyruvate carboxylase. *The Biochemical Journal*. 413 (3), pp. 369-387.

Jocken, J.W.E., Moro, C., Goossens, G.H., Hansen, D., Mairal, A., Hesselink, M.K.C., Langin, D., van Loon, L.J.C., and Blaak, E.E. (2010) Skeletal Muscle Lipase Content and Activity in Obesity and Type 2 Diabetes. *The Journal of Clinical Endocrinology & Metabolism*. 95 (12), pp. 5449-5453.

Junho, C., Caio-Silva, W., Trentin-Sonoda, M., and Carneiro-Ramos, M.S. (2020) An Overview of the Role of Calcium/Calmodulin-Dependent Protein Kinase in Cardiorenal Syndrome. *Frontiers in Physiology*. 11, 735.

- Kamei, Y., Mizukami, J., Miura, S., Suzuki, M., Takahashi, N., Kawada, T., Taniguchi, T., and Ezaki, O. (2003) A forkhead transcription factor FKHR up-regulates lipoprotein lipase expression in skeletal muscle. *FEBS Letters*. 536 (1-3), pp. 232-236.
- Kanaley, J.A., Shadid, S., Sheehan, M.T., Guo, Z., and Jensen, M.D. (2009) Relationship between plasma free fatty acid, intramyocellular triglycerides and long-chain acylcarnitines in resting humans. *The Journal of Physiology*. 587 (Pt 24), pp. 5939-5950.
- Kayar, S.R., Hoppeler, H., Howald, H., Claassen, H. and Oberholzer, F. (1986) Acute effects of endurance exercise on mitochondrial distribution and skeletal muscle morphology. *European Journal of Applied Physiology and Occupational Physiology*. 54 (6), pp. 578-584.
- Kelley, D.E., Goodpaster, B., Wing, R.R., and Simoneau, J.A. (1999) Skeletal muscle fatty acid metabolism in association with insulin resistance, obesity, and weight loss. *The American Journal of Physiology*. 277 (6), pp. E1130-E1141.
- Kelley, D.E., Reilly, J.P., Veneman, T., and Mandarino, L.J. (1990) Effects of insulin on skeletal muscle glucose storage, oxidation, and glycolysis in humans. *The American Journal of Physiology*. 258 (6 Pt 1), pp. E923-E929.
- Kennedy, E.P. (1961) Biosynthesis of complex lipids. *Federation Proceedings*. 20, pp. 934-940.
- Kerner, J., and Hoppel, C. (2000) Fatty acid import into mitochondria. *Biochimica et Biophysica Acta*. 1486 (1), pp. 1-17.
- Kersten, S., Seydoux, J., Peters, J.M., Gonzalez, F.J., Desvergne, B., and Wahli, W. (1999) Peroxisome proliferator-activated receptor alpha mediates the adaptive response to fasting. *The Journal of Clinical Investigation*. 103 (11), pp. 1489-1498.
- Kim, J.K., Fillmore, J.J., Sunshine, M.J., Albrecht, B., Higashimori, T., Kim, D.W., Liu, Z.X., Soos, T.J., Cline, G.W., O'Brien, W.R., Littman, D.R., and Shulman, G.I. (2004) PKC-theta knockout mice are protected from fat-induced insulin resistance. *The Journal of Clinical Investigation*. 114 (6), pp. 823-827.

- Kjaer, M., Howlett, K., Langfort, J., Zimmerman-Belsing, T., Lorentsen, J., Bulow, J., Ihlemann, J., Feldt-Rasmussen, U., and Galbo, H. (2000) Adrenaline and glycogenolysis in skeletal muscle during exercise: a study in adrenalectomised humans. *The Journal of Physiology*. 528 (2), pp. 371-378.
- Knight, Z.A., Gonzalez, B., Feldman, M.E., Zunder, E.R., Goldenberg, D.D., Williams, O., Loewith, R., Stokoe, D., Balla, A., Toth, B., Balla, T., Weiss, W.A., Williams, R.L., and Shokat, K.M. (2006) A pharmacological map of the PI3-K family defines a role for p110alpha in insulin signaling. *Cell*. 125 (4), pp. 733-747.
- Konishi, H., Kuroda, S., and Kikkawa, U. (1994) The pleckstrin homology domain of RAC protein kinase associates with the regulatory domain of protein kinase C zeta. *Biochemical and Biophysical Research Communications*. 205 (3), pp. 1770-1775.
- Korotchkina, L.G., and Patel, M.S. (1995) Mutagenesis studies of the phosphorylation sites of recombinant human pyruvate dehydrogenase. Site-specific regulation. *The Journal of Biological Chemistry*. 270 (24), pp. 14297-14304.
- Kragh-Hansen, U. (1981) Molecular Aspects of Ligand Binding to Serum Albumin. *Pharmacological Reviews*. 33 (1), pp. 17-53.
- Krintel, C., Osmark, P., Larsen, M.R., Resjö, S., Logan, D.T., and Holm, C. (2008) Ser649 and Ser650 are the major determinants of protein kinase A-mediated activation of human hormone-sensitive lipase against lipid substrates. *PLoS one*. 3 (11), e3756.
- Krssak, M., Falk Petersen, K., Dresner, A., DiPietro, L., Vogel, S.M., Rothman, D.L., Roden, M., and Shulman, G.I. (1999) Intramyocellular lipid concentrations are correlated with insulin sensitivity in humans: a ¹H NMR spectroscopy study. *Diabetologia*. 42 (1), pp. 113-116.
- Kuerschner, L., Moessinger, C., and Thiele, C. (2008) Imaging of lipid biosynthesis: how a neutral lipid enters lipid droplets. *Traffic (Copenhagen, Denmark)*. 9 (3), pp. 338-352.

- Kuo, Y.C., Huang, K.Y., Yang, C.H., Yang, Y.S., Lee, W.Y., and Chiang, C.W. (2008) Regulation of phosphorylation of Thr-308 of Akt, cell proliferation, and survival by the B55alpha regulatory subunit targeting of the protein phosphatase 2A holoenzyme to Akt. *The Journal of Biological Chemistry*. 283 (4), pp. 1882-1892.
- Kusminski, C.M., Shetty, S., Orci, L., Unger, R.H., and Scherer, P.E. (2009) Diabetes and apoptosis: lipotoxicity. *Apoptosis: An International Journal on Programmed Cell Death*. 14 (12), pp. 1484-1495.
- Kuzmiak-Glancy, S., and Willis, W.T. (2014) Skeletal muscle fuel selection occurs at the mitochondrial level. *The Journal of Experimental Biology*. 217 (Pt 11), pp. 1993-2003.
- Kwon, H.S., Huang, B., Unterman, T.G., and Harris, R.A. (2004) Protein kinase B-alpha inhibits human pyruvate dehydrogenase kinase-4 gene induction by dexamethasone through inactivation of FOXO transcription factors. *Diabetes*. 53 (4), pp. 899-910.
- Langendorf, C.G., Ngoei, K., Scott, J.W., Ling, N., Issa, S., Gorman, M.A., Parker, M.W., Sakamoto, K., Oakhill, J.S., and Kemp, B.E. (2016) Structural basis of allosteric and synergistic activation of AMPK by furan-2-phosphonic derivative C2 binding. *Nature Communications*. 7, 10912.
- Langin, D. (2006) Adipose tissue lipolysis as a metabolic pathway to define pharmacological strategies against obesity and the metabolic syndrome. *Pharmacological Research*. 53 (6), pp. 482-491.
- Lanzi, S., Codecasa, F., Cornacchia, M., Maestrini, S., Salvadori, A., Brunani, A., and Malatesta, D. (2014) Fat oxidation, hormonal and plasma metabolite kinetics during a submaximal incremental test in lean and obese adults. *PloS One*. 9 (2), e88707.
- Lara-Castro, C., Newcomer, B.R., Rowell, J., Wallace, P., Shaughnessy, S.M., Munoz, A.J., Shiflett, A.M., Rigsby, D.Y., Lawrence, J.C., Bohning, D.E., Buchthal, S., and Garvey, W.T. (2008) Effects of short-term very low-calorie diet on intramyocellular lipid and insulin sensitivity in nondiabetic and type 2 diabetic subjects. *Metabolism: Clinical and Experimental*. 57 (1), pp. 1-8.

- Larsen, S., Ara, I., Rabøl, R., Andersen, J.L., Boushel, R., Dela, F., and Helge, J.W. (2009) Are substrate use during exercise and mitochondrial respiratory capacity decreased in arm and leg muscle in type 2 diabetes?. *Diabetologia*. 52 (7), pp. 1400-1408.
- Larson-Meyer, D.E., Borkhsenius, O.N., Gullett, J.C., Russell, R.R., Devries, M.C., Smith, S.R., and Ravussin, E. (2008) Effect of dietary fat on serum and intramyocellular lipids and running performance. *Medicine and Science in Sports and Exercise*. 40 (5), pp. 892-902.
- Lattka, E., Illig, T., Koletzko, B., and Heinrich, J. (2010) Genetic variants of the FADS1 FADS2 gene cluster as related to essential fatty acid metabolism. *Current Opinion in Lipidology*. 21 (1), pp. 64-69.
- Lee, C.H., Olson, P., and Evans, R.M. (2003) Minireview: lipid metabolism, metabolic diseases, and peroxisome proliferator-activated receptors. *Endocrinology*. 144 (6), pp. 2201-2207.
- Lee, S., Boesch, C., Kuk, J.L., and Arslanian, S. (2013) Effects of an overnight intravenous lipid infusion on intramyocellular lipid content and insulin sensitivity in African-American versus Caucasian adolescents. *Metabolism: Clinical and Experimental*. 62 (3), pp. 417-423.
- Lewis, R.E., Cao, L., Perregaux, D., and Czech, M.P. (1990) Threonine 1336 of the human insulin receptor is a major target for phosphorylation by protein kinase C. *Biochemistry*. 29 (7), pp. 1807-1813.
- Li, J., and Cheng, J.X. (2014) Direct visualization of de novo lipogenesis in single living cells. *Scientific Reports*. 4, 6807.
- Liu, H., and Chen, Y.G. (2022) The Interplay Between TGF- β Signaling and Cell Metabolism. *Frontiers in Cell and Developmental Biology*. 10, 846723.
- Lucić, V., Greif, G.J., and Kennedy, M.B. (2008) Detailed state model of CaMKII activation and autophosphorylation. *European Biophysics Journal: EBJ*. 38 (1), pp. 83-98.
- Lund, S., Holman, G.D., Schmitz, O., and Pedersen, O. (1995) Contraction stimulates translocation of glucose transporter GLUT4 in skeletal muscle

through a mechanism distinct from that of insulin. *Proceedings of the National Academy of Sciences of the United States of America*. 92 (13), pp. 5817-5821.

Lund, J., Helle, S.A., Li, Y., Løvsetten, N.G., Stadheim, H.K., Jensen, J., Kase, E.T., Thoresen, G.H., and Rustan, A.C. (2018) Higher lipid turnover and oxidation in cultured human myotubes from athletic versus sedentary young male subjects. *Scientific Reports*. 8 (1), 17549.

Lundell, L.S., Massart, J., Altıntaş, A., Krook, A., and Zierath, J.R. (2019) Regulation of glucose uptake and inflammation markers by FOXO1 and FOXO3 in skeletal muscle. *Molecular Metabolism*. 20, pp. 79-88.

Ly, L.D., Xu, S., Choi, S.K., Ha, C.M., Thoudam, T., Cha, S.K., Wiederkehr, A., Wollheim, C.B., Lee, I.K., and Park, K.S. (2017) Oxidative stress and calcium dysregulation by palmitate in type 2 diabetes. *Experimental & Molecular Medicine*. 49 (2), e291.

Mahfouz, R., Houry, R., Blachnio-Zabielska, A., Turban, S., Loiseau, N., Lipina, C., Stretton, C., Bourron, O., Ferré, P., Foufelle, F., Hundal, H.S., and Hajduch, E. (2014) Characterising the inhibitory actions of ceramide upon insulin signaling in different skeletal muscle cell models: a mechanistic insight. *PloS One*. 9 (7), e101865.

Malenfant, P., Joanisse, D.R., Thériault, R., Goodpaster, B.H., Kelley, D.E., and Simoneau, J.A. (2001) Fat content in individual muscle fibers of lean and obese subjects. *International Journal of Obesity and Related Metabolic Disorders: Journal of The International Association for The Study of Obesity*. 25 (9), pp. 1316–1321.

Malisoux, L., Francaux, M., Nielens, H., and Theisen, D. (2006) Stretch-shortening cycle exercises: an effective training paradigm to enhance power output of human single muscle fibers. *Journal of Applied Physiology (Bethesda, Md.: 1985)*. 100 (3), pp. 771-779.

Maréchal, L., Laviolette, M., Rodrigue-Way, A., Sow, B., Brochu, M., Caron, V., and Tremblay, A. (2018) The CD36-PPAR γ Pathway in Metabolic Disorders. *International Journal of Molecular Sciences*. 19 (5), 1529.

Mason, R.R., Meex, R.C., Russell, A.P., Canny, B.J., and Watt, M.J. (2014) Cellular localization and associations of the major lipolytic proteins in human skeletal muscle at rest and during exercise. *PloS One*. 9 (7), e103062.

Medler, S. (2019) Mixing it up: the biological significance of hybrid skeletal muscle fibers. *The Journal of Experimental Biology*. 222 (Pt 23), jeb200832.

Mejhert, N., Gabriel, K.R., Frendo-Cumbo, S., Krahmer, N., Song, J., Kuruvilla, L., Chitraju, C., Boland, S., Jang, D.K., von Grotthuss, M., Costanzo, M.C., Rydén, M., Olzmann, J.A., Flannick, J., Burt, N.P., Farese, R.V., Jr., and Walther, T.C. (2022) The Lipid Droplet Knowledge Portal: A resource for systematic analyses of lipid droplet biology. *Developmental Cell*. 57 (3), pp. 387-397.

Mejhert, N., Kuruvilla, L., Gabriel, K.R., Elliott, S.D., Guie, M.A., Wang, H., Lai, Z.W., Lane, E.A., Christiano, R., Danial, N.N., Farese, R.V., Jr., and Walther, T.C. (2020) Partitioning of MLX-Family Transcription Factors to Lipid Droplets Regulates Metabolic Gene Expression. *Molecular Cell*. 77 (6), pp. 1251-1264

Miao, B., Skidan, I., Yang, J., Lugovskoy, A., Reibarkh, M., Long, K., Brazell, T., Durugkar, K.A., Maki, J., Ramana, C.V., Schaffhausen, B., Wagner, G., Torchilin, V., Yuan, J., and Degterev, A. (2010) Small molecule inhibition of phosphatidylinositol-3,4,5-triphosphate (PIP3) binding to pleckstrin homology domains. *Proceedings of the National Academy of Sciences of the United States of America*. 107 (46), pp. 20126-20131.

Middelbeek, R.J., Chambers, M.A., Tantiwong, P., Treebak, J.T., An, D., Hirshman, M.F., Musi, N., and Goodyear, L.J. (2013) Insulin stimulation regulates AS160 and TBC1D1 phosphorylation sites in human skeletal muscle. *Nutrition & Diabetes*. 3 (6), e74.

Mikines, K.J., Farrell, P.A., Sonne, B., Tronier, B., and Galbo, H. (1988) Postexercise dose-response relationship between plasma glucose and insulin secretion. *Journal of Applied Physiology*. 64 (3), pp. 988-999.

Mikines, K.J., Richter, E.A., Dela, F., and Galbo, H. (1991) Seven Days of Bed Rest Decrease Insulin Action on Glucose Uptake in Leg and Whole Body. *Journal of Applied Physiology*. 70 (3), pp. 1245-1254.

Moller, D.E., Yokota, A., Caro, J.F. and Flier, J.S. (1989) Tissue-specific Expression of Two Alternatively Spliced Insulin Receptor mRNAs in Man. *Molecular Endocrinology*. 3 (8), pp. 1263-1269.

Montell, E., Turini, M., Marotta, M., Roberts, M., Noé, V., Ciudad, C.J., Macé, K., and Gómez-Foix, A.M. (2001) DAG accumulation from saturated fatty acids desensitizes insulin stimulation of glucose uptake in muscle cells. *American Journal of Physiology. Endocrinology and Metabolism*. 280 (2), pp. E229-E237.

Mogensen, M., Sahlin, K., Fernström, M., Glinborg, D., Vind, B.F., Beck-Nielsen, H., and Højlund, K. (2007) Mitochondrial respiration is decreased in skeletal muscle of patients with type 2 diabetes. *Diabetes*. 56 (6), pp. 1592-1599.

Moro, C., Galgani, J.E., Luu, L., Pasarica, M., Mairal, A., Bajpeyi, S., Schmitz, G., Langin, D., Liebisch, G. and Smith, S.R. (2009) Influence of gender, obesity, and muscle lipase activity on intramyocellular lipids in sedentary individuals. *The Journal of Clinical Endocrinology and Metabolism*. 94 (9), pp. 3440-3447.

Mootha, V.K., Lindgren, C.M., Eriksson, K.F., Subramanian, A., Sihag, S., Lehar, J., Puigserver, P., Carlsson, E., Ridderstråle, M., Laurila, E., Houstis, N., Daly, M.J., Patterson, N., Mesirov, J.P., Golub, T.R., Tamayo, P., Spiegelman, B., Lander, E.S., Hirschhorn, J.N., Altshuler, D., and Groop, L.C. (2003) PGC-1alpha-responsive genes involved in oxidative phosphorylation are coordinately downregulated in human diabetes. *Nature Genetics*. 34 (3), pp. 267-273.

Muoio, D.M., MacLean, P.S., Lang, D.B., Li, S., Houmard, J.A., Way, J.M., Winegar, D.A., Corton, J.C., Dohm, G.L., and Kraus, W.E. (2002) Fatty acid homeostasis and induction of lipid regulatory genes in skeletal muscles of peroxisome proliferator-activated receptor (PPAR) alpha knock-out mice. Evidence for compensatory regulation by PPAR delta. *The Journal of Biological Chemistry*. 277 (29), pp. 26089-26097.

Murphy, D.J. (2012) The dynamic roles of intracellular lipid droplets: from archaea to mammals. *Protoplasma*. 249 (3), pp. 541-585.

Nahlé, Z., Hsieh, M., Pietka, T., Coburn, C.T., Grimaldi, P.A., Zhang, M.Q., Das, D., and Abumrad, N.A. (2008) CD36-dependent regulation of muscle FoxO1 and PDK4 in the PPAR delta/beta-mediated adaptation to metabolic stress. *The Journal of Biological Chemistry*. 283 (21), pp. 14317-14326.

Newton A.C. (2018) Protein kinase C: perfectly balanced. *Critical Reviews in Biochemistry and Molecular Biology*. 53 (2), pp. 208-230.

NICE (2012) Type 2 diabetes: prevention in people at high risk. Available from: <https://www.nice.org.uk/guidance/ph38/resources/type-2-diabetes-prevention-in-people-at-high-risk-pdf-1996304192197>. [Accessed: 04/06/2022].

Nickerson, J.G., Alkhateeb, H., Benton, C.R., Lally, J., Nickerson, J., Han, X.X., Wilson, M.H., Jain, S.S., Snook, L.A., Glatz, J., Chabowski, A., Luiken, J., and Bonen, A. (2009) Greater transport efficiencies of the membrane fatty acid transporters FAT/CD36 and FATP4 compared with FABPpm and FATP1 and differential effects on fatty acid esterification and oxidation in rat skeletal muscle. *The Journal of Biological Chemistry*. 284 (24), pp. 16522-16530.

Niculite, C.M., Enciu, A.M., and Hinescu, M.E. (2019) CD 36: Focus on Epigenetic and Post-Transcriptional Regulation. *Frontiers in Genetics*. 10, 680.

Nielsen, J., Mogensen, M., Vind, B. F., Sahlin, K., Højlund, K., Schrøder, H. D., & Ortenblad, N. (2010). Increased subsarcolemmal lipids in type 2 diabetes: effect of training on localization of lipids, mitochondria, and glycogen in sedentary human skeletal muscle. *American journal of physiology. Endocrinology and metabolism*. 298 (3), pp. E706-E713.

Nikolić, N., and Aas, V. (2019) Electrical Pulse Stimulation of Primary Human Skeletal Muscle Cells. *Methods in Molecular Biology (Clifton, N.J.)*. 1889, pp. 17–24.

Odland, L.M., Howlett, R.A., Heigenhauser, G.J., Hultman, E., and Spriet, L.L. (1998) Skeletal muscle malonyl-CoA content at the onset of exercise at varying

power outputs in humans. *The American journal of Physiology*. 274 (6), pp. E1080-E1085.

Ojuka, E.O., Goyaram, V., and Smith, J.A. (2012) The role of CaMKII in regulating GLUT4 expression in skeletal muscle. *American journal of physiology. Endocrinology and Metabolism*. 303 (3), pp. E322-E331.

Ørtenblad, N., Nielsen, J., Boushel, R., Söderlund, K., Saltin, B., and Holmberg, H.C. (2018) The Muscle Fiber Profiles, Mitochondrial Content, and Enzyme Activities of the Exceptionally Well-Trained Arm and Leg Muscles of Elite Cross-Country Skiers. *Frontiers in Physiology*. 9, 1031.

Palmer, B.F., and Clegg, D.J. (2022) Metabolic Flexibility and Its Impact on Health Outcomes. *Mayo Clinic Proceedings*. 97 (4), pp. 761-776.

Pan, D.A., Lillioja, S., Kriketos, A.D., Milner, M.R., Baur, L.A., Bogardus, C., Jenkins, A.B., and Storlien, L.H. (1997) Skeletal muscle triglyceride levels are inversely related to insulin action. *Diabetes*. 46 (6), pp. 983-988.

Pan, X., Eathiraj, S., Munson, M., and Lambright, D.G. (2006) TBC-domain GAPs for Rab GTPases accelerate GTP hydrolysis by a dual-finger mechanism. *Nature*. 442 (7100), pp. 303-306.

Pande, S.V. (1975) A mitochondrial carnitine acylcarnitine translocase system. *Proceedings of the National Academy of Sciences of the U.S.A.* 72 (3), pp. 883-887.

Parikh, H.M., Elgzyri, T., Alibegovic, A., Hiscock, N., Ekström, O., Eriksson, K.F., Vaag, A., Groop, L.C., Ström, K., and Hansson, O. (2021) Relationship between insulin sensitivity and gene expression in human skeletal muscle. *BMC Endocrine Disorders*. 21 (1), 32.

Patel, M.S., Nemeria, N.S., Furey, W., and Jordan F. (2014) The pyruvate dehydrogenase complexes: structure-based function and regulation. *Journal of Biological Chemistry*. 289 (24), pp. 16615-16623.

Peck, B., Huot, J., Renzi, T., Arthur, S., Turner, M.J., and Marino, J.S. (2018) Mice lacking PKC- θ in skeletal muscle have reduced intramyocellular lipid accumulation and increased insulin responsiveness in skeletal

muscle. *American Journal of Physiology. Regulatory, Integrative and Comparative Physiology*. 314 (3), pp. R468-R477

Perreault, L., Newsom, S.A., Strauss, A., Kerege, A., Kahn, D.E., Harrison, K.A., Snell-Bergeon, J.K., Nemkov, T., D'Alessandro, A., Jackman, M.R., MacLean, P.S., and Bergman, B.C. (2018) Intracellular localization of diacylglycerols and sphingolipids influences insulin sensitivity and mitochondrial function in human skeletal muscle. *JCI Insight*. 3 (3), e96805.

Phielix, E., Meex, R., Ouwens, D.M., Sparks, L., Hoeks, J., Schaart, G., Moonen-Kornips, E., Hesselink, M.K., and Schrauwen, P. (2012) High oxidative capacity due to chronic exercise training attenuates lipid-induced insulin resistance. *Diabetes*. 61 (10), pp. 2472-2478.

Phillips, D.I., Caddy, S., Ilic, V., Fielding, B.A., Frayn, K.N., Borthwick, A.C., and Taylor, R. (1996) Intramuscular triglyceride and muscle insulin sensitivity: evidence for a relationship in nondiabetic subjects. *Metabolism: Clinical and Experimental*. 45 (8), pp. 947-950.

Plotkin, D.L., Roberts, M.D., Haun, C.T., and Schoenfeld, B.J. (2021) Muscle Fiber Type Transitions with Exercise Training: Shifting Perspectives. *Sports (Basel, Switzerland)*. 9 (9), 127.

Powell, D.J., Turban, S., Gray, A., Hajduch, E., and Hundal, H.S. (2004) Intracellular ceramide synthesis and protein kinase C ζ activation play an essential role in palmitate-induced insulin resistance in rat L6 skeletal muscle cells. *The Biochemical Journal*. 382 (Pt 2), pp. 619-629.

Prats, C., Donsmark, M., Qvortrup, K., Londos, C., Sztalryd, C., Holm, C., Galbo, H., and Ploug, T. (2006) Decrease in intramuscular lipid droplets and translocation of HSL in response to muscle contraction and epinephrine. *Journal of Lipid Research*. 47 (11), pp. 2392-2399.

Puchałowicz, K., and Rać, M.E. (2020) The Multifunctionality of CD36 in Diabetes Mellitus and Its Complications-Update in Pathogenesis, Treatment and Monitoring. *Cells*. 9 (8), 1877.

Purdom, T., Kravitz, L., Dokladny, K., and Mermier, C. (2018) Understanding the factors that effect maximal fat oxidation. *Journal of the International Society of Sports Nutrition*. 15, 3.

Randle, P.J., Garland, P.B., Hales, C.N., and Newsholme, E.A. (1963) The glucose fatty-acid cycle. Its role in insulin sensitivity and the metabolic disturbances of diabetes mellitus. *Lancet (London, England)*. 1 (7285), pp. 785-789.

Rathinaswamy, M.K., Dalwadi, U., Fleming, K.D., Adams, C., Stariha, J., Pardon, E., Baek, M., Vadas, O., DiMaio, F., Steyaert, J., Hansen, S.D., Yip, C.K., and Burke, J.E. (2021) Structure of the phosphoinositide 3-kinase (PI3K) p110 γ -p101 complex reveals molecular mechanism of GPCR activation. *Science Advances*. 7 (35), eabj4282.

Reggiani, C., Bottinelli, R., and Stienen, G.J. (2000) Sarcomeric Myosin Isoforms: Fine Tuning of a Molecular Motor. *News In Physiological Sciences: An International Journal of Physiology Produced Jointly by The International Union of Physiological Sciences and The American Physiological Society*. 15, pp. 26-33.

Reidy, P.T., McKenzie, A.I., Mahmassani, Z., Morrow, V.R., Yonemura, N.M., Hopkins, P.N., Marcus, R.L., Rondina, M.T., Lin, Y.K., and Drummond, M.J. (2018) Skeletal muscle ceramides and relationship with insulin sensitivity after 2 weeks of simulated sedentary behaviour and recovery in healthy older adults. *The Journal of Physiology*. 596 (21), pp. 5217-5236.

Renne, M.F., and Hariri, H. (2021) Lipid Droplet-Organelle Contact Sites as Hubs for Fatty Acid Metabolism, Trafficking, and Metabolic Channeling. *Frontiers In Cell and Developmental Biology*. 9, 726261.

Reue, K., and Wang, H. (2019) Mammalian lipin phosphatidic acid phosphatases in lipid synthesis and beyond: metabolic and inflammatory disorders. *Journal of Lipid Research*. 60 (4), pp. 728-733.

Richter, E.A., and Hargreaves, M. (2013) Exercise, GLUT4, and skeletal muscle glucose uptake. *Physiological Reviews*. 93 (3), pp. 993-1017.

- Richter, E.A., and Ruderman, N.B. (2009) AMPK and the biochemistry of exercise: implications for human health and disease. *The Biochemical Journal*. 418 (2), pp. 261-275.
- Roberts, D.J., and Miyamoto, S. (2015) Hexokinase II integrates energy metabolism and cellular protection: Acting on mitochondria and TORCing to autophagy. *Cell Death and Differentiation*. 22 (2), pp. 248-257.
- Röder, P.V., Wu, B., Liu, Y., and Han, W. (2016) Pancreatic regulation of glucose homeostasis. *Experimental & Molecular Medicine*. 48 (3), e219.
- Romijn, J.A., Coyle, E.F., Sidossis, L.S., Gastaldelli, A., Horowitz, J.F., Endert, E., and Wolfe, R.R. (1993) Regulation of endogenous fat and carbohydrate metabolism in relation to exercise intensity and duration. *The American Journal of Physiology*. 265 (3 Pt 1), pp. E380-E391.
- Rose, A.J., Kiens, B., and Richter, E.A. (2006) Ca²⁺-calmodulin-dependent protein kinase expression and signalling in skeletal muscle during exercise. *The Journal of Physiology*. 574 (Pt 3), pp. 889-903.
- Ruberg, F.L., Chen, Z., Hua, N., Bigornia, S., Guo, Z., Hallock, K., Jara, H., LaValley, M., Phinikaridou, A., Qiao, Y., Viereck, J., Apovian, C.M., and Hamilton, J.A. (2010) The relationship of ectopic lipid accumulation to cardiac and vascular function in obesity and metabolic syndrome. *Obesity (Silver Spring)*. 18 (6), pp. 1116-1121.
- Rui, L. (2014) Energy metabolism in the liver. *Comprehensive Physiology*. 4 (1), pp. 177-197.
- Rustaeus, S., Lindberg, K., Stillemark, P., Claesson, C., Asp, L., Larsson, T., Borén, J., and Olofsson, S.O. (1999) Assembly of Very Low Density Lipoprotein: A Two-Step Process of Apolipoprotein B Core Lipidation. *The Journal of Nutrition*. 129 (2), pp. 463S-466S.
- Rynders, C.A., Blanc, S., DeJong, N., Bessesen, D.H., and Bergouignan, A. (2018) Sedentary behaviour is a key determinant of metabolic inflexibility. *The Journal of Physiology*. 596 (8), pp. 1319-1330.

- Sabaratnam, R., Pedersen, A.J., Eskildsen, T.V., Kristensen, J.M., Wojtaszewski, J., and Højlund, K. (2019) Exercise Induction of Key Transcriptional Regulators of Metabolic Adaptation in Muscle Is Preserved in Type 2 Diabetes. *The Journal of Clinical Endocrinology and Metabolism*. 104 (10), pp. 4909-4920.
- Sacchetti, M., Saltin, B., Osada, T., and van Hall, G. (2002) Intramuscular fatty acid metabolism in contracting and non-contracting human skeletal muscle. *The Journal of Physiology*. 540 (Pt 1), pp. 387-395.
- Sacchetti, M., Saltin, B., Olsen, D.B., and van Hall, G. (2004) High triacylglycerol turnover rate in human skeletal muscle. *The Journal of Physiology*. 561 (Pt 3), pp. 883-891.
- Saggerson, D., Ghadiminejad, I., and Awan, M. (1992) Regulation of Mitochondrial Carnitine Palmitoyl Transferases from Liver and Extrahepatic Tissues. *Advances in Enzyme Regulation*. 32, pp. 285-306.
- Saha, A.K., Vavvas, D., Kurowski, T.G., Apazidis, A., Witters, L.A., Shafrir, E., and Ruderman, N.B. (1997) Malonyl-CoA regulation in skeletal muscle: its link to cell citrate and the glucose-fatty acid cycle. *The American Journal of Physiology*. 272 (4 Pt 1), pp. E641-E648.
- Sakurai, Y., Tamura, Y., Takeno, K., Kumashiro, N., Sato, F., Kakehi, S., Ikeda, S., Ogura, Y., Saga, N., Naito, H., Katamoto, S., Fujitani, Y., Hirose, T., Kawamori, R., and Watada, H. (2011) Determinants of intramyocellular lipid accumulation after dietary fat loading in non-obese men. *Journal of Diabetes Investigation*. 2 (4), pp. 310-317.
- Salo, V.T., Belevich, I., Li, S., Karhinen, L., Vihinen, H., Vigouroux, C., Magré, J., Thiele, C., Hölttä-Vuori, M., Jokitalo, E., and Ikonen, E. (2016) Seipin regulates ER-lipid droplet contacts and cargo delivery. *The EMBO J*. 35 (24), pp. 2699-2716.
- Sanchez, A.M., Candau, R.B., and Bernardi, H. (2014) FoxO transcription factors: their roles in the maintenance of skeletal muscle homeostasis. *Cellular and Molecular Life Sciences: CMLS*. 71 (9), pp. 1657-1671.

Sano, H., Kane, S., Sano, E., Miinea, C.P., Asara, J.M., Lane, W.S., Garner, C.W., and Lienhard, G.E. (2003) Insulin-stimulated phosphorylation of a Rab GTPase-activating protein regulates GLUT4 translocation. *The Journal of Biological Chemistry*. 278 (17), pp. 14599-14602.

Schenk, S., and Horowitz, J.F. (2007) Acute exercise increases triglyceride synthesis in skeletal muscle and prevents fatty acid-induced insulin resistance. *Journal of Clinical Investigation*. 117 (6), pp. 1690-1698.

Schiaffino, S., and Reggiani, C. (2011) Fiber types in mammalian skeletal muscles. *Physiological Reviews*. 91 (4), pp. 1447-1531.

Schmitz-Peiffer, C., and Biden, T.J. (2008) Protein kinase C function in muscle, liver, and beta-cells and its therapeutic implications for type 2 diabetes. *Diabetes*. 57 (7), pp. 1774-1783.

Schönfeld, P. and Wojtczak, L. (2016) Short- and medium-chain fatty acids in energy metabolism: the cellular perspective. *Journal of Lipid Research*. 57 (6), pp. 943-954.

Schönfeld, P., and Reiser, G. (2013) Why does brain metabolism not favor burning of fatty acids to provide energy? Reflections on disadvantages of the use of free fatty acids as fuel for brain. *Journal of Cerebral Blood Flow and Metabolism: Official Journal of The International Society of Cerebral Blood Flow and Metabolism*. 33 (10), pp. 1493-1499.

Schuldiner, M., and Bohnert, M. (2017) A different kind of love – lipid droplet contact sites. *Biochimica et Biophysica Acta (BBA) - Molecular and Cell Biology of Lipids*. 1862 (10, Part B), pp. 1188-1196.

Schulz, L.O., and Chaudhari, L.S. (2015) High-Risk Populations: The Pimas of Arizona and Mexico. *Current Obesity Reports*. 4 (1), pp. 92-98.

Serrano, N., Colenso-Semple, L.M., Lazauskus, K.K., Siu, J.W., Bagley, J.R., Lockie, R.G., Costa, P.B., and Galpin, A.J. (2019) Extraordinary fast-twitch fiber abundance in elite weightlifters. *PloS One*. 14 (3), e0207975.

Shaw, C.S., Shepherd, S.O., Wagenmakers, A.J., Hansen, D., Dendale, P., and van Loon, L.J. (2012) Prolonged exercise training increases intramuscular

lipid content and perilipin 2 expression in type I muscle fibers of patients with type 2 diabetes. *American Journal of Physiology. Endocrinology and Metabolism*. 303 (9), pp. E1158-E1165.

Shindou, H., Hishikawa, D., Harayama, T., Yuki, K., and Shimizu, T. (2009) Recent progress on acyl CoA: lysophospholipid acyltransferase research. *Journal of Lipid Research*. 50 (Suppl), pp. S46-S51.

Sidossis, L.S., and Wolfe, R.R. (1996) Glucose and insulin-induced inhibition of fatty acid oxidation: the glucose-fatty acid cycle reversed. *The American Journal of Physiology*. 270 (4 Pt 1), pp. E733-E738.

Sinha, R., Dufour, S., Petersen, K.F., LeBon, V., Enoksson, S., Ma, Y.Z., Savoye, M., Rothman, D.L., Shulman, G.I., and Caprio, S. (2002) Assessment of skeletal muscle triglyceride content by ¹H nuclear magnetic resonance spectroscopy in lean and obese adolescents: relationships to insulin sensitivity, total body fat, and central adiposity. *Diabetes*. 51 (4), pp. 1022-1027.

Sjöros, T., Vähä-Ypyä, H., Laine, S., Garthwaite, T., Lahesmaa, M., Laurila, S.M., Latva-Rasku, A., Savolainen, A., Miikkulainen, A., Löyttyniemi, E., Sievänen, H., Kalliokoski, K.K., Knuuti, J., Vasankari, T., and Heinonen, I. (2020) Both sedentary time and physical activity are associated with cardiometabolic health in overweight adults in a 1 month accelerometer measurement. *Scientific Reports*. 10 (1), 20578.

Smerdu, V., Karsch-Mizrachi, I., Campione, M., Leinwand, L., and Schiaffino, S. (1994) Type IIx myosin heavy chain transcripts are expressed in type IIb fibers of human skeletal muscle. *The American Journal of Physiology*. 267 (6 Pt 1), pp. C1723-C1728.

Solinas, G., Borén, J., and Dulloo, A.G. (2015) De novo lipogenesis in metabolic homeostasis: More friend than foe? *Molecular Metabolism*. 4 (5), pp. 367-377.

Spriet L.L. (2014) New insights into the interaction of carbohydrate and fat metabolism during exercise. *Sports Medicine (Auckland, N.Z.)*. 44 (Suppl 1), pp. S87-S96.

Spriet, L.L. (1992) Anaerobic metabolism in human skeletal muscle during short-term, intense activity. *Canadian Journal of Physiology and Pharmacology*. 70 (1), pp. 157-165.

Sriwijitkamol, A., Coletta, D.K., Wajcberg, E., Balbontin, G.B., Reyna, S.M., Barrientes, J., Eagan, P.A., Jenkinson, C.P., Cersosimo, E., DeFronzo, R.A., Sakamoto, K., and Musi, N. (2007) Effect of acute exercise on AMPK signaling in skeletal muscle of subjects with type 2 diabetes: a time-course and dose-response study. *Diabetes*. 56 (3), pp. 836-848.

Staron, R.S., Hikida, R.S., Murray, T.F., Hagerman, F.C., and Hagerman, M.T. (1989) Lipid depletion and repletion in skeletal muscle following a marathon. *Journal of the Neurological Sciences*. 94 (1-3), pp. 29-40.

Steinberg, G.R., and Carling, D. (2019) AMP-activated protein kinase: the current landscape for drug development. *Nature Reviews. Drug Discovery*. 18 (7), pp. 527-551.

Steinberg, S.F. (2008) Structural basis of protein kinase C isoform function. *Physiological Reviews*. 88 (4), pp. 1341-1378.

Stellingwerff, T., Boon, H., Jonkers, R.A., Senden, J.M., Spriet, L.L., Koopman, R., and van Loon, L.J. (2007) Significant intramyocellular lipid use during prolonged cycling in endurance-trained males as assessed by three different methodologies. *American Journal of Physiology. Endocrinology and Metabolism*. 292 (6), pp. E1715-E1723.

Stenmark, H. (2009) Rab GTPases as coordinators of vesicle traffic. *Nature Reviews Molecular Cell Biology*. 10 (8), pp. 513-525.

Storch, J., and Thumser, A.E. (2010) Tissue-specific functions in the fatty acid-binding protein family. *The Journal of Biological Chemistry*. 285 (43), pp. 32679-32683.

Storlien, L., Oakes, N.D., and Kelley, D.E. (2004) Metabolic flexibility. *The Proceedings of The Nutrition Society*. 63 (2), pp. 363-368.

Stratford, S., Hoehn, K.L., Liu, F., and Summers, S.A. (2004) Regulation of insulin action by ceramide: dual mechanisms linking ceramide accumulation to

the inhibition of Akt/protein kinase B. *The Journal of Biological Chemistry*. 279 (35), pp. 36608-36615.

Stuart, C.A., Shangraw, R.E., Prince, M.J., Peters, E.J., and Wolfe, R.R. (1988) Bed-rest-induced insulin resistance occurs primarily in muscle. *Metabolism*. 37 (8), pp. 802-806.

Suganami T., Tanaka, M., Ogawa, Y. (2012) Adipose tissue inflammation and ectopic lipid accumulation. *Endocrine Journal*. 59 (10), pp. 849-857.

Sugden, M.C., Kraus, A., Harris, R.A., and Holness, M.J. (2000) Fibre-type specific modification of the activity and regulation of skeletal muscle pyruvate dehydrogenase kinase (PDK) by prolonged starvation and refeeding is associated with targeted regulation of PDK isoenzyme 4 expression. *The Biochemical Journal*. 346 (Pt 3), pp. 651-657.

Sugi, H., Minoda, H., Inayoshi, Y., Yumoto, F., Miyakawa, T., Miyauchi, Y., Tanokura, M., Akimoto, T., Kobayashi, T., Chaen, S., and Sugiura, S. (2008) Direct demonstration of the cross-bridge recovery stroke in muscle thick filaments in aqueous solution by using the hydration chamber. *Proceedings of the National Academy of Sciences of the United States of America*. 105 (45), pp. 17396-17401.

Sun, J., Aluvila, S., Kotaria, R., Mayor, J.A., Walters, D.E., and Kaplan, R.S. (2010) Mitochondrial and Plasma Membrane Citrate Transporters: Discovery of Selective Inhibitors and Application to Structure/Function Analysis. *Molecular and Cellular Pharmacology*. 2 (3), pp. 101-110.

Sutherland, C., Leighton, I.A., and Cohen, P. (1993) Inactivation of glycogen synthase kinase-3 beta by phosphorylation: new kinase connections in insulin and growth-factor signalling. *The Biochemical Journal*. 296 (Pt 1), pp. 15-19.

Szendroedi, J., Yoshimura, T., Phielix, E., Koliaki, C., Marcucci, M., Zhang, D., Jelenik, T., Müller, J., Herder, C., Nowotny, P., Shulman, G.I., and Roden, M. (2014) Role of diacylglycerol activation of PKC θ in lipid-induced muscle insulin resistance in humans. *Proceedings of the National Academy of Sciences of the United States of America*. 111 (26), pp. 9597-9602.

Talanian, J.L., Holloway, G.P., Snook, L.A., Heigenhauser, G.J., Bonen, A., and Spriet, L.L. (2010) Exercise training increases sarcolemmal and mitochondrial fatty acid transport proteins in human skeletal muscle. *American Journal of Physiology. Endocrinology and Metabolism*. 299 (2), E180-E188.

Talanian, J.L., Tunstall, R.J., Watt, M.J., Duong, M., Perry, C.G., Steinberg, G.R., Kemp, B.E., Heigenhauser, G.J., and Spriet, L.L. (2006) Adrenergic regulation of HSL serine phosphorylation and activity in human skeletal muscle during the onset of exercise. *American Journal of Physiology. Regulatory, Integrative and Comparative Physiology*. 291 (4), R1094-R1099.

Talbot, J., and Maves, L. (2016) Skeletal muscle fiber type: using insights from muscle developmental biology to dissect targets for susceptibility and resistance to muscle disease. *Wiley Interdisciplinary Reviews. Developmental Biology*. 5 (4), pp. 518-534.

Tan, C.Y., and Vidal-Puig, A. (2008) Adipose tissue expandability: the metabolic problems of obesity may arise from the inability to become more obese. *Biochemical Society Transactions*. 36 (Pt 5), pp. 935-940.

Tanaka, T., Yamamoto, J., Iwasaki, S., Asaba, H., Hamura, H., Ikeda, Y., Watanabe, M., Magoori, K., Ioka, R. X., Tachibana, K., Watanabe, Y., Uchiyama, Y., Sumi, K., Iguchi, H., Ito, S., Doi, T., Hamakubo, T., Naito, M., Auwerx, J., Yanagisawa, M., Kodama, T. and Sakai, J. (2003) Activation of peroxisome proliferator-activated receptor delta induces fatty acid beta-oxidation in skeletal muscle and attenuates metabolic syndrome. *Proceedings of the National Academy of Sciences of the United States of America*. 100 (26), pp. 15924-15929.

Tan-Chen, S., Guitton, J., Bourron, O., Le Stunff, H., and Hajdouch, E. (2020) Sphingolipid Metabolism and Signaling in Skeletal Muscle: From Physiology to Physiopathology. *Frontiers in Endocrinology*. 11, 491.

Taylor, A.W., Essén, B., and Saltin, B. (1974) Myosin ATPase in skeletal muscle of healthy men. *Acta Physiologica Scandinavica*. 91 (4), pp. 568-570.

Tegtmeyer, L.C., Rust, S., van Scherpenzeel, M., Ng, B.G., Losfeld, M.E., Timal, S., Raymond, K., He, P., Ichikawa, M., Veltman, J., Huijben, K., Shin,

Y.S., Sharma, V., Adamowicz, M., Lammens, M., Reunert, J., Witten, A., Schrapers, E., Matthijs, G., Jaeken, J., Rymen, D., Stojkovic, T., Laforêt, P., Petit, F., Aumaitre, O., Czarnowska, E., Piraud, M., Podskarbi, T., Stanley, C.A., Matalon, R., Burda, P., Seyyedi, S., Debus, V., Socha, P., Sykut-Cegielska, J., van Spronsen, F., de Meirleir, L., Vajro, P., DeClue, T., Ficicioglu, C., Wada, Y., Wevers, R.A., Vanderschaeghe, D., Callewaert, N., Fingerhut, R., van Schaftingen, E., Freeze, H.H., Morava, E., Lefeber, D.J., and Marquardt, T. (2014) Multiple phenotypes in phosphoglucomutase 1 deficiency. *The New England Journal of Medicine*. 370 (6), pp. 533-542.

Tesch, P.A., and Karlsson, J. (1985) Muscle fiber types and size in trained and untrained muscles of elite athletes. *Journal of Applied Physiology (Bethesda, Md.: 1985)*. 59 (6), pp. 1716-1720.

Thai, M.V., Guruswamy, S., Cao, K.T., Pessin, J.E., and Olson, A.L. (1998) Myocyte enhancer factor 2 (MEF2)-binding site is required for GLUT4 gene expression in transgenic mice. Regulation of MEF2 DNA binding activity in insulin-deficient diabetes. *The Journal of Biological Chemistry*. 273 (23), pp. 14285-14292.

Thiam, A.R., Farese, R.V. Jr., and Walther, T.C. (2013) The biophysics and cell biology of lipid droplets. *Nature Reviews Molecular Cell Biology*. 14 (12), pp. 775-786.

Tornqvist, H., and Belfrage, P. (1976) Purification and some properties of a monoacylglycerol-hydrolyzing enzyme of rat adipose tissue. *The Journal of Biological Chemistry*. 251 (3), pp. 813-819.

Tovar-Méndez, A., Hirani, T.A., Miernyk, J.A., and Randall, D.D. (2005) Analysis of the catalytic mechanism of pyruvate dehydrogenase kinase. *Archives of Biochemistry and Biophysics*. 434 (1), pp. 159-168.

Trappe, S., Luden, N., Minchev, K., Raue, U., Jemiolo, B., and Trappe, T.A. (2015) Skeletal muscle signature of a champion sprint runner. *Journal of Applied Physiology (Bethesda, Md.: 1985)*. 118 (12), pp. 1460-1466.

Trebbak, J.T., Glund, S., Deshmukh, A., Klein, D.K., Long, Y.C., Jensen, T.E., Jørgensen, S.B., Viollet, B., Andersson, L., Neumann, D., Wallimann, T.,

- Richter, E.A., Chibalin, A.V., Zierath, J.R., and Wojtaszewski, J.F. (2006) AMPK-mediated AS160 phosphorylation in skeletal muscle is dependent on AMPK catalytic and regulatory subunits. *Diabetes*. 55 (7), pp. 2051-2058.
- Tsintzas, K., Jewell, K., Kamran, M., Laithwaite, D., Boonsong, T., Littlewood, J., Macdonald, I., and Bennett, A. (2006) Differential regulation of metabolic genes in skeletal muscle during starvation and refeeding in humans. *The Journal of Physiology*. 575 (Pt 1), pp. 291-303.
- Turpin-Nolan, S.M., Hammerschmidt, P., Chen, W., Jais, A., Timper, K., Awazawa, M., Brodesser, S., and Brüning, J.C. (2019) CerS1-Derived C_{18:0} Ceramide in Skeletal Muscle Promotes Obesity-Induced Insulin Resistance. *Cell Reports*. 26 (1), pp. 1–10.e7.
- Uchida, Y., and Park, K. (2021) Ceramides in Skin Health and Disease: An Update. *American Journal of Clinical Dermatology*. 22 (6), pp. 853-866.
- Unger, R.H., Clark, G.O., Scherer, P.E., and Orci L. (2010) Lipid homeostasis, lipotoxicity and the metabolic syndrome. *Biochimica et Biophysica Acta*. 1801 (3), pp. 209-214.
- Vaag, A.A., Handberg, A., Skøtt, P., Richter, E.A., and Beck-Nielsen, H. (1994) Glucose-fatty acid cycle operates in humans at the levels of both whole body and skeletal muscle during low and high physiological plasma insulin concentrations. *European Journal of Endocrinology*. 130 (1), pp. 70-79.
- Van Der Vusse, G.J., Glatz, J.F., Stam, H.C., and Reneman, R.S. (1992) Fatty Acid Homeostasis in the Normoxic and Ischemic Heart. *Physiological Review*. 72 (4), pp. 881-940.
- van Loon, L.J., Greenhaff, P.L., Constantin-Teodosiu, D., Saris, W.H., and Wagenmakers, A.J. (2001) The effects of increasing exercise intensity on muscle fuel utilisation in humans. *The Journal of Physiology*. 536 (Pt1), pp. 295-304.
- van Loon L.J. (2004) Use of intramuscular triacylglycerol as a substrate source during exercise in humans. *Journal of Applied Physiology (Bethesda, Md.: 1985)*. 97 (4), pp. 1170-1187.

- Vance, J.E. (2015) Phospholipid synthesis and transport in mammalian cells. *Traffic (Copenhagen, Denmark)*. 16 (1), pp. 1-18.
- Varga, T., Czimmerer, Z., and Nagy, L. (2011) PPARs are a unique set of fatty acid regulated transcription factors controlling both lipid metabolism and inflammation. *Biochimica et Biophysica Acta*. 1812 (8), pp. 1007-1022.
- Verbrugge, S.A.J., Alhusen, J.A., Kempin, S., Pillon, N.J., Rozman, J., Wackerhage, H., and Kleinert, M. (2022) Genes controlling skeletal muscle glucose uptake and their regulation by endurance and resistance exercise. *Journal of Cellular Biochemistry*. 123 (2), pp. 202-214.
- Violante, S., Ijlst, L., van Lenthe, H., de Almeida, I.T., Wanders, R.J., and Ventura, F.V. (2010) Carnitine palmitoyltransferase 2: New insights on the substrate specificity and implications for acylcarnitine profiling. *Biochimica et Biophysica Acta*. 1802 (9), pp. 728-732.
- Višnjić, D., Lalić, H., Dembitz, V., Tomić, B., and Smoljo, T. (2021) AICAr, a Widely Used AMPK Activator with Important AMPK-Independent Effects: A Systematic Review. *Cells*. 10 (5), 1095.
- Wahren, J., Felig, P., Ahlborg, G., and Jorfeldt, L. (1971) Glucose metabolism during leg exercise in man. *The Journal of Clinical Investigation*. 50 (12), pp. 2715-2725.
- Wakil, S.J., Stoops, J.K., and Joshi, V.C. (1983) Fatty acid synthesis and its regulation. *Annual review of biochemistry*. 52, pp. 537-579.
- Walther, T.C., and Farese, R.V. Jr. (2009) The life of lipid droplets. *Biochimica et Biophysica Acta (BBA) - Molecular and Cell Biology of Lipids*. 1791 (6), pp. 459-466.
- Walther, T.C., and Farese, R.V. Jr. (2012) Lipid droplets and cellular lipid metabolism. *Annual Review of Biochemistry*. 81, pp. 687-714.
- Wanders, R., Vaz, F.M., Waterham, H.R., and Ferdinandusse, S. (2020) Fatty Acid Oxidation in Peroxisomes: Enzymology, Metabolic Crosstalk with Other Organelles and Peroxisomal Disorders. *Advances in Experimental Medicine and Biology*. 1299, pp. 55-70.

- Wang, H., Airola, M.V., and Reue, K. (2017) How lipid droplets "TAG" along: Glycerolipid synthetic enzymes and lipid storage. *Biochimica et Biophysica Acta. Molecular and Cell Biology of Lipids*. 1862 (10 Pt B), pp. 1131-1145.
- Wang, L., Qian, H., Nian, Y., Han, Y., Ren, Z., Zhang, H., Hu, L., Prasad, B., Laganowsky, A., Yan, N., and Zhou, M. (2020) Structure and mechanism of human diacylglycerol O-acyltransferase 1. *Nature*. 581 (7808), pp. 329-332.
- Wasserman D.H. (2009) Four grams of glucose. *American Journal of Physiology. Endocrinology and metabolism*. 296 (1), pp. E11-E21.
- Watt, K.I., Henstridge, D.C., Ziemann, M., Sim, C.B., Montgomery, M.K., Samocha-Bonet, D., Parker, B.L., Dodd, G.T., Bond, S.T., Salmi, T.M., Lee, R.S., Thomson, R.E., Hagg, A., Davey, J.R., Qian, H., Koopman, R., El-Osta, A., Greenfield, J.R., Watt, M.J., Febbraio, M.A., Drew, B.G., Cox, A.G., Porrello, E.R., Harvey, K.F., and Gregorevic, P. (2021) Yap regulates skeletal muscle fatty acid oxidation and adiposity in metabolic disease. *Nature Communications*. 12 (1), 2887.
- Watt, M.J., and Spriet, L.L. (2004) Regulation and role of hormone-sensitive lipase activity in human skeletal muscle. *The Proceedings of the Nutrition Society*. 63 (2), pp. 315-322.
- Watt, M.J., Heigenhauser, G.J., and Spriet, L.L. (2003) Effects of dynamic exercise intensity on the activation of hormone-sensitive lipase in human skeletal muscle. *The Journal of Physiology*. 547 (Pt 1), pp. 301-308.
- Watt, M.J., Heigenhauser, G.J., Dyck, D.J., and Spriet, L.L. (2002) Intramuscular triacylglycerol, glycogen and acetyl group metabolism during 4 h of moderate exercise in man. *The Journal of Physiology*. 541 (3), pp. 969-978.
- White, M.F. (2002) IRS Proteins and the Common Path to Diabetes. *American Journal of Physiology: Endocrinology and Metabolism*. 283 (3), pp. e413-e422.
- Wilfling, F., Haas, J.T., Walther, T.C., and Farese, R.V., Jr. (2014) Lipid droplet biogenesis. *Current Opinion in Cell Biology*. 29, pp. 39-45.

- Wilfling, F., Wang, H., Haas, J.T., Krahmer, N., Gould, T.J., Uchida, A., Cheng, J.X., Graham, M., Christiano, R., Fröhlich, F., Liu, X., Buhman, K.K., Coleman, R.A., Bewersdorf, J., Farese, R.V., Jr, and Walther, T.C. (2013) Triacylglycerol synthesis enzymes mediate lipid droplet growth by relocating from the ER to lipid droplets. *Developmental Cell*. 24 (4), pp. 384-399.
- Wilson, J.E. (2003) Isozymes of mammalian hexokinase: structure, subcellular localization and metabolic function. *Journal of Experimental Biology*. 206 (12), pp. 2049-2057.
- Wilson, J.M., Loenneke, J.P., Jo, E., Wilson, G.J., Zourdos, M.C., and Kim, J.S. (2012) The effects of endurance, strength, and power training on muscle fiber type shifting. *Journal of Strength and Conditioning Research*. 26 (6), pp. 1724-1729.
- Winkler, F.K., D'Arcy, A., and Hunziker, W. (1990) Structure of human pancreatic lipase. *Nature*. 343 (6260), pp. 771-774.
- Witczak, C.A., Fujii, N., Hirshman, M.F., and Goodyear, L.J. (2007) Ca²⁺/calmodulin-dependent protein kinase kinase- α regulates skeletal muscle glucose uptake independent of AMP-activated protein kinase and Akt activation. *Diabetes*. 56 (5), pp. 1403-1409.
- Wojtaszewski, J.F., Lynge, J., Jakobsen, A.B., Goodyear, L.J., and Richter, E.A. (1999) Differential regulation of MAP kinase by contraction and insulin in skeletal muscle: metabolic implications. *The American Journal of Physiology*. 277 (4), pp. E724-E732.
- Woods, A., Johnstone, S.R., Dickerson, K., Leiper, F.C., Fryer, L.G., Neumann, D., Schlattner, U., Wallimann, T., Carlson, M., and Carling, D. (2003) LKB1 is the upstream kinase in the AMP-activated protein kinase cascade. *Current Biology: CB*. 13 (22), pp. 2004–2008.
- Wright, D.C., Hucker, K.A., Holloszy, J.O., and Han, D.H. (2004) Ca²⁺ and AMPK both mediate stimulation of glucose transport by muscle contractions. *Diabetes*. 53 (2), pp. 330-335.
- Xiao, B., Heath, R., Saiu, P., Leiper, F.C., Leone, P., Jing, C., Walker, P.A., Haire, L., Eccleston, J.F., Davis, C.T., Martin, S.R., Carling, D., and Gamblin,

- S.J. (2007) Structural basis for AMP binding to mammalian AMP-activated protein kinase. *Nature*. 449 (7161), pp. 496-500.
- Yamazaki, N., Shinohara, Y., Shima, A., Yamanaka, Y., and Terada, H. (1996) Isolation and characterization of cDNA and genomic clones encoding human muscle type carnitine palmitoyltransferase I. *Biochimica et Biophysica Acta*. 1307 (2), pp. 157-161.
- Yli-Jokipii, K.M., Schwab, U.S., Tahvonen, R.L., Kurvinen, J.P., Mykkänen, H.M., and Kallio, H.P. (2003) Chylomicron and VLDL TAG structures and postprandial lipid response induced by lard and modified lard. *Lipids*. 38 (7), pp. 693-703.
- Yoon, M.S. (2017) The Role of Mammalian Target of Rapamycin (mTOR) in Insulin Signaling. *Nutrients*. 9 (11), 1176.
- Youn, J.H., Gulve, E.A., and Holloszy, J.O. (1991) Calcium stimulates glucose transport in skeletal muscle by a pathway independent of contraction. *The American Journal of Physiology*. 260 (3 Pt 1), pp. C555-C561.
- Young, M.E., Goodwin, G.W., Ying, J., Guthrie, P., Wilson, C.R., Laws, F.A., and Taegtmeyer, H. (2001) Regulation of cardiac and skeletal muscle malonyl-CoA decarboxylase by fatty acids. *American Journal of Physiology: Endocrinology and Metabolism*. 280 (3), pp. E471-E479.
- Zacharewicz, E., Hesselink, M., and Schrauwen, P. (2018) Exercise counteracts lipotoxicity by improving lipid turnover and lipid droplet quality. *Journal of Internal Medicine*. 284 (5), pp. 505-518.
- Zderic, T.W., Davidson, C.J., Schenk, S., Byerley, L.O. and Coyle, E.F. (2004) High-fat diet elevates resting intramuscular triglyceride concentration and whole body lipolysis during exercise. *American Journal of Physiology: Endocrinology and Metabolism*. 286 (2), pp. E217-E225.
- Zhang, X., Tang, N., Hadden, T.J., and Rishi, A.K. (2011) Akt, FoxO and regulation of apoptosis. *Biochimica et Biophysica Acta*. 1813 (11), pp. 1978-1986.

Zierler, K.L. (1976) Fatty Acids as Substrates for Heart and Skeletal Muscle. *Circulation Research*. 38 (6), pp. 459-463.

Zimmermann, R., Strauss, J.G., Haemmerle, G., Schoiswohl, G., Birner-Gruenberger, R., Riederer, M., Lass, A., Neuberger, G., Eisenhaber, F., Hermetter, A., and Zechner, R. (2004) Fat mobilization in adipose tissue is promoted by adipose triglyceride lipase. *Science (New York, N.Y.)*. 306 (5700), pp. 1383-1386.

Zouhal, H., Jacob, C., Delamarche, P., and Gratas-Delamarche, A. (2008) Catecholamines and the effects of exercise, training and gender. *Sports Medicine (Auckland, N.Z.)*, 38 (5), pp. 401-423.

2. General Methods

This chapter describes the principles and protocols for the methods that are common to each experimental chapter (**Chapters 3, 4, and 5**). Study specific protocols and methods are detailed in the relevant chapters.

2.1 Hyperinsulinaemic-Euglycemic Clamp Technique in the Measurement of Whole-Body Glucose Disposal

2.1.1 Overview of the Hyperinsulinaemic-Euglycaemic Clamp

The hyperinsulinaemic-euglycaemic clamp technique (DeFronzo, Tobin and Andres, 1979) is a method for the assessment of whole-body tissue sensitivity to insulin in fasting participants.

First, a loading dose of exogenous insulin (Human Actrapid, EMEA/H/C/000424; Novo Nordisk A/S, Bagsværd, Denmark) is infused into the participant for 10 minutes through a cannulated antecubital vein to raise plasma insulin concentration. Then insulin is infused at a constant rate, equivalent to 60 mIU/m²/min, to maintain a supraphysiological circulating plasma insulin concentration. This hyperinsulinaemic state blunts hepatic glucose output and stimulates cellular uptake and utilisation of endogenous glucose (Brehm and Roden, 2007). Concurrently, exogenous glucose (20% Dextrose infusion, Baxter Healthcare, Thetford, UK) is infused at a variable rate to achieve and maintain a fixed arterialised venous blood glucose concentration (4.5 mmol/l).

Once the glucose infusion rate reaches a steady-state the rate at which the exogenous glucose is infused will represent the rate at which glucose is being transported into the tissues for that specific plasma insulin concentration. In the studies described herein the use of this technique was primarily performed, and otherwise closely supervised by, Dr. Liz Simpson.

2.1.2 Calculating the M value

The M value represents the milligrams of glucose per kilogram of body weight (mg/ kg/ min) disposed into tissues per minute during the steady state period of the hyperinsulinaemic-euglycaemic clamp for the specific fixed insulin infusion rate at which the clamp is performed.

To calculate the M value, whole blood glucose concentration is measured at 5-minute intervals. The difference in blood glucose concentration between each successive interval and the glucose infusion rate (*GIR*; the variable rate at which exogenous glucose is infused), are also recorded at these 5-minute intervals. The volume of glucose solution infused (*GSI*) during each 5-minute interval is then calculated as follows:

$$GSI (ml) = \frac{GIR (ml/hr)}{60} \times 5$$

(Equation 2-1)

Glucose has a molecular weight of 180.156 g/mol and in the protocols described here 20% w/v solutions were used. To calculate the moles of glucose (*GI*) in the volume of glucose solution infused during the 5-minute interval:

$$GI (mol) = \frac{GSI \times 0.2}{180}$$

$$GI (mmol) = GI (mol) \times 1000$$

(Equation 2-2, 2-3)

To calculate the amount of glucose disposed (*GD*) during a 5-minute interval:

$$GD (mmol/min) = GI (mmol) \times (BG1 - BG0)$$

(Equation 2-4)

Where (*BG1 - BG0*) is the difference in the blood glucose concentration measured at the end of the 5-minute interval (*BG1*) and the beginning of the 5-minute interval (*BG0*). These 5-minute interval glucose disposal values are

then used to calculate 15-minute averages ($\bar{x}GD$) which are standardised to body weight:

$$\bar{x}GD \text{ (mmol/min/kg)} = \frac{\bar{x}GD \text{ (mmol/min)}}{\text{Bodyweight (kg)}} \quad \text{(Equation 2-5)}$$

The final M value is then calculated by multiplying the $\bar{x}GD$ by the molecular weight of glucose as shown in **Equation 2-5**:

$$M \text{ value (mg/min/kg)} = \bar{x}GD \text{ (mmol/min/kg)} \times 180 \quad \text{(Equation 2-6)}$$

2.2 Determination of Body Composition using Dual-Energy X-ray Absorptiometry (DEXA)



Figure 2-1: The Lunar Prodigy DEXA by GE Medical Systems that was used to determine body composition in the participants of the chronic bed rest study detailed in Chapter 3.

Dual energy X-ray absorptiometry (DEXA) is a technique for the assessment of body composition. The principle behind this technique is that the body consists of multiple components which vary in density and that this variation differentially alters the transmission of X-ray photons produced by the flow of

an electrical current through tungsten (Lorenz, 1928; Pietrobelli *et al.*, 1996). The components recognized by DEXA are fat mass, lean mass, and bone mineral content (BMC) as a product of bone density and bone area (Jain and Vokes, 2017). Here lean tissue mass is inclusive of muscle, skin and viscera and can be defined as the fat free mass (FFM) minus the mass of the BMC. As shown in **Figure 2-1**, DEXA scanners primarily consist of a flat table/bed, which contains the main electrical hardware and the X-ray source, and the scanner C-arm which contains the detector.

For the collection of the body composition data presented here, which was conducted by qualified technical personnel within the David Greenfield Human Physiology unit and the Institute for Space Medicine and Physiology in Toulouse, participants were instructed to lie supine on the DEXA table, with their arms away from their trunk and legs separated. The X-ray source was turned on and two beams of high and low energy were transmitted through the participant (Blake and Fogelman, 1997). The photon intensity reaching the detector for each section of the participant scanned was dependent upon the distance through which the X-ray beams travelled and the attenuation these beams experienced as they passed through the participant's different tissue compartments (Allen and Krohn, 2014).

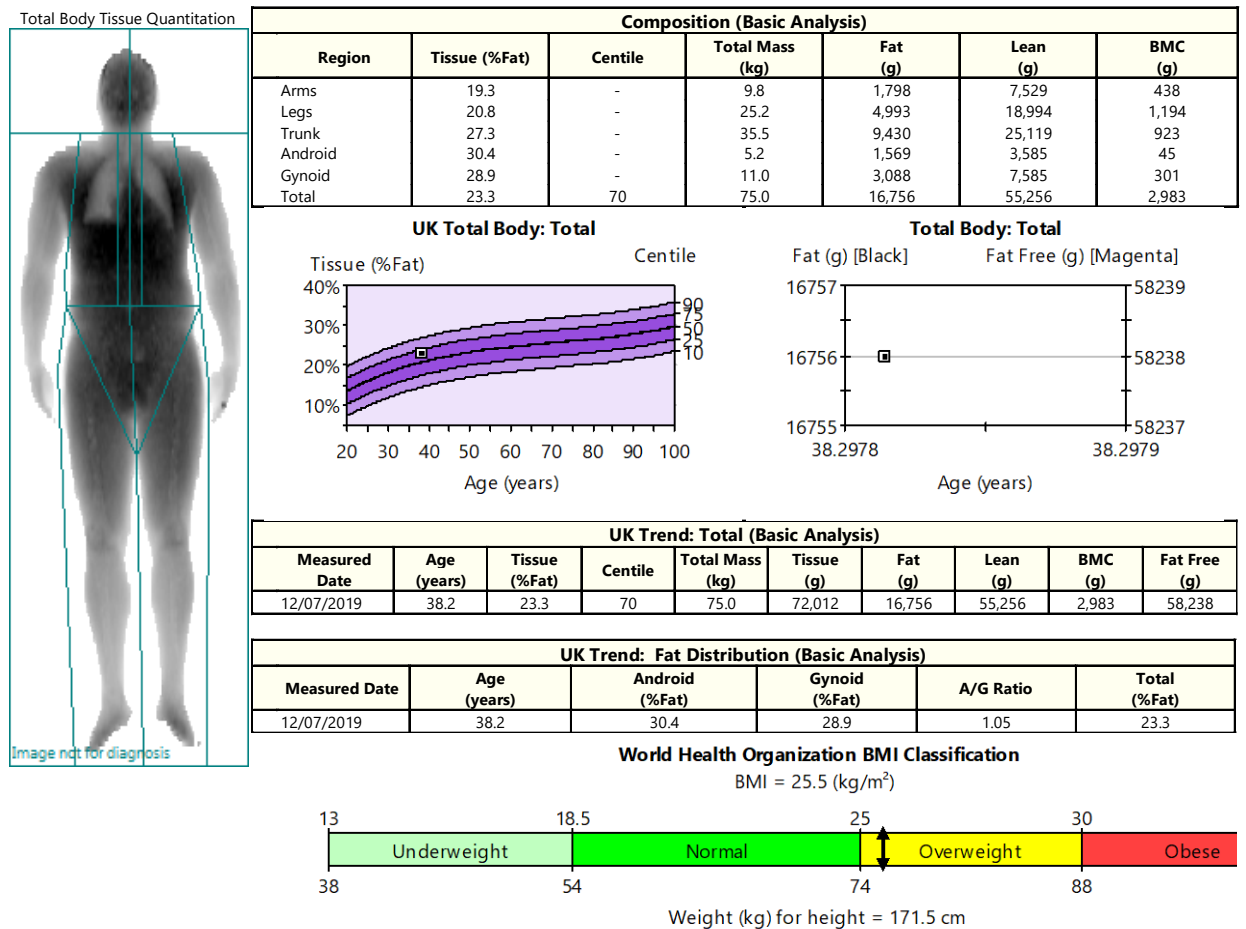


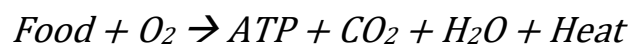
Figure 2-2: Example output for DEXA determination of body composition.

The detector then converted these photon intensities to pixel data. For each pixel an R value representing a ratio of the attenuation experienced by the low energy X-ray beam relative to the high energy beam was calculated by the DEXA system (Pietrobelli *et al.*, 1998). The R value for bone is significantly higher than for lean tissue and fat. In DEXA systems these R values are compared to known thresholds for each component relative to the beam intensities and participant thickness (determined by the height and weight of the participant) such that each pixel can be characterised as containing data from photons attenuated principally by bone, fat, or lean tissue mass (Wang *et al.*, 2010). Using these pixels, two-dimensional scans of the participants were created and the total mass of each component and ancillary data on component mass per distinct region were reported (see **Figure 2-2**). These regions included the head, android and gynoid regions as well as the right/left leg, right/left arm, and right/left side of the trunk.

The T- and Z-scores for each participant were also reported. The T-score represents the number of standard deviations of a participant's total component mass above or below the average value for a young, healthy adult of the same sex. The Z-score represents the standard deviation of a participant's total component mass above or below the average for an age-matched UK reference population of the same sex.

2.3 Indirect Calorimetry

In the body, the generation of energy in the form of adenosine triphosphate (ATP), which is necessary to perform all work, is a metabolic process which requires the consistent supply of glucose and fatty acids as the primary energy substrates and oxygen (O₂) to release the energy stored in these substrates. This reaction releases heat and produces CO₂ and H₂O as by-products such that:



(Equation 2-7)

Indirect calorimetry was used to calculate the O₂ consumption and CO₂ production in participants through the measurement of expired O₂ and CO₂ content of the breath. These measurements were used for the estimation of energy expenditure using the Weir equation and the rate of substrate oxidation using the respiratory exchange ratio (RER) (Haugen, Chen, and Li, 2007).

2.3.1 Indirect Calorimetry in the Estimation of Substrate Oxidation

Carbohydrates, fats, and proteins differ in the stoichiometric amount of O₂ consumed to fully oxidise them and the CO₂ produced as a product of this oxidation. The RER is the ratio of CO₂ production to O₂ consumption during aerobic respiration at the whole-body level and acts as a numeric indicator of the relative contribution of carbohydrates, fats, and proteins to oxidative ATP production:

$$RER = \frac{VCO_2}{VO_2}$$

(Equation 2-8)

During indirect calorimetry, VO_2 consumed and VCO_2 excreted in the breath are calculated by measuring the total volume of inspired (V_i) and expired (V_e) air and then multiplying those values by the fraction of inspired and expired O_2 (FiO_2 and FeO_2) and inspired and expired CO_2 ($FiCO_2$ and $FeCO_2$) in that air, respectively, such that:

$$VO_2 = (V_i \times FiO_2) - (V_e \times FeO_2)$$

$$VCO_2 = (V_e \times FeCO_2) - (V_i \times FiCO_2)$$

(Equation 2-9, 2-10)

Under normal physiological conditions both carbohydrates and fats are oxidised at rest and during physical activity. However, theoretically, if only glucose is oxidised at rest in the equation $C_6H_{12}O_6 + 6O_2 \rightarrow 6H_2O + 6CO_2$, then the RER can be expressed as $(RER = (6/6) = 1)$, given that six mols of O_2 are consumed and six mols of CO_2 are produced for each mole of glucose oxidised. The RER of carbohydrates is therefore = 1. The theoretical, exclusive oxidation of fat molecules at rest yields an RER value ≈ 0.7 , depending on the degree of saturation of the fatty acid (Frayn, 1983). In indirect calorimetry measurements, the closer the RER value is to 1 or 0.7 the greater the contribution of carbohydrates or fats to energy production, respectively. An RER ≈ 0.80 indicates that proteins are predominantly being used, or that a mixture of substrates is being oxidised, for energy production. Physiologically normal RER values fall between 0.7 – 1.1.

2.3.2 Indirect Calorimetry in the Estimation of Energy Expenditure

The measurements of VO_2 and VCO_2 can also be used to estimate total energy expenditure (TEE) using the Weir equation:

$$\dot{M} \text{ (kcal/day)} = 1440 \times ([3.94 \times VO_2 \text{ (litres/min)}] + [1.11 \times VCO_2 \text{ (litres/min)}]) - [2.17 \times uN_2 \text{ (g/day)}]$$

(Equation 2-11)

With 3.94 and 1.11 relating to the calorie value of carbohydrate (Zuntz, 1897) and protein (Cathcart and Cuthbertson, 1931) oxidation per litre of oxygen (Weir, 1949). Urinary nitrogen (uN_2) is typically excluded from this

equation, as it contributes a negligible amount ($\approx 1-2\%$) to energy expenditure (Ferrannini, 1988), such that:

$$\dot{M} \text{ (kcal/day)} = 1440 \times ([3.94 \times VO_2 \text{ (litres/min)}] + [1.11 \times VCO_2 \text{ (litres/min)}])$$

(Equation 2-12)

TEE is a measure of the amount of food energy in calories or kilojoules (kJ) expended per day. TEE has three main components, which can be influenced by an individual's stature (height/weight), body composition (lean/fat mass), age, biological sex, and ethnicity (Dugas *et al.*, 2011). (1) Resting metabolic rate (RMR) is the energy expenditure when the body is at rest. This includes the basal metabolic rate (BMR), the minimum amount of energy that must be expended to maintain the normal bodily functions and homeostatic processes that sustain life. (2) Diet-induced thermogenesis represents the energy expended to metabolise and absorb food, with the production of ATP and heat. (3) The energy expended during various forms of physical activity, activity energy expenditure (AEE). The modified (non-protein) Weir equation is used to estimate the RMR; which is also often referred to as resting energy expenditure (REE).

2.3.3 Indirect Calorimetry Protocol for The Estimation of RMR and Whole-Body Substrate Oxidation

The Quark RMR (COSMED srl, Rome, Italy) ventilated hood indirect calorimeter was used to estimate RMR, RER and the rate of carbohydrate and fat oxidation in participants at rest when fasted and under hyperinsulinaemic-euglycaemic clamp conditions during the 3-day bed-rest study, with the GEM system (GEMNutrition Ltd., Daresbury, United Kingdom) used during the 56-day bedrest and NAFLD studies. This technique was performed by Dr. Liz Simpson on participants lying supine (**Chapter 3**) or in semi-Fowler's position (**Chapter 4**) at rest.

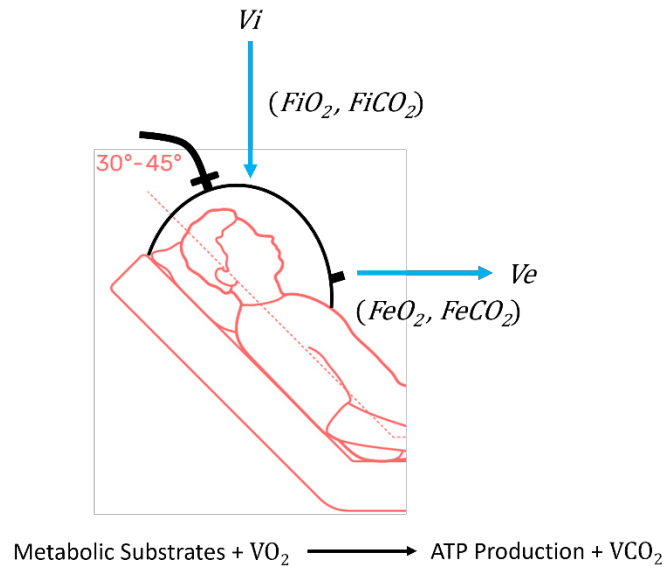


Figure 2-3: Example schematic of the ventilated hood indirect calorimetry system. The participant in red is shown lying in semi-Fowler's position with their head covered by a bubble canopy hood. Participant image adapted from (Dimensions.com, 2022).

The O_2 and CO_2 analysers were calibrated using 2 reference gas mixtures before each measurement, with the flow turbine being calibrated on the morning of each study day using a standard 3-litre syringe. Each participant had rested quietly for more than 15 minutes before the ventilated hood was placed over their head and neck. After a few minutes acclimatising under the hood, formal data collection began. The Quark RMR operates using an open circuit system with mixing chamber (Schoffelen and Plasqui, 2018). When under the hood, participants breathe in atmospheric air that is being drawn into the hood and exhale into the stream of air being extracted by a 0-18 mm bidirectional turbine that controls flow rate (see **Figure 2-3**). VO_2 and VCO_2 are then calculated from measurements of O_2 concentration using a paramagnetic O_2 analyser and CO_2 concentration using a nondispersive infrared detector (see **Section 2.3.1**).

Measurements were performed before and during the last 15 minutes of the hyperinsulinaemic-euglycaemic clamp protocol. Carbohydrate and fat oxidation were standardised for the lean body mass of the participants. The contribution of nitrogen excretion in urine to energy expenditure was excluded, instead the table of nonprotein respiratory quotient developed by Péronnet and

Maissicotte was used to estimate the percentage of carbohydrate/fat oxidation based on the RER (Péronnet and Massicotte, 1991). The Péronnet and Maissicotte equations for nonprotein carbohydrate and fat oxidation are:

$$\text{Carbohydrate (g/min)} = (4.585 \times VCO_2) - (3.226 \times VO_2)$$

$$\text{Fat (g/min)} = (1.695 \times VO_2) - (1.701 \times VCO_2)$$

(Equation 2-13, 2-14)

2.4 Physical Activity Level Assessment Using Accelerometry

Accelerometers were used to calculate the daily AEE and TEE of participants under free-living conditions. This information was particularly important for participants in the bed rest studies detailed in **Chapter 3** as free-living daily energy expenditure informed the daily calorific intake of each participant during bed rest to maintain a balance between energy intake and energy expenditure. These data were collected by Dr. Simpson, Dr. Shur, and the MEDES research team in the studies described in **Chapter 3**, and by Dr. Simpson in the study described in **Chapter 4**.

The accelerometers used in the studies presented herein were tri-axial, capable of recording the lateral (x), vertical (y), and longitudinal (z) movements of the participants that they were fitted on (Yang and Hsu, 2010; Lugade *et al.*, 2014) using micro-electromechanical systems (MEMS) (Yang and Hsu, 2010). MEMS are designed with polysilicon microstructures that form sensory units consisting of proof masses, objects of known mass, connected to the inside of the casing by thin cantilevers (Szermer *et al.*, 2021). The proof masses are positioned equidistant between fixed supports. The air gaps between these proof masses and their supports allow these units to act as capacitors. When the participant is immobile the proof masses do not move. However, as the participant moves, the casing of the accelerometer moves in tandem, and the force of this movement is transferred to the cantilevers. The force transferred to the cantilevers corresponds to the force of acceleration experienced by and displacing the proof masses in each axis. As the masses move, the thickness

of the air gaps changes such that the masses are closer to one of the fixed supports than the other. This creates a change in the electrical charge which is proportional to the participant's acceleration. These changes in charge are converted to 12-bit acceleration waveforms. The accelerometers also functioned as electrocardiograms that recorded ECG traces to monitor the physiological effect of this activity on the heart rate of the participants.

Actiheart physical activity monitors were used for accelerometry measurements in the acute bed rest study described in **Chapter 3** whilst ActiGraph monitors were used for the same purpose in the chronic bed rest study described in **Chapter 3** and the study described in **Chapter 4**. These monitors were worn at the hip and the software associated with them operates in an analogous manner. The specifics of the Actiheart software will be discussed here as an example of the principles by which heart rate and activity count measurements made by these devices are converted to energy expenditure.

During the initial set-up of the Actiheart software, the height, weight, date of birth and biological sex of each participant was programmed into the software. The RMR and sleeping heart rate were also entered into the system. Actiheart software can estimate participant RMR using Schofield equations (Schofield, 1985) which integrate sex, age, and weight such that, for example:

$$RMR \text{ (Male, 18-30 y/o)} = (0.063 \times \text{Weight}) + 2.896$$

$$RMR \text{ (Female, 30-60 y/o)} = (0.062 \times \text{Weight}) + 2.036$$

(Equation 2-15, 2-16)

However, in the studies described in **Chapter 3** measured RMR values calculated from indirect calorimetry were used, see **Section 2.3**, which is accepted by the software. The intervals during which accelerometers record movement and heart rate data are referred to as epochs. The frequency, intensity, and duration of the acceleration frequencies recorded during each epoch were converted to discrete activity counts, with the exclusion of very low frequency signals.

Heart rate and activity count measurements are combined to derive AEE using the Branched Model, which takes into account calibration coefficients derived from multi linear regression equations. This model, which is expanded upon in great detail elsewhere (Brage *et al.*, 2004), is ideal for calculating AEE via accelerometry as using just heart rate or activity count measurements alone inevitably under- or overestimates AEE, respectively, for accelerometers worn at the hip (Ellis *et al.*, 2016).

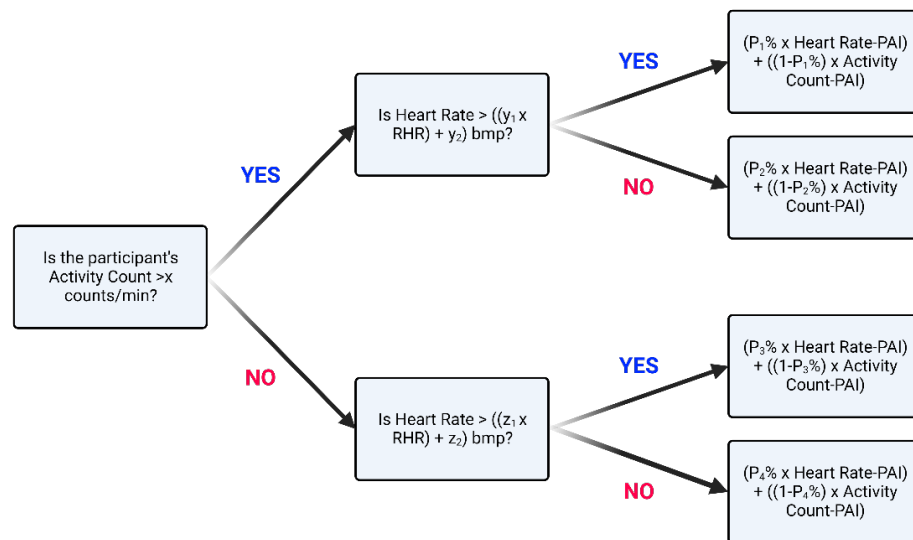


Figure 2-4: Branched equation decision tree for determination of AEE using both heart rate and activity count measurements.

The calculation tree for the Branched Model is shown in **Figure 2-4** and is split into three stages:

1. In the first stage x Activity Counts/minute distinguishes between participants performing physical activity and those at rest.
2. In the second stage the y and z parameters then create heart rate thresholds in the presence and absence of physical activity, respectively, with z representing parameters around the flex heart rate. The flex heart rate is an average of the greatest heart rate during rest and the lowest heart rate during exercise, creating a threshold below which energy is almost exclusively expended as part of the RMR and

above which it is in part expended via physical activity (Leonard, 2003). Where heart rate is $> ((y_1 \times RHR) + y_2)$ beats per minute (bpm) the participant is typically running versus walking if heart rate is $< ((y_1 \times RHR) + y_2)$ bpm, with RHR representing resting heart rate.

3. In the third stage AEE is calculated by integrating physical activity intensity (PAI), which is a minute-to-minute metric measured in kJ/kg/min, with the time/epoch taken for the measurement to be made. This is with respect to P_1 - P_4 , which are different weightings of heart rate and activity count data such that, for example, $P_1 = 0.90$, $P_2 = 0.50$, $P_3 = 0.50$, $P_4 = 0.10$. The *Heart Rate-PAI* and *Activity Count-PAI* terms are given by group calibration multi linear regression equations categorised by age and sex and stored within the software. These validated equations are derived from incremental treadmill exercise studies conducted with Actiheart (heart rate and activity count), peak VO_2 , and direct calorimetry measurements (Brage *et al.*, 2004; Corder *et al.*, 2005; Brage *et al.*, 2005; Assah *et al.*, 2011).

The AEE calculated in this way is added to the inputted RMR to determine daily TEE. Where heart rate data is lost or corrupted this can affect calculations of AEE. To overcome this Actiheart software can perform a cleaning process to recover this missing data. This process has three stages. Firstly, the software identifies “suspect” values, which are either those where heart rate is < 30 bpm or those in which heart rate is > 30 bpm but increases by more than 100 bpm for a 1-minute epoch, or more than 132 and 160 bpm for 30 and 15 second epochs, respectively. Secondly, the software calculates the “filtered heart rate” value which is the average heart rate of the 4 minutes preceding each suspect value. Where any suspect minute value is greater than 1.75x the filtered heart rate it is set to 0. Lastly, where each suspect minute value has been set to 0, each minimum and maximum interbeat interval (IBI) in the preceding minute is used to calculate a recovered heart rate value. The IBI is the interval between individual heart beats within a selected range/epoch. The IBI can act as a surrogate measure of heart rate such that if for example, the time between heart beats is 1 second on average, there will be 60 bpm.

This recovered heart rate value is then compared to the last valid heart rate reading before the suspect minute value. If the recovered heart rate value is within 30 bpm of the last valid reading It will be used to replace the 0 value for the suspect minute value.

This cleaning process is only applied where suspect values or 0 value readings constitute less than 5 recorded minutes. Where such gaps are longer than 5 minutes the values are left as 0 and the cleaning process is disabled. Actiheart software identifies major gaps in daily energy expenditure data by screening for any continuous 2-hour periods in which activity recordings are absent. These gaps can be due to poor adherence to study protocols by the participant or to temporary faults with the device. An autofill option is available which will automatically fill these gaps with the average value of AEE recordings for that day. In the studies presented herein this “autofill” option was not used.

2.5 Estimating Resting Metabolic Rate from equations

The Harris-Benedict equation estimates BMR in calories expended per day and is derived from data collected from a healthy sample population of 136 men, 103 women and 94 infants whose varying height, weight, age, and biological sex were factored into the equation (Harris and Benedict, 1918). As this was a very specific population, the Harris-Benedict equation is not necessarily an accurate predictor of BMR in individuals who are significantly different from the original study population (Haugen, Chen and Li, 2007). The equation was later re-evaluated and modified (Roza and Shizgal, 1984) with the inclusion of data from 94 healthy subjects spanning a wider age range such that:

$$BMR (kcal/day) = 88.362 + (13.397\omega) + (4.799s) - (5.677a)$$

(Equation 2-17)

Where ω , s and a are the weight (kg), stature (cm) and age, respectively, of the participant being assessed, and the constants are values from multiple regression equations calculated using the biometric data of the study populations. This equation acts as a suitable predictor of BMR for

participants aged 21-70, standing 151-200 cm tall and weighing 25-125 kg. The modified Harris-Benedict equation was used to calculate the BMR of participants during the run-in phase of the bed rest studies detailed in **Chapter 3**. This enabled daily energy requirements to be estimated and individually tailored menu plans to be designed. These participants were young, healthy, physically active males within the demographic range of the equation. Participant characteristics are shown in the relevant chapters.

2.6 Blood Analyses

During the hyperinsulinaemic-euglycaemic clamp protocol, a cannula was inserted retrograde into a superficial vein on the dorsal surface of the hand for serial blood sampling. The cannulated hand was kept warm in an air temperature of between 50-55 °C to arterialise venous blood.

Blood samples taken for analysis of plasma FFA concentration were collected into lithium heparin microtubes (Sarstedt Inc., Nümbrecht, Germany), supplemented with 0.5 µl tetrahydrolipstatin and 7.5 µl EGTA - reduced glutathione additive, and immediately centrifuged at 2000 x g for 10 minutes at 4 °C. Following centrifugation, the plasma was aliquoted and then frozen at -80 °C. Tetrahydrolipstatin is a potent non-competitive inhibitor of pancreatic and gastric lipases (Krebs *et al.*, 2000); it binds irreversibly to the serine residues in the active sites of these enzymes, thereby inhibiting the breakdown of triacylglycerides in the plasma samples. EGTA is an anticoagulant (Nielsen, 1985). Blood extracted for analysis of TAG and insulin concentration in serum was collected into microtubes containing a clot activator (Sarstedt Inc., Nümbrecht, Germany), left to clot for 15 minutes, and centrifuged as described above, before being frozen at -80°C. Blood analyses were performed by Sally Corden.

2.6.1 Serum Insulin Concentration

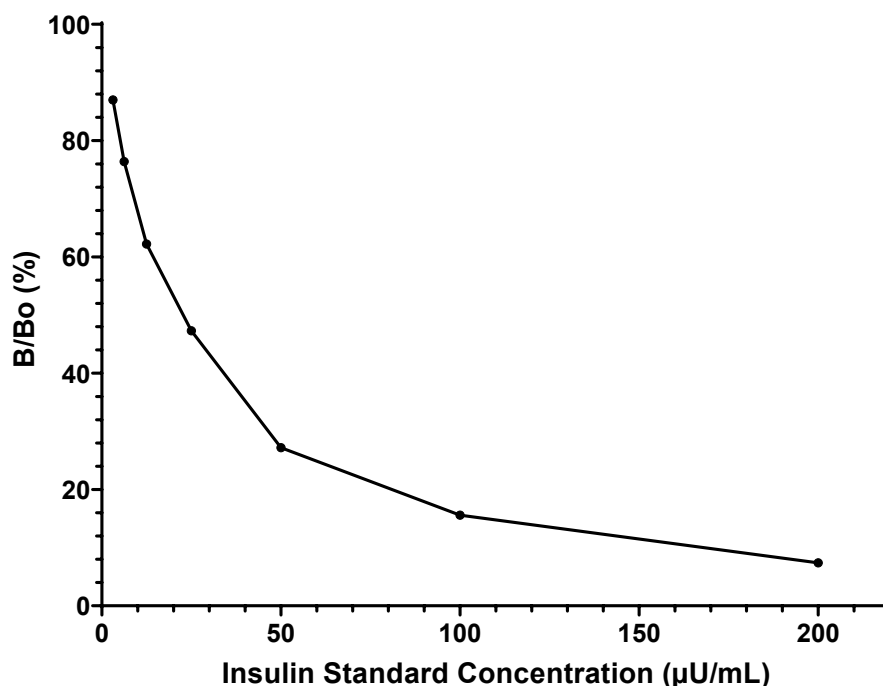


Figure 2-5: Standard insulin concentration curve generated from example assay results presented in the HI-14K insulin radioimmunoassay kit.

Serum insulin concentrations were determined in vitro using the double-antibody radioimmunoassay technique (Yalow and Berson, 1960; Morgan and Lazarow, 1963) with a human insulin specific radioimmunoassay kit (HI-14K, EMD Millipore Corporation, MI, USA).

Briefly, assay buffer (0.05M Phosphosaline pH 7.4 containing 0.025M EDTA, 0.08% Sodium Azide, and 1% BSA) was added to seven glass tubes. The kit provides a 2 ml stock solution of 200 µU/ml purified and unlabelled human insulin in assay buffer for use in making six standard insulin concentrations of 100, 50, 25, 12.5, 6.25 and 3.125 µU/ml. From these six standard solutions and a control solution (containing no unlabelled insulin), 100 µL was added to each of the six glass tubes, respectively, in addition to 100 µL of radioactively labelled, hydrated insulin (¹²⁵I-insulin). The iodine-125 (¹²⁵I) radioisotope readily incorporates into the tyrosine residues of human insulin and emits gamma radiation. The same volume (100 µL) of guinea pig anti-human, insulin specific antibody was then added to these tubes which

were vortexed, covered and left to incubate at room temperature for 24 hours. In this dual antigen, single antibody system, 125 I-insulin and unlabelled insulin compete for the limited binding sites on the anti-human insulin antibodies. This results in the formation of two separate insulin fractions, a bound fraction of insulin-antibody complexes and a free fraction of insulin in suspension. The concentration of 125 I-insulin antigen is kept constant in each tube whilst the concentration of unlabelled insulin is increased sequentially from tube to tube. As the concentration of unlabelled insulin increases, these unlabelled insulin antigens will outcompete the radioactively labelled insulin for the binding sites on the antibodies such that the bound fraction becomes decreasingly radioactive.

Following the 24-hour incubation, 1 ml of cold precipitating reagent (Goat anti-Guinea Pig IgG serum, 3% PEG and 0.05% Triton X-100 in 0.05M Phosphosaline, 0.025M EDTA, 0.08% Sodium Azide) containing a secondary antibody was added to each tube to separate the bound and free insulin fractions. The tubes were then vortexed at 4 °C and incubated for 20 minutes before being centrifuged to obtain a pellet of bound insulin-antibody complexes and free insulin in the supernatant. Following centrifugation, the supernatant was decanted from all tubes and the tubes were dried. The radioactivity of the bound insulin fraction in the pellet was then measured in counts per minute (CPM) using a gamma counter. CPM is a measure of the detection rate of ionising radiation, in this case gamma rays. CPM values were used to calculate B/B_0 which is a ratio that represents the CPM from bound 125 I-insulin in the sample or standard pellet (B)/ CPM from the 125 I-insulin only control pellet (B_0). The greater this ratio, the greater the radioactivity of the pellet from the standards or participant sera and the lower the concentration of unlabelled insulin in the standards or participant sera samples. A standard binding curve was generated from these data with the B/B_0 on the y-axis and the unlabelled human insulin standard concentrations on the x-axis (see **Figure 2-5**).

The above procedure was repeated but with the known standard concentrations of human insulin being replaced with the serum samples from the participants, which contained unknown concentrations of insulin. These unknown insulin concentrations in participant serum samples were then

estimated using the standard curve. Serum samples were all analysed in duplicate. The assay is homologous – the antibodies were raised against human insulin and 125 I-insulin was prepared with human insulin- and has negligible cross-reactivity (<0.2%) with proinsulin in the serum.

2.6.2 Total Plasma Free Fatty Acid Concentration

An enzymatic-colourimetric approach with a WAKO NEFA chemical reagent kit (WAKO Chemicals GmbH, Neuss, Germany), was used to determine total plasma FFA concentrations as described in detail elsewhere (Jeevanandam *et al.*, 1989).

The principle of this assay is based on two reactions. In the first, FFAs are converted to fatty acyl-CoA ($FFA + CoA + ATP \rightleftharpoons Acyl-CoA + AMP + PP_i$), which is the active form that is involved in downstream metabolic processes, in a reaction catalysed by acyl-CoA synthetase enzymes. In the second reaction acyl-CoA is oxidised to form 2,3-trans-Enoyl-CoA and hydrogen peroxide ($Acyl-CoA + O_2 \rightleftharpoons 2,3-trans-Enoyl-CoA + H_2O_2$) in a reaction catalysed by Acyl-CoA oxidase. The hydrogen peroxide produced because of these reactions catalyses a subsequent condensation reaction that produces a purple adduct measurable at 550 nm. Changes in optical density/absorbance were measured using an automated benchtop analyser (ABX Pentra 400, Horiba Medical, Montpellier, France). A standard solution of FFA provided as part of the kit was serially diluted to generate a standard curve from which the FFA concentrations in participant plasma samples were derived. The greater the optical density, the greater the FFA concentration in each plasma sample.

2.6.3 Plasma Triglyceride Concentration

Plasma triglyceride concentrations were determined using an enzymatic-colourimetric assay with a triglyceride reagent kit (WAKO Chemicals GmbH, Neuss, Germany). The kit contained two reagents, enzyme colour reagent A (50 U/mL glycerol kinase, 8.0 mmol/L adenosine 5'-triphosphate disodium salt, 5.6 U/mL glycerol-3-phosphate oxidase, 150 U/mL catalase, 0.4 mmol/L of N-(3-sulfopropyl)-3-methoxy-5-methylaniline and 2.0 U/mL ascorbate oxidase in 50 U/mL Good's buffer (pH 7)) and enzyme colour reagent B (250 U/mL

lipoprotein lipase, 25 U/mL horseradish peroxidase and 4.6 mmol/L 4-aminoantipyrine in 50 U/mL Good's buffer (pH 7.1)).

Plasma contains free glycerol that can affect the results of a triglyceride assay. Samples were first mixed with reagent A which contains glycerol kinase, glycerol-3-phosphate oxidase and catalase enzymes that catalyse a sequence of reactions which decompose free glycerol in the plasma samples, leaving only the glycerol which is part of TAGs. The principle of the assay following the decomposition of free glycerol is based on a three-step enzymatic reaction that begins when reagent B is added to the mixture. In the first reaction lipoprotein lipases in reagent B hydrolyse triglycerides to form glycerol and three fatty acids ($Triglyceride + H_2O \rightarrow Glycerol + 3 Fatty Acids$). In the second reaction glycerol is converted to glycerol-3-phosphate in an ATP-dependent reaction catalysed by glycerol kinase ($Glycerol + ATP \rightarrow Glycerol-3-phosphate + ADP$). Finally, glycerol-3-phosphate is oxidised in a reaction catalysed by glycerol-3-phosphate oxidase to form dihydroxyacetone phosphate and hydrogen peroxide ($Glycerol-3-phosphate + O_2 \rightarrow Dihydroxyacetone phosphate + H_2O_2$). Reagent A contains 0.4 mmol/L of N-(3-sulfopropyl)-3-methoxy-5-methylaniline and reagent B contains 4.6 mmol/L of 4-aminoantipyrine. The hydrogen peroxide produced by the oxidation of glycerol-3-phosphate causes these two compounds to undergo a condensation reaction catalysed by horseradish peroxidase that results in the formation of a blue pigment. The optical density of this pigment was measured using the ABX Pentra 400 automated benchtop analyser (Horiba Medical, Montpellier, France) at a sub wavelength of 700 nm and main wavelength of 600 nm. To determine the concentration of triglyceride in participant plasma, absorbances were compared to a curve of known standard triglyceride concentrations.

2.7 Quantification of IMCL content using Magnetic Resonance Spectroscopy (MRS)

Proton magnetic resonance spectroscopy (^1H -MRS) is a method for the quantification of molecules in substances, and metabolites in living tissues, based on the properties of the hydrogen (^1H) atoms within them (Machann *et al.*, 2003). This technique was used for the non-invasive determination of IMCL content in the vastus lateralis of the participants of the acute bed rest study detailed in **Chapter 3** and in both healthy controls and participants with NAFLD as detailed in **Chapter 4**. Imaging was performed using magnetic resonance imaging (MRI) scanners at the Sir Peter Mansfield Imaging Centre (SPMIC), University of Nottingham.

Participants were asked questions from a safety assessment form to ensure that they had no metallic objects in or on their body. Once all safety criteria were met they were instructed to lie supine on the bed of the scanner and radiofrequency coils were placed on top of them, covering from the ankle to the neck.

A ^1H atom has a single proton in its nucleus, which is orbited by a single electron. This proton applies a spin to the nucleus and this spin generates a magnetic dipole in the atom. In the absence of an external magnetic field (B_0) ^1H atoms have nuclear spins with random orientations. When the B_0 was applied to the participants by the MRI scanner, the nuclear spins of their ^1H atoms first aligned parallel to the direction of B_0 , which is known as the α spin state or low energy state (Posse *et al.*, 2013). Then radiofrequency radiation produced by the surface coils was applied to these ^1H atoms. When the pulse power was sufficient, this radiation was absorbed and provided enough energy to shift the ^1H atoms from the α spin state to what is called the β spin state, in which the atoms align antiparallel to B_0 . When all the ^1H atoms transition to the higher energy β spin state they are said to be in “resonance”.

Over time the energy absorbed by these nuclei is lost as they return to their original orientations during the T_1 and T_2 relaxation phases. The energy released by the nuclei during T_1 and T_2 for each participant was detected by a receiving coil to generate output visualised as ^1H -MRS spectra.

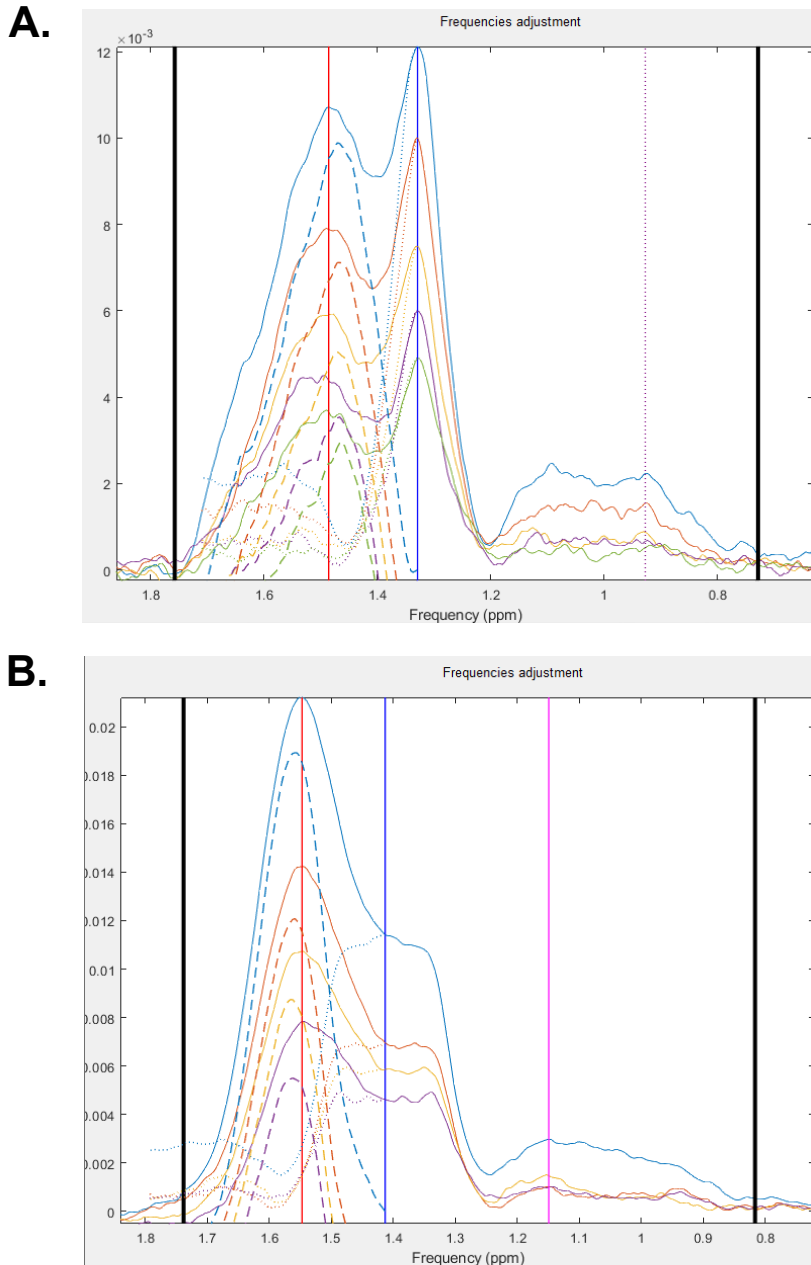


Figure 2-6: Example ^1H -MRS spectra of the vastus lateralis. Resonances are shown by the gaussian line shapes in the frequency domain, with each lineshape representing the same spectra at a different echo time. The vertical red line marks the methylene peak of EMCL. The vertical blue line marks the methylene peak of IMCL. **(A)** Spectra in which the methylene IMCL peak at 1.33 ppm is well resolved from the EMCL peak at 1.49 ppm. **(B)** Spectra in which the EMCL and IMCL peaks overlap.

There were several considerations for the quantification of lipid content in skeletal muscle using ^1H -MRS. In ^1H -MRS spectra lipid resonances are detected between 0.9-1.6 ppm and must be resolved into those peaks arising

from intra- vs. extra-myocellular lipid. IMCL and EMCL signals can be distinguished by the slight differences in their resonance frequencies, the resolution of which is complicated by the angle of the muscle relative to B_0 during acquisition (Schick *et al.*, 1993). Because LDs which compose the majority of IMCL are spherical and free in the aqueous cytosol of myocytes, the ^1H atoms in these LDs can freely align with B_0 . Therefore the methylene, IMCL- $(\text{CH}_2)_n$, and methyl, IMCL- CH_3 , resonance peaks of the IMCL spectral lineshape at around 1.28 ppm and 0.885 ppm respectively are always present on ^1H -MRS spectra of skeletal muscle and are unaffected by the orientation of the muscle relative to B_0 (see **Figure 2-6A**) (Boesch *et al.*, 1997).

However, fat depots in adipocytes (EMCL) form sheets or cylindrical shaped structures localised between and along skeletal muscle fibres. The nuclei of ^1H atoms in EMCL cannot spin as freely as those in IMCL. Thus, EMCL resonance signals depend on the pennation angle of the muscle fibres within the area of the area being assessed (voxel) and the angle of the whole muscle relative to B_0 . The methylene resonance peak of EMCL, EMCL- $(\text{CH}_2)_n$, is best resolved at 1.5 ppm (Schick *et al.*, 1993) when the muscle fibres within the voxel are parallel to B_0 , but this peak can broaden as much as to 1.2 ppm when these fibres are perpendicular to B_0 (Szczepaniak *et al.*, 2002). The resonance signals of IMCL are independent of orientation so as the angle of the muscle relative to B_0 increases, the methylene EMCL resonance peak will broaden and shift into the IMCL resonances such that the signals for the two compartments overlap and become indistinguishable without the use of fitting algorithms (see **Fig 2-6B**). The ^1H -MRS data for the quantification of IMCL presented herein were determined using spectra acquired from receiving coils positioned abutting the quadriceps femoris of study participants. The legs of these participants were positioned parallel to B_0 for each acquisition.

Another consideration was water suppression. Water is the most abundant component of muscle, composing as much as 78% of the voxel volume, whilst the other detectable components in ^1H spectra compose roughly 2% (Sjøgaard and Saltin, 1982). The ^1H nuclei in water are more densely concentrated than in any other metabolite and, in unsuppressed ^1H spectra, there is a large water peak between 4.4-5.0 ppm. This phenomenon

necessitates the use of methods to suppress water in these spectra so that the area under the other metabolites can be resolved and calculated (Ogg, Kingsley, and Taylor, 1994). For the data presented herein both water-suppressed, and unsuppressed spectra were acquired from the same voxels. The water peaks in the unsuppressed spectra were used as internal standards to scale the metabolite peaks, and to correct for the variations in signal intensity or any experimental variation, in the suppressed spectra. The algorithms for water suppression and line fitting, based on muscle orientation relative to B_0 , applied during spectra processing were developed by Dr. Olivier Mougin (SPMIC) based on existing methodologies (Khuu *et al.*, 2009).

2.8 Histochemical Quantification of IMCL Content

2.8.1 Fluorescent Staining of Lipid in Vastus Lateralis Muscle Cryosections with Bodipy 493/503

The method for the quantification of IMCL content used in the studies presented herein, with the fluorescent dye Bodipy 493/503 (D3922; Fisher Scientific, Paisley, UK), has been described previously (Prats *et al.*, 2013). Frozen vastus lateralis samples were embedded in OCT mounting medium (361603E; VWR International, Lutterworth, UK) before being secured to the object holder of a Leica CM3050 S Research Cryostat (Leica Biosystems, Wetzlar, Germany). Cryostat chamber temperature was maintained at $-20\text{ }^{\circ}\text{C}$ whilst the object temperature was maintained at $-18\text{ }^{\circ}\text{C}$. Then, transverse sections of $14\text{ }\mu\text{m}$ thickness were trimmed consecutively and collected from each frozen muscle biopsy block. These sections were mounted on SuperFrost Plus adhesion microscope slides (631-0108P; VWR International, Lutterworth, UK).

To prevent the sections from air drying after cutting, sections on each slide were immediately immersed in 50 mL of ice-cold 4% paraformaldehyde Zamboni's fixative (Apoteket, Copenhagen, Denmark) supplemented with 2.5 ml of 2% glyceraldehyde in 0.05M phosphate buffer (pH 7.4) and were left to fix for 60 minutes. After immersing the sections in cold Sørensen's Phosphate Buffer (SPB) (0.1 M, pH 7.4) for 20 minutes to wash off the fixative, they were then incubated for 30 minutes in $20\text{ }\mu\text{g/mL}$ Bodipy 493/503 in 50 mL of cold

SPB. After the incubation with Bodipy 493/503, the sections were immersed in cold SPB again for 20 minutes as a final wash. Samples were always kept cold before imaging to prevent the leakage of intracellular lipid from the muscle fibres into the extracellular space, which can occur when frozen muscle biopsies thaw.

These stained muscle sections were then mounted in Vectashield mounting medium for fluorescence (H-1000; 2BScientific, Upper Heyford, UK), covered by 1.5 mm cover slips (MIC3124; Scientific Laboratory Supplies, Nottingham, UK), and sealed with nail polish before being placed on ice and enclosed to limit any exposure to external light.

2.8.2 Image Acquisition

Zeiss confocal laser scanning microscopes (Carl Zeiss AG, Jena, Germany), operating ZEN Black Edition software (Carl Zeiss AG, Jena, Germany) were used in the studies described here to image Bodipy stained muscle sections at 20x magnification. In all studies, the Bodipy 493/503 fluorophore was excited using the 488 nm argon-ion laser line (Macho, Mishal and Uriel, 1996). Pinhole size was maintained at 0.96 AU. Z-stacks were imaged from the top to the bottom of each section and consisted of 5 segments of total thickness 3.642 μm , 910.54 nm between segments, obtained for a single region within each muscle sample. Each z-stack constituted a single tile and numerous tiles were stitched together to generate a complete image of each section. The most structurally intact sections from each vastus lateralis muscle sample were imaged. From each captured image, a maximum projection was generated using the “*Orthogonal Projection*” processing function in ZEN Blue Edition software (Carl Zeiss AG, Jena, Germany). These maximum projections were then exported as Tiff Format (64 bit) (Big Tiff) image files. These files were analysed in the FIJI (Fiji Is Just ImageJ) software package (Schindelin *et al.*, 2012).

Biopsy sections do not have perfectly even surfaces and the penetrance of fluorescent dye into different regions of the tissue during the staining process can vary. Therefore, within each segment of the z-stacks composing a captured image there will be areas where the visualised intensity is lower

than in other segments of the stack. A maximum projection is a combination of all the segments within the z-stacks of an image, such that all regions of the projection represent the maximal visualised intensity as calculated from the segments within the stack.

Note that, for each biopsy sample, section cutting, staining, and imaging were performed on the same day. This was because it has been demonstrated that freezing sections after fixation, for later histochemical staining, or after staining, for later imaging, results in significantly reduced LD count and decreased staining intensity (Prats *et al.*, 2013). Also, biopsies were taken at the same time for each time point in each study discussed here, thereby accounting for any possible diurnal variation in IMCL content (Held *et al.*, 2020).

2.8.3 Image Analysis

When Tiff format maximum projections were opened in FIJI, a “*Gaussian Blur*” of radius 1.00 was applied to sharpen each image and allow for better detection of LDs amongst other stained neutral lipid. The “*Auto Local Threshold*” function was then used to binarise each image with the application of the Bernsen Algorithm (radius=50) (Bernsen, 1986) such that well stained lipids (LDs) were detected and highlighted in white as particles whilst weakly stained or unstained structures were converted to black background.

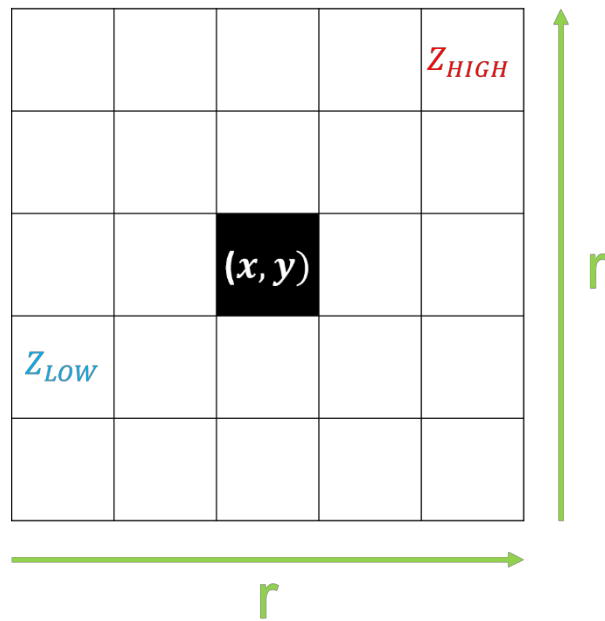


Figure 2-7: Example diagram of variables used in the binarisation of pixels via the Bernsen algorithm. A single pixel (x, y) is bounded by a user defined region ($r \times r$). Z_{LOW} is the pixel with the lowest grey value within the defined region, Z_{HIGH} is the pixel with the highest grey value within the region.

The Bernsen algorithm is a widely used and robust (Tantakitti *et al.*, 2012; Korzynska *et al.*, 2013; Potter *et al.*, 2016; Kim *et al.*, 2017) method for the binarisation of images using thresholding formulae. Binarisation methods convert greyscale images, which are composed of pixels with grey levels ranging on a spectrum from 0-255, to images composed entirely of black (0) and white (1) pixels. There are two broad binarisation categories, global binarisation and local binarization. Global binarisation thresholding methods use a single threshold value for the whole image and are optimal when measuring the differences in staining intensity between stained objects. Local binarisation methods calculate a unique threshold value for each greyscale pixel within an image based on the grey level values of neighbouring pixels. Local binarisation methods are most useful when investigating the number or size of stained objects, irrespective of staining intensity. Using the Bernsen algorithm, the threshold value for each pixel ($T(x, y)$) is calculated with the following formula:

$$T(x,y) = \frac{(Z_{LOW}+Z_{HIGH})}{2}$$

(Equation 2-18)

Where Z_{LOW} is the lowest grey level pixel value in a defined square ($r \times r$) neighbourhood/radius centred around a single pixel (x, y) and Z_{HIGH} is the highest grey level pixel value in the radius centred around the same single pixel (see **Figure 2-7**). The threshold value is thus determined by the mean of the sum of the lowest grey value in a defined radius and the highest grey value in a defined radius. This measure ($T(x, y)$) is also called the midgrey value. Within the $r \times r$ radius, the local contrast ($C(x, y)$) is also calculated as:

$$C(x,y) = Z_{HIGH} - Z_{LOW}$$

(Equation 2-19)

If the local contrast ($C(x, y)$) value is greater than a user defined contrast threshold, also called “Parameter 1” in the FIJI interface, (usually 15) then the midgrey value ($T(x, y)$) is used as the threshold value for the single pixel defined as (x, y) . In this case, If the grey level value of pixel $(x, y) > T(x, y)$ then pixel (x, y) will be assigned to the foreground as a white particle. If the grey level value of pixel $(x, y) < T(x, y)$ then pixel (x, y) will be assigned to the background. However, if $C(x, y)$ is lower than the user defined contrast threshold then all pixels in the region $r \times r$ will be assigned as background. This algorithm is automatically applied to as many pixels as necessary to binarise an entire image used the “*Auto Local Threshold*” function.

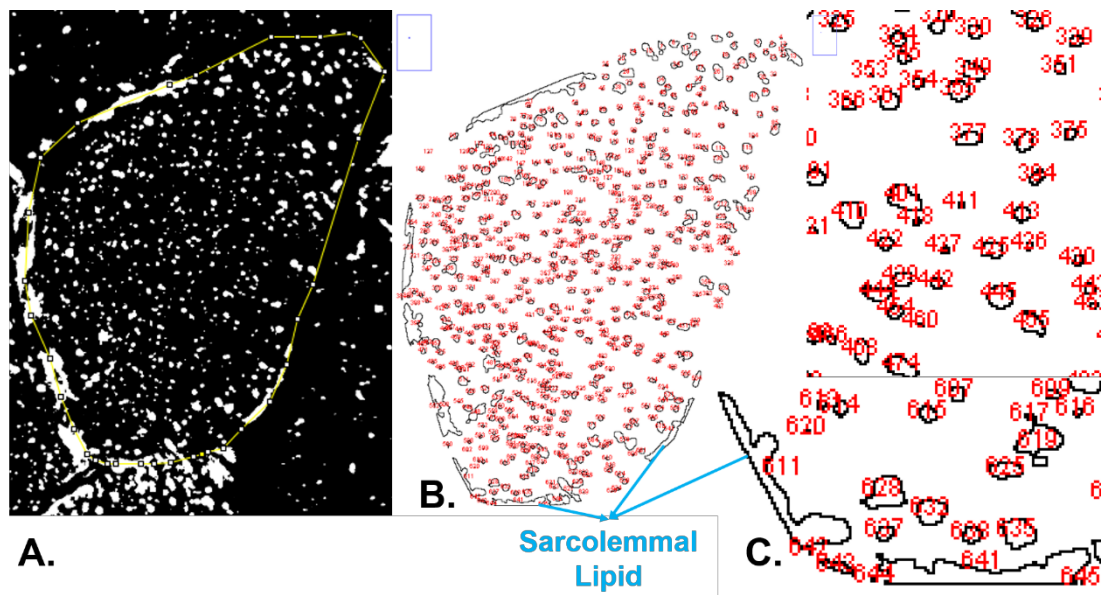


Figure 2-8: (A) Binarised image of muscle biopsy sample with a single fibre bounded by an ROI in yellow. (B) Visual output of the particles identified within the ROI using the showing the “Analyse Particles” tool. Particles are labelled in red. (C) Magnification of the visual output showing labelled LDs within the fibre and sarcolemmal lipid at the periphery.

Then, with the “Polygon Selection” tool, regions of interest (ROIs) were manually drawn, and the “Analyse Particles” tool was used to measure the value of several variables within these regions from which parameters including LD count, LD size and IMCL content were calculated for each sample. These variables were total tissue area, which is the sum of the area in micrometres of the section bounded by the ROI/ROIs, total LD count, which is the sum of all the LDs within the total tissue area, and total LD area, which is the total area within the tissue that contains lipid. For the assessment of LD count and size, the circularity filter is set to 0.50-1.00 to exclude sarcolemmal lipid and only include intracellular LDs in the analysis (Covington *et al.*, 2017). FIJI calculates the circularity of each detected particle using the formula:

$$Particle\ Circularity = 4\pi\left(\frac{A}{C^2}\right)$$

(Equation 2-20)

Where C equals the circumference of the particle and A equals the area of the particle. This formula is essentially a ratio between circle area and circle circumference based on the relationship $C^2 = 4\pi A$. Thus, the closer the circularity value for a particle is to 1 the more circular it is, with 1 being a perfect circle and 0 being a perfectly straight line. The circularity filter allows a user to specify the circularity range within which individual particles must fall to be detected and recorded within the output of the “*Analyse Particles*” tool. For the quantification of LD count and LD size a circularity filter of 0.50-1.00 was applied to favour the inclusion of intracellular LDs whilst excluding sarcolemmal lipid (see **Figure 2-8** and **Figure 2-9**). Without the adjustment for circularity, particle analysis calculates significantly inflated values for LD count and LD size. The impact of such errors, particularly on LD size calculations, is greatly exacerbated by the fact that participants can express broadly different quantities of lipid localised to the sarcolemma. This filter is not applied in the calculation of the ratio of lipid area to whole tissue area (percentage IMCL content).

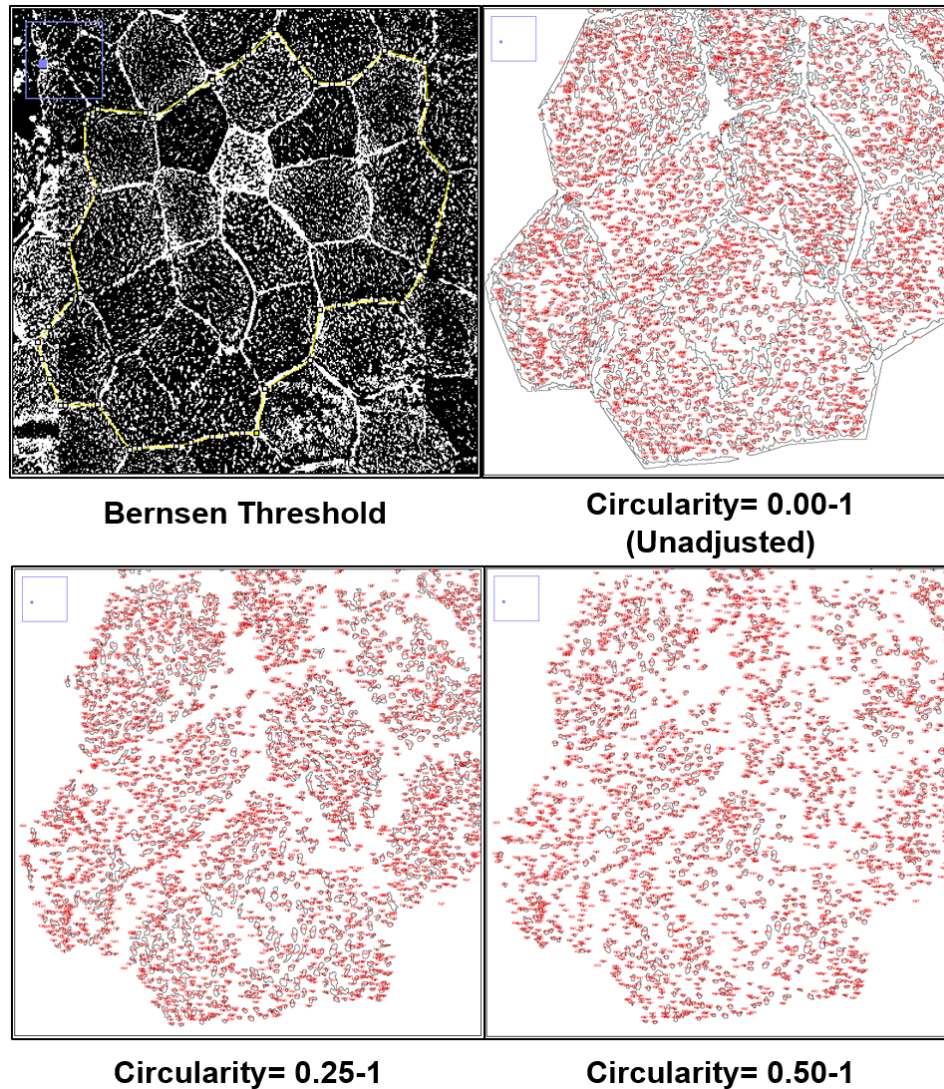


Figure 2-9: Images showing the variation in the particles recorded in the “Analyze Particles” output based on the range of the circularity filter.

LD count is a relative measure that is manually calculated as $\frac{\text{Total LD Count}}{\text{Total Tissue Area}}$ within each ROI and is presented herein as droplets per square micrometre (droplets/ μm^2) of muscle tissue. LD size is automatically calculated by the FIJI software as a mean of the size of every droplet within the ROI, here LD size is presented as the mean size of the droplets in micrometres. For IMCL staining images here, a single pixel has an area of $0.0244 \mu\text{m}^2$. Pixel aspect ratio for all muscle sample maximum projections was $1 \mu\text{m} = 6.3983$ pixels. The total lipid area within each sample (percentage IMCL content) is also calculated automatically as $\frac{\text{Total LD Area}}{\text{Total Tissue Area}}$ within each ROI.

2.8.4 Comparison of Image Analysis Methods

2.8.4.1 Single Fibre (SF) and Field of View (FOV)

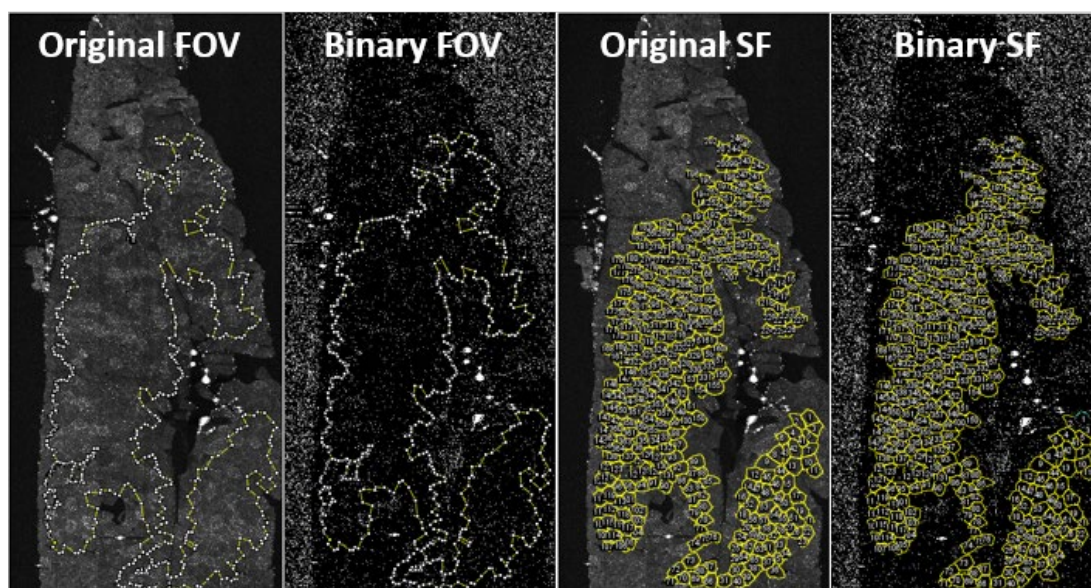


Figure 2-10: Representative images of the FOV and SF techniques used to validate the image analyses in the quantification of IMCL.

For muscle biopsy samples with tight cohesion between individual fibres, ROIs encompassing several hundred individual muscle fibres within a large field of view can be drawn for subsequent particle analysis. This method was used to analyse images from the chronic bed rest study detailed in **Chapter 3**. Where samples have fibres which are less cohesive and more interspersed, even marginally, the use of a method in which unique ROIs are drawn around each individual fibre to guarantee accurate calculation of the relevant parameters is necessary. Such a method was used to analyse images from the acute bed rest study detailed in **Chapter 3**. The principal study parameters in the studies presented here are LD count, LD size and percentage IMCL content which are defined in **Section 2.8.3**. Other important parameters include Total Tissue Area, which is the size in micrometres of the tissue within a ROI, Total LD Count, which is the total number of LDs within the Total Tissue Area, and Total LD Area, which is the total area within the section of tissue selected by the ROI that is occupied by lipid.

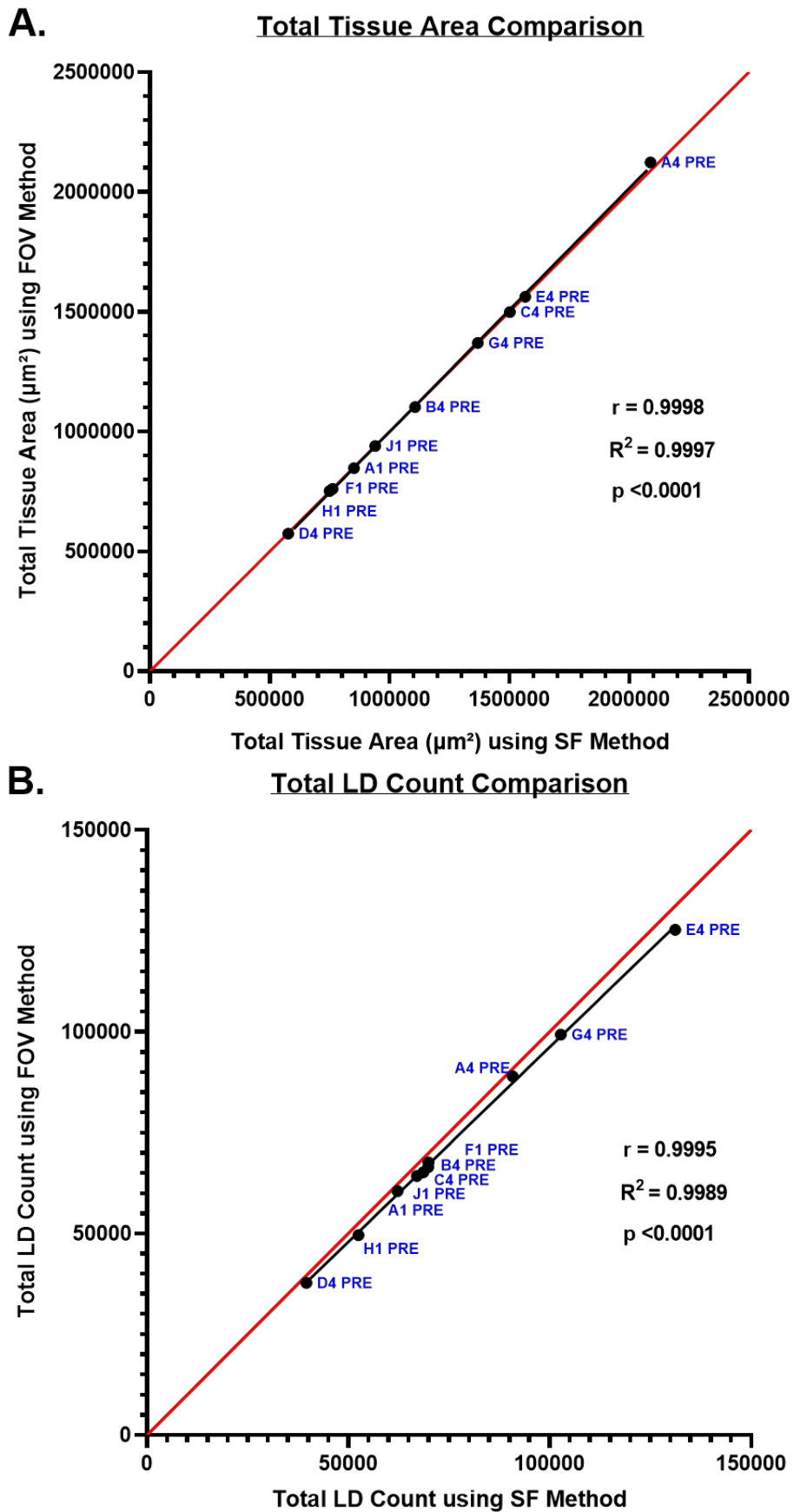
To determine the validity of directly comparing data generated by the two differing methods for image analysis, 10 randomly selected maximal

projections generated using pre bed rest samples from the chronic bed rest study described in **Chapter 3** were analysed using both the field of view (FOV) method -in which a single ROI encompasses a large section of the muscle tissue- and the single fibre (SF) method -in which unique ROIs are drawn around individual fibres- to compare the variability between these methods in the means calculated for the study parameters (see **Figure 2-10**). Data were compared without the application of the circularity filter. A total of 228 ± 29 individual fibres were analysed for each of the 10 tested samples.

2.8.4.2 Analysis of SF and FOV Method Correlation

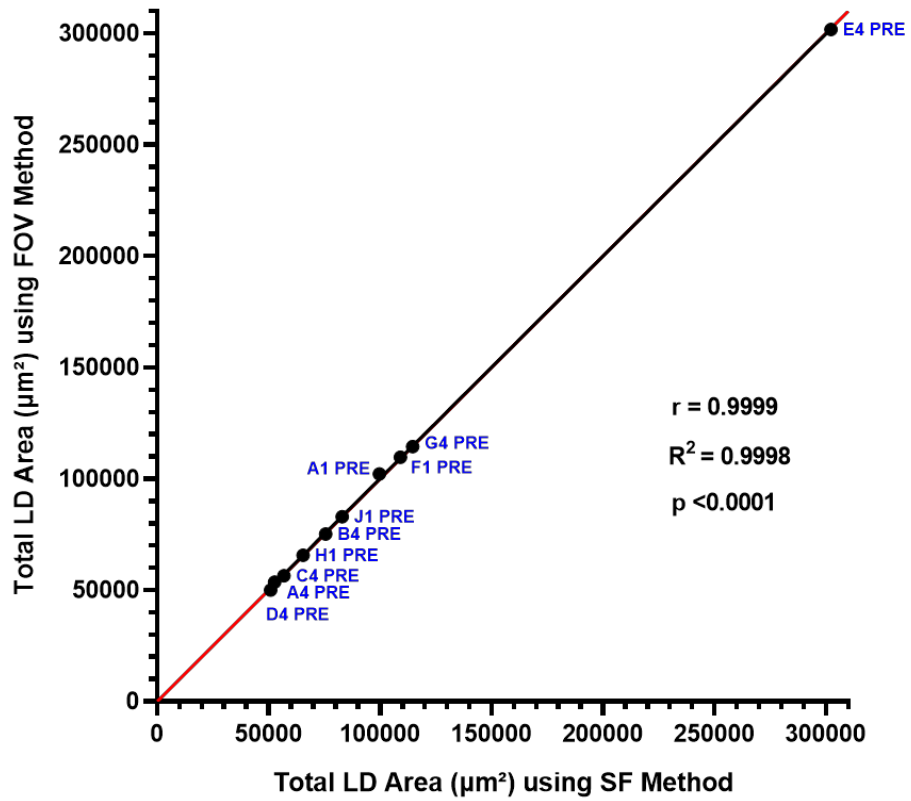
Correlations between values determined by the SF and FOV methods were calculated in GraphPad Prism 8 software and are presented as correlation coefficient (r) and R-squared (R^2) values. The correlation coefficient was computed by comparing the value of a parameter measured by the SF method (x-axis) with the value of that same parameter in the same sample as measured using the FOV method (y-axis). All r values are Pearson correlation coefficients as Gaussian distribution was assumed. p values were generated from two-tailed correlation coefficient hypothesis tests. In addition, to identify any statistically significant differences between the values generated by the FOV and SF methods for tabulated data of the principal study parameters, paired, two tailed t-tests were also used.

2.8.4.3 Between-Method Agreement



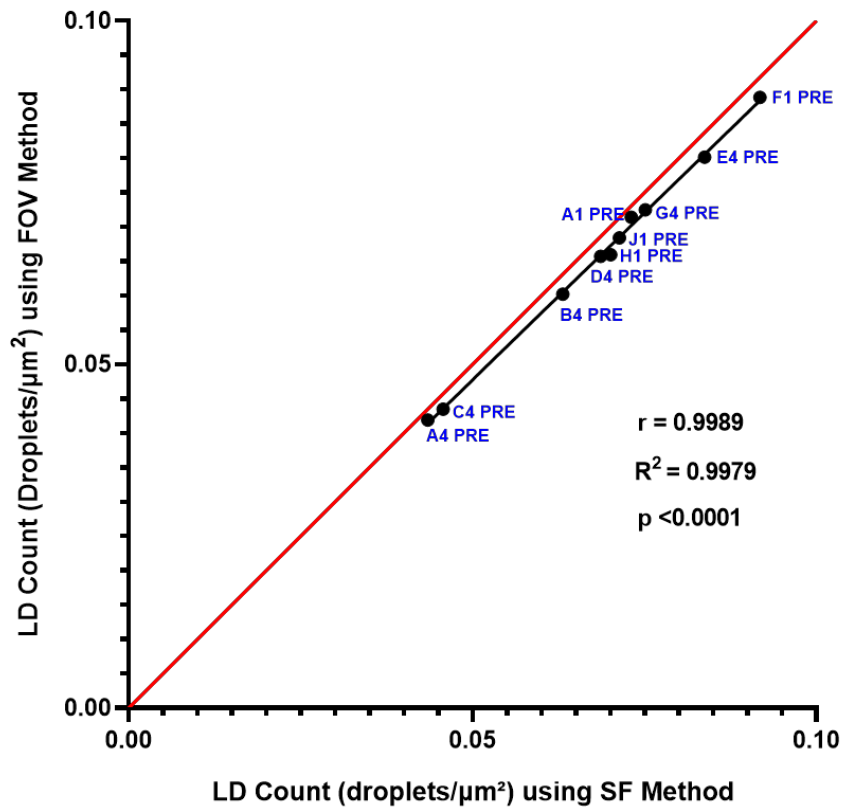
C.

Total LD Area Comparison



D.

LD Count (droplets/ μm^2) Comparison



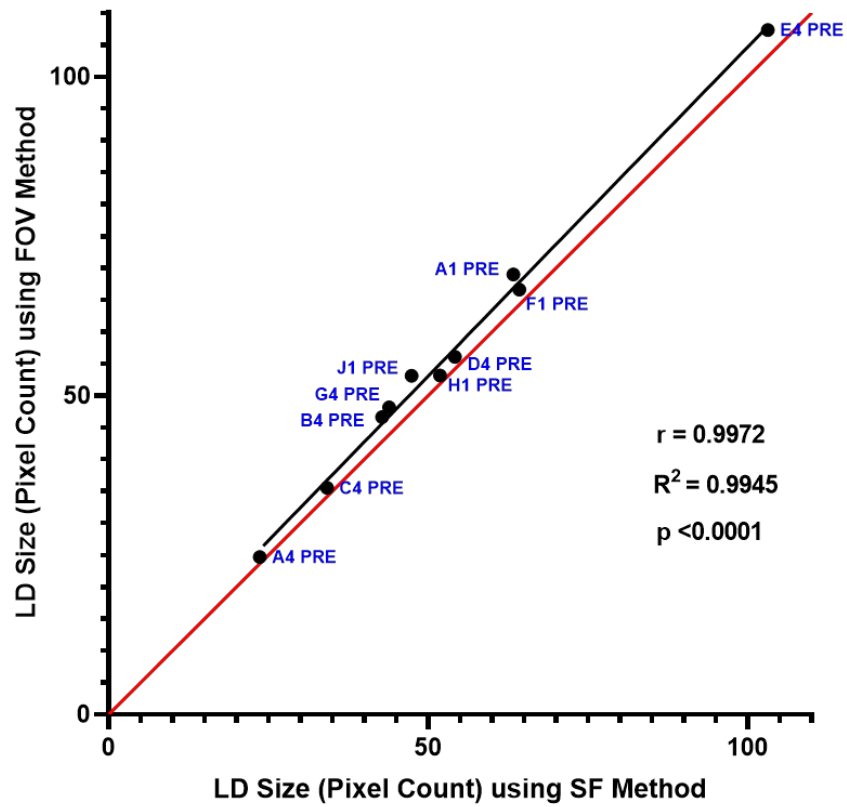
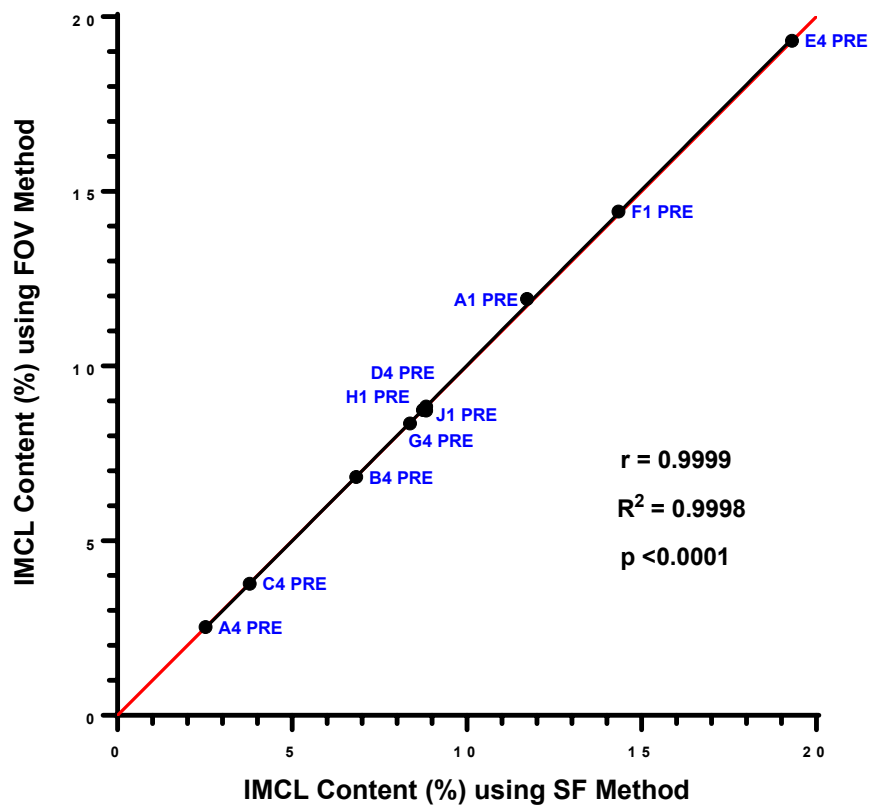
F.**LD Size Comparison****F.****IMCL Content Comparison**

Figure 2-11: Comparison of parameter means in various samples using the SF and FOV methods, $n = 10$ samples for all parameters. The parameter which was measured is shown in each graph title. Each point is labelled with the pre bed rest sample designation in blue. Lines of identity are shown in red. (D-F) Principal study parameters.

Figure 2-11 shows scatter plots comparing measurements made by the SF method (x-axis) and measurements made by the FOV method (y-axis). Correlation coefficient (r) values between the FOV and SF methods for each measured parameter were all >0.99 . Visually this can be seen by the points for measurements of each parameter falling close to the lines of identity shown in red. Linear regression lines are fitted between the points for each parameter to represent the R^2 values calculated during correlation analysis. Correlation coefficient hypothesis tests between the two methods for each parameter reported p values <0.0001 indicating that there is a significant linear relationship between x (the value of the parameters as measured using the SF method) and y (the value of the same parameters as measured using the FOV method) and that the data from these muscle samples is representative of the population. For each of the 10 samples analysed there was a significant linear relationship between the values calculated for each parameter using the FOV method and the values calculated for those same parameters using the SF method.

Sample	Parameter					
	LD Count (LDs/μm ²)		LD Size (Pixels)		IMCL Content	
	SF Method	FOV Method	SF Method	FOV Method	SF Method	FOV Method
A4 PRE	0.043	0.042	23.6	24.7	2.52	2.53
A1 PRE	0.073	0.071	63.3	69	11.7	11.9
B4 PRE	0.063	0.06	42.8	46.6	6.83	6.82
C4 PRE	0.046	0.043	34.2	35.5	3.79	3.77
D4 PRE	0.069	0.066	54.2	56.1	8.83	8.72
E4 PRE	0.084	0.08	103.1	107.3	19.3	19.3
F1 PRE	0.092	0.089	64.2	66.6	14.3	14.4
G4 PRE	0.075	0.072	43.9	48.2	8.37	8.36
H1 PRE	0.07	0.066	51.9	53.2	8.75	8.74
J1 PRE	0.071	0.068	47.4	53.1	8.84	8.84
Mean ± SE	0.069 ± 0.005	0.066 ± 0.005	52.9 ± 6.82	56.0 ± 7.06	9.33 ± 1.55	9.34 ± 1.56
P-value	<0.0001		0.0003		0.5493	

Table 2-1: Table of data showing the comparison of principal study parameter measurements in all samples using the SF and FOV methods. Paired, two-tailed T-tests.

The agreement between the two methods when measuring Total Tissue Area, Total LD Area, Total LD count, LD count, LD Size and IMCL Content is very strong. T-tests comparing the FOV and SF values for the principal study parameters showed that there were some statistically significant differences in the mean values for LD count and LD size but not IMCL content (see **Table 2-1**). The difference in LD count and LD size quantification between the two methods is roughly 5%; there is no statistically significant differences in the values calculated by these methods for Total Tissue Area, Total LD Area and Total LD count. Overall, there is minimal variability between these methods. Given that any variability can be further reduced by improving the geometric alignment between the ROIs created for these methods, and that 228 ± 29.004 individual fibres were analysed for each of the 10 samples tested such that the ROIs used were enough to be representative of each vastus lateralis biopsy, the differences between the measurements generated using these two

methods are not significant. Thus, images analysed using the SF method can be compared with those analysed using the FOV method.

2.8.4.4 Validation of Automated ROI selection and Particle Analysis

As outlined in **Section 2.8.4.1**, the SF method is sometimes used for the analysis of total IMCL content instead of the FOV method in those samples where muscle fibres are not adequately cohesive. The SF method is also necessary for the determination of fibre-type specific IMCL content as detailed in **Section 2.9**.

Manually selecting and analysing each of the hundreds of fibres within a single image from the ROI manager during SF analysis is laborious. To overcome this, macros were written to fully automate the sequential selection and particle analysis of all muscle fibre ROIs within the ROI manager.

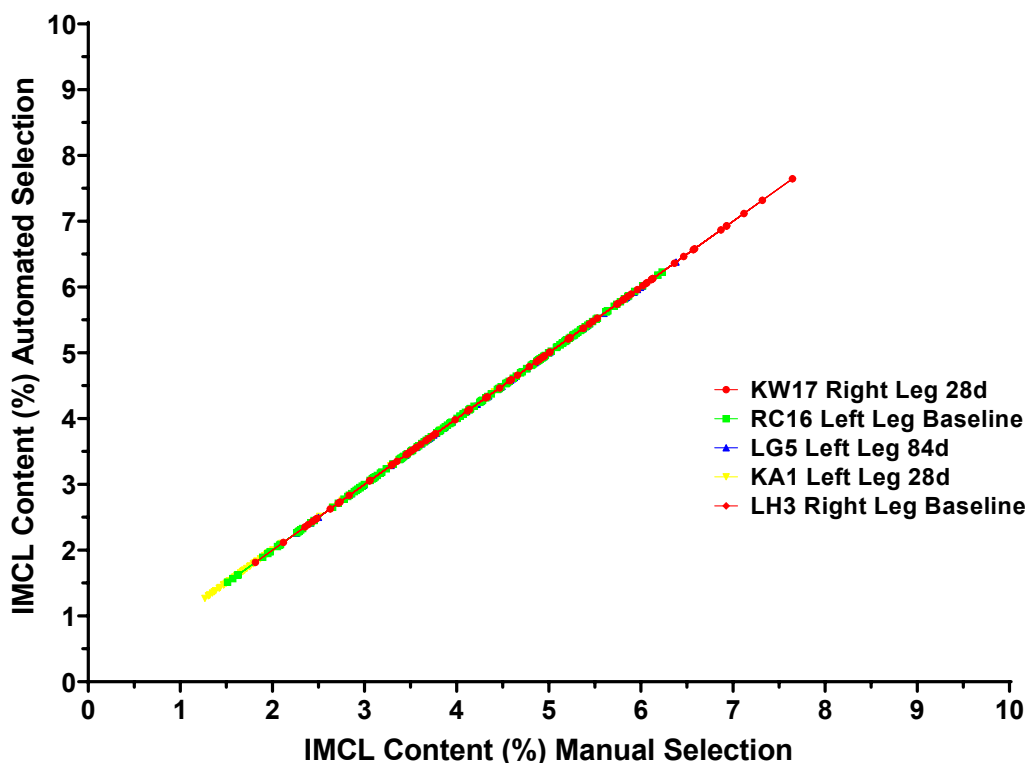


Figure 2-12: Comparison of manual vs automated ROI selection and SF muscle IMCL content analysis. For all samples r and R^2 are equal to 1 for all the fibres analysed.

To ensure that these macros for automated circularity adjusted and unadjusted particle analysis produced the same results as those generated by manual selection and analysis, 5 samples from the study detailed in **Chapter 4** were randomly selected. Manual and automated selection, and muscle fibre IMCL content determination was compared as shown in **Figure 2-12**. The two methods produced identical results for each muscle fibre in all samples, hence the overlapping perfect straight lines. Thus, automated selection and analysis of muscle fibre ROIs is used in cases where the SF method is necessitated in all studies described here.

2.8.5 Repeatability of IMCL Quantification with Bodipy 493/503

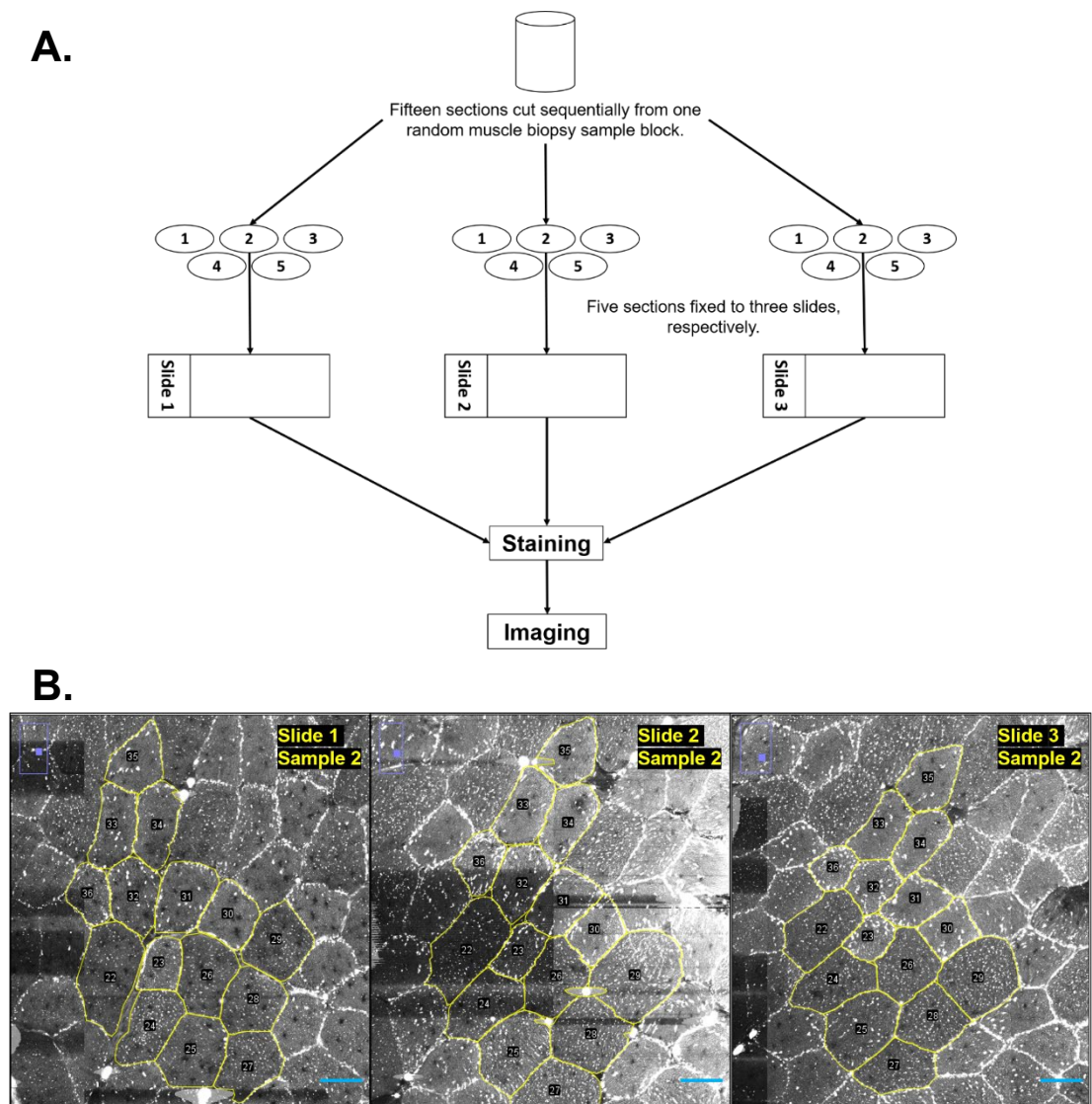
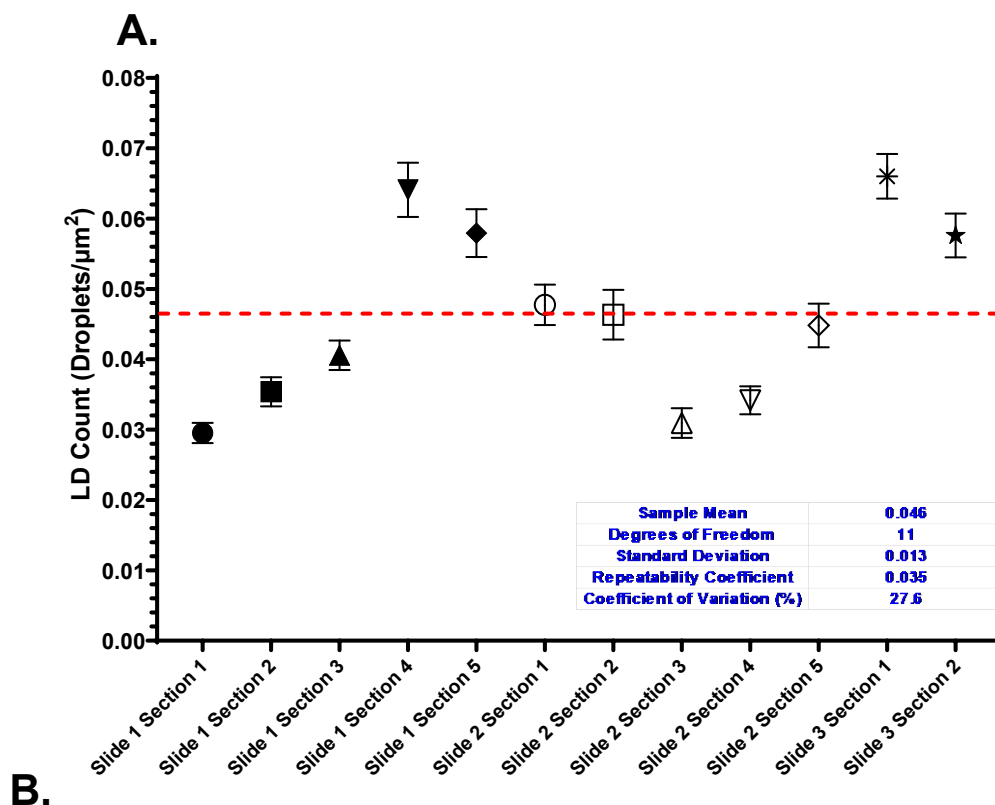


Figure 2-13: (A) Flow diagram of repeatability test protocol. (B) Example of the same fibres identified in different sections on different slides. Bars are 50 μ m.

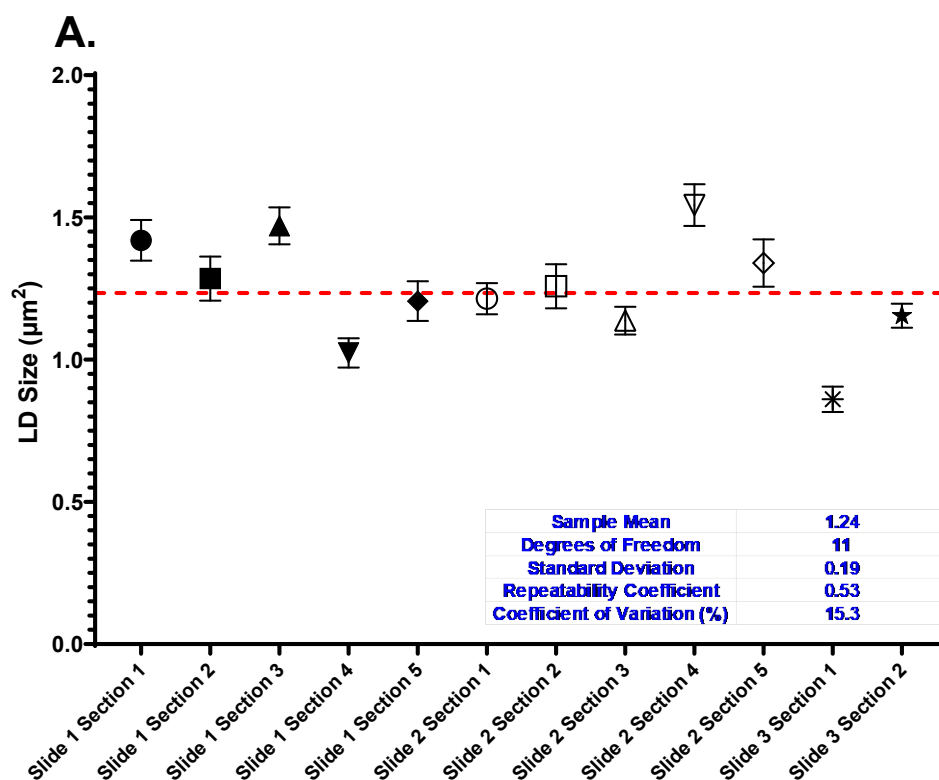
For assessment of repeatability, measurements of the same subject/sample must be made in quick succession by the same operator using the same methods and equipment (Nakagawa and Schielzeth, 2010). To assess the repeatability of the IMCL quantification protocol, LD count, LD size and percentage IMCL content were measured in multiple sections from a single randomly selected vastus lateralis biopsy sample block (see **Figure 2-13A**). Fifteen 14 μm thick sections were cut from this block sequentially and acted as technical replicates. These sections were transferred to three SuperFrost Plus adhesion microscope slides, fixed to these slides with Zamboni's fixative, stained with Bodipy 493/503 and imaged on the same day as previously described (see **Section 2.7.1**). All fifteen sections were stained but sections 3, 4, and 5 on slide 3 were not imaged due to time constraints on the day. At least two sections on each slide are required to assess repeatability or reproducibility (Bartlett and Frost, 2008), thus data for sections 1 and 2 on slide 3 are shown here.

For images acquired for each technical replicate from each slide the same 39 fibres were identified, and ROIs were created (see **Figure 2-13B**). LD count, LD size and percentage IMCL content parameters were calculated for every fibre ROI in a section. These fibre-level data were then pooled to generate mean values of these parameters at the section level for each of these replicates. Data at the section level was then pooled to create an overall sample level mean for each parameter. Repeatability was quantified using the repeatability coefficient and coefficient of variation of the sample means.



Section	LD Count (Droplets/ μm^2)	Deviation from Sample Mean	Deviation ²
Slide 1 Section 1	0.030	-0.01673	0.00028
Slide 1 Section 2	0.035	-0.01089	0.00012
Slide 1 Section 3	0.041	-0.00569	3.23E-05
Slide 1 Section 4	0.064	0.01783	0.00032
Slide 1 Section 5	0.058	0.01168	0.00014
Slide 2 Section 1	0.048	0.00148	2.20E-06
Slide 2 Section 2	0.046	0.00007	5.38E-09
Slide 2 Section 3	0.031	-0.01533	0.00023
Slide 2 Section 4	0.034	-0.01210	0.00015
Slide 2 Section 5	0.045	-0.00146	2.12E-06
Slide 3 Section 1	0.066	0.01975	0.00039
Slide 3 Section 2	0.058	0.01135	0.00013
Sum	0.56	0	0.00179

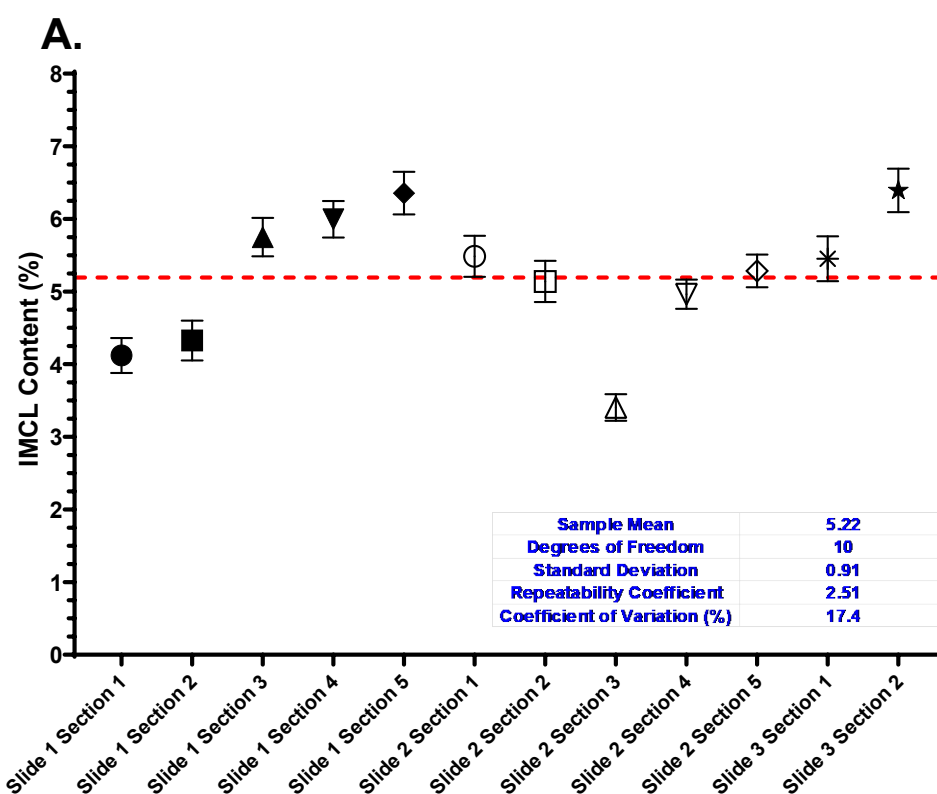
Figure 2-14: (A) Graph showing pooled LD count data for each section/replicate. Bars are mean \pm SEM. Sample mean, which is visually represented by the red dotted line, represents the average LD count across all replicates. (B) Table of descriptive statistics for each replicate shown in graph A.



B.

Section	LD Size (μm^2)	Deviation from Sample Mean	Deviation ²
Slide 1 Section 1	1.42	0.1764	0.03111
Slide 1 Section 2	1.29	0.0424	0.00179
Slide 1 Section 3	1.47	0.2284	0.05215
Slide 1 Section 4	1.02	-0.2186	0.04780
Slide 1 Section 5	1.21	-0.0366	0.00134
Slide 2 Section 1	1.21	-0.0286	0.00082
Slide 2 Section 2	1.26	0.0154	0.00024
Slide 2 Section 3	1.14	-0.1056	0.01116
Slide 2 Section 4	1.54	0.3004	0.09022
Slide 2 Section 5	1.34	0.0974	0.00948
Slide 3 Section 1	0.86	-0.3820	0.14595
Slide 3 Section 2	1.15	-0.0886	0.00786
Sum	14.9	0	0.39991

Figure 2-15: (A) Graph showing pooled LD size data for each section/replicate. Bars are mean \pm SEM. **Sample mean, which is visually represented by the red dotted line, represents the average LD size across all replicates. (B) Table of descriptive statistics for each replicate shown in graph A.**

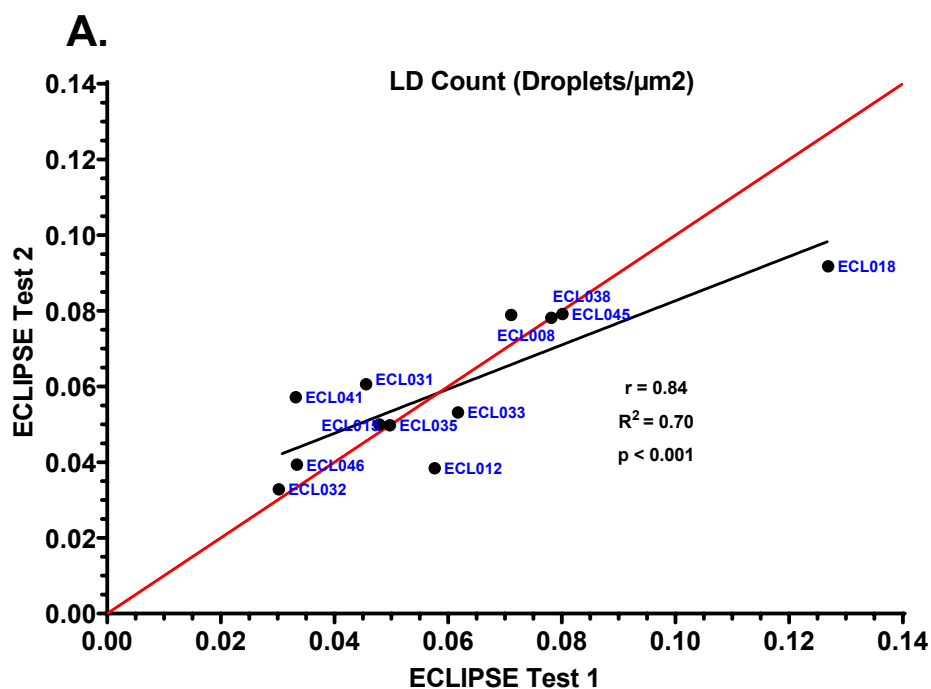


B.

Section	IMCL Content (%)	Deviation from Sample Mean	Deviation ²
Slide 1 Section 1	4.12	-1.1023	1.21514
Slide 1 Section 2	4.33	-0.8963	0.80341
Slide 1 Section 3	5.75	0.5277	0.27843
Slide 1 Section 4	6.00	0.7727	0.59701
Slide 1 Section 5	6.36	1.1327	1.28293
Slide 2 Section 1	5.49	0.2637	0.06952
Slide 2 Section 2	5.14	-0.0833	0.00694
Slide 2 Section 3	3.40	-1.8183	3.30634
Slide 2 Section 4	4.96	-0.2583	0.06674
Slide 2 Section 5	5.29	0.0627	0.00393
Slide 3 Section 1	5.45	0.2297	0.05275
Slide 3 Section 2	6.39	1.1697	1.36812
Sum	62.7	0	9.05126

Figure 2-16: (A) Graph showing pooled IMCL content data for each section/replicate. Bars are mean \pm SEM. Sample mean, which is visually represented by the red dotted line, represents the average IMCL content across all replicates. (B) Table of descriptive statistics for each replicate shown in graph A.

The coefficient of repeatability (Standard Deviation*2.77) is an index of measurement error. In the data above there is 95% confidence that the difference between two repeated measurements of LD count, LD size, and IMCL content in the same sample using the histochemical method described herein will fall below 0.035 droplets/ μm^2 , 0.53 μm^2 , and 2.51%, respectively (see **Figures 2-14B, 2-15B, and 2-16B**). The coefficient of variation for measurement of LD count, LD size, and IMCL content was 27.6%, 15.3%, and 17.4%, respectively. Given that, to the best knowledge of the present author, no investigators have published repeatability data from histochemical IMCL staining methods it is impossible to relativise these findings. Given that LDs are spherical and that more than 168 μm (12, 14 μm sections) of tissue was cut from each transverse-orientated sample, it is highly unlikely that the same LDs were imaged every 2-3 sections, which in part explains the variability observed in these repeated measurements.



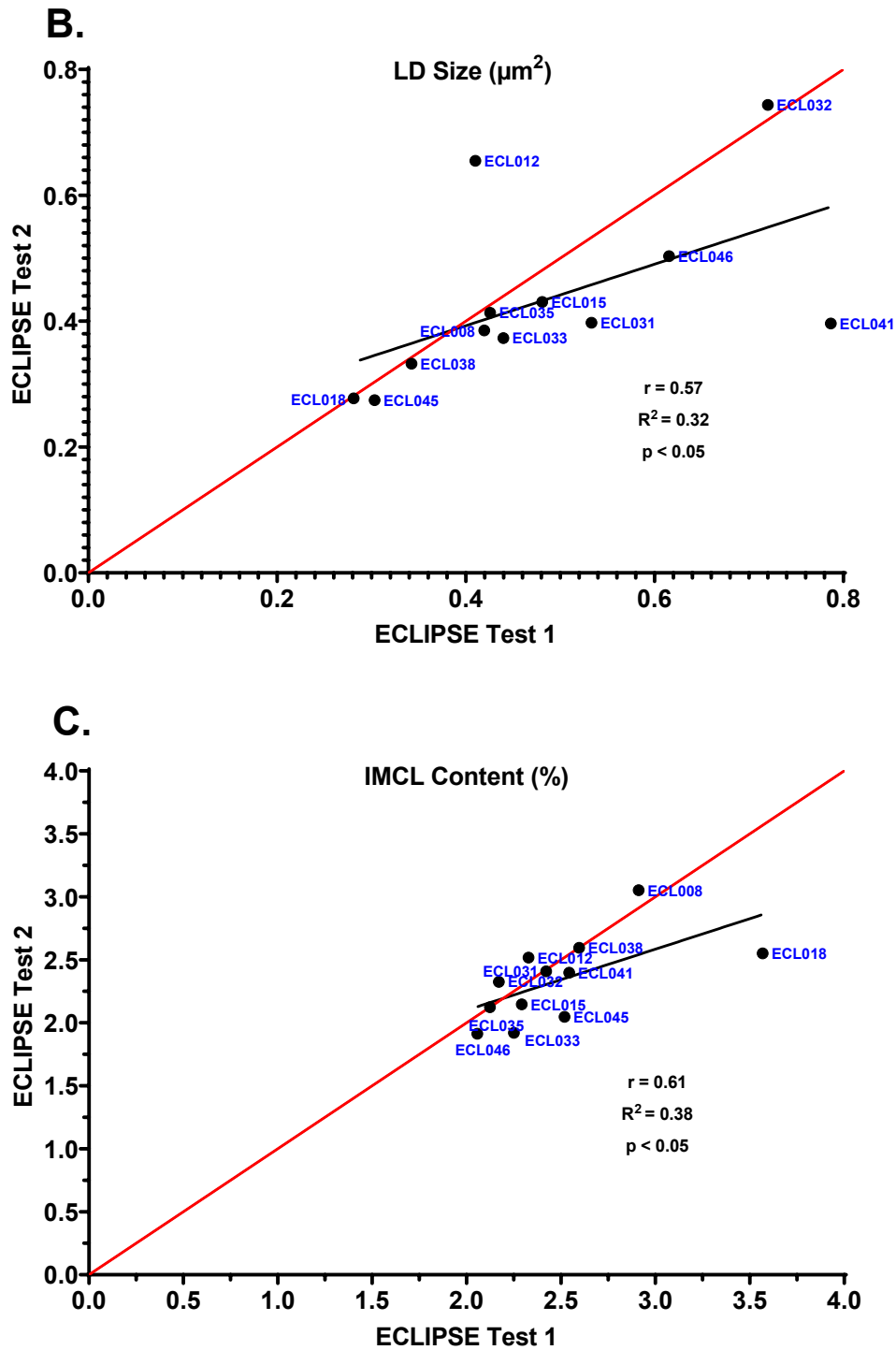


Figure 2-17: Comparison of (A) LD count, (B) LD size, and (C) IMCL content measurements of two independent sections each from a single muscle sample obtained from participants of the ECLIPSE study. For all parameters $n = 12$ pairs. Each point is labelled with the ECLIPSE sample designation in blue. Lines of identity are shown in red.

Sample	Parameter					
	LD Count (LDs/ μm^2)		LD Size (μm^2)		IMCL Content (%)	
	Test 1	Test 2	Test 1	Test 2	Test 1	Test 2
ECL008	0.071	0.079	0.42	0.39	2.91	3.05
ECL015	0.048	0.050	0.48	0.43	2.29	2.15
ECL018	0.127	0.092	0.28	0.28	3.57	2.55
ECL031	0.046	0.061	0.53	0.40	2.42	2.41
ECL032	0.030	0.033	0.72	0.74	2.17	2.33
ECL035	0.050	0.050	0.43	0.41	2.12	2.12
ECL041	0.033	0.057	0.79	0.40	2.54	2.40
ECL046	0.033	0.039	0.62	0.50	2.06	1.91
ECL012	0.058	0.038	0.41	0.65	2.33	2.52
ECL033	0.062	0.053	0.44	0.37	2.25	1.92
ECL038	0.078	0.078	0.34	0.33	2.60	2.60
ECL045	0.080	0.079	0.30	0.27	2.52	2.05
Mean \pm SE	0.060 \pm 0.008	0.059 \pm 0.005	0.48 \pm 0.05	0.43 \pm 0.04	2.48 \pm 0.12	2.33 \pm 0.09
P-value	0.91		0.27		0.16	

Table 2-2: Table of data showing the comparison of LD count, LD size, and IMCL content measurements in two sections of the same sample from the ECLIPSE study. P values relate to the results of paired, two-tailed, t-tests. SE; Standard Error.

To follow these repeatability analyses, sections from 12 samples obtained from participants in the ECLIPSE study described in **Chapter 4** were cut, stained, imaged, and returned to storage in liquid nitrogen (Test 1). A week later these same samples were cut, stained, and imaged again (Test 2). All sections were analysed to measure and compare LD count, LD size, and IMCL content between Test 1 and Test 2. The results of these analyses are shown in scatter plots comparing measurements during Test 1 (x-axis) and measurements made during Test 2 (y-axis) (see **Figure 2-17**). There was a positive linear relationship between Test 1 and Test 2 for all study parameters, with all correlation coefficient hypothesis tests being significant ($p < 0.05$). Two-tailed paired t-tests revealed that there were no significant differences between

the measurements of LD count ($p = 0.91$), LD size ($p = 0.27$), and IMCL content ($p = 0.16$) in the first set of sections from the ECLIPSE study compared to the second set of sections (see **Table 2-2**). The percentage difference in measurement was greatest in mean IMCL content, with it being 6% greater in Test 1 than Test 2 (2.48% vs. 2.33%, respectively).

2.9 Immunohistochemical Determination of Muscle

Fibre Type

2.9.1 Cryosectioning

Cryosectioning of samples for fibre type analysis was performed in the same manner as previously specified for the fluorescent staining of lipid with Bodipy 493/503 in **Section 2.8.1**. Once cut, sections were stored at $-80\text{ }^{\circ}\text{C}$ until staining.

2.9.2 Staining

Sections were removed from storage at $-80\text{ }^{\circ}\text{C}$ and kept frozen with dry ice before being fixed in 2% formaldehyde Zamboni's fixative, contained within glass Coplin staining jars, for 30 minutes at room temperature. This was followed by a wash with 0.1 M SPB to remove excess fixative. Once washed and dry, an ImmEdge pen (H-4000; 2BScientific, Upper Heyford, UK) was used to draw a single circular area enclosing all the sections on each slide. ImmEdge pens contain a hydrophobic solution that, when applied to a slide and left to dry, forms a residue which is insoluble to acetone, ethanol, and water. The hydrophobic nature of this residue allows it to confine immunofluorescent reagents added to the slides to the area in which the sections are located. Once drawn, 200 μl of 0.1% triton x-100 in immunobuffer (0.25% bovine serum albumin, 50 mM glycine, 0.033% saponin and 0.05% sodium azide in SPB) was added to the sections within the enclosed area and these sections were incubated for 10 minutes in preparation for immunofluorescence labelling.

Sections were then washed twice for 5 minutes each time with immunobuffer. To fibre type, the sections were incubated for 3 hours in 200 μl

immunobuffer solution containing unconjugated primary antibodies targeting three different myosin heavy chain isoforms. These antibodies were: 1/500 of 33 µg/mL monoclonal mouse anti-slow twitch myosin heavy chain type I IgG2b (BA-D5; Developmental Studies Hybridoma Bank (DSHB), Iowa City, United States); 1/200 of 64 µg/mL monoclonal mouse anti-fast twitch myosin heavy chain type IIA IgG1 (SC-71; DSHB, Iowa City, United States); and 1/25 monoclonal mouse anti-fast twitch myosin heavy chain type IIX IgM (6H1; DSHB, Iowa City, United States). Also included was 1/700 of 0.5 mg/mL polyclonal rabbit anti-Laminin IgG (L9393-5ML, Sigma-Aldrich, Gillingham, UK) for co-immunostaining of laminin to mark cell boundaries. The primary antibody incubation period was followed by three washes in immunobuffer, each wash lasting five minutes.

Sections were then incubated for 2 hours in 200 µl immunobuffer solution containing secondary antibodies. These antibodies were: 2 mg/mL polyclonal goat anti-mouse IgG2b specific for the IgG γ -2 heavy chain and conjugated to Alexa Fluor 594 (A-21145; Thermo Fisher Scientific, Loughborough, UK); 2 mg/mL polyclonal goat anti-mouse IgG1 specific for the IgG γ -1 heavy chain and conjugated to Alexa Fluor 488 (A-21121; Thermo Fisher Scientific, Loughborough, UK); 2 mg/mL polyclonal goat anti-mouse IgM specific for the μ heavy chain of IgM and conjugated to Alexa Fluor 647 (A-21238; Thermo Fisher Scientific, Loughborough, UK); and 2 mg/mL polyclonal goat anti-rabbit IgG specific for IgG γ heavy and light chains and conjugated to Alexa Fluor 647 (A-32733; Thermo Fisher Scientific, Loughborough, UK). All secondary antibodies were present at a dilution of 1/500 in the immunobuffer. After this secondary antibody incubation period, sections were washed thrice with immunobuffer again for 5 minutes each wash. This was followed by a single 5-minute wash with 0.1 M SPB.

After removing excess SPB from the area delineated in Dako residue, stained muscle sections were mounted in Vectashield mounting medium for fluorescence, covered by 1.5 mm cover slips, and sealed with nail polish before being covered to limit any exposure to external light. Stained sections were then kept at -4 °C overnight and then at -20 °C until imaging.

2.9.3 Image Acquisition

Image acquisition was performed at 10x magnification. The entirety of the most intact section on each slide was captured. Excitation wavelengths of 493 nm, 577 nm and 653 nm were used to excite Alexa Fluors 488, 568 and 647 respectively conjugated to the secondary antibodies. The specific microscope and/or scanner settings used to image muscle fibre types for each study will be discussed in greater detail in the relevant chapters.

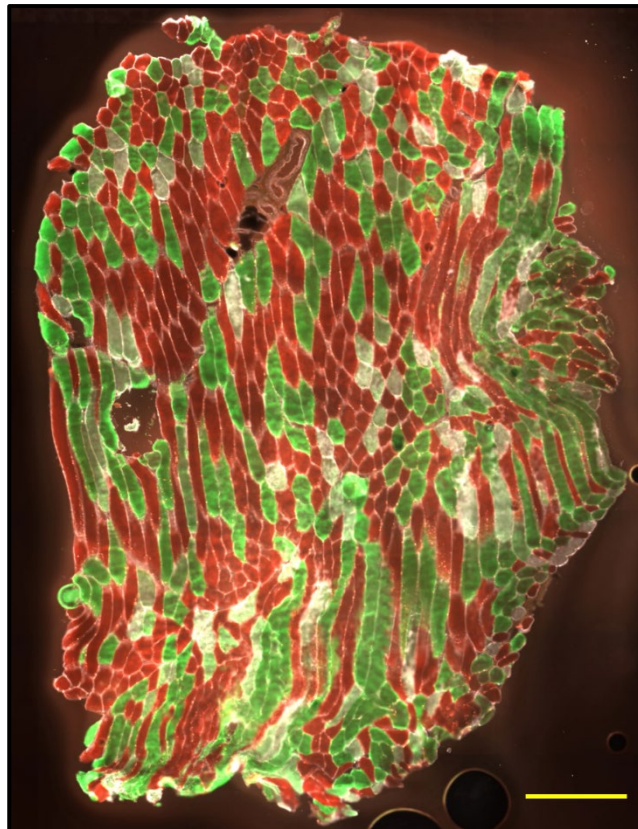


Figure 2-18: Image showing the result of the immunohistochemical staining described in Section 2.9.2 on a test sample. Type I fibres are shown in red. Type IIA fibres are shown in green. Type IIX fibres are shown in white. Bar is 500 μm .

An example image from test staining performed before the staining of samples described in **Chapter 3** is shown in **Figure 2-18**.

2.9.4 Fibre Type and IMCL Matching

Scanned fibre type images were opened in ZEN Blue software for ready switching between channel views and geometric rotation/mirroring of the image as necessary, while IMCL images were opened in FIJI to outline

individual fibres in ROIs. Using the “*Analyse Particles*” tool, study parameters including LD count, LD size and percentage IMCL content were calculated as previously described in **Section 2.8.3** from the ROIs of individual fibres within each sample. Data from the particle analysis of each fibre was transferred to Microsoft Excel (Microsoft Corporation, Redmond, Washington State, United States) and these individual fibres were then sorted and grouped by MHC isoform to calculate the mean value of the study parameters for each MHC isoform in each vastus lateralis sample.

2.10 Statistical Analysis

Graphing and statistical analysis of all data presented here was performed using the GraphPad Prism (GraphPad Software Inc., San Diego, CA, USA) and the Statistical Package for the Social Sciences (SPSS) software packages (IBM, Armonk, NY, USA). Data was assessed for variance and normality and where appropriate non-parametric tests (Friedman Test as an alternative to ANOVA) were used as outlined in the relevant studies. For all tests, the threshold for statistical significance was set to $p\text{-value} \leq 0.05$.

2.11 References

Ainsworth, B.E., Haskell, W.L., Leon, A.S., Jacobs, D.R., Jr., Montoye, H.J., Sallis, J.F. and Paffenbarger, R.S., Jr. (1993) Compendium of physical activities: classification of energy costs of human physical activities. *Medicine and Science in Sports and Exercise*. 25 (1), pp. 71-80.

Allen, M.R. and Krohn, K. (2014) Chapter 5 – Skeletal Imaging. *Basic and Applied Bone Biology*. Academic Press; Illustrated edition.

Assah, F. K., Ekelund, U., Brage, S., Wright, A., Mbanya, J. C., and Wareham, N. J. (2011) Accuracy and validity of a combined heart rate and motion sensor for the measurement of free-living physical activity energy expenditure in adults in Cameroon. *International Journal of Epidemiology*. 40 (1), pp. 112-120.

Bakker, E.A., Hartman, Y.A.W., Hopman, M.T.E., Hopkins, N.D., Graves, L.E.F., Dunstan, D.W., Healy, G.N., Eijsvogels, T.M.H. and Thijssen D.H.J. (2020) Validity and reliability of subjective methods to assess sedentary behaviour in adults: a systematic review and meta-analysis. *International Journal of Behavioral Nutrition and Physical Activity*. 17 (1), 75.

Bartlett, J.W. and Frost, C. (2008) Reliability, repeatability and reproducibility: analysis of measurement errors in continuous variables. *Ultrasound in obstetrics & gynecology: the official journal of the International Society of Ultrasound in Obstetrics and Gynecology*. 31 (4), pp. 466-475.

Blake, G.M. and Fogelman, I. (1997) Technical principles of dual energy x-ray absorptiometry. *Seminars in Nuclear Medicine*. 27 (3), pp. 210-228.

Bergström, J. (1962) Muscle electrolytes in man: determined by neutron activation analysis on needle biopsy specimens. A study on normal subjects, kidney patients and patients with chronic diarrhea. *Scandinavian Journal of Clinical & Laboratory Investigation*. Supplement 68 (11-13), pp. 511-513.

Bernsen, J., (1986) Dynamic thresholding of gray level images. *Proceedings of the International Conference on Pattern Recognition (ICPR '86)*. pp. 1251-1255.

- Boesch, C., Slotboom, J., Hoppeler, H. and Kreis, R. (1997) In vivo determination of intra-myocellular lipids in human muscle by means of localized ¹H-MR-spectroscopy. *Magnetic Resonance in Medicine*. 37 (4), pp. 484-493.
- Brage, S., Brage, N., Franks, P.W., Ekelund, U., Wong, M.Y., Andersen, L.B., Froberg, K., and Wareham, N.J. (2004) Branched equation modeling of simultaneous accelerometry and heart rate monitoring improves estimate of directly measured physical activity energy expenditure. *Journal of Applied Physiology (Bethesda, Md.: 1985)*. 96 (1), pp. 343-351.
- Brage, S., Brage, N., Franks, P.W., Ekelund, U., and Wareham, N.J. (2005) Reliability and validity of the combined heart rate and movement sensor Actiheart. *European Journal of Clinical Nutrition*. 59 (4), pp. 561-570.
- Brehm, A., Roden, M. (2007) Glucose Clamp Technique. In Roden (Ed.), *Clinical Diabetes Research: Methods and Techniques* (pp. 43-68). ProQuest Ebook Central <https://ebookcentral.proquest.com>.
- Cathcart, E.P. and Cuthbertson, D.P. (1931) The composition and distribution of the fatty substances of the human subject. *The Journal of Physiology*. 72 (3), pp. 349-360.
- Chu, A.H. and Moy, F.M. (2015) Reliability and validity of the Malay International Physical Activity Questionnaire (IPAQ-M) among a Malay population in Malaysia. *Asia-Pacific Journal of Public Health*. 27 (2), pp. 2381-2389.
- Cleland, C., Ferguson, S., Ellis, G. and Hunter, R.F. (2018) Validity of the International Physical Activity Questionnaire (IPAQ) for assessing moderate-to-vigorous physical activity and sedentary behaviour of older adults in the United Kingdom. *BMC Medical Research Methodology*. 18 (1), 176.
- Craig, C.L., Marshall, A.L., Sjöström, M., Bauman, A.E., Booth, M.L., Ainsworth, B.E., Pratt, M., Ekelund, U., Yngve, A., Sallis, J.F. and Oja, P. (2003) International physical activity questionnaire: 12-country reliability and validity. *Medicine and Science in Sports and Exercise*. 35 (8), pp. 1381-1395.

Corder, K., Brage, S., Wareham, N. J., and Ekelund, U. (2005) Comparison of PAEE from combined and separate heart rate and movement models in children. *Medicine and Science in Sports and Exercise*. 37 (10), pp. 1761-1767.

Covington, J.D., Johannsen, D. L., Coen, P.M., Burk, D.H., Obanda, D.N., Ebenezer, P.J., Tam, C.S., Goodpaster, B.H., Ravussin, E. and Bajpeyi, S. (2017) Intramyocellular Lipid Droplet Size Rather Than Total Lipid Content is Related to Insulin Sensitivity After 8 Weeks of Overfeeding. *Obesity (Silver Spring, Md.)*. 25 (12), pp. 2079-2087.

Deng, H.B., Macfarlane, D.J., Thomas, G.N., Lao, X.Q., Jiang, C.Q., Cheng, K.K. and Lam, T.H. (2008) Reliability and validity of the IPAQ-Chinese: the Guangzhou Biobank Cohort study. *Medicine and Science in Sports and Exercise*. 40 (2), pp. 303-307.

Dimensions.com (2022) *Semi-Fowler's Position*. Available from: <https://www.dimensions.com/element/semi-fowlers-position>. [Accessed: 10/02/2022].

Dugas, L.R., Harders, R., Merrill, S., Ebersole, K., Shoham, D.A., Rush, E.C., Assah, F.K., Forrester, T., Durazo-Arvizu, R.A. and Luke, A. (2011) Energy expenditure in adults living in developing compared with industrialized countries: a meta-analysis of doubly labeled water studies. *The American Journal of Clinical Nutrition*. 93 (2), pp. 427-441.

Ellis, K., Kerr, J., Godbole, S., Staudenmayer, J., and Lanckriet, G. (2016) Hip and Wrist Accelerometer Algorithms for Free-Living Behavior Classification. *Medicine and science in sports and exercise*. 48 (5), pp. 933-940.

Ferrannini, E. (1988) The theoretical bases of indirect calorimetry: A review. *Metabolism*. 37 (3), pp. 287-301.

Frayn, K.N. (1983) Calculation of substrate oxidation rates in vivo from gaseous exchange. *Journal of Applied Physiology: Respiratory, Environmental and Exercise Physiology*. 55 (2), pp. 628-634.

- Harris, J.A. and Benedict, F.G. (1918) A Biometric Study of Human Basal Metabolism. *Proceedings of the National Academy of Sciences of the United States of America*. 4 (12), pp. 370-373.
- Haugen, H.A., Chan, L.N. and Li, F. (2007) Indirect calorimetry: a practical guide for clinicians. *Nutrition in clinical practice: official publication of the American Society for Parenteral and Enteral Nutrition*. 22 (4), pp. 377-388.
- Jain, R.K. and Vokes, T. (2017) Dual-energy X-ray Absorptiometry. *Journal of Clinical Densitometry: The Official Journal of the International Society for Clinical Densitometry*. 20 (3), pp. 291-303.
- Jeevanandam, M., Hsu, Y.C., Ramias, L. and Schiller, W.R. (1989) A rapid, automated micromethod for measuring free fatty acids in plasma/serum. *Clinical Chemistry*. 35 (11), pp. 2228-2231.
- Khuu, A., Ren, J., Dimitrov, I., Woessner, D., Murdoch, J., Sherry, A.D. and Malloy, C.R. (2009) Orientation of lipid strands in the extracellular compartment of muscle: effect on quantitation of intramyocellular lipids. *Magnetic Resonance in Medicine*. 61 (1), pp. 16-21.
- Kim, F.H., Moylan, S.P., Garboczi, E.J. and Slotwinski, J.A. (2017) Investigation of pore structure in cobalt chrome additively manufactured parts using X-ray computed tomography and three-dimensional image analysis. *Additive Manufacturing*. 17, pp. 23-38.
- Korzynska, A., Roszkowiak, L., Lopez, C., Bosch, R., Witkowski, L. and Lejeune, M. (2013) Validation of various adaptive threshold methods of segmentation applied to follicular lymphoma digital images stained with 3,3'-Diaminobenzidine & Haematoxylin. *Diagnostic Pathology*. 8, 48.
- Kurtze, N., Rangul, V. and Hustvedt, B.E. (2008) Reliability and validity of the international physical activity questionnaire in the Nord-Trøndelag health study (HUNT) population of men. *BMC Medical Research Methodology*. 8 (1), 63.
- Lee, P.H., Macfarlane, D.J., Lam, T.H. and Stewart, S.M. (2011). Validity of the International Physical Activity Questionnaire Short Form (IPAQ-SF): a systematic review. *The International Journal of Behavioral Nutrition and Physical Activity*. 8, 115.

- Leonard, W.R. (2003) Measuring human energy expenditure: what have we learned from the flex-heart rate method? *American Journal of Human Biology: The Official Journal of The Human Biology Council*. 15 (4), pp. 479-489.
- Lorenz E. (1928) The Spectrum of X-Rays from the Back of a Tungsten Target. *Proceedings of the National Academy of Sciences of the United States of America*. 14 (7), pp. 582-588.
- Lugade, V., Fortune, E., Morrow, M. and Kaufman, K. (2014) Validity of using tri-axial accelerometers to measure human movement - Part I: Posture and movement detection. *Medical Engineering & Physics*. 36 (2), pp. 169-176.
- Machann, J., Steidle, G., Thamer, C., Mader, I. and Schick, F. (2003) In Vivo Proton NMR Studies in Skeletal Musculature. *Annual Reports on NMR Spectroscopy*. 50, pp. 1-74.
- Morgan, C.R. and Lazarow, A (1963) Immunoassay of Insulin: Two Antibody System. Plasma Insulin Levels of Normal, Subdiabetic and Diabetic Rats. *Diabetes*. 12 (2), pp. 115-126.
- Nakagawa, S., and Schielzeth, H. (2010) Repeatability for Gaussian and non-Gaussian data: a practical guide for biologists. *Biological Reviews of The Cambridge Philosophical Society*. 85 (4), pp. 935-956.
- Nielsen, H. (1985) Influence of five different anticoagulants on human blood monocyte isolation and functional activities. *Acta Pathologica, Microbiologica, et Immunologica Scandinavica. Section C, Immunology*. 93 (2), pp. 49-52.
- Ogg, R.J., Kingsley, P.B. and Taylor, J.S. (1994) WET, a T1- and B1-insensitive water-suppression method for in vivo localized ¹H NMR spectroscopy. *Journal of Magnetic Resonance. Series B*. 104 (1), pp. 1-10.
- Oyeyemi, A.L., Bello, U.M., Philemon, S.T., Aliyu, H.N., Majidadi, R.W. and Oyeyemi, A.Y. (2014) Examining the reliability and validity of a modified version of the International Physical Activity Questionnaire, long form (IPAQ-LF) in Nigeria: a cross-sectional study. *BMJ Open*. 4 (12), e005820.
- Papathanasiou, G., Georgoudis, G., Papandreou, M., Spyropoulos, P., Georgakopoulos, D., Kalfakakou, V. and Evangelou, A. (2009) Reliability

measures of the short International Physical Activity Questionnaire (IPAQ) in Greek young adults. *Hellenic Journal of Cardiology*. 50 (4), pp. 283-294.

Papathanasiou, G., Georgoudis, G., Georgakopoulos, D., Katsouras, C., Kalfakakou, V. and Evangelou, A. (2010) Criterion-related validity of the short International Physical Activity Questionnaire against exercise capacity in young adults. *European Journal of Cardiovascular Prevention and Rehabilitation*. 17 (4), pp. 380-386.

Péronnet, F. and Massicotte, D. (1991) Table of nonprotein respiratory quotient: an update. *Canadian Journal of Sport*. 16 (1), pp. 23-29.

Pietrobelli, A., Formica, C., Wang, Z. and Heymsfield, S.B. (1996) Dual-energy X-ray absorptiometry body composition model: review of physical concepts. *The American Journal of Physiology*. 271 (6 Pt 1), pp, E941-E951.

Pietrobelli, A., Gallagher, D., Baumgartner, R., Ross, R. and Heymsfield, S.B. (1998) Lean R value for DXA two-component soft-tissue model: influence of age and tissue or organ type. *Applied Radiation and Isotopes: Including Data, Instrumentation and Methods for Use in Agriculture, Industry and Medicine*. 49 (5-6), pp. 743-744.

Posse, S., Otazo, R., Dager, S.R. and Alger, J. (2013) MR spectroscopic imaging: principles and recent advances. *Journal of Magnetic Resonance Imaging: JMRI*. 37 (6), pp. 1301-1325.

Potter, L.E., Paylor, J.W., Suh, J.S., Tenorio, G., Caliaperumal, J., Colbourne, F., Baker, G., Winship, I. and Kerr, B.J. (2016) Altered excitatory-inhibitory balance within somatosensory cortex is associated with enhanced plasticity and pain sensitivity in a mouse model of multiple sclerosis. *Journal of Neuroinflammation*. 13 (1), 142.

Roza, A.M. and Shizgal, H.M. (1984) The Harris Benedict equation reevaluated: resting energy requirements and the body cell mass. *The American Journal of Clinical Nutrition*. 40 (1), pp. 168-182.

Ryan, D.J., Wullems. J.A., Stebbings, G.K., Morse, C.I., Stewart, C.E. and Onambele-Pearson, G.L. (2018) Reliability and validity of the international physical activity questionnaire compared to calibrated accelerometer cut-off

points in the quantification of sedentary behaviour and physical activity in older adults. *PLoS ONE*. 13 (4), e0195712.

Schick, F., Eismann, B., Jung, W.I., Bongers, H., Bunse, M. and Lutz, O. (1993) Comparison of localized proton NMR signals of skeletal muscle and fat tissue in vivo: two lipid compartments in muscle tissue. *Magnetic Resonance in Medicine*. 29 (2), pp. 158-167.

Schindelin J, Arganda-Carreras I, Frise E, Kaynig V, Longair M, Pietzsch T, Preibisch S, Rueden C, Saalfeld S, Schmid B, Tinevez JY, White DJ, Hartenstein V, Eliceiri K, Tomancak P, Cardona A. (2012) Fiji: an open-source platform for biological-image analysis. *Nature Methods*. 9 (7), pp. 676-82.

Schoffelen, P. and Plasqui, G. (2018) Classical experiments in whole-body metabolism: open-circuit respirometry-diluted flow chamber, hood, or facemask systems. *European Journal of Applied Physiology*. 118 (1), pp. 33-49.

Schofield, W.N. (1985) Predicting basal metabolic rate, new standards and review of previous work. *Human Nutrition. Clinical Nutrition*. 39 (Suppl. 1), pp. 5-41.

Sjøgaard, G. and Saltin, B. (1982) Extra- and intracellular water spaces in muscles of man at rest and with dynamic exercise. *The American Journal of Physiology*. 243 (3), pp. R271-R280.

Szczepaniak, L.S., Dobbins, R.L., Stein, D.T. and McGarry, J.D. (2002) Bulk magnetic susceptibility effects on the assessment of intra- and extramyocellular lipids in vivo. *Magnetic Resonance in Medicine*. 47 (3), pp. 607-610.

Szermer, M., Zając, P., Amrozik, P., Maj, C., Jankowski, M., Jabłoński, G., Kiełbik, R., Nazdrowicz, J., Napieralska, M., and Sakowicz, B. (2021) A Capacitive 3-Axis MEMS Accelerometer for Medipost: A Portable System Dedicated to Monitoring Imbalance Disorders. *Sensors (Basel, Switzerland)*. 21 (10), 3564.

Tantakitti, F., Burk-Rafel, J., Cheng, F., Egnatchik, R., Owen, T., Hoffman, M., Weiss, D.N. and Ratner, D.M. (2012) Nanoscale clustering of carbohydrate

thiols in mixed self-assembled monolayers on gold. *Langmuir: the ACS journal of surfaces and colloids*. 28 (17), pp. 6950-6959.

Tognarelli, J.M., Dawood, M., Shariff, M.I., Grover, V.P., Crossey, M.M., Cox, I.J., Taylor-Robinson, S.D. and McPhail, M.J. (2015) Magnetic Resonance Spectroscopy: Principles and Techniques: Lessons for Clinicians. *Journal of Clinical and Experimental Hepatology*. 5 (4), pp. 320-328.

Tomioka, K., Iwamoto, J., Saeki, K. and Okamoto, N. (2011) Reliability and validity of the International Physical Activity Questionnaire (IPAQ) in elderly adults: the Fujiwara-kyo Study. *Journal of Epidemiology*. 21 (6), pp. 459-465.

Wang, Z., Heymsfield, S.B., Chen, Z., Zhu, S. and Pierson, R.N. (2010) Estimation of percentage body fat by dual-energy x-ray absorptiometry: evaluation by in vivo human elemental composition. *Physics in Medicine and Biology*. 55 (9), pp. 2619-2635.

Wanner, M., Probst-Hensch, N., Kriemler, S., Meier, F., Autenrieth, C. and Martin, B.W. (2016) Validation of the long international physical activity questionnaire: Influence of age and language region. *Preventive Medicine Reports*. 3, pp. 250-256.

Weir, J.B. (1949) New methods for calculating metabolic rate with special reference to protein metabolism. *The Journal of Physiology*. 109 (1-2), pp. 1-9.

Yalow, R.S. and Berson, S.A. (1960) Immunoassay of endogenous plasma insulin in man. *The Journal of Clinical Investigation*. 39 (7), pp. 1157-1175.

Yang, C.C., and Hsu, Y.L. (2010) A review of accelerometry-based wearable motion detectors for physical activity monitoring. *Sensors (Basel, Switzerland)*. 10 (8), pp. 7772-7788.

Zuntz, N. (1897) Ueber den Stoffverbrauch des Hundes bei Muskelarbeit. *Archiv für die gesamte Physiologie des Menschen und der Tiere*. 68, pp. 191-211.

3. The effect of 3 and 56 days of bed rest on IMCL content and glucose disposal in healthy male volunteers maintained in energy balance

3.1 Introduction

Physical inactivity has been associated with the presentation of metabolic impairments that are major risk factors for cardiovascular disease (Katzmarzyk *et al.*, 2009) and T2DM (Hu, 2003). Global inactivity levels, particularly those in high-income countries (gross national income per capita of \$12,696 or greater (World Bank, 2022)), are projected to rise in the coming decades (Guthold *et al.*, 2018) due to a variety of factors including: the proportional increase in desk jobs that require minimal physical activity (Brownson, Boehmer, and Luke, 2005), increased screen time amongst children and adolescents (Healy *et al.*, 2008; Hale and Guan, 2015) and the progressive urbanisation of populations in low income countries (Assah *et al.*, 2011). Thus, physical inactivity will be an increasingly significant factor in the disease burden of the global population (Lee *et al.*, 2012; Ozemeka, Lavieb, and Rognmoc, 2019). Improving our understanding of the mechanisms which control physiological adaptations to physical inactivity is crucial to developing effective countermeasures against the metabolic impairments that present during states of inactivity.

Bed rest has been used to study low level physical activity and hospitalisation for decades and is also used to simulate the microgravity conditions experienced in space (Hargens and Vico, 2016). Given that bed rest is most commonly necessitated during hospitalisation and that the average length of stay for patients in the UK is 6-7 days (Eurostat, 2019; Ward *et al.*, 2021), with the global median length of stay being 6 days (Kiss *et al.*, 2021), a long-term (chronic) period of bed rest can be defined as lasting longer than 7 consecutive days.

Both short- and long-term bed rest studies have universally identified decreased whole-body, insulin-mediated GD as a hallmark consequence of bed rest (Lipman *et al.*, 1970; Brower, 2009; Coker *et al.*, 2014; Rudwill *et al.*, 2018). This decrease in whole-body GD is the result of impaired glucose tolerance, primarily caused by peripheral insulin resistance (Stuart *et al.*, 1988; Mikines *et al.*, 1991). Impaired glucose tolerance acts as a precursor to the development of T2DM and various chronic cardiovascular diseases including ischaemic heart disease, the leading cause of death worldwide (World Health Organisation, 2016). Skeletal muscle is responsible for the disposal of upwards of 80% of intravenously infused glucose under hyperinsulinaemic-euglycaemic clamp conditions (see **Section 1.3**) (Wasserman, 2009; DeFronzo and Tripathy, 2009). Attenuation of the contraction-stimulated glucose uptake pathway (Yu *et al.*, 2015; Bergouignan *et al.*, 2016) and the decrease in the expression of key regulators of the insulin-stimulated glucose uptake pathway, including Akt1, TBC1D4, and GLUT4, in skeletal muscle (Biensø *et al.*, 2012; Dirks *et al.*, 2018) are some of the mechanistic drivers contributing to the development of peripheral insulin resistance and decreased whole-body GD during bed rest, and have been proposed to play a role in chronic disease development (Doehner *et al.*, 2010; Kampmann *et al.*, 2021).

Recent work has focussed on elucidating the potential role of IMCL accumulation in contributing to the impairment of whole-body GD during 7 to 28 days of bed rest (Cree *et al.*, 2010; Dirks *et al.*, 2016). There is a well-established negative association between IMCL content and GD in sedentary lean and obese individuals; the greater the skeletal muscle lipid content an individual has, the lower their muscle and whole-body GD (Phillips *et al.*, 1996; Pan *et al.*, 1997; Krssak *et al.*, 1999; Goodpaster *et al.*, 2001; Bajpeyi *et al.*, 2014). As previously described, see **Section 1.5**, this relationship has been proposed to be mechanistically explained by the accumulation of IMCL, including DAG and ceramide species, which are involved in downstream antagonism of the canonical insulin signalling pathway (Bosma *et al.*, 2012; Chavez and Summers, 2012; Petersen *et al.*, 2016; Søgaard *et al.*, 2019). IMCL accumulation has also been implicated in increasing PDK activity

(Petersen *et al.*, 2015), resulting in decreased pyruvate flux into the TCA cycle (Kiilerich *et al.*, 2010; Constantin-Teodosiu *et al.*, 2012).

In the context of bed rest and inactivity, the hypothesis proposed by some authors is that IMCL accumulates as a result of a bed-rest induced reduction in mitochondrial content decreasing FA oxidation (Blanc *et al.*, 2000a; Bergouignan *et al.*, 2011; Bilet *et al.*, 2020). The accumulation of IMCL in this way is then thought to perturb glucose metabolism via aforementioned mechanisms, thereby contributing to decreased insulin-mediated whole-body GD. More simply of course, if energy intake is not reduced in bed rest the ensuing positive energy balance will also result in IMCL deposition, independent of any impact of bed rest on lipid oxidation rates. More specifically, for participants in bed rest studies, decreased daily energy expenditure, which predominantly arises from decreased AEE (see **Section 2.3.2**) (Ritz *et al.*, 1998; Bergouignan *et al.*, 2010), produces a state of positive energy balance unless their diets are strictly controlled to maintain energy balance (Blanc *et al.*, 2000b; Hamburg *et al.*, 2007; Biolo *et al.*, 2008; Bergouignan *et al.*, 2011). Moreover, the hypothesis that IMCL accumulation during bed rest is a driver of impaired GD is contested by evidence showing that, under conditions of energy balance, IMCL did not accumulate during an acute 7-day period of bed rest, regardless of changes in mitochondrial content, muscle oxidative capacity, and significantly reduced whole-body GD (Dirks *et al.*, 2016). Thus, the accumulation of IMCL in the context of bed rest may be a direct consequence of participants being in states of positive energy balance rather than a result of any changes in mitochondrial content or impairments in FA oxidation due to bed rest *per sé*. Whether the results observed following 7 days of bed rest (Dirks *et al.*, 2016), impaired whole-body GD in the face of unchanged IMCL content, remain consistent in the chronic bed rest setting requires investigation.

Mechanistically, positive energy balance elevates plasma FFA concentrations, resulting in greater FA uptake by the skeletal muscles and greater incorporation of these FAs into the TAG pool stored in LDs, which are the main constituents of IMCL (Bachmann *et al.*, 2001; Zderic *et al.*, 2004; Sakurai *et al.*, 2011; Hoeks *et al.*, 2012; Phielix *et al.*, 2012). Studies suggest that increases in IMCL content are primarily underpinned by increases in LD size, which is negatively correlated with insulin sensitivity; smaller, numerous droplets are observed in the skeletal muscle of highly insulin sensitive individuals and larger, less numerous droplets are observed in the skeletal muscles as insulin sensitivity decreases (He, Goodpaster, and Kelley, 2004; Nielsen *et al.*, 2017; Covington *et al.*, 2017). This increase in LD size and decrease in LD count is likely the result of the fusion of droplets within LD clusters (Borén *et al.*, 2013).

It is important to note that, in healthy participants, bed rest cannot replicate the pathology of chronic disease or metabolic multimorbidities. The aetiology of impaired whole-body GD, its association with IMCL accumulation and its contribution to the development of insulin resistance may be vastly different in the context of inactivity than it is in the context of disease.

In contrast to inactivity, exercise is known to robustly improve insulin-mediated GD in general (Heath *et al.*, 1983; Ferrara *et al.*, 2006; O'Gorman *et al.*, 2006) and within a few days following bed rest (Tabata *et al.*, 1999), mainly by improving the skeletal muscle expression and translocation of GLUT4 and other key mediators of the insulin-mediated glucose uptake pathway (Dela *et al.*, 1994; Tabata *et al.*, 1999; Dagaard *et al.*, 2000; Frøsig *et al.*, 2007). Exercise is also known to increase the rate of lipid oxidation and acutely decrease IMCL content (Horowitz and Klein, 2000; Watt *et al.*, 2002; Lund *et al.*, 2018). What remains to be elucidated is whether there is any association between exercise-induced improvements in whole-body GD following bed rest and changes in IMCL content during this same time frame.

3.2 Study Aims

It has been demonstrated that IMCL content does not change following an acute, 7-day, period of bed rest conducted with participants in energy balance, though both impaired GD and altered mitochondrial content and substrate oxidation present in this context. Whether these observations are consistent in chronic bed rest is unknown. Also, whilst exercise is known to improve whole-body GD post immobilisation, the role of IMCL in this process requires elucidation.

The work presented in this chapter aimed to investigate the association between changes in GD and changes in LD count, LD size, and IMCL content during acute (3 days) and chronic (56 days) periods of bed rest, with four research questions in mind:

1. Are any changes in LD count, LD size, and IMCL content observed during chronic (56 days) bed rest consistent with those observed following an acute (3 days) period of bed rest conducted under conditions of energy balance?
2. Are any observed changes in LD parameters and IMCL content associated with changes in substrate oxidation and/or plasma lipid availability?
3. If the decline in insulin-mediated whole-body GD during either acute or chronic bed rest is associated with IMCL accumulation or changes in LD size and count, are these changes muscle fibre-type specific?
4. Is the increase in insulin-mediated GD observed following exercise intervention post-bed rest associated with a reduction in IMCL content, and is this reduction muscle fibre-type specific?

3.3 Materials and Methods

3.3.1 Study Overview and Ethics Statement

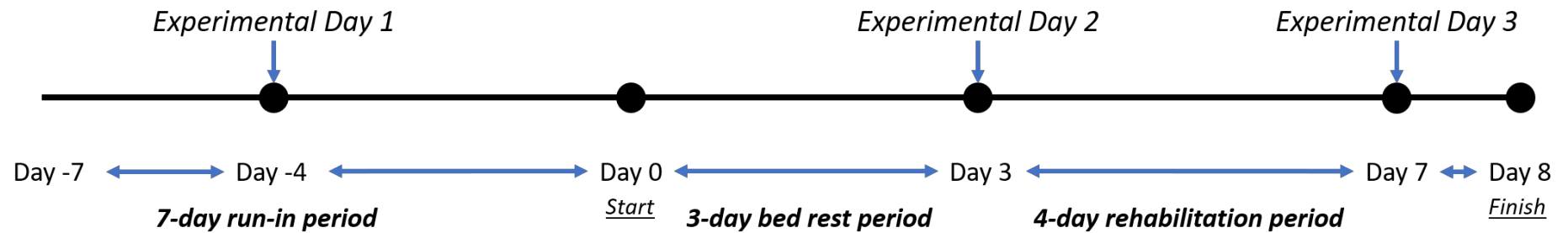
An acute bed rest study of 3 days duration was conducted at the David Greenfield Human Physiology Unit, University of Nottingham. There were 10 participants, all of whom were healthy young men. A chronic bed rest study lasting 60 days was conducted at the Space Clinic of L'Institut de Médecine et de Physiologie Spatiales (MEDES) based in Toulouse, France. There were 20 participants in this study, all of whom were healthy males. Participants in both studies were lean, had no history of any neuromuscular disorders, were non-smokers and were not taking any prescribed medications.

The primary end-point measurements in both studies were IMCL content, which was quantified by fluorescent staining of LDs in cryosections from vastus lateralis biopsies obtained from the participants, whole-body GD, determined using the hyperinsulinaemic-euglycaemic clamp technique, and whole-body carbohydrate and FA oxidation, determined by indirect calorimetry. DEXA scans were performed to determine total lean mass and fat mass. Blood samples were taken and analysed to measure fasting insulin, FFA, and TAG concentrations.

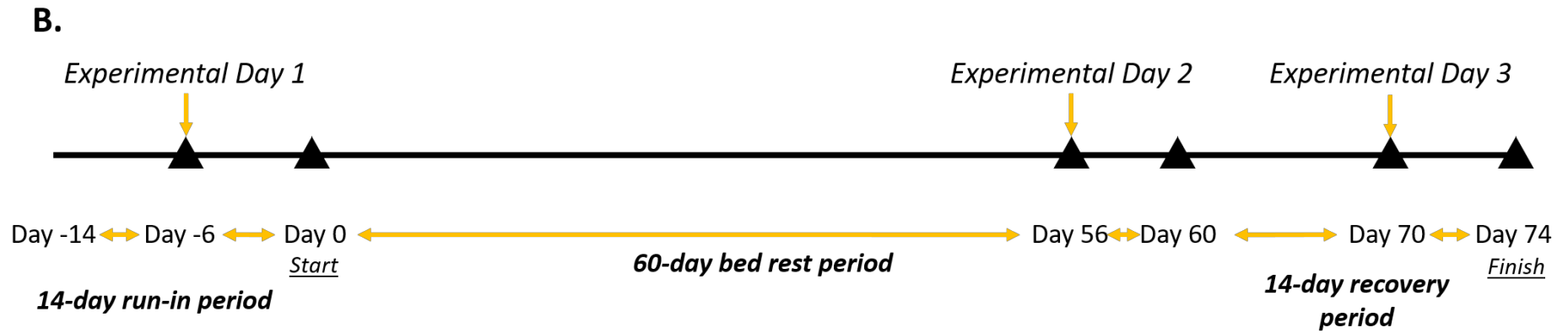
All participants from both studies were of sound physical and mental health and were made fully aware of the study protocols before giving informed consent to undergo the experimental procedures described herein. The acute bed rest study was approved by the University of Nottingham Medical School Ethics Committee in May of 2017 (Ethics reference no: 6-1704). The chronic bed rest study was approved by CPP Sud-Ouest et Outre-Mer I (Ethics reference no ID RCB: 2016-A00401–50), an ethics committee associated with Rangueil University Hospital, a subsidiary of the University Hospital of Toulouse.

3.3.2 Study Protocols

A.



- *Experimental Days: DEXA Scan (Day 1 only), Hyperinsulinaemic-euglycaemic Clamp, Vastus Lateralis Biopsy, and Indirect Calorimetry.*



- *Experimental Days: DEXA Scans, Hyperinsulinaemic-euglycaemic Clamp (Experimental Day 1 and 2), Vastus Lateralis Biopsy, and Indirect Calorimetry.*
- *DEXA scans performed periodically during the 60-day bed rest period.*

Figure 3-1: Timelines for the experimental protocols of the (A) acute (3 days) bed rest study and (B) chronic (60 days) bed rest study.

3.3.2.1 3 Days Bed Rest

There were three phases in this study: a 7-day run-in period, 3 days of strict bed rest at -6° head-down tilt (HDT) and finally a 4-day period of remobilisation (see **Figure 3-1A**). BMI was calculated from the measured heights and weights of the participants at screening. Baseline habitual physical activity for all participants was evaluated using a standardised and extensively validated (Kurtze, Rangul, and Hustvedt, 2008; Papathanasiou *et al.*, 2010; Tomioka *et al.*, 2011) compilation of self-reported measures referred to as the International Physical Activity Questionnaire (IPAQ) (Craig *et al.*, 2003). The IPAQ is based on a comprehensive assessment of the intensity and duration of daily physical activity related to work, recreation, sitting and mode of transportation amongst others, with each task being assigned a Metabolic Equivalent of Task (MET) value, which indicates the energy cost of that activity (Ainsworth *et al.*, 1993). The MET values for each of these activities are then multiplied by the total time that the activity is engaged in over a week and these scores are combined to calculate a total score expressed as MET minutes per week (MET-min/week). The greater this combined score, the more physically active a participant is. Based on the mean IPAQ score of $7,368 \pm 4,032$ (SD) MET-min/week recorded for the participants of this 3-day bed rest study, they were categorised as physically active prior to the bed rest intervention.

For the entirety of the study (run-in, bed rest, and remobilisation periods) participants were placed on an individually tailored, precisely controlled diet (30% of total energy intake provided by fat, 55% by carbohydrates, 15% by protein). Energy intake during the bed rest period was reduced to account for the decreased AEE, to avoid states of positive energy balance, and to prevent any significant changes in the weight of the participants during the study. To facilitate this, each participant was fitted with an Actiheart activity monitor (CamNtech Ltd., Fenstanton, UK) to collect heart rate and accelerometry data, and estimate AEE in the run-in phase, which was used to characterise habitual physical activity level (PAL) (see **Section 2.4**). For each participant, the modified Harris-Benedict equation was used to estimate baseline RMR (Harris and Benedict, 1918; Roza and Shizgal, 1984). The PAL is a factor reflecting the amount of physical activity a person engages in daily and is

calculated as a ratio of TEE to RMR, with a PAL of less than 1.4 representing a state of inactivity. The calculated RMRs for each participant were multiplied by 1.4 to estimate TEE during the run-in phase. These TEE calculations acted as estimates of the daily dietary intake required to maintain energy balance whilst participants were at home and maintaining habitual physical activity levels. Baseline RMR for each participant was multiplied by 1.2 to estimate TEE and derive the daily dietary energy intake allowed for each participant when accounting for reduced physical activity during the bed rest period, and by 1.4 when participants resumed ambulation. The PAL thresholds defined here are derived from European Space Agency (ESA) bed rest standardisation guidelines for nutrient intake during bed rest at -6° HDT (International Academy of Astronautics, 2014).

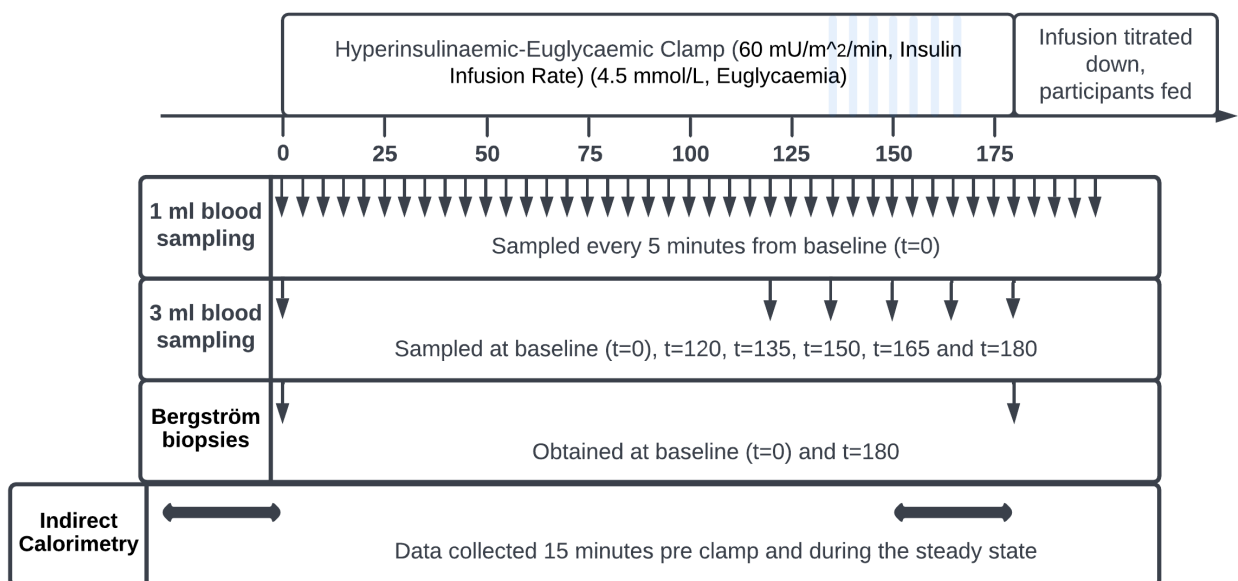


Figure 3-2: Schematic of the experimental days. Striped, light blue area shows the steady state phase of the hyperinsulinaemic-euglycaemic clamp.

During “experimental days”, biopsies were taken, ventilated hood indirect calorimetry was performed using the Quark RMR calorimeter (COSMED srl, Bicester, UK) to calculate carbohydrate and fat oxidation rates (see **Section 2.3**), and the hyperinsulinaemic-euglycaemic clamp technique was performed to determine whole-body GD (see **Figure 3-2**). For the 3-day bed rest study the experimental days were on day 4 of the run-in period, the

third (and final) day of the bed rest period, and the final day of the remobilisation period (see **Figure 3-1A**).

Baseline body composition for each participant was determined using DEXA with the Lunar Prodigy DF+ 16075 (GE Healthcare, Buckinghamshire, UK) on day -4 during the run-in period as described in **Section 2.2**. For each experimental day, participants had fasted overnight and, before the hyperinsulinaemic-euglycaemic clamp protocol was performed, vastus lateralis biopsies were taken from one leg using the Bergström needle (5 mm) biopsy procedure (Bergström, 1962). Two passes were made to obtain ~300 mg of tissue. Following this, participants were cannulated, and 3 ml samples of arterialised venous blood were collected at baseline and at intervals of 15 minutes from t=120 till the end of the clamp thereafter during the 3-hour infusion time to measure the concentration of several factors including insulin, FFAs, and TAGs (see **Figure 3-2**). Insulin (Human Actrapid, EMEA/H/C/000424; Novo Nordisk A/S, Bagsværd, Denmark) was infused at a constant rate of 60 mU/m²/min for 3 hours through the antecubital cannula and arterialised venous blood glucose concentration was maintained at 4.5 mmol/L by varying the infusion rate of 20% (w/v) glucose (Baxter Healthcare, Thetford, UK) (see **Section 2.1.1**). Blood glucose concentration was measured every 5 minutes (see **Figure 3-2**) and these measurements were used to calculate GD during the clamp as described in **Section 2.1.2**. GD was defined as the M values calculated from the clamp data standardised to the baseline lean body mass measurements collected at day -4 using DEXA. At t=180 minutes of the clamp, vastus lateralis biopsies were obtained from each participant as previously described, but this time taken from the contralateral leg. After the biopsy at t=180 minutes the infusion of insulin was stopped, the participants were fed, and the glucose infusion titrated down until blood glucose concentration was stable without requiring the infusion of exogenous glucose (see **Figure 3-2**). Hyperinsulinaemic-euglycaemic clamps and Bergström biopsies were performed in the same manner on the other two experimental days, day 3 (post bed rest) and day 7 (post remobilisation), with biopsies being taken from the exercised leg at the post remobilisation time point (see **Figure 3-1A**).

For each participant, some of the muscle biopsy tissue was immediately frozen in liquid nitrogen after collection, for subsequent biochemical analysis, whilst the remaining tissue was embedded in OCT cryo-embedding compound (361603E; VWR International, Lutterworth, UK) and frozen in isopentane (Fisher Scientific, Loughborough, UK), for subsequent histochemical analysis. These frozen biopsy samples were placed in labelled tubes and stored fully submerged in liquid nitrogen within a cryogenic storage dewar.

During remobilisation days, participants were ambulatory and performed 5 sets of 30 maximal isokinetic knee extensions of the dominant leg under strict supervision whilst secured to an isokinetic dynamometer (Cybex, HUMAC NORM, Computer Sports Medicine Inc., Stoughton, Massachusetts, United States), with the non-dominant leg left untrained as a control. Flexion of the knee was from a 90° angle to a 180° angle at an angular velocity of 90°/s and with each set separated by a 1-minute rest. This specific exercise protocol was used as it has been demonstrated to recruit all muscle fibre types and effectively restore lost muscle mass and functional strength following two-week periods of voluntary single-leg limb immobilisation in young healthy male participants by altering the expression of genes associated with muscle catabolism and hypertrophy (Jones *et al.*, 2004).

3.3.2.2 56 Days Bed Rest

Following a 14-day run-in period, participants underwent 60 days of strict bed rest in -6° HDT position. This was followed by a medically supervised, 14-day period of recovery (see **Figure 3-1B**). For ten days, prior to the start of the run-in period, while participants were still free-living, heart rate and habitual PAL for each participant were recorded 24 hours a day by an ActiGraph GT3X activity monitor (ActiGraph LLC, Pensacola, FL, USA) (see **Section 2.4**). After this, at the start of the run-in period (Day -14), RMR was estimated by indirect calorimetry. Accelerometry data from the ActiGraph was used to ensure that participants maintained the same PALs during the run-in phase when they were based at MEDES as they did at home, to prevent deconditioning. For each participant, daily energy requirements (TEE) during the study were calculated by multiplying the RMR values estimated by indirect calorimetry by a PAL of 1.4 during the run-in phase and 1.2 during the bed rest phase.

Individualised meal plans were designed for each of the participants to maintain energy balance and prevent any significant fluctuations in weight during the run-in and bed rest stages of the study. Serial DEXA scans (Hologic, QDR4500C, MA, USA) were also performed to inform any necessary adjustments to diets during the bed rest period.

The experimental days in this study were day -6 during the run-in period (pre-bed rest, baseline measurements), day 56 of the bed rest intervention (post bed rest) and day 10 of the recovery period (see **Figure 3-1B**). Hyperinsulinaemic-euglycaemic clamp conditions were the same as those described in **Section 3.3.2.1** and vastus lateralis biopsies were taken using the same method. However, while biopsies were taken both before and after the hyperinsulinaemic-euglycaemic clamps, post-clamp biopsies were not mounted for histochemistry. As in the 3-day study, some vastus lateralis biopsy samples were immediately frozen in liquid nitrogen and some muscle tissue was mounted in OCT compound, forming blocks that were subsequently stored at -80 °C.

Recovery programmes designed to restore upright posture, unassisted balance, and gait control were overseen by the ESA Space Medicine and Remobilisation team and were tailored for the individual needs of each participant. Programmes generally consisted of stretches and simple movements/rotations designed to strengthen core and lower limb muscles during the first ten days of recovery before progressing to push ups, kettlebell swings and submaximal treadmill runs thereafter.

It is important to note that during the 60-day bed rest period the participants were split into two groups of 10, one group being a Placebo group, the other being a “Cocktail” group. Participants randomly allocated to the Cocktail group were prescribed a regimen of pills with a nutrient content that has been described in detail elsewhere (Damiot *et al.*, 2019). Briefly, the regimen consisted of three components. The first was a daily 741 mg polyphenol mix (323.4 mg flavonols, 135.6 mg flavanols, 108.0 mg flavanones, 78.0 mg oligostilbènes, 50.4 mg acide hydroxycinnamiques, and 45.6 mg phenylpropanoïdes) provided by 6 pills, two taken with breakfast, two with

lunch, and two with dinner. The second component was 138 mg vitamin E with 80 µg of selenium which was contained within a single pill orally ingested once daily after breakfast. For the final component, participants were also given three pills daily, taken orally during breakfast, lunch, and dinner to provide 3g of omega-3 (1.1 g of eicosapentaenoic acid and 1.0 g of docosahexaenoic acid). This cocktail was designed to reduce inactivity-induced skeletal muscle oxidative damage and deconditioning but failed to alter muscle CSA, muscle fibre-type distribution, markers of oxidative stress, and the expression of molecules involved in the protein synthesis pathway, as described elsewhere (Arc-Chagnaud *et al.*, 2020). Also, whilst the mRNA expression of 18 genes involved in the regulation of inflammation and oxidative damage changed in response to 56 days of bed rest, the changes in only 2 of these genes (Heat Shock 70-kDa Protein 8 (HSPA8) and Immunoglobulin (CD79A)-Binding Protein 1) was different between the Placebo and Cocktail groups (Shur *et al.*, 2022). Given the matched anthropometric measurements between the two groups at baseline and the lack of any differences in the endpoint measurements, in the data presented here the Placebo and Cocktail groups are combined to form a single chronic bed rest group of 20 participants.

3.3.4 Quantification of IMCL Content

Staining of LDs with the fluorescent dye Bodipy 493/503 was used to quantify IMCL content in vastus lateralis biopsies taken from participants of both the acute bed rest and chronic bed rest studies as detailed in **Sections 2.8.1, 2.8.2 and 2.8.3.**

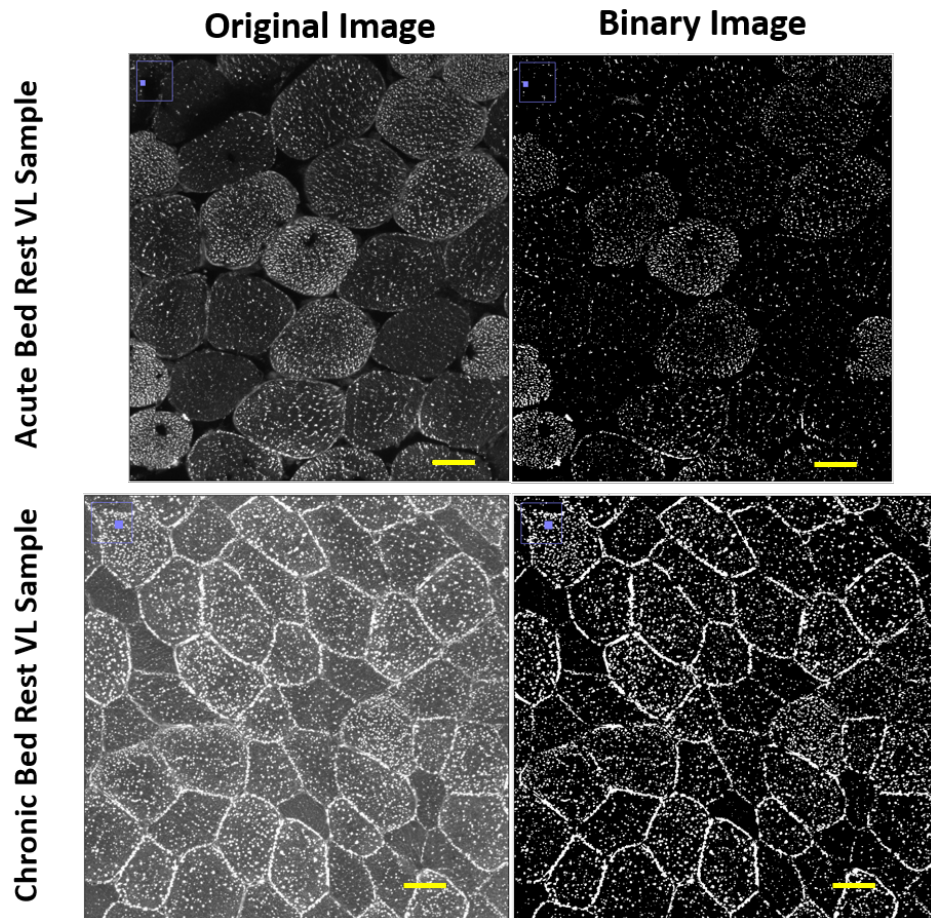


Figure 3-3: Representative images of Bodipy 493/503 staining in the acute and chronic bed rest studies taken at 20x magnification. Bars are 40 μ m.

A Zeiss LSM 700, Axio Imager 2 confocal microscope (Carl Zeiss AG, Jena, Germany) operating ZEN Black Edition software (Carl Zeiss AG, Jena, Germany) was used to image Bodipy 493/503 stained sections at 20x magnification through a 20x/0.8 M27 Plan-Apochromat objective with a 25 mm field of view and 45.06 mm parfocal length. The 488 nm argon laser line was used to excite the Bodipy fluorophore. Pinhole size was maintained at 0.96 AU.

As outlined in **Section 2.8.3**, IMCL content within each sample was calculated as the percentage of the total area of each section occupied by lipid. LD count was calculated as total LD count/ total tissue area. LD size was calculated as a mean of the size of every droplet within the ROI(s) of each muscle section.

In total, 57 vastus lateralis biopsy samples from the chronic bed rest study were stained, imaged, and analysed. For the acute bed rest study 45 biopsies were stained, imaged, and analysed in total but only data from the 21 pre-clamp biopsies are presented here.

3.3.5 Immunohistochemical Staining of MHC for Muscle Fibre Typing

3.3.5.1 Cryosectioning and Staining

Cryosectioning of samples for fibre type analysis was performed in the same manner as previously specified in **Section 2.8.1**. The sections were then stored at -80 °C overnight until staining. Immunohistochemical staining of these cryosections was performed the following morning as specified in **Section 2.9.2**.

3.3.5.2 Image Acquisition

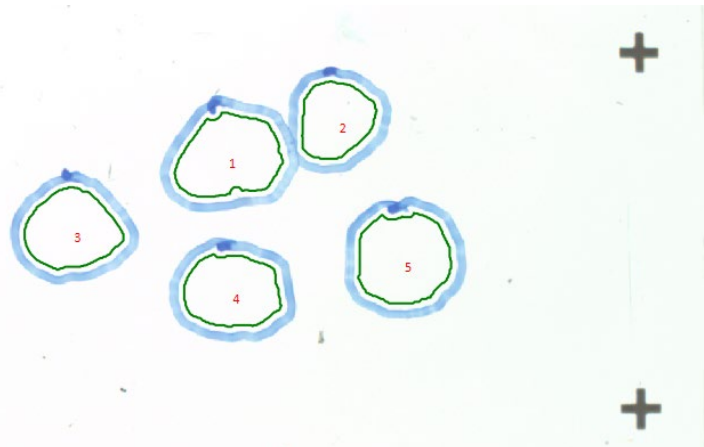


Figure 3-4: Representative scan preview image of individual vastus lateralis sample section identification in ZEN software before Axio image acquisition. Blue borders were manually drawn around individual sections on each slide. The inner green borders represent the area recognised by the software as an area which will be imaged.

Image acquisition was performed at 10x magnification using the 10x/0.45 M27 plan-apochromatic objective of a Zeiss Axio Scan.Z1 slides scanner (Carl Zeiss AG, Jena, Germany) equipped with an AxioCam MR Rev 3 camera and interfaced with ZEN software (Carl Zeiss AG, Jena, Germany). A felt tip pen was used to draw around each section on each slide such that these sections could all be individually identified by the ZEN software operated by the scanner

(see **Figure 3-4**). The entirety of the most intact section on each slide from each sample was captured. Excitation wavelengths of 493 nm, 577 nm and 653 nm emitted by the LED modules of the slide scanner were used to excite Alexa Fluors 488, 568 and 647 respectively conjugated to the secondary antibodies. All other acquisition settings were the same for each fluorophore. Fluorophore emissions for the MHC Type I isoform were captured in channel 1 and are presented here in red. Fluorophore emissions for the MHC Type IIA isoform were captured in channel 2 and are presented in green while emissions from the fluorophores conjugated to MHC Type IIX antibodies were captured in channel 3 and are presented here in grey. As the secondary antibodies for the Type IIX isoform and laminin share the same fluorophore (Alexa Fluor 647), laminin is also presented here in grey. For scanned sections, analysis was carried out in the FIJI and ZEN Blue software packages.

3.3.5.3 Fibre Type and IMCL Matching

1.	Acute (3-Days) Bed Rest		
	Type I	Type IIA	Type IIX
Pre-Bed Rest	27 ± 5	22 ± 5	7 ± 2
Post Bed Rest	33 ± 7	28 ± 5	11 ± 3
Post Rehab	31 ± 7	22 ± 5	7 ± 1

2.	Chronic (56-Days) Bed Rest		
	Type I	Type IIA	Type IIX
Pre-Bed Rest	93 ± 14	51 ± 7	13 ± 3
Post Bed Rest	70 ± 9	60 ± 6	16 ± 3

Tables 3-2 and 3-3: Mean number of fibres counted and matched per MHC isoform, per time point for all samples of the acute and chronic bed rest studies. Values are mean ± SEM.

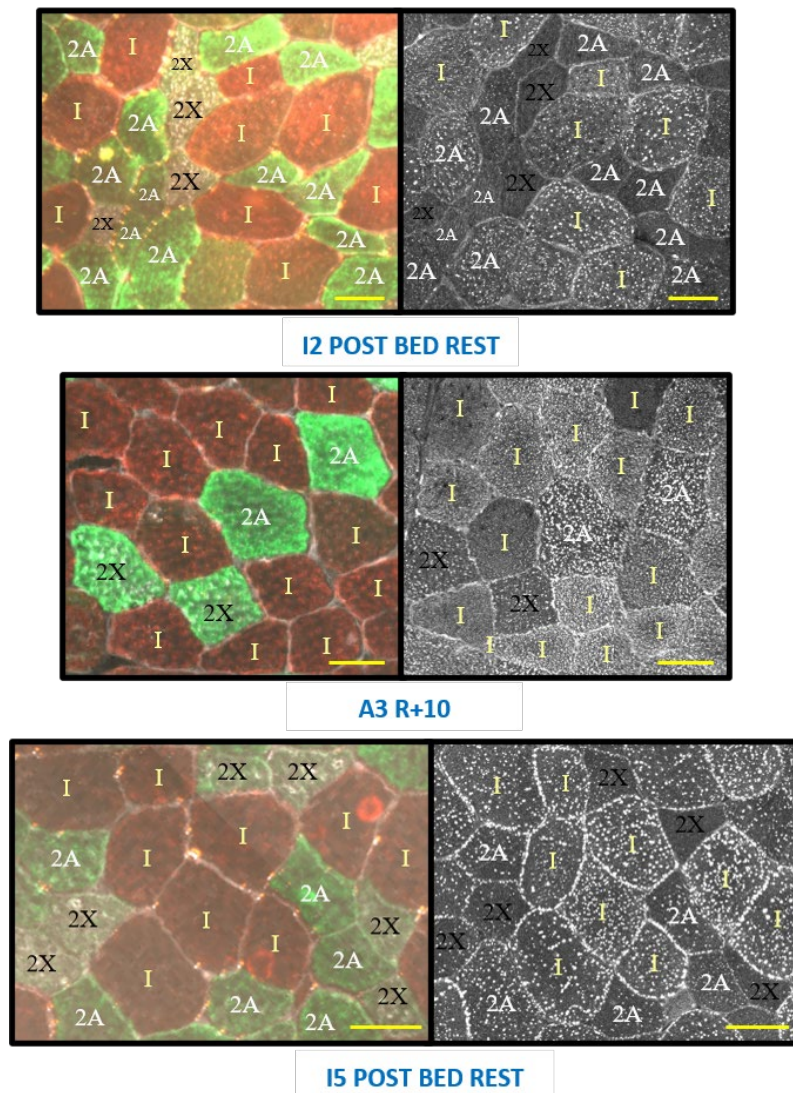


Figure 3-5: Matching of IMCL content in individual fibres to MHC isoform. For each pair of images, immunohistochemical staining of MHC is shown in the left panel whilst fluorescent staining of lipid with Bodipy 493/503 is shown in the right panel. Sample designations are shown beneath each set of images in blue. Bars are 50 μ m.

The number of fibres counted during the fibre type analysis for the acute and chronic bed rest studies is shown in **Tables 3-2 and 3-3**. Lipid parameters in muscle fibres from each of the imaged biopsy samples were matched to fibre type as detailed in **Section 2.9.4**. Examples of this matching for the acute and chronic bed rest studies are shown in **Figure 3-5**.

3.3.6 Blood Analyses

Fasting insulin, FFA and triglyceride concentrations were measured in blood samples collected on the mornings of each of the experimental days following

an overnight fast. Serum insulin concentrations were measured using the radioimmunoassay technique with a standard kit (HI-14K, EMD Millipore Corporation, MI, USA) as described in **Section 2.6.1**. Plasma FFA and TAG concentrations were measured using enzymatic-colourimetric assay kits (WAKO Chemicals GmbH, Neuss, Germany) and an automated analyser (ABX Pentra 400, Horiba Medical, Montpellier, France) respectively (see **Sections 2.6.2** and **2.6.3**).

3.3.7 Statistical Analysis

One-way ANOVA was used for comparing IMCL quantification and steady state GD data at the pre bed rest, post bed rest and post remobilisation time points in the acute bed rest study. In the chronic bed rest study paired, two-tailed t-tests were used to analyse differences in LD count, LD size, IMCL content and steady state GD between the pre bed rest and post bed rest time points. Wilcoxin tests were used to compare differences in fasting insulin, TAG, and FFA measurements at the different time points. Two-way ANOVA was used for the analysis of muscle fibre-type specific IMCL data, and substrate oxidation data from indirect calorimetry, in both studies. Tukey's test was used for post hoc multiple comparison between time points and fibre types.

For both studies, the Shapiro-Wilk and Kolmogorov-Smirnov tests were used to assess the normality of the data. Mauchly's sphericity test was used to assess whether the variance in the differences in LD count, LD size and percentage IMCL content between all the pairs being compared were equal. Where Mauchly's W was <0.75 , the Geisser-Greenhouse correction was used to calculate individual variance between the pairs being compared.

Where data failed the tests for normality the Freidman test, with Dunn's pairwise post hoc tests, was used as a non-parametric alternative to assess the significance of differences in LD count, LD size and percentage IMCL content between time points. Where this was applicabe the Freidman statistic is stated.

3.4 Results

3.4.1 Participant Characteristics

	Acute (3 Days) Bed Rest (n = 10)		Chronic (56 Days) Bed Rest (n = 20)	
Mean Age (Years)	24 ± 4.0		34 ± 8.1	
Baseline IPAQ Score	7,368 ± 4,032		9,562 ± 2,469	
	Pre-Bed Rest	Post Bed Rest	Pre-Bed Rest	Post Bed Rest
BMI (kg/m ²)	22.7 ± 1.9	22.7 ± 1.9	23.7 ± 6.7	23.4 ± 1.8
Weight (kg)	70.7 ± 10.1	70.6 ± 10.1	73.5 ± 27.3	72.6 ± 7.2
Lean mass (DEXA) (kg)	56.6 ± 6.6	—	54.1 ± 5.8	50.2 ± 5.4
Fat mass (DEXA) (kg)	10.9 ± 3.2	—	19.2 ± 4.0	20.4 ± 4.0

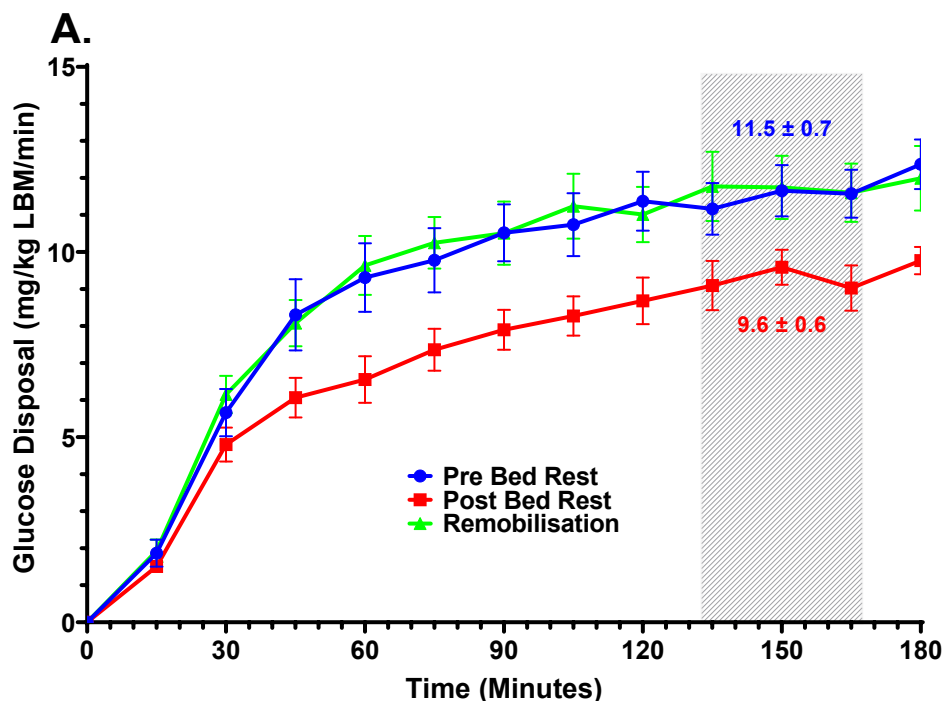
Table 3-1: Table of participant characteristics for both the acute and chronic bed rest studies. Dashes represent measurements that were not made during the study. Values are mean ± SD.

Participants in the acute and chronic bed rest studies were matched for baseline BMI and lean mass. There were significant differences in the ages (24 ± 4.0 years vs. 34 ± 8.1 years, $p < 0.001$) and baseline fat mass (10.9 ± 3.8 kg versus 19.2 ± 4.0 kg, $p < 0.001$) measurements in the participants of the acute bed rest study compared to those in the chronic bed rest study (see **Table 3-1**). Participants in the chronic bed rest study were a decade older on average and carried double the fat mass of their counterparts in the acute bed rest study. No significant differences between the two groups were observed in measurements of BMI, weight, lean mass, or pre-study habitual physical activity as measured by the IPAQ score. Lean mass and fat mass were not measured post bed rest in the acute bed rest study.

All participants in the acute bed rest study completed the run-in, 3 days bed rest and remobilisation phases of the study. Complete sets of mounted biopsy samples were not available at each time point for IMCL quantification using Bodipy 493/503. Six, seven and eight biopsies from the pre-bed rest, post bed rest and post remobilisation time points were available, respectively; all were analysed.

All participants of the chronic bed rest study completed the run-in, 60 days bed rest and post-recovery phases of the study. A single mounted biopsy was unavailable at each time point, leaving a total of 57 samples (19 at each time point) for IMCL quantification with Bodipy 493/503. All were cut, stained, imaged, and analysed but only IMCL and LD data from the pre-bed rest and post bed rest time points are reported here as energy balance was not maintained, hyperinsulinaemic-euglycaemic clamps were not performed, and exercise regimes were individualised, not standardised, during the recovery phase of the study.

3.4.2 Whole-Body Glucose Disposal: 3 Days Bed Rest



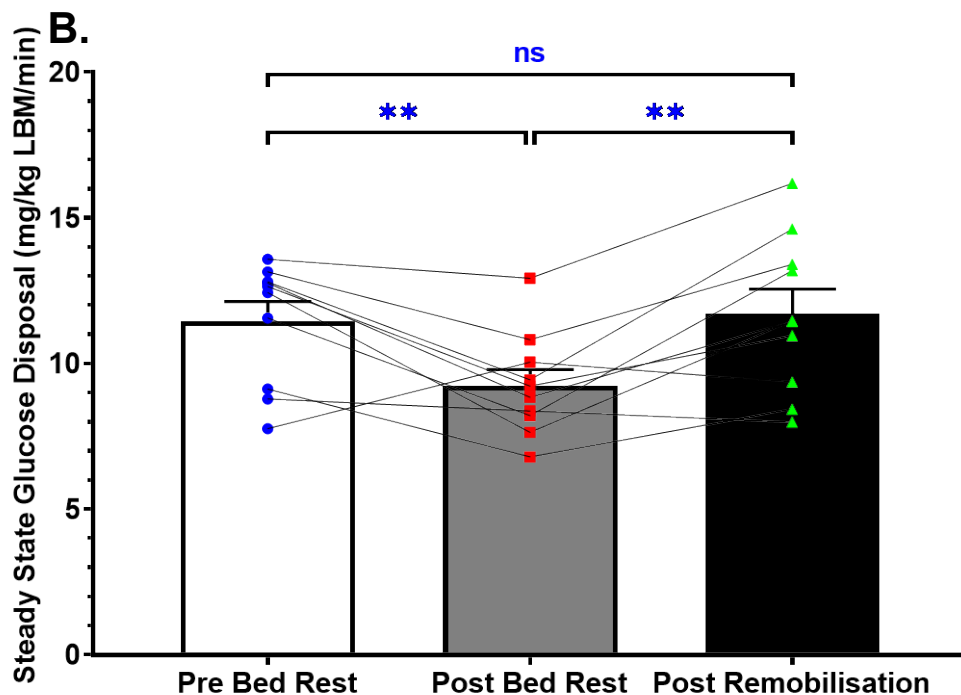


Figure 3-6: Whole-body glucose disposal during the time course of the 180-minute hyperinsulinaemic-euglycaemic clamp protocol (A). Shaded area shows the steady state ($t=135$ to $t=165$). Mean glucose disposal during the steady state (B). Glucose disposal is standardised to lean body mass (LBM) and $n = 10$ at all time points. Bars are SEM.

Using values measured during the steady state between $t=135$ and $t=165$ minutes of the hyperinsulinaemic-euglycaemic clamp, a decrease in mean insulin-mediated whole-body GD from 11.5 ± 0.68 mg/kg/min to 9.30 ± 0.58 mg/kg/min was observed across all 10 participants of the acute bed rest study following 3 days of bed rest at -6° HDT ($p < 0.01$) (see **Figure 3-6B**). The resumption of ambulation and unilateral leg exercises significantly increased mean insulin-mediated whole-body GD to 11.7 ± 0.86 mg/kg/min ($p < 0.01$) post remobilisation, restoring it to baseline levels.

3.4.3 Whole-Body Glucose Disposal: 56 Days Bed Rest

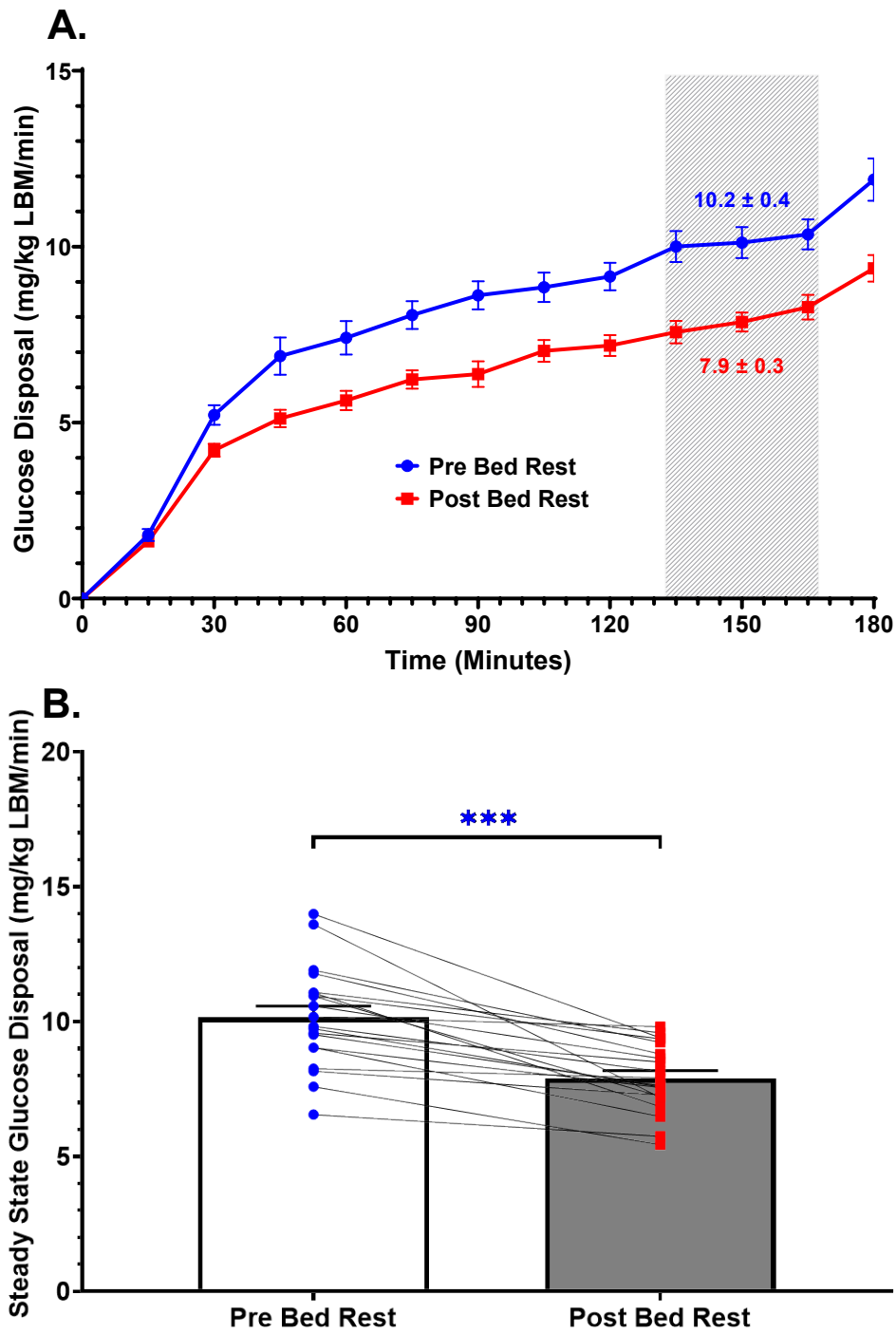


Figure 3-7: Whole-body glucose disposal during the time course of the 180-minute hyperinsulinaemic-euglycaemic clamp protocol (A). Shaded area shows the steady state ($t=135$ to $t=165$). Glucose disposal during the steady state (B). Glucose disposal is standardised to lean body mass (LBM), $n = 20$ at all time points. Bars are SEM.

A significant decrease of 22% in mean insulin-mediated whole-body GD from the pre-bed rest to the post bed rest time point (10.2 ± 0.42 mg/kg/min vs. 7.90 ± 0.28 mg/kg/min, respectively; $p < 0.001$) was observed in the 20 participants of the chronic bed rest study following 56 days of bed rest (see **Figure 3-7A, 3-7B**).

3.4.4 Substrate Oxidation: 3 Days Bed Rest

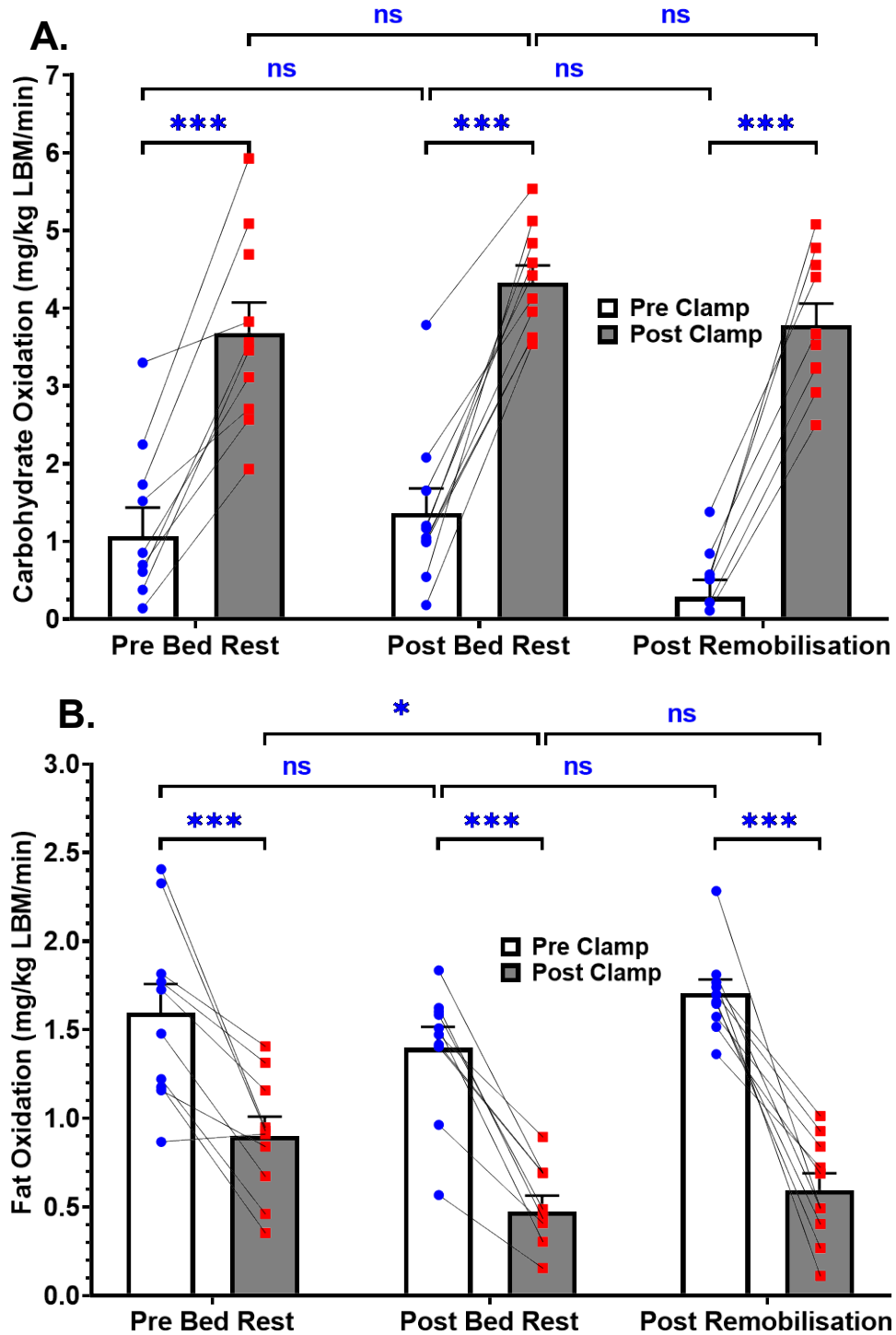


Figure 3-8: (A) Carbohydrate and (B) fat oxidation before and during the hyperinsulinaemic-euglycaemic clamp protocol. Statistically significant differences are presented as *. Values are mean \pm SEM and are standardised to lean body mass (LBM).

At each time point, carbohydrate oxidation during the hyperinsulinaemic-euglycaemic clamp was greater than before the clamp ($p < 0.001$) (see **Figure 3-8A**). Mean carbohydrate oxidation in response to insulin infusion during the clamp protocol was not significantly different between the pre bed rest, post bed rest and post remobilisation time points (3.69 ± 0.39 mg/kg LBM/min vs. 4.34 ± 0.22 mg/kg LBM/min, vs. 3.79 ± 0.27 mg/kg LBM/min, respectively; $p = 0.17$).

The insulin-stimulated suppression of fat oxidation during the clamp protocol was significant relative to pre clamp fat oxidation at all time points ($p \leq 0.001$) (see **Figure 3-8B**). Following 3 days of bed rest fat oxidation during the clamp protocol was suppressed to a greater extent than under the same conditions at the pre bed rest time point (1.13 ± 0.14 mg/kg LBM/min, pre bed rest, post clamp vs. 0.59 ± 0.11 mg/kg LBM/min, post bed rest, post clamp; $p < 0.05$) but returned to baseline levels post remobilisation.

3.4.5 Substrate Oxidation: 56 Days Bed Rest

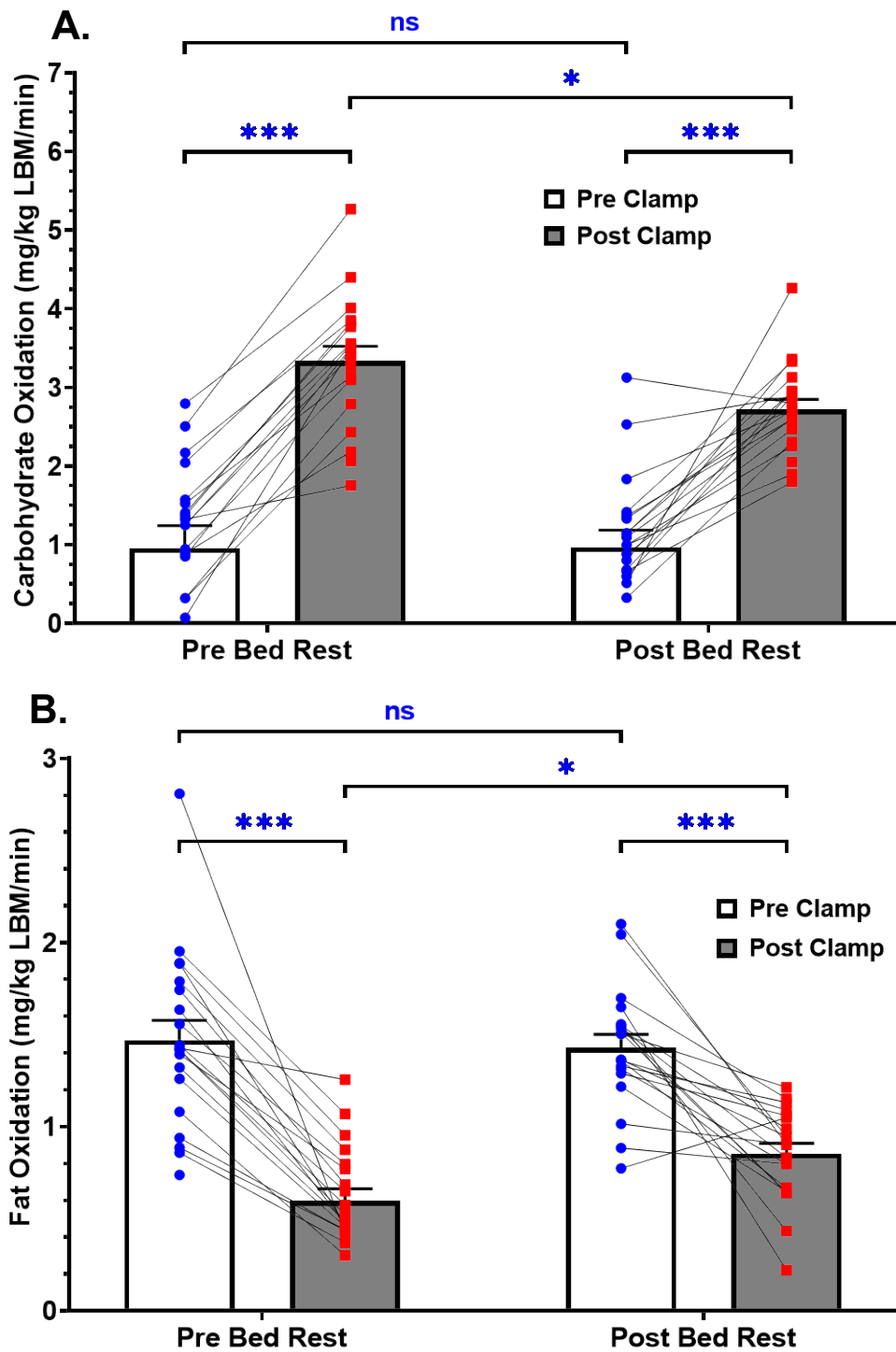


Figure 3-9: (A) Carbohydrate and (B) fat oxidation before and during the hyperinsulinaemic-euglycaemic clamp protocol. Statistically significant differences are presented as *. Values are mean \pm SEM and standardised to LBM.

A significant increase in carbohydrate oxidation in response to insulin infusion during the hyperinsulinaemic-euglycaemic clamp protocol compared to pre clamp fasted measurements was observed at both the pre bed rest and post bed rest time points ($p < 0.001$) (see **Figure 3-9A**). After 56 days of bed rest, mean carbohydrate oxidation during the clamp protocol was significantly lower than carbohydrate oxidation during the clamp protocol at the pre bed rest time point (2.72 ± 0.13 vs. 3.34 ± 0.18 mg/kg LBM/min, respectively; $p < 0.05$).

At both the pre bed rest and post bed rest time points, a significant suppression in fat oxidation was observed during the clamp protocol in response to insulin infusion, relative to pre clamp measurements of fat oxidation ($p < 0.001$) (see **Figure 3-9B**). After 56 days of bed rest insulin-stimulated suppression of fat oxidation was blunted, such that fat oxidation during the clamp protocol at the post bed rest time point was significantly greater than fat oxidation during the clamp protocol at the pre bed rest time point (0.85 ± 0.06 mg/kg LBM/min vs. 0.60 ± 0.07 mg/kg LBM/min, respectively; $p < 0.05$).

3.4.6 Fasting Insulin, TAG, and FFA Concentration

	Acute Bed Rest			Chronic Bed Rest	
	Pre Bed Rest	Post Bed Rest	Post Remobilisation	Pre Bed Rest	Post Bed Rest
Fasting Insulin Concentration (mIU/L)	6 ± 2	9 ± 2	7 ± 1	18 ± 2	22 ± 2 **
Fasting Triglyceride Concentration (mmol/L)	0.69 ± 0.05	0.76 ± 0.06	0.54 ± 0.05 * †	0.66 ± 0.10	0.61 ± 0.07
Fasting FFA Concentration (mmol/L)	0.53 ± 0.04	0.57 ± 0.06	0.38 ± 0.05 * †	0.43 ± 0.03	0.44 ± 0.40

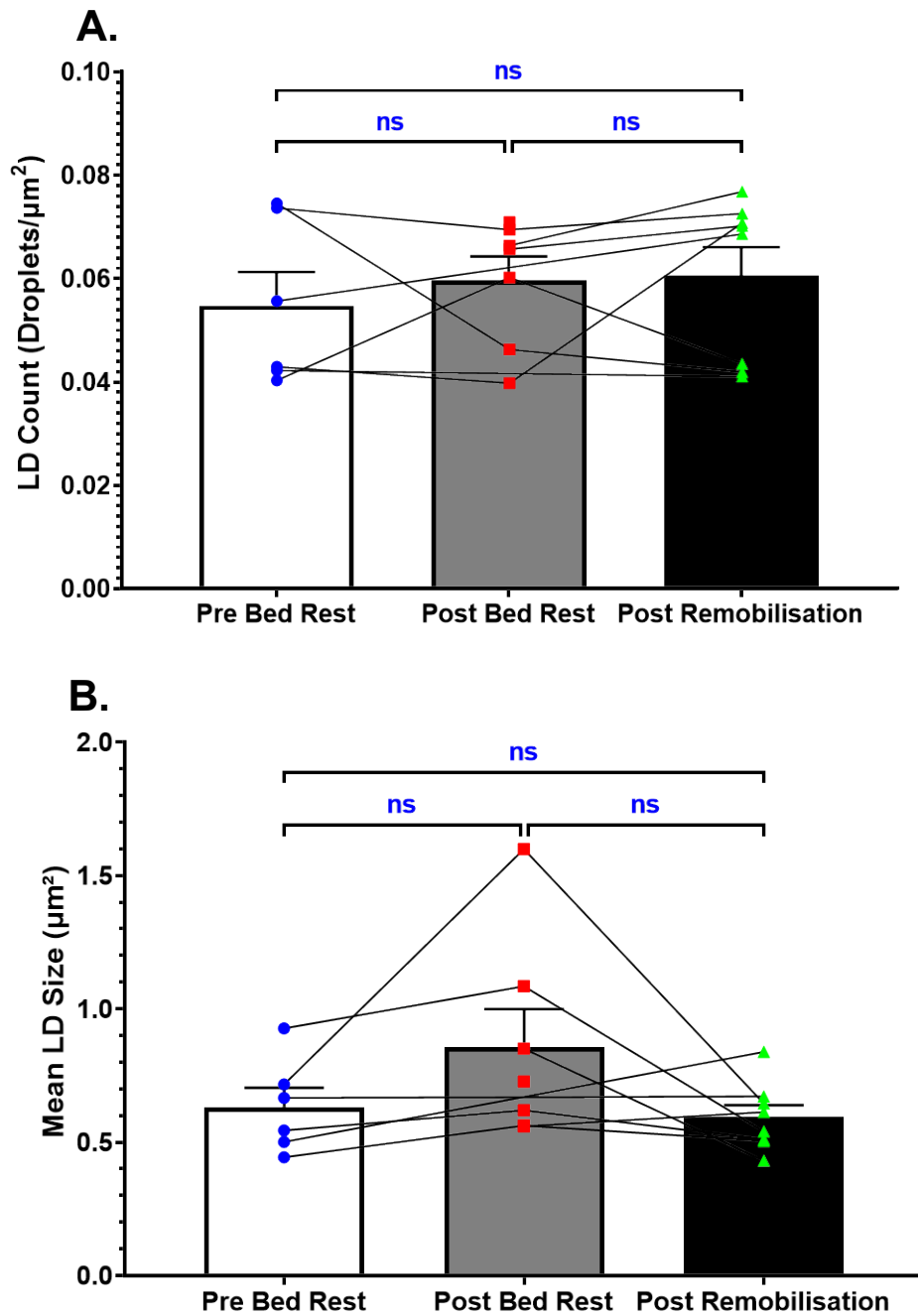
Table 3-4: Table of fasting insulin, triglyceride and FFA concentrations in participants of both the acute and chronic bed rest studies at all time points. All values are mean \pm SEM. Comparisons vs. Pre Bed Rest are represented as *, vs. Post Bed Rest as †.

Fasting insulin concentration in the participants of the acute bed rest study did not change significantly between the pre bed rest, post bed rest and post remobilisation time points ($p = 0.46$) (see **Table 3-4**). However, after 56 days of bed rest, a 25% increase in fasting insulin concentration was observed in the participants of the chronic bed rest study compared to pre-bed rest measurements ($p < 0.01$).

In the acute bed rest study, no significant difference in fasting triglyceride concentration was observed from pre-bed rest to post bed rest ($p = 0.58$). However, fasting triglyceride concentration was significantly lower following remobilisation compared to the pre-bed rest time point ($p < 0.05$) and the post bed rest time point ($p < 0.05$). In the chronic bed rest study, there was no significant difference in fasting plasma triglyceride concentration between the pre-bed rest and post bed rest time points ($p = 0.51$).

Fasting FFA concentration in the acute bed rest participants measured at the post remobilisation time point was significantly lower than FFA concentration at the pre-bed rest and post bed rest time points ($p < 0.05$). There were no differences in fasting FFA concentration between the pre-bed rest and post bed rest time points ($p = 0.80$). In the chronic bed rest study, no significant difference in fasting FFA concentration was observed between the pre-bed rest and post bed rest time points ($p = 0.80$).

3.4.7 IMCL Content: 3 Days Bed Rest



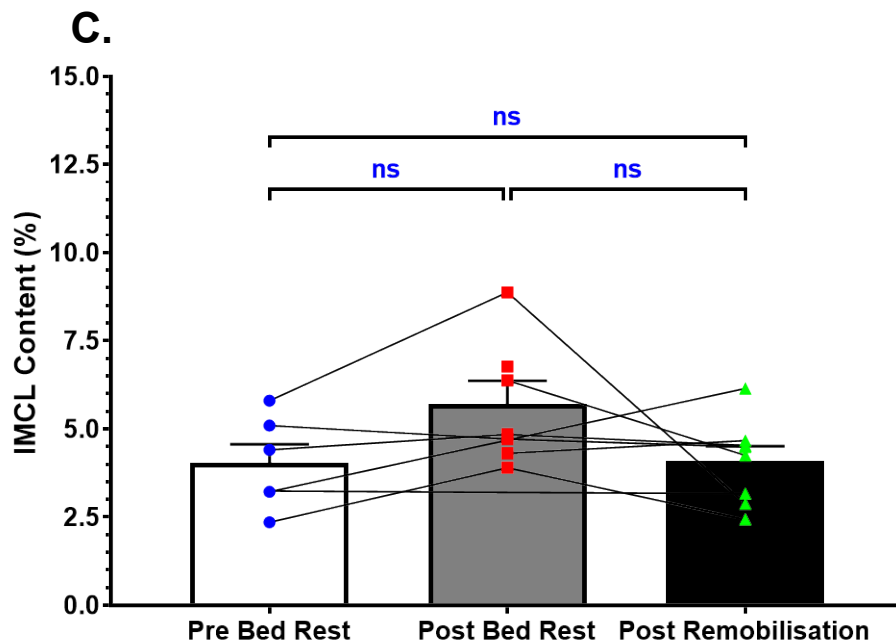


Figure 3-10: (A) LD count, (B) LD size and (C) the percentage IMCL content in the vastus lateralis muscle biopsies before and after 3 days of -6° HDT bed rest and after remobilisation. All data are generated from pre-clamp samples for each participant, at each time point. Values are mean \pm SEM. For all measures, $n = 6$ pre bed rest, $n = 7$ post bed rest and $n = 8$ post remobilisation.

Figure 3-10 shows the LD count (**A**), LD size (**B**), and the contribution of lipid to total fibre content (**C**) in vastus lateralis biopsies before 3 days of bed rest, after 3 days of bed rest and after a remobilisation period of 4 days. No significant changes in the relative number of LDs were observed as an effect of bed rest or remobilisation between the pre-bed rest, post bed rest, and post remobilisation time points (0.055 ± 0.007 LDs/ μm^2 vs. 0.060 ± 0.005 LDs/ μm^2 vs. 0.061 ± 0.005 LDs/ μm^2 , respectively; Freidman test statistic $\chi^2(2) = 0.5$, $p = 0.78$).

No differences in LD size were observed between the time points ($p = 0.12$). Significant changes in LD size between the pre-bed rest and post bed rest time points were not observed ($0.63 \pm 0.07 \mu\text{m}^2$ vs. $0.86 \pm 0.14 \mu\text{m}^2$, respectively; $p = 0.43$) after 3 days of bed rest. After bed rest, LD size did not change following remobilisation ($0.86 \pm 0.14 \mu\text{m}^2$ vs. $0.59 \pm 0.04 \mu\text{m}^2$, $p = 0.32$).

The IMCL content within the vastus lateralis muscle did not change between the pre-bed rest, post bed rest and post remobilisation time points ($4.0 \pm 0.5\%$ vs. $5.7 \pm 0.7\%$ vs. $4.1 \pm 0.4\%$, respectively; $p = 0.14$).

3.4.8 IMCL Content by Fibre Type: 3 Days Bed Rest

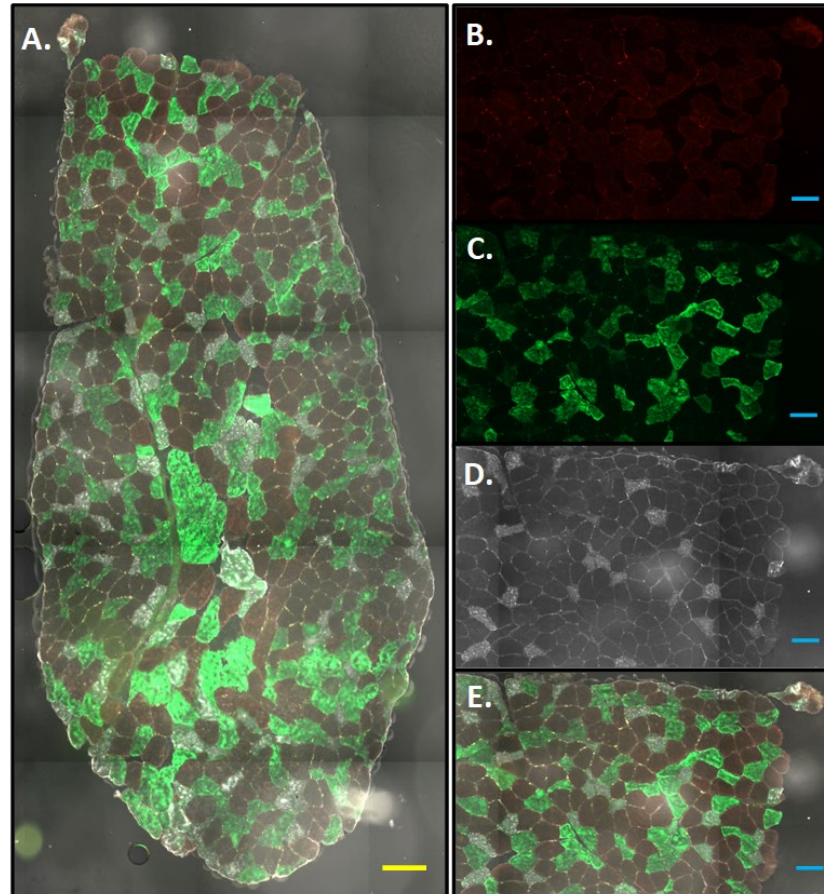
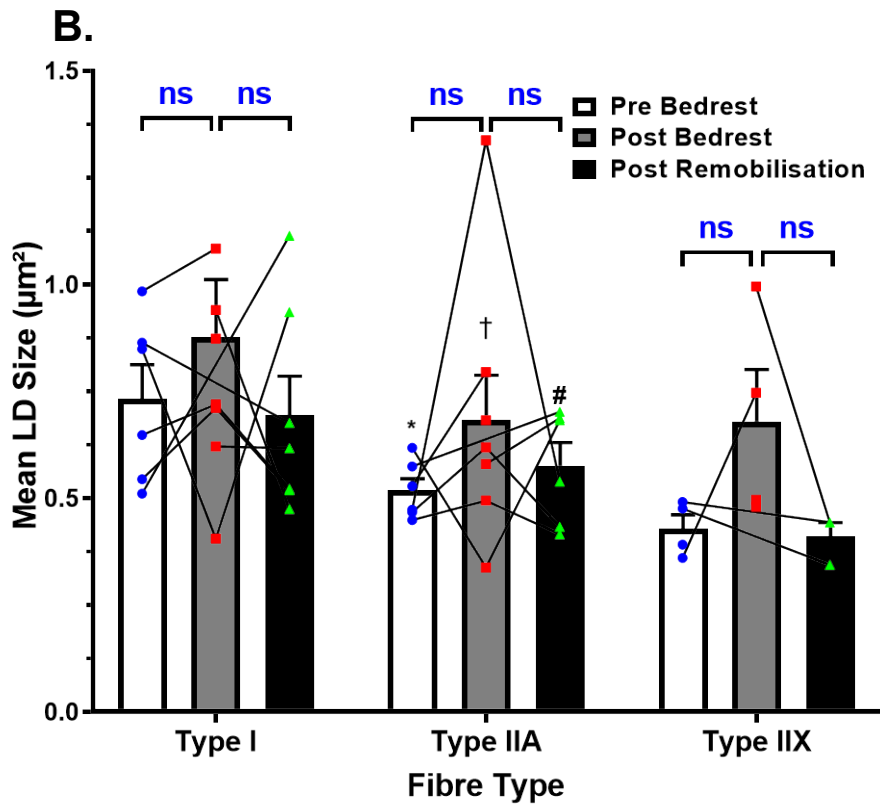
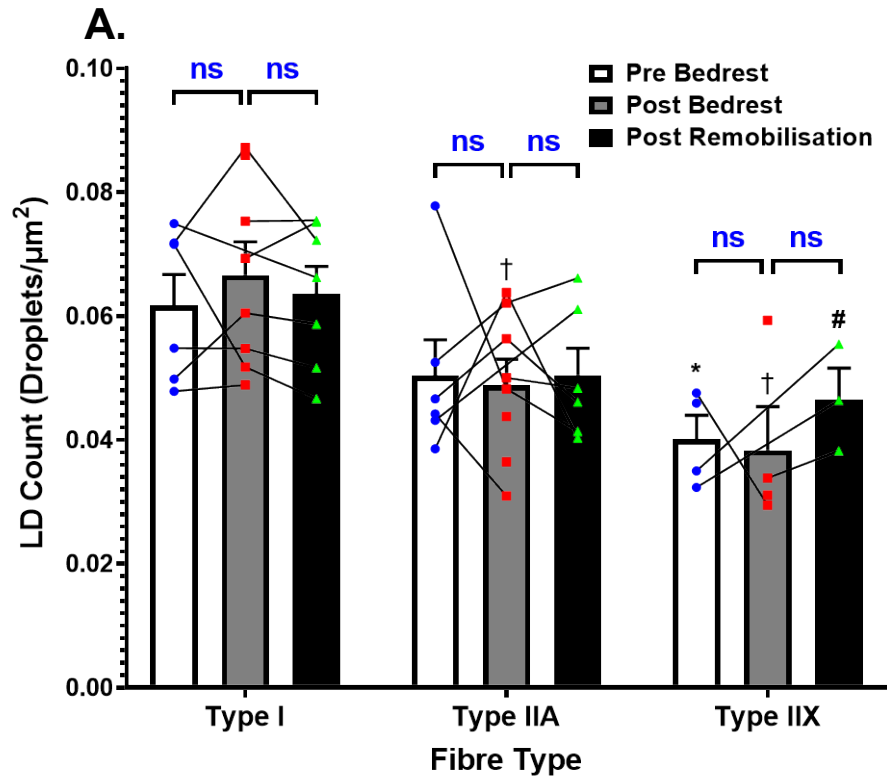


Figure 3-11: Representative images of fibre type staining. (B) The immunohistochemical staining of the MHC Type 1 (Type I) isoform in red. (C) The immunohistochemical staining of MHC Type IIA in green and (D) MHC Type IIX and laminin in grey. **Figures 3-11E and 3-11A** show the combination of all channels in a segment of a sample and in the whole sample, respectively. Yellow scale bar is 150 μm , blue scale bars are 100 μm .

Example images of the fibre type staining are shown in **Figure 3-11**. **Figures 3-11B, 3-11C** and **3-11D** show staining of the individual fibre types and laminin while figures **3-11E** and **3-11A** show the staining of all fibre types combined, in a segment of a sample and the entire sample, respectively.



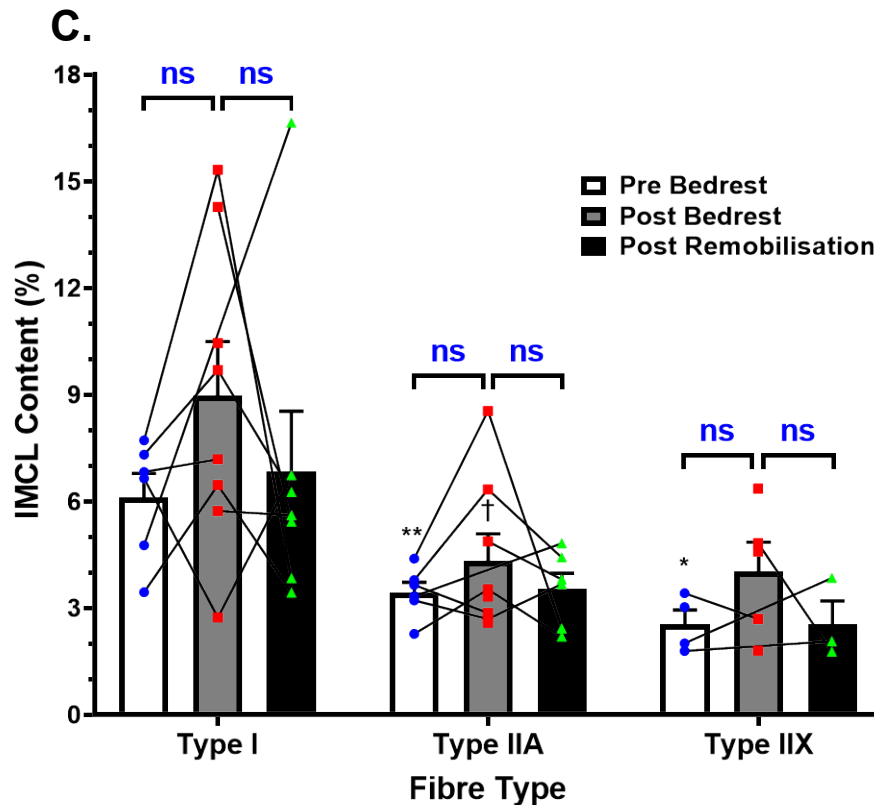


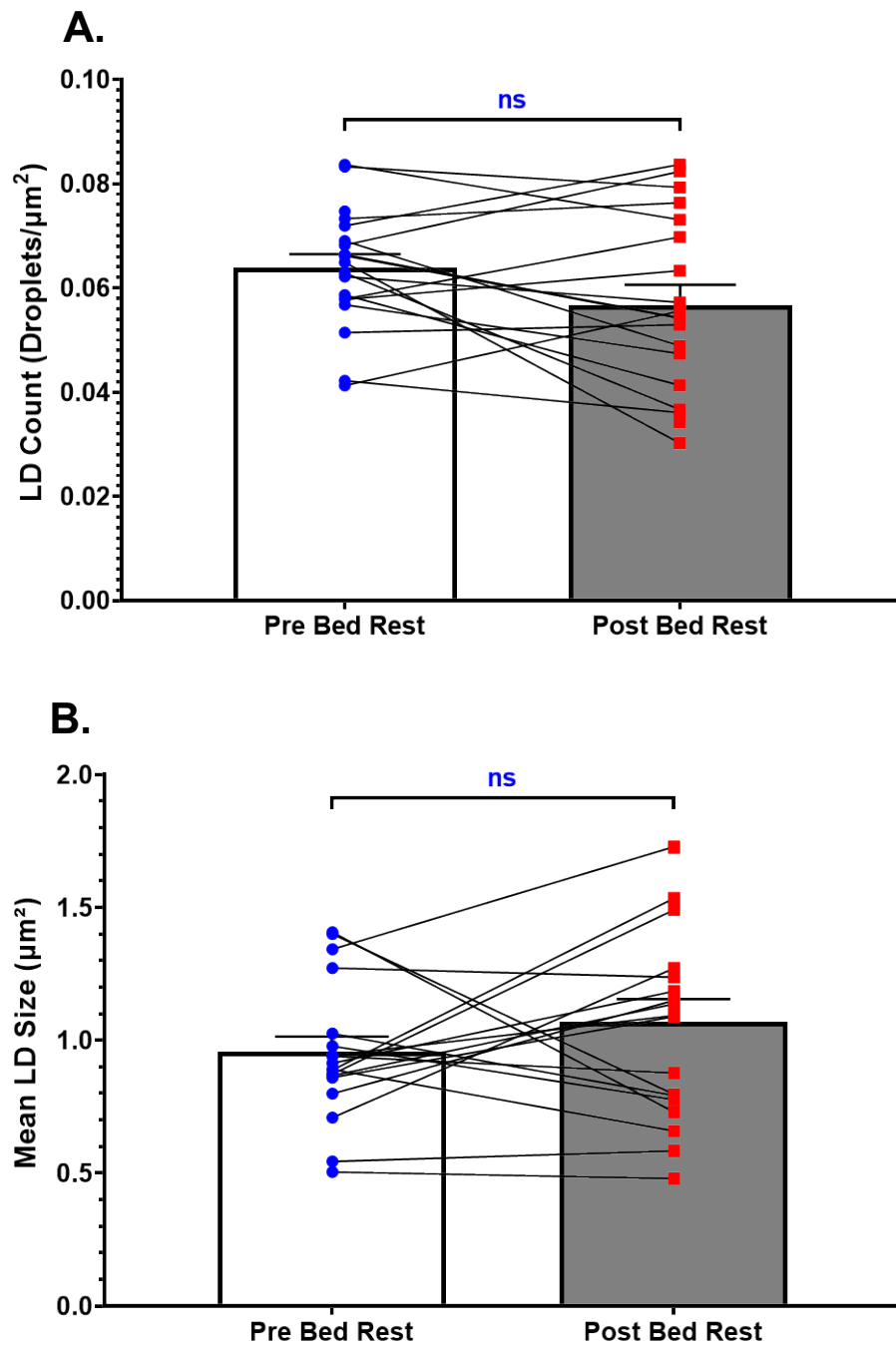
Figure 3-12 Fibre type specific differences in LD parameters and IMCL content after 3 days of bed rest. (A) LD count. (B) LD Size. (C) IMCL content. Statistically significant differences vs. Type I Pre-Bed Rest are represented as *, vs. Type I Post Bed Rest are represented as † and vs. Type I Post Rehab are represented as #. Results presented as mean \pm SEM.

Figure 3-12 shows the fibre type specific changes in LD count (A), LD size (B), and IMCL content (C) following 3 days of bed rest and 4 days of remobilisation. While LD count varied significantly between fibre types ($p < 0.01$), being greatest in Type I fibres and lowest in Type IIX fibres across all time points, the time point variables of 3 days bed rest and 4 days remobilisation had no significant effect on the LD count within these individual fibre types ($p = 0.64$).

Muscle fibre type also had a significant effect on LD size ($p < 0.001$), such that droplets were largest in Type I fibres and smallest in Type IIX fibres. However, the bed rest intervention and subsequent remobilisation did not. Within each fibre type, there was no significant difference in LD size pre bed rest compared to post bed rest and post remobilisation ($p = 0.35$).

Similarly, there was no significant effect of bed rest or remobilisation on IMCL content in any fibre type ($p = 0.38$). Differences between the fibre types in lipid content were significant ($p < 0.01$), IMCL content was greatest in Type I fibres and lowest in Type IIX fibres.

3.4.9 IMCL Content: 56 Days Bed Rest



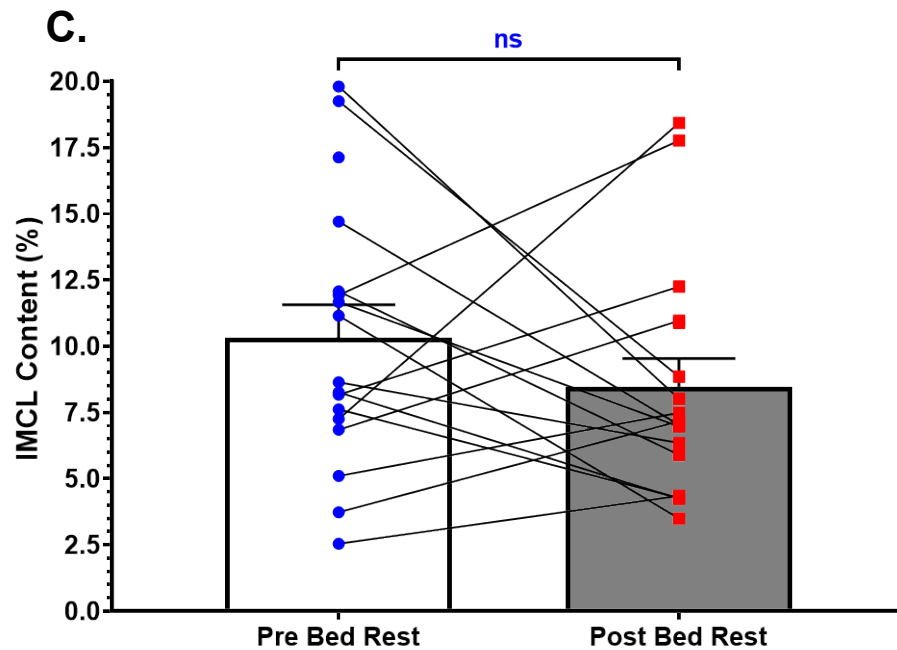


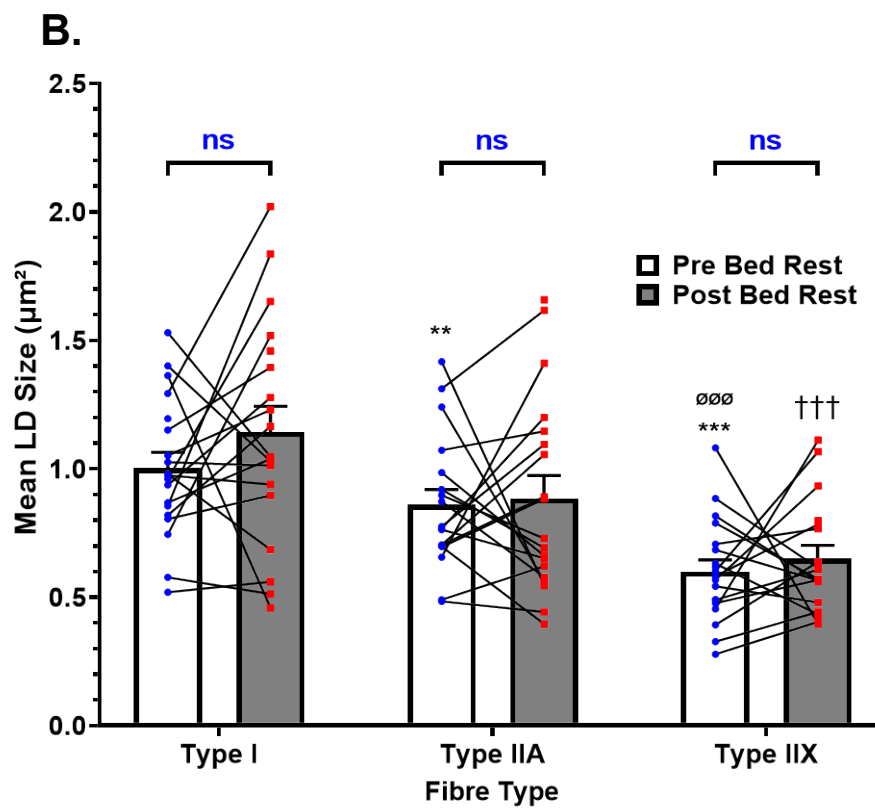
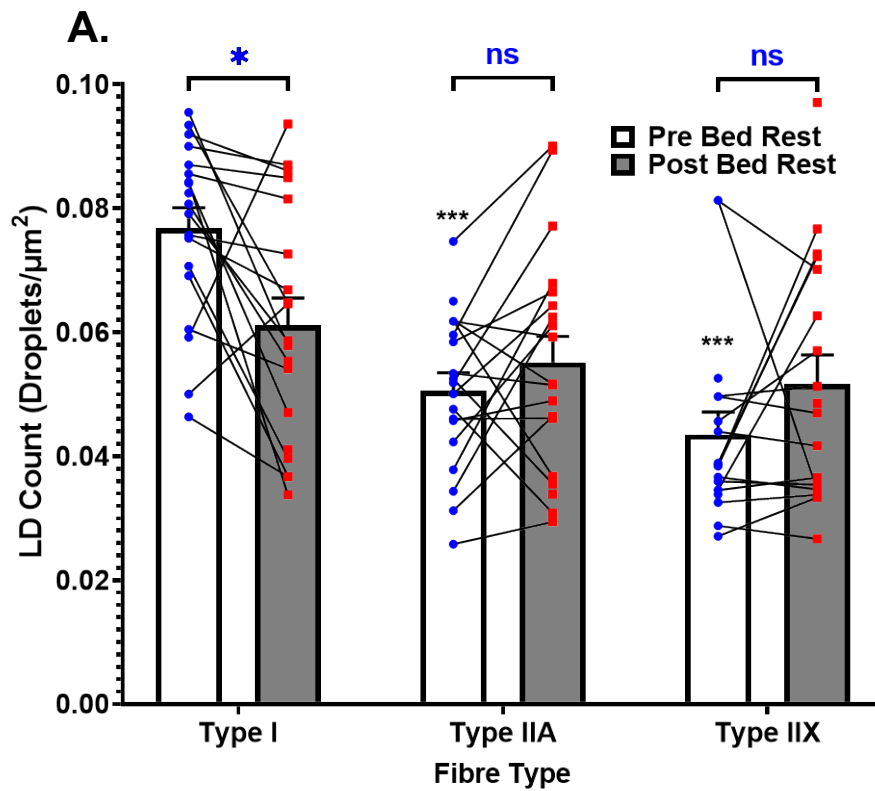
Figure 3-13: (A) LD count, (B) LD size and (C) the IMCL content in the vastus lateralis muscle tissue before and after 56 days of bed rest. Values are mean \pm SEM, $n = 19$ for both time points.

Figure 3-13 shows the mean LD count (A), LD size (B), and the contribution of lipid to total fibre content (IMCL content) (C), 6 days before the bed rest period and 56 days into the bed rest period. For LD count, mean values were 0.064 ± 0.003 LDs/ μm^2 pre-bed rest and 0.057 ± 0.004 LDs/ μm^2 post bed rest, with no significant differences observed ($p = 0.13$).

LD size was not significantly different between the pre-bed rest and post bed rest time points ($0.96 \pm 0.06 \mu\text{m}^2$ vs. $1.07 \pm 0.09 \mu\text{m}^2$, respectively; $p = 0.38$).

Differences in IMCL content between the two time points were also not significant, mean IMCL content was $11.3 \pm 1.6\%$ pre-bed rest and $9.7 \pm 1.5\%$ post bed rest ($p = 0.60$).

3.4.10 IMCL Content by Fibre Type: 56 Days Bed Rest



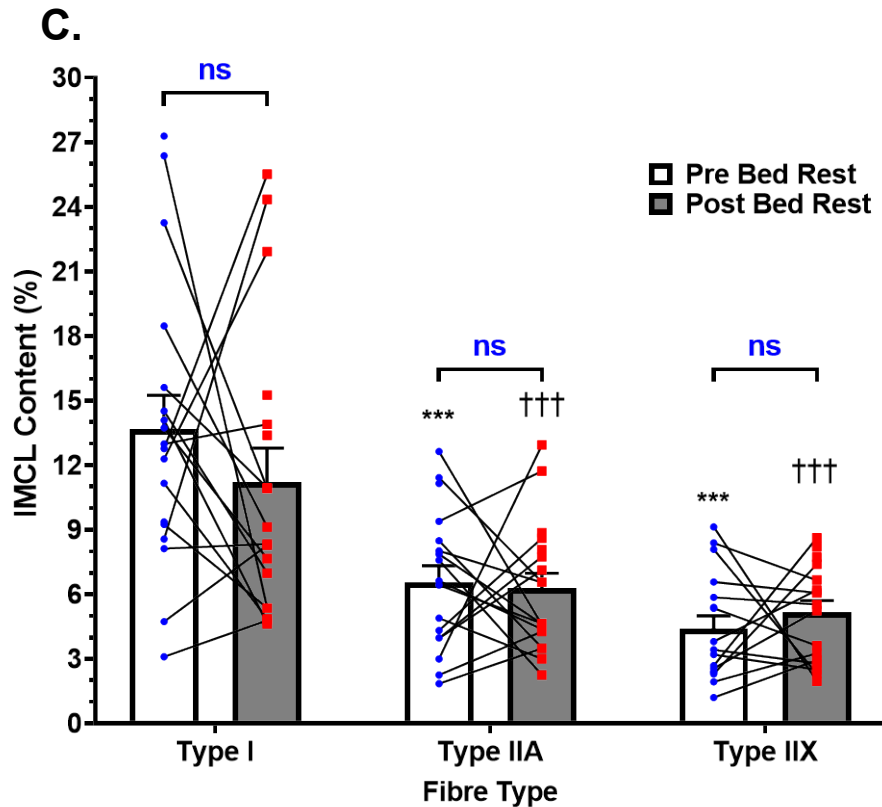


Figure 3-14: Fibre type specific differences in LD parameters and IMCL content before and after 56 days of bed rest. (A) LD count. (B) LD Size. (C) IMCL content. Statistically significant differences vs. Type I Pre-Bed Rest are represented as *, vs. Type I Post Bed Rest are represented as † and vs. Type IIA Pre-Bed Rest are represented as ∅. Values are mean ± SEM, n = 19 for both time points.

Figure 3-14 shows the fibre type specific changes in LD count (**A**), LD size (**B**), and IMCL content (**C**) before and after 56 days of bed rest. There was no overall significant time point effect on LD count ($p = 0.84$). However, the number of LDs per micrometre of tissue in Type I fibres specifically following 56 days of bed rest was significantly lower than at the pre bed rest time point ($p < 0.05$). Significant between-fibre type differences in LD count were observed ($p < 0.001$), with LDs being significantly more numerous in Type I fibres than Type IIA and IIX fibres at both time points.

Fibre type also had a significant effect on observed differences in LD size ($p < 0.001$) and IMCL content ($p < 0.001$). LD size was greatest in Type I fibres and smallest in Type IIX fibres, but not significantly different post bed rest compared to pre bed rest at any time point ($p = 0.61$). The 56-day bed rest intervention had no effect on the lipid content within the muscle fibres such that all differences between time points were insignificant ($p = 0.88$).

3.5 Discussion

It has been reported that IMCL content does not change following 7 days of bed rest in participants maintained in energy balance, though GD and mitochondrial content are significantly reduced during this acute period of inactivity (Dirks *et al.*, 2016). No previous work has investigated how whole-body GD, total substrate oxidation and IMCL content are altered following a chronic period of bed rest. Understanding how these elements interact in a chronic setting is crucial to elucidating the pathophysiology of metabolic dysfunction resulting from inactivity.

The main aim of the work presented in this chapter was to determine whether IMCL content in lean, healthy, male participants changed similarly during acute (3 days) and chronic periods (56 days) of bed rest, under conditions in which energy balance was maintained by reducing energy intake. Another aim was to determine whether any such changes were associated with alterations in insulin-mediated whole-body GD or substrate oxidation rates during those periods. Specifically in the acute bed rest study, an additional aim was to determine whether the changes in insulin-mediated whole-body GD following a standardised remobilisation protocol were associated with any changes in IMCL content.

A multitude of bed rest studies are described in the literature but very few of these focus on quantifying changes in IMCL content in non-obese participants under conditions in which energy balanced is maintained. Indeed, the data presented here are the first to characterise changes in total and fibre-type specific LD count, LD size, and IMCL content in lean males following short- and long-term periods of bed rest. The novel data presented here suggest that, under conditions of energy balance, LD count, LD size, and IMCL content do not change during bed rest, even after 56 days or following remobilisation. Also, in tandem insulin-mediated whole-body GD in the participants of both studies fell by 17% and 22% following 3 and 56 days of bed rest, respectively, but these declines were unassociated with any changes in LD parameters or IMCL content. This decrease in whole-body GD was reversed by remobilisation in the acute bed rest study, again independent of

any changes in IMCL content. Such declines in whole-body GD are characteristic findings in bed rest studies that reflect peripheral insulin resistance at the level of the skeletal muscles which leads to impaired glucose disposal at the whole-body level (Mikines *et al.*, 1991), given that skeletal muscles are the site for the disposal of greater than 80% of intravenously infused glucose (Thiebaud *et al.*, 1982).

The key findings of this work were that, after 56 days of bed rest, participants in the chronic bed rest study presented with fasting hyperinsulinaemia and had become metabolically inflexible (see **Section 1.4**) (Rudwill *et al.*, 2018), presenting with impaired insulin-mediated suppression of fat oxidation concurrent with decreased carbohydrate oxidation under the same insulin-mediated conditions. This was in stark contrast to the acute bed rest study in which fat oxidation during the hyperinsulinaemic-euglycaemic clamp protocol was suppressed to a greater extent following 3 days of bed rest compared to baseline measurements. Fasting carbohydrate and fat oxidation remained unchanged post bed rest relative to baseline in both studies. Crucially, these substrate oxidation data could not be explained by IMCL content, FFA availability, or TAG availability, all of which remained unchanged post bed rest in both studies. These novel data directly contradict evidence of impaired fasting and postprandial fat oxidation following chronic bed rest (Bergouignan *et al.*, 2006). Also, given that the significant decreases in whole-body glucose disposal in both studies presented in the absence of increases in IMCL content, these findings contest the hypothesis that inactivity per sé impairs basal fat oxidation, leading to IMCL accumulation that contributes to reductions in whole-body GD and the development of insulin resistance (Blanc *et al.*, 2000a; Bergouignan *et al.*, 2011; Bilet *et al.*, 2020). The data presented here also greatly expand upon findings from a comparable study conducted under conditions of energy balance which found no changes in the lipid area percentage in Type I or Type II fibres and no changes in lipotoxic DAG and ceramide species content following 7 days of bed rest, even with significant reductions in mitochondrial content (Dirks *et al.*, 2016). It is clear that the previously described hypothesis does not hold true in the context of bed rest conducted under conditions of energy balance.

At the fibre-type level, it has been demonstrated that the IMCL content of Type I fibres from obese insulin resistant women is significantly greater than the IMCL content of Type I fibres from insulin sensitive women (Coen *et al.*, 2010). Also, while Dirks and her colleagues observed no changes in the lipid area of Type I and Type II fibres after 7 days of bed rest, they did observe that LD size in Type I muscle fibres increased and LD size in Type II muscle fibres decreased after 7 days of bed rest, such that LD size was significantly greater in Type I fibres than it was in Type II fibres post bed rest (Dirks *et al.*, 2016). These data suggest that, while total IMCL content may not change in response to inactivity, there may be a shift in IMCL at the fibre-type level which favours the increase in LD size within Type I fibres (Berg, Larsson and Tesch, 1997; Trappe *et al.*, 2004) and contributes to impairments in insulin sensitivity. In the acute bed rest study presented in this report, no significant within fibre-type changes were observed in LD count, LD size, or IMCL content following 3 days of bed rest and 4 days of remobilisation. Moreover, no within fibre-type differences were observed in LD count, LD size, or IMCL content between the pre-bed rest and post bed rest time points in the chronic bed rest study. Contrary to Dirks' previous work, these data point to neither acute nor chronic bed rest being associated with any fibre-type specific changes in IMCL content that would contribute to the impairment of insulin-mediated whole-body GD during bed rest conducted under energy balanced conditions.

A positive energy balance caused by overfeeding can be a major confounding variable when measuring changes in IMCL content during bed rest; it has been demonstrated that high fat and high carbohydrate diets can increase IMCL content in healthy young males by 20-30% after only 60 hours of bed rest (Stettler *et al.*, 2005). This is likely explained by changes in circulating TAG and FFA availability and the decreased metabolic rates and daily energy expenditure of participants during bed rest. When energy balance is not maintained during bed rest, circulating TAG concentrations increase (Yanagibori *et al.*, 1998; Stettler *et al.*, 2005; Biolo *et al.*, 2008; Bergouignan *et al.*, 2009). These TAGs are hydrolysed by LPLs on the luminal surface of endothelial cells (Braun and Severson, 1992), releasing FFAs that are transported into the skeletal muscles (Jain *et al.*, 2015). The increased FFA

availability and low metabolic rates result in FFAs being preferentially stored as part of the IMCL pool instead of being oxidised, which explains the accumulation of IMCL observed in states of positive energy balance. In both the acute and chronic bed rest study presented here, fasting TAG and FFA concentrations were not significantly different post bed rest compared to pre-bed rest and the participants of both studies remained weight stable between these time points. These data indicate that these participants were not overfed and were in fact maintained in energy balance for the duration of both studies.

In the acute bed rest study, a 17% reduction in insulin-mediated whole-body glucose disposal was observed following 3 days of bed rest, which was reversed by 4 days of remobilisation. IMCL content in exercising muscle significantly decreases immediately following acute bouts of exercise due to increased utilisation of FAs stored in IMCL pools (Schrauwen-Hinderling *et al.*, 2003; White *et al.*, 2003; Ith *et al.*, 2010). IMCL content is increased in response to chronic exercise and these increases are concomitant with improved insulin sensitivity (Dubé *et al.*, 2008; Shepherd *et al.*, 2013). Indeed, a previous study has shown that IMCL content is increased in male participants after just 3 days of isokinetic maximal knee flexion and extension at 60°/s and 180°/s (Zhu *et al.*, 2015). However, to date few studies have investigated the effect of exercise on IMCL content immediately following bed rest. In the acute bed rest study presented here IMCL content measured post-bed rest was not significantly different to IMCL content quantified after a remobilisation protocol lasting 4 consecutive days. These data suggest that exercise-induced improvements in insulin-mediated whole-body glucose disposal are not associated with changes in IMCL content. However, fasting plasma FFA concentrations were significantly lower at the post remobilisation time point than at baseline and post bed rest. This is likely explained by increased FFA utilisation, which increases in response to exercise intensity (Turcotte, Richter and Kiens, 1992; Romijn *et al.*, 1993).

3.6 Conclusion

Bed rest, under conditions of energy balance, induced significant and similar decrements in insulin-mediated glucose disposal after 3 and 56 days that could not be explained by an increase in IMCL content. Crucially, differing alterations in substrate oxidation between the acute bed rest and chronic bed rest setting could not be explained by circulating lipid availability or muscle lipid content. Furthermore, exercise following bed rest restored insulin-mediated glucose disposal but did not impact upon IMCL content. It would appear therefore that under these experimental conditions, changes in insulin sensitivity can be readily dissociated from IMCL content. Greater caution needs to be taken when considering the mechanistic link between IMCL content and insulin sensitivity, particularly when experimental designs do not control for energy intake and more work must be done to understand the aetiology of altered substrate oxidation in this context.

3.7 References

Ainsworth, B.E., Haskell, W.L., Leon, A.S., Jacobs, D.R., Jr., Montoye, H.J., Sallis, J.F., and Paffenbarger, R.S., Jr. (1993) Compendium of physical activities: classification of energy costs of human physical activities. *Medicine and Science in Sports and Exercise*. 25 (1), pp. 71-80.

Arc-Chagnaud, C., Py, G., Fovet, T., Roumanille, R., Demangel, R., Pagano, A.F., Delobel, P., Blanc, S., Jasmin, B.J., Blottner, D., Salanova, M., Gomez-Cabrera, M.C., Viña, J., Brioché, T., and Chopard, A. (2020) Evaluation of an Antioxidant and Anti-inflammatory Cocktail Against Human Hypoactivity-Induced Skeletal Muscle Deconditioning. *Frontiers in Physiology*. 11, 71.

Assah, F.K., Ekelund, U., Brage, S., Mbanja, J.C., and Wareham, N.J. (2011) Urbanization, physical activity, and metabolic health in sub-Saharan Africa. *Diabetes Care*. 34 (2), pp. 491-496.

Bachmann, O.P., Dahl, D.B., Brechtel, K., Machann, J., Haap, M., Maier, T., Loviscach, M., Stumvoll, M., Claussen, C.D., Schick, F., Häring, H.U., and Jacob, S. (2001) Effects of Intravenous and Dietary Lipid Challenge on Intramyocellular Lipid Content and the Relation with Insulin Sensitivity in Humans. *Diabetes*. 50 (11), pp. 2579-2584.

Bajpeyi, S., Myrland, C.K., Covington, J.D., Obanda, D., Cefalu, W.T., Smith, S.R., Rustan, A.C., and Ravussin, E. (2014) Lipid in skeletal muscle myotubes is associated to the donors' insulin sensitivity and physical activity phenotypes. *Obesity (Silver Spring, Md.)*. 22 (2), pp. 426-434.

Berg, H.E., Larsson, L., and Tesch, P.A. (1997) Lower limb skeletal muscle function after 6 wk of bed rest. *Journal of Applied Physiology*. 82 (1), pp. 182-188.

Bergouignan, A., Latouche, C., Heywood, S., Grace, M.S., Reddy-Luthmoodoo, M., Natoli, A.K., Owen, N., Dunstan, D.W., and Kingwell, B.A. (2016) Frequent interruptions of sedentary time modulates contraction- and insulin-stimulated glucose uptake pathways in muscle: Ancillary analysis from randomized clinical trials. *Scientific Reports*. 6, e32044.

Bergouignan, A., Momken, I., Schoeller, D.A., Normand, S., Zahariev, A., Lescure, B., Simon, C., and Blanc, S. (2010) Regulation of energy balance during long-term

physical inactivity induced by bed rest with and without exercise training. *The Journal of Clinical Endocrinology and Metabolism*. 95 (3), pp. 1045-1053.

Bergouignan, A., Rudwill, F., Simon, C., and Blanc, S. (2011). Physical inactivity as the culprit of metabolic inflexibility: evidence from bed-rest studies. *Journal of Applied Physiology*. 111 (4), pp. 1201-1210.

Bergouignan, A., Trudel, G., Simon, C., Chopard, A., Schoeller, D.A., Momken, I., Votruba, S.B., Desage, M., Burdige, G.C., Gauquelin-Koch, G., Normand, S., and Blanc, S. (2009) Physical inactivity differentially alters dietary oleate and palmitate trafficking. *Diabetes*. 58 (2), pp. 367-376.

Bergström, J. (1962) Muscle electrolytes in man: determined by neutron activation analysis on needle biopsy specimens. A study on normal subjects, kidney patients and patients with chronic diarrhea. *Scandinavian Journal of Clinical & Laboratory Investigation*. Supplement 68 (11-13), pp. 511-513.

Biensø, R.S., Ringholm, S., Kiilerich, K., Aachmann-Andersen, N.J., Krogh-Madsen, R., Guerra, B., Plomgaard, P., van Hall, G., Treebak, J.T., Saltin, B., Lundby, C., Calbet, J.A., Pilegaard, H., and Wojtaszewski, J.F. (2012) GLUT4 and glycogen synthase are key players in bed rest-induced insulin resistance. *Diabetes*. 61 (5), pp. 1090-1099.

Bilet, L., Phielix, E., van de Weijer, T., Gemmink, A., Bosma, M., Moonen-Kornips, E., Jorgensen, J. A., Schaart, G., Zhang, D., Meijer, K., Hopman, M., Hesselink, M., Ouwens, D. M., Shulman, G.I., Schrauwen-Hinderling, V.B., and Schrauwen, P. (2020) One-leg inactivity induces a reduction in mitochondrial oxidative capacity, intramyocellular lipid accumulation and reduced insulin signalling upon lipid infusion: a human study with unilateral limb suspension. *Diabetologia*. 63 (6), pp. 1211-1222.

Biolo, G., Agostini, F., Simunic, B., Sturma, M., Torelli, L., Preiser, J.C., Deby-Dupont, G., Magni, P., Strollo, F., di Prampero, P., Guarnieri, G., Mekjavic, I.B., Pisot, R., and Narici, M.V. (2008) Positive energy balance is associated with accelerated muscle atrophy and increased erythrocyte glutathione turnover during 5 wk of bed rest. *The American Journal of Clinical Nutrition*. 88 (4), pp. 950-958.

Blanc, S., Normand, S., Pachiaudi, C., Duvareille, M., and Gharib, C. (2000b). Leptin responses to physical inactivity induced by simulated weightlessness. *American Journal of Physiology: Regulatory, Integrative and Comparative Physiology*. 279 (3), pp. R891-R898.

- Blanc, S., Normand, S., Pachiaudi, C., Fortrat, J.O., Laville, M., and Gharib, C. (2000a) Fuel homeostasis during physical inactivity induced by bed rest. *The Journal of Clinical Endocrinology and Metabolism*. 85 (6), pp. 2223-2233.
- Bloomfield, S. (1997) Changes in musculoskeletal structure and function with prolonged bed rest. *Medicine and Science in Sports and Exercise*. 29 (2), pp. 197-206.
- Borén, J., Taskinen, M.R., Olofsson, S.O., and Levin, M. (2013) Ectopic lipid storage and insulin resistance: a harmful relationship. *Journal of Internal Medicine*. 274 (1), pp. 25-40.
- Bosma, M., Kersten, S., Hesselink, M.K., and Schrauwen, P. (2012) Re-evaluating lipotoxic triggers in skeletal muscle: relating intramyocellular lipid metabolism to insulin sensitivity. *Progress in Lipid Research*. 51 (1), pp. 36-49.
- Braun, J. E. A., and Severson D.L. (1992) Regulation of the synthesis, processing and translocation of lipoprotein lipase. *The Biochemical Journal*. 287 (2), pp. 337-347.
- Brocca, L., Cannavino, J., Coletto, L., Biolo, G., Sandri, M., Bottinelli, R., and Pellegrino, M.A. (2012) The time course of the adaptations of human muscle proteome to bed rest and the underlying mechanisms. *Journal of Physiology*. 590 (20), pp. 5211-5230.
- Brooks, N.E., Cloutier, G.J., Cadena, S.M., Layne, J.E., Nelsen, C.A., Freed, A.M., Roubenoff, R., and Castaneda-Sceppa, C. (2008) Resistance training and timed essential amino acids protect against the loss of muscle mass and strength during 28 days of bed rest and energy deficit. *Journal of Applied Physiology*. 105 (1), pp. 241-248.
- Brower, R.G. (2009) Consequences of bed rest. *Critical Care Medicine*. 37 (10 Suppl.), pp. S422-S428.
- Brownson, R.C., Boehmer, T.K., and Luke, D.A. (2005) Declining rates of physical activity in the United States: what are the contributors? *Annual Review Public Health*. 26, pp. 421-443.
- Chavez, J.A., and Summers, S.A. (2012) A ceramide-centric view of insulin resistance. *Cell Metabolism*. 15 (5), pp. 585-594.
- Chee, C., Shannon, C.E., Burns, A., Selby, A.L., Wilkinson, D., Smith, K., Greenhaff, P.L., and Stephens, F.B. (2016) Relative Contribution of Intramyocellular Lipid to Whole-Body Fat Oxidation Is Reduced With Age but Subsarcolemmal Lipid

Accumulation and Insulin Resistance Are Only Associated With Overweight Individuals. *Diabetes*. 65 (4), pp. 840-850.

Coen, P.M., Dubé, J.J., Amati, F., Stefanovic-Racic, M., Ferrell, R.E., Toledo, F.G., and Goodpaster, B.H. (2010) Insulin resistance is associated with higher intramyocellular triglycerides in type I but not type II myocytes concomitant with higher ceramide content. *Diabetes*. 59 (1), pp. 80-88.

Coker, R.H., Hays, N.P., Williams, R.H., Xu, L., Wolfe, R.R., and Evans, W.J. (2014) Bed rest worsens impairments in fat and glucose metabolism in older, overweight adults. *The Journals of Gerontology. Series A, Biological Sciences and Medical Sciences*. 69 (3), pp. 363-370.

Constantin-Teodosiu, D., Constantin, D., Stephens, F., Laithwaite, D., and Greenhaff, P.L. (2012) The role of FOXO and PPAR transcription factors in diet-mediated inhibition of PDC activation and carbohydrate oxidation during exercise in humans and the role of pharmacological activation of PDC in overriding these changes. *Diabetes*. 61 (5), pp. 1017-1024.

Covington, J.D., Johannsen, D.L., Coen, P.M., Burk, D.H., Obanda, D.N., Ebenezer, P.J., Tam, C.S., Goodpaster, B.H., Ravussin, E., and Bajpeyi, S. (2017) Intramyocellular Lipid Droplet Size Rather Than Total Lipid Content is Related to Insulin Sensitivity After 8 Weeks of Overfeeding. *Obesity (Silver Spring, Md.)*. 25 (12), pp. 2079-2087.

Craig, C.L., Marshall, A.L., Sjöström, M., Bauman, A.E., Booth, M.L., Ainsworth, B.E., Pratt, M., Ekelund, U., Yngve, A., Sallis, J.F., and Oja, P. (2003) International physical activity questionnaire: 12-country reliability and validity. *Medicine and Science in Sports and Exercise*. 35 (8), pp. 1381-1395.

Cree, M.G., Paddon-Jones, D., Newcomer, B.R., Ronsen, O., Aarsland, A., Wolfe, R.R., and Ferrando, A. (2010) Twenty-eight-day bed rest with hypercortisolemia induces peripheral insulin resistance and increases intramuscular triglycerides. *Metabolism: Clinical and Experimental*. 59 (5), pp. 703-710.

Damiot, A., Demangel, R., Noone, J., Chery, I., Zahariev, A., Normand, S., Brioché, T., Crampes, F., de Glisezinski, I., Lefai, E., Bareille, M. P., Chopard, A., Draï, J., Collin-Chavagnac, D., Heer, M., Gauquelin-Koch, G., Prost, M., Simon, P., Py, G., Blanc, S., Simon, C., Bergouignan, A. and O'Gorman, D.J. (2019) A nutrient cocktail prevents lipid metabolism alterations induced by 20 days of daily steps reduction and

fructose overfeeding: result from a randomized study. *Journal of Applied Physiology (Bethesda, Md : 1985)*. 126 (1), pp. 88-101.

Daugaard, J.R., Nielsen, J.N., Kristiansen, S., Andersen, J.L., Hargreaves, M., and Richter, E.A. (2000) Fiber type-specific expression of GLUT4 in human skeletal muscle: influence of exercise training. *Diabetes*. 49 (7), pp. 1092-1095.

DeFronzo, R.A., and Tripathy, D. (2009) Skeletal muscle insulin resistance is the primary defect in type 2 diabetes. *Diabetes Care*. 32 (Supplement 2), pp. S157-S163.

Dela, F., Ploug, T., Handberg, A., Petersen, L.N., Larsen, J.J., Mikines, K.J., and Galbo, H. (1994) Physical training increases muscle GLUT4 protein and mRNA in patients with NIDDM. *Diabetes*. 43 (7), pp. 862-865.

Dirks, M.L., Wall, B.T., van de Valk, B., Holloway, T.M., Holloway, G.P., Chabowski, A., Goossens, G.H., and van Loon, L.J. (2016) One Week of Bed Rest Leads to Substantial Muscle Atrophy and Induces Whole-Body Insulin Resistance in the Absence of Skeletal Muscle Lipid Accumulation. *Diabetes*. 65 (10), pp. 2862-2875.

Dirks, M.L., Stephens, F.B., Jackman, S.R., Galera Gordo, J., Machin, D.J., Pulsford, R.M., van Loon, L., and Wall, B.T. (2018) A single day of bed rest, irrespective of energy balance, does not affect skeletal muscle gene expression or insulin sensitivity. *Experimental Physiology*. 103 (6), pp. 860–875.

Djurhuus, C.B., Gravholt, C.H., Nielsen, S., Pedersen, S.B., Møller, N., and Schmitz, O. (2004) Additive effects of cortisol and growth hormone on regional and systemic lipolysis in humans. *American Journal of Physiology: Endocrinology and Metabolism*. 286 (3), pp. E488-E494.

Doehner, W., Gathercole, D., Cicoira, M., Krack, A., Coats, A.J., Camici, P.G., and Anker, S.D. (2010) Reduced glucose transporter GLUT4 in skeletal muscle predicts insulin resistance in non-diabetic chronic heart failure patients independently of body composition. *International Journal of Cardiology*. 138 (1), pp. 19-24.

Dubé, J.J., Amati, F., Stefanovic-Racic, M., Toledo, F.G., Sauers, S.E., and Goodpaster, B.H. (2008) Exercise-induced alterations in intramyocellular lipids and insulin resistance: the athlete's paradox revisited. *American journal of physiology. Endocrinology and Metabolism*. 294 (5), pp. E882-E888.

Eurostat (2019) *In-patient average length of stay (days)*. [Accessed: 21/04/2022]. Available from: https://ec.europa.eu/eurostat/databrowser/view/hlth_co_inpst/default/table?lang=en.

- Ferrando, A.A., Stuart, C.A., Sheffield-Moore, M., and Wolfe, R.R. (1999) Inactivity amplifies the catabolic response of skeletal muscle to cortisol. *The Journal of Clinical Endocrinology and Metabolism*. 84 (10), pp. 3515-3521.
- Ferrara, C.M., Goldberg, A.P., Ortmeyer, H.K., and Ryan, A.S. (2006) Effects of aerobic and resistive exercise training on glucose disposal and skeletal muscle metabolism in older men. *The Journals of Gerontology. Series A, Biological Sciences and Medical Sciences*. 61 (5), pp. 480-487.
- Frøsig, C., Rose, A.J., Treebak, J.T., Kiens, B., Richter, E.A., and Wojtaszewski, J.F. (2007) Effects of endurance exercise training on insulin signaling in human skeletal muscle: interactions at the level of phosphatidylinositol 3-kinase, Akt, and AS160. *Diabetes*. 56 (8), pp. 2093-2102.
- Guthold, R., Stevens, G.A., Riley, L.M., and Bull, F.C. (2018) Worldwide trends in insufficient physical activity from 2001 to 2016: a pooled analysis of 358 population-based surveys with 1·9 million participants. *The Lancet: Global Health*. 6 (10), pp. e1077-e1086.
- Hale, L. and Guan, S. (2015) Screen time and sleep among school-aged children and adolescents: a systematic literature review. *Sleep Medicine Reviews*. 21, pp. 50-58.
- Hamburg, N.M., McMackin, C.J., Huang, A.L., Shenouda, S.M., Widlansky, M.E., Schulz, E., Gokce, N., Ruderman, N.B., Keaney, J.F., Jr and Vita, J.A. (2007) Physical inactivity rapidly induces insulin resistance and microvascular dysfunction in healthy volunteers. *Arteriosclerosis, Thrombosis, and Vascular Biology*. 27 (12), pp. 2650-2656.
- Hargens, A.R., and Vico, L. (2016) Long-duration bed rest as an analog to microgravity. *Journal of Applied Physiology*. 120 (8), pp. 891-903.
- Harris, J.A., and Benedict, F.G. (1918) A Biometric Study of Human Basal Metabolism. *Proceedings of the National Academy of Sciences of the United States of America*. 4 (12), pp. 370-373.
- Healy, G.N., Dunstan, D.W., Salmon, J., Shaw, J.E., Zimmet, P.Z., and Owen N. (2008) Television time and continuous metabolic risk in physically active adults. *Medicine and Science in Sports and Exercise*. 40 (4), pp. 639-645.
- Heath, G.W., Gavin, J.R., Hinderliter, J.M., Hagberg, J.M., Bloomfield, S.A., and Holloszy, J.O. (1983) Effects of Exercise and Lack of Exercise on Glucose Tolerance

and Insulin Sensitivity. *Journal of Applied Physiology: Respiratory, Environmental and Exercise Physiology*. 55 (2), pp. 512-517.

Heer, M., Baecker, N., Wnendt, S., Fischer, A., Biolo, G., and Frings-Meuthen, P. (2014) How fast is recovery of impaired glucose tolerance after 21-day bed rest (NUC study) in healthy adults?. *The Scientific World Journal*. 2014, 803083.

Hoeks, J., Mensink, M., Hesselink, M.K.C., Ekroos, K., and Schrauwen, P. (2012) Long- and medium-chain fatty acids induce insulin resistance to a similar extent in humans despite marked differences in muscle fat accumulation. *Journal of Clinical Endocrinology and Metabolism*. 97 (1), pp. 208-216.

Horowitz, J.F., and Klein, S. (2000) Lipid metabolism during endurance exercise. *The American Journal of Clinical Nutrition*. 72 (2 Suppl), pp. 558S-563S.

Hu, F.B. (2003) Sedentary lifestyle and risk of obesity and type 2 diabetes. *Lipids*. 38 (2), pp. 103-108.

International Academy of Astronautics (2014) *Guidelines for Standardization of Bed Rest Studies in the Spaceflight Context*. Section 7.1.1, pp. 32-33. [Accessed 15/10/2020].

https://www.nasa.gov/sites/default/files/atoms/files/bed_rest_studies_complete.pdf

Ith, M., Huber, P.M., Egger, A., Schmid, J. P., Kreis, R., Christ, E., and Boesch, C. (2010) Standardized protocol for a depletion of intramyocellular lipids (IMCL). *NMR in Biomedicine*. 23 (5), pp. 532-538.

Jain, S.S., Luiken, J.J., Snook, L.A., Han, X.X., Holloway, G.P., Glatz, J.F., and Bonen, A. (2015) Fatty acid transport and transporters in muscle are critically regulated by Akt2. *FEBS letters*. 589 (19 Pt B), pp. 2769-2775.

Jessen, N. and Goodyear, L.J. (2005) Contraction signaling to glucose transport in skeletal muscle. *Journal of Applied Physiology (Bethesda, Md.: 1985)*. 99 (1), pp. 330-337. Jones, S.W., Hill, R.J., Krasney, P.A., O'Conner, B., Peirce, N., and Greenhaff, P.L. (2004) Disuse atrophy and exercise rehabilitation in humans profoundly affects the expression of genes associated with the regulation of skeletal muscle mass. *FASEB journal: official publication of the Federation of American Societies for Experimental Biology*. 18 (9), pp. 1025-1027.

Kampmann, U., Christensen, B., Nielsen, T.S., Pedersen, S.B., Ørskov, L., Lund, S., Møller, N., and Jessen, N. (2011) GLUT4 and UBC9 protein expression is reduced in

muscle from type 2 diabetic patients with severe insulin resistance. *PLoS One*. 6 (11), e27854.

Katzmarzyk, P.T., Church, T.S., Craig, C.L., and Bouchard, C. (2009) Sitting time and mortality from all causes, cardiovascular disease, and cancer. *Medicine and Science in Sports and Exercise*. 41 (5), pp. 998-1005.

Kiilerich, K., Gudmundsson, M., Birk, J.B., Lundby, C., Taudorf, S., Plomgaard, P., Saltin, B., Pedersen, P.A., Wojtaszewski, J.F., and Pilegaard, H. (2010) Low muscle glycogen and elevated plasma free fatty acid modify but do not prevent exercise-induced PDH activation in human skeletal muscle. *Diabetes*. 59 (1), pp. 26-32.

Kiss, N., Hiesmayr, M., Sulz, I., Bauer, P., Heinze, G., Mouhieddine, M., Schuh, C., Tarantino, S., and Simon, J. (2021) Predicting Hospital Length of Stay at Admission Using Global and Country-Specific Competing Risk Analysis of Structural, Patient, and Nutrition-Related Data from Nutrition Day 2007-2015. *Nutrients*. 13 (11), 4111.

Krssak, M., Falk Petersen, K., Dresner, A., DiPietro, L., Vogel, S.M., Rothman, D.L., Roden, M., and Shulman, G.I. (1999) Intramyocellular lipid concentrations are correlated with insulin sensitivity in humans: a ¹H NMR spectroscopy study. *Diabetologia*. 42 (1), pp. 113-116.

Kurtze, N., Rangul, V., and Hustvedt, B.E. (2008) Reliability and validity of the international physical activity questionnaire in the Nord-Trøndelag health study (HUNT) population of men. *BMC Medical Research Methodology*. 8 (1), 63.

LeBlanc, A.D., Schneider, V.S., Evans, H.J., Pientok, C., Rowe, R., and Spector, E. (2012) Regional changes in muscle mass following 17 weeks of bed rest. *Journal of Applied Physiology*. 73 (5), pp. 2172-2178.

Lee, I.M., Shiroma, E.J., Lobelo, F., Puska, P., Blair, S.N., Katzmarzyk, P.T., and Lancet Physical Activity Series Working Group (2012) Effect of physical inactivity on major non-communicable diseases worldwide: an analysis of burden of disease and life expectancy. *Lancet (London, England)*. 380 (9838), pp. 219-229.

Lipman, R.L., Schnure, J.J., Bradley, E.M., and Lecocq, F.R. (1970) Impairment of peripheral glucose utilization in normal subjects by prolonged bed rest. *The Journal of Laboratory and Clinical Medicine*. 76 (2), pp. 221-230.

Lund, J., Helle, S.A., Li, Y., Løvsletten, N.G., Stadheim, H.K., Jensen, J., Kase, E.T., Thoresen, G.H., and Rustan, A.C. (2018) Higher lipid turnover and oxidation in

cultured human myotubes from athletic versus sedentary young male subjects. *Scientific Reports*. 8, 17549.

Macho, A., Mishal, Z., and Uriel, J. (1996) Molar quantification by flow cytometry of fatty acid binding to cells using dipyrrometheneboron difluoride derivatives. *Cytometry*. 23 (2), 166-173.

Mikines, K.J., Richter, E.A., Dela, F., and Galbo, H. (1991) Seven Days of Bed Rest Decrease Insulin Action on Glucose Uptake in Leg and Whole Body. *Journal of Applied Physiology*. 70 (3), pp. 1245-1254.

Misra, M., Bredella, M.A., Tsai, P., Mendes, N., Miller, K.K., and Klibanski, A. (2008) Lower growth hormone and higher cortisol are associated with greater visceral adiposity, intramyocellular lipids, and insulin resistance in overweight girls. *American Journal of Physiology: Endocrinology and Metabolism*. 295 (2), pp. E385-E392.

Nielsen, J., Christensen, A.E., Nellesmann, B., and Christensen, B. (2017) Lipid droplet size and location in human skeletal muscle fibers are associated with insulin sensitivity. *American Journal of Physiology: Endocrinology and Metabolism*. 313 (6), pp. E721-E730.

Nielsen, M.F., Caumo, A., Chandramouli, V., Schumann, W.C., Cobelli, C., Landau, B.R., Vilstrup, H., Rizza, R.A., and Schmitz, O. (2004) Impaired basal glucose effectiveness but unaltered fasting glucose release and gluconeogenesis during short-term hypercortisolemia in healthy subjects. *American Journal of Physiology: Endocrinology and metabolism*. 286 (1), pp. E102-E110.

O'Gorman, D.J., Karlsson, H.K., McQuaid, S., Yousif, O., Rahman, Y., Gasparro, D., Glund, S., Chibalin, A.V., Zierath, J.R., and Nolan, J.J. (2006) Exercise training increases insulin-stimulated glucose disposal and GLUT4 (SLC2A4) protein content in patients with type 2 diabetes. *Diabetologia*. 49 (12), pp. 2983-2992.

Ozemeka, C., Lavieb, C.J., and Rognmoc, Ø. (2019) Global physical activity levels - Need for intervention. *Progress in Cardiovascular Diseases*. 62 (2), pp. 102-107.

Pan, D.A., Lillioja, S., Kriketos, A.D., Milner, M.R., Baur, L.A., Bogardus, C., Jenkins, A.B., and Storlien, L.H. (1997) Skeletal muscle triglyceride levels are inversely related to insulin action. *Diabetes*. 46 (6), pp. 983-988.

Papathanasiou, G., Georgoudis, G., Georgakopoulos, D., Katsouras, C., Kalfakakou, V., and Evangelou, A. (2010) Criterion-related validity of the short International

Physical Activity Questionnaire against exercise capacity in young adults. *European Journal of Cardiovascular Prevention and Rehabilitation*. 17 (4), pp. 380-386.

Petersen, K.F., Morino, K., Alves, T.C., Kibbey, R.G., Dufour, S., Sono, S., Yoo, P.S., Cline, G.W., and Shulman, G.I. (2015) Effect of aging on muscle mitochondrial substrate utilization in humans. *Proceedings of the National Academy of Sciences of the United States of America*. 112 (36), pp. 11330-11334.

Petersen, M.C., Madiraju, A.K., Gassaway, B.M., Marcel, M., Nasiri, A.R., Butrico, G., Marcucci, M.J., Zhang, D., Abulizi, A., Zhang, X.M., Philbrick, W., Hubbard, S.R., Jurczak, M.J., Samuel, V.T., Rinehart, J., and Shulman, G.I. (2016) Insulin receptor Thr1160 phosphorylation mediates lipid-induced hepatic insulin resistance. *The Journal of Clinical Investigation*. 126 (11), pp. 4361-4371.

Phielix, E., Meex, R., Ouwens, D. M., Sparks, L., Hoeks, J., Schaart, G., Moonen-Kornips, E., Hesselink, M.K.C, and Schrauwen, P. (2012) High Oxidative Capacity Due to Chronic Exercise. *Diabetes*. 61 (10), pp. 2472-2478.

Phillips, D.I., Caddy, S., Ilic, V., Fielding, B.A., Frayn, K.N., Borthwick, A.C., and Taylor, R. (1996) Intramuscular triglyceride and muscle insulin sensitivity: evidence for a relationship in nondiabetic subjects. *Metabolism: Clinical and Experimental*. 45 (8), pp. 947-950.

Prats, C., Gomez-Cabello, A., Nordby, P., Andersen, J.L., Helge, J.W., Dela, F., Baba, O., and Ploug, T. (2013) An optimized histochemical method to assess skeletal muscle glycogen and lipid stores reveals two metabolically distinct populations of type I muscle fibers. *PloS one*. 8 (10), p. e77774.

Rittweger, J., Beller, G., Armbrecht, G., Mulder, E., Buehring, B., Gast, U., Dimeo, F., Schubert, H., de Haan, A., Stegeman, D.F., Schiessl, H., and Felsenberg (2010) Prevention of bone loss during 56 days of strict bed rest by side-alternating resistive vibration exercise. *Bone*. 46 (1), pp. 137-147.

Ritz, P., Acheson, K., Gachon, P., Vico, L., Bernard, J.J., Alexandre, C., and Beaufrère, B. (1998) Energy and substrate metabolism during a 42-day bed-rest in a head-down tilt position in humans. *European Journal of Applied Physiology and Occupational Physiology*. 78, pp. 308-314.

Romijn, J.A., Coyle, E.F., Sidossis, L.S., Gastaldelli, A., Horowitz, J.F., Endert, E., and Wolfe, R.R. (1993) Regulation of endogenous fat and carbohydrate metabolism

in relation to exercise intensity and duration. *The American Journal of Physiology*. 265 (3 Pt 1), pp. E380-E391.

Roza, A.M., and Shizgal, H.M. (1984) The Harris Benedict equation reevaluated: resting energy requirements and the body cell mass. *The American Journal of Clinical Nutrition*. 40 (1), pp. 168-182.

Rudwill, F., O'Gorman, D., Lefai, E., Chery, I., Zahariev, A., Normand, S., Pagano, A.F., Chopard, A., Damiot, A., Laurens, C., Hodson, L., Canet-Soulas, E., Heer, M., Meuthen, P.F., Buehlmeier, J., Baecker, N., Meiller, L., Gauquelin-Koch, G., Blanc, S., Simon, C., and Bergouignan, A. (2018) Metabolic Inflexibility Is an Early Marker of Bed-Rest-Induced Glucose Intolerance Even When Fat Mass Is Stable. *The Journal of Clinical Endocrinology and Metabolism*. 103 (5), pp. 1910-1920.

Sakurai, Y., Tamura, Y., Takeno, K., Kumashiro, N., Sato, F., Kakehi, S., Ikeda, S., Ogura, Y., Saga, N., Naito, H., Katamoto, S., Fujitani, Y., Hirose, T., Kawamori, R., and Watada, H. (2011) Determinants of intramyocellular lipid accumulation after dietary fat loading in non-obese men. *Journal of Diabetes Investigation*. 2 (4), pp. 310-317.

Schindelin, J., Arganda-Carreras, I., Frise, E., Kaynig, V., Longair, M., Pietzsch, T., Preibisch, S., Rueden, C., Saalfeld, S., Schmid, B., Tinevez, J. Y., White, D. J., Hartenstein, V., Eliceiri, K., Tomancak, P., and Cardona, A. (2012) Fiji: an open-source platform for biological-image analysis. *Nature Methods*. 9 (7), pp. 676-682. Schindelin J, Arganda-Carreras I, Frise E, Kaynig V, Longair M, Pietzsch T, Preibisch S, Rueden C, Saalfeld S, Schmid B, Tinevez JY, White DJ, Hartenstein V, Eliceiri K, Tomancak P, Cardona A. (2012) Fiji: an open-source platform for biological-image analysis. *Nature Methods*. 9 (7), pp. 676-82.

Schrauwen-Hinderling, V.B., van Loon, L.J., Koopman, R., Nicolay, K., Saris, W.H., and Kooi, M.E. (2003) Intramyocellular lipid content is increased after exercise in nonexercising human skeletal muscle. *Journal of applied physiology (Bethesda, Md: 1985)*. 95 (6), pp. 2328-2332.

Shur, N.F., Simpson, E.J., Crossland, H., Chivaka, P.K., Constantin, D., Cordon, S.M., Constantin-Teodosiu, D., Stephens, F.B., Lobo, D.N., Szewczyk, N., Narici, M., Prats, C., Macdonald, I.A., and Greenhaff, P.L. (2022) Human adaptation to immobilization: Novel insights of impacts on glucose disposal and fuel utilization. *Journal Of Cachexia, Sarcopenia and Muscle*. 13 (6), pp. 2999-3013.

Shepherd, S.O., Cocks, M., Tipton, K.D., Ranasinghe, A.M., Barker, T.A., Burniston, J.G., Wagenmakers, A.J., and Shaw, C.S. (2013) Sprint interval and traditional endurance training increase net intramuscular triglyceride breakdown and expression of perilipin 2 and 5. *The Journal of Physiology*. 591 (3), pp. 657-675.

Søgaard, D., Baranowski, M., Larsen, S., Taulo Lund, M., Munk Scheuer, C., Vestergaard Abildskov, C., Greve Dideriksen, S., Dela, F., and Wulff Helge, J. (2019). Muscle-Saturated Bioactive Lipids Are Increased with Aging and Influenced by High-Intensity Interval Training. *International Journal Of Molecular Sciences*., 20 (5), 1240.

Stettler, R., Ith, M., Acheson, K. J., Décombaz, J., Boesch, C., Tappy, L., and Binnert, C. (2005) Interaction between dietary lipids and physical inactivity on insulin sensitivity and on intramyocellular lipids in healthy men. *Diabetes Care*. 28 (6), pp. 1404-1409.

Stuart, C.A., Shangraw, R.E., Prince, M.J., Peters, E.J., and Wolfe, R.R. (1988) Bed-rest-induced insulin resistance occurs primarily in muscle. *Metabolism*. 37 (8), pp. 802-806.

Tabata, I., Suzuki, Y., Fukunaga, T., Yokozeki, T., Akima, H., and Funato, K. (1999) Resistance training affects GLUT-4 content in skeletal muscle of humans after 19 days of head-down bed rest. *Journal of Applied Physiology*. 86 (3), pp. 909-914

Thiebaut, D., Jacot, E., DeFronzo, R.A., Maeder, E., Jequier, E., and Felber, J.P. (1982) The effect of graded doses of insulin on total glucose uptake, glucose oxidation, and glucose storage in man. *Diabetes*. 31 (11), pp. 957-963.

Thomas, D.D., Corkey, B.E., Istfan, N.W. and Apovian, C.M. (2019) Hyperinsulinemia: An Early Indicator of Metabolic Dysfunction. *Journal of the Endocrine Society*. 3 (9), pp. 1727-1747.

Tomioka, K., Iwamoto, J., Saeki, K., and Okamoto, N. (2011) Reliability and validity of the International Physical Activity Questionnaire (IPAQ) in elderly adults: the Fujiwara-kyo Study. *Journal of Epidemiology*. 21 (6), pp. 459-465.

Trappe, S., Trappe, T., Gallagher, P., Harber, M., Alkner, B., and Tesch, P. (2004) Human single muscle fibre function with 84 day bed-rest and resistance exercise. *The Journal of Physiology*. 557 (Pt 2), pp. 501-513.

Turcotte, L.P., Richter, E.A., and Kiens, B. (1992) Increased plasma FFA uptake and oxidation during prolonged exercise in trained vs. untrained humans. *The American Journal of Physiology*. 262 (6 Pt 1), pp. E791-E799.

- Van Der Vusse, G.J., and Roemen, T.H. (1995) Gradient of Fatty Acids from Blood Plasma to Skeletal Muscle in Dogs. *Journal of Applied Physiology*. 78 (5), pp. 1839-1943.
- Ward, T.L., Raybould, S. J., Mondal, A., Lambert, J., and Patel, B. (2021) Predicting the length of stay at admission for emergency general surgery patients a cohort study. *Annals Of Medicine and Surgery (2012)*. 62, pp. 127-130.
- Wasserman, D.H. (2009) Four grams of glucose. *American Journal of Physiology. Endocrinology and metabolism*. 296 (1), pp. E11-E21.
- Watt, M.J., Heigenhauser, G.J., Dyck, D.J., and Spriet, L.L. (2002) Intramuscular triacylglycerol, glycogen and acetyl group metabolism during 4 h of moderate exercise in man. *The Journal of Physiology*. 541 (3), pp. 969-978.
- White, L.J., Ferguson, M.A., McCoy, S.C., and Kim, H. (2003) Intramyocellular lipid changes in men and women during aerobic exercise: a (1)H-magnetic resonance spectroscopy study. *The Journal of Clinical Endocrinology and Metabolism*. 88 (12), pp. 5638-5643.
- World Bank (202220) Country and lending groups. *World Bank, Washington, DC*. [Accessed: 1208/0410/20220]. Available from: <https://datahelpdesk.worldbank.org/knowledgebase/articles/906519>.
- World Health Organisation, (2016) Global Estimates 2016: Deaths by Cause, Age, Sex, by Country and by Region. *Geneva: World Health Organisation*.
- Yanagibori, R., Kondo, K., Suzuki, Y., Kawakubo, K., Iwamoto, T., Itakura, H., and Gunji, A. (1998) Effect of 20 days' bed rest on the reverse cholesterol transport system in healthy young subjects. *Journal of Internal Medicine*. 243 (4), pp. 307–312.
- Yanagibori, R., Suzuki, Y., Kawakubo, K., Makita, Y., and Gunji, A. (1994) Carbohydrate and lipid metabolism after 20 days of bed rest. *Acta Physiologica Scandinavica Supplementum*. 616, pp. 51-57.
- Yu, H., Fujii, N.L., Toyoda, T., An, D., Farese, R.V., Leitges, M., Hirshman, M.F., Mul, J.D., and Goodyear, L.J. (2015) Contraction stimulates muscle glucose uptake independent of atypical PKC. *Physiological Reports*. 3 (11), e12565.
- Zderic, T.W., Davidson, C.J., Schenk, S., Byerley, L.O., and Coyle, E.F. (2004) High-fat diet elevates resting intramuscular triglyceride concentration and whole-body lipolysis during exercise. *American Journal of Physiology: Endocrinology and Metabolism*. 286 (2), pp. E217-E225.

Zhu, R., Wen, C., Li, J., Harris, M. B., Liu, Y.Y., and Kuo, C.H. (2015) Lipid storage changes in human skeletal muscle during detraining. *Frontiers in Physiology*. 6, 309.

4. Does IMCL accumulation contribute to impaired whole-body glucose disposal and peripheral insulin sensitivity in males with NAFLD?

4.1 Introduction

The term “non-alcoholic fatty liver disease” (NAFLD) describes a condition characterised by intrahepatic triglyceride (IHTG) content greater than 5.56%, determined using $^1\text{H-MRS}$, which is unrelated to excessive alcohol consumption (Bril *et al.*, 2017). NAFLD is associated with components of the metabolic syndrome including dyslipidaemia, inflammation, and whole-body and peripheral insulin resistance (Godoy-Matos, Silva Júnior, and Valerio, 2020). As IHTG accumulates, patients with NAFLD can develop non-alcoholic steatohepatitis (NASH), an advanced form of NAFLD in which chronic hepatic inflammation promotes hepatic fibrosis and, eventually, cirrhosis (Benedict and Zhang, 2017). Thus, the term “NAFLD” can encompass a broad spectrum of disease (Rinella, 2015) ranging from simple hepatic steatosis at the most benign, which is ameliorable with weight loss (Romero-Gómez, Zelber-Sagi, and Trenell, 2017; Kenneally, Sier and Moore, 2017), to end-stage liver failure at the most severe, caused by irreversible cirrhosis, for which the only recourse is liver transplantation (Pais *et al.*, 2016).

Worldwide, amongst the general population, the prevalence of NAFLD is roughly 25% (Younossi, 2019), though it can vary greatly from continent to continent, being highest in South America at 30% and lowest in Africa at 13% (Younossi *et al.*, 2016). NAFLD is closely associated with obesity (BMI>30 kg/m²), which is increasingly endemic due to the global transition toward less healthy, calorie dense diets (Kearney, 2010; Popkin, Adair, and Ng, 2012) and global decreases in physical activity levels (Pietiläinen *et al.*, 2008; Healy *et al.*, 2008). Chronic over-consumption of energy predisposes the liver to

steatosis, and obesity is perhaps the biggest risk factor for NAFLD, with simple steatosis prevalent in 33% of obese individuals and NAFLD presenting in 57-98% of overweight and obese individuals worldwide (Ong *et al.*, 2005; Machado, Marques-Vidal, and Cortez-Pinto, 2006; Vernon, Baranova, and Younossi, 2011). Indeed, NAFLD prevalence is increasing proportionally with obesity status worldwide (Fan, Kim and Wong, 2017; Younossi *et al.*, 2019). In comparison, the prevalence of NAFLD amongst lean individuals (BMI<25 kg/m²) is estimated to be around 16% (Wattacheri and Sanyal, 2016).

The crosstalk between the adipose tissue, liver, and skeletal muscles in overfed states is central to the pathogenesis of NAFLD as it is currently understood (da Silva Rosa *et al.*, 2020). Chronic dietary intake of energy beyond what is necessary to match energy expenditure elevates serum TAG and FA concentrations and creates a state of positive energy balance (Chow and Hall, 2014; Wehmeyer *et al.*, 2016) that promotes the hypertrophy and hyperplasia of adipocytes and the expansion of white adipose tissue depots (Tchoukalova *et al.*, 2010). If this state is maintained then serum TAG and FA availability can overwhelm the FA uptake capacity of the adipose tissue, thereby increasing lipid uptake and ectopic storage in the liver and skeletal muscles, and it is proposed that, in the context of overfeeding and obesity, this promotes the development of insulin resistance in these tissues (Unger, 2003; Mittendorfer, 2011). Also, in the context of chronic overfeeding and obesity, adipocytes secrete molecules, including TNF- α , Retinol Binding Protein 4, Interleukin 1 β and Interleukin 6 which, through autocrine, paracrine, and endocrine signalling, promote adipose and systemic insulin resistance and inflammation (Plomgaard *et al.*, 2005; Smith and Kahn, 2016; Zatterale *et al.*, 2020). Insulin reduces lipolytic activity in adipocytes by inhibiting the enzymatic action of HSL, which is responsible for the hydrolysis of TAG and DAG (Foley, 1988). Thus, a characteristic feature of adipose tissue insulin resistance is elevated basal lipolysis which may increase the secretion of FA into the circulation, thereby further funnelling FA to the liver and skeletal muscles (Morigny *et al.*, 2015).

The preferential deposition of fat in visceral depots, rather than subcutaneous depots (McLaughlin *et al.*, 2011), in response to overfeeding is

of particular concern in the context of NAFLD. The deposition of fat in visceral adipose tissue (VAT) is strongly associated with increased incidence of T2DM (Vague, 1956; Banerji *et al.*, 1997) and with impaired whole-body GD, independent of age, sex, and total body fat mass (Björntorp, 1993; Brochu *et al.*, 2000). The lipolysis of TAG stored in VAT releases FAs directly into the hepatic portal vein (Björntorp, 1990), exposing the liver to high concentrations of FA. In lean adults, 5-10% of FAs delivered to the liver originate from VAT lipolysis, which is 4-fold greater in obese adults and increases in line with visceral fat mass (Nielsen *et al.*, 2004). The consequence of visceral obesity is increased IHTG accumulation, and increased fibrosis and inflammation that worsens NAFLD (van der Poorten *et al.*, 2008; Mirza, 2011; Yu *et al.*, 2015).

Liver fat content is determined by the balance between hepatic FA uptake and DNL, which increase fat content, and hepatic FA oxidation and lipoprotein production, which decrease fat content (Koo, 2013). In NAFLD, the disruption of one or more of these processes can create a chronic imbalance in hepatic FA homeostasis that predisposes the liver to the retention and accumulation of lipid as IHTG. Activity state is also a major determinant of IHTG content. Exercise increases muscle FA oxidation and, depending on the intensity and duration, can significantly reduce circulating FA concentration, thereby decreasing the amount of FA available for deposition in the liver (Maunder, Plews, and Kilding, 2018). Exercise also increases hepatic fat oxidation and decreases FA synthesis, responses which serve to decrease IHTG content (van der Windt *et al.*, 2018).

Hepatic mitochondrial oxidation increases to compensate for the onset of pathological IHTG accumulation (Sunny *et al.*, 2011). Recent evidence suggests that hepatic oxidation of dietary FAs can also be impaired (Naguib *et al.*, 2020) as NAFLD progresses. Thus, hepatic FA oxidation can be increased or reduced depending on the severity of NAFLD. Though the mechanisms underpinning this are not completely understood, it has been found that PPAR- α expression is reduced in patients with NAFLD (Kohjima *et al.*, 2007), with the extent of this reduction relative to the normal population acting as a marker of NAFLD severity (Francque *et al.*, 2015). FA oxidation primarily occurs in mitochondria but in response to pathological IHTG accumulation beyond the

oxidative capacity of the mitochondria alone, and/or impaired mitochondrial function, FA oxidation by the peroxisomes and cytochromes increases to compensate. Peroxisomes are primarily involved in the oxidation of VLCFAs, which can be oxidised by the cytochrome P450 CYP4A omega hydrolase system in reactions that generate hydrogen peroxide molecules (Rao and Reddy, 2001). The reactive oxygen species produced in this case, in conjunction with the elevated angiotensin II expression present in moderate to severe NAFLD (Cichoż-Lach and Michalak, 2014), increase oxidative stress in hepatocytes, causing damage that promotes fibrogenesis. Dysfunctional FA oxidation can also lead to the accumulation of DAG and ceramide species which antagonise the insulin signalling pathway and may contribute to the development of hepatic insulin resistance (Petersen *et al.*, 2016; Petersen and Shulman, 2017).

Skeletal muscle insulin resistance decreases glucose uptake in this tissue and diverts glucose to liver (Petersen *et al.*, 2007; Rabøl *et al.*, 2011) where it is metabolised to form acetyl-CoA. This excess acetyl-CoA is then converted to FAs via DNL (see **Section 1.2.2**) and contributes to the pathological accumulation of IHTG in NAFLD (Smith *et al.*, 2020). One mechanism via which insulin resistance at the level of the skeletal muscles is thought to develop is as a consequence of increased FA delivery, due to increased circulating FA availability from excess energy intake and/or from excess adipose tissue lipolysis, which leads to increased FA uptake by these tissues and the accumulation of IMCL (Yu *et al.*, 2002). Indeed, increasing serum FA concentration in vivo by hypercaloric or high-fat feeding, or by lipid infusion, has been shown to increase IMCL content, decrease whole-body glucose disposal and significantly impair skeletal muscle glucose uptake in humans (Nuutila *et al.*, 1992; Bachmann *et al.*, 2001; Hoeks *et al.*, 2012; Zderic *et al.*, 2014). As in hepatocytes, this “lipid-induced insulin resistance” in myocytes is thought to result from the antagonism of the canonical insulin signalling pathway by lipotoxic DAG and ceramide species (Yu *et al.*, 2002; Bosma *et al.*, 2012; Chavez and Summers, 2012).

In the context of NAFLD, it is clear that adipose insulin resistance reduces clearance of glucose from the blood by this tissue, leading to a greater

proportion being taken up by the liver (Korenblat *et al.*, 2008; Czech *et al.*, 2020). Together with increased lipolytic activity in adipose tissue enhancing FA delivery to the liver (Björntorp, 1990; Morigny *et al.*, 2015), both processes contribute to IHTG accumulation. Existing evidence also shows that IHTG accumulation, resulting from increased FA delivery (Fabbrini, Sullivan and Klein, 2010), enhanced DNL (Smith *et al.*, 2020), perturbed FA oxidation (Sunny *et al.*, 2011; Cichoż-Lach and Michalak, 2014) and decreased VLDL production (Higuchi *et al.*, 2011) promotes hepatic insulin resistance which is in turn associated with obesity, T2DM and the cluster of disorders which define the metabolic syndrome (Godoy-Matos, Silva Júnior, and Valerio, 2020).

An inverse association between IHTG content and muscle insulin sensitivity has been reported (Korenblat *et al.*, 2008). Korenblat and colleagues conducted a study in which IHTG content was measured by ¹H-MRS in 42 sedentary obese, middle-aged (41 ± 11 years) men ($n = 11$) and women ($n = 31$) who did not present with diabetes. They also used a two-step hyperinsulinaemic-euglycaemic clamp to assess tissue glucose disposal concurrent with the infusion of isotopically labelled glucose and palmitate tracers. They found that participants had a wide range of IHTG content, ranging from 0.7% to 45.5%. Using multivariate linear regression analysis in which age, BMI, and percentage body fat were all included factors, they found that IHTG content was the best predictor of skeletal muscle, liver, and adipose tissue insulin sensitivity, with visceral adiposity identified as the second major predictor in skeletal muscle and in the liver. Though theorised, whether lipid content in the skeletal muscles of individuals with NAFLD is indeed elevated relative to healthy controls (which is thought to contribute to muscle lipid-induced insulin resistance), remains unclear based on current evidence but can be reasonably assumed.

4.2 Study Aims

This study evaluated differences in IMCL content between healthy participants with liver fat content less than 5.56% and participants with NAFLD to investigate the association between IMCL content and measures of whole-body and leg glucose disposal, with the aim of determining whether IMCL content is associated with whole body and leg insulin resistance in NAFLD.

4.3 Materials and Methods

4.3.1 Study Overview and Ethics Statement

Some of the data presented in this chapter formed part of the “Effect of Carnitine on Liver Fat and Glucose Metabolism” (ECLIPSE) study, which was conducted at the David Greenfield Human Physiology Unit and SPMIC (University of Nottingham). All IMCL data generated are specific to this chapter. All participants were males aged 18-50 years and were allocated to one of two groups. A control group of healthy men with liver IHTG content less than 5.56% or a NAFLD group of males presenting with IHTG content greater than 5.56%; the 95th percentile of the normal population, indicative of the pathological IHTG accumulation that is diagnostic of NAFLD (Bril *et al.*, 2017). Consumption of less than 21 units of alcohol per week was a strict inclusion criterion for recruitment to either group. Exclusion criteria included diabetes mellitus, viral hepatitis or liver autoantibodies identified on serological screening, metallic medical implants (MRI contraindication), use of medication known to influence liver fat content and history of cardiovascular disease.

The primary end-point measurement in both groups was IMCL content, which was quantified by both fluorescent staining of LDs in cryosections of vastus lateralis biopsies and from ¹H-MRS spectra generated from non-invasive scanning of the vastus lateralis. Insulin-stimulated whole-body glucose disposal and leg glucose disposal were assessed via a hyperinsulinaemic-euglycaemic clamp protocol (60 mU/m² insulin infusion rate), with leg glucose disposal determined by sampling of venous and arterialed-venous blood for glucose concentration in combination with leg blood flow measurements. DEXA scans were performed to determine body composition and allowed standardisation of measures to lean body mass.

The study protocol was approved by a National Research Ethics Committee, Integrated Research Application System Project ID: 228690; Clinical Trials Identifier: NCT03439917. All participants were made fully aware of the study protocols and judged capable of consenting before signing consent forms and undergoing any of the experimental procedures described here.

4.3.2 Study Protocol

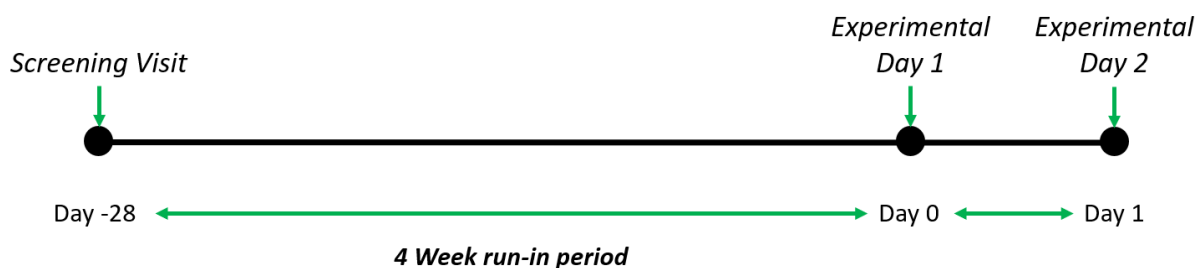


Figure 4-1: Timeline for the screening and baseline experimental days in the ECLIPSE study.

Those recruited to this study were invited to attend a screening visit at the David Greenfield Human Physiology Unit. Participants that met the eligibility criteria were then invited to attend the baseline experimental day (Day 0), scheduled ~4 weeks after initial screening (see **Figure 4-1**). Some participants were recruited from the Nottingham University Hospitals database whilst others were recruited after presenting with elevated liver enzymes on assessment by their general practitioner.

4.3.2.1 Screening Visit

The initial screening for each participant involved signing consent documentation, blood tests, anthropometric measurements, and ultrasound scanning of the liver to measure liver fat content. Participants with liver lipid deposits visible on ultrasound were initially allocated to the NAFLD group. Eligible participants for the NAFLD group had to present with liver stiffness less than 8kPa as assessed using transient elastography.

To assess energy intake and expenditure, participants in both groups were asked to record their dietary intake and wear triaxial ActiGraph GT3X accelerometers (ActiGraph LLC, Pensacola, FL, USA) worn at the waist for physical activity monitoring for 7 days following the screening visit. Both measurements were returned to researchers before the first experimental visit. Dietary records were analysed using a food composition database (Nutritics, Dublin, Ireland), with the activity data interrogated using the manufacturer's software (Actilife V6; ActiGraph LLC, Pensacola, FL, USA). The participants' physical activity levels were subsequently used as multipliers for resting

energy expenditure, estimated from standard equations (Schofield, 1985) (see **Section 2.4**), to calculate daily energy requirements.

4.3.2.2 Experimental Day 1

The first experimental day commenced ~4 weeks after the screening visit. Participants were asked to fast overnight and to not consume alcohol or engage in any strenuous physical activity in the 48 hours preceding the start of the experimental day. A 3 Tesla (3T) Philips Achieva MRI Scanner (Philips Healthcare, Netherlands) was used to scan the liver and vastus lateralis muscle of each participant to generate ¹H-MRS spectra from which IHTG and IMCL content were determined. Participant suitability for the control and NAFLD groups was confirmed at this point. Those with clinically normal liver fat (<5.56% IHTG) were allocated to the healthy control group. The diagnostic criteria for allocating participants to the NAFLD group included IHTG content greater than 5.56% not associated with excessive alcohol consumption and clinically significant fibrosis.

4.3.2.3 Experimental Day 2

During the second experimental day participants first underwent whole-body DEXA scans to determine body composition. This was followed by a two-step hyperinsulinaemic-euglycaemic clamp to assess whole-body and hepatic insulin sensitivity (DeFronzo, Tobin, and Andres, 1979). A two-step clamp involves first infusing a low dose of insulin to assess endogenous glucose release by the liver and to ensure it is completely blunted in preparation for the second, high-dose, insulin infusion during which insulin-mediated whole-body GD is assessed (**see Section 2.1**). Following local anaesthesia with 1% lidocaine, vastus lateralis biopsies were obtained from one leg via the Bergström percutaneous needle (5 mm) method (Bergström, 1962) immediately prior to the start of the clamp and at the end of the clamp. These biopsies were mounted on metal chucks using OCT compound (VWR International, Lutterworth, United Kingdom), frozen in liquid nitrogen, and stored at -80 °C.

4.3.3 Body Composition

Body composition was assessed using DEXA with a Lunar Prodigy DF+ 16075 scanner (GE Healthcare, Madison, WI, USA). Participants were instructed to lie supine on the DEXA table, with their arms away from their trunk and legs separated, and to stay still until the conclusion of the scanning process. Scans were analysed using enCORE software (GE Healthcare, Madison, WI, USA) which reports results for whole-body (total) and regional lean mass, fat mass, and bone mass. The regions being: right and left leg, right and left arm, right and left trunk. Android and gynoid fat masses were determined from manufacturer defined ROIs located at the level of the umbilicus and at the hips and upper thighs, respectively. Android fat is comprised of both visceral and subcutaneous fat, with gynoid fat comprised mainly of subcutaneous fat. The android/gynoid (A/G) ratio was defined as android fat mass divided by gynoid fat mass. Appendicular lean mass was calculated as the sum of the lean muscle mass of both arms and legs.

4.3.4 Whole-Body Glucose Disposal

The principles of the hyperinsulinaemic-euglycaemic clamp technique and the calculation of glucose disposal rate (M value) are discussed in **Section 2.1**. In this study whole-body glucose disposal in both groups was assessed in the final stage of a two-step hyperinsulinaemic euglycaemic clamp protocol (total clamp duration 240 minutes). A dorsal hand vein and the antecubital and femoral veins of the participants were cannulated. In the first step, insulin was intravenously infused at a rate of 15 mU/m²/min (Human Actrapid, EMEA/H/C/000424; Novo Nordisk A/S, Bagsværd, Denmark) through the antecubital cannula for 120 minutes. This first, low-dose infusion was conducted to determine endogenous glucose production but only steady-state data from the second step is discussed here. In this second step, the insulin infusion rate was increased to a constant 60 mU/m²/min for another 120 minutes. During both steps, arterialised-venous whole blood glucose was maintained at 4.5 mmol/L by frequent assessment of whole blood glucose concentration at 5-minute intervals (glucose oxidase method; YSI2300) and varying the infusion rate of 20% (w/v) glucose (Baxter Healthcare, Thetford,

UK). Blood samples of 1 ml were obtained from the cannulated hand of each participant at 5-minute intervals throughout of the clamp until the end of the protocol to monitor blood glucose during the time course of the clamp. For each participant, whole-body glucose disposal was calculated as a mean of the 15-minute M values (see **Section 2.1.2**) during the steady-state of the high dose infusion of the hyperinsulinaemic-euglycaemic clamp protocol at the t=180 minutes, t=190 and t=210 time points. After t=240, the insulin infusion was stopped, the participant fed, and the glucose infusion rate continued to be titrated until blood glucose concentration was stable without requiring the infusion of exogenous glucose. At this point the clamp protocol was stopped.

4.3.5 Leg Glucose Disposal

Before the start of the clamp and at t=210, t=225 and t=240 during the second step, arterialised blood and venous blood samples were obtained to calculate arterialised venous-venous (AV) differences in blood glucose concentration across the leg. Blood velocity in, and the mean diameter (across the cardiac cycle) of, the femoral vein was measured to calculate blood flow in the leg at these same time points. Mean leg glucose disposal (milligrams of glucose, per kilogram lean mass of the right leg, per minute) was calculated as the product of the (AV) differences in blood glucose concentration and blood flow in the cannulated leg at the t=210, t=225 and t=240 time points during the second step of the clamp standardised to the lean mass of the right leg of each participant (see **Equation 4-1** and **4-2**).

$$\text{Glucose Uptake (mg/min)} = \frac{\text{AV Differences (mmol/L)} \times \text{Blood Flow (ml/m)} \times 240 \text{ min}}{1000}$$

$$\text{Glucose Uptake (mg/kg RLeg LBM/min)} = \frac{\text{Glucose Uptake (mg/min)}}{\text{Right Leg Lean Mass}}$$

(Equation 4-1, 4-2)

4.3.6 Determination of IMCL:EMCL Ratio Using ¹H-MRS

Participants were positioned supine on the bed of a 3 Tesla (3T) Achieva MRI Scanner (Philips Healthcare, Best, Netherlands). The left leg of each participant was positioned parallel to the magnetic field and held in place by a stabiliser (see Section 2.7). An imaging receive coil was placed in contact with

the quadriceps femoris and ^1H -MRS spectra were obtained from the vastus lateralis muscle. Initial scanning time was 110 minutes followed by a 30-minute break and final 20 minutes of scanning using a 7T-Achieva MRI Scanner (Philips Healthcare, Best, Netherlands). Both water suppressed and non-water suppressed spectra were obtained. Resonances at 1.5 ppm originated from the EMCL-(CH₂)_n protons of extramyocellular lipids and resonances at 1.3 ppm originated from the IMCL-(CH₂)_n protons of intramyocellular lipids. IMCL:EMCL ratio was determined as a proportion of the area under the IMCL resonance peak to that under the EMCL resonance peak.

4.3.7 IMCL Quantification with Bodipy 493/503

The cryosectioning of vastus lateralis biopsies was performed using a Leica CM3050 S cryostat (Leica Microsystems GmbH, Wetzlar, Germany) as previously described (**Section 2.8.1**). A Zeiss LSM 880, AxioObserver confocal laser scanning microscope (Carl Zeiss AG, Jena, Germany) was used to image Bodipy 493/503 stained lipid in the sections at 20x magnification. All image acquisition settings in this study were the same as those defined in **Section 2.8.2** and image analysis to quantify LD count, LD size, and IMCL content in these sections was performed as described in **Section 2.8.3**.

4.3.8 Immunohistochemical Staining for Fibre Type

Cryosectioning and immunohistochemical staining of vastus lateralis biopsies from both groups was performed as described in **Sections 2.9.1** and **2.9.2**, respectively. Imaging was performed using a Zeiss LSM 880, AxioObserver confocal laser scanning microscope (Carl Zeiss AG, Jena, Germany). Sections were imaged at 20x magnification through an EC Plan-Neofluar M27 objective with a 25 mm field of view and 45.06 mm parfocal length. The 488 nm, 561 nm, and 633 nm laser lines at 3% power were used for the excitation of Alexa Fluors 488, 594, and 647 conjugated to secondary antibodies against Type IIA, Type I and Type IIX MHC isoforms, respectively. Fluorescence emissions for the MHC Type I isoform were collected between 589-619 nm and recorded in channel 1. Fluorescence emissions for the MHC Type IIA isoform were collected between 501-550 nm and recorded in channel 2 and emissions for the MHC Type IIX isoform were collected between 646-700 and recorded in

channel 3. Pixel scaling was 0.16 μm x 0.16 μm , each pixel being 0.026 μm^2 . Individual tiles were stitched together to create final images of entire biopsy sections. These images were matched to the IMCL staining images to categorise the lipid content of fibres by the predominant MHC isoform as described in **Section 2.9.4**.

4.3.9 Statistical Analyses

The normality of data was assessed using the Shapiro-Wilk and Kolmogorov-Smirnov goodness of fit tests. The variance in the distribution of data between the groups was assessed using F-tests. Where the variance in data between the two groups was significantly different, Welch's unpaired t-test was used to compare group means. The differences between group means for normally distributed data with equal variances were assessed using the two-tailed unpaired Student's t-test. Relationships among anthropometric characteristics, measures of IMCL content and indices of insulin sensitivity were evaluated using linear regression analysis, with the significance of these relationships being assessed with the Pearson correlation coefficient. In all cases two-tailed P values less than 0.05 were considered statistically significant. Statistical analyses were performed using IBM SPSS version 27 (IBM, Armonk, NY, USA) and Prism version 9.0.2 (GraphPad, San Diego, CA, USA). Asterisks represent p values such that * and † are $p < 0.05$, ** is $p < 0.01$, *** is $p < 0.001$, and **ns** means "not significant".

4.4 Results

4.4.1 Participant Characteristics

	Control Group (n = 8)	NAFLD Group (n = 11)	P value
Age (years)	30 ± 8.7	39 ± 9.3	= 0.05 (NS)
Height (m)	1.76 ± 0.04	1.79 ± 0.06	>0.05 (NS)
Weight (kg)	77.8 ± 6.50	106.7 ± 17.0	<0.001 (***) ^W
BMI (kg/m ²)	25.1 ± 2.50	33.2 ± 4.40	<0.001 (***)
IHTG (%)	1.37 ± 1.07	26.4 ± 11.7	<0.0001 (***) ^W
Body Fat (%)	22.7 ± 9.40	35.6 ± 6.40	<0.01 (**)
Lean Body Mass (kg)	56.5 ± 5.40	65.1 ± 8.10	<0.05 (*)
Trunk Lean Mass (kg)	25.9 ± 2.20	30.6 ± 4.20	<0.05 (*)
Leg Lean Mass (kg)	19.4 ± 1.60	22.4 ± 3.10	<0.05 (*)
Arm Lean Mass (kg)	7.54 ± 1.15	7.87 ± 1.23	>0.05 (NS)
Appendicular Lean Mass (ALM) (kg)	27.0 ± 2.70	30.2 ± 4.00	>0.05 (NS)
Whole Body Fat Mass (kg)	17.6 ± 8.20	37.4 ± 11.6	<0.001 (***)
Trunk Fat Mass (kg)	9.28 ± 4.06	21.6 ± 6.20	<0.001 (***)
Leg Fat Mass (kg)	6.15 ± 3.35	10.4 ± 3.20	<0.05 (*)
Arm Fat Mass (kg)	1.46 ± 0.81	4.03 ± 1.73	<0.001 (**)
Android/Gynoid Fat Ratio	1.01 ± 0.16	1.25 ± 0.14	<0.01 (**)
Android Fat (% Body Fat Mass)	28.1 ± 11.0	47.1 ± 7.30	<0.001 (***)
Gynoid Fat (% Body Fat Mass)	27.4 ± 9.00	37.9 ± 6.60	<0.5 (*)

Table 4-1: Participant characteristics for the control and NAFLD groups. Regional data left unshaded. Values are mean ± SD. ^W = Welch's t-test.

The participants with NAFLD had greater lean body mass than the control participants. Whole body fat mass in the participants with NAFLD was two-fold

greater than in healthy controls and this difference in fat mass was maintained in the trunk, arms, and legs. The NAFLD participants were obese while their healthy counterparts straddled the boundary between normal weight and overweight ($25.1 \pm 2.54 \text{ kg/m}^2$). The android and gynoid (A/G) fat ratio, a measure of visceral fat deposition around the abdomen, was greater in participants with NAFLD than in healthy controls. There were no differences in height and appendicular lean mass between the two groups. Of the participants in the original dataset, 8 participants in the control group and 11 participants in the NAFLD group yielded tissue suitable for fluorescent and immunohistochemical staining. Each of these 19 samples were cut, stained, imaged, and analysed in the data presented here.

4.4.2 Whole-Body Glucose Disposal

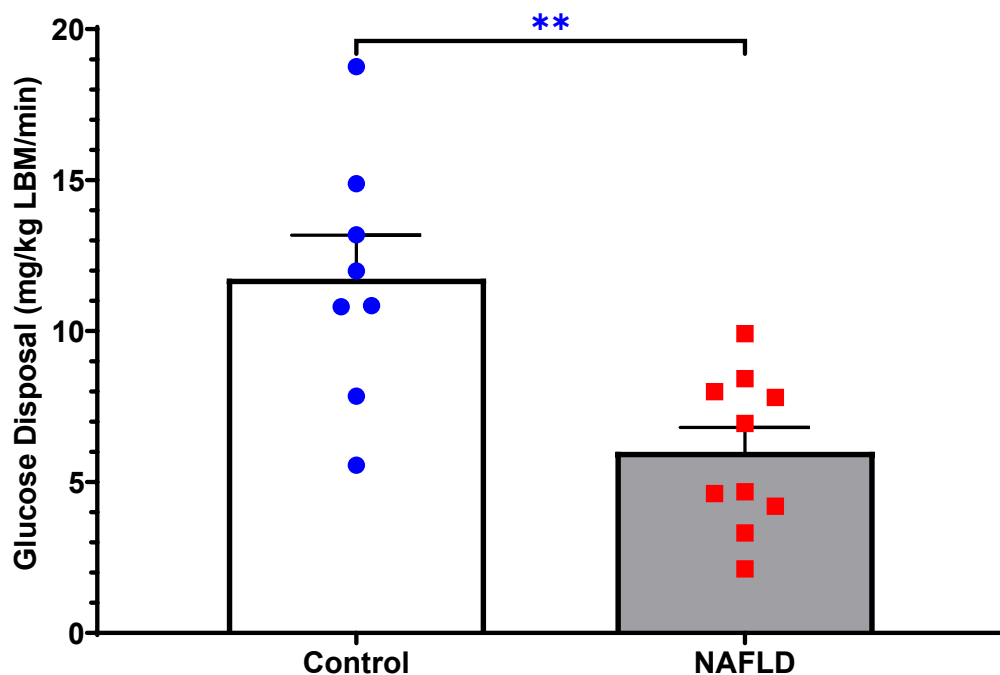


Figure 4-2: Mean whole-body glucose disposal in control and NAFLD groups during the steady state ($t=195$ to $t=225$) of the hyperinsulinaemic-euglycaemic clamp protocol. Values are mean \pm SEM and are standardised to LBM.

Mean steady-state insulin-mediated whole-body glucose disposal in the NAFLD group was 51% of that in the control group ($6.0 \pm 0.8 \text{ mg/kg LBM/min}$ vs. $11.7 \pm 1.4 \text{ mg/kg LBM/min}$, respectively; $p < 0.01$).

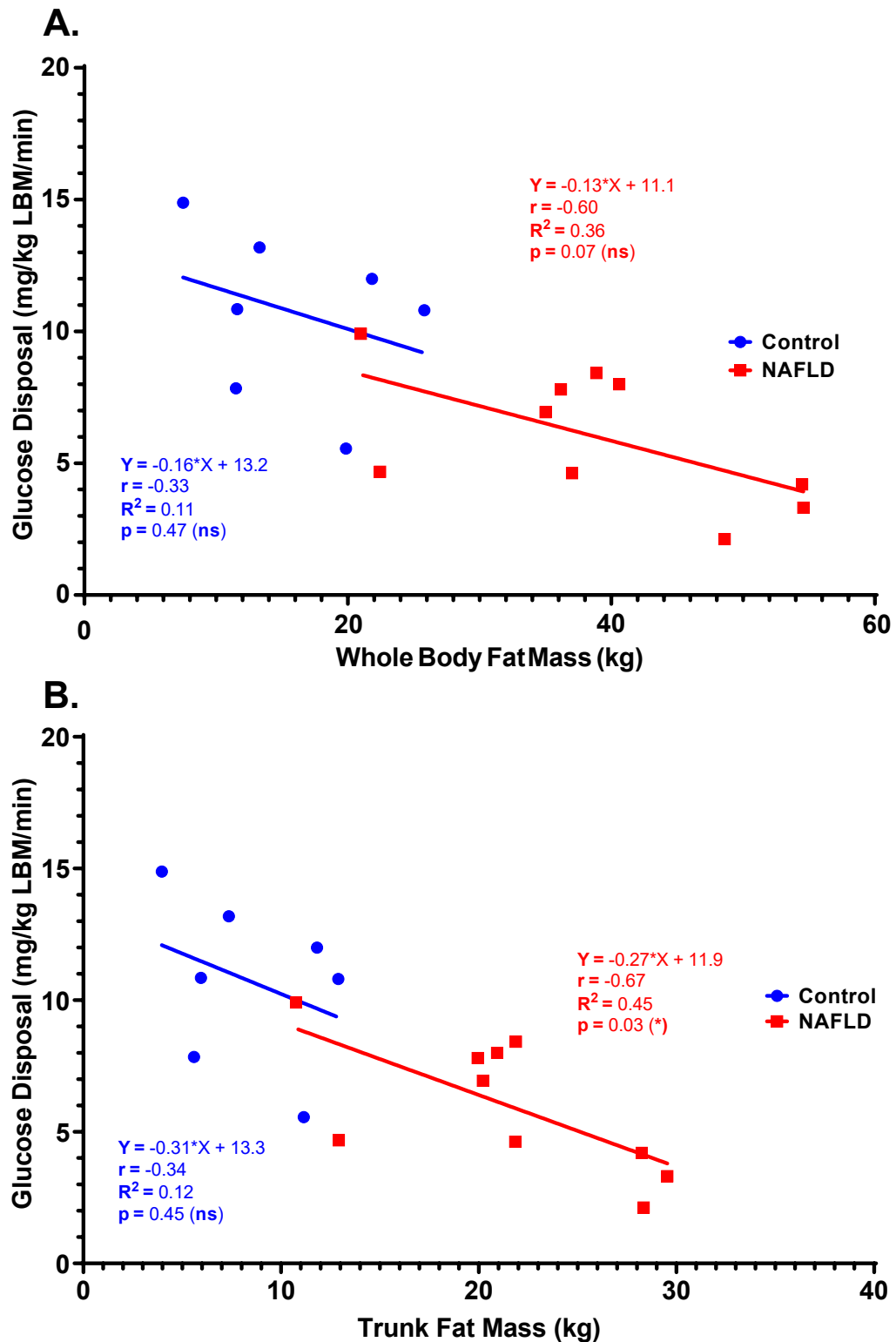


Figure 4-3: Association between (A) whole body fat mass and (B) trunk fat mass with whole body glucose disposal in both control and NAFLD participants using Pearson correlation. For the control group, $n = 7$ and for the NAFLD group $n = 10$.

For the control group, neither whole-body ($r = -0.33$; $p = 0.47$) nor trunk fat mass ($r = -0.34$; $p = 0.45$) was associated with whole-body glucose disposal (see **Figure 4-3A** and **4-3B**). In the NAFLD group, a trend for whole body fat mass to be correlated with glucose disposal was observed ($r = -0.60$; $p = 0.07$). However, a significant inverse relationship was observed when fat localised to the trunk region of NAFLD participants was compared with whole-body glucose disposal ($r = -0.67$; $p < 0.05$).

4.4.3 Leg Glucose Disposal

	Control Group	NAFLD Group	P value
AV Difference (mmol/L)	0.83 ± 0.45	0.39 ± 0.27	0.027 (*)
Blood Flow (cm³/min)	541.7 ± 297.6	313.7 ± 149.3	0.06 (ns)

Table 4-2: Blood flow and AV differences in glucose concentration across the leg in control and NAFLD participants shown as means of values measured at the $t=120$, $t=210$, and $t=225$ time points. Values are mean ± SD.

The AV difference in leg glucose during the steady-state period was less in the NAFLD group than in the control group ($p < 0.05$). At the same time there was a trend for femoral artery blood flow during the steady-state period of the insulin clamp to be less in NAFLD patients compared to controls ($p = 0.06$).

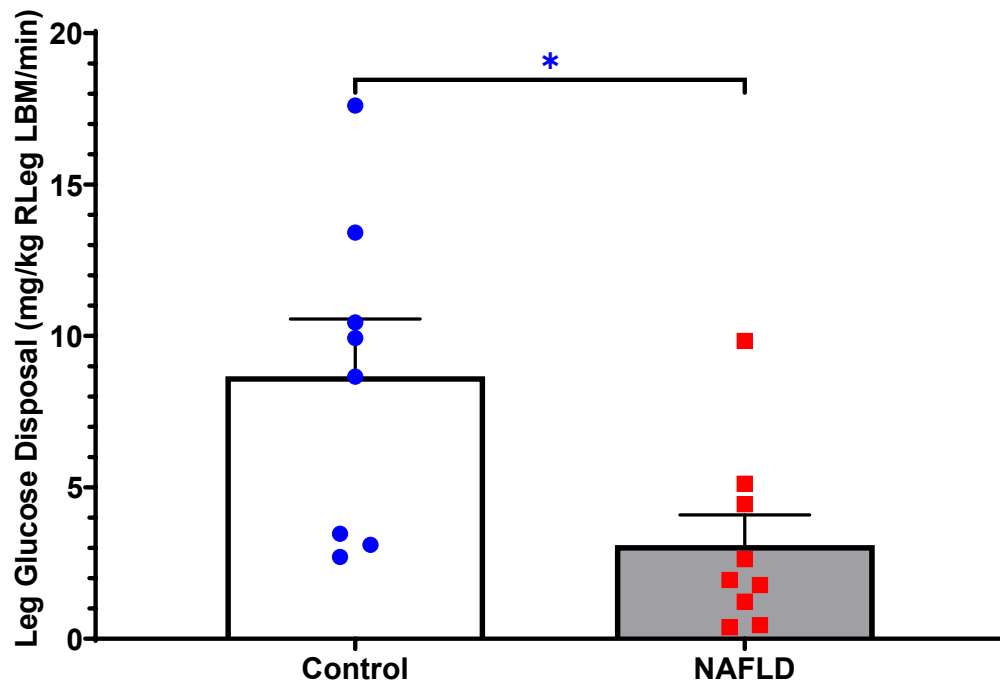


Figure 4-4: Leg glucose disposal in control and NAFLD group participants during the steady state of the hyperinsulinaemic-euglycaemic clamp protocol. Values are mean \pm SEM and are standardised to the lean mass of the right leg (kg RLeg LBM) of each participant. For the control group, $n=8$ and for the NAFLD group $n=9$.

Leg glucose disposal was less in the NAFLD group compared to the control group (3.01 ± 1.00 mg/kg RLeg LBM/min vs. 8.67 ± 1.89 mg/kg RLeg LBM/min, respectively; $p < 0.05$).

4.4.4 ¹H-MRS Quantification of IMCL:EMCL Ratio

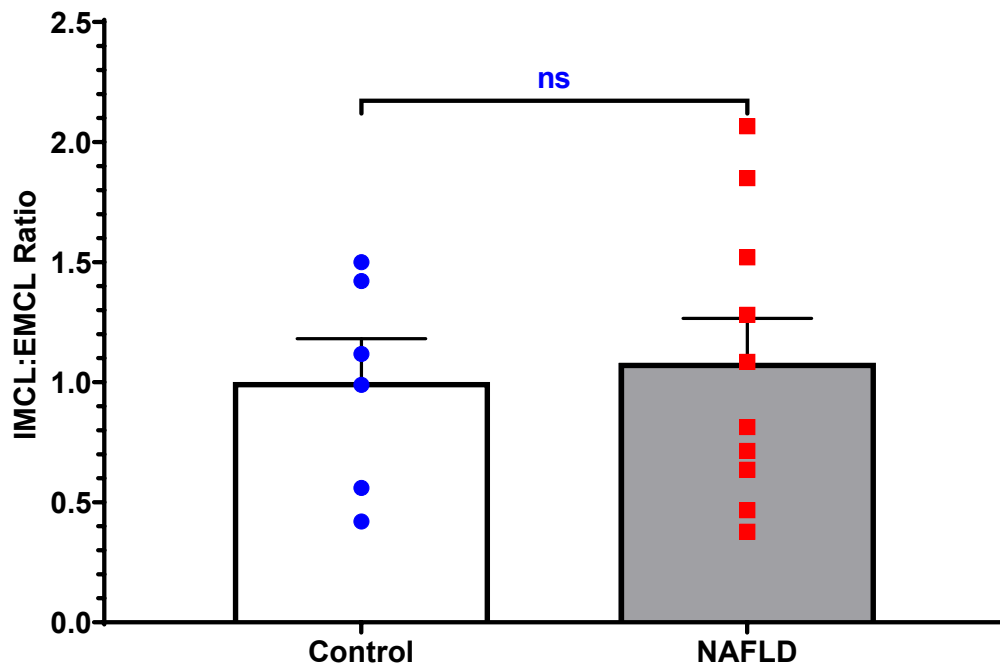
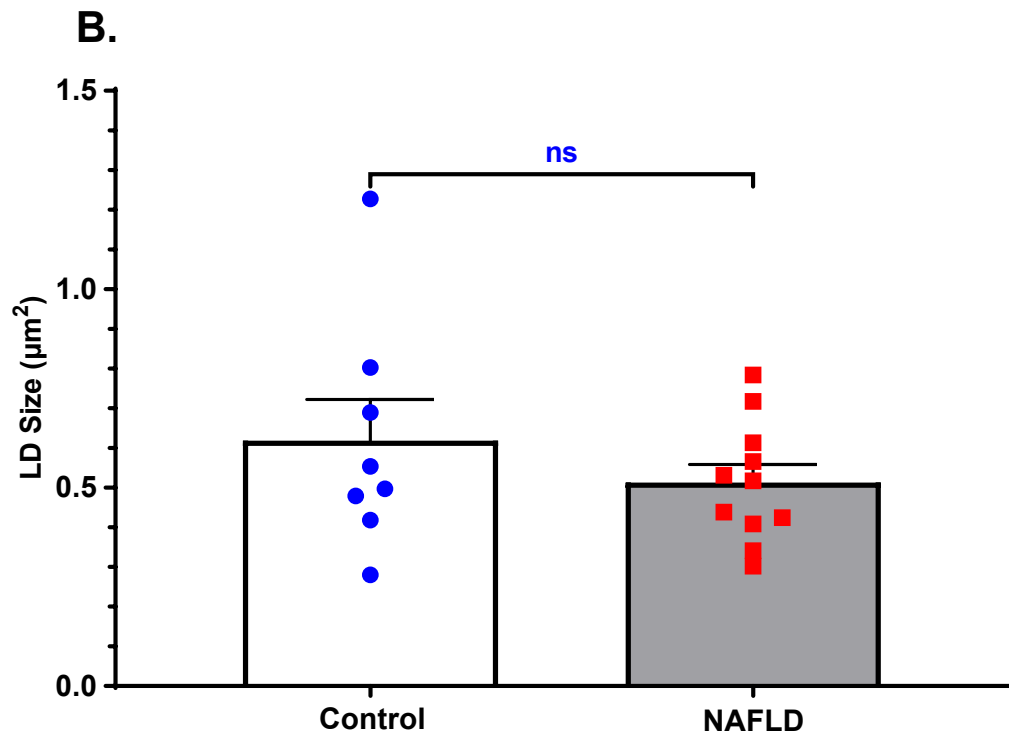
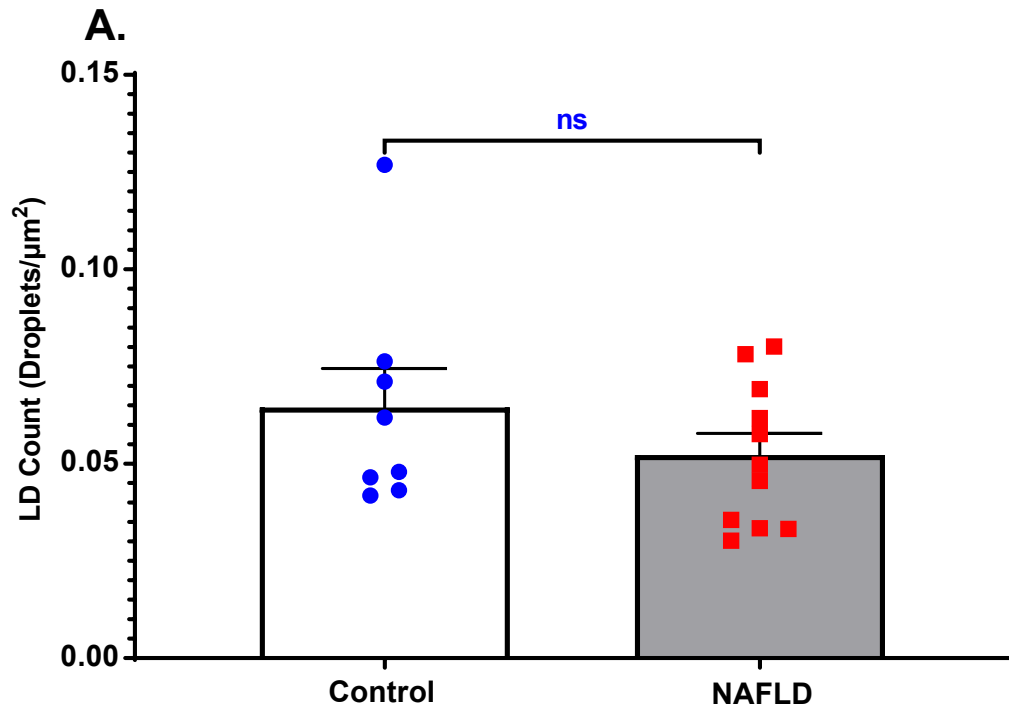


Figure 4-5: IMCL:EMCL ratio estimated from $-(CH_2)_n-$ and terminal $-CH_3$ resonances in ¹H-MR spectra of the vastus lateralis muscle from both the control group and NAFLD group participants. Values are mean \pm SEM, $n=6$ control group and $n=10$ NAFLD group.

There were no differences in IMCL:EMCL ratio measured using ¹H-MRS between the healthy participants in the control group and the participants with NAFLD (1.00 ± 0.18 vs. 1.08 ± 0.18 , respectively; $p = 0.78$).

4.4.5 Histochemical Quantification of IMCL Content



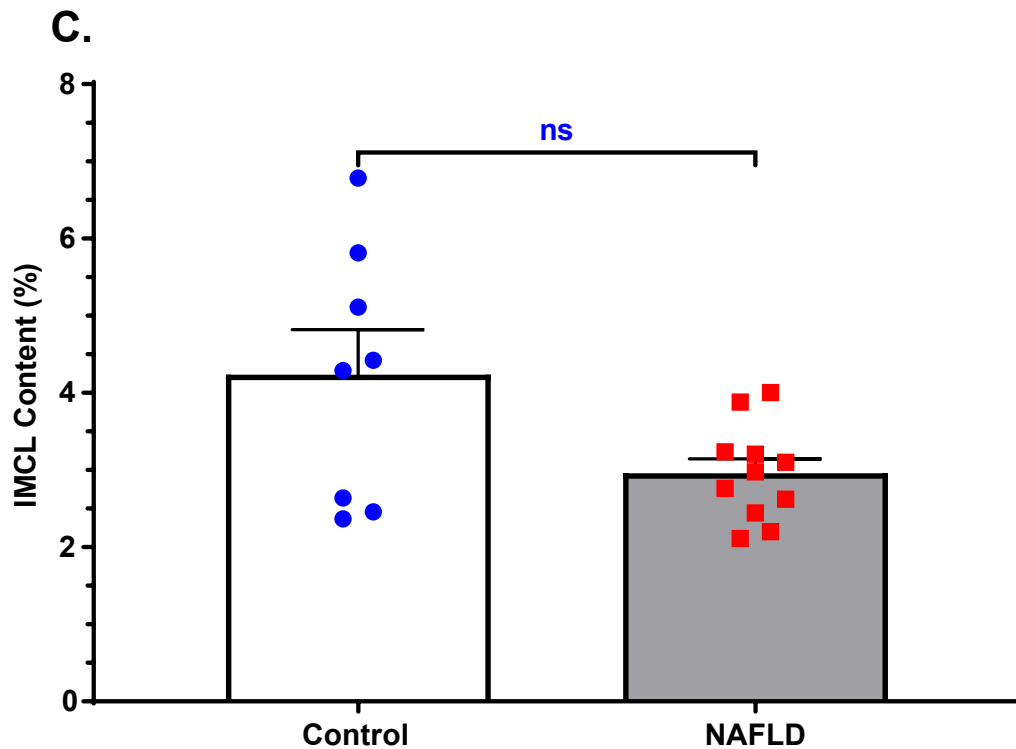
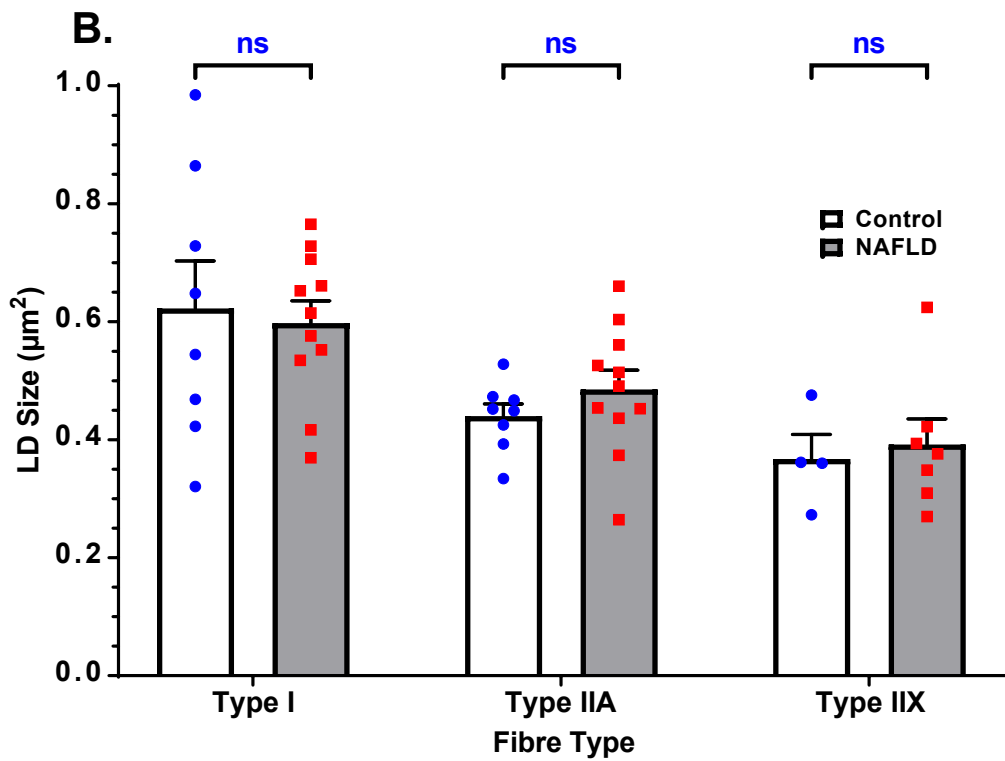
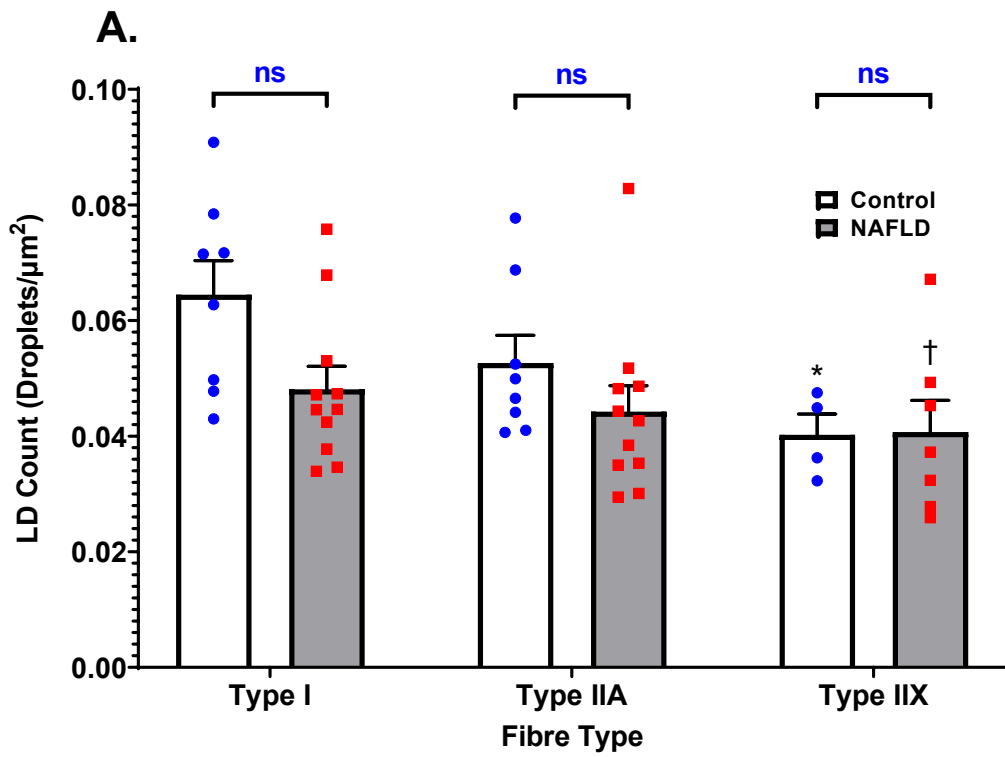


Figure 4-6: The (A) LD count, (B) LD size, and (C) IMCL content in vastus lateralis muscle biopsies taken from control and NAFLD participants. Values are mean \pm SEM. For all measures, $n=8$ control group and $n=11$ NAFLD group.

Figure 4-6 shows the LD count (A), LD size (B) and the (C) percentage of lipid in vastus lateralis muscle biopsies from healthy control participants and NAFLD participants as determined by histochemical staining of neutral lipid in these biopsies with Bodipy 493/503. There were no differences between control and NAFLD groups in the number of LDs per square micrometre of muscle tissue (0.06 ± 0.01 LDs/ μm^2 vs. 0.05 ± 0.01 LDs/ μm^2 , respectively; $p = 0.27$). There were also no differences in the size of LDs in vastus lateralis biopsies from both groups (0.62 ± 0.10 μm^2 , control group, vs. 0.51 ± 0.05 μm^2 , NAFLD group; $p = 0.32$) or the area of muscle tissue occupied by lipid between the two groups ($4.23 \pm 0.58\%$ control group vs. $2.96 \pm 0.19\%$ NAFLD group, $p = 0.07$).

4.4.6 IMCL Content by Fibre Type



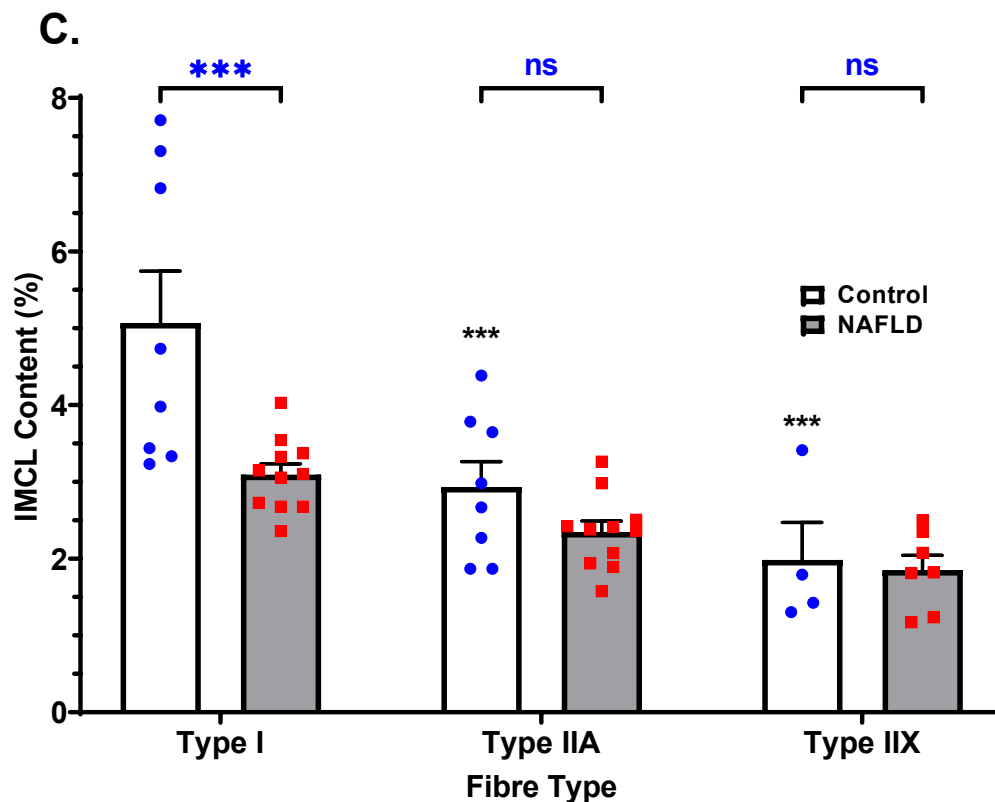


Figure 4-7: Fibre type specific (A) LD count, (B) LD size, and (C) IMCL content in the control and NAFLD groups. Statistically significant differences vs. Type I Control are represented as *, vs. Type I NAFLD as †. Values are mean ± SEM.

There were no differences between the control participants and NAFLD patients in Type I, IIA, and IIX fibre type specific LD count ($p = 0.07$, **Figure 4-7A**) and LD size ($p = 0.71$, **Figure 4-7B**). Within the control group, LD size was greater in type I fibres compared with Type IIX fibres ($p < 0.05$), which was mirrored in the NAFLD group where LD size in Type I fibres was greater than in Type IIX fibres ($p < 0.05$). The IMCL content of Type I fibres in control participants was greater than in NAFLD participants (5.07 ± 0.67 vs. 3.09 ± 0.14 , $p < 0.001$, **Figure 4-7C**). No between-group differences were seen in the IMCL content of Type IIA and IIX fibres. Within the control group, IMCL content in Type I fibres was greater than in type IIA ($p < 0.001$) and Type IIX ($p < 0.001$) fibres.

4.4.7 Association Between IMCL Content and Glucose Disposal

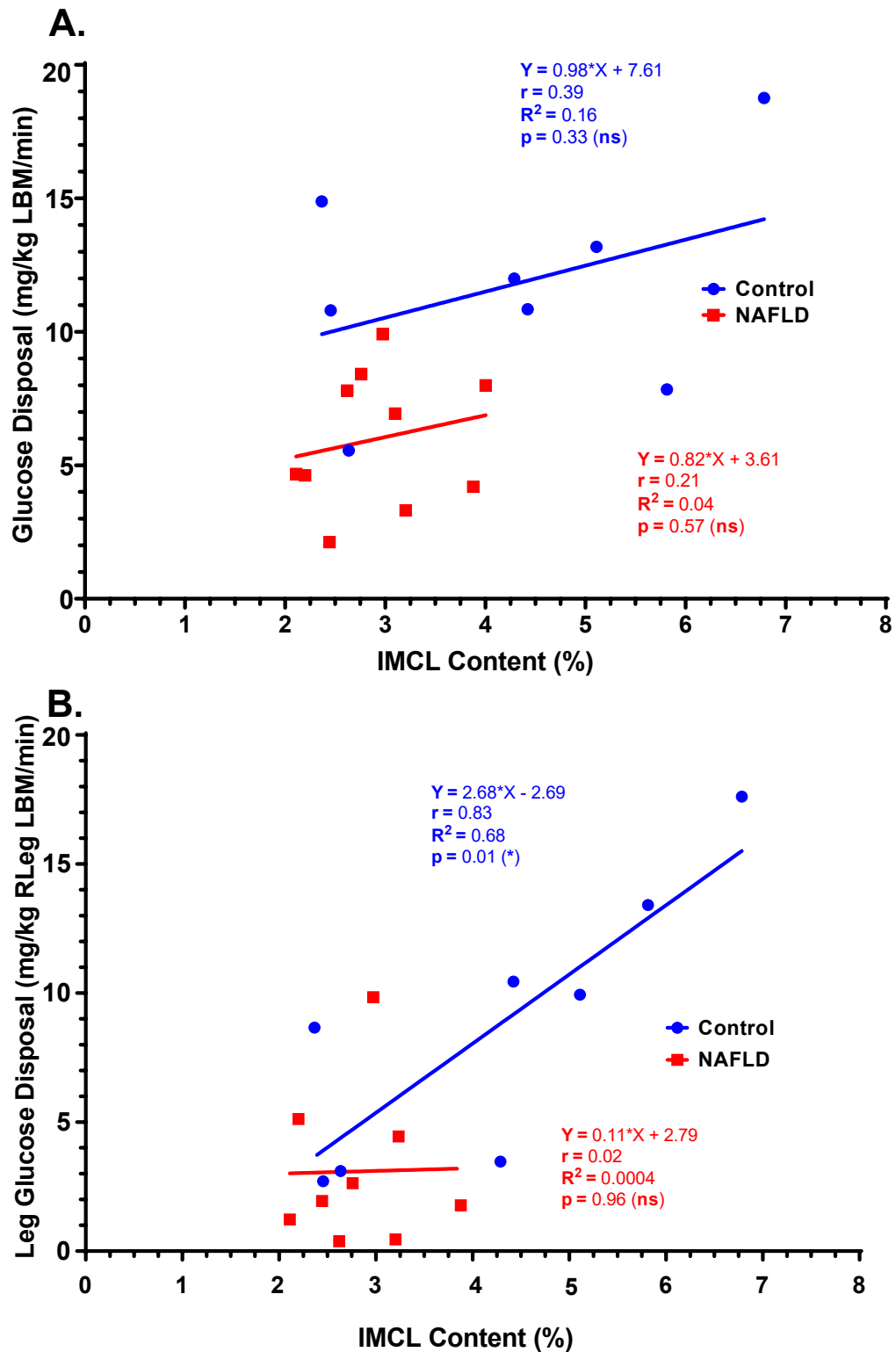


Figure 4-8: Association between (A) whole-body glucose disposal and (B) leg glucose disposal with IMCL content determined by histochemical staining. For the control group, $n = 7$ and for the NAFLD group $n = 10$.

In the participants with NAFLD, IMCL content was not associated with measures of whole-body ($r = 0.21$; $p = 0.57$) or leg glucose disposal ($r = 0.02$; $p = 0.96$). Similarly, in the healthy control participants, whole-body glucose disposal was not associated with muscle lipid content ($r = 0.39$; $p = 0.33$). However, there was a significant association between IMCL content and leg glucose disposal in the healthy controls ($r = 0.83$; $p < 0.05$).

4.5 Discussion

This study is the first to characterise differences in the number and size of skeletal muscle LDs in participants with NAFLD at the fibre-type level and the first to compare histochemical quantification of IMCL content with MRS measurements of IMCL:EMCL ratio in this context. The principal finding from this study was that GD was lower in the participants with NAFLD than in the control group despite myocellular fat content being no different between the two groups. This was evident both with IMCL content measured histochemically (see **Figure 4-6C**) and with the IMCL:EMCL ratio determined using ^1H -MRS (see **Figure 4-5**). This finding suggests that, in the context of NAFLD, elevated IMCL content may not have a causative role in the establishment of muscle insulin resistance or in the development of pathological IHTG accumulation and whole-body insulin resistance. Indeed, the strongest association found here was a negative association between trunk fat mass and whole-body GD.

Though decrements in whole-body GD are a well reported feature of NAFLD, very few studies have measured and compared IMCL content in both individuals with NAFLD and in healthy controls. Indeed, what little evidence exists in this regard is contradictory. It has been reported that there were no baseline differences in IMCL content in healthy controls versus non-obese NAFLD patients (Pugh *et al.*, 2014), that IMCL content is greater in overweight NAFLD patients than in healthy individuals (Oh *et al.*, 2014), and that greater IMCL content in obese NAFLD patients relative to healthy individuals is only present in those younger than 30 years of age (Oshida *et al.*, 2019). These reports have all used MRS in the quantification of IMCL content which allows for the delineation of intramyocellular and extramyocellular lipid stores but

cannot discern the number and size of LDs, which constitute the vast majority of the IMCL pool, and their relative abundance in different muscle fibre types. The findings of this study show that IMCL content in the Type I muscle fibres of those with NAFLD is less than in healthy controls, though this difference is not evident in Type IIA and Type IIX fibres (see **Figure 4-7C**).

IMCL content measured histochemically was not associated with leg glucose disposal in the NAFLD group but was positively associated with leg glucose disposal in the healthy control participants (see **Figure 4-8B**). This discrepancy may be explained by the differing levels of habitual physical activity between the two groups. The participants in the control group were physically active and it has recently been demonstrated that physical activity level in healthy, male non-athletes is positively correlated with IMCL content, which is in turn positively associated with insulin sensitivity, such that IMCL accumulation in this demographic has no association with muscle or whole-body insulin resistance (Yamasaki *et al.*, 2020). In contrast individuals with obese NAFLD are typically sedentary as well as overfed, with sedentary time being strongly associated with NAFLD progression (Goncalves *et al.*, 2013; Croci *et al.*, 2019). Physical activity improves mitochondrial function (Sorriento, Di Vaia, and Iaccarino, 2021), increases muscle insulin sensitivity (Rabøl *et al.*, 2011), and decreases IHTG content independent of changes in body weight (Sargeant *et al.*, 2018) and it is encouraged as an effective non-pharmacological countermeasure to ameliorate the insulin resistance and metabolic dysfunctions presenting in NAFLD (Koliaki *et al.*, 2015; Hoene *et al.*, 2021). The differences in the associations described in this chapter could also be explained by the fact that the range of IMCL content amongst the control participants was significantly greater than that of their counterparts with NAFLD (see **Figure 4-8B**).

Clearly, reduced whole-body insulin sensitivity and muscle glucose disposal in the obese participants with NAFLD, compared to the healthy controls, were not due to differences in IMCL content. What then can explain the development of these metabolic impairments in NAFLD?

As mentioned in the introduction to this chapter, visceral fat accumulation is associated with insulin resistance (Björntorp, 1993; Ruderman *et al.*, 1998; Brochu *et al.*, 2000) and is a predictor of NAFLD severity independent of BMI (Pang *et al.*, 2015; Shida *et al.*, 2020). Visceral fat was not measured directly in this study but, within a range of 0.5 to 1.5, A/G ratio has been shown to be strongly correlated with visceral fat area and liver fat content (Bouchi *et al.*, 2016). Android adiposity and the A/G ratio are associated with insulin resistance and dyslipidaemia in all age groups (Aucouturier *et al.*, 2009; Kang *et al.*, 2011; Samsell *et al.*, 2014; Petersen *et al.*, 2015; Sari *et al.*, 2019) and in a cross-sectional study involving 67 normal-weight and 659 overweight NAFLD patients, the A/G ratio was found to be the best predictor of NAFLD (Alferink *et al.*, 2019). In this study the A/G ratio of the NAFLD participants was significantly greater than that of the control group (See **Table 4-1**), indicating that the deposition of fat in visceral stores rather than subcutaneous and muscle stores was greater amongst the NAFLD participants. Supporting this is the fact that trunk fat mass in the NAFLD group was double that of trunk fat mass in the control group (See **Table 4-1**). From these data it is clear that visceral adiposity was greater in the NAFLD participants, and that this visceral adiposity contributed to the whole-body insulin resistance observed in that group. This preferential deposition of lipid into visceral stores and the liver may partly explain why IMCL content is not elevated in the NAFLD group relative to the healthy controls.

Another important consideration is that up to 70% of NAFLD susceptibility can be attributed to inherited risk factors (Dongiovanni, and Valenti, 2016). Individuals predisposed to NAFLD present with variations of genes (including UCP2, IRS1, APOB, FATP3, and PNPLA3) which are involved in the regulation of hepatic LD remodelling, VLDL secretion, insulin signalling, and hepatic LD β -oxidation (Meroni *et al.*, 2021). These variations lead to greater hepatic FA uptake, reduced hepatic production and secretion of VLDLs containing FA, increased hepatic LD count and size, and perturbed hepatic FA oxidation (Dongiovanni, Anstee, and Valenti, 2013; Desterke, and Chiappini, 2019). These data suggest that in those with NAFLD there may be a genetic predisposition to FA deposition in the VAT and liver, independent of

overfeeding, which may spare the skeletal muscles from the accumulation of lipid. As previously mentioned, FAs from the lipolysis of TAG stored in VAT are secreted directly into the hepatic portal vein (Björntorp, 1990; Nielsen *et al.*, 2004), transported into hepatocytes increasing IHTG content and promoting hepatic and systemic insulin resistance (Rytka *et al.*, 2011). This is compounded with the secretion of pro-inflammatory cytokines by macrophages recruited to dead adipocytes in VAT, these cytokines promote adipose and systemic inflammation that can contribute to NAFLD progression (Zatterale *et al.*, 2020).

Several studies have provided evidence that IHTG accumulation is independently correlated with liver and skeletal muscle insulin resistance in NAFLD, though it remains unclear whether hepatic steatosis is the result of skeletal muscle insulin resistance (Flannery *et al.*, 2012) or a cause of it (Uno *et al.*, 2006; Misu *et al.*, 2010). Kato and colleagues demonstrated that in obese individuals with NAFLD, IHTG content was strongly correlated with liver and skeletal muscle insulin resistance whilst IMCL content, measured by MRS and standardised to creatine, was not correlated with skeletal muscle insulin resistance in 69 participants (Kato *et al.*, 2014). This is supported by evidence that, in obese individuals, hepatic fat content is correlated with characteristics of the metabolic syndrome such as hepatic and whole-body insulin resistance, while IMCL content is not (Kotronen *et al.*, 2008; Visser *et al.*, 2011). Thus, in the context of obese NAFLD, it is likely that IHTG accumulation independently contributes to whole-body insulin resistance, with IMCL content having no primary role in the development of this metabolic dysfunction (Korenblat *et al.*, 2008).

4.6 Conclusion

In summary, this study compares the differences in IMCL content between healthy individuals with normal liver fat content and individuals with NAFLD, demonstrating that IMCL content, measured histochemically and using ¹H-MRS, is not different between the two groups and does not contribute to the lowerleg whole-body and leg glucose disposal in obese NAFLD when compared to control. The impairments in glucose disposal can be partly

explained by greater visceral adiposity and IHTG content in the group with NAFLD and differences in habitual physical activity as previously discussed.

4.7 References

Adams, L.A., Anstee, Q.M., Tilg, H. and Targher, G. (2017) Non-alcoholic fatty liver disease and its relationship with cardiovascular disease and other extrahepatic diseases. *Gut*. 66 (6), pp. 1138-1153.

Alferink, L., Trajanoska, K., Erler, N. S., Schoufour, J. D., de Knegt, R. J., Ikram, M. A., Janssen, H., Franco, O. H., Metselaar, H. J., Rivadeneira, F., & Darwish Murad, S. (2019) Nonalcoholic Fatty Liver Disease in The Rotterdam Study: About Muscle Mass, Sarcopenia, Fat Mass, and Fat Distribution. *Journal of Bone and Mineral Research : The Official Journal of The American Society for Bone And Mineral Research*. 34 (7), pp. 1254-1263.

Aucouturier, J., Meyer, M., Thivel, D., Taillardat, M. and Duché, P. (2009) Effect of android to gynoid fat ratio on insulin resistance in obese youth. *Archives of Pediatrics & Adolescent Medicine*. 163 (9), pp. 826-831.

Bachmann, O.P., Dahl, D.B., Brechtel, K., Machann, J., Haap, M., Maier, T., Loviscach, M., Stumvoll, M., Claussen, C.D., Schick, F., Häring, H.U. and Jacob, S. (2001) Effects of Intravenous and Dietary Lipid Challenge on Intramyocellular Lipid Content and the Relation with Insulin Sensitivity in Humans. *Diabetes*. 50 (11), pp. 2579-2584.

Bae, J.C., Rhee, E.J., Lee, W.Y., Park, S.E., Park, C.Y., Oh, K.W., Park, S.W. and Kim, SW. (2011) Combined effect of nonalcoholic fatty liver disease and impaired fasting glucose on the development of type 2 diabetes: a 4-year retrospective longitudinal study. *Diabetes Care*. 34 (3), pp. 727-729.

Banerji, M.A., Lebowitz, J., Chaiken, R.L., Gordon, D., Kral, J.G. and Lebovitz, H.E. (1997) Relationship of visceral adipose tissue and glucose disposal is independent of sex in black NIDDM subjects. *The American Journal of Physiology*. 273 (2 Pt 1), pp. E425-E432.

Baron, A.D., Brechtel, G., Wallace, P. and Edelman, S.V. (1988) Rates and tissue sites of non-insulin- and insulin-mediated glucose uptake in humans. *The American Journal of Physiology*. 255 (6 Pt 1), pp. E769-E774.

Benedict, M. and Zhang, X. (2017) Non-alcoholic fatty liver disease: An expanded review. *World Journal of Hepatology*. 9 (16), pp. 715-732.

Bergström, J. (1962) Muscle electrolytes in man: determined by neutron activation analysis on needle biopsy specimens. A study on normal subjects, kidney patients and patients with chronic diarrhea. *Scandinavian Journal of Clinical & Laboratory Investigation*. Supplement 68 (11-13), pp. 511-513.

Björntorp, P. (1990) "Portal" adipose tissue as a generator of risk factors for cardiovascular disease and diabetes. *Arteriosclerosis (Dallas, Tex.)*. 10 (4), pp. 493-496.

Björntorp, P. (1993) Visceral obesity: a "civilization syndrome". *Obesity Research*. 1 (3), pp. 206-222.

Borel, A.L., Nazare, J.A., Smith, J., Aschner, P., Barter, P., Van Gaal, L., Eng Tan, C., Wittchen, H.U., Matsuzawa, Y., Kadowaki, T., Ross, R., Brulle-Wohlhueter, C., Alméras, N., Haffner, S. M., Balkau, B. and Després, J.P. (2015) Visceral, subcutaneous abdominal adiposity and liver fat content distribution in normal glucose tolerance, impaired fasting glucose and/or impaired glucose tolerance. *International Journal of Obesity (2005)*. 39 (3), pp. 495-501.

Bosma, M., Kersten, S., Hesselink, M.K. and Schrauwen, P. (2012) Re-evaluating lipotoxic triggers in skeletal muscle: relating intramyocellular lipid metabolism to insulin sensitivity. *Progress in Lipid Research*. 51 (1), pp. 36-49.

Bouchi, R., Nakano, Y., Ohara, N., Takeuchi, T., Murakami, M., Asakawa, M., Sasahara, Y., Numasawa, M., Minami, I., Izumiyama, H., Hashimoto, K., Yoshimoto, T. and Ogawa, Y. (2016) Clinical relevance of dual-energy X-ray absorptiometry (DXA) as a simultaneous evaluation of fatty liver disease and atherosclerosis in patients with type 2 diabetes. *Cardiovascular Diabetology*. 15, 64.

- Bril, F., Barb, D., Portillo-Sanchez, P., Biernacki, D., Lomonaco, R., Suman, A., Weber, M.H., Budd, J.T., Lupi, M.E. and Cusi, K. (2017) Metabolic and histological implications of intrahepatic triglyceride content in nonalcoholic fatty liver disease. *Hepatology (Baltimore, Md.)*. 65 (4), 1132-1144.
- Brochu, M., Starling, R.D., Tchernof, A., Matthews, D.E., Garcia-Rubi, E. and Poehlman, E.T. (2000) Visceral adipose tissue is an independent correlate of glucose disposal in older obese postmenopausal women. *The Journal of Clinical Endocrinology and Metabolism*. 85 (7), pp. 2378-2384.
- Campos, R., Masquio, D., Corgosinho, F.C., Caranti, D.A., Ganen, A.P., Tock, L., Oyama, L.M. and Dâmaso, A.R. (2019) Effects of magnitude of visceral adipose tissue reduction: Impact on insulin resistance, hyperleptinemia and cardiometabolic risk in adolescents with obesity after long-term weight-loss therapy. *Diabetes & Vascular Disease Research*. 16 (2), pp. 196-206.
- Chavez, J.A. and Summers, S.A. (2012) A ceramide-centric view of insulin resistance. *Cell Metabolism*. 15 (5), pp. 585-594.
- Chow, C.C., and Hall, K.D. (2014) Short and long-term energy intake patterns and their implications for human body weight regulation. *Physiology & Behaviour*. 134, pp. 60-65.
- Cichoż-Lach, H. and Michalak, A. (2014) Oxidative stress as a crucial factor in liver diseases. *World Journal of Gastroenterology*. 20 (25), pp. 8082-8091.
- Croci, I., Coombes, J.S., Bucher Sandbakk, S., Keating, S.E., Nauman, J., Macdonald, G.A., and Wisloff, U. (2019) Non-alcoholic fatty liver disease: Prevalence and all-cause mortality according to sedentary behaviour and cardiorespiratory fitness. The HUNT Study. *Progress in Cardiovascular Diseases*. 62 (2), pp. 127-134.
- Czech, M.P. (2020) Mechanisms of insulin resistance related to white, beige, and brown adipocytes. *Molecular Metabolism*. 34, pp. 27-42.
- da Silva Rosa, S.C., Nayak, N., Caymo, A.M. and Gordon, J.W. (2020) Mechanisms of muscle insulin resistance and the cross-talk with liver and adipose tissue. *Physiological Reports*. 8 (19), e14607.

- DeFronzo, R.A., Tobin, J.D. and Andres, R. (1979) Glucose clamp technique: a method for quantifying insulin secretion and resistance. *The American Journal of Physiology*. 237 (3), pp. E214-E223.
- DeFronzo, R.A., Gunnarsson, R., Björkman, O., Olsson, M. and Wahren, J. (1985) Effects of insulin on peripheral and splanchnic glucose metabolism in noninsulin-dependent (type II) diabetes mellitus. *The Journal Of Clinical Investigation*. 76 (1), pp. 149-155.
- Desterke, C., and Chiappini, F. (2019) Lipid Related Genes Altered in NASH Connect Inflammation in Liver Pathogenesis Progression to HCC: A Canonical Pathway. *International Journal of Molecular Sciences*. 20 (22), 5594.
- Dongiovanni, P., Anstee, Q.M., and Valenti, L. (2013) Genetic predisposition in NAFLD and NASH: impact on severity of liver disease and response to treatment. *Current Pharmaceutical Design*. 19 (29), pp. 5219-5238.
- Dongiovanni, P., and Valenti, L. (2016) Genetics of nonalcoholic fatty liver disease. *Metabolism: Clinical and Experimental*. 65 (8), pp. 1026-1037.
- Fan, J.G., Kim, S.U. and Wong, V.W. (2017) New trends on obesity and NAFLD in Asia. *Journal of Hepatology*. 67 (4), pp. 862-873.
- Fabbrini, E., Magkos, F., Mohammed, B. S., Pietka, T., Abumrad, N. A., Patterson, B. W., Okunade, A. and Klein, S. (2009) Intrahepatic fat, not visceral fat, is linked with metabolic complications of obesity. *Proceedings of the National Academy of Sciences of the United States of America*. 106 (36), pp. 15430-15435.
- Fabbrini, E., Sullivan, S. and Klein, S. (2010) Obesity and nonalcoholic fatty liver disease: biochemical, metabolic, and clinical implications. *Hepatology (Baltimore, Md.)*. 51 (2), pp. 679-689.
- Ferrannini, E., Iozzo, P., Virtanen, K.A., Honka, M.J., Bucci, M. and Nuutila, P. (2018) Adipose tissue and skeletal muscle insulin-mediated glucose uptake in insulin resistance: role of blood flow and diabetes. *The American Journal of Clinical Nutrition*. 108 (4), pp. 749-758.

Flannery, C., Dufour, S., Rabøl, R., Shulman, G.I. and Petersen, K.F. (2012) Skeletal muscle insulin resistance promotes increased hepatic de novo lipogenesis, hyperlipidemia, and hepatic steatosis in the elderly. *Diabetes*. 61 (11), pp. 2711-2717.

Foley, J.E. (1988) Mechanisms of impaired insulin action in isolated adipocytes from obese and diabetic subjects. *Diabetes/Metabolism Reviews*. 4 (5), pp. 487-505.

Francque, S., Verrijken, A., Caron, S., Prawitt, J., Paumelle, R., Derudas, B., Lefebvre, P., Taskinen, M.R., Van Hul, W., Mertens, I., Hubens, G., Van Marck, E., Michielsen, P., Van Gaal, L. and Staels, B. (2015) PPAR α gene expression correlates with severity and histological treatment response in patients with non-alcoholic steatohepatitis. *Journal of Hepatology*. 63 (1), pp. 164-173.

Godoy-Matos, A.F., Silva Júnior, W.S. and Valerio, C.M. (2020) NAFLD as a continuum: from obesity to metabolic syndrome and diabetes. *Diabetology & Metabolic Syndrome*. 12, 60.

Goncalves, I.O., Oliveira, P.J., Ascensao, A., and Magalhaes, J. (2013) Exercise as a therapeutic tool to prevent mitochondrial degeneration in nonalcoholic steatohepatitis. *European Journal of Clinical Investigation*. 43 (11), pp. 1184-1194.

Healy, G.N., Dunstan, D.W., Salmon, J., Shaw, J.E., Zimmet, P.Z. and Owen N. (2008) Television time and continuous metabolic risk in physically active adults. *Medicine and Science in Sports and Exercise*. 40 (4), pp. 639-645.

Hernández Mijares, A. and Jensen, M.D. (1995) Contribution of blood flow to leg glucose uptake during a mixed meal. *Diabetes*. 44 (10), pp. 1165-1169.

Hoeks, J., Mensink, M., Hesselink, M.K.C., Ekroos, K. and Schrauwen, P. (2012) Long- and medium-chain fatty acids induce insulin resistance to a similar extent in humans despite marked differences in muscle fat accumulation. *Journal of Clinical Endocrinology and Metabolism*. 97 (1), pp. 208-216.

Hoene, M., Kappler, L., Kollipara, L., Hu, C., Imler, M., Bleher, D., Hoffmann, C., Beckers, J., Hrabě de Angelis, M., Häring, H.U., Birkenfeld, A.L., Peter, A.,

Sickmann, A., Xu, G., Lehmann, R., and Weigert, C. (2021) Exercise prevents fatty liver by modifying the compensatory response of mitochondrial metabolism to excess substrate availability. *Molecular Metabolism*. 54, 101359.

Janochova, K., Haluzik, M. and Buzga, M. (2019) Visceral fat and insulin resistance - what we know?. *Biomedical Papers Of The Medical Faculty Of The University Palacky, Olomouc, Czechoslovakia*. 163 (1), pp. 19-27.

Kang, S.M., Yoon, J.W., Ahn, H.Y., Kim, S.Y., Lee, K.H., Shin, H., Choi, S.H., Park, K.S., Jang, H.C. and Lim, S. (2011) Android fat depot is more closely associated with metabolic syndrome than abdominal visceral fat in elderly people. *PloS One*. 6 (11), e27694.

Kato, K., Takamura, T., Takeshita, Y., Ryu, Y., Misu, H., Ota, T., Tokuyama, K., Nagasaka, S., Matsuhisa, M., Matsui, O. and Kaneko, S. (2014) Ectopic fat accumulation and distant organ-specific insulin resistance in Japanese people with nonalcoholic fatty liver disease. *PloS One*. 9 (3), e92170.

Kearney, J. (2010) Food consumption trends and drivers. *Philosophical Transactions of the Royal Society of London. Series B, Biological Sciences*. 365 (1554), pp. 2793-2807.

Kenneally, S., Sier, J.H., and Moore, J.B. (2017) Efficacy of dietary and physical activity intervention in non-alcoholic fatty liver disease: a systematic review. *BMJ Open Gastroenterology*. 4 (1), e000139.

Kersten, S. and Stienstra, R. (2017) The role and regulation of the peroxisome proliferator activated receptor alpha in human liver. *Biochimie*. 136, pp. 75-84.

Kohjima, M., Enjoji, M., Higuchi, N., Kato, M., Kotoh, K., Yoshimoto, T., Fujino, T., Yada, M., Yada, R., Harada, N., Takayanagi, R. and Nakamuta, M. (2007) Re-evaluation of fatty acid metabolism-related gene expression in nonalcoholic fatty liver disease. *International Journal of Molecular Medicine*. 20 (3), pp. 351-358.

Koliaki, C., Szendroedi, J., Kaul, K., Jelenik, T., Nowotny, P., Jankowiak, F., Herder, C., Carstensen, M., Krausch, M., Knoefel, W.T., Schlensak, M., and Roden, M. (2015) Adaptation of hepatic mitochondrial function in humans with

non-alcoholic fatty liver is lost in steatohepatitis. *Cell Metabolism*. 21 (5), pp. 739-746.

Koo, S.H. (2013) Nonalcoholic fatty liver disease: molecular mechanisms for the hepatic steatosis. *Clinical and Molecular Hepatology*. 19 (3), pp. 210-215.

Korenblat, K.M., Fabbrini, E., Mohammed, B.S., and Klein, S. (2008) Liver, muscle, and adipose tissue insulin action is directly related to intrahepatic triglyceride content in obese subjects. *Gastroenterology*. 134 (5), pp. 1369-1375.

Kotronen, A., Seppälä-Lindroos, A., Bergholm, R., and Yki-Järvinen, H. (2008) Tissue specificity of insulin resistance in humans: fat in the liver rather than muscle is associated with features of the metabolic syndrome. *Diabetologia*. 51 (1), pp. 130-138.

Krssak, M., Falk Petersen, K., Dresner, A., DiPietro, L., Vogel, S.M., Rothman, D.L., Roden, M., and Shulman, G.I. (1999) Intramyocellular lipid concentrations are correlated with insulin sensitivity in humans: a ¹H NMR spectroscopy study. *Diabetologia*. 42 (1), pp. 113-116.

Machado, M.V., Marques-Vidal, P., and Cortez-Pinto, H. (2006) Hepatic histology in obese patients undergoing bariatric surgery. *Journal of Hepatology*. 45 (4), pp. 600-606.

Machado, M.V., Ferreira, D.M., Castro, R.E., Silvestre, A.R., Evangelista, T., Coutinho, J., Carepa, F., Costa, A., Rodrigues, C.M. and Cortez-Pinto, H. (2012) Liver and muscle in morbid obesity: the interplay of fatty liver and insulin resistance. *PloS one*. 7 (2), e31738.

Maunder, E., Plews, D.J., and Kilding, A.E. (2018) Contextualising Maximal Fat Oxidation During Exercise: Determinants and Normative Values. *Frontiers in physiology*, 9, 599.

McLaughlin, T., Lamendola, C., Liu, A. and Abbasi, F. (2011) Preferential fat deposition in subcutaneous versus visceral depots is associated with insulin sensitivity. *The Journal of Clinical Endocrinology and Metabolism*. 96 (11), pp. E1756-E1760.

Meroni, M., Longo, M., Tria, G., and Dongiovanni, P. (2021) Genetics Is of the Essence to Face NAFLD. *Biomedicines*. 9 (10), 1359.

Mirza, M.S. (2011) Obesity, Visceral Fat, and NAFLD: Querying the Role of Adipokines in the Progression of Nonalcoholic Fatty Liver Disease. *ISRN Gastroenterology*. 2011, 592404.

Misu, H., Takamura, T., Takayama, H., Hayashi, H., Matsuzawa-Nagata, N., Kurita, S., Ishikura, K., Ando, H., Takeshita, Y., Ota, T., Sakurai, M., Yamashita, T., Mizukoshi, E., Yamashita, T., Honda, M., Miyamoto, K., Kubota, T., Kubota, N., Kadowaki, T., Kim, H.J., Lee, I.K, Minokoshi, Y., Saito, Y., Takahashi, K., Yamada, Y., Takakura, N. and Kaneko, S. (2010) A liver-derived secretory protein, selenoprotein P, causes insulin resistance. *Cell Metabolism*. 12 (5), pp. 483-495.

Mittendorfer, B. (2011) Origins of metabolic complications in obesity: adipose tissue and free fatty acid trafficking. *Current Opinion in Clinical Nutrition and Metabolic Care*. 14 (6), 535-541.

Morigny, P., Houssier, M., Mouisel, E. and Langin, D. (2016) Adipocyte lipolysis and insulin resistance. *Biochimie*. 125, pp. 259-266.

Naguib, G., Morris, N., Yang, S., Fryzek, N., Haynes-Williams, V., Huang, W. A., Norman-Wheeler, J. and Rotman, Y. (2020) Dietary fatty acid oxidation is decreased in non-alcoholic fatty liver disease: A palmitate breath test study. *Liver International : Official Journal of The International Association for The Study of The Liver*. 40 (3), pp. 590-597.

Nielsen, S., Guo, Z., Johnson, C.M., Hensrud, D.D. and Jensen, M.D. (2004) Splanchnic lipolysis in human obesity. *The Journal of Clinical Investigation*. 113 (11), pp. 1582-1588.

Nuutila, P., Koivisto, V.A., Knuuti, J., Ruotsalainen, U., Teräs, M., Haaparanta, M., Bergman, J., Solin, O., Voipio-Pulkki, L.M. and Wegelius, U. (1992) Glucose-free fatty acid cycle operates in human heart and skeletal muscle in vivo. *The Journal of Clinical Investigation*. 89 (6), 1767-1774.

Oh, S., Shida, T., Sawai, A., Maruyama, T., Eguchi, K., Isobe, T., Okamoto, Y., Someya, N., Tanaka, K., Arai, E., Tozawa, A. and Shoda, J. (2014)

Acceleration training for managing nonalcoholic fatty liver disease: a pilot study. *Therapeutics and Clinical Risk Management*.10, pp. 925-936.

Ong, J.P., Elariny, H., Collantes, R., Younoszai, A., Chandhoke, V., Reines, H.D., Goodman, Z.D. and Younossi, Z.M. (2005) Predictors of nonalcoholic steatohepatitis and advanced fibrosis in morbidly obese patients. *Obesity Surgery*. 15 (3), pp. 310–315.

Oshida, N., Shida, T., Oh, S., Kim, T., Isobe, T., Okamoto, Y., Kamimaki, T., Okada, K., Suzuki, H., Ariizumi, S.I., Yamamoto, M. and Shoda, J. (2019) Urinary Levels of Titin-N Fragment, a Skeletal Muscle Damage Marker, are Increased in Subjects with Nonalcoholic Fatty Liver Disease. *Scientific Reports*. 9 (1), p. 19498.

Pais, R., Barritt, A.S., 4th, Calmus, Y., Scatton, O., Runge, T., Lebray, P., Poynard, T., Ratziu, V. and Conti, F. (2016) NAFLD and liver transplantation: Current burden and expected challenges. *Journal of Hepatology*. 65 (6), pp. 1245-1257.

Pang, Q., Zhang, J.Y., Song, S.D., Qu, K., Xu, X. S., Liu, S.S. and Liu, C. (2015) Central obesity and nonalcoholic fatty liver disease risk after adjusting for body mass index. *World Journal Of Gastroenterology*. 21 (5), pp. 1650-1662.

Petersen, K.F., Dufour, S., Savage, D.B., Bilz, S., Solomon, G., Yonemitsu, S., Cline, G.W., Befroy, D., Zeman, L., Kahn, B.B., Papademetris, X., Rothman, D.L. and Shulman, G.I. (2007) The role of skeletal muscle insulin resistance in the pathogenesis of the metabolic syndrome. *Proceedings of the National Academy of Sciences of the United States of America*. 104 (31), pp. 12587-12594.

Peterson, M.D., Al Snih, S., Serra-Rexach, J.A. and Burant, C. (2015) Android Adiposity and Lack of Moderate and Vigorous Physical Activity Are Associated With Insulin Resistance and Diabetes in Aging Adults. *The Journals Of Gerontology. Series A, Biological Sciences and Medical Sciences*. 70 (8), pp. 1009-1017.

Petersen, M.C., Madiraju, A.K., Gassaway, B.M., Marcel, M., Nasiri, A.R., Butrico, G., Marcucci, M.J., Zhang, D., Abulizi, A., Zhang, X.M., Philbrick, W., Hubbard, S.R., Jurczak, M.J., Samuel, V.T., Rinehart, J. and Shulman, G.I. (2016) Insulin receptor Thr1160 phosphorylation mediates lipid-induced hepatic insulin resistance. *The Journal of Clinical Investigation*. 126 (11), pp. 4361-4371.

Petersen, M.C. and Shulman, G.I. (2017) Roles of Diacylglycerols and Ceramides in Hepatic Insulin Resistance. *Trends in Pharmacological Sciences*. 38 (7), pp. 649-665.

Pietiläinen, K.H., Kaprio, J., Borg, P., Plasqui, G., Yki-Järvinen, H., Kujala, U.M., Rose, R.J., Westerterp, K.R. and Rissanen, A. (2008) Physical inactivity and obesity: a vicious circle. *Obesity (Silver Spring, Md.)*. 16 (2), pp. 409-414.

Plomgaard, P., Bouzakri, K., Krogh-Madsen, R., Mittendorfer, B., Zierath, J.R. and Pedersen, B.K. (2005) Tumor necrosis factor-alpha induces skeletal muscle insulin resistance in healthy human subjects via inhibition of Akt substrate 160 phosphorylation. *Diabetes*. 54 (10), pp. 2939-2945.

Popkin, B.M., Adair, L.S. and Ng, S.W. (2012) Global nutrition transition and the pandemic of obesity in developing countries. *Nutrition Reviews*. 70 (1), pp. 3-21.

Pugh, C.J., Spring, V.S., Kemp, G.J., Richardson, P., Shojaee-Moradie, F., Umpleby, A.M., Green, D.J., Cable, N.T., Jones, H. and Cuthbertson, D.J. (2014) Exercise training reverses endothelial dysfunction in nonalcoholic fatty liver disease. *American Journal of Physiology. Heart and Circulatory Physiology*. 307 (9), pp. H1298-H1306.

Rabøl, R., Petersen, K.F., Dufour, S., Flannery, C., and Shulman, G.I. (2011) Reversal of muscle insulin resistance with exercise reduces postprandial hepatic de novo lipogenesis in insulin resistant individuals. *Proceedings of the National Academy of Sciences of the United States of America*. 108 (33), pp. 13705-13709.

Rao, M.S. and Reddy, J.K. (2001) Peroxisomal beta-oxidation and steatohepatitis. *Seminars in Liver Disease*. 21 (1), pp. 43-55.

Romero-Gómez, M., Zelber-Sagi, S. and Trenell, M. (2017) Treatment of NAFLD with diet, physical activity and exercise. *Journal of Hepatology*. 67 (4), pp. 829-846.

Rytka, J.M., Wueest, S., Schoenle, E.J. and Konrad, D. (2011) The portal theory supported by venous drainage-selective fat transplantation. *Diabetes*. 60 (1), pp. 56-63.

Samsell, L., Regier, M., Walton, C. and Cottrell, L. (2014) Importance of android/gynoid fat ratio in predicting metabolic and cardiovascular disease risk in normal weight as well as overweight and obese children. *Journal of Obesity*. 2014, 846578.

Sargeant, J.A., Gray, L.J., Bodicoat, D.H., Willis, S.A., Stensel, D.J., Nimmo, M.A., Aithal, G.P., and King, J.A. (2018) The effect of exercise training on intrahepatic triglyceride and hepatic insulin sensitivity: a systematic review and meta-analysis. *Obesity Reviews: An Official Journal of The International Association for The Study of Obesity*. 19 (10), pp. 1446-1459.

Sari, C.I., Eikelis, N., Head, G.A., Schlaich, M., Meikle, P., Lambert, G. and Lambert, E. (2019) Android Fat Deposition and Its Association With Cardiovascular Risk Factors in Overweight Young Males. *Frontiers in Physiology*. 10, 1162.

Schofield, W.N. (1985) Predicting basal metabolic rate, new standards and review of previous work. *Human Nutrition. Clinical Nutrition*. 39 (Suppl. 1), pp. 5-41.

Shida, T., Oshida, N., Suzuki, H., Okada, K., Watahiki, T., Oh, S., Kim, T., Isobe, T., Okamoto, Y., Ariizumi, S. I., Yamamoto, M. and Shoda, J. (2020) Clinical and anthropometric characteristics of non-obese non-alcoholic fatty liver disease subjects in Japan. *Hepatology research : the official journal of the Japan Society of Hepatology*. 50 (9), pp. 1032-1046.

Sinha, R., Dufour, S., Petersen, K.F., LeBon, V., Enoksson, S., Ma, Y.Z., Savoye, M., Rothman, D.L., Shulman, G.I. and Caprio, S. (2002) Assessment of skeletal muscle triglyceride content by (1)H nuclear magnetic resonance spectroscopy in lean and obese adolescents: relationships to insulin

sensitivity, total body fat, and central adiposity. *Diabetes*. 51 (4), pp. 1022-1027.

Smith, U. and Kahn, B.B. (2016) Adipose tissue regulates insulin sensitivity: role of adipogenesis, de novo lipogenesis and novel lipids. *Journal of Internal Medicine*. 280 (5), pp. 465-475.

Smith, G.I., Shankaran, M., Yoshino, M., Schweitzer, G.G., Chondronikola, M., Beals, J.W., Okunade, A.L., Patterson, B. W., Nyangau, E., Field, T., Sirlin, C. B., Talukdar, S., Hellerstein, M.K. and Klein, S. (2020) Insulin resistance drives hepatic de novo lipogenesis in nonalcoholic fatty liver disease. *The Journal of Clinical Investigation*. 130 (3), pp. 1453-1460.

Sorriento, D., Di Vaia, E., and Iaccarino, G. (2021) Physical Exercise: A Novel Tool to Protect Mitochondrial Health. *Frontiers in Physiology*. 12, 660068.

Sunny, N.E., Parks, E.J., Browning, J.D. and Burgess, S.C. (2011) Excessive hepatic mitochondrial TCA cycle and gluconeogenesis in humans with nonalcoholic fatty liver disease. *Cell Metabolism*. 14 (6), pp. 804-810.

Tchoukalova, Y.D., Votruba, S.B., Tchkonina, T., Giorgadze, N., Kirkland, J.L. and Jensen, M.D. (2010) Regional differences in cellular mechanisms of adipose tissue gain with overfeeding. *Proceedings of the National Academy of Sciences of the United States of America*. 107 (42), pp. 18226-18231.

Unger, R.H. (2003) Lipid overload and overflow: metabolic trauma and the metabolic syndrome. *Trends in Endocrinology and Metabolism: TEM*. 14 (9), pp. 398-403.

Uno, K., Katagiri, H., Yamada, T., Ishigaki, Y., Ogihara, T., Imai, J., Hasegawa, Y., Gao, J., Kaneko, K., Iwasaki, H., Ishihara, H., Sasano, H., Inukai, K., Mizuguchi, H., Asano, T., Shiota, M., Nakazato, M. and Oka, Y. (2006) Neuronal pathway from the liver modulates energy expenditure and systemic insulin sensitivity. *Science (New York, N.Y.)*. 312 (5780), pp. 1656-1659.

Vague, J. (1956) The degree of masculine differentiation of obesities: a factor determining predisposition to diabetes, atherosclerosis, gout, and uric calculous disease. *The American Journal of Clinical Nutrition*. 4 (1), pp. 20-34.

van der Poorten, D., Milner, K.L., Hui, J., Hodge, A., Trenell, M.I., Kench, J.G., London, R., Peduto, T., Chisholm, D.J. and George, J. (2008) Visceral fat: a key mediator of steatohepatitis in metabolic liver disease. *Hepatology (Baltimore, Md.)*. 48 (2), pp. 449-457.

van der Windt, D.J., Sud, V., Zhang, H., Tsung, A., and Huang, H. (2018) The Effects of Physical Exercise on Fatty Liver Disease. *Gene Expression*. 18 (2), pp. 89-101.

Vernon, G., Baranova, A. and Younossi, Z.M. (2011) Systematic review: the epidemiology and natural history of non-alcoholic fatty liver disease and non-alcoholic steatohepatitis in adults. *Alimentary Pharmacology & Therapeutics*. 34 (3), pp. 274-285.

Videla, L.A. and Pettinelli, P. (2012) Misregulation of PPAR Functioning and Its Pathogenic Consequences Associated with Nonalcoholic Fatty Liver Disease in Human Obesity. *PPAR Research*. 2012, 107434.

Wattacheril, J. and Sanyal, A.J. (2016) Lean NAFLD: An Underrecognized Outlier. *Current Hepatology Reports*. 15 (2), pp. 134-139.

Wehmeyer, M.H., Zyriax, B.C., Jagemann, B., Roth, E., Windler, E., Schulze Zur Wiesch, J., Lohse, A.W. and Kluwe, J. (2016) Nonalcoholic fatty liver disease is associated with excessive calorie intake rather than a distinctive dietary pattern. *Medicine*. 95 (23), e3887.

Yamasaki, N., Tamura, Y., Takeno, K., Kakehi, S., Someya, Y., Funayama, T., Furukawa, Y., Kaga, H., Suzuki, R., Sugimoto, D., Kadowaki, S., Sato, M., Nakagata, T., Nishitani-Yokoyama, M., Shimada, K., Daida, H., Aoki, S., Satoh, H., Kawamori, R., and Watada, H. (2020) Both higher fitness level and higher current physical activity level may be required for intramyocellular lipid accumulation in non-athlete men. *Scientific Reports*. 10 (1), 4102.

Younossi, Z.M., Koenig, A.B., Abdelatif, D., Fazel, Y., Henry, L. and Wymer, M. (2016) Global epidemiology of nonalcoholic fatty liver disease-Meta-analytic assessment of prevalence, incidence, and outcomes. *Hepatology (Baltimore, Md.)*, 64 (1), pp. 73-84.

Younossi, Z.M. (2019) Non-alcoholic fatty liver disease - A global public health perspective. *Journal of Hepatology*. 70 (3), pp. 531-544.

Younossi, Z.M., Tacke, F., Arrese, M., Chander Sharma, B., Mostafa, I., Bugianesi, E., Wai-Sun Wong, V., Yilmaz, Y., George, J., Fan, J. and Vos, M.B. (2019) Global Perspectives on Nonalcoholic Fatty Liver Disease and Nonalcoholic Steatohepatitis. *Hepatology (Baltimore, Md.)*. 69 (6), pp. 2672-2682.

Yu, C., Chen, Y., Cline, G.W., Zhang, D., Zong, H., Wang, Y., Bergeron, R., Kim, J.K., Cushman, S.W., Cooney, G.J., Atcheson, B., White, M.F., Kraegen, E.W. and Shulman, G.I. (2002) Mechanism by which fatty acids inhibit insulin activation of insulin receptor substrate-1 (IRS-1)-associated phosphatidylinositol 3-kinase activity in muscle. *The Journal of Biological Chemistry*. 277 (52), pp. 50230-50236.

Yu, S.J., Kim, W., Kim, D., Yoon, J.H., Lee, K., Kim, J.H., Cho, E.J., Lee, J.H., Kim, H.Y., Kim, Y.J. and Kim, C.Y. (2015) Visceral Obesity Predicts Significant Fibrosis in Patients With Nonalcoholic Fatty Liver Disease. *Medicine*. 94 (48), e2159.

Zatterale, F., Longo, M., Naderi, J., Raciti, G.A., Desiderio, A., Miele, C. and Beguinot, F. (2020) Chronic Adipose Tissue Inflammation Linking Obesity to Insulin Resistance and Type 2 Diabetes. *Frontiers in Physiology*. 10, 1607.

Zderic, T.W., Davidson, C.J., Schenk, S., Byerley, L.O. and Coyle, E.F. (2004) High-fat diet elevates resting intramuscular triglyceride concentration and whole-body lipolysis during exercise. *American Journal of Physiology: Endocrinology and Metabolism*. 286 (2), pp. E217-E225.

5. Effect of Diclofenac administration on IMCL content during 12 weeks of resistance exercise training in young, healthy male volunteers

5.1 Introduction

Non-steroidal anti-inflammatory drugs (NSAIDs) are drugs that have antipyretic, anti-inflammatory, and analgesic properties, making them suitable in the treatment of various conditions from simple musculoskeletal pain (Hatt *et al.*, 2018), to arthritis (Harirforoosh and Jamali, 2009) and osteoarthritis (Curtis *et al.*, 2019), to the treatment of psychiatric disorders and neurodegenerative disease characterised by neuroinflammation (Perrone *et al.*, 2020). Recent evidence suggests that NSAIDs may also be useful in cancer prevention (Hayashi *et al.*, 2019; Ramos-Inza *et al.*, 2021).

Using supernatant from cell-free guinea-pig lung homogenates Vane showed that the early NSAIDs indomethacin, aspirin, and sodium salicylate inhibited the biosynthesis of prostaglandins $F_{2\alpha}$ and E_2 from arachidonic acid in a dose-dependent manner, thereby providing evidence that these drugs function by antagonising the enzymes which catalyse this biosynthetic process (Vane, 1971). This led to the identification of cyclooxygenase (COX) enzymes as the molecular target of NSAIDs, with the general structure and function of these enzymes being elucidated through a wellspring of research published in the late 20th century (Vane, Bakhle, and Botting, 1998).

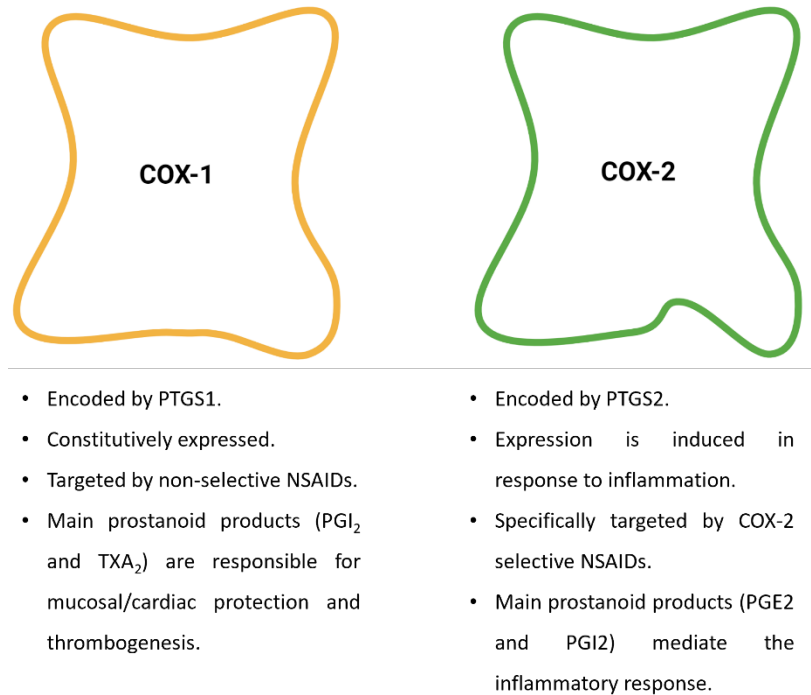


Figure 5-1: Overview of COX isoform expression, function and targeting by NSAIDs.

There are two COX isoenzymes: COX-1 and COX-2 (see **Figure 5-1**). These isoforms are obligate homodimeric membrane proteins (Chandrasekharan and Simmons, 2004) embedded in the luminal surface of the endoplasmic reticulum, in the nuclear envelope, mitochondria, and other organelles (Liou *et al.*, 2001). They are encoded by prostaglandin G/H synthase 1 (PTGS1) (Yokoyama and Tanabe, 1989) and prostaglandin G/H synthase and cyclooxygenase (PTGS2) (Hla and Neilson, 1992), respectively. COX-1 is synthesised and expressed constitutively in almost all tissues, being most abundant in blood vessels, smooth muscle, interstitial cells, and platelets (Crofford, 1997). COX-2 is only constitutively expressed, under normal conditions, in the central nervous system (Minghetti, 2004), the kidneys (Nørregaard, Kwon, and Frøkiær, 2015) and the female reproductive system (Sirois *et al.*, 2014), but is otherwise undetectable in most healthy tissue. COX-2 is predominantly an inducible protein, with its expression in most tissue only increasing in response to cytokines, hormones, water-electrolyte imbalances, or homeostatic disorders in inflammation (Griswold and Adams, 1996).

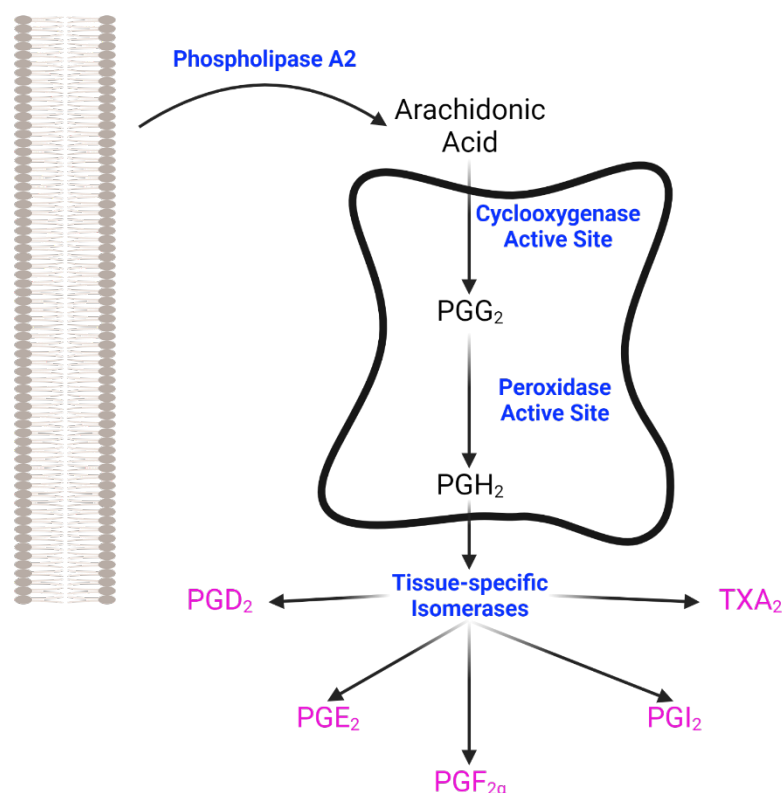


Figure 5-2: Schematic diagram of COX-mediated prostaglandin biosynthesis. Enzymes which catalyse this process are presented in blue. Bioactive prostanoids, the end-product of this pathway, are presented in pink.

Arachidonic acid is a 20-carbon polyunsaturated FA which is liberated from endoplasmic reticulum and nuclear membrane phospholipids by the catalytic activity of phospholipase A2 (PLA₂) hydrolases (Burke and Dennis, 2009) (see **Figure 5-2**). This is the initial and rate-limiting step in prostaglandin synthesis through COX. Then, in the C-terminal catalytic domain of COXs, the cyclooxygenase active site catalyses the double dioxygenation of arachidonic acid to form prostaglandin G₂ (PGG₂) and the peroxidase active site catalyses the reduction of PGG₂ to prostaglandin H₂ (PGH₂) (van der Donk, Tsai, and Kulmacz, 2002; Blobaum and Marnett, 2007). PGH₂ then dissociates from COX and undergoes tissue-specific isomerisation to form one of five bioactive prostanoids: Prostaglandin E₂ (PGE₂), I₂ (PGI₂), D₂ (PGD₂), F_{2α} (PGF_{2α}) or thromboxane A₂ (TXA₂). Prostanoids are lipid mediators which bind to G-coupled prostanoid receptors that propagate intracellular signalling pathways

which regulate homeostatic and inflammatory responses in multiple organ systems (Biringer, 2021). By diffusing into the COX protein through the channel formed by the dimer and creating bonds with the amino acid residues in the active sites of COX isoenzymes, NSAIDs compete with arachidonic acid and inhibit prostaglandin synthesis (Vane, 1971; Vane and Botting, 1995). PGE₂ is the main prostanoid mediator of inflammatory responses in most tissues, its decreased synthesis via the inhibition of COX is the main mechanism by which NSAIDs exert their analgesic and anti-inflammatory properties (Ricciotti and FitzGerald, 2011).

Broadly speaking NSAIDs can be separated into two categories. Non-selective NSAIDs which antagonise both COX isoforms and COX-2 selective NSAIDs which function by targeting a side pocket in the active site of the enzyme that is inaccessible in the COX-1 variant (Kurumbail *et al.*, 1996). COX-2 selective NSAIDs are designed to produce an anti-inflammatory response with a decreased risk of the gastric side effects associated with non-selective NSAIDs (Noble, King, and Olutade, 2000; Simmons, Wagner, and Westover, 2000). COX-1 is a key part of the biosynthetic pathways that create PGI₂ (Wallace, 2008). PGI₂ decreases the secretion of H⁺ ions from parietal cells within the gastric mucosa, which in turn increases bicarbonate secretion, thereby enhancing the neutralisation of gastric acid and sparing of the stomach lining (Allen and Flemström, 2005). Inhibition of COX-1 by non-selective COX inhibitors reduces PGI₂ synthesis, which can result in damage to, and ulceration of, the gastric mucosa (Drini, 2017).

Diclofenac (2-(2,6-dichloranilino) phenylacetic acid) is a non-selective NSAID derived from phenylacetic acid. It was first synthesised by Alfred Sallman and Rudolf Pfister before being released to the general market in 1973 by Novartis (Sallman, 1986). Diclofenac preferentially inhibits COX-2 enzymatic activity and is one of the most potent inhibitors of COX in general, significantly reducing the synthesis of the main prostanoid inflammatory mediator PGE₂ (Ku *et al.*, 1986) and, at high concentrations, inhibiting phospholipase A2 activity (Mäkelä, Kuusi, and Schröder, 1997) and promoting the re-incorporation of arachidonic acid into membrane phospholipids (Ku *et al.*, 1986). Globally, diclofenac is the most widely used NSAID (McGettigan

and Henry, 2013) and is typically administered orally at a dosage of 150 mg daily (Derry *et al.*, 2009), which has been demonstrated to be a highly efficacious dosage in the management of pain in most cases relative to other NSAIDs, especially in osteoarthritis (da Costa *et al.*, 2017).

NSAIDs, particularly diclofenac, are widely used by amateur and elite athletes (Mazzarino *et al.*, 2010; Brennan *et al.*, 2021) off-label pre- and post-endurance or strength training with the intention of reducing inflammation, reducing pain, and allowing users to exercise at greater workloads with greater frequency (Warden, 2009; O'Connor *et al.*, 2019). A report from Doping Control at the 2000 Olympic games revealed that the most used medications were NSAIDs, with 706 (25.6%) of the 2,167 athletes that declared a substance having used them during the event (Corrigan and Kazlauskas, 2003). Usage of NSAIDs was even more pronounced amongst the players competing in the 2014 FIFA World Cup. Of the 2,346 medications taken during that tournament, 1,030 (43.9%) were NSAIDs, mostly diclofenac with 611 reported uses (Vaso *et al.*, 2015). However, evidence favouring the use of NSAIDs in this context is lacking, especially in young individuals accustomed to high-intensity training (Holgado *et al.*, 2018). Indeed, a meta-analysis of 23 studies reported that across different NSAID classifications, NSAID doses, and exercise regimens there was no difference between time to exhaustion and self-perceived indices of pain between controls and groups taking NSAIDs to aid in performance (Cornu *et al.*, 2020). The paucity of data demonstrating empirical benefits of NSAID usage to performance and the known analgesic and anti-inflammatory effects of these drugs mean that they are considered performance enabling rather than performance enhancing, such that NSAIDs are currently not included on the World Anti-Doping Agency (WADA) list of prohibited drugs.

TaqMan array microfluidic gene card data generated by the present author's research group at the University of Nottingham found that the muscle mRNA abundance of genes associated with lipid metabolism were markedly altered in young, trained males administered diclofenac for 84 days during a resistance training programme when compared to matched volunteers engaged in resistance exercise training alone (Greenhaff *et al.*, Unpublished). From these unpublished data two questions arose to be addressed by the

present author. Firstly, via what mechanism does diclofenac alter muscle lipid metabolism? Secondly, do these diclofenac-induced changes in muscle lipid metabolism translate to changes in IMCL content?

Diclofenac has several cellular effects that are independent of its inhibition of COX (Gan, 2010), the most salient in the context of this chapter is its ability to bind to and activate PPAR- γ (Adamson *et al.*, 2002) (see **Section 1.4.5.1**). PPAR- γ is a nuclear receptor encoded by PPARG (Fajas *et al.*, 1997). When a ligand binds to PPAR- γ , it forms a heterodimer with Retinoid X Receptor Alpha (RXR α) (Tontonoz *et al.*, 1994) and this heterodimer acts as a transcription factor that enters the nucleus, binds to PPAR response elements, and promotes the transcription of downstream genes involved in myriad metabolic, immune, and regulatory functions in an array of cell types (Hernandez-Quiles, Broekema, and Kalkhoven, 2021). Of interest here is that this transactivation promotes lipid metabolism processes (Vamecq, and Latruffe, 1999) and is substantially enhanced by the binding of transcriptional coactivators like Peroxisome Proliferator-Activated Receptor-Gamma Coactivator (PGC)-1 α to the PPAR- γ /RXR α heterodimer. The PGC-1 α coactivator is encoded by the PPARGC1A gene, increases in expression with PPAR- γ , and has pleiotropic effects as a key regulator of energy metabolism (Lin, Handschin, and Spiegelman, 2005; Liang and Ward, 2006; Espinoza *et al.*, 2010). Amongst NSAIDs diclofenac is supreme in its affinity for PPAR- γ in vitro, indeed it displays 4-fold greater binding affinity for the receptor than the endogenous ligand 15-Deoxy- Δ -^{12,14}-prostaglandin J2 (Adamson *et al.*, 2002; Yamazaki *et al.*, 2002; Kojo *et al.*, 2003).

Also linking diclofenac to lipid metabolism are novel findings showing that COX proteins can be found localised to the phospholipid monolayer of LDs, and that Group X PLA₂ hydrolases are implicated in both LD biogenesis (Pucer *et al.*, 2013) and the liberation of arachidonic acid from LD monolayers, which may in turn influence LD lipolysis (Jarc, and Petan, 2020). Thus, in addition to their recognised functions, mounting evidence shows that LDs may also act as sites that produce eicosanoids, a superfamily of lipid mediators including prostanoids, epoxyeicosatrienoic acids, and leukotrienes, which can all be derived from arachidonic acid (Accioly *et al.*, 2008; Bozza *et al.*, 2011).

This connection is underappreciated as to date no study has investigated the effect of diclofenac, or NSAIDs in general, on lipid metabolism and IMCL content in response to exercise in humans. Research concerning NSAIDs in exercise typically focuses on their role in the amelioration of exercise-induced muscle soreness and inflammation, based on their inhibition of COX, and their potential effects on muscle strength and hypertrophy during resistance training. Accordingly, a study investigating the effect of high, 400 mg Ibuprofen thrice daily, and low, 75 mg aspirin once daily, NSAID dosing during an 8-week resistance training intervention in young men and women found that NSAIDs can attenuate strength and hypertrophic gains (Lilja *et al.*, 2017), and interestingly in the context of this chapter, may reduce mitochondrial content and function (Cardinale *et al.*, 2017).

Very few studies report the effect of resistance exercise on IMCL content relative to the wealth of quality data available on the effect of endurance exercise on IMCL (Devries *et al.*, 2007; Shepherd *et al.*, 2013; Bajpeyi *et al.*, 2012; Nakagawa and Hattori, 2017; Kakehi *et al.*, 2020). In one study, a single bout of resistance exercise was reported to reduce IMCL content by a mean of 27% in the Type I muscle fibres of 8 males, with no changes observed in the IMCL content of Type II fibres (Koopman *et al.*, 2006). This likely reflected enhanced mobilisation and oxidation of muscle LD FA stores in response to the increased energy demand during the resistance exercise protocol. Another study found that 28 days of unilateral leg extensions in male participants that were sedentary at baseline increased IMCL content in both the trained and untrained leg and that after three weeks of detraining IMCL content in the trained leg only remained elevated (Zhu *et al.*, 2015). This increase in IMCL content likely represented an adaptation induced by the resistance training. Whether a similar resistance training protocol would increase IMCL content in recreationally active or trained individuals is unknown.

Where exercise-induced changes in IMCL content have been reported such changes are concomitant with changes in the expression of PLIN proteins, particularly PLIN5 (Amati *et al.*, 2011; Peters *et al.*, 2012; Shepherd *et al.*, 2013; Gemmink, Schrauwen, and Hesselink, 2020). Like all PLINs PLIN5 plays an integral role in LD biogenesis and LD function. PLIN5

specifically interacts with ATGL, which is responsible for the rate-limiting step in TAG lipolysis (see **Section 1.2.3**), inhibiting its enzymatic activity and limiting basal LD TAG lipolysis (Wang *et al.*, 2011). However, all these observations concern endurance training with sedentary or insulin resistant participants. The effect of resistance exercise and diclofenac administration on IMCL content and PLIN expression in trained individuals remains unknown.

5.2 Study Aims

Few studies investigate the effect of resistance exercise on IMCL and PLIN content and muscle gene expression. To date no prior work has investigated the impact of diclofenac administration concurrent with resistance exercise on IMCL and PLIN content and muscle gene expression even though diclofenac has been shown to be a potent activator of PPAR- γ , which mediates several pathways involved in lipid oxidation and fatty acid synthesis. The aims of this study were:

1. To investigate the effect of 12-weeks resistance exercise training on IMCL content, PLIN 5 content, and muscle mRNA expression of genes linked to the control of FA oxidation in healthy young males.
2. To investigate the effect of diclofenac administration and resistance exercise on IMCL content, PLIN 5 content, and muscle mRNA expression of genes thought to control lipid metabolism in healthy young males.

5.3 Materials and Methods

5.3.1 Study Overview and Ethics Statement

Eighteen healthy, young males were recruited to participate in this study, which was conducted at the David Greenfield Human Physiology Unit, University of Nottingham. All were non-smokers and omnivorous. To reduce between participant variation in end-point measurements to training, it was a requirement for inclusion that each participant was male and had engaged in

structured resistance exercise or trained in a sport 2-3 days minimum per week for at least two years prior to the start of the study.

This study was approved by the University of Nottingham Medical School Ethics Committee (Ethics reference no: I 07 2011). Those recruited to the study underwent a routine medical screening and completed a general health questionnaire. All were of sound physical and mental health and were provided detailed information on the study protocols and requirements for maintaining compliance for the duration of the study prior to signing any informed consent documentation or undergoing any of the procedures described herein.

5.3.2 Study Protocol

	Placebo Group (n = 8)	Diclofenac Group (n = 9)
Mean Age (Years)	24 ± 4.8	25 ± 4.2
Weight (kg)	78.7 ± 8.5	80.6 ± 9.6
BMI (kg/m²)	23.5 ± 2.5	24.8 ± 2.7

Table 5-1: Baseline anthropometric characteristics in the participants of the placebo group and the Diclofenac group. Values are mean ± SD.

This was a randomised, placebo controlled, double-blind study. Of the 18 participants recruited 9 were randomly allocated to a placebo group and 9 were randomly allocated to a diclofenac group (see **Table 5-1**). However, one participant allocated to the placebo group dropped out during the study, thus reducing the total number of participants in this group to 8. Participants in both groups were matched for isometric strength at baseline.

For 84 days participants in both the placebo group and diclofenac group engaged in 3 exercise sessions a week during which they performed 5x30 sets of maximal isokinetic concentric knee extensions in the non-dominant leg at

an angular velocity of 90°/s using the HUMAC NORM isokinetic dynamometer (Computer Sports Medicine Inc., Stoughton, Massachusetts, United States). Between each set participants rested for 3 minutes. The total number of maximal knee extensions was therefore 150 per session, 450 per week, and 5400 during the whole intervention. As discussed in **Section 3.3.2.1** this specific knee extension regimen has been demonstrated to stimulate discernible anabolic responses in young healthy males (Jones *et al.*, 2004). During the study each participant was asked and reminded to maintain their habitual exercise training routines, apart from any leg resistance exercises. For the duration of the study participants were also instructed to cease any dietary supplementation, including the consumption of protein powders and creatine which are anabolic agents.

Following baseline measurements and over the course of the exercise intervention, participants in the placebo group were given lactose capsules (Placebo) whilst those in the diclofenac group were given capsules containing 75 mg diclofenac sodium and 15 mg lansoprazole, to be taken daily. These capsules were provided by Clinical Trials Services, Nottingham University Hospital Pharmacy Department in identical bottles, such that investigators and volunteers were blind to the treatment groups during the study. To minimise reported side-effects, a moderate dose of 75 mg/day diclofenac was used. The large-scale CLASS randomised control trial, investigating the gastrointestinal side effects of long-term NSAID administration, demonstrated that 6 months of 75 mg diclofenac administration twice daily in rheumatoid arthritis and osteoarthritis patients was well tolerated (Silverstein *et al.*, 2000). The capsule formulations in this study also contained lansoprazole, which is commonly used in tandem with chronic NSAID administration to limit the release of H⁺ ions from stomach parietal cells, thereby minimising damage to the gastric mucosa (Sugano *et al.*, 2011). Participants were also instructed to consume their capsules with a meal. At the end of every month blood samples were taken to measure the concentration of the hepatic injury marker alanine aminotransferase and monitor the presentation of any side effects. None of the participants presented with a hypersensitivity response to diclofenac or with any diclofenac-associated side effects over the course of the intervention.

Vastus lateralis biopsies were obtained from the non-dominant leg of participants using the Bergström needle biopsy technique in a resting, fasted state at baseline before the start of the training and drug intervention (baseline), 24 hours after the first training session (24h) and then at 7 days (7d), 28 days (28d), and 84 days (84d). Participants were asked to refrain from engaging in strenuous exercise or consuming alcohol in the 2 days preceding biopsy acquisition. Muscle biopsies were snap frozen in liquid nitrogen or mounted using OCT mounting medium (361603E; VWR International, Lutterworth, UK) for histochemical analysis and then frozen. All biopsies were stored in liquid nitrogen. A total of 40 muscle samples were obtained from the participants in the Placebo group across all time points whilst a total of 45 samples were obtained from the participants in the Diclofenac group. However, only 29 of the Placebo and 33 of the Diclofenac muscle tissue samples yielded were suitable for histochemical determination of IMCL content and muscle fibre type. All these suitable muscle biopsies were cut, stained, imaged, and analysed.

5.3.3 Measures of Muscle Strength and Function

An isometric knee extension machine within the David Greenfield Human Physiology Unit was used to measure isometric strength of the concentric trained leg of each participant following the exercise sessions conducted at the Baseline, 24h, 28d, and 84d time points. Participants performed three static maximal voluntary contractions with the knee flexed at 90° and the greatest recording of the three was used for data analysis. Total work output, the sum of the mechanical energy generated and dissipated as positive and negative work, respectively, by the concentric limb during each exercise session was calculated as the work done during the 150 contractions in newton metres (Nm). Here total work output is presented in kilojoules, with 1 Nm being equal 0.001 kJ.

5.3.4 Quantification of IMCL Content

Cutting, staining, and imaging of vastus lateralis muscle obtained from participants in both groups and at all time points was performed as detailed in **Sections 2.8.1** and **2.8.2**. Image acquisition was performed using a Zeiss LSM

880, AxioObserver confocal laser scanning microscope (Carl Zeiss AG, Jena, Germany) and image analysis was conducted as described in **Section 2.8.3**. Concurrent with the collection of sections for IMCL staining, for each sample, sections were also cut and frozen for subsequent fibre type staining.

5.3.5 Immunohistochemical Staining for Identification of Muscle Fibre Types

Primary and secondary antibody staining of MHC I, IIA, and IIX isoforms and laminin was performed as described in **Section 2.9.2**. Imaging of MHC fibre type was completed using a Zeiss LSM 880 as described in **Section 4.3.8** and analysis of these images was performed as described in **Section 2.9.4**.

5.3.6 Immunohistochemical Staining for Quantification of PLIN5 Content

5.3.6.1 Staining

Vastus Lateralis sections were fixed to SuperFrost Plus adhesion microscope slides (631-0108P; VWR International, Lutterworth, UK) via immersion in cold 4% paraformaldehyde Zamboni's fixative (#1459A; Newcomer Supply, Middleton, WI, USA) supplemented with 2.5 ml of 2% glycerinaldehyde in 0.05 M phosphate buffer (pH 7.4) and were left to fix for 60 minutes. These sections were then washed for five minutes twice using 0.1 M SPB. Using an ImmEdge pen (H-4000; 2BScientific, Upper Heyford, UK), circles were drawn around the sections on each slide. Then the sections were incubated for 10 minutes in 200 uL of 0.1% triton x-100 in immunobuffer (0.25% bovine serum albumin, 50 mM glycine, 0.033% saponin and, 0.05% sodium azide in SPB), with the hydrophobic residues of the ImmEdge pen keeping the solution in the delineated circle. The triton/immunobuffer solution was then removed and sections were washed twice, five minutes each time, with immunobuffer alone.

Anti-Perilipin 5 (C-terminus) guinea pig polyclonal (GP31; Progen Biotechnik, Heidelberg, Germany) antibodies were diluted in immunobuffer at a ratio of 1:100 and sections on each slide were incubated in 200 uL of this primary antibody solution for 3 hours at room temperature and covered from light. After this primary antibody incubation, sections were washed thrice for

five minutes with immunobuffer alone. This was followed by a 2-hour incubation in 200 μ L of a secondary antibody solution containing Goat anti-Guinea Pig IgG (H+L) (A-21450; Thermo Fisher Scientific, Loughborough, UK) in immunobuffer at a ratio of 1:400 whilst sections were covered from external light. To complete the PLIN5 staining, the sections were washed thrice with immunobuffer again for three minutes each time.

Immediately after the final immunobuffer wash, the vastus lateralis sections were submerged in cold 0.1 M SPB, followed by a 30-minute incubation period in 50 mL of 20 μ g/mL Bodipy 493/503. After a 20-minute final wash in SPB, the sections were mounted in Vectashield Antifade Mounting Medium for fluorescence (H-1000-10; 2BScientific, Upper Heyford, UK), covered by 1.5 mm cover slips, sealed with nail polish, placed on ice, and covered from external light before imaging.

5.3.6.2 Image Acquisition

Images of co-localised IMCL and PLIN were obtained at 40x magnification using the EC Plan-Neofluar 40x/1.30 Oil Ph3 M27 objective of a Zeiss LSM 800 confocal microscope (Carl Zeiss AG, Jena, Germany). The 488 nm argon-ion laser line was used to excite the Bodipy 493/503 fluorophore, with a detection wavelength of 491-557 nm, whilst the helium-neon 633 laser line was used to excite fluorophore 633 conjugated to PLIN 5, with a detection wavelength of 659-751 nm. Scaling was 0.0064 μ m² per pixel. Sections were imaged from top to bottom as tiles of 3.642 μ m thick Z stacks composed of 5 slices (910.54 nm between each slice) (see **Section 2.8.2**). Maximum projections of each sample section image were generated using the “*Orthogonal Projection*” processing function in ZEN Blue Edition as described in **Section 2.8.2**. The IMCL images in channel 1 and the PLIN5 images in channel 2 were exported separately as BigTiff format files with lossless compression.

5.3.6.3 Image Analysis

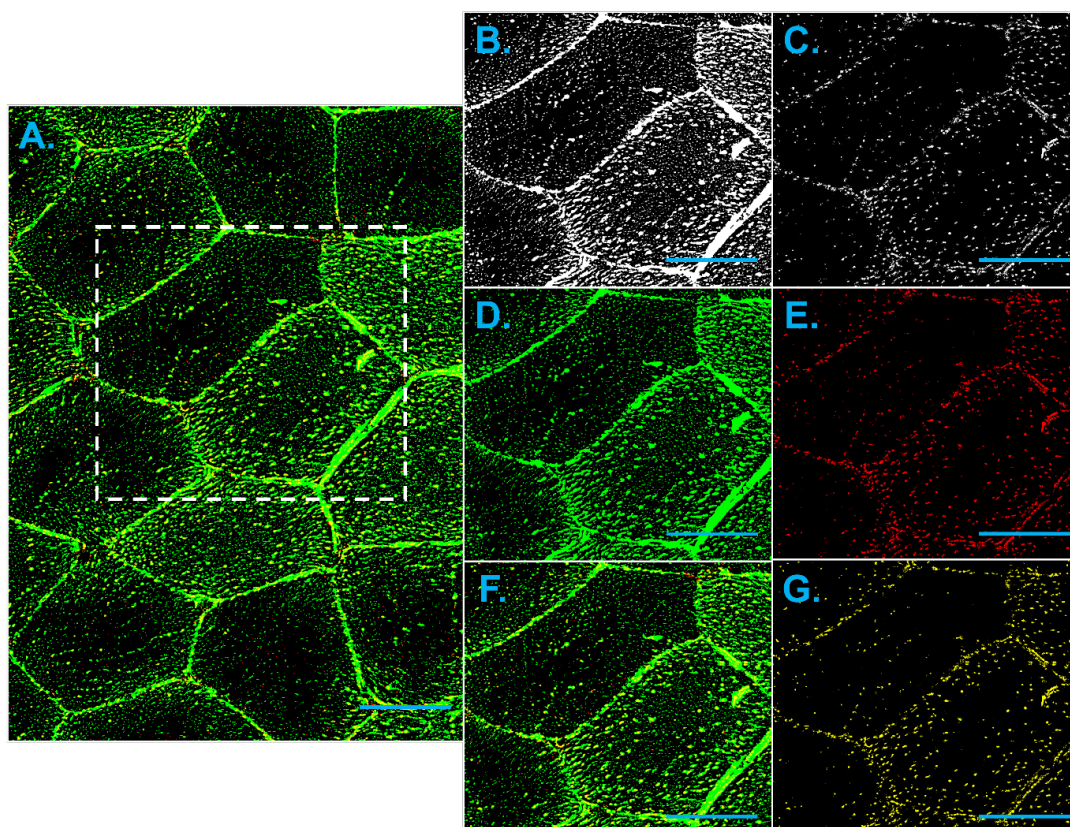


Figure 5-3: Representative images of vastus lateralis muscle fibres co-stained for IMCL and PLIN5. (A, F) Composite images showing lipid in green, PLIN5 in red and overlapped particles in yellow. Binary images of muscle fibres stained for (B) IMCL content and (C) PLIN5 expression. Green and red channel for (D) IMCL and (E) PLIN5 respectively and (G) the colocalisation map showing only those particles that overlap in the green, IMCL, and red, PLIN5, channels. Bars are 50 μ m.

For each sample the IMCL and PLIN5 files were opened side by side in FIJI. A gaussian blur of radius 1 was applied to both the IMCL and PLIN images and they were converted to binary using the Bernsen algorithm auto local thresholding method as described in **Section 2.8.3** (see **Figures 5-3B** and **5-3C**). Using the “AND” operator in the “Image Calculator” tool located in the “Process” tab of FIJI, composite images displaying only those pixels that were present at the exact same (x , y) coordinates in the Bodipy images and the PLIN5 images were generated (see **Figure 5-3G**).

To calculate the percentage of LDs that were colocalised with PLIN5 (PLIN5+ LDs), the number of LDs identified within the ROIs of the

colocalization maps (**Figure 5-3G**) was divided by the total number of droplets in the IMCL images (**Figure 5-3D**) within the same ROIs. Total PLIN5 content in each section was defined as the area delineated by an ROI that was positively stained for PLIN 5 relative to the total area (**Figure 5-3E**).

5.3.7 Muscle mRNA Expression

5.3.7.1 RNA Extraction and Reverse Transcription

Four muscle biopsy samples from a total of 85 could not be analysed for mRNA expression due to limited tissue availability. For each available snap frozen biopsy, 30 mg of muscle tissue was homogenised in a tube containing 1 mL TRI Reagent solution (AM9738; Invitrogen, Waltham, Massachusetts, United States) for RNA extraction. To this homogenised TRI Reagent mixture, 100 mL of bromochloropropane (BCP) was added, followed by a 10-minute incubation period. This mixture was then centrifuged at 12,000 xg for 10 minutes at 4 °C. This centrifugation resulted in the formation of three distinct phases in the tube: an aqueous phase containing total RNA at the top; an interphase containing DNA; and an organic phase of phenol/BCP, fats and other water-insoluble molecules at the bottom of the tube. The aqueous phase was transferred to a fresh tube, 500 uL of isopropanol was added and the solution was left to incubate for 10 minutes to precipitate total RNA. This solution was then centrifuged at 12,000 xg for 8 minutes at 4 °C to produce an RNA pellet. The supernatant was discarded, the pellet was washed in 1 mL of 70% ethanol to remove salt and other impurities and the tube was centrifuged again at 7,500 xg for 5 minutes. The ethanol supernatant was discarded, and the remaining pellet was left to dry before being dissolved in nuclease free buffer solution.

Using SuperScript III reverse transcriptase (18080400; Invitrogen, Paisley, United Kingdom) and random primers (Promega, Southampton, United Kingdom), 1 µg of total RNA from each sample was reverse transcribed to form single-stranded cDNA which was subsequently frozen at -80 °C.

5.3.7.2 Reverse Transcription Quantitative PCR

For each sample, PCR reaction mixtures consisting of 50 μ L Universal PCR Master Mix (4304437; Applied Biosystems, Waltham, Massachusetts, United States), 10 μ L (200 ng) of sample cDNA and 40 μ L of RNase-free water were prepared. The Master Mix contained AmpliTaq Gold DNA Polymerase, deoxynucleotide triphosphates, uracil-DNA glycosylase and a modified ROX dye as a passive internal reference.

Then 100 μ L of each PCR reaction mix was added to the left arm of each fill reservoir of a TaqMan array plate. Plates were then centrifuged twice for 1 minute at 1,200 rpm (3,000 xg) in a Heraeus Multifuge 3S-R Refrigerated Centrifuge (Thermo Scientific, Waltham, Massachusetts, United States) to evenly distribute the PCR mixtures across of the wells of the plate. The wells of these plates were coated with lyophilised TaqMan 5' nuclease assays (forward and reverse primers, quencher dyes and minor groove binders) targeting 93 gene transcripts linked to energy metabolism, inflammation, stress responses and myogenicity. Of the 93 genes, 50 were selected based on evidence that the abundance of their mRNA transcripts is altered in response to acute eccentric exercise (Chen *et al.*, 2003) or to 10 weeks of isokinetic knee extensions in young males, similar to the protocol described here (Murton *et al.*, 2014). The remaining 43 genes were selected because they are known to transcribe transcription factors, regulators of skeletal muscle inflammation (Crossland *et al.*, 2008), or regulators of energy metabolism (Mallinson *et al.*, 2009). These assays included reporter dyes which emitted fluorescent signals during PCR amplification that were proportional to the abundance of the target genes when reconstituted in the PCR mix containing participant cDNA.

After centrifugation the plates were prepared for analysis by using a specialised sealer (Model 4331770, Rev. A5; Applied Biosystems, Waltham, Massachusetts, United States) to isolate the wells and then by trimming off the fill consumable sections, which contain the fill reservoirs. Plates were then loaded into the ABI PRISM 7900 HT real-time PCR system operating Sequence Detection Systems (SDS) 2.1 software (Applied Biosystems, Waltham, Massachusetts, United States). The thermal cycling protocol

included an initial 2-minute incubation at 50 °C for uracil-DNA glycosylase activation followed by 10 minutes at 94.5 °C for enzyme activation. These activation steps were followed by PCR cycles consisting of alternating 30 seconds, 97 °C incubations to denature DNA and 60 seconds, 59.7 °C incubations to extend and anneal cDNA strands, each for 40 cycles.

Cards were analysed using the “Relative Quantification $\Delta\Delta C_t$ ” function in the SDS software. The quantification cycle/ cycle threshold (C_t) is the number of PCR cycles necessary for the fluorescent signal of a specific nucleic acid to exceed the threshold level, which represents the intensity of the background fluorescence. The lower the C_t , the greater the abundance of that nucleic acid in the original participant sample. Relative gene expression quantification ($\Delta\Delta C_t$) involves calculation of the difference in the C_t values of the target genes relative to the C_t value of an endogenous control gene for each sample (ΔC_t). In the data presented here the hydroxymethylbilane synthase (HMBS) gene was selected as the endogenous control gene amongst the 93 targets, the C_t value of each of the other 92 genes for each sample at all time points was normalised to the C_t value of HMBS to calculate ΔC_t . The HMBS gene encodes a protein of the same name which catalyses the deamination of porphobilinogen molecules in condensation reactions that result in the formation of tetrapyrrole 1-hydroxymethylbilane, this process is essential in the biosynthesis of haem (Battersby, 2000). The most important characteristic of a control gene is that it remains stable, with minimal variation in expression between samples (Silver *et al.*, 2006). Control genes should also be well expressed in the tissue of interest. Fittingly, HMBS is well expressed in skeletal muscle (Porter *et al.*, 2017) and has been extensively validated as the optimal reference gene for normalisation of gene expression data due to its high expression stability in various tissues (Cicinnati *et al.*, 2008; Zhang *et al.*, 2014) including skeletal muscle (Mallinson *et al.*, 2020). Indeed, there were no significant differences in HMBS expression between the placebo and diclofenac groups during muscle mRNA expression data analysis (Mallinson *et al.*, 2020).

These ΔC_t values were then normalised to the ΔC_t of a reference sample to calculate $\Delta\Delta C_t$. In this case the ΔC_t values of the target genes from biopsies

taken at 24h, 7d, 28d and 84d were normalised to the ΔC_t values of the target genes in biopsies taken at baseline in both groups. $\Delta\Delta C_t$ was expressed as fold change of the target gene at the 24h, 7d, 28d and 84d time points relative to baseline, such that where *Fold Change* > 1 mRNA abundance of the target genes was greater at the later time points than at baseline and where $0 < \textit{Fold Change} < 1$ the mRNA abundance of the target gene at the 24h, 7d, 28d and 84d time points was less than at baseline. Statistical significance of mRNA expression fold changes at these time points relative to baseline was determined using paired t-tests. $\text{Log}_2(\textit{Fold Change})$ was also calculated such that:

$$2^{\text{Log}_2(\textit{Fold Change})} = \textit{Fold Change}$$

Where $\text{Log}_2(\textit{Fold Change})$ values > 1 indicated increased mRNA abundance of the target gene at the 24h, 7d, 28d or 84d time points relative to baseline, values = 0 indicated no change and values < 1 indicated decreased mRNA expression at these later time points relative to baseline. Data filtering was set with a fold change cut-off of 1.5 and p-value threshold of $p < 0.05$ to select for the most significantly altered genes. These genes were then used as the input for the subsequent core IPA analysis.

During analysis, the Relative Quantification Manager application (Applied Biosystems, Waltham, Massachusetts, United States) was used to normalise the threshold level across all TaqMan plates prior to the calculation of C_t values for each gene target for every sample. Fold change, $\text{Log}_2(\textit{Fold Change})$ and p value data from gene expression analysis were transferred to spreadsheets in Microsoft Excel (Microsoft Corporation, Redmond, Washington State, United States).

5.3.7.3 Ingenuity Pathway Analysis (IPA)

To better understand the abundance changes of the 93 target gene mRNA transcripts and how the genes together influenced changes in the pathways that regulate various biological functions during the intervention, fold change and p value data from RT-PCR were uploaded to Ingenuity Pathway Analysis (IPA) software (Qiagen, Hilden, Germany). It is important to note that only

those genes identified by IPA as being linked with lipid metabolism will be discussed here to address the aims outlined in **Section 5.2**.

IPA is an online bioinformatics program that allows users to upload data from gene expression analyses and identify gene expression patterns to better understand and predict the downstream effect of changes in gene expression on biochemical pathways and biological/diseases responses to experimental interventions. It is powered by data stored in a repository called the Ingenuity Knowledge Base (IKB) which contains millions of findings from the literature concerning changes in gene expression. This repository has two components, Ingenuity Findings, and Ingenuity Modelled Knowledge. Ingenuity Findings contains experimental data on changes in gene expression compiled and reviewed both manually and automatically from peer-reviewed journal articles. Ingenuity Modelled Knowledge contains models and projections of biochemical and disease pathways and contains third-party information on mRNA, biomarkers, and clinical trials. IPA compares the observed changes in gene expression from the uploaded RT-PCR experimental data with IKB databases on known molecular interactions and activity state regulators in published literature.

For muscle gene expression data uploaded to IPA, right-tailed Fisher's Exact Tests, with the Benjamini-Hochberg procedure for multiple testing, were used to calculate the "p-value of overlap" to identify significantly enriched function pathways where $p < 0.05$. This test compared the proportion of altered genes in the uploaded data set involved in a specific biological function (i.e., accumulation of lipid), respective of the magnitude and direction of these alterations, with all the genes from a reference IKB data set which are known to be involved in that biological function. The null hypothesis of these tests was that for each biological function, any overlap between the genes in the uploaded data set and those in the IKB reference data set was due to chance. To control for any enrichment of false positive results when undertaking multiple comparisons (type II errors) IPA utilises Bonferroni's corrected p-value set at $p < 0.05$. Activation z-scores were calculated to predict gene, regulator, and biological function activation/inhibition states. Where a z-score was ≥ 2 , activation was predicted; where it was ≤ -2 , inhibition was predicted. The

regulation z-scores and overlap p values accounted for the fact that only the expression of the 93 target genes was investigated, rather than global gene expression.

The output received from IPA was multi-directional gene networks showing significantly increased/decreased mRNA abundance in response to the intervention and the biological functions that were predicted to be upregulated or downregulated as a result.

5.3.8 Statistical Analysis

Group and time point effects on LD count, LD size and IMCL content, at the total and fibre-type specific level, between and within the Placebo and diclofenac groups were assessed using two-way ANOVA. Differences between the groups in PLIN content and the proportion of PLIN5+ LDs at all time points were assessed using multiple unpaired T-tests. The Shapiro-Wilks test was used to evaluate the normality of data. For graphed data **ns** means “not significant” in relation to the groups at the time points indicated.

5.4 Results

5.4.1 Muscle Strength and Function

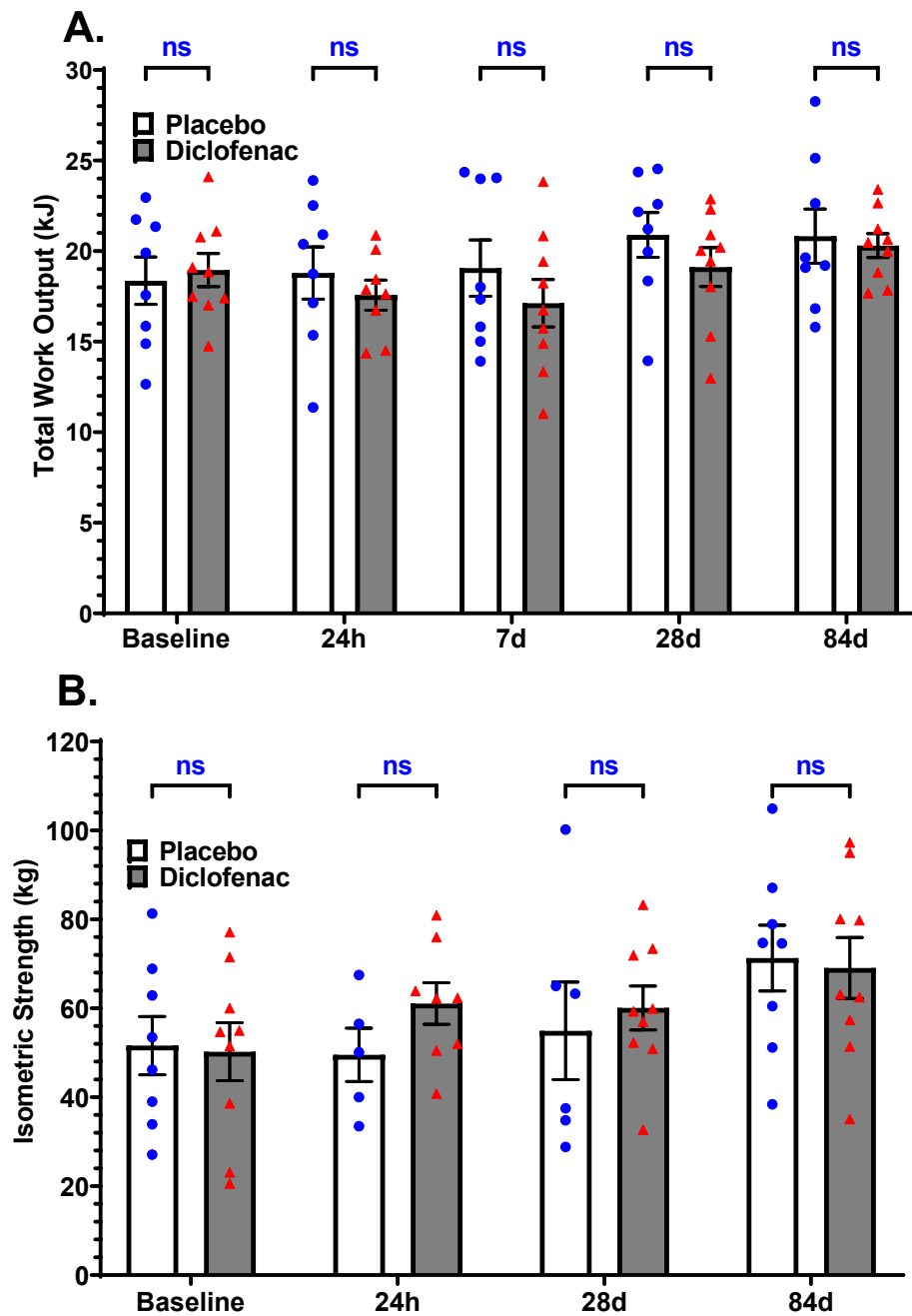
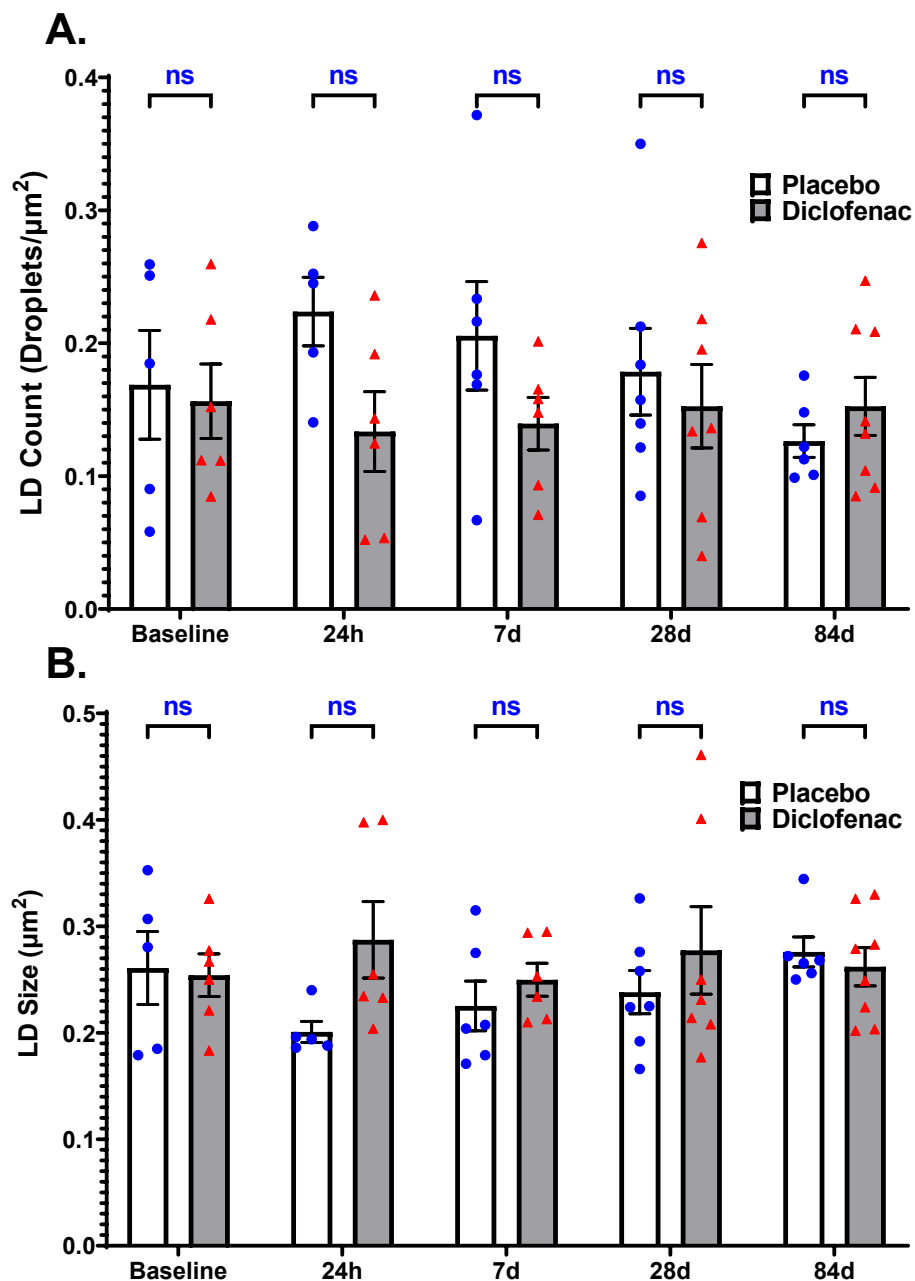


Figure 5-4: Mean total work output (A) and isometric strength (B) of the concentric trained legs of the participants in the Placebo and Diclofenac groups during the exercise interventions conducted at the Baseline, 24h, 7d, 28d, and 84d time points. Values are mean \pm SEM.

Both total work output (18.4 ± 1.31 kJ Placebo vs. 19.0 ± 0.92 kJ Diclofenac; $p = 0.71$) and isometric strength (51.6 ± 6.57 kg Placebo vs. 50.2 ± 6.52 kg Diclofenac; $p = 0.88$) measured during the baseline exercise training intervention were not different between the Placebo and Diclofenac groups. Total work output was no different between the two groups at any time point ($p = 0.49$), but there was a significant timepoint effect ($p < 0.05$). This was mirrored in measurements of isometric strength which were no different between the two groups ($p = 0.88$), but which did increase over time ($p < 0.01$).

5.4.2 Histochemical Quantification of IMCL Content



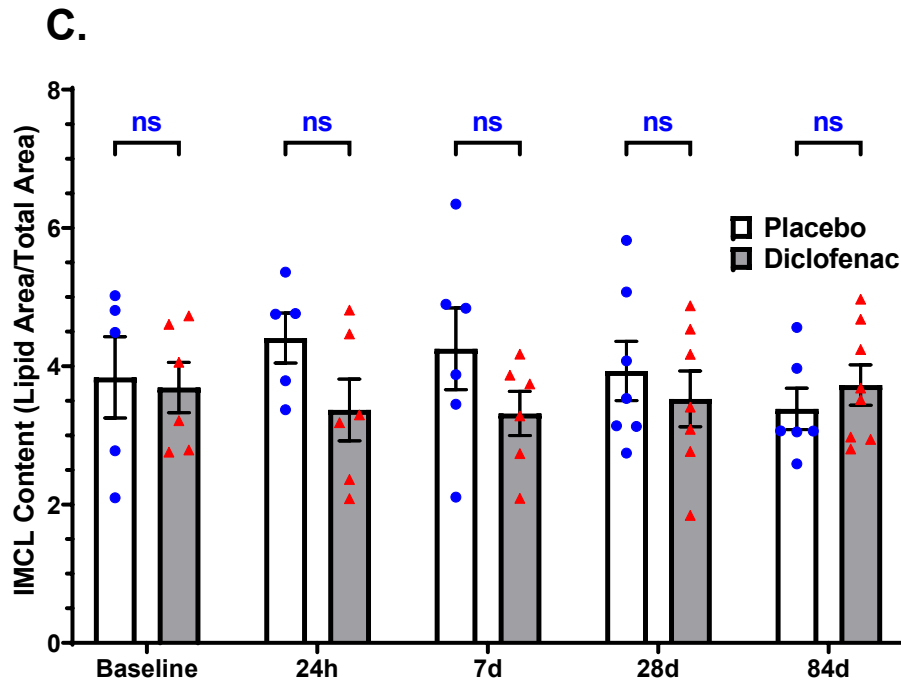
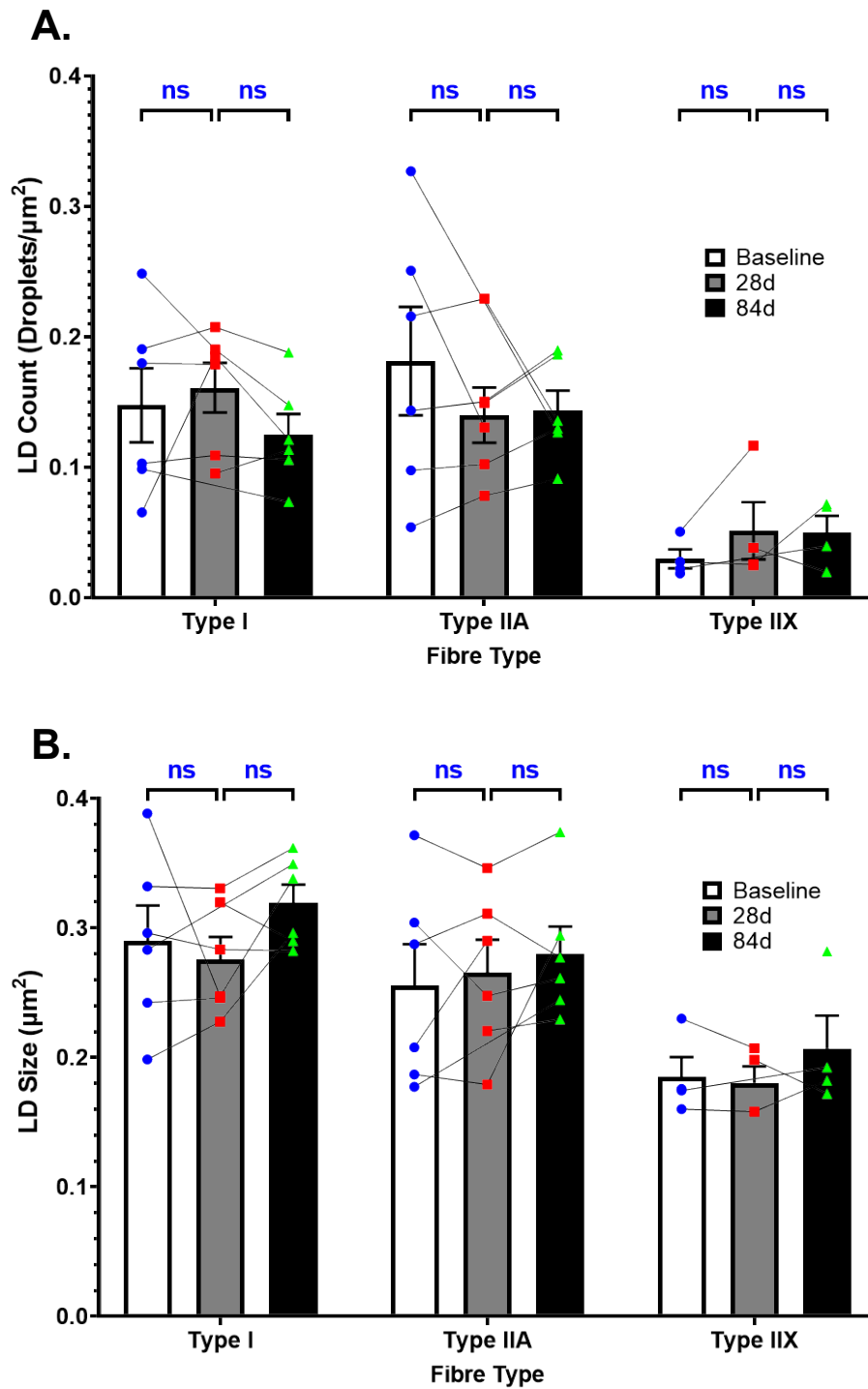


Figure 5-5: Mean vastus lateralis muscle (A) LD count, (B) LD Size and (C) IMCL content of participants in both the placebo group and the Diclofenac group at all time points. Values are mean \pm SEM.

Figure 5-5 shows mean LD count, LD size and IMCL content in the placebo and diclofenac intervention groups at all time points of the study. At baseline, both LD parameters and IMCL content were not significantly different between the participants in the placebo group and those in the diclofenac group.

There was no effect of intervention group on LD count ($p = 0.18$), with no significant difference in LD count observed between the two groups at all time points. There was also no time point effect, with mean LD count remaining unchanged from baseline through to 84d for both groups ($p = 0.40$). For both the placebo and diclofenac groups, LD size did not change between time points from baseline ($p = 0.51$). There was also no effect of group ($p = 0.22$), with no significant difference in mean LD size observed between the participants of the placebo and diclofenac groups at any time point. Similarly, IMCL content was unchanged, with no main effect of group ($p = 0.21$) or time point effect ($p = 0.81$) observed.

5.4.3 IMCL Content by Muscle Fibre Type (Placebo Group)



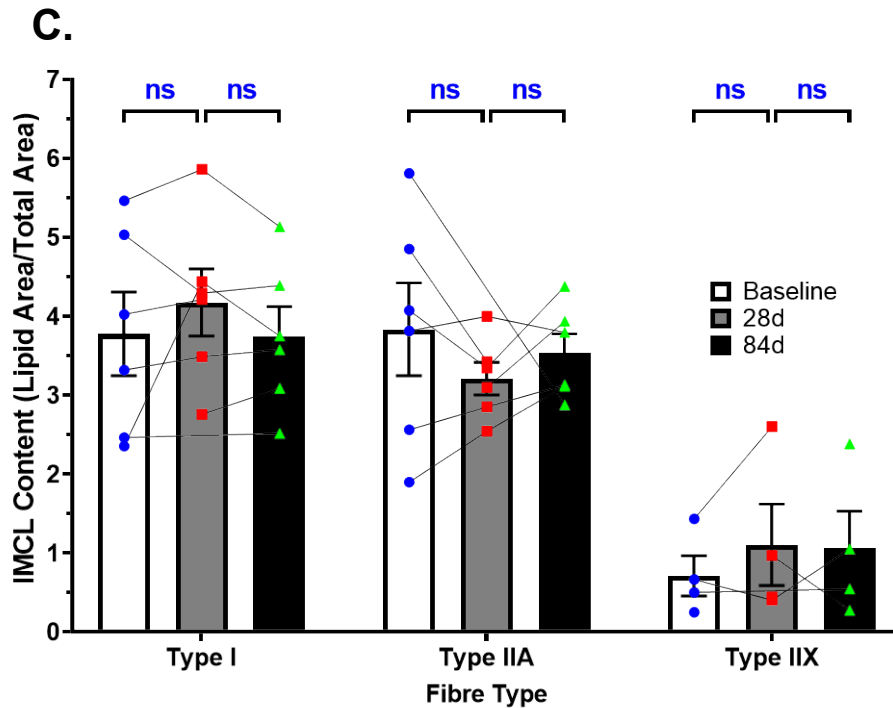
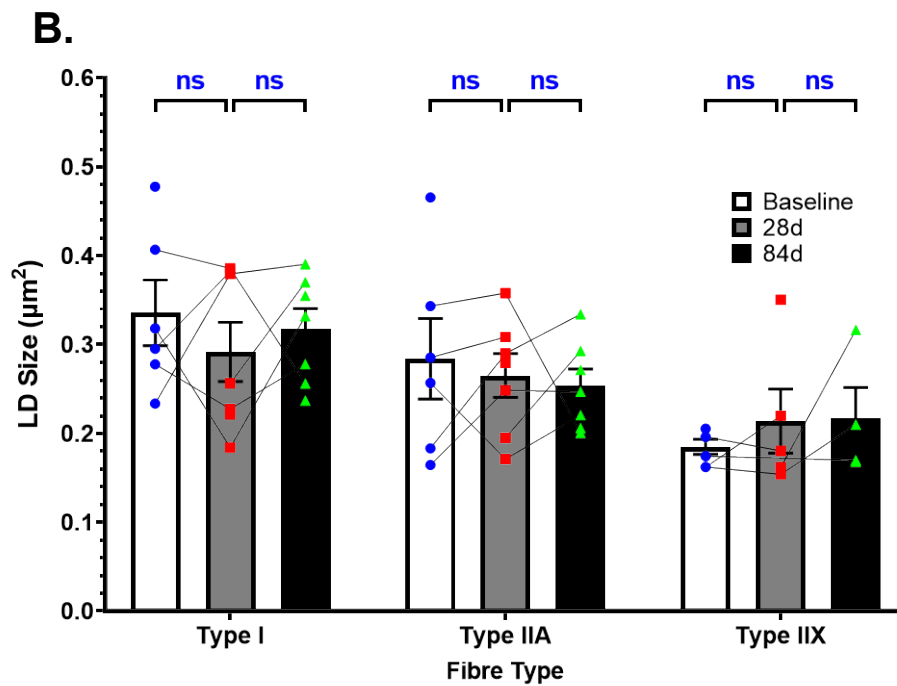
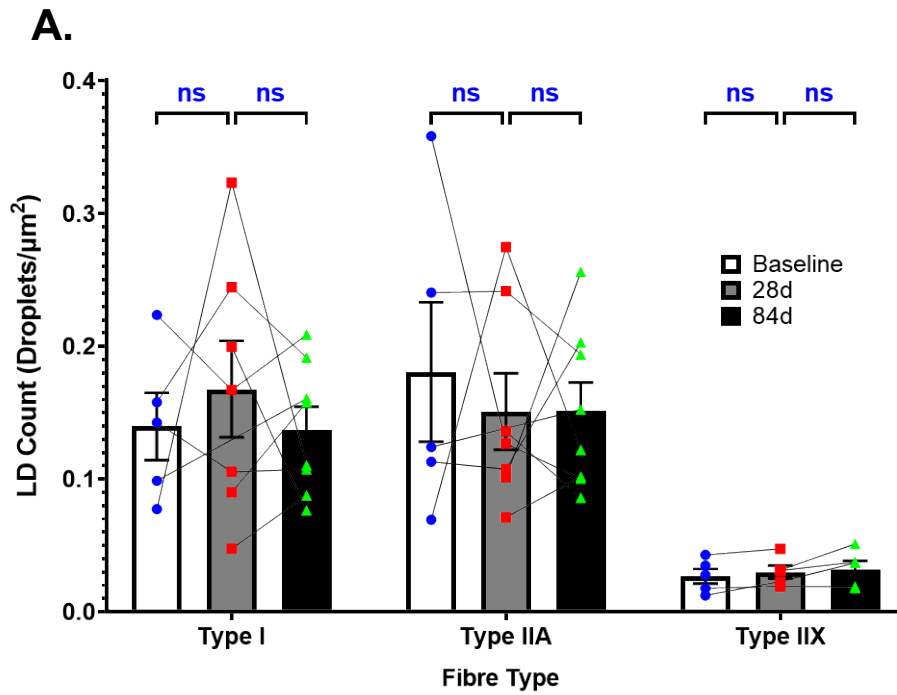


Figure 5-6: Fibre type specific differences in mean (A) LD count, (B) LD size and (C) IMCL content at the baseline, 28d, and 84d time points for the participants in the placebo group. Values are mean \pm SEM.

There was a significant effect of muscle fibre type on mean LD count ($p < 0.01$), LD size ($p < 0.01$) and IMCL content ($p < 0.001$) such that the relative number and size of LDs in type IIX fibres was significantly smaller than in type I and type IIA fibres, which in turn resulted in IMCL content also being lowest in IIX fibres also. However, there was no significant effect of the exercise intervention on LD count ($p = 0.79$), LD size ($p = 0.34$), and IMCL content ($p = 0.68$), none of which changed between the baseline, 28d, and 84d time points.

5.4.4 IMCL Content by Muscle Fibre Type (Diclofenac Group)



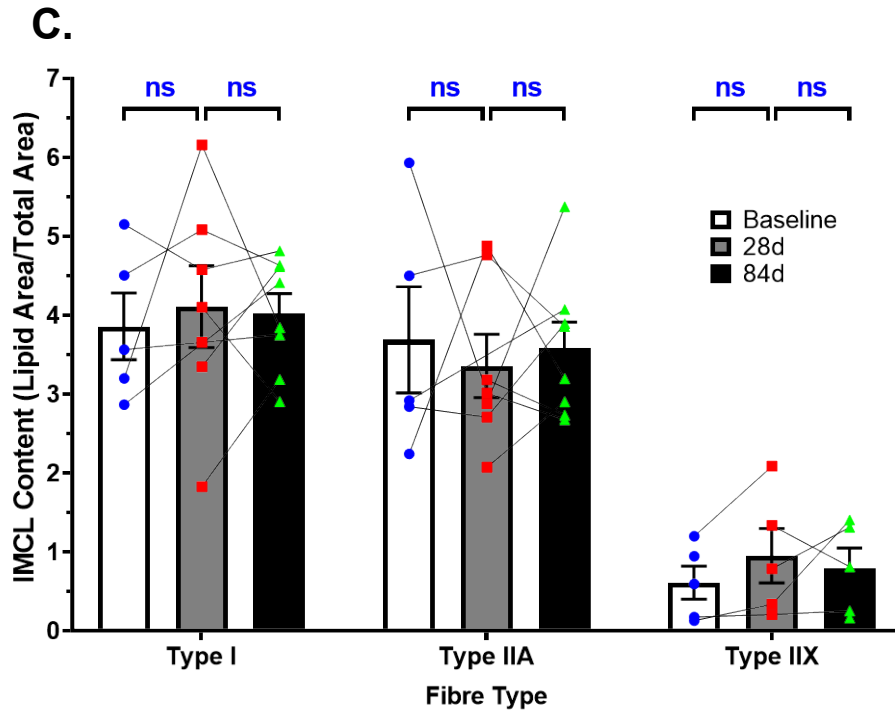


Figure 5-7: Fibre type specific differences in mean (A) LD count, (B) LD size and (C) IMCL content at the baseline, 28d, and 84d time points for the participants in the Diclofenac group. Values are mean \pm SEM.

Figure 5-7 shows the fibre type specific changes in mean LD count (**A**), LD size (**B**) and IMCL content (**C**) at the baseline, 28d, and 84d time points of the exercise intervention protocol in participants concurrently ingesting diclofenac. Though a significant effect of muscle fibre type was observed for LD count ($p < 0.001$), LD size ($p < 0.001$) and IMCL content ($p < 0.001$), with the mean value of these parameters being significantly lower in type IIX fibres than type I and type IIA fibres, there was no observed effect of the intervention on these parameters. There was no time point effect on LD count ($p = 0.86$), LD size ($p = 0.92$) or IMCL content ($p = 0.84$).

5.4.5 PLIN 5 Content and Colocalisation with LDs

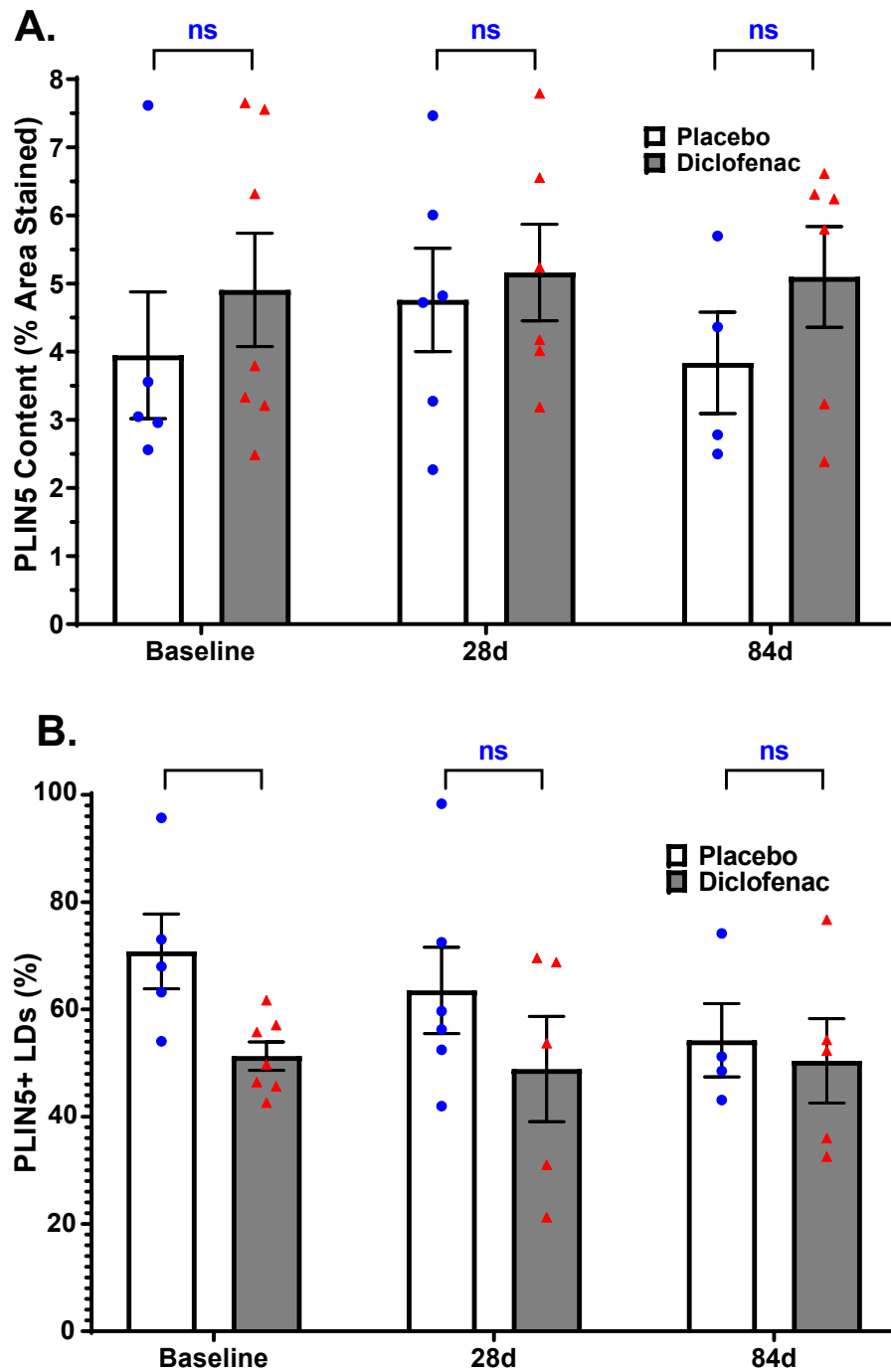


Figure 5-8: (A) Mean PLIN 5 content as a percentage of total muscle fibre area and (B) the percentage of LDs in the total LD pool that were coated with PLIN 5 in both placebo and Diclofenac participants.

Mean PLIN 5 content, as a percentage of total muscle fibre area, was not significantly different between the placebo and diclofenac groups at baseline

($3.95 \pm 0.93\%$ Placebo vs. $4.91 \pm 0.83\%$ Diclofenac; $p = 0.46$), 28 days ($4.76 \pm 0.76\%$ Placebo vs. $5.16 \pm 0.71\%$ Diclofenac; $p = 0.71$) or 84 days ($3.84 \pm 0.74\%$ vs. 5.10 ± 0.74 , $p = 0.27$). However, at baseline the percentage of LDs associated with PLIN5 in the placebo group was greater than that in the diclofenac group ($70.81 \pm 6.97\%$ vs. $51.30 \pm 2.65\%$; $p = 0.46$). No such significant differences were observed at the 28d ($63.54 \pm 8.06\%$ Placebo vs. $48.88 \pm 9.83\%$ Diclofenac; $p = 0.28$) and 84d ($54.24 \pm 6.85\%$ vs. 50.40 ± 7.87 diclofenac; $p = 0.72$) time points.

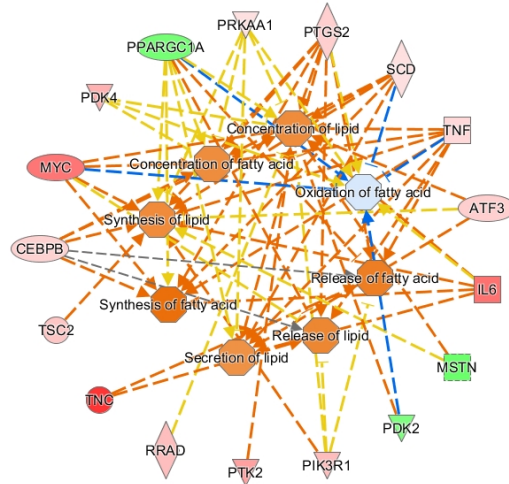
5.4.6 Predicted Metabolic Events for Lipid Metabolism per Changes in mRNA Abundance Relative to Baseline

Genes with Altered mRNA Abundance	
Gene Abbreviation	Gene Name
AKT1	AKT Serine/Threonine Kinase 1
ATF3	Activating Transcription Factor 3
CEBPB	CCAAT Enhancer Binding Protein Beta
CYR61	Cysteine-rich Angiogenic Inducer 61
FABP3	Fatty Acid Binding Protein 3
FBXO32	F-Box Protein 32
FOXO1	Forkhead Box Protein O1
IGF1	Insulin-Like Growth Factor 1
IL18	Interleukin-18
IL6	Interleukin-6
MET	MET Proto-Oncogene, Receptor Tyrosine Kinase
MSTN	Myostatin
MYC	MYC Proto-Oncogene, BHLH Transcription Factor
MYH1	Myosin Heavy Chain 1
MYOG	Myogenin
PAX3	Paired Box 3
PDK2	Pyruvate Dehydrogenase Kinase 2
PDK4	Pyruvate Dehydrogenase Kinase 4
PIK3R1	Phosphoinositide-3-Kinase Regulatory Subunit 1
PPARGC1A	PPARG Coactivator 1 Alpha
PRKAA1	Protein Kinase AMP-Activated Catalytic Subunit Alpha 1
PTGD2	Prostaglandin D2
PTGS2	Prostaglandin D2 Synthase
PTK2	Protein Tyrosine Kinase 2
RRAD	Ras Related Glycolysis Inhibitor and Calcium Channel Regulator
SCD	Stearoyl-CoA Desaturase
SIRT1	Sirtuin 1
SRF	Serum Response Factor
TNC	Tenascin C
TNF	Tumor Necrosis Factor
TSC2	TSC Complex Subunit 2
TXNIP	Thioredoxin Interacting Protein
VEGFA	Vascular Endothelial Growth Factor A
VEGFD	Vascular Endothelial Growth Factor D

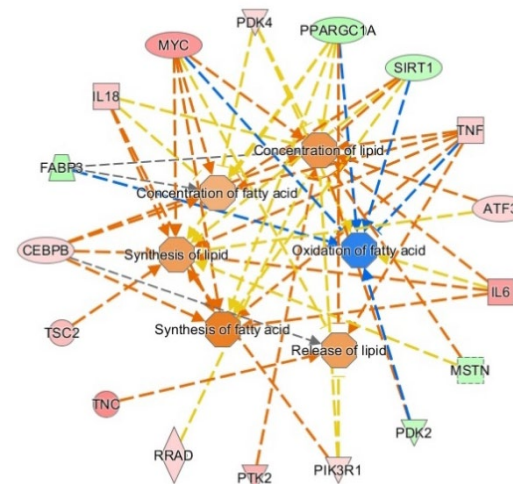
Table 5-2: Table of all genes related to lipid metabolism that had altered mRNA expression post-intervention relative to baseline.

Network Shapes	Path Designer Shapes
Canonical Pathway	Canonical Pathway
Complex/Group/Other	Complex/Group/Other
Chemical/Drug/Toxicant	Chemical/Toxicant
Cytokine	Cytokine
Disease	Disease
Enzyme	Enzyme
Function	Function
Fusion gene/product	Fusion gene/product
G-protein Coupled Receptor	G-protein Coupled Receptor
Growth Factor	Growth Factor
Ion Channel	Ion Channel
Kinase	Kinase
Ligand-dependent Nuclear Receptor	Ligand-dependent Nuclear Receptor
Mature microRNA	Mature microRNA
microRNA	microRNA
Other	Other
Peptidase	Peptidase
Phosphatase	Phosphatase
Transcription Regulator	Transcription Regulator
Translation Regulator	Translation Regulator
Transmembrane Receptor	Transmembrane Receptor
Transporter	Transporter

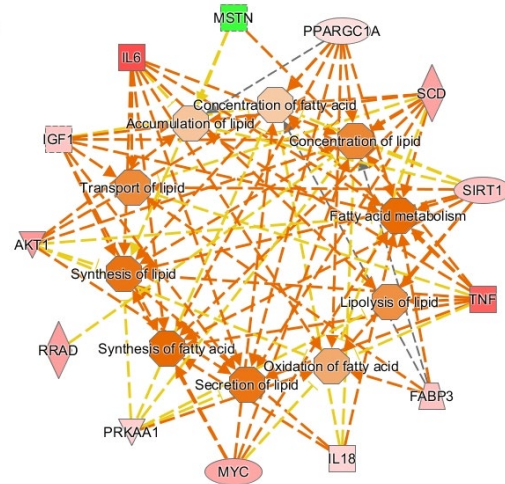
Placebo 24 hours



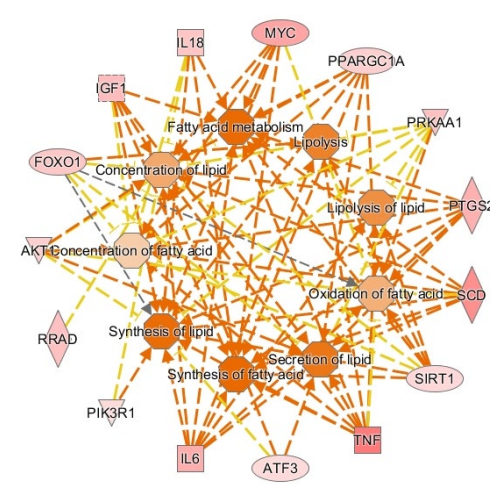
Placebo 7 days



Diclofenac 24 hours



Diclofenac 7 days



Prediction Legend

more extreme in dataset less

Increased measurement (red circle) Decreased measurement (green circle)

more confidence less

Predicted activation (orange arrow) Predicted inhibition (blue arrow)

Findings inconsistent with state of downstream molecule (yellow arrow)

Effect not predicted (black arrow)

Glow indicates activity when opposite of measurement (red/green glow)

Predicted Relationships

Leads to activation (orange arrow)

Leads to inhibition (blue arrow)

Findings inconsistent with state of downstream molecule (yellow arrow)

Effect not predicted (black arrow)

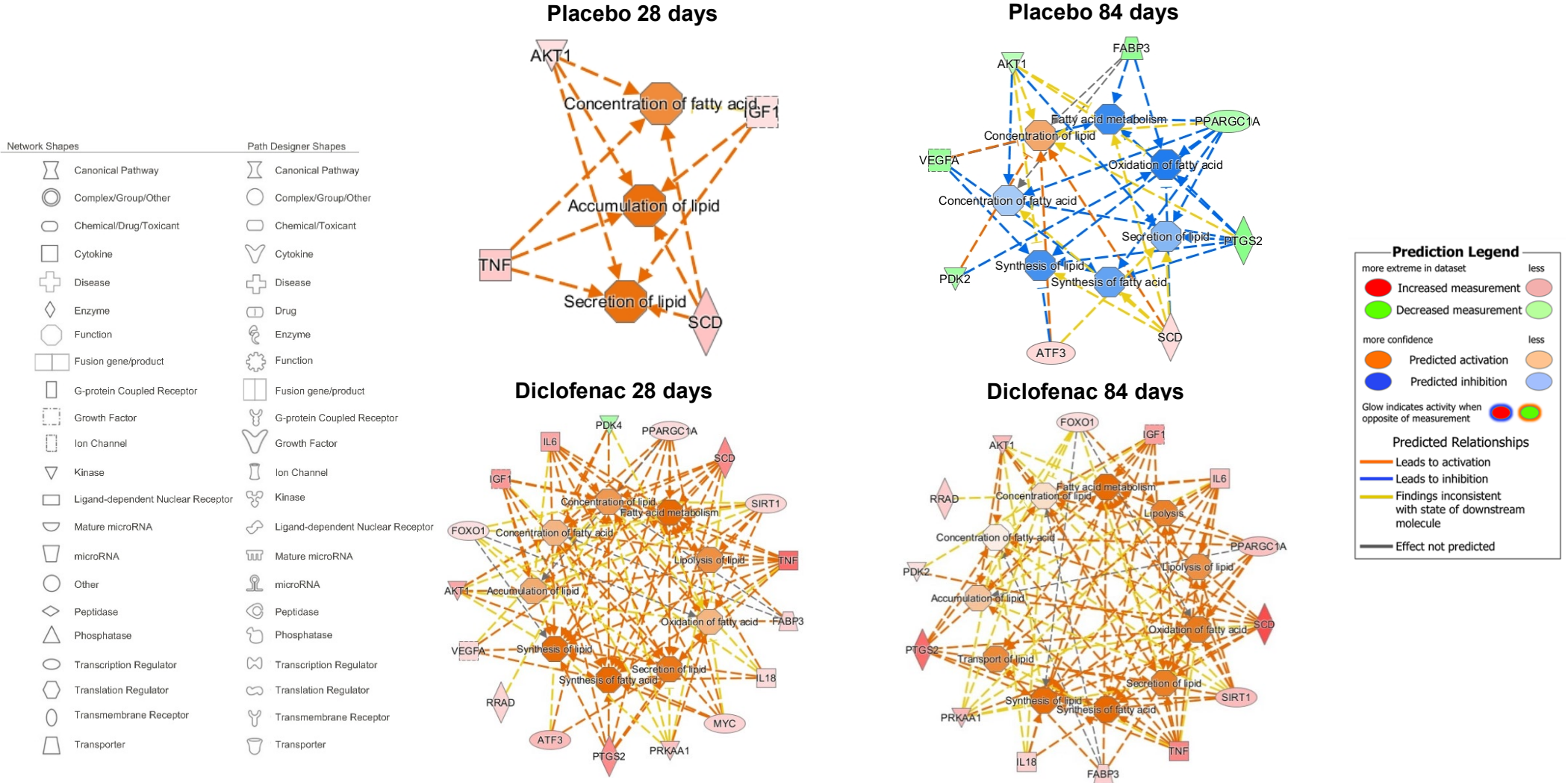


Figure 5-9: Schematics of gene networks and IPA predicted changes in metabolic events related to lipid metabolic in both groups.

In this study the mRNA expression of genes associated with functions such as “tissue development”, “carbohydrate metabolism” and “organismal injury and abnormalities” was significantly altered in both groups during the concentric exercise intervention, as published elsewhere (Mallinson *et al.*, 2020). However, for the purposes of this chapter only those differentially altered genes and cellular events associated with lipid metabolism will be presented and discussed. In total, 34 lipid associated genes had significantly altered mRNA abundance at the intervention time points relative to baseline (see **Table 5-2**). Full lists of the genes altered at the 24h, 7 days, 28 days, and 84 days’ time points relative to baseline, including fold changes and p values, in the placebo group are presented in **Appendix A**. Similar lists for the diclofenac group are presented in **Appendix B**.

Figure 5-9 shows schematic representations of log fold changes in the mRNA abundance of genes associated with lipid metabolism (outer ring shapes), and the resulting predicted effects on cellular events involved to lipid metabolism (inner ring shapes), in both groups at the time points shown relative to baseline (see Network Shapes in **Figure 5-9**). The greater the intensity of the colour filling the shapes of the genes the greater the magnitude of the change in the expression of their mRNA transcripts, the deeper the colour of the cellular events the greater the confidence in the predicted activation or inhibition of that event (see Prediction Legend in **Figure 5-9**).

For the placebo group, at the 24h time point, robust decreases in PPARGC1A, PDK2, and MSTN mRNA abundance relative to baseline was evident in conjunction with an increase in abundance of 13 other mRNAs, most notably MYC, TNC, and IL6. These changes in expression were collectively associated with a predicted activation of a number of lipid metabolism cellular events and, uniquely, with the inhibition of FA oxidation (see **Figure 5-9**). At 7 days PPARGC1A, SIRT1, FABP3, PDK2, and MSTN were reduced in expression relative to baseline, whilst 12 other mRNAs were increased in expression (see **Appendix A**). Collectively these events predicted synthesis and storage of lipid alongside the robust inhibition of fatty acid oxidation, maintained from the 24h timepoint. At 28 days change in mRNA expression had waned, with only 4 mRNA transcripts (AKT1, IGF1, TNF, and SCD)

presenting with altered expression, being elevated above baseline levels, but this was still associated with a robust prediction of storage and accumulation of lipid. By 84 days the pattern of change in gene expression from baseline had changed considerably from earlier timepoints with decreases in PDK2, VEGFA, AKT1, FABP3, PPARGC1A, and PTGS2 mRNA abundance relative to baseline being recorded and increases in only ATF3 and SCD relative to baseline. Collectively this was associated with predictions of an inhibition in a number of cellular events associated with lipid metabolism in direct contrast to earlier predictions.

For the diclofenac group, at the 24h time point, the mRNA abundance of 13 genes was altered leading to the predicted activation of an array of processes involved in lipid metabolism including lipid synthesis, lipid storage, and FA oxidation (see **Figure 5-9**). Of these 13 genes, only the mRNA abundance of MSTN was decreased. At 7 days the mRNA expression of 15 genes was altered relative to baseline, with the magnitude of the fold changes being greatest for TNF, SCD, IL6, and PTGS2 (see **Appendix B**), leading to the predicted activation of lipid metabolism processes. By 28 days the mRNA abundance of 17 genes had changed relative to baseline, all but one increasing, with TNF, SCD, PTGS2, and IL6 being the most changed. Only PDK4 had decreased mRNA expression at this time point. Together, these changes predicted the activation of processes associated with lipid metabolism as previously mentioned. Finally, at 84 days 14 genes all had significantly elevated mRNA abundance relative to baseline, with SCD, PTGS2, TNF, and IGF1 being the most increased (see **Appendix B**).

There was a stark divergence between the placebo and diclofenac groups in the predicted activation status of cellular events linked to lipid metabolism at the 84d time point. At this time point inhibition of lipid metabolism, synthesis, storage, and oxidation was predicted in the placebo group whilst the robust activation of lipid metabolism processes observed in the diclofenac group was maintained throughout the intervention.

5.5 Discussion

Few studies investigate the effect of resistance exercise on IMCL content. It has been shown that a single bout of resistance exercise can transiently decrease IMCL content (Koopman *et al.*, 2006), owing to enhanced FA oxidation during exercise, and that 28 days of unilateral leg extensions can increase resting IMCL content in participants sedentary at baseline (Zhu *et al.*, 2015). Little is known about the effect of resistance exercise on PLIN5 content. The data presented here are the first to show that, in trained healthy young males, 12 weeks of structured lower limb resistance exercise does not elicit changes in total or fibre-type specific IMCL content or PLIN5 expression. IMCL and PLIN5 content have not previously been determined following 12 weeks of resistance exercise. Also, the concurrent administration of diclofenac, an NSAID known to interact with PPAR- γ in vitro, led to previously unidentified changes in mRNA expression that predicted the robust, sustained activation of metabolic events linked to lipid metabolism. This contrasts with the placebo group in which changes in mRNA abundance at the 84d time point predicted the inhibition of cellular events linked to lipid metabolism. Also, muscle strength and muscle mass adaptations were observed in the participants of this study. Both isometric strength and work done increased over time, with strength being significantly greater in both groups at the 84d timepoint relative to baseline. Data previously published elsewhere shows that both mean leg muscle cross-sectional area and volume also increased over time in the participants of this study (Mallinson *et al.*, 2020).

There is no universal effect of exercise on IMCL content. Rather the magnitude of the change depends upon the metabolic health of the participants, their training status at baseline, and the exercise modality (Moro, Bajpeyi, and Smith, 2008; Bajpeyi *et al.*, 2012). It is important to note that in almost all exercise intervention studies, changes in LD parameters and IMCL content are observed in participants that are sedentary on recruitment and at baseline. However, the participants recruited to this study were habitual exercisers, recruited to reduce the risk that any changes in muscle CSA or strength that could result from acute neural adaptations to resistance exercise

(Škarabot *et al.*, 2021), as is often seen in sedentary individuals. Trained individuals have distinctive LD characteristics, their LDs tend to be significantly more numerous and either the same size or smaller than those in sedentary individuals (Tarnopolsky *et al.*, 2007; Daemen *et al.*, 2018). The greater surface area to volume ratio in this arrangement is an adaptation that allows FAs to be released from LDs more readily during exercise and these FAs act as substrates for ATP generation via β -oxidation in conjunction with plasma FAs (Van Loon *et al.*, 2003; Shepherd *et al.*, 2013). This phenomenon can be seen here in the fact that baseline LD count in both the placebo and diclofenac groups was roughly double that observed at the pre bed rest time point for participants recruited to the bed rest studies detailed in **Chapter 3** and at baseline in the control and NAFLD groups detailed in **Chapter 4** (see **Appendix C**). Also, mean LD size at baseline in both the placebo and diclofenac groups was less than half that observed in the participants of the studies described in **Chapter 3** and **Chapter 4** (see **Appendix C**). In addition, it has been shown that resistance training-induced elevation in IMCL content persists even after three weeks of detraining (Zhu *et al.*, 2015). Taken together these data suggest that in the study detailed here changes in IMCL content were not observed in response to the exercise intervention in either the placebo or diclofenac group because both groups already had an IMCL profile typical to trained individuals. It is unlikely that the resistance stimulus alone provided during the intervention would change IMCL content further in this cohort.

The effect of resistance exercise training on the PLIN5 content of trained individuals is not well understood. What is known is that PLIN protein expression is positively correlated with IMCL content in other exercise modalities (Amati *et al.*, 2011; Peters *et al.*, 2012). It has been demonstrated that 6 weeks of sprint interval and endurance training increases PLIN5 content in both the Type I and Type IIA muscle fibres of healthy males sedentary at baseline (Shepherd *et al.*, 2013) and that in individuals with T2DM, exercise training specifically increases PLIN5 expression, without any alterations in any of the other PLIN isoforms (Daemen *et al.*, 2018). It is unsurprising then that

PLIN5 content also did not change in either the placebo group or diclofenac group here.

In the data presented here, PPARGC1A mRNA abundance in the placebo group was lower at 24h, 7 days and 84 days than at baseline and was not significantly different from baseline at 28 days. This is consistent with another report that in trained muscle acute resistance exercise intervention did not increase PPARGC1A expression through the canonical gene promoter (Popov *et al.*, 2017). However, PPARGC1A mRNA abundance was increased above baseline at all time points relative to baseline in the group supplementing 75 mg diclofenac daily. Taken together these data indicate that diclofenac induces increased expression of PGC-1 α , the protein product of the PPARGC1A gene, likely via its binding to and activation of PPAR- γ for which PGC-1 α is the main coactivator. This is supported by the observation that the mRNA abundance of silent information regulator 2 homolog 1 (SIRT1) was also elevated at all time points relative to baseline in the diclofenac group, but did not change or was decreased (at 7 days) relative to baseline in the placebo group. SIRT1 encodes a protein called Sirtuin 1 which is an NAD⁺ dependent histone acetylase that deacetylates PGC-1 α and increases its transcriptional activity (Rodgers *et al.*, 2005). Sirtuin 1 and PGC-1 α have also been shown to increase myonuclear numbers in muscle in response to resistance exercise (Radak *et al.*, 2020).

Lending credence to the hypothesis of diclofenac-induced activation of PGC-1 α being the main driver of consistently predicted activation of lipid metabolism processes, several mRNA transcripts of genes known to be activated by or to interact with PGC-1 α were elevated in the diclofenac group over the course of the training intervention. PGC-1 α expression increases with the expression of fatty acid binding proteins (FABPs) (Mulya *et al.*, 2017; Supruniuk, Miklosz, and Chabowski, 2017). Here the mRNA abundance of FABP3, a gene encoding Heart-type FABP (H-FABP), which is expressed in the sarcolemma and binds reversibly with FAs, transporting them to the mitochondrial for β -oxidation (Furuhashi, and Hotamisligil, 2008), was measured. FABP3 mRNA abundance at the 24h, 28d and 84d time points in the diclofenac group increased relative to baseline measurements but was

unchanged or decreased (at 84 days) in the placebo group. Also, PGC-1 α has been shown to co-activate the transcription of FOXO-1 by binding to O-GlcNAc Transferase (Housley *et al.*, 2009), and to interact with the catalytic subunit of AMPK, which is encoded by Protein Kinase AMP-Activated Catalytic Subunit Alpha 1 (PRKAA1) (Irrcher *et al.*, 2008; Cantó and Auwerx, 2009). The mRNA abundance of FOXO-1 did not change significantly during the intervention in the placebo group but was increased post 7 days in the diclofenac group. The mRNA abundance of PRKAA1 was increased at all time points in the diclofenac group but only at the 24h time point in the placebo group.

Changes in skeletal muscle lipid composition were reported in a study during which 8 mg of Rosiglitazone, a more potent agonist of PPAR- γ than diclofenac (Adamson *et al.*, 2002) that acts as an insulin sensitising medication in individuals with Type 2 Diabetes Mellitus (Lebovitz *et al.*, 2001), was administered twice daily to 7 males with impaired glucose tolerance (IGT) (Mai *et al.*, 2012). During this study the skeletal muscle lipid profile changed such that the percentage of saturated LCFAs decreased whilst the percentage of unsaturated FAs increased as determined by gas chromatography, though the overall size of the lipid pool was unaltered. This transition was explained by the observed elevation in the myocellular mRNA expression of Stearoyl-CoA desaturase-1 (SCD1) and Sterol regulatory element-binding protein 1 (SREBP-1), the main transcriptional regulator of SCD1 (Ntambi, 1999). SCD1 is an enzyme encoded by the SCD gene and it is the rate limiting enzyme in the conversion of saturated fatty acids to monounsaturated fatty acids as it catalyses the formation of a double bond at the cis- Δ -9 position (Igal, 2016). It is via this process that palmitate is converted to palmitoleate, and stearate is converted to oleate. Rosiglitazone has also been shown to bind PPAR- γ and increase its expression and the expression of SCD1 mRNA in healthy participants that have no impairments in insulin sensitivity (Yao-Borengasser *et al.*, 2008).

For the first time, a novel mechanism of action of diclofenac is proposed here for future research. The binding of diclofenac to PPAR- γ may upregulate the expression and activity of PGC-1 α , a key mediator of energy metabolism, resulting in both greater FA transport into the muscle via increased FABP3

expression and greater utilisation of this FA, with no net change in IMCL content. Diclofenac may therefore confer a performance enhancing benefit by increasing the rate of ATP production through FAs during exercise. In this vein, it is interesting to note that the mRNA expression of both VEGF-A and VEGF-D, which encode proteins that are key mediators of skeletal muscle angiogenesis (Rissanen *et al.*, 2003; Wagner, 2011), was increased at the 28d time point relative to baseline in the diclofenac group. Whether this same effect can be seen in sedentary individuals with or without exercise intervention, or with other NSAIDs, requires further investigation. Though the magnitude of this response is likely to be greatest with diclofenac given its great affinity for PPAR- γ .

It is important to highlight that whilst the canonical mechanism of action of diclofenac is the reduction of prostaglandin synthesis via antagonism of COX proteins, preferentially COX-2, diclofenac did not induce any changes in skeletal muscle PTGS2 mRNA abundance after 24 hours but did increase PPARGC1A mRNA abundance by roughly 1.5 times baseline after just 24 hours. This is in line with in vitro findings that diclofenac is a rapid and potent activator of PPAR- γ , which is shown here to be via its upregulation of PGC-1 α transcription which precedes significant changes in the mRNA abundance of the COX-2 gene PTGS2.

It should be noted that plasma FFA concentration is inversely correlated with PGC-1 α mRNA expression in human skeletal muscle (Richardson *et al.*, 2005). Thus, an effect of any diet induced changes in FFA concentration on PGC-1 α and lipid metabolism during the course of the study described here cannot be completely excluded. However, the magnitude of the differences observed in the expression of PGC-1 α and its metabolic co-factors/targets between the placebo and diclofenac groups suggest that diclofenac was the main cause of the observed changes.

5.6 Conclusion

This study reports for the first time that chronic (12 weeks) resistance exercise does not alter IMCL or PLIN5 content in healthy, young, trained males. Another key finding is that diclofenac, as an established partial agonist of PPAR- γ in

vitro, significantly increases PGC-1 α mRNA abundance and in so doing is predicted to propagate the robust activation of pathways associated with lipid metabolism in vivo in humans. However, this effect does not have any impact on overall intramyocellular lipid content or the expression of PLIN5, which is involved in regulating LD biogenesis and lipolysis. Whether diclofenac-induced changes in the mRNA abundance of lipid metabolism genes alters muscle fuel oxidation such that FA oxidation is enhanced cannot be determined by the data presented here. However, this should be investigated further as any such effects could fundamentally change our understanding of diclofenac's role in the context of exercise enhancement.

5.7 References

Accioly, M.T., Pacheco, P., Maya-Monteiro, C.M., Carrossini, N., Robbs, B.K., Oliveira, S.S., Kaufmann, C., Morgado-Diaz, J.A., Bozza, P.T., and Viola, J.P. (2008) Lipid bodies are reservoirs of cyclooxygenase-2 and sites of prostaglandin-E2 synthesis in colon cancer cells. *Cancer Research*. 68 (6), pp. 1732-1740.

Adamson, D.J., Frew, D., Tatoud, R., Wolf, C.R., and Palmer, C.N. (2002) Diclofenac antagonizes peroxisome proliferator-activated receptor-gamma signaling. *Molecular Pharmacology*. 61 (1), pp. 7-12.

Allen, A. and Flemström, G. (2005) Gastroduodenal mucus bicarbonate barrier: protection against acid and pepsin. *American journal of physiology. Cell Physiology*. 288 (1), pp. C1-C19.

Amati, F., Dubé, J.J., Alvarez-Carnero, E., Edreira, M.M., Chomentowski, P., Coen, P.M., Switzer, G.E., Bickel, P.E., Stefanovic-Racic, M., Toledo, F.G., and Goodpaster, B.H. (2011) Skeletal muscle triglycerides, diacylglycerols, and ceramides in insulin resistance: another paradox in endurance-trained athletes?. *Diabetes*. 60 (10), pp. 2588-2597.

Atzeni, F., Masala, I.F. and Sarzi-Puttini, P. (2018) A Review of Chronic Musculoskeletal Pain: Central and Peripheral Effects of Diclofenac. *Pain and Therapy*. 7 (2), pp. 163-177.

Bajpeyi, S., Reed, M.A., Molskness, S., Newton, C., Tanner, C.J., McCartney, J.S., and Houmard, J.A. (2012) Effect of short-term exercise training on intramyocellular lipid content. *Applied Physiology, Nutrition, and Metabolism: Physiologie Appliquee, Nutrition et Metabolisme*. 37 (5), pp. 822-828.

Battersby, A.R. (2000) Tetrapyrroles: the pigments of life. *Natural Product Reports*. 17 (6), pp. 507-526.

Bergström, J. (1962) Muscle electrolytes in man: determined by neutron activation analysis on needle biopsy specimens. A study on normal subjects, kidney patients and patients with chronic diarrhea. *Scandinavian Journal of Clinical & Laboratory Investigation*. Supplement 68 (11-13), pp. 511-513.

- Biringer, R.G. (2021) A Review of Prostanoid Receptors: Expression, Characterization, Regulation, and Mechanism of Action. *Journal of Cell Communication and Signaling*. 15 (2), pp. 155-184.
- Blobaum, A.L., and Marnett, L.J. (2007) Structural and functional basis of cyclooxygenase inhibition. *Journal of Medicinal Chemistry*. 50 (7), pp. 1425-1441.
- Brennan, R., Wazaify, M., Shawabkeh, H., Boardley, I., McVeigh, J., and Van Hout, M.C. (2021) A Scoping Review of Non-Medical and Extra-Medical Use of Non-Steroidal Anti-Inflammatory Drugs (NSAIDs). *Drug Safety*. 44 (9), pp. 917-928.
- Bozza, P.T., Bakker-Abreu, I., Navarro-Xavier, R.A., and Bandeira-Melo, C. (2011) Lipid body function in eicosanoid synthesis: an update. *Prostaglandins, Leukotrienes, and Essential Fatty Acids*. 85 (5), pp. 205-213.
- Burke, J.E. and Dennis, E.A. (2009) Phospholipase A2 structure/function, mechanism, and signaling. *Journal of Lipid Research*. 50 Suppl(Suppl), pp. S237-S242.
- Cantó, C. and Auwerx, J. (2009) PGC-1alpha, SIRT1 and AMPK, an energy sensing network that controls energy expenditure. *Current Opinion in Lipidology*. 20 (2), pp. 98-105.
- Cardinale, D.A., Lilja, M., Mandić, M., Gustafsson, T., Larsen, F.J., and Lundberg, T.R. (2017) Resistance Training with Co-ingestion of Anti-inflammatory Drugs Attenuates Mitochondrial Function. *Frontiers in Physiology*. 8, 1074.
- Chandrasekharan, N.V. and Simmons, D.L. (2004) The cyclooxygenases. *Genome Biology*. 5 (9), 241.
- Chen, Y.W., Hubal, M.J., Hoffman, E.P., Thompson, P.D., and Clarkson, P.M. (2003) Molecular responses of human muscle to eccentric exercise. *Journal of Applied Physiology (Bethesda, Md.: 1985)*. 95 (6), pp. 2485-2494.
- Cicinnati, V.R., Shen, Q., Sotiropoulos, G.C., Radtke, A., Gerken, G., and Beckebaum, S. (2008) Validation of putative reference genes for gene

expression studies in human hepatocellular carcinoma using real-time quantitative RT-PCR. *BMC Cancer*. 8, 350.

Cornu, C., Grange, C., Regalin, A., Munier, J., Ounissi, S., Reynaud, N., Kassai-Koupai, B., Sallet, P., and Nony, P. (2020) Effect of Non-Steroidal Anti-Inflammatory Drugs on Sport Performance Indices in Healthy People: a Meta-Analysis of Randomized Controlled Trials. *Sports Medicine – Open*. 6 (1), 20.

Corrigan, B., and Kazlauskas, R. (2003) Medication use in athletes selected for doping control at the Sydney Olympics (2000). *Clinical Journal of Sport Medicine: Official Journal of The Canadian Academy of Sport Medicine*. 13 (1), pp. 33-40.

Crofford, L.J. (1997) COX-1 and COX-2 tissue expression: implications and predictions. *The Journal of Rheumatology*. Supplement 49, pp. 15-19.

Crossland, H., Constantin-Teodosiu, D., Gardiner, S.M., Constantin, D., and Greenhaff, P.L. (2008) A potential role for Akt/FOXO signalling in both protein loss and the impairment of muscle carbohydrate oxidation during sepsis in rodent skeletal muscle. *The Journal of Physiology*. 586 (22), pp. 5589-5600.

Curtis, E., Fuggle, N., Shaw, S., Spooner, L., Ntani, G., Parsons, C., Corp, N., Honvo, G., Baird, J., Maggi, S., Dennison, E., Bruyère, O., Reginster, J.Y., and Cooper, C. (2019) Safety of Cyclooxygenase-2 Inhibitors in Osteoarthritis: Outcomes of a Systematic Review and Meta-Analysis. *Drugs & Aging*. 36 (Suppl 1), pp. 25-44.

da Costa, B.R., Reichenbach, S., Keller, N., Nartey, L., Wandel, S., Jüni, P., and Trelle, S. (2017) Effectiveness of non-steroidal anti-inflammatory drugs for the treatment of pain in knee and hip osteoarthritis: a network meta-analysis. *Lancet (London, England)*. 390 (10090), pp. e21-e33.

Daemen, S., Gemmink, A., Brouwers, B., Meex, R., Huntjens, P. R., Schaart, G., Moonen-Kornips, E., Jörgensen, J., Hoeks, J., Schrauwen, P. and Hesselink, M. (2018) Distinct lipid droplet characteristics and distribution unmask the apparent contradiction of the athlete's paradox. *Molecular Metabolism*. 17, pp. 71-81.

Derry, P., Derry, S., Moore, R.A., and McQuay, H.J. (2009) Single dose oral diclofenac for acute postoperative pain in adults. *The Cochrane Database of Systematic Reviews*. (2), CD004768.

Devries, M.C., Lowther, S.A., Glover, A.W., Hamadeh, M.J., and Tarnopolsky, M.A. (2007) IMCL area density, but not IMCL utilization, is higher in women during moderate-intensity endurance exercise, compared with men. *American Journal of Physiology. Regulatory, Integrative and Comparative Physiology*. 293 (6), pp. R2336-R2342.

Drini, M. (2017) Peptic ulcer disease and non-steroidal anti-inflammatory drugs. *Australian Prescriber*. 40 (3), pp. 91-93.

Espinoza, D.O., Boros, L.G., Crunkhorn, S., Gami, H., and Patti, M.E. (2010) Dual modulation of both lipid oxidation and synthesis by peroxisome proliferator-activated receptor-gamma coactivator-1alpha and -1beta in cultured myotubes. *FASEB Journal: Official Publication of The Federation of American Societies for Experimental Biology*. 24 (4), pp. 1003-1014.

Fajas, L., Auboeuf, D., Raspé, E., Schoonjans, K., Lefebvre, A.M., Saladin, R., Najib, J., Laville, M., Fruchart, J.C., Deeb, S., Vidal-Puig, A., Flier, J., Briggs, M.R., Staels, B., Vidal, H., and Auwerx, J. (1997) The organization, promoter analysis, and expression of the human PPARgamma gene. *The Journal of Biological Chemistry*. 272 (30), pp. 18779-18789.

Farrell, L., Hollingsworth, B., Propper, C., and Shields, M.A. (2014) The socioeconomic gradient in physical inactivity: evidence from one million adults in England. *Social Science & Medicine (1982)*. 123, pp. 55-63.

Furuhashi, M., and Hotamisligil, G.S. (2008) Fatty acid-binding proteins: role in metabolic diseases and potential as drug targets. *Nature Reviews. Drug Discovery*. 7 (6), pp. 489-503.

Gan, T.J. (2010) Diclofenac: an update on its mechanism of action and safety profile. *Current Medical Research and Opinion*. 26 (7), pp. 1715-1731.

Goodpaster, B.H., He, J., Watkins, S., and Kelley, D.E. (2001) Skeletal muscle lipid content and insulin resistance: evidence for a paradox in endurance-

trained athletes. *The Journal of Clinical Endocrinology and Metabolism*. 86 (12), pp. 5755-5761.

Griswold, D.E. and Adams, J.L. (1996) Constitutive cyclooxygenase (COX-1) and inducible cyclooxygenase (COX-2): rationale for selective inhibition and progress to date. *Medicinal Research Reviews*. 16 (2), pp. 181-206.

Gemmink, A., Schrauwen, P., and Hesselink, M. (2020) Exercising your fat (metabolism) into shape: a muscle-centred view. *Diabetologia*. 63 (8), pp. 1453-1463.

Harirforoosh, S. and Jamali, F. (2009) Renal adverse effects of nonsteroidal anti-inflammatory drugs. *Expert Opinion on Drug Safety*. 8 (6), pp. 669-681.

Harris, R.C. (2000) Cyclooxygenase-2 in the kidney. *Journal of the American Society of Nephrology: JASN*. 11 (12), pp. 2387-2394.

Harris, T., Limb, E.S., Hosking, F., Carey, I., DeWilde, S., Furness, C., Wahlich, C., Ahmad, S., Kerry, S., Whincup, P., Victor, C., Ussher, M., Iliffe, S., Ekelund, U., Fox-Rushby, J., Ibison, J., and Cook, D.G. (2019) Effect of pedometer-based walking interventions on long-term health outcomes: Prospective 4-year follow-up of two randomised controlled trials using routine primary care data. *PLoS Medicine*. 16 (6), e1002836.

Hatt, K.M., Vijapura, A., Maitin, I.B., and Cruz, E. (2018) Safety Considerations in Prescription of NSAIDs for Musculoskeletal Pain: A Narrative Review. *PM & R: The Journal of Injury, Function, and Rehabilitation*. 10 (12), pp. 1404-1411.

Hayashi, T., Fujita, K., Matsushita, M., and Nonomura, N. (2019) Main Inflammatory Cells and Potentials of Anti-Inflammatory Agents in Prostate Cancer. *Cancers*. 11 (8), 1153.

Hernandez-Quiles, M., Broekema, M. F., and Kalkhoven, E. (2021) PPARgamma in Metabolism, Immunity, and Cancer: Unified and Diverse Mechanisms of Action. *Frontiers in Endocrinology*. 12, 624112.

Hla, T. and Neilson, K. (1992) Human cyclooxygenase-2 cDNA. *Proceedings of the National Academy of Sciences of the United States of America*. 89 (16), pp. 7384-7388.

- Holgado, D., Hopker, J., Sanabria, D., and Zabala, M. (2018) Analgesics and Sport Performance: Beyond the Pain-Modulating Effects. *PM & R: The Journal of Injury, Function, And Rehabilitation*. 10 (1), pp. 72-82.
- Housley, M.P., Udeshi, N.D., Rodgers, J.T., Shabanowitz, J., Puigserver, P., Hunt, D.F., and Hart, G.W. (2009) A PGC-1alpha-O-GlcNAc transferase complex regulates FoxO transcription factor activity in response to glucose. *The Journal of Biological Chemistry*. 284 (8), pp. 5148-5157.
- Igal, R.A. (2016) Stearoyl CoA desaturase-1: New insights into a central regulator of cancer metabolism. *Biochimica et Biophysica Acta*. 1861 (12 Pt A), pp. 1865-1880.
- Irrcher, I., Ljubcic, V., Kirwan, A.F., and Hood, D.A. (2008) AMP-activated protein kinase-regulated activation of the PGC-1alpha promoter in skeletal muscle cells. *PLoS One*. 3 (10), e3614.
- Jarc, E., and Petan, T. (2020) A twist of FATE: Lipid droplets and inflammatory lipid mediators. *Biochimie*. 169, pp. 69-87.
- Jones, S.W., Hill, R.J., Krasney, P.A., O'Conner, B., Peirce, N. and Greenhaff, P.L. (2004) Disuse atrophy and exercise rehabilitation in humans profoundly affects the expression of genes associated with the regulation of skeletal muscle mass. *FASEB Journal: Official Publication of The Federation of American Societies for Experimental Biology*. 18 (9), pp. 1025-1027.
- Takehi, S., Tamura, Y., Takeno, K., Ikeda, S.I., Ogura, Y., Saga, N., Miyatsuka, T., Naito, H., Kawamori, R., and Watada, H. (2020) Endurance Runners with Intramyocellular Lipid Accumulation and High Insulin Sensitivity Have Enhanced Expression of Genes Related to Lipid Metabolism in Muscle. *Journal of Clinical Medicine*. 9 (12), 3951.
- Kojo, H., Fukagawa, M., Tajima, K., Suzuki, A., Fujimura, T., Aramori, I., Hayashi, K., and Nishimura, S. (2003) Evaluation of human peroxisome proliferator-activated receptor (PPAR) subtype selectivity of a variety of anti-inflammatory drugs based on a novel assay for PPAR delta(beta). *Journal of Pharmacological Sciences*. 93 (3), pp. 347-355.

Koopman, R., Manders, R.J., Jonkers, R.A., Hul, G.B., Kuipers, H., and van Loon, L.J. (2006) Intramyocellular lipid and glycogen content are reduced following resistance exercise in untrained healthy males. *European Journal of Applied Physiology*. 96 (5), pp. 525-534.

Ku, E.C., Lee, W., Kothari, H.V. and Scholer, D.W. (1986) Effect of diclofenac sodium on the arachidonic acid cascade. *The American Journal of Medicine*. 80 (4B), pp. 18-23.

Kurumbail, R.G., Stevens, A.M., Gierse, J.K., McDonald, J.J., Stegeman, R.A., Pak, J.Y., Gildehaus, D., Miyashiro, J.M., Penning, T.D., Seibert, K., Isakson, P.C., and Stallings, W.C. (1996) Structural basis for selective inhibition of cyclooxygenase-2 by anti-inflammatory agents. *Nature*. 384 (6610), pp. 644-648.

Lebovitz, H.E., Dole, J.F., Patwardhan, R., Rappaport, E.B., Freed, M.I., and Rosiglitazone Clinical Trials Study Group (2001) Rosiglitazone monotherapy is effective in patients with type 2 diabetes. *The Journal of Clinical Endocrinology and Metabolism*. 86 (1), pp. 280-288.

Liang, H., and Ward, W.F. (2006) PGC-1 α : a key regulator of energy metabolism. *Advances in Physiology Education*. 30 (4), pp. 145-151.

Lilja, M., Mandić, M., Apró, W., Melin, M., Olsson, K., Rosenborg, S., Gustafsson, T., and Lundberg, T.R. (2018) High doses of anti-inflammatory drugs compromise muscle strength and hypertrophic adaptations to resistance training in young adults. *Acta Physiologica (Oxford, England)*. 222 (2), 10.1111/apha.

Lin, J., Handschin, C., and Spiegelman, B.M. (2005) Metabolic control through the PGC-1 family of transcription coactivators. *Cell Metabolism*. 1 (6), pp. 361-370.

Liou, J.Y., Deng, W.G., Gilroy, D.W., Shyue, S.K., and Wu, K.K. (2001) Colocalization and interaction of cyclooxygenase-2 with caveolin-1 in human fibroblasts. *The Journal of Biological Chemistry*. 276 (37), pp. 34975-34982.

Mai, K., Andres, J., Bobbert, T., Assmann, A., Biedasek, K., Diederich, S., Graham, I., Larson, T.R., Pfeiffer, A.F., and Spranger, J. (2012) Rosiglitazone

increases fatty acid Δ 9-desaturation and decreases elongase activity index in human skeletal muscle in vivo. *Metabolism: Clinical and Experimental*. 61 (1), pp. 108-116.

Mäkelä, A., Kuusi, T., and Schröder, T. (1997) Inhibition of serum phospholipase-A2 in acute pancreatitis by pharmacological agents in vitro. *Scandinavian Journal of Clinical and Laboratory Investigation*. 57 (5), pp. 401-407.

Mallinson, J.E., Constantin-Teodosiu, D., Sidaway, J., Westwood, F.R., and Greenhaff, P.L. (2009) Blunted Akt/FOXO signalling and activation of genes controlling atrophy and fuel use in statin myopathy. *The Journal of Physiology*. 587 (1), pp. 219-230.

Mallinson, J.E., Taylor, T., Constantin-Teodosiu, D., Billeter-Clark, R., Constantin, D., Franchi, M.V., Narici, M.V., Auer, D., and Greenhaff, P.L. (2020) Longitudinal hypertrophic and transcriptional responses to high-load eccentric-concentric vs concentric training in males. *Scandinavian Journal of Medicine & Science in Sports*. 30 (11), pp. 2101-2115.

Mazzarino, M., Braganò, M.C., Donati, F., de la Torre, X., and Botrè, F. (2010) Effects of propyphenazone and other non-steroidal anti-inflammatory agents on the synthetic and endogenous androgenic anabolic steroids urinary excretion and/or instrumental detection. *Analytica Chimica Acta*. 657 (1), pp. 60-68.

McGettigan, P., and Henry, D. (2013) Use of non-steroidal anti-inflammatory drugs that elevate cardiovascular risk: an examination of sales and essential medicines lists in low-, middle-, and high-income countries. *PLoS Medicine*. 10 (2), e1001388.

Minghetti, L. (2004) Cyclooxygenase-2 (COX-2) in inflammatory and degenerative brain diseases. *Journal of Neuropathology and Experimental Neurology*. 63 (9), pp. 901-910.

Moro, C., Bajpeyi, S., and Smith, S.R. (2008) Determinants of intramyocellular triglyceride turnover: implications for insulin sensitivity. *American Journal of Physiology. Endocrinology and Metabolism*. 294 (2), pp. E203-E213.

Mulya, A., Haus, J.M., Solomon, T.P., Kelly, K.R., Malin, S.K., Rocco, M., Barkoukis, H., and Kirwan, J.P. (2017) Exercise training-induced improvement in skeletal muscle PGC-1 α -mediated fat metabolism is independent of dietary glycemic index. *Obesity (Silver Spring, Md.)*. 25 (4), pp. 721-729.

Murton, A.J., Billeter, R., Stephens, F.B., Des Etages, S.G., Graber, F., Hill, R.J., Marimuthu, K., and Greenhaff, P.L. (2014) Transient transcriptional events in human skeletal muscle at the outset of concentric resistance exercise training. *Journal of Applied Physiology (Bethesda, Md.: 1985)*. 116 (1), pp. 113-125.

Nakagawa, Y., and Hattori, M. (2017) Intramyocellular lipids of muscle type in athletes of different sport disciplines. *Open Access Journal of Sports Medicine*. 8, pp. 161-166.

Noble, S.L., King, D.S., and Olutade, J.I. (2000) Cyclooxygenase-2 enzyme inhibitors: place in therapy. *American Family Physician*. 61 (12), pp. 3669-3676.

Nørregaard, R., Kwon, T.H. and Frøkiær, J. (2015) Physiology and pathophysiology of cyclooxygenase-2 and prostaglandin E₂ in the kidney. *Kidney Research and Clinical Practice*. 34 (4), pp. 194-200.

Ntambi, J.M. (1999) Regulation of stearyl-CoA desaturase by polyunsaturated fatty acids and cholesterol. *Journal of Lipid Research*. 40 (9), pp. 1549-1558.

O'Connor, S., McCaffrey, N., Whyte, E., Moran, K., and Lacey, P. (2019) Nonsteroidal anti-inflammatory drug use, knowledge, and behaviors around their use and misuse in Irish collegiate student-athletes. *The Physician and Sports Medicine*. 47 (3), pp. 318-322.

Perrone, M.G., Centonze, A., Miciaccia, M., Ferorelli, S., and Scilimati, A. (2020) Cyclooxygenase Inhibition Safety and Efficacy in Inflammation-Based Psychiatric Disorders. *Molecules (Basel, Switzerland)*. 25 (22), 5388.

Peters, S.J., Samjoo, I.A., Devries, M.C., Stevic, I., Robertshaw, H.A., and Tarnopolsky, M.A. (2012) Perilipin family (PLIN) proteins in human skeletal muscle: the effect of sex, obesity, and endurance training. *Applied physiology*,

nutrition, and metabolism = Physiologie appliquee, nutrition et metabolisme. 37 (4), pp. 724-735.

Popov, D.V., Lysenko, E.A., Makhnovskii, P.A., Kurochkina, N.S., and Vinogradova, O.L. (2017) Regulation of *PPARGC1A* gene expression in trained and untrained human skeletal muscle. *Physiological Reports.* 5 (23), e13543.

Porter, C., Constantin-Teodosiu, D., Constantin, D., Leighton, B., Poucher, S.M., and Greenhaff, P.L. (2017) Muscle carnitine availability plays a central role in regulating fuel metabolism in the rodent. *The Journal of Physiology.* 595 (17), pp. 5765-5780.

Porter, C., Reidy, P.T., Bhattarai, N., Sidossis, L.S., and Rasmussen, B.B. (2015) Resistance Exercise Training Alters Mitochondrial Function in Human Skeletal Muscle. *Medicine and Science in Sports and Exercise.* 47 (9), pp. 1922-1931.

Pucer, A., Brglez, V., Payré, C., Pungercar, J., Lambeau, G., and Petan, T. (2013) Group X secreted phospholipase A(2) induces lipid droplet formation and prolongs breast cancer cell survival. *Molecular Cancer.* 12 (1), 111.

Radak, Z., Suzuki, K., Posa, A., Petrovszky, Z., Koltai, E., and Boldogh, I. (2020) The systemic role of SIRT1 in exercise mediated adaptation. *Redox Biology.* 35, 101467.

Ramos-Inza, S., Ruberte, A.C., Sanmartín, C., Sharma, A.K. and Plano, D. (2021) NSAIDs: Old Acquaintance in the Pipeline for Cancer Treatment and Prevention—Structural Modulation, Mechanisms of Action, and Bright Future. *Journal of Medicinal Chemistry.* 64 (22), pp. 16380-16421.

Ricciotti, E., and FitzGerald, G.A. (2011) Prostaglandins and inflammation. *Arteriosclerosis, Thrombosis, And Vascular Biology.* 31 (5), pp. 986-1000.

Rissanen, T.T., Markkanen, J.E., Gruchala, M., Heikura, T., Puranen, A., Kettunen, M. I., Kholová, I., Kauppinen, R. A., Achen, M. G., Stacker, S. A., Alitalo, K., and Ylä-Herttuala, S. (2003) VEGF-D is the strongest angiogenic

and lymphangiogenic effector among VEGFs delivered into skeletal muscle via adenoviruses. *Circulation Research*. 92 (10), pp. 1098-1106.

Rodgers, J.T., Lerin, C., Haas, W., Gygi, S.P., Spiegelman, B.M., and Puigserver, P. (2005) Nutrient control of glucose homeostasis through a complex of PGC-1alpha and SIRT1. *Nature*. 434 (7029), pp. 113-118.

Sallmann, A.R. (1986) The history of diclofenac. *The American Journal of Medicine*. 80 (4B), pp. 29-33.

Shepherd, S.O., Cocks, M., Tipton, K.D., Ranasinghe, A.M., Barker, T.A., Burniston, J.G., Wagenmakers, A.J. and Shaw, C.S. (2013) Sprint interval and traditional endurance training increase net intramuscular triglyceride breakdown and expression of perilipin 2 and 5. *The Journal of Physiology*. 591 (3), pp. 657-675.

Silver, N., Best, S., Jiang, J., and Thein, S.L. (2006) Selection of housekeeping genes for gene expression studies in human reticulocytes using real-time PCR. *BMC Molecular Biology*. 7, 33.

Silverstein, F.E., Faich, G., Goldstein, J.L., Simon, L.S., Pincus, T., Whelton, A., Makuch, R., Eisen, G., Agrawal, N.M., Stenson, W.F., Burr, A.M., Zhao, W.W., Kent, J.D., Lefkowitz, J.B., Verburg, K.M., and Geis, G.S. (2000) Gastrointestinal toxicity with celecoxib vs nonsteroidal anti-inflammatory drugs for osteoarthritis and rheumatoid arthritis: the CLASS study: A randomized controlled trial. Celecoxib Long-term Arthritis Safety Study. *JAMA*. 284 (10), pp. 1247-1255.

Simmons, D.L., Wagner, D., and Westover, K. (2000) Nonsteroidal anti-inflammatory drugs, acetaminophen, cyclooxygenase 2, and fever. *Clinical Infectious Diseases: An Official Publication of The Infectious Diseases Society of America*. 31 (Suppl. 5), pp, S211-S218.

Sirois, J., Sayasith, K., Brown, K.A., Stock, A.E., Bouchard, N., and Doré, M. (2004) Cyclooxygenase-2 and its role in ovulation: a 2004 account. *Human Reproduction Update*. 10 (5), pp. 373-385.

- Škarabot, J., Brownstein, C.G., Casolo, A., Del Vecchio, A., and Ansdell, P. (2021) The knowns and unknowns of neural adaptations to resistance training. *European Journal of Applied Physiology*. 121 (3), pp. 675-685.
- Sugano, K., Matsumoto, Y., Itabashi, T., Abe, S., Sakaki, N., Ashida, K., Mizokami, Y., Chiba, T., Matsui, S., Kanto, T., Shimada, K., Uchiyama, S., Uemura, N., and Hiramatsu, N. (2011) Lansoprazole for secondary prevention of gastric or duodenal ulcers associated with long-term low-dose aspirin therapy: results of a prospective, multicenter, double-blind, randomized, double-dummy, active-controlled trial. *Journal of Gastroenterology*. 46 (6), pp. 724-735.
- Supruniuk, E., Mikłosz, A., and Chabowski, A. (2017) The Implication of PGC-1 α on Fatty Acid Transport across Plasma and Mitochondrial Membranes in the Insulin Sensitive Tissues. *Frontiers in Physiology*. 8, p. 923.
- Tarnopolsky, M.A., Rennie, C.D., Robertshaw, H.A., Fedak-Tarnopolsky, S.N., Devries, M.C., and Hamadeh, M.J. (2007) Influence of endurance exercise training and sex on intramyocellular lipid and mitochondrial ultrastructure, substrate use, and mitochondrial enzyme activity. *American journal of physiology. Regulatory, integrative and comparative physiology*. 292 (3), pp. R1271-R1278.
- Tiwari, S., Mishra, M., Salemi, M.R., Phinney, B.S., Newens, J.L., and Gomes, A.V. (2020) Gender-specific changes in energy metabolism and protein degradation as major pathways affected in livers of mice treated with ibuprofen. *Scientific Reports*. 10 (1), 3386.
- Tontonoz, P., Graves, R.A., Budavari, A.I., Erdjument-Bromage, H., Lui, M., Hu, E., Tempst, P., and Spiegelman, B.M. (1994) Adipocyte-specific transcription factor ARF6 is a heterodimeric complex of two nuclear hormone receptors, PPAR gamma and RXR alpha. *Nucleic Acids Research*. 22 (25), pp. 5628-5634.
- van der Donk, W.A., Tsai, A.L., and Kulmacz, R.J. (2002) The cyclooxygenase reaction mechanism. *Biochemistry*. 41 (52), pp. 15451-15458.

- van Loon, L.J., Koopman, R., Stegen, J.H., Wagenmakers, A.J., Keizer, H.A., and Saris, W.H. (2003) Intramyocellular lipids form an important substrate source during moderate intensity exercise in endurance-trained males in a fasted state. *The Journal of physiology*. 553 (Pt 2), pp. 611-625.
- Vamecq, J., and Latruffe, N. (1999) Medical significance of peroxisome proliferator-activated receptors. *Lancet*. 354 (9173), pp. 141-148.
- Vane, J.R. (1971) Inhibition of prostaglandin synthesis as a mechanism of action for aspirin-like drugs. *Nature: New Biology*. 231 (25), pp. 232-235.
- Vane, J.R. and Botting, R.M. (1995) New insights into the mode of action of anti-inflammatory drugs. *Inflammation Research: Official Journal of The European Histamine Research Society*. 44 (1), pp. 1-10.
- Vane, J.R., Bakhle, Y.S., and Botting, R.M. (1998) Cyclooxygenases 1 and 2. *Annual Review of Pharmacology and Toxicology*. 38, pp. 97-120.
- Vaso, M., Weber, A., Tscholl, P.M., Junge, A. and Dvorak, J. (2015) Use and abuse of medication during 2014 FIFA World Cup Brazil: a retrospective survey. *BMJ Open*. 5 (9), e007608.
- Wagner, P.D. (2011) The critical role of VEGF in skeletal muscle angiogenesis and blood flow. *Biochemical Society Transactions*. 39 (6), pp. 1556-1559.
- Wallace, J.L. (2008) Prostaglandins, NSAIDs, and gastric mucosal protection: why doesn't the stomach digest itself?. *Physiological Reviews*. 88 (4), pp. 1547-1565.
- Wang, H., Bell, M., Sreenivasan, U., Sreenevasan, U., Hu, H., Liu, J., Dalen, K., Londos, C., Yamaguchi, T., Rizzo, M.A., Coleman, R., Gong, D., Brasaemle, D., and Sztalryd, C. (2011) Unique regulation of adipose triglyceride lipase (ATGL) by perilipin 5, a lipid droplet-associated protein. *The Journal of Biological Chemistry*. 286 (18), pp. 15707-15715.
- Warden, S.J. (2009) Prophylactic misuse and recommended use of non-steroidal anti-inflammatory drugs by athletes. *British Journal of Sports Medicine*. 43 (8), pp. 548-549.

Wolins, N.E., Quaynor, B.K., Skinner, J.R., Tzekov, A., Croce, M.A., Gropler, M.C., Varma, V., Yao-Borengasser, A., Rasouli, N., Kern, P.A., Finck, B.N. and Bickel, P.E. (2006) OXPAT/PAT-1 is a PPAR-induced lipid droplet protein that promotes fatty acid utilization. *Diabetes*. 55 (12), pp. 3418-3428.

Yamazaki, R., Kusunoki, N., Matsuzaki, T., Hashimoto, S., and Kawai, S. (2002) Nonsteroidal anti-inflammatory drugs induce apoptosis in association with activation of peroxisome proliferator-activated receptor gamma in rheumatoid synovial cells. *The Journal of Pharmacology and Experimental Therapeutics*. 302 (1), pp. 18-25.

Yao-Borengasser, A., Rassouli, N., Varma, V., Bodles, A.M., Rasouli, N., Unal, R., Phanavanh, B., Ranganathan, G., McGehee, R.E., Jr, and Kern, P.A. (2008) Stearoyl-coenzyme A desaturase 1 gene expression increases after pioglitazone treatment and is associated with peroxisomal proliferator-activated receptor-gamma responsiveness. *The Journal of Clinical Endocrinology and Metabolism*. 93 (11), pp. 4431-4439.

Yokoyama, C. and Tanabe, T. (1989) Cloning of human gene encoding prostaglandin endoperoxide synthase and primary structure of the enzyme. *Biochemical and Biophysical Research Communications*. 165 (2), pp. 888-894.

Zhang, J., Tang, H., Zhang, Y., Deng, R., Shao, L., Liu, Y., Li, F., Wang, X., and Zhou, L. (2014) Identification of suitable reference genes for quantitative RT-PCR during 3T3-L1 adipocyte differentiation. *International Journal of Molecular Medicine*. 33 (5), pp. 1209-1218.

Zhu, R., Wen, C., Li, J., Harris, M.B., Liu, Y.Y., and Kuo, C.H. (2015) Lipid storage changes in human skeletal muscle during detraining. *Frontiers in Physiology*. 6, 309.

6. General Discussion

6.1 Thesis Overview

Skeletal muscle is the main site for the insulin-mediated disposal of glucose (Wasserman, 2009; DeFronzo and Tripathy, 2009) and oxidation of IMCL-derived FAs provides the majority of energy for muscle at rest and during low-moderate intensity exercise (van Loon, 2004a; Gemmink, Schrauwen, and Hesselink, 2020). Though there has been an exponential increase in research concerning the structure, function, and localisation of LDs in skeletal muscle, which compose the bulk of IMCL, the role of IMCL in the integration of fuel metabolism under physiological stress and pathophysiology remains poorly understood. The work presented in this thesis endeavoured to advance our understanding of the role of IMCL in metabolic adaptation to acute and chronic immobilisation and exercise intervention, and in the insulin resistance characteristic of NAFLD.

6.1.1 Role of IMCL in Physiological Adaptations to Inactivity

Several streams of evidence published in the late 1990s contributed to the identification of a strong association between IMCL content, determined histochemically (Phillips *et al.*, 1996), biochemically (Pan *et al.*, 1997), and using ¹H-MRS (Krssak *et al.*, 1999), and impairments in whole-body insulin sensitivity. It has since been proposed that inactivity-induced reductions in skeletal muscle FA oxidation may lead to the accumulation of IMCL and that this accumulation contributes to the development of the insulin resistance observed following bed rest (Blanc *et al.*, 2000a; Bilet *et al.*, 2020). However, as highlighted by Bergouignan and colleagues, historically, one of the major challenges in establishing a cause-and-effect relationship between physical inactivity, IMCL accumulation, the development of whole-body insulin resistance, and other metabolic dysfunctions associated with diseases like T2DM, has been maintaining participants in energy balance, particularly during chronic interventions (Bergouignan *et al.*, 2011). Many bed rest studies report findings in participants that were in positive energy balance for the duration of the bed rest intervention or neglect to discuss if and how energy balance was

maintained (Mikines *et al.*, 1989; Dolkas and Greenleaf, 1997; Blanc *et al.*, 2000b; Hamburg *et al.*, 2007). This has left a gap in our understanding of whether inactivity per se alters IMCL content. Therefore, **Chapter 3** aimed to determine whether IMCL content changed during acute (3 days) and chronic (56 days) bed rest when the energy intake of the participants was decreased to 1.2xRMR to account for the decreased energy expenditure during the bed rest period and to strictly maintain energy balance. By concurrently measuring whole-body glucose disposal in these studies, the existence of an association between IMCL content and bed rest-induced whole-body insulin resistance was investigated. This was done to determine if an association exists between changes in IMCL content and changes in whole-body glucose disposal in this context. Another aim was to determine whether IMCL content changes in response to exercise remobilisation post bed rest and if these changes are associated with any exercise-induced increase in whole-body glucose disposal. Indirect calorimetry was also used to quantify changes in basal and insulin-mediated fuel oxidation before and after bed rest.

The main novel findings were that IMCL content in the healthy male participants maintained in energy balance was unchanged following both 3 and 56 days of bed rest. In addition, whole-body glucose disposal was reduced at the post bed rest time points in both studies but restored to baseline levels by 4 days of exercise remobilisation in the 3-day bed rest study. Therefore, bed rest-induced insulin resistance was dissociated from IMCL content. Participants in the chronic bed rest study also became metabolically inflexible, with the insulin-mediated suppression of fat oxidation during the hyperinsulinaemic-euglycaemic clamp being blunted following 56 days of bed rest.

Taken together the results presented in **Chapter 3** naturally raise an important question. If immobilisation does not increase IMCL content, thereby potentially generating lipotoxic intermediates that antagonise the canonical insulin signalling pathway as postulated by some authors (see **Section 1.5**), what are the mechanisms by which immobilisation induces whole-body insulin resistance, and so rapidly? The work presented here establishes that 3 days of bed rest is sufficient to induce whole-body insulin resistance. It has been

reported that just 24 hours of forearm casting induces a precipitous decline in forearm glucose uptake in the immobilised limb (Burns *et al.*, 2021). This finding demonstrated that immobilisation-induced reductions in glucose disposal at the skeletal muscle level are rapid and likely precede reductions in the protein expression of GLUT4 and hexokinase, and the decreased muscle Akt phosphorylation, observed after 7 days of bed rest when whole-body insulin resistance has developed (Biensø *et al.*, 2012; Dirks *et al.*, 2016). Previous studies have found that glucose disposal at the whole-body level and the muscle mRNA expression of GLUT4 and other key components of the insulin-mediated glucose uptake pathway are unchanged following 24 hours (Dirks *et al.*, 2018) and 2 days of bed rest (Duran-Valdez *et al.*, 2008). Muscle glucose disposal was not measured here or in the aforementioned 24 hours and 2-day bed rest studies, but it is reasonable to conclude from the available evidence that decrements in muscle glucose disposal during bed rest precede the development of whole-body insulin resistance at 3 days (Mikines *et al.*, 1991; Burns *et al.*, 2021).

Therefore, insulin resistance in the context of immobilisation is almost certainly initiated by the attenuation of the contraction-mediated glucose uptake pathway (see **Section 1.3.2**), given that muscular contractions increase the expression of genes involved in glucose uptake (Verbrugge *et al.*, 2022), promote the increased expression and translocation of GLUT4 to the sarcolemma independent of insulin (Lund *et al.*, 1995), and sensitise the skeletal muscle to the action of insulin (Bergouignan *et al.*, 2016). This is supported by evidence that participants who perform structured resistance exercise on non-consecutive days concurrent with bed rest are completely protected from immobilisation-induced decrements in whole-body glucose disposal (Kenny *et al.*, 2017). Still the precise mechanisms underpinning this potential association between contraction-mediated glucose uptake and skeletal muscle and whole-body insulin resistance require elucidation.

6.1.2 Role of IMCL Content in the Insulin Resistance Observed in NAFLD

There are few studies in the literature that measure IMCL content in humans with NAFLD (Pugh *et al.*, 2014; Oh *et al.*, 2014; Oshida *et al.*, 2019) and, as of writing, none which compare IMCL content between those with NAFLD and young healthy controls. Indeed, differences in the association between IMCL content and measures of skeletal muscle and whole-body glucose disposal in these groups remain unexplored.

Thiazolidinediones, potent insulin sensitisers that act as modulators of PPAR- γ , are often used in the prevention and treatment of NAFLD (Chang, Park, and Park, 2013) and in the amelioration of the symptoms observed in NASH (He *et al.*, 2016). They function by decreasing lipolysis (Miyazaki *et al.*, 2002), reducing muscle LCFA content (DeFronzo, 2010), and promoting the redistribution of FA stored in IMCL and IHTG to subcutaneous stores (Mayerson *et al.*, 2002), thereby improving both muscle, liver, and whole-body insulin sensitivity. Indeed, Thiazolidinedione-induced reductions in muscle LCFA content are strongly associated with improved whole-body glucose disposal (Bajaj *et al.*, 2010) and muscle forms part of an axis with the liver and adipose tissue that controls responses to changes in plasma FA availability caused by overfeeding, a major contributor to the aetiology of NAFLD. Therefore, it is reasonable to hypothesise that IMCL content is elevated in those with NAFLD relative to healthy individuals and that IMCL contributes to the development of the insulin resistance commonly observed in this disease. **Chapter 4** aimed to test this hypothesis by measuring IMCL content, skeletal muscle glucose disposal, and whole-body glucose disposal in young, healthy, male, control participants and in a group of participants with NAFLD. The main findings were that IMCL content was not different between the two groups and that whilst the NAFLD participants presented with both skeletal muscle and whole-body insulin resistance the control participants did not. These findings suggest, for the first time, that IMCL accumulation is not necessarily a feature of NAFLD and does not contribute to the development of insulin resistance in this disease.

For the NAFLD participants described in **Chapter 4**, the observed muscle insulin resistance may have resulted from habitual sedentary behaviour (Crocì *et al.*, 2019). The whole-body insulin resistance could have resulted from a combination of this sedentarism and increased plasma FA availability from visceral adipose tissue lipolysis, which primarily affects the liver (van der Poorten *et al.*, 2008), and chronic overfeeding (Machado *et al.*, 2012).

6.1.3 Effect of Chronic Resistance Exercise and Diclofenac on IMCL Content and Muscle Fuel Oxidation

Few studies investigate the effect of resistance exercise training on IMCL and muscle PLIN content, and none have investigated the effect of chronic resistance exercise on IMCL and PLIN content in trained human males. Therefore, the first aim of the work presented in **Chapter 5** was to investigate the effect of 12 weeks resistance exercise training, by maximal isokinetic concentric knee extensions, on IMCL and PLIN5 content in young, healthy, trained males. The secondary aim was centred around the use of diclofenac concurrent with resistance exercise in this population. Diclofenac is an NSAID that preferentially inhibits COX-2 and is often used off-label as a performance enabling drug by elite athletes and non-athletes (Sallmann, 1986; Brennan *et al.*, 2021). It has been shown in previous reports that diclofenac has great affinity for PPAR- γ , one of the key regulators of muscle fuel metabolism and a potent promoter of FA oxidation (Adamson *et al.*, 2002). However, this interaction between diclofenac and PPAR- γ in humans has gone completely unexplored generally and within the context in which diclofenac is often used, exercise. Thus, the secondary aim was to investigate the effect of 75 mg/day diclofenac administration concurrent with chronic resistance exercise on the muscle mRNA expression of genes which control lipid metabolism.

The main finding of this work was that IMCL content was unchanged following 84 days of resistance exercise in young, trained males. A previous study has reported that IMCL content was increased by 72%, per $^1\text{H-MRS}$ imaging of the vastus lateralis, in the legs of 8 young, lean, male participants that were untrained at baseline following 28 days of unilateral leg extensions (Zhu *et al.*, 2015). The participants in the study described in **Chapter 5** were

well-trained at baseline and already had LD count, LD size, and IMCL content characteristic of training adaptation (see **Appendix C**). This perhaps explains why IMCL content did not change in these participants following 84 days of resistance exercise. In addition, it was found that diclofenac administration altered the muscle mRNA abundance of genes associated with lipid metabolism. Consolidation of these mRNA abundance changes and analysis by IPA revealed predictions of robust, consistent, diclofenac-induced activation of cellular events associated with lipid metabolism from 24 hours after the start of the exercise intervention through till the end at 84 days. In stark contrast, at 84 days in the control group that did not receive diclofenac, cellular events associated with lipid metabolism were predicted to be inhibited. These data provide the first indication that alongside its well characterised inhibition of COX enzymes, diclofenac also binds to and activates PPAR- γ in humans.

IMCL accumulation is typically a sign of lipid overspill from the adipose tissue and is well associated with obesity, T2DM and the metabolic dysfunctions associated with these states, including whole-body and skeletal muscle insulin resistance (Van Loon *et al.*, 2004b; Ingram *et al.*, 2011). Commonality amongst the chapters in this thesis exists in the fact that IMCL content did not change in response to bed rest and exercise and was no different in healthy individuals compared to those with NAFLD. There is mounting evidence in this field of research that absolute IMCL content alone is not the most accurate predictor of muscle and whole-body insulin resistance in non-athletes (Barrett *et al.*, 2022). Instead, the field is pivoting towards the measurement of IMCL turnover rates, which have been shown to be highest in athletes and lowest in obese individuals with diabetes (Perreault *et al.*, 2010; Bergman *et al.*, 2018), and of muscle DAG and ceramide species content (Chow *et al.*, 2014).

6.2 Considerations Emerging from This Work

From reflections upon the work presented in this thesis, several considerations concerning the methodologies and study protocols arise which will be used to inform future work.

Central to the findings presented herein were results generated from histochemical staining of muscle biopsies with Bodipy 493/503 and from the determination of whole-body glucose disposal using the hyperinsulinaemic-euglycaemic clamp technique. The Bodipy 493/503 method has the unique advantage of allowing for the identification of muscle fibre types and the stratification of IMCL content by these fibre-types. Also, other methods for IMCL quantification have noteworthy disadvantages. Electron microscopy only allows for the analysis of microsegments of muscle, not the hundreds of fibres viewable with confocal microscopy, the quantification of total muscle TAG content using biochemical methods is confounded by intra-individual variations in tissue adiposity, and in magnetic resonance methodologies the EMCL resonance peaks can contaminate the IMCL response peaks (see **Section 2.7**) (Schrauwen-Hinderling *et al.*, 2006). Even so it is important to note that the methods used in this study cannot rule out the involvement of lipotoxic lipid species, principally DAGs and ceramides, in the development of inactivity-induced muscle and whole-body insulin resistance or in the pathological IHTG accumulation in NAFLD.

To the best knowledge of the present author no reports have been published on the effects of chronic resistance exercise training on IMCL content in healthy, young, sedentary males. What research does exist in the literature focuses on a single bout of resistance exercise in the aforementioned population (Koopman *et al.*, 2006; Tsintzas *et al.*, 2017) or on the overweight elderly (Bucci *et al.*, 2016). Also, as aforementioned, one study reports increased IMCL content in response to 28 days of resistance exercise training in a cohort of healthy young males that were sedentary at baseline (Zhu *et al.*, 2015). As detailed in **Section 5.6** the participants presented with LD parameters that are characteristic of the trained phenotype (see **Appendix C**). Therefore, future work should include untrained participants to discern whether chronic resistance exercise impacts on IMCL content in untrained individuals.

It is not possible to detangle the effects of ambulation and resistance exercise on the restoration of whole-body glucose disposal following the 3 days bed rest period detailed in **Chapter 3**. The effects of bed rest on metabolic health are more widely studied than the restoration of skeletal

muscle and whole-body glucose uptake following bed rest. A 21-day bed rest study of 7 young men found that participants required between 5-14 days to regain their baseline glucose tolerance, as determined by OGTT, during recovery periods in which there was no structured exercise, only the resumption of ambulation (Heer *et al.*, 2014). However, in that study the effects of exercise in the restoration of glucose disposal following bed rest were not assessed.

Lastly, the muscle sections cut for histochemical staining were transverse sections with muscle fascicles and fibres clearly visible during imaging. A limitation of the retrospective analyses performed here was using samples for histochemistry collected by others. Ease of cutting these samples depended upon their size and, more importantly, their orientation in the OCT compound before they were mounted and frozen in liquid nitrogen. Where a sample is small, only 20 ± 5 fibres can be analysed. Where the orientation of the muscle sample is incorrect such that cutting initially produces longitudinal sections, the sample must be reorientated within the cryostat which may damage it, and which results in excess loss of tissue to ensure that appropriate sections are collected. Some samples yielded by the participants were too small or orientated incorrectly after collection, making them unsuitable for histochemical analysis in the worst cases. It must be noted that the muscle biopsies were also needed for metabolite and muscle mRNA analyses as well as the histochemical analyses that formed the core of this thesis. The multiple demands on tissue availability were a major factor in the size of the biopsies available for histochemical analysis.

6.3 Future Directions

6.3.1 Impact of Inactivity with Overfeeding on Fibre-Type Specific IMCL Content and Lipotoxic Intermediates

To add to the conclusion reached in **Chapter 3**, that inactivity per se does not cause IMCL accumulation, further work is required. This could take the form of another chronic bed rest study in which, rather than being maintained in energy balance for the duration of the bed rest period, participants would be maintained in a state of positive energy balance which would presumably increase IMCL content. There is little in the way of studies that have purposefully increased energy intake in this way, with a one-day bed rest study reporting no changes in muscle insulin sensitivity with overfeeding (Dirks *et al.*, 2018), and none that have done so with the measurement of IMCL content. To elucidate the mechanisms via which potential increases in IMCL content during bed rest with overfeeding could contribute to impaired skeletal muscle glucose disposal, the DAG and ceramide content of muscle biopsies must be measured. As discussed in **Section 1.5.4** the myocellular localisation of these lipotoxic intermediates serves as a marker of their functional activation (Szendroedi *et al.*, 2014; Perreault *et al.*, 2018). Therefore, not only total DAG and ceramide content but sarcolemmal and cytosolic-specific DAG and ceramide content.

Any future work concerning bed rest with overfeeding could also consider the work of Stettler and his colleagues who showed that macronutrient composition is a major determinant of changes in IMCL content and insulin-mediated glucose disposal during bed rest, even when energy balance is maintained (Stettler *et al.*, 2005). They conducted a crossover study of 8 healthy, young males with three arms, each lasting 60 hours: (1) Bed rest with high-fat feeding (45% of total macronutrient diet composition), (2) Bed rest with high-carbohydrate feeding (70% of total macronutrient diet composition) and (3) High-fat feeding concurrent with ambulation and moderate exercise. For reference, macronutrient composition of the meals provided to the participants of the bed rest studies described in **Chapter 3** was 50-60% carbohydrates,

~30% fat and ~15% protein. Stettler and colleagues found that high-fat feeding, under conditions of energy balance, decreased insulin-mediated whole-body glucose disposal by a mean of 24% relative to baseline but that high-carbohydrate feeding did not. Interestingly both high-fat and high-carbohydrate feeding increased IMCL content as measured by ¹H-MRS by 32% and 17%, respectively, and IMCL content was also increased during the high-fat feeding concurrent with exercise arm. Future work, using histochemical determination of IMCL content and muscle fibre-type will allow for the identification of fibre-type specific changes in IMCL content in response to bed rest with overfeeding. Distinction by fibre type is of great relevance given that Type I muscle fibres have a greater capacity for glucose uptake as evidenced by their higher protein expression of insulin receptor, GLUT4, PDH, and GS (Albers *et al.*, 2015) and because the content of IMCL in Type I fibres alone has been correlated with insulin resistance (Coen *et al.*, 2010). This would also allow for the determination of fibre type specific changes in LD count and size, with increases in LD size in Type I fibres being associated with inactivity-induced insulin resistance (Coen *et al.*, 2010; Dirks *et al.*, 2016).

Given that walking constitutes a significant proportion of AEE amongst the general population (Farrell *et al.*, 2014; Harris *et al.*, 2019) this follow up study could also be conducted using a reduced step count model. Meta-analyses of physical activity studies report that healthy adults typically walk at least 7-8,000 steps daily at a pace of 2.5 mph or greater (Tudor-Locke *et al.*, 2011), which constitutes mild-to-vigorous physical activity (Zheng *et al.*, 2022). Hence the common recommendation for adults is to walk at least 10,000 steps per day to reduce their relative risk of cardiovascular disease, dysglycaemia, and all-cause mortality (Hall *et al.*, 2020). Previous work in young and older healthy participants has demonstrated that reducing participant daily step count by $\geq 75\%$ relative to their habitual step count or lowering step count to a maximum of around 1,500 steps per day can reduce insulin sensitivity, as evidenced by attenuated whole-body glucose disposal rates (Krogh-Madsen *et al.*, 2010; Dwyer *et al.*, 2011; Knudsen *et al.*, 2012; Reidy *et al.*, 2018; Sjöros *et al.*, 2020). As detailed elsewhere these reduced step count models are representative of real world sedentarism than bed rest (Perkin *et al.*, 2016).

Thus, future work could involve taking two groups of young, healthy participants matched in anthropometric characteristics and reducing their daily step counts by 75-90% relative to their habitual activity for 7 days, the boundary for acute inactivity as discussed in **Chapter 3**. One group would have their daily energy intake matched to their reduced energy expenditure, measured by hip-worn accelerometers (see **Section 2.4**), to maintain energy balance whilst the other would have their daily energy intake increased to overfeeding. This initial intervention would be followed by a washout period and crossover of the participants. Muscle biopsies would be obtained and the hyperinsulinaemic-euglycaemic clamp technique would be performed on all participants at baseline and at the end of each intervention period to measure muscle lipid content and whole-body glucose disposal. The aim would be to determine if overfeeding in conjunction with reducing step count increased participant IMCL content and if this increased IMCL content exacerbated the attenuation of whole-body glucose disposal observed when participants were reducing their step count whilst in energy balance.

6.3.2 Does Chronic Diclofenac Administration Alter Skeletal Muscle Fuel Oxidation at Rest and in Response to Exercise?

The work presented in **Chapter 5** identified diclofenac-induced increases in the mRNA abundance of lipid metabolism genes, but whether these changes in mRNA expression translate to changes in metabolic physiology could not be determined. Critical to future work in this area will be determining if chronic administration of diclofenac does in fact alter whole-body fuel oxidation in humans, given the IPA predictions of robustly increased FA oxidation. This would require the use of indirect calorimetry to measure the pulmonary gas exchange, VO_2 consumption and VCO_2 production, of study participants as detailed in **Section 2.3**. Indirect calorimetry alone cannot distinguish between the oxidation of intracellular, LD-derived, FAs and the oxidation of FAs taken up from the plasma. This is an important distinction that could provide insight into whether diclofenac increases FA mobilisation from LDs or increases FA uptake by myocytes or both, given that the mRNA abundance of both FA transporter genes and genes involved in LD function are increased by the

NSAID (See **Appendix B**). Making this distinction would require the continuous infusion of ^{13}C -labelled palmitate and $^2\text{H}_2$ -labelled glucose tracers concurrent with indirect calorimetry measures as previously described (Van Loon *et al.*, 2001). As the ^{13}C -labelled palmitate tracer is oxidised, the rate at which ^{13}C appears in the expired air of the participants increases. The enrichment of expired air with these labelled isotopes can be measured as a ratio of ^{13}C to ^{12}C using gas chromatography, mass spectrometry (Patterson, 1997). Also, blood sampling during the infusion would be performed to measure the rate of appearance and disappearance of these isotope-labelled tracers (Magkos and Mittendorfer, 2009). These measurements would be made both at rest and during resistance or endurance exercise when muscle fuel oxidation is altered (see **Section 1.4**).

In addition, the establishment of a causal relationship between diclofenac administration, activation of PPAR- γ and PGC-1 α , and the increased transcription of the host of genes involved in the regulation of FA oxidation detailed in **Chapter 5** and **Appendix A and B** fundamentally depends upon the identification of concomitant changes in muscle protein expression and activation. In future work protein expression would be determined by immunoblotting for PPAR- γ and PPAR- δ (Loviscach *et al.*, 2000), PGC-1 α and its main targets described in **Chapters 1 and 5** (Silvennoinen *et al.*, 2015), and for FOXO and PDK (Chien, Greenhaff, and Constantin-Teodosiu, 2020), analyses that have been performed previously in human skeletal muscle. PPAR- δ mRNA expression and protein expression should also be measured given that PPAR- δ has a greater role in skeletal muscle fuel selection than PPAR- γ , which is an important effector not just in skeletal muscle as detailed in this thesis but also in adipocytes (Crossland, Constantin-Teodosiu, and Greenhaff, 2021).

Use of isolated muscle from participant biopsies for primary cell culture should also be considered. Part of the hypothesis presented here for future work is that diclofenac acts as an agonist of PPAR- γ in human skeletal muscle, a function which until the work presented in this thesis had not been postulated. Diclofenac has great affinity for PPAR- γ in vitro in DU-145 human prostate cancer cells (Adamson *et al.*, 2002), rheumatoid synovial cells (Yamazaki *et*

al., 2002) and others (Kojo *et al.*, 2003), but the affinity of diclofenac for PPAR- γ in human skeletal muscle in vitro and the resultant cellular changes of this interaction remain unexplored. Thus, future work should include an element in which diclofenac, 15-deoxy- Δ 12,14-prostaglandin J2, the endogenous PPAR- γ ligand (Li, Guo, and Wu, 2019), and rosiglitazone, the most extensively studied PPAR- γ agonist (Lecka-Czernik *et al.*, 2007), are administered to human muscle cell lines and the relative affinity of these agonists for PPAR- γ is directly compared. In this vein it is important to note that diclofenac is a member of the propionic acid-derived NSAIDs chemical group alongside indomethacin and ibuprofen (Bushra and Aslam, 2010). It is reasonable to speculate that the structural properties which may allow diclofenac to interact with PPAR- γ in skeletal muscle may be common to all drugs within that class. Indeed, it has been demonstrated in DU-145 cells that indomethacin also has binding affinity for PPAR- γ (Adamson *et al.*, 2002). An investigation of the affinity of propionic acid-derived NSAIDs for skeletal muscle PPAR- γ and the chemical properties that allow for this binding would greatly expand upon our understanding of NSAID function.

6.3.3 Lipotoxic Intermediates Content in the Skeletal Muscles of individuals with NAFLD

In the hepatocytes of individuals with obese NAFLD, like those described in **Chapter 4**, the content of several DAG species is positively correlated with insulin resistance as determined by the Homeostatic Model Assessment for Insulin Resistance (HOMA-IR) (Magkos *et al.*, 2012; Luukkonen *et al.*, 2016). Indeed, a study by Kumashiro and colleagues identified cytoplasmic DAG concentration in hepatocytes as the variable with the greatest association with insulin resistance in those with NAFLD (Kumashiro *et al.*, 2011). The connection between ceramides and the development of hepatic and whole-body insulin resistance in NAFLD is tenuous, with conflicting data generated principally from rodent models (Petersen and Shulman, 2017). To the best knowledge of the present author, muscle and liver DAG and ceramide content have not both been measured concurrently in humans with NAFLD, only in rodent models of NAFLD (Perry *et al.*, 2013; Perry *et al.*, 2015). The participants with obese NAFLD described in **Chapter 4** presented with skeletal

muscle insulin resistance. Given the aforementioned accumulation of lipotoxic species in hepatocytes in this phenotype and the fact that skeletal muscle DAG and ceramide concentrations are typically elevated in obese individuals, there may be differences in abundance at the level of these intermediates between healthy individuals and those with NAFLD that went undetected here. Thus, future work in this area should measure the content of DAG and ceramide species localised to the sarcoplasm and sarcolemma in those with NAFLD and in healthy controls.

6.4 References

- Adamson, D.J., Frew, D., Tatoud, R., Wolf, C.R., and Palmer, C.N. (2002) Diclofenac antagonizes peroxisome proliferator-activated receptor-gamma signaling. *Molecular Pharmacology*. 61 (1), 7-12.
- Albers, P.H., Pedersen, A.J., Birk, J.B., Kristensen, D.E., Vind, B.F., Baba, O., Nøhr, J., Højlund, K., and Wojtaszewski, J.F. (2015) Human muscle fiber type-specific insulin signaling: impact of obesity and type 2 diabetes. *Diabetes*. 64 (2), pp. 485-497.
- Bajaj, M., Baig, R., Suraamornkul, S., Hardies, L.J., Coletta, D.K., Cline, G.W., Monroy, A., Koul, S., Sriwijitkamol, A., Musi, N., Shulman, G.I., and DeFronzo, R.A. (2010). Effects of pioglitazone on intramyocellular fat metabolism in patients with type 2 diabetes mellitus. *The Journal of Clinical Endocrinology and Metabolism*. 95 (4), pp. 1916-1923.
- Bergouignan, A., Rudwill, F., Simon, C., and Blanc, S. (2011) Physical inactivity as the culprit of metabolic inflexibility: evidence from bed-rest studies. *Journal of Applied Physiology (Bethesda, Md.: 1985)*. 111 (4), pp. 1201-1210.
- Bergouignan, A., Latouche, C., Heywood, S., Grace, M.S., Reddy-Luthmoodoo, M., Natoli, A.K., Owen, N., Dunstan, D.W., and Kingwell, B.A. (2016) Frequent interruptions of sedentary time modulates contraction- and insulin-stimulated glucose uptake pathways in muscle: Ancillary analysis from randomized clinical trials. *Scientific Reports*. 6, 32044.
- Bergman, B.C., Perreault, L., Strauss, A., Bacon, S., Kerege, A., Harrison, K., Brozinick, J.T., Hunerdosse, D.M., Playdon, M.C., Holmes, W., Bui, H.H., Sanders, P., Siddall, P., Wei, T., Thomas, M.K., Kuo, M.S., and Eckel, R.H. (2018). Intramuscular triglyceride synthesis: importance in muscle lipid partitioning in humans. *American Journal of Physiology. Endocrinology and Metabolism*. 314 (2), pp. E152-E164.
- Biensø, R.S., Ringholm, S., Kiilerich, K., Aachmann-Andersen, N.J., Krogh-Madsen, R., Guerra, B., Plomgaard, P., van Hall, G., Treebak, J.T., Saltin, B.,

Lundby, C., Calbet, J.A., Pilegaard, H., and Wojtaszewski, J.F. (2012) GLUT4 and glycogen synthase are key players in bed rest-induced insulin resistance. *Diabetes*. 61 (5), pp. 1090-1099.

Bilet, L., Phielix, E., van de Weijer, T., Gemmink, A., Bosma, M., Moonen-Kornips, E., Jorgensen, J. A., Schaart, G., Zhang, D., Meijer, K., Hopman, M., Hesselink, M., Ouwens, D. M., Shulman, G.I., Schrauwen-Hinderling, V.B., and Schrauwen, P. (2020) One-leg inactivity induces a reduction in mitochondrial oxidative capacity, intramyocellular lipid accumulation and reduced insulin signalling upon lipid infusion: a human study with unilateral limb suspension. *Diabetologia*. 63 (6), pp. 1211-1222.

Blanc, S., Normand, S., Pachiardi, C., Fortrat, J.O., Laville, M., and Gharib, C. (2000a) Fuel homeostasis during physical inactivity induced by bed rest. *The Journal of Clinical Endocrinology and Metabolism*. 85 (6), pp. 2223-2233.

Blanc, S., Normand, S., Pachiardi, C., Duvareille, M., and Gharib, C. (2000b) Leptin responses to physical inactivity induced by simulated weightlessness. *American Journal of Physiology. Regulatory, Integrative and Comparative Physiology*. 279 (3), pp. R891-R898.

Bucci, M., Huovinen, V., Guzzardi, M.A., Koskinen, S., Raiko, J. R., Lipponen, H., Ahsan, S., Badeau, R.M., Honka, M.J., Koffert, J., Savisto, N., Salonen, M.K., Andersson, J., Kullberg, J., Sandboge, S., Iozzo, P., Eriksson, J.G., and Nuutila, P. (2016) Resistance training improves skeletal muscle insulin sensitivity in elderly offspring of overweight and obese mothers. *Diabetologia*. 59 (1), pp. 77-86.

Burns, A.M., Nixon, A., Mallinson, J., Cordon, S.M., Stephens, F.B., and Greenhaff, P.L. (2021) Immobilisation induces sizeable and sustained reductions in forearm glucose uptake in just 24 h but does not change lipid uptake in healthy men. *The Journal of Physiology*. 599 (8), pp. 2197-2210.

Bushra, R., and Aslam, N. (2010) An overview of clinical pharmacology of Ibuprofen. *Oman Medical Journal*. 25 (3), pp. 155-1661.

Brennan, R., Wazaify, M., Shawabkeh, H., Boardley, I., McVeigh, J., and Van Hout, M.C. (2021) A Scoping Review of Non-Medical and Extra-Medical Use

of Non-Steroidal Anti-Inflammatory Drugs (NSAIDs). *Drug Safety*. 44 (9), pp. 917-928.

Chang, E., Park, C.Y., and Park, S.W. (2013) Role of thiazolidinediones, insulin sensitizers, in non-alcoholic fatty liver disease. *Journal of Diabetes Investigation*. 4 (6), pp. 517-524.

Chien, H.C., Greenhaff, P.L., and Constantin-Teodosiu, D. (2020) PPAR δ and FOXO1 Mediate Palmitate-Induced Inhibition of Muscle Pyruvate Dehydrogenase Complex and CHO Oxidation, Events Reversed by Electrical Pulse Stimulation. *International Journal of Molecular Sciences*. 21 (16), 5942.

Chow, L.S., Mashek, D.G., Austin, E., Eberly, L.E., Persson, X.M., Mashek, M.T., Seaquist, E.R., and Jensen, M.D. (2014) Training status diverges muscle diacylglycerol accumulation during free fatty acid elevation. *American Journal of Physiology. Endocrinology and Metabolism*. 307 (1), pp. E124-E131.

Coen, P.M., Dubé, J. J., Amati, F., Stefanovic-Racic, M., Ferrell, R.E., Toledo, F.G., and Goodpaster, B.H. (2010) Insulin resistance is associated with higher intramyocellular triglycerides in type I but not type II myocytes concomitant with higher ceramide content. *Diabetes*. 59 (1), pp. 80-88.

DeFronzo, R.A., and Tripathy, D. (2009) Skeletal muscle insulin resistance is the primary defect in type 2 diabetes. *Diabetes Care*. 32 (Supplement 2), pp. S157-S163.

DeFronzo, R.A. (2010) Insulin resistance, lipotoxicity, type 2 diabetes and atherosclerosis: the missing links. The Claude Bernard Lecture 2009. *Diabetologia*. 53 (7), pp. 1270-1287.

Dolkas, C.B., and Greenleaf, J.E. (1977) Insulin and glucose responses during bed rest with isotonic and isometric exercise. *Journal of applied physiology: Respiratory, Environmental and Exercise Physiology*. 43 (6), pp. 1033-1038.

Duran-Valdez, E., de Serna, D.G., Schneider, S., Amorim, F., Burge, M., and Schade, D.S. (2008) Metabolic effects of 2 days of strict bed rest. *Endocrine Practice: Official Journal of The American College of Endocrinology and The American Association of Clinical Endocrinologists*. 14 (5), pp. 564-569.

Dirks, M.L., Stephens, F.B., Jackman, S.R., Galera Gordo, J., Machin, D.J., Pulsford, R.M., van Loon, L., and Wall, B.T. (2018) A single day of bed rest, irrespective of energy balance, does not affect skeletal muscle gene expression or insulin sensitivity. *Experimental Physiology*. 103 (6), pp. 860-875.

Dwyer, T., Ponsonby, A.L., Ukoumunne, O.C., Pezic, A., Venn, A., Dunstan, D., Barr, E., Blair, S., Cochrane, J., Zimmet, P., and Shaw, J. (2011) Association of change in daily step count over five years with insulin sensitivity and adiposity: population based cohort study. *BMJ (Clinical Research ed.)*. 342, c7249.

Gemmink, A., Schrauwen, P., and Hesselink, M. (2020) Exercising your fat (metabolism) into shape: a muscle-centred view. *Diabetologia*. 63 (8), pp. 1453-1463.

Hall, K.S., Hyde, E.T., Bassett, D.R., Carlson, S.A., Carnethon, M.R., Ekelund, U., Evenson, K.R., Galuska, D.A., Kraus, W.E., Lee, I.M., Matthews, C.E., Omura, J.D., Paluch, A.E., Thomas, W.I., and Fulton, J.E. (2020) Systematic review of the prospective association of daily step counts with risk of mortality, cardiovascular disease, and dysglycemia. *The International Journal of Behavioral Nutrition and Physical Activity*. 17 (1), 78.

Hamburg, N.M., McMackin, C.J., Huang, A.L., Shenouda, S.M., Widlansky, M.E., Schulz, E., Gokce, N., Ruderman, N.B., Keaney, J.F., Jr, and Vita, J.A. (2007) Physical inactivity rapidly induces insulin resistance and microvascular dysfunction in healthy volunteers. *Arteriosclerosis, Thrombosis, and Vascular Biology*. 27 (12), pp. 2650-2656.

He, L., Liu, X., Wang, L., and Yang, Z. (2016) Thiazolidinediones for nonalcoholic steatohepatitis: A meta-analysis of randomized clinical trials. *Medicine*. 95 (42), e4947.

Heer, M., Baecker, N., Wnendt, S., Fischer, A., Biolo, G., and Frings-Meuthen, P. (2014) How fast is recovery of impaired glucose tolerance after 21-day bed rest (NUC study) in healthy adults? *The Scientific World Journal*. 2014, 803083.

Holten, M.K., Zacho, M., Gaster, M., Juel, C., Wojtaszewski, J.F., and Dela, F. (2004) Strength training increases insulin-mediated glucose uptake, GLUT4 content, and insulin signaling in skeletal muscle in patients with type 2 diabetes. *Diabetes*. 53 (2), 294-305.

Ingram, K.H., Lara-Castro, C., Gower, B.A., Makowsky, R., Allison, D.B., Newcomer, B.R., Munoz, A.J., Beasley, T.M., Lawrence, J.C., Lopez-Ben, R., Rigsby, D.Y., and Garvey, W.T. (2011) Intramyocellular lipid and insulin resistance: differential relationships in European and African Americans. *Obesity (Silver Spring, Md.)*. 19 (7), pp. 1469-1475.

Kenny, H.C., Rudwill, F., Breen, L., Salanova, M., Blottner, D., Heise, T., Heer, M., Blanc, S., and O'Gorman, D.J. (2017) Bed rest and resistive vibration exercise unveil novel links between skeletal muscle mitochondrial function and insulin resistance. *Diabetologia*. 60 (8), pp. 1491-1501.

Knudsen, S.H., Hansen, L.S., Pedersen, M., Dejgaard, T., Hansen, J., Hall, G.V., Thomsen, C., Solomon, T.P., Pedersen, B.K., and Krogh-Madsen, R. (2012) Changes in insulin sensitivity precede changes in body composition during 14 days of step reduction combined with overfeeding in healthy young men. *Journal of Applied Physiology (Bethesda, Md.: 1985)*. 113 (1), pp. 7-15.

Koopman, R., Manders, R.J., Jonkers, R.A., Hul, G.B., Kuipers, H., and van Loon, L.J. (2006) Intramyocellular lipid and glycogen content are reduced following resistance exercise in untrained healthy males. *European Journal of Applied Physiology*. 96 (5), pp. 525-534.

Krogh-Madsen, R., Thyfault, J.P., Broholm, C., Mortensen, O.H., Olsen, R.H., Mounier, R., Plomgaard, P., van Hall, G., Booth, F.W., and Pedersen, B.K. (2010) A 2-wk reduction of ambulatory activity attenuates peripheral insulin sensitivity. *Journal of Applied Physiology (Bethesda, Md.: 1985)*. 108 (5), pp. 1034-1040.

Krssak, M., Falk Petersen, K., Dresner, A., DiPietro, L., Vogel, S.M., Rothman, D.L., Roden, M., and Shulman, G.I. (1999) Intramyocellular lipid concentrations are correlated with insulin sensitivity in humans: a ¹H NMR spectroscopy study. *Diabetologia*. 42 (1), pp. 113-116.

Kumashiro, N., Erion, D.M., Zhang, D., Kahn, M., Beddow, S.A., Chu, X., Still, C.D., Gerhard, G.S., Han, X., Dziura, J., Petersen, K.F., Samuel, V.T., and Shulman, G.I. (2011) Cellular mechanism of insulin resistance in nonalcoholic fatty liver disease. *Proceedings of the National Academy of Sciences of the United States of America*. 108 (39), pp. 16381-16385.

Lecka-Czernik, B., Ackert-Bicknell, C., Adamo, M.L., Marmolejos, V., Churchill, G.A., Shockley, K.R., Reid, I.R., Grey, A., and Rosen, C.J. (2007) Activation of peroxisome proliferator-activated receptor gamma (PPARgamma) by rosiglitazone suppresses components of the insulin-like growth factor regulatory system in vitro and in vivo. *Endocrinology*. 148 (2), pp. 903-911.

Li, J., Guo, C., and Wu, J. (2019) 15-Deoxy- Δ -^{12,14}-Prostaglandin J2 (15d-PGJ2), an Endogenous Ligand of PPAR- γ : Function and Mechanism. *PPAR Research*. 2019, 7242030.

Loviscach, M., Rehman, N., Carter, L., Mudaliar, S., Mohadeen, P., Ciaraldi, T.P., Veerkamp, J.H., and Henry, R.R. (2000) Distribution of peroxisome proliferator-activated receptors (PPARs) in human skeletal muscle and adipose tissue: relation to insulin action. *Diabetologia*. 43 (3), pp. 304-311.

Lund, S., Holman, G. D., Schmitz, O., and Pedersen, O. (1995) Contraction stimulates translocation of glucose transporter GLUT4 in skeletal muscle through a mechanism distinct from that of insulin. *Proceedings of the National Academy of Sciences of the United States of America*. 92 (13), pp. 5817-5821.

Luukkonen, P.K., Zhou, Y., Sädevirta, S., Leivonen, M., Arola, J., Orešič, M., Hyötyläinen, T., and Yki-Järvinen, H. (2016) Hepatic ceramides dissociate steatosis and insulin resistance in patients with non-alcoholic fatty liver disease. *Journal of Hepatology*. 64 (5), pp. 1167-1175.

Machado, M.V., Ferreira, D.M., Castro, R.E., Silvestre, A.R., Evangelista, T., Coutinho, J., Carepa, F., Costa, A., Rodrigues, C.M. and Cortez-Pinto, H. (2012) Liver and muscle in morbid obesity: the interplay of fatty liver and insulin resistance. *PloS one*. 7 (2), e31738.

Magkos, F., and Mittendorfer, B. (2009) Stable isotope-labeled tracers for the investigation of fatty acid and triglyceride metabolism in humans in vivo. *Clinical Lipidology*. 4 (2), pp. 215-230.

Magkos, F., Su, X., Bradley, D., Fabbrini, E., Conte, C., Eagon, J.C., Varela, J.E., Brunt, E.M., Patterson, B.W., and Klein, S. (2012) Intrahepatic diacylglycerol content is associated with hepatic insulin resistance in obese subjects. *Gastroenterology*. 142 (7), pp. 1444–1446.

Mayerson, A.B., Hundal, R.S., Dufour, S., Lebon, V., Befroy, D., Cline, G.W., Enocksson, S., Inzucchi, S.E., Shulman, G.I., and Petersen, K.F. (2002) The effects of rosiglitazone on insulin sensitivity, lipolysis, and hepatic and skeletal muscle triglyceride content in patients with type 2 diabetes. *Diabetes*. 51 (3), pp. 797-802.

Mikines, K.J., Dela, F., Tronier, B., and Galbo, H. (1989) Effect of 7 days of bed rest on dose-response relation between plasma glucose and insulin secretion. *The American Journal of Physiology*. 257 (1 Pt 1), pp. E43-E48.

Mikines, K.J., Richter, E.A., Dela, F. and Galbo, H. (1991) Seven Days of Bed Rest Decrease Insulin Action on Glucose Uptake in Leg and Whole Body. *Journal of Applied Physiology*. 70 (3), pp. 1245-1254.

Miyazaki, Y., Glass, L., Triplitt, C., Wajcberg, E., Mandarino, L.J., and DeFronzo, R.A. (2002) Abdominal fat distribution and peripheral and hepatic insulin resistance in type 2 diabetes mellitus. *American Journal of Physiology. Endocrinology and Metabolism*. 283 (6), pp. E1135-E1143.

Oh, S., Shida, T., Sawai, A., Maruyama, T., Eguchi, K., Isobe, T., Okamoto, Y., Someya, N., Tanaka, K., Arai, E., Tozawa, A. and Shoda, J. (2014) Acceleration training for managing nonalcoholic fatty liver disease: a pilot study. *Therapeutics and Clinical Risk Management*. 10, pp. 925-936.

Oshida, N., Shida, T., Oh, S., Kim, T., Isobe, T., Okamoto, Y., Kamimaki, T., Okada, K., Suzuki, H., Ariizumi, S.I., Yamamoto, M. and Shoda, J. (2019) Urinary Levels of Titin-N Fragment, a Skeletal Muscle Damage Marker, are Increased in Subjects with Nonalcoholic Fatty Liver Disease. *Scientific Reports*. 9 (1), p. 19498.

Pan, D.A., Lillioja, S., Kriketos, A.D., Milner, M.R., Baur, L.A., Bogardus, C., Jenkins, A.B., and Storlien, L.H. (1997) Skeletal muscle triglyceride levels are inversely related to insulin action. *Diabetes*. 46 (6), pp. 983-988.

Patterson, B.W. (1997) Use of stable isotopically labeled tracers for studies of metabolic kinetics: an overview. *Metabolism: Clinical and Experimental*. 46 (3), pp. 322-329.

Perreault, L., Newsom, S.A., Strauss, A., Kerege, A., Kahn, D.E., Harrison, K.A., Snell-Bergeon, J.K., Nemkov, T., D'Alessandro, A., Jackman, M.R., MacLean, P.S., and Bergman, B.C. (2018) Intracellular localization of diacylglycerols and sphingolipids influences insulin sensitivity and mitochondrial function in human skeletal muscle. *JCI Insight*. 3 (3), e96805.

Perreault, L., Bergman, B.C., Hunerdosse, D.M., Playdon, M.C., and Eckel, R.H. (2010) Inflexibility in intramuscular triglyceride fractional synthesis distinguishes prediabetes from obesity in humans. *Obesity (Silver Spring, Md.)*. 18 (8), pp. 1524-1531.

Perreault, L., Newsom, S.A., Strauss, A., Kerege, A., Kahn, D.E., Harrison, K.A., Snell-Bergeon, J.K., Nemkov, T., D'Alessandro, A., Jackman, M.R., MacLean, P.S., and Bergman, B.C. (2018) Intracellular localization of diacylglycerols and sphingolipids influences insulin sensitivity and mitochondrial function in human skeletal muscle. *JCI Insight*. 3 (3), e96805.

Perry, R.J., Kim, T., Zhang, X.M., Lee, H.Y., Pesta, D., Popov, V.B., Zhang, D., Rahimi, Y., Jurczak, M.J., Cline, G.W., Spiegel, D.A., and Shulman, G.I. (2013) Reversal of hypertriglyceridemia, fatty liver disease, and insulin resistance by a liver-targeted mitochondrial uncoupler. *Cell Metabolism*. 18 (5), pp. 740-748.

Perry, R.J., Zhang, D., Zhang, X.M., Boyer, J.L., and Shulman, G.I. (2015) Controlled-release mitochondrial protonophore reverses diabetes and steatohepatitis in rats. *Science (New York, N.Y.)*. 347 (6227), pp. 1253-1256.

Pesta, D. and Gnaiger, E. (2012) High-resolution respirometry: OXPHOS protocols for human cells and permeabilized fibers from small biopsies of human muscle. *Methods in molecular Biology (Clifton, N.J.)*. 810, pp. 25-58.

Petersen, M.C., and Shulman, G.I. (2017) Roles of Diacylglycerols and Ceramides in Hepatic Insulin Resistance. *Trends in Pharmacological Sciences*. 38 (7), pp. 649-665.

Phillips, D.I., Caddy, S., Ilic, V., Fielding, B.A., Frayn, K.N., Borthwick, A.C., and Taylor, R. (1996) Intramuscular triglyceride and muscle insulin sensitivity: evidence for a relationship in nondiabetic subjects. *Metabolism: Clinical and Experimental*. 45 (8), pp. 947-950.

Pugh, C.J., Spring, V.S., Kemp, G.J., Richardson, P., Shojaee-Moradie, F., Umpleby, A.M., Green, D.J., Cable, N.T., Jones, H., and Cuthbertson, D.J. (2014) Exercise training reverses endothelial dysfunction in nonalcoholic fatty liver disease. *American Journal of Physiology. Heart and Circulatory Physiology*. 307 (9), pp. H1298-H1306.

Reidy, P.T., McKenzie, A.I., Mahmassani, Z., Morrow, V.R., Yonemura, N.M., Hopkins, P.N., Marcus, R.L., Rondina, M.T., Lin, Y.K., and Drummond, M.J. (2018) Skeletal muscle ceramides and relationship with insulin sensitivity after 2 weeks of simulated sedentary behaviour and recovery in healthy older adults. *The Journal of Physiology*. 596 (21), pp. 5217-5236.

Sallmann, A.R. (1986) The history of diclofenac. *The American Journal of Medicine*. 80 (4B), pp. 29-33.

Schrauwen-Hinderling, V.B., Hesselink, M.K., Schrauwen, P., and Kooi, M.E. (2006) Intramyocellular lipid content in human skeletal muscle. *Obesity (Silver Spring, Md.)*. 14 (3), pp. 357-367.

Sjöros, T., Vähä-Ypyä, H., Laine, S., Garthwaite, T., Laheesmaa, M., Laurila, S.M., Latva-Rasku, A., Savolainen, A., Miikkulainen, A., Löyttyniemi, E., Sievänen, H., Kalliokoski, K.K., Knuti, J., Vasankari, T., and Heinonen, I.H.A. (2020) Both sedentary time and physical activity are associated with cardiometabolic health in overweight adults in a 1 month accelerometer measurement. *Scientific Reports*. 10 (1), 20578.

Silvennoinen, M., Ahtiainen, J.P., Hulmi, J.J., Pekkala, S., Taipale, R.S., Nindl, B.C., Laine, T., Häkkinen, K., Selänne, H., Kyröläinen, H., and Kainulainen, H. (2015) PGC-1 isoforms and their target genes are expressed differently in

human skeletal muscle following resistance and endurance exercise. *Physiological Reports*. 3 (10), e12563.

Smorawiński, J., Kaciuba-Uściłko, H., Nazar, K., Kubala, P., Kamińska, E., Ziemia, A. W., Adrian, J., and Greenleaf, J.E. (2000) Effects of three-day bed rest on metabolic, hormonal and circulatory responses to an oral glucose load in endurance or strength trained athletes and untrained subjects. *Journal Of Physiology and Pharmacology: An Official Journal of The Polish Physiological Society*. 51 (2), pp. 279-289.

Stephens, B.R., Granados, K., Zderic, T.W., Hamilton, M.T., and Braun, B. (2011) Effects of 1 day of inactivity on insulin action in healthy men and women: interaction with energy intake. *Metabolism: Clinical and Experimental*. 60 (7), pp. 941-949.

Stettler, R., Ith, M., Acheson, K.J., Décombaz, J., Boesch, C., Tappy, L., and Binnert, C. (2005) Interaction between dietary lipids and physical inactivity on insulin sensitivity and on intramyocellular lipids in healthy men. *Diabetes Care*. 28 (6), pp. 1404-1409.

Szendroedi, J., Yoshimura, T., Phielix, E., Koliaki, C., Marcucci, M., Zhang, D., Jelenik, T., Müller, J., Herder, C., Nowotny, P., Shulman, G.I., and Roden, M. (2014) Role of diacylglycerol activation of PKC θ in lipid-induced muscle insulin resistance in humans. *Proceedings of the National Academy of Sciences of the United States of America*. 111 (26), pp. 9597-9602.

Tsintzas, K., Stephens, F.B., Snijders, T., Wall, B.T., Cooper, S., Mallinson, J., Verdijk, L.B., and van Loon, L. (2017) Intramyocellular lipid content and lipogenic gene expression responses following a single bout of resistance type exercise differ between young and older men. *Experimental Gerontology*. 93, pp. 36-45.

Tudor-Locke, C., Craig, C.L., Brown, W.J., Clemes, S.A., De Cocker, K., Giles-Corti, B., Hatano, Y., Inoue, S., Matsudo, S.M., Mutrie, N., Oppert, J.M., Rowe, D.A., Schmidt, M.D., Schofield, G.M., Spence, J.C., Teixeira, P.J., Tully, M.A., and Blair, S.N. (2011) How many steps/day are enough? For adults. *The International Journal of Behavioral Nutrition and Physical Activity*. 8, 79.

- van Loon, L.J., Greenhaff, P.L., Constantin-Teodosiu, D., Saris, W.H., and Wagenmakers, A.J. (2001) The effects of increasing exercise intensity on muscle fuel utilisation in humans. *The Journal of Physiology*. 536 (Pt 1), pp. 295-304.
- van Loon, L.J. (2004a) Use of intramuscular triacylglycerol as a substrate source during exercise in humans. *Journal of Applied Physiology (Bethesda, Md.: 1985)*. 97 (4), pp. 1170-1187.
- van Loon, L.J., Koopman, R., Manders, R., van der Weegen, W., van Kranenburg, G.P., and Keizer, H.A. (2004b) Intramyocellular lipid content in type 2 diabetes patients compared with overweight sedentary men and highly trained endurance athletes. *American Journal of Physiology. Endocrinology and Metabolism*. 287 (3), pp. E558-E565.
- van der Poorten, D., Milner, K.L., Hui, J., Hodge, A., Trenell, M.I., Kench, J.G., London, R., Peduto, T., Chisholm, D.J. and George, J. (2008) Visceral fat: a key mediator of steatohepatitis in metabolic liver disease. *Hepatology (Baltimore, Md.)*. 48 (2), pp. 449-457.
- Verbrugge, S.A.J., Alhusen, J.A., Kempin, S., Pillon, N.J., Rozman, J., Wackerhage, H., and Kleinert, M. (2022) Genes controlling skeletal muscle glucose uptake and their regulation by endurance and resistance exercise. *Journal of Cellular Biochemistry*. 123 (2), pp. 202-214.
- Wasserman D.H. (2009) Four grams of glucose. *American Journal of Physiology. Endocrinology and Metabolism*. 296 (1), pp. E11-E21.
- Yamazaki, R., Kusunoki, N., Matsuzaki, T., Hashimoto, S., and Kawai, S. (2002) Nonsteroidal anti-inflammatory drugs induce apoptosis in association with activation of peroxisome proliferator-activated receptor gamma in rheumatoid synovial cells. *The Journal of Pharmacology and Experimental Therapeutics*. 302 (1), pp. 18-25.
- Zheng, P., Ducharme, S.W., Moore, C.C., Tudor-Locke, C., and Aguiar, E.J. (2022) Classification of moderate-intensity overground walking speed in 21- to 85-year-old adults. *Journal of Sports Sciences*. 40 (15), pp. 1732-1740.

Zhu, R., Wen, C., Li, J., Harris, M.B., Liu, Y.Y., and Kuo, C.H. (2015) Lipid storage changes in human skeletal muscle during detraining. *Frontiers in Physiology*. 6, 309.

7. Appendices

Appendix A

7-1.

Change in mRNA Expression: 24h vs. Baseline		
Gene	Log Fold Change	P value
PPARGC1A	-1.144	1.01E-11
TNF	0.7	8.96E-09
PIK3R1	1.227	8.53E-08
CEBPB	0.817	0.000000231
TNC	3.777	0.00000181
MSTN	-1.222	0.00000204
SCD	0.547	0.00000204
PTK2	1.726	0.00000682
PDK4	1.444	0.0000128
IL6	2.593	0.0000235
PRKAA1	0.511	0.000211
PDK2	-1.06	0.000348
TSC2	1.045	0.000399
PTGS2	0.879	0.000516
ATF3	0.9	0.0011
MYC	2.526	0.00597

7-2.

Change in mRNA Expression: 7 Days vs. Baseline		
Gene	Log Fold Change	P value
PPARGC1A	-0.639	1.23E-09
TNF	0.906	7.65E-09
MSTN	-0.525	2.75E-08
SIRT1	-0.51	2.83E-08
TNC	2.136	0.00000113
CEBPB	0.692	0.00000114
PTK2	1.392	0.00000427
PDK4	0.695	0.00000901
PIK3R1	0.658	0.0000477
IL6	1.785	0.0000691
PDK2	-0.517	0.000276
ATF3	0.766	0.000783
MYC	1.879	0.00282
TSC2	1.198	0.0393

7-3.

Change in mRNA Expression: 28 Days vs. Baseline		
Gene	Log Fold Change	P value
IGF1	0.503	0.0000972
AKT1	0.582	0.000188
TNF	0.99	0.000514

7-4.

Change in mRNA Expression: 84 Days vs. Baseline		
Gene	Log Fold Change	P value
PPARGC1A	-0.682	7.5E-09
AKT1	-0.584	0.000000114
VEGFA	-0.847	0.00000463
SCD	0.664	0.00653

Tables 7-1, 7-2, 7-3, 7-4: Tables showing the change in mRNA expression from baseline (Log Fold Change) in lipid metabolism associated genes relative to baseline at the (7-2) 24 hours, (7-3) 7 days, (7-4) 28 days, and (7-5) 84 days time points in the placebo group. For each time point comparison, genes are ordered in descending order from most significantly altered to least significantly altered based on p value.

Appendix B

7-5.

Change in mRNA Expression: 24h vs. Baseline		
Gene	Log Fold Change	P value
MSTN	-1.359	4.65E-11
TNF	2.646	0.000000278
IGF1	0.957	0.000000574
AKT1	1.722	0.00000107
PPARGC1A	0.542	0.0000225
PRKAA1	0.793	0.000286
MYC	1.469	0.000664
SCD	1.562	0.00158
IL6	3	0.00161
SIRT1	1.033	0.00187
IL18	0.722	0.0426

7-6.

Change in mRNA Expression: 7 Days vs. Baseline		
Gene	Log Fold Change	P value
AKT1	0.799	2.86E-11
TNF	2.223	3.58E-09
FOXO1	0.911	5.07E-09
PIK3R1	0.576	6.3E-09
IGF1	1.107	1.06E-08
PPARGC1A	0.804	0.000000293
SIRT1	0.635	0.000000341
IL6	1.352	0.0000126
PRKAA1	1.035	0.0000224
PTGS2	1.299	0.0000696
SCD	1.849	0.000106
IL18	0.952	0.000404
ATF3	0.593	0.0017

7-7. Change in mRNA Expression: 28 Days vs. Baseline

Gene	Log Fold Change	P value
AKT1	1.488	2.86E-11
IGF1	1.735	8.37E-10
PPARGC1A	0.601	1.34E-09
FOXO1	0.501	5.07E-09
SIRT1	0.677	2.51E-08
TNF	2.484	2.53E-08
VEGFA	0.607	0.000000324
IL6	1.464	0.00000167
PTGS2	1.93	0.00000423
PDK4	-0.607	0.0000202
PRKAA1	1.037	0.0000224
IL18	0.616	0.0000243
SCD	1.992	0.000106
MYC	0.738	0.00029
ATF3	1.153	0.0017

7-8. Change in mRNA Expression: 84 Days vs. Baseline

Gene	Log Fold Change	P value
PPARGC1A	1.05	9.88E-09
AKT1	1.142	7.43E-08
TNF	2.025	0.000000278
FOXO1	0.559	0.000000315
IGF1	1.606	0.000000574
SIRT1	1.138	0.0000252
PRKAA1	1.227	0.000286
IL6	1.046	0.000292
PDK2	0.505	0.000407
PTGS2	2.437	0.000698
SCD	2.988	0.00158
IL18	0.754	0.00423

Tables 7-5, 7-6, 7-7, 7-8: Tables showing the change in mRNA expression from baseline (Log Fold Change) in lipid metabolism associated genes relative to baseline at the (5-6) 24 hours, (5-7) 7 days, (5-8) 28 days and (5-9) 84 days' time points in the diclofenac group. For each time point comparison, genes are ordered in descending order from most significantly altered to least significantly altered based on p value.

Appendix C

Baseline LD Count, LD Size and IMCL content data for the distinct groups of all studies described throughout. All bars are mean \pm SEM. * Significant difference vs. Acute BR, Chronic BR, Control and NAFLD. †, Significant difference vs. all other groups.

